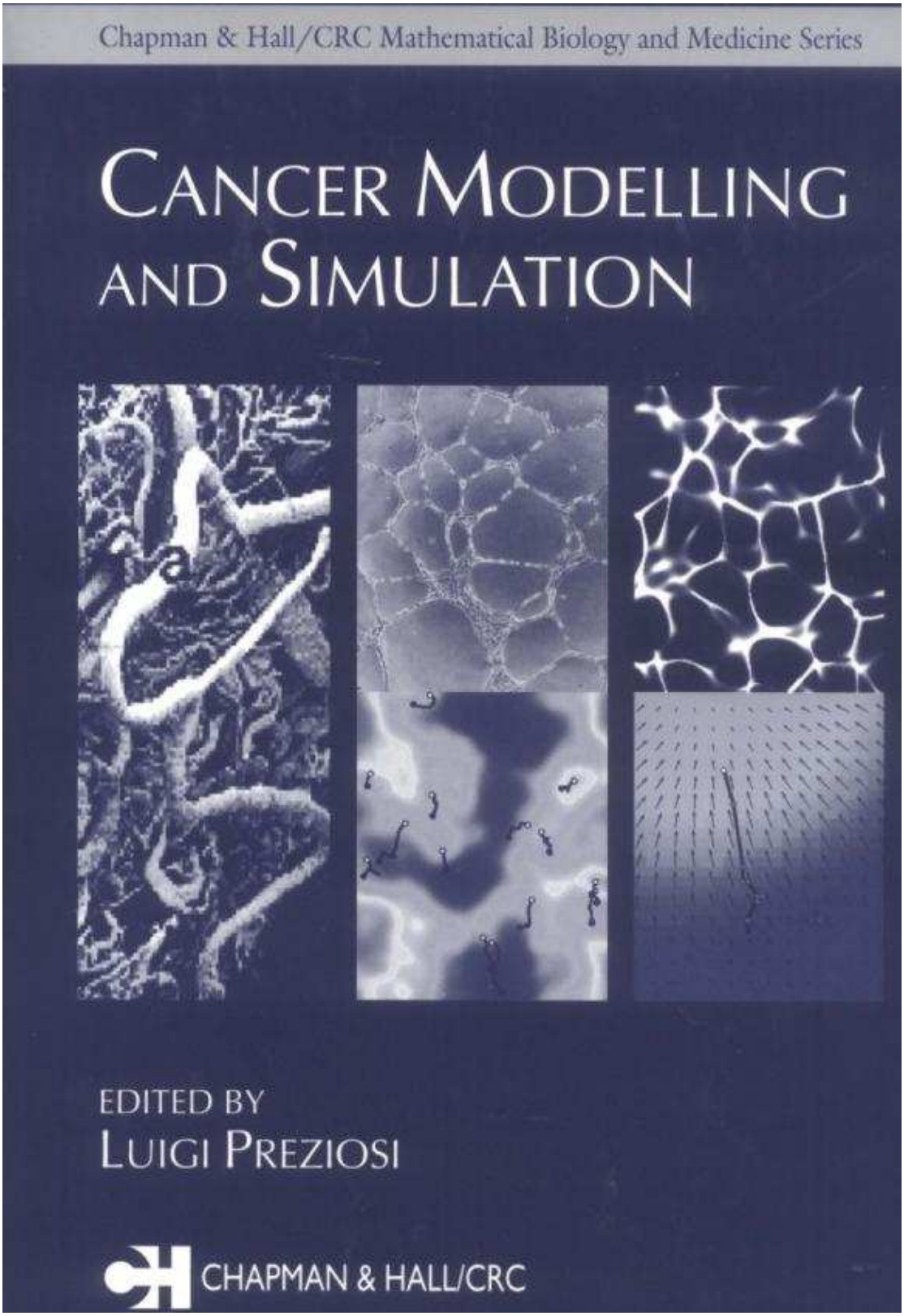

Asd for AEK FC

Chapman & Hall/CRC Mathematical Biology and Medicine Series

Cancer Modelling and Simulation

EDITED BY
Luigi Preziosi

CHAPMAN & HALL/CRC

A CRC Press Company
Boca Raton London New York Washington, D.C.

Pictured on the cover: left, vasculature surrounding a tumour; center (top), *in vitro* vasculogenesis; center (bottom), trajectories of some endothelial cells involved in vasculogenesis on a background of the simulated concentration field of chemoattractant produced by the endothelial cells; right (top), results of the vasculogenesis simulation; right (bottom), comparison of the experimental trajectory of an endothelial cell with the field of concentration gradients of chemoattractant.

Library of Congress Cataloging-in-Publication Data

Cancer modelling and simulation / edited by Luigi Preziosi.
p. cm. — (Chapman & Hall/CRC mathematical biology and medicine series; v.3)
Includes bibliographical references and index.
ISBN 1-58488-361-8
1. Cancer—Mathematical models. 2. Cancer—Computer simulation. I. Preziosi, Luigi. II. Series.

RC267.C3645 2003
616.99′4′00113—dc21 2003046137

International Standard Book Number 1-58488-361-8
Library of Congress Card Number 2003046137
Printed in the United States of America 1 2 3 4 5 6 7 8 9 0
Printed on acid-free paper

Preface

Tumour evolution is a very complex process, involving many different phenomena, which occur at different scales. In fact, the phenomenological description strongly depends on the enlargement used in the real or ideal microscope used by the biologist or by the modeller. A biologist, a bio-chemist, or a medical doctor would probably describe the phenomena occurring during the evolution of tumours using three natural viewpoints: the sub-cellular level, the cellular level, and the tissue level. From the modelling point of view a connection can be approximately drawn between the description levels above and the microscopic, mesoscopic, and macroscopic scales.

So, the microscopic scale refers to those phenomena that occur at the sub-cellular level and therefore to activities that take place within the cell or at the cell membrane, e.g., DNA synthesis and degradation, gene expression, alteration mechanisms of the cell cycle, absorption of vital nutrients, activation or inactivation of receptors, transduction of chemical signals between cells that regulate cellular activities, such as duplication, motion, adhesion, or detachment.

The mesoscopic scale refers to the cellular level and therefore to the main activities of the cell populations, e.g., statistical description of the progression and activation state, interactions among tumour cells and the other types of cells present in the body such as endothelial cells, macrophages, lymphocytes, proliferative and destructive interactions, aggregation and disaggregation properties, and intravasation and extravasation processes.

The macroscopic scale refers to the tissue level and therefore to those phenomena which are typical of continuum systems, e.g., cell migration, convection and diffusion of nutrients and chemical factors, mechanical responses, interactions with external tissues, capsule formation and rupture, diffusion of metastases, and phase transitions (from free to bound cells and vice versa).

Of course what happens at a certain scale is strongly linked to what happens at the other scales. Therefore it is impossible to completely describe a phenomenon without taking into account others occurring at a smaller or a larger scale. This means that like a set of Chinese boxes, mathematical models and methods characteristic of different scales could be interlaced to achieve a better description of the phenomena. For instance, in the avascular phase tumour cells are packed in a multicellular spheroid not yet connected to the host's blood supply. Looking at this stage from the tissue level the evolution depends, for instance, on the distribution of oxygen, glucose, and other nutrients and on the production and reception of growth modulating chemical

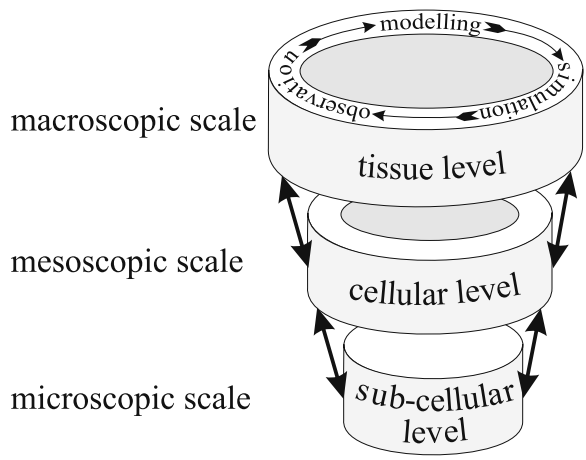

Figure 0.1

substances, phenomena involving the sub-cellular level. This phase can be described by mass balance equation and reaction-diffusion equations that can be derived not only on the basis of principles of continuum mechanics but also on the basis of cell-based models. Actually, in the latter modelling framework it is easier to introduce cellular and sub-cellular mechanisms, while in the former framework it is easier to deal with macroscopic mechanisms, such as the interaction with external tissues. Going on with the evolutionary process, at a certain stage of maturation tumour cells start producing particular chemical factors switching on the process of angiogenesis. By this process new blood vessels grow into a tissue from surrounding parent vessels. This crucial triggering mechanism, leading to the vascular growth phase, is therefore also regulated by phenomena occurring at the sub-cellular and cellular level. Finally, the detachment of metastases is regulated by the adhesion properties of the cells.

In addition to the just-mentioned connections among different observation and modelling levels, research at each single level would certainly profit from the interactions among different branches of science. In fact, the ideal modelling cycle should develop as follows: from the phenomenological observation of a certain phenomenon in real patients, scientists in bio-medicine try to conceive a more convenient and relatively harmless biological model, which can be *in vivo*, e.g., mouse, chicken embryo, or *in vitro*. They can then perform a series of experiments on that model. Either directly from the phenomenological

observation or through the biological model, mathematicians and physicists can generate mathematical models aimed at describing the phenomenon of interest. The analysis of the properties of the solution by proper mathematical methods will then give a qualitative description of the dynamics resulting in a deeper insight into the problem. The model can then be implemented numerically to give rise to *in silico* models of the phenomenon. The quality of the modelling process can be tested validating the results of the simulations with the experiments. If the comparison is considered satisfactory, then the modelling cycle closes successfully. If not, one or more steps of the modelling process need be refined and the cycle continues. Needless to say that, vice versa simulations need to agree with the qualitative properties of the solution, otherwise the numerical code is not accurate enough and that the theoretical predictions need to agree with the experiments, otherwise the mathematical model is not satisfactory.

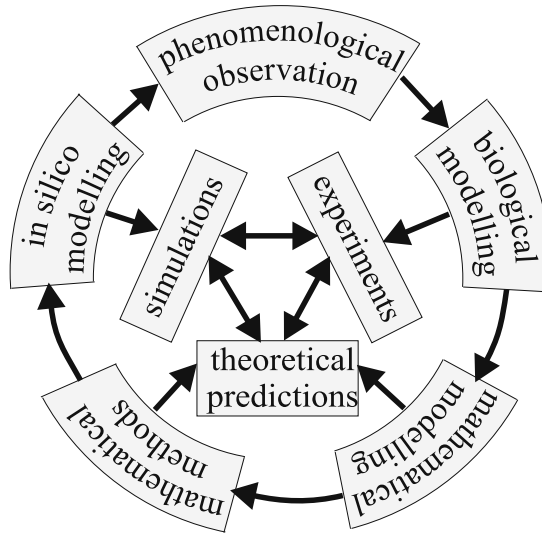

Figure 0.2

This book is embedded in the cultural framework explained above and is written in the belief that the use of mathematical modelling and computer simulations can help cancer research. In fact, the path that goes from clinical experience to the laboratories and back to the clinic starts from a very practical situation and passes through progressive abstractions and simplification steps to gain insight into the complex phenomena occurring during tumour

evolution and growth. The acquisition of this knowledge is then tested back through experimental phases of increasing complexity and hopefully applied in the clinical practice. It is common knowledge that this stepwise process also means a different level of ethical involvement.

It is true that including mathematical modelling and computer simulations in the path mentioned above can speed up the process, provide insight into the mechanisms that control tumour evolution and growth, and, hence, suggest directions for new therapies. The theoretical predictions generated from the models and their simulations can help optimise the experimental protocol by identifying the most promising candidates for further clinical investigation. In fact, the ease with which physical parameters can be manipulated in a computer simulation and the speed with which large numbers of simulations can be performed can help reduce the number of animal experiments to be carried out and identify new experimental programmes and optimal tumour therapy schedules.

However, the development of mathematical models of tumour growth requires the knowledge of different backgrounds, in particular the understanding of the biological phenomena involved and the skill in using several mathematical tools to obtain both qualitative and quantitative results.

The aim of this book is to collect some of the modelling techniques and the mathematical methods that allow the reader to gain deeper insight into the dynamics of tumour development and growth after being given the biological background. The aim is to deal with the whole modelling process and to propose a unified treatment of the whole subject in a way that modelling, analytical, and computational methods are linked together toward the final objective of providing a virtual representation of physical reality.

The first three chapters give the phenomenological description of the main processes involved in tumour development and growth. Specifically, the first chapter describes the process of angiogenesis, the second some of the sub-cellular mechanisms that direct tumour behaviour, and the third the fundamental mechanisms of diffusion in an avascular and a vascular tumour. Chapter 4 introduces at a tutorial level some of the basic techniques used to deduce models describing the growth of tumour masses in the avascular phase, and to study the existence of stationary solution and their stability properties. Chapter 5 gives the fundamentals of continuum mechanics of growing media and of multicomponent systems usually applied to deduce tumour models. Chapter 6 gives a review of mathematical models for the description of angiogenesis, keeping in mind both the mesoscopic and the macroscopic description. Chapter 7 looks more deeply into the mechanisms of angiogenesis studying the interactions between the sub-cellular and the tissue level, going toward the definition of antiangiogenic strategies. The following three chapters deal with the mechanisms of detachment, intravasation, transport, and extravasation of metastases from the multicell spheroid, both from an experimental and a theoretical viewpoint. More precisely, Chapter 8 deals with the fundamentals of the adhesion mechanisms and the experiments that can be performed to test

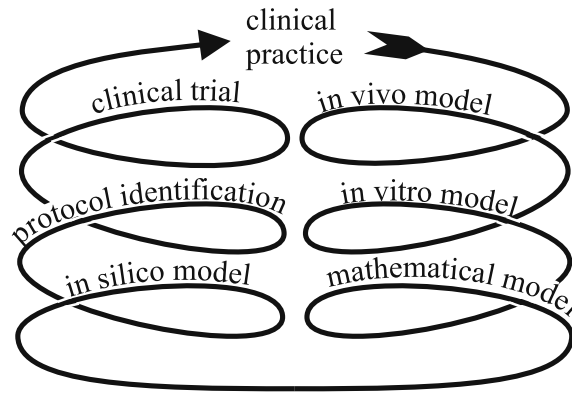

Figure 0.3

adhesion properties, Chapter 9 with the interactions between the endothelium and the tumour cells which are circulating in the body, and Chapter 10 with a review of the invasion models existing in the literature. Chapter 11 deals with the competition between a tumour and the immune system and with a review of the models deduced at the cellular level. Chapter 12 describes the general problem of hypersensitivity to chemotherapy and how *in silico* models can help optimise therapies. Finally, the last chapter explains some of the most used mathematical methods that can be applied to tumour models which write as systems of reaction-diffusion equations, like those introduced in Chapters 4, 6, and 10.

This book is addressed to curricula in applied mathematics, bio-physics, bio-mathematics, and theoretical biology and medicine. It is then proposed as an advanced textbook for graduate interdisciplinary courses having as a common point the interest in modelling and simulating tumoural systems. Of course, the contents of the volume develops keeping in mind the different backgrounds of the readers. In this respect mathematicians and physicists will find some chapters easier than others as they might have stronger backgrounds in these particular fields. The opposite will occur for biologists and medical doctors. The aim of the volume is, however, to give both types of readers a common language, a common starting block, and a complete knowledge of the mathematical and biological aspects of tumour growth. It is thought that this will help them in breaking down the barriers which often hamper

inter-disciplinary activities. In addition, by reading this volume, the readers will acquire a wide panorama of the topic, broadening their horizons in the related fields.

The contents of the volume refer in part to the lectures held during the summer schools organised in the framework of a Research Training Network funded by the European Community on "Using Mathematical Modelling and Computer Simulation to Improve Cancer Therapy."

CONTRIBUTORS

Zvia Agur
Institute for Medical Biomathematics
Bene Ataroth (Israel)
Optimata Ltd., Tel-Aviv (Israel)

Davide Ambrosi
Dept. of Mathematics
Politecnico di Torino (Italy)

Alexander R.A. Anderson
The SIMBIOS Centre, Dept. of Mathematics
University of Dundee (Scotland)

Levon Arakelyan
Institute for Medical Biomathematics
Bene Ataroth (Israel)

Marco Arese
Dept. of Molecular Angiogenesis
Institute for Cancer Research and Treatment
and Department of Oncological Sciences,
University of Torino School of Medicine,
Candiolo (Italy)

Enrica Audero
Dept. of Molecular Angiogenesis
Institute for Cancer Research and Treatment
and Department of Oncological Sciences,
University of Torino School of Medicine,
Candiolo (Italy)

Nicola Bellomo
Dept. of Mathematics
Politecnico di Torino (Italy)

Maria Letizia Bertotti
Dept. of Mathematics
Università di Palermo (Italy)

Federico Bussolino
Dept. of Molecular Angiogenesis
Institute for Cancer Research and Treatment
and Department of Oncological Sciences,
University of Torino School of Medicine,
Candiolo (Italy)

Helen M. Byrne
Centre for Mathematical Medicine
School of Mathematical Sciences
University of Nottingham (U.K.)

Filippo Castiglione
Institute for Medical Biomathematics
Bene Ataroth (Israel)

Mark A.J. Chaplain
The SIMBIOS Centre, Dept. Mathematics
University of Dundee (Scotland)

Roxana Chotard–Ghodsnia
Biomécanique et Génie Biomédical,
Universitè de Technologie de Compiègne
Laboratoire de Rhéologie, Universitè J. Fourier
and CNRS, Grenoble (France)

Peteris Daugulis
Institute for Medical Biomathematics
Bene Ataroth (Israel)

Agnes Drochon
Biomécanique et Génie Biomédical
Universitè de Technologie de Compiègne, (France)

Alain Duperray
Laboratoire de Migration Cellulaire et
Infiltration Tumorale, Institut A. Bonniot,
Faculté de Médecine, Grenoble (France)

Yuval Ginosar
Institute for Medical Biomathematics
Bene Ataroth (Israel)

Enrico Giraudo
Dept. of Molecular Angiogenesis
Institute for Cancer Research and Treatment
and Department of Oncological Sciences,
University of Torino School of Medicine,
Candiolo (Italy)

Miguel Angel Herrero
Dept. of Applied Mathematics
Universidad Complutense de Madrid (Spain)

Hila Harpak
Institute for Medical Biomathematics
Bene Ataroth (Israel)

Rakesh Jain
Dept. of Radiation Oncology
Massachusetts General Hospital and Harvard
Medical School, Boston (U.S.A.)

Yuri Kogan
Institute for Medical Biomathematics
Bene Ataroth (Israel)

Sophie Lelièvre
Dept. of Basic Medical Sciences
Purdue University (U.S.A.)

Howard Levine
Dept. of Mathematics
Iowa State University (U.S.A.)

Anne Leyrat
Laboratoire de Rhéologie
Universitè J. Fourier and CNRS
Grenoble (France)

Serena Marchiò
Dept. of Molecular Angiogenesis
Institute for Cancer Research and Treatment
and Department of Oncological Sciences,
University of Torino School of Medicine,
Candiolo (Italy)

Yifat Merbl
Institute for Medical Biomathematics
Bene Ataroth (Israel)

Stefania Mitola
Dept. of Molecular Angiogenesis
Institute for Cancer Research and Treatment
and Department of Oncological Sciences,
University of Torino School of Medicine,
Candiolo (Italy)

Francesco Mollica
Istituto CNR per la Tecnologia dei Materiali
Compositi, Napoli (Italy)

Santo Motta
Dept. of Mathematics,
Università di Catania (Italy)
Institute of Immunology, Singapore
University, (Repubblic of Singapore)

Paolo Netti
Dept. of Materials and Production Eng.
University of Naples 'Federico II', Napoli (Italy)

Cédric Plachot
Dept. of Basic Medical Sciences
Purdue University (U.S.A.)

Luca Primo
Dept. of Molecular Angiogenesis
Institute for Cancer Research and Treatment
and Department of Oncological Sciences,
University of Torino School of Medicine,
Candiolo (Italy)

Vera Selitser
Institute for Medical Biomathematics
Bene Ataroth (Israel)

Guido Serini
Dept. of Molecular Angiogenesis
Institute for Cancer Research and Treatment
and Department of Oncological Sciences,
University of Torino School of Medicine,
Candiolo (Italy)

Brian Sleeman
School of Mathematics
University of Leeds (U.K.)

Vladimir Vainstain
Institute for Medical Biomathematics
Bene Ataroth (Israel)
Optimata Ltd., Tel-Aviv (Israel)

Claude Verdier
Laboratoire de Rhéologie
Universitè J. Fourier and CNRS
Grenoble (France)

List of Abbreviations

ACI	Adoptive Cellular Immunotherapy
ADF	Actin-Depolymerizing Factor
AFM	Atomic Force Microscopy
Ag	Antigen
Ang1	Angiopoietin-1
APC	Antigen Processing Cell
ATP	Adenosine Tri-Phosphate
AVD	Average Vessel Density
Bcl-2	B-Cell Leukemia/Lymphoma 2
BDNF	Brain-Derived Neutrophic Factor
bHLH	basic Helix-Loop-Helix
BL	Basal Lamina
BSA	Bovine Serum Albumin
CA	Cellular Automata
CAM	Cellular Adhesion Molecule
cAMP	cyclic Adenosine MonoPhospate
CD62E	E-cadherin
CD62L	L-cadherin
CD62P	P-cadherin
Dd	Dictyostelium discoideum
DNMT1	DNA MetylTransferase 1
E-cadherin	Epithelial cadherin
EC	Endothelial Cells
ECF	Eosinophil Chemotactic Factor
ECM	Extra-Cellular Matrix
EGF	Epidermal Growth Factor
EVD	Effective Vascular Density
FGF	Fibroblast Growth Factor
FGFR	Fibroblast Growth Factor Receptor
FHN	FitzHugh-Nagumo (equation)
FRAP	Fluorescence Recovery After Photobleaching

GAG	GlycosAminoGlycans
GDP	Guanosine Di Phosphate
GL	Ginzburg-Landau (equation)
GMP	Guanosine Mono Phosphate
GSK-3β	Glycogen-Synthetase Kinase-3β
GTP	Guanosine Tri Phosphate
HAT	Histone AcetylTransferase
HDAC	Histone DeAcetylase
HH	Hodgkin-Huxley (equation)
HIF-1	Hypoxia-Inducible transcription Factor 1
HLA	Human Leukocyte Antigens
HMT	Histone Methyl Tranferase
IC	Immuno-Complex
ICAM	Intercellular Adhesion Molecule-1 (or CD54)
IFN-γ	Interferon gamma
IgE	Immunoglobulin of class E
IL	Interleukin
kDa	kiloDalton
LAD	Leukocyte Adhesion Deficiency
LAK	Lymphokine Activated Killer cell
Lef	Lymphoid Enhancer-binding Factor
LFA-1	Lymphocyte Function-Associated Antigen-1
LPS	LipoPolySaccharides
MA	Macrophage
MBD	Methyl Binding Domain
MBP	Methyl Binding Protein
MC	Mast Cell
MDE	Matrix Degrading Enzyme
MeCBP2	Methyl-CpG Binding Protein 2
MHC	Major Histocompatibility Complex
MLL	Mixed Lineage Leukemia/trithorax protein
MMP	Matrix Metalloprotease
MORF	MOZ Related Factor
MOZ	Monocytic leukemia zinc-finger
MW	Molecular Weight
N-cadherin	Neuronal cadherin
NCF	Neutrophil Chemotactic Factor
nm	nanometer
NuRD	Nucleosome Remodeling and Deacetylation
ODE	Ordinary Differential Equation

PA	Plasminogen Activator
P-cadherin	Placental cadherin
PD	Pharmaco-Dynamics
PDE	Partial Differential Equation
PDGF	Platelet Derived Growth Factor
PECAM-1	Platelet Endothelial Cell Adhesion Molecules-1
PI(3)	Phosphatidylinositol-3
PK	Pharmaco-Kinetics
PKC	Protein Kinase C
PLB	Plasma B (cell)
PlGF	Placental derived Growth Factor
PMN	PolyMorphonuclear Neutrophil
PSGL-1	P-Selectin Glycoprotein Ligand-1
RD	Reaction-Diffusion (equation)
R_F	retardation factor
RICM	Reflexion Interference Contrast Microscopy
ROCK	Rho-associated, coiled-coil-forming protein kinase
SFA	Surface Force Apparatus
SFM	Scanning Force Microscope
SWI/SNF	SWItching/Sucrose Non-Fermenting
TCF	T-Cell Factor
TCM	Tumour Conditioned Medium
TGF	Tumour Growth Factor
T-GF	T-cell Growth Factor
TGFβ	Transforming Growth Factor β
Th-1	T helper cell of type 1
TIL	Tumour Infiltrated Lymphocyte
TIMP	Tissue Inhibiting Metallo Protease
TMP	TransMural Pressure
TNF	Tumor Necrosis Factor
TW	Travelling Wave
VCAM-1	Vascular Cell Adhesion Molecule-1
VE-cadherin	Vascular Endothelium cadherin
VEGF	Vascular Endothelial Growth Factor
VEGFR-1	Vascular Endothelial Growth Factor receptor-1
VHL	Von Hippel-Lindau protein
VLA-4	Very Late Antigen-4 (or CD49d/CD29)

Contents

3 Interstitial Transport in Solid Tumours

Paolo A Netti[1] *and Rakesh K. Jain*[2]

[1]Department of Materials and Production Engineering, University of Naples 'Federico II', Naples (Italy)

[2]Edwin Steele Laboratory, Department of Radiation Oncology, Massachusetts General Hospital and Harvard Medical School, Boston (U.S.A.)

4 Modelling Avascular Tumour Growth

Helen M. Byrne

Centre for Mathematical Medicine School of Mathematical Sciences, University of Nottingham (U.K.)

Chapter 1

Biological Aspects of Tumour Angiogenesis

Federico Bussolino, Marco Arese, Enrica Audero, Enrico Giraudo, Serena Marchiò, Stefania Mitola, Luca Primo, and Guido Serini

Institute for Cancer Research and Treatment and Department of Oncological Sciences, University of Torino School of Medicine, Candiolo (Italy)

1.1 Vasculogenesis, Angiogenesis, and Arteriogenesis

The development of the cardiovascular system is regulated by vasculogenesis, which typically occurs during embryonic development, and by angiogenesis which regulates the growth of vessels both in the embryo and in the adult. Key cellular elements of vasculogenesis are the hemangioblast and the angioblast which differentiate from the mesoderm under the control of fibroblast growth factor (FGF)-2 and vascular endothelial growth factor (VEGF)-A [1]– [4]. In the more peripheral mat

zone hemangioblasts form blood islands, i.e., cellular aggregations made of external endothelial cells (ECs) and internal precursors of hematopoietic cells [5], [6]. ECs originating from these structures organise into a primitive plexus of homogeneously sized vessels, which vascularise tissues of endodermal origin. In the more internal zona pellucida the angioblasts give rise to ECs which participate to heart organogenesis and locally self-assemble into a primitive capillary plexus contributing to the formation of the large blood vessels, such as aorta and cardinal vein [5], [6] (Figure 1.1). Little is known about the mechanisms governing EC fate; basic helix-loop-helix (bHLH) transcription factors, Ets-1, Fra1, Hex, Vezf1, Hox, and GATA family members of transcription factors may be involved [7]. The fate of ECs to become integrated into arteries or veins is mediated by the bHLH transcription factor gridlock at the angioblast stage [8], and, subsequently, by members of the ephrin family [9], [10], signals that are also involved in guidance of axons and repulsion of neurons.

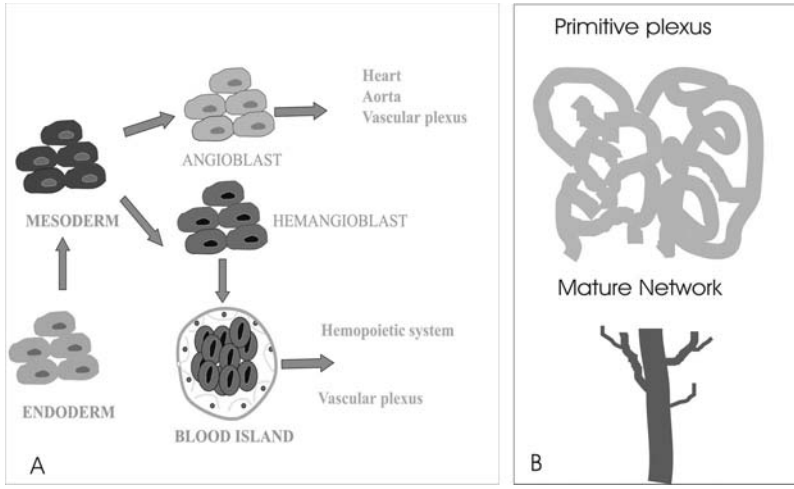

Figure 1.1

Vasculogenesis. Panel A. Differentiation of mesodermic precursor stimulated by soluble mediators released by endoderm into angioblasts and hemangioblasts that originate a primitive vascular plexus and the later the hematopoietic system too. Panel B. Remodelling of primitive plexus by angiogenic mechanism.

In the embryo, the initial capillary meshwork is then remodelled by angiogenesis into a mature and functional vascular bed comprised of arteries, capillaries, and veins [11]. Angiogenic remodelling co-ordinates with the establishment of blood flow and can occur through sprouting [11], intussusception, i.e., by internal division of the vessel lumen [12] (Figure 1.2), or vascular fusion [13].

Angiogenesis also includes penetration by sprouting of vessels into avascular

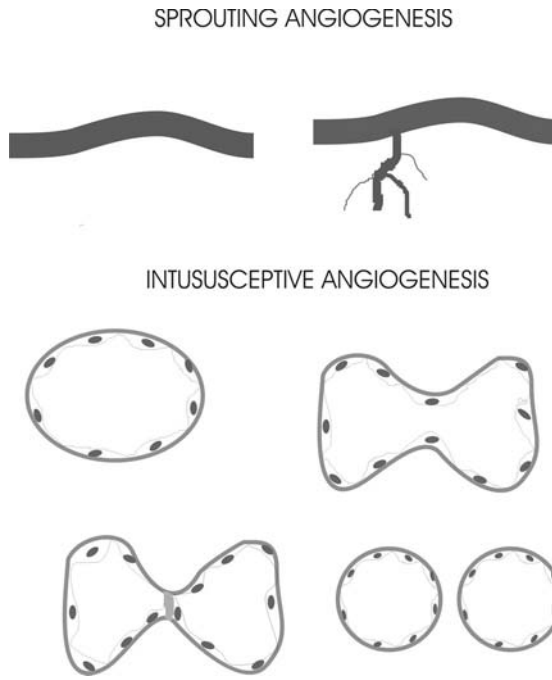

Figure 1.2
Different modalities of angiogenesis in fetal and adult life.

regions of the embryo and recruitment of mural cells [14]. In the adult, angiogenesis characterises some physiological situations, such as the vascularisation of ovary and uterus during the menstrual cycle, of mammary glands during lactation, and of granulation tissue during wound healing [15]. Not less significant is the role of angiogenesis in pathological settings, such as tumours, chronic inflammatory diseases (e.g., rheumatoid arthritis and psoriasis), vasculopathies (e.g., diabetic microangiopathy), degenerative disorders (e.g., atherosclerosis and cirrhosis), and tissue injury occurring in ischemia [15]. Five biological phases of angiogenesis have been established and characterised by different, overlapping genetic programs: initiation, progression, differentiation, maturation, and remodelling and guidance. Initiation is characterised by changes in the EC shape and by increased permeability. The progression phase includes the degradation of extracellular matrix, and migration and proliferation of ECs. During differentiation, ECs stop to growth, survive in suboptimal conditions, and differentiate into primitive blood vessels. The maturation phase implies formation of new extracellular matrix, recruitment of pericytes and smooth muscle cells (SMCs), and remodelling of the primitive vascular network. In the guidance phase, the architecture of the mature vasculature tree is delineated both during development and in the adult organism [16], [17]. All these steps are in part regulated by vascular endothelium-specific growth factors that now include members of the VEGF,

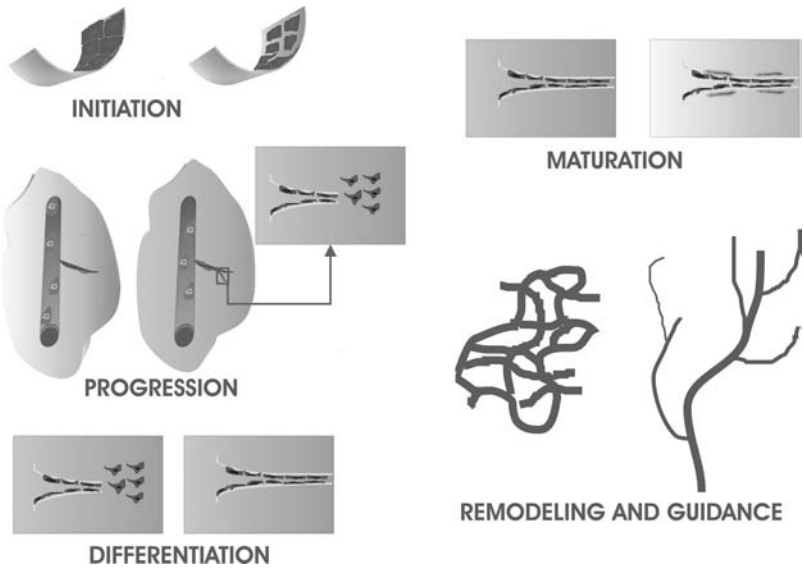

Figure 1.3

Five overlapping steps of sprouting angiogenesis: initiation, progression, differentiation, maturation, and remodelling and guidance.

Angiopoietin (Ang), ephrin [10], [11], and semaphorin families [18] (Serini G., in preparation) (Figure 1.3). An emerging rule is that all these molecules have to act in concert to allow the formation of functional vasculature.

In the adult new vessels arise mainly through angiogenesis, although vasculogenesis may occur [19]. However, a further process leading to vessel formation in the adult life is arteriogenesis, a process triggered by arterial occlusion and characterised by the enlargement of pre-existing arteriolar connections into true collateral arteries [20]. These vessels, bypassing the site of occlusion, have the ability to markedly grow and increase their lumen providing an enhanced perfusion to the jeopardised ischemic regions caused by arterial occlusions. It is worth noting that proliferation of collateral arteries is not a process of passive dilatation, but of active proliferation and remodelling. Under normal flow conditions and depending on the pressure gradient between the interconnecting arterial networks, there is only minimal net forward flow, but small amounts of flow may oscillate within the network. In a sudden arterial occlusion or a slowly progressing stenosis, a steep pressure gradient along the shortest path within the interconnecting network develops that increases blood flow velocity and hence fluid shear stress in these vessels that now assume the new function as collaterals. Such a sustained increase in shear results in the upregulation of distinct processes in the collateral arteries, including increased endothelial production of cytokines, attraction of circulating monocytes, and production of nitric oxide [21]– [23]. These events in turn create an inflammatory environment and produce fairly large amounts of growth factors, particularly FGF-2 [24]. The inva-

sion of monocytes is soon followed by the first wave of mitosis of ECs and smooth muscle cells (SMCs). The perivascular inflammation in turn creates the space for the greatly expanding collateral vessel that can increase its diameter up to 20 times. The old structure is largely dismantled and primarily replaced by new intimal and medial SMCs. Finally, arteriogenesis results in a new functional artery originating from a pre-existing arteriole.

1.2 Inducers of Angiogenesis: The Example of the VEGF Family

Direct angiogenic inducers cause ECs to migrate, proliferate, and differentiate into nascent blood vessels, which require the involvement of other molecules (e.g., Angs) to acquire whole function and stability.

Before 1989, the prototypic members of the fibroblast growth factor family, were the leading candidates as positive regulators of angiogenesis; they are potent angiogenic inducers both *in vitro* and *in vivo* and widely distributed in tissues and organs. However, cloning of genes encoding fibroblast growth factor-1 and -2 in 1986 demonstrated that both molecules lack a classic secretory signal peptide. Thus, these molecules are not typical secreted proteins and indeed they have been shown to be mostly cell-associated [25]. In 1989, the definitive isolation and cloning of VEGF-A as a diffusible EC-specific mitogen, as well as a permeability-enhancing factor, had the potential to fill, at least in part, the gap of our understanding the regulation of angiogenesis [26]. The family of VEGF consists of six genes, which encode specific proteins: VEGF-A, -B, -C, -D, -E, and placental derived growth factor (PlGF) [11], [27], [28]. They are dimeric glycoproteins produced by mesenchymal cells, structurally related to platelet derived growth factor, and capable of binding with different affinities to three related receptor tyrosine kinases VEGF receptor-1 (VEGFR-1), VEGFR-2, and VEGFR-3. VEGF-A is expressed as different splice variants, including in humans 121-, 145-, 165-, 189-, and 206-amino acid residues, the 121- and 165-isoforms being the most frequently expressed variants. Exon 7 in the VEGF-A gene encodes a structural motif mediating binding to heparin. The 121-amino acid isoform, in which exon 7 as well as exon 6 are excluded, is freely diffusible. In contrast, the 189- and 206-amino acid isoforms contain additional stretches of basic residues responsible for their retention in the extracellular matrix. VEGF-A induces EC chemotaxis, chemokinesis, survival, and proliferation. VEGF-A also controls hematopoietic differentiation during development [3], [4], [29], as well as monocyte [30], osteoclast, and osteoblast [31] behaviour. The biological significance of VEGF molecules other than VEGF-A is largely unknown. VEGF-C (and probably also VEGF-D) seems to be the most important effector of lymphangiogenesis by activating VEGFR-3 [32]. PlGF, which does not play major roles in physiological angiogenesis, is an important inducer of vascularisation of tumours

and ischemic tissues [33].

One the most important regulators of VEGF-A expression is oxygen tension. In response to reduced oxygen levels, cells overexpress the hypoxia-inducible transcription factor 1 (HIF-1), which translocates into the nucleus where it binds to hypoxia-response elements of genomic DNA, thereby activating the expression of numerous hypoxia-responsive genes, including VEGF-A. Induction of VEGF-A production by low oxygen tension justifies the fact that this molecule is highly expressed in many situations where an increase in vascularisation is required to compensate low oxygenation, e.g., necrotic area of solid tumour or ischemic tissues. The most elegant demonstration of the need for fine regulation of VEGF levels is represented by postnatal retinal vascularisation in rodents. Angiogenic sprouting into the initially avascular and hypoxic retina depends upon its VEGF expression [34]. In the presence of oxygen, HIF-1α is bound to the tumour suppressor Von Hippel-Lindau (VHL) protein. This interaction causes HIF-1α to become ubiquitylated and targeted to the proteasome, where it is degraded. Mutations in VHL, that are associated with renal cancer and cerebellar hemangioblastomas, prevent its ubiquitylation, resulting in an accumulation of HIF-1 and continuous activation of VEGF gene which promotes tumour angiogenesis [35]. Besides, the effect of hypoxia is amplified in the presence of mutations of the Ras protooncogene, suggesting a strict relationship between oncogenesis and angiogenesis [36], [37].

Three structurally related receptor tyrosine kinases for the VEGF family members have been identified to date (see Table 1.1): VEGFR-1 (Flt-1; binds VEGF-A, PlGF, and VEGF-B); VEGFR-2 (KDR in humans or Flk-1 in the mouse; binds VEGF-A, VEGF-C, VEGF-D, and VEGF-E); and VEGFR-3 (Flt-4; binds VEGF-C and VEGF-D). Generally, VEGFR-1 and -2 are expressed in vascular ECs and all three receptors are crucial for vascular development during embryogenesis. The structural hallmarks of VEGF receptors include seven immunoglobulin (Ig)-like domains in the extracellular portion and a split tyrosine kinase domain containing an intervening noncatalytic 70-amino-acid residue sequence. The extracellular domain of VEGFR-3 is composed of two large domains bound by a disulphide bridge. The third Ig-like loops in VEGFR-1 and -2 are responsible for binding VEGF-A, whereas the first three loops are required for receptor dimerization. The tyrosine kinase domains of the three receptors are highly related (80% similarity) [11], [27], [28].

An emerging topic of interest in the field of VEGF receptors is the requirement of co-receptors capable of modulating their activity and specificity. Integrin $\alpha v\beta 3$ functions as a co-receptor in VEGFR signal transduction. Indeed, VEGFR-2 forms complexes with $\alpha v\beta 3$ integrin, which is specifically expressed on angiogenic ECs. Activation of $\alpha v\beta 3$ by plating cells on one of its ligand vitronectin or fibrin, one of more abundant protein in remodelled extracellular matrix during angiogenesis, results in an increased VEGFR-2 kinase activity and augmented VEGF-A-mediated mitogenicity [38]. Homotypic adhesive interactions between ECs negatively regulate VEGFR-2 tyrosine phosphorylation and a neutralising antivascular endothelial (VE)-cadherin antibody increases VEGFR-2 responsiveness to VEGF-A, suggesting that VE-cadherin could act as co-receptor as well. On the other hand, targeted inactivation of VE-cadherin in mice severely impairs vascular development causing em-

bryonic death and indicating the need for a fine-tuned balance of VEGFR-2 activity during vasculogenesis [39]. Neuropilins (Npns) are the third class of co-receptors. Originally implicated in repulsive growth cone guidance in the developing nervous system, Npn-1 and -2 have been recently suggested to play a role in the development of the vascular system [40], [41] and in angiogenesis [42], [43]. In past years, it has been shown that neuropilins also bind specific isoforms of VEGF-A. In 1998, Klagsbrun's group [44] reported that VEGF-A165 binds to Npn-1. Subsequently, VEGF-A 145, PlGF-2, VEGF-B, and VEGF-E have all been shown to bind to Npn-1 or -2. Exon 7 in VEGF-A is involved in Npn binding, thereby excluding VEGF121 from this interaction [27], [28]. Finally, the fourth class of co-receptors are extracellular matrix heparan sulphates. They either may be a reservoir of VEGF-A or could allow a better ligand/receptor interaction. VEGF-A exon 7 confers heparin-binding ability to VEGF-A isoforms 165, 189, and 206 [27], [28].

VEGF receptor signal transduction appears to rely upon the canonical pathways activated by most receptor tyrosine kinases [45]. After binding specific receptors with high affinity (pM range), VEGF triggers their dimerization and autophosphorylation on specific cytoplasmic tyrosine residues, which mediate the recruitment of adaptors and enzymes (e.g., Grb, Nck, VRAP, Sck, phospholipase C γ, CrK, phospatidylinositol 3-kinase, SHP-2) and lead to early and late biological responses by activating Ras, mitogen activate protein kinase, and protein kinase B pathways (for an extensive review see Reference 28). The observed biological activities (migration, proliferation, and survival) exerted on adult ECs are mainly mediated by VEGFR-2, while the function played by VEGFR-1 is not well defined yet [27], [28]. Studies on null mice indicate that both receptors are required for embryo vasculogenesis [46], [47]. During development, VEGFR-1 is crucial for negative regulation of the hemangioblast pool. Such a negative regulation appears to be independent of VEGFR-1 kinase activity and may be mediated through the binding and sequestering of VEGF-A. This is compatible with the observation that dosing VEGF-A is required for a proper vascular development [4]. Therefore, both in the embryo and the adult life VEGFR-1 activity seems to be generally devoted to the regulation of VEGF-A/VEGFR-2 activities.

1.3 The Tissue-Specific Angiogenic Inducers

Depending on the phenotypic features and the growth rate of the different tissue compartments, the endothelium of the various vascular beds is diverse and distinct [48], [49]. This happens despite the fact that the expression of VEGF and Ang (see above) is almost ubiquitous. The morphology and architecture of ECs also differs among different capillary beds. For example, fenestrae are associated with highly permeable vessels, such as those serving the endocrine tissues. The contribution of tissue microenvironment to EC phenotypic characteristics has been

Table 1.1 Direct and indirect angiogenic inducers.
+ Molecules that induce the *in vitro* migration and/or proliferation of endothelial cells .
++ Molecules that extert their angiogenic activity in specific anatomical districts or in selected conditions
+++ Molecules unable to directly induce the *in vitro* migration and/or proliferation of endothelial cells
*** Molecules that induce angiogenesis *in vitro*, i.e., promote the differentiation of endothelial cell cultured in tri-dimensional structures.**
PDGF shows that activity, but does not induce angiogenesis *in vivo*.

Direct inducers+	**Endothelial cell receptor involved**	**Proliferation**	**Migration**
VEGF-A*	Tyrosine kinase receptors (VEGFR-1, Flt-1; VEGFR-2, Flk-1/KDR)	Yes	Yes
VEGF -C	Tyrosine kinase receptors (VEGFR-3, Flt-4; VEGFR-2, Flk-1/KDR)	Weak	Yes
VEGF -D	Tyrosine kinase receptors (VEGFR-3, Flt-4; VEGFR-2, Flk-1/KDR)	Weak	Yes
VEGF -E	Tyrosine kinase receptors (VEGFR-3, Flt-4; VEGFR-2, Flk-1/KDR)	Weak	Yes
Basic and acid fibroblast growth factor*	Tyrosine kinase receptors (FGFR-1, flg-1; FGFR-2, bek)	Yes	Yes
Transforming growth factor-α and epidermal growth factor*	Tyrosine kinase receptors (erb-1, erb-2)	Yes	Yes
Platelet-derived endothelial cell growth factor	Unknown	Yes	No
Hepatocyte growth factor *	Tyrosine kinase receptor (met)	Yes	Yes
IL-8	Chemokine receptor(s)	Yes	Yes
Neutrophil-activating peptide-2	Chemokine receptor(s)	No	Yes
Epithelial cell-derived neutrophil-activating protein-78	Chemokine receptor(s)	No	Yes
Melanoma growth-stimulatory activity-α	Chemokine receptor(s)	No	Yes
Stroma-derived factor-1α	Chemokine receptor(s)	No	Yes
Growth-related oncogenes α and γ	Chemokine receptor(s)	No	Yes

Granulocyte-colony stimulating factor	Type 1 cytokine receptor	Weak	Yes
Placental growth factor-1 and -2	Tyrosine kinase receptor (VEGFR-1, Flt-1)	Weak	Yes
Proliferin	IGF-II/mannose 6-phosphate receptor	-	Yes
B61 (ephrin-A1)	Tyrosine kinase receptor (EphA2, eck)	No	Yes
Soluble form of VCAM-1	Integrin $\alpha 4\beta 1$	No	Yes
Leptina	Ob receptor	Yes	Yes
Timosin $\alpha 1$	Unknown	Unknown	Yes
TWEAK (member of TNF family)	TWEAK receptor	Yes	Yes
TRANCE	RANK	Yes	Yes
Soluble form of Selectine-E	Sialil Lewis X/A ?	Unknown	Yes
CYR61	Integrin $\alpha v\beta 3$. Other receptors?	-	-
Connective-tissue growth factor	Integrin $\alpha v\beta 3$. Other receptors?	No Anti-apoptotic	Yes
IL-13	IL-13 receptor	Not tested	Not tested
IL-18	IL-18 receptor	-	Yes
HIV-1 Tat	VEGFR2, $\alpha v\beta 3$, $\alpha v\beta 5$	Weak	Yes
Platelet activating factor (PAF)	Seven transmembrane domains receptor	No	Yes
Adenosine	A2A receptor	Yes	Yes
Nicotine	Ach receptor	Yes	Not tested
Local angiogenic inducers++			
Prolactin	Type 1 cytokine receptor		
Growth hormone	Type 1 cytokine receptor		
Placental lactogen	Type 1 cytokine receptor		
EG-VEGF	Seven transmembrane domains receptor	Yes	Yes
Indirect inducers +++		No	No
Tumor necrosis factor-α	p55, tumor necrosis factor-α receptor	No	No
Transforming growth factor-β*	Serine/treonine kinase receptors (types I and II)	No	No
Angiogenin	Unknown	No	No
Copper binding peptide from the SPARC protein	Unknown	No	No
Prostaglandin E1	Seven transmembrane domains receptor (EP2 e/o EP3)	No	No

clearly demonstrated by studies on grafted tissues and tumour xenografts implanted at various anatomic sites [50], [51]. Recently, it has been found a new angiogenic inducer, which specifically activates microvascular ECs of endocrine tissues and has been therefore named endocrine gland derived VEGF. It is not structurally related to VEGF family and transduces through a G protein-coupled receptor [52]. The biological activity of this molecule is indistinguishable from that of VEGF-A, but only in specific cell and tissue contexts. A similar role is played by other molecules, such as proliferin, placental lactogen, and growth hormone, which are also angiogenic in specific tissues [53].

The existence of local activators of angiogenesis suggests that vasculature formation could be controlled at two different levels, VEGF-A controlling the initiation of neovascularisation and local molecules refining the system to establish and maintain differentiated EC structure and function.

1.4 Molecules Stabilising Nascent Capillaries: The Example of Angiopoietins

It has been well established that nascent capillaries are not physiologically active and can regress when extracellular matrix is perturbed [54], [55]. Therefore, VEGF-A as well as other angiogenic inducers must cooperate with stabilising molecules. Some of them, such as transforming growth factor β (TGFβ) are not exclusively specific for this function. It is interesting to point out that point mutations of TGFβ receptor subunits endoglin and activin are responsible of hemorrhagic telangiectasia [56], a syndrome characterised by blood vessel dilatation and formation of artery-vein shunt with disappearance of capillaries.

Angiopoietins (Ang) were discovered as ligands for the Tie family of receptor tyrosine kinases that are selectively expressed by vascular ECs. There are four members of the Ang family. Although Ang3 and Ang4 may represent widely diverged counterparts of the same gene locus in mouse and man. Ang1 promotes *in vitro* EC sprouting, survival, and migration. On the contrary, Ang2 blocks the activation of Tie2 induced by Ang1, suggesting that it may be a naturally occurring inhibitor of Ang1/Tie2 activity [10].

The most important insights into the physiological roles of Ang1 and its receptor Tie2 came from the analysis of null mice [57]– [60]. Ang1-/- or Tie2-/- mice show a decreased number of ECs, simplification of the vascular branching pattern, and failure to recruit pericytes and SMCs. Transgenic overexpression of Ang1 in the skin results in a pronounced hyper-vascularisation characterised by a modest increases in vessel number and marked increase in vessel size. Consistent with its action as an Ang1/Tie2 inhibitor, over-expression of Ang2 results in vascular defects similar to those observed in Ang1 or Tie2 knockout mice. These studies suggest that angiopoietins play their major role during vascular remodelling and maturation from

simple endothelial tubes into more elaborate vascular tree composed of several cell types. Furthermore, they contribute to the maintenance of vessel integrity through the establishment of appropriate cell-cell and cell-matrix connections [17].

In addition to their effects on vascular morphology, transgenic overexpression of Ang1 results in a reduced responsiveness to leakage induced by inflammatory agents and VEGF [61], [62]. On the contrary, VEGF-A overexpression leads to immature, leaky, and haemorrhagic vessels [63]. These findings confirm the ability of Ang1 to maximise interactions between ECs and their surrounding support cells and matrix.

1.5 Natural Inhibitors of Angiogenesis

There are different classes of natural inhibitors of angiogenesis that exert their activity by inhibiting EC motility and growth (see Table 1.2). By counteracting angiogenic inducers, inhibitors guarantee a fine homeostatic balance, which finally results in a regulated angiogenic process. Events reducing the concentration of inhibitors or increasing that of stimulators trigger a deregulated vascular proliferation, as found in tumours, chronic inflammatory diseases, and retinopathies. The first negative controller of angiogenesis in is the oncosuppressor protein p53, responsible for the reduction of VEGF-A synthesis and thrombospondin secretion [64]. Thrombospondin is a multifunctional inhibitor of angiogenesis, which acts by modulating EC adhesiveness and motility or trapping angiogenesis inducers [64]. Thus, p53 mutations favour the initiation of tumour angiogenesis by impairing the regulation of thrombospondin synthesis. A second class of inhibitors includes protein fragments. Angiostatin was the first protein fragment to be found to behave as an angiogenesis inhibitor. Angiostatin is a 38 kDa fragment of plasminogen [65]. The antiangiogenic protein fragment described was endostatin that corresponds to the C-terminal fragment of collagen XVIII [66]. The class of antiangiogenic protein fragment includes also a fragment of 16 kDa of prolactin, one of 6 kDa of platelet factor 4, and fragments of hepatocyte growth factor, epidermal growth factor, thrombospondin-1, kininogen, antithrombin III, and prothrombin [67].

The third class of angiogenesis inhibitors includes some chemokines belonging to both Cys/Cys and Cys/X/Cys subclasses, which selectively inhibit cell cycle [68].

1.6 Angiogenesis and Cancer Progression

In cancer new vessels are required to provide cancer cells with nutrients and are targets for invading cancer cells themselves. At the beginning of its natural his-

Table 1.2 Angiogenesis inhibitors: (a) Oncosuppressor genes.

Inhibitor	Mechanism
TP53	Induction of TSP-1 synthesis
RB	Induction of TSP-1 synthesis
VHL	Induction of TSP-1 synthesis
Locus Loh2, mouse chormosome 16	Induction of unknown angiogenesis inhibitors
Unidentified gene on human choromosome 10q	Induction of TSP-1 synthesis

(b) Criptic molecules derived from larger precursors

Inhibitor	Mechanism
Angiostatin (plasminogen fragment)	Inhibition of endothelial growth and motility
Endostatin (collagene XVIII fragment)	Inhibition of endothelial growth and motility
Alternative form of HGF	Unknown
Antithrombin fragment	Inhibition of EC growth and motility
Prothrombin fragments	Inhibition of endothelial growth
High molecular weight kininogen fragment	Inhibition of endothelial motility
16 kDa prolactin fragment	Inhibition of endothelial growth and motility
16 kDa placental lactogen fragment	Inhibition of endothelial growth
16 kDa GH fragment	Inhibition of endothelial growth

(c) Soluble mediators

Soluble mediators	
Interferon α	Inhibition of endothelial growth and motility
Platelet factor 4	Inhibition of endothelial motility and VEGF-A activity
Interferon-γ (IFN-γ)-inducible protein-10	Inhibition of endothelial growth and differentiation
IFN-inducible T-cell α-chemoattractant	Inhibition of endothelial growth
Monokine induced by IFN-γ	Inhibition of endothelial growth
gro-β	Inhibition of endothelial growth
C6kine	Not determined
TSP-1	Inhibition of endothelial growth, motility, and adhesion
Tissue type metallo-protease inhibitors (Type 1, 2 e 3)	Type 1 is an inhibitor of EC motility Type 2 is an inhibitor of EC motility and growth Type 3 acts with an unknown mechanism
Heparinase	Heparan sulphates depletion
Semaphorin III A	Inhibition of VEGF-A165 activity
2-methossiestradiol	Inhibition of endothelial growth and motility
IL-4	Inhibition of endothelial motility
Corticotropin-releasing factor	Inhibition of endothelial motility and growth
Dopamine	Inhibition of VEGFR-2
Parathyroid hormone related peptide	Inhibition of endothelial growth and motility
Proliferin-related protein	Inhibition of endothelial motility

tory, a cancer is not vascularised, and it does not grow beyond 2 mm in size unless vascularisation has occurred. The switch to the angiogenic phenotype is a critical point in tumour progression [69] and depends on the additive effect of progressive genetic alterations [70]. Before this switch occurs, most tumours are restricted to a microscopic size. A prominent example is represented by the early *in situ* carcinoma, where neighbouring mature microvessels are quiescent, and metastases are virtually absent. After the angiogenic switch, e.g., in the later stages of *in situ* breast carcinoma, neo-vascular sprouts breach the basement membrane [71], and tumour cells can grow around each new capillary vessel, enter the circulation, and cause metastases. Furthermore, the angiogenic switch is also active in determining the translation of micrometastases from a dormant to an aggressive status [69].

One EC can support more than 50 to 100 tumour cells. Thus, the microvascular EC recruited by a tumour has become an important second target in cancer therapy. Treating both the cancer cell and the EC in a tumour may be more effective than treating the cancer cell alone [72]. The interactions between tumour cells and blood vessels may be supported by:

1. the ability of tumour cells to directly modify the homeostasis of inducers and inhibitors of angiogenesis [15];

2. the ability of tumour cells to disturb this balance through stromal and inflammatory cells [73], [74];

3. the possibility of tumour cells to grow around pre-existing vessels [75];

4. the colonisation of nascent vessels by CD34+ cells which differentiate in ECs [76];

5. the formation of capillaries by tumour cells themselves through a trandifferentiation process [77]; and

6. the transient and dynamic participation of tumour cells to vessel walls [78] (Figure 1.4).

The first model implies the selection of a tumour cell clone having the biological feature to support the switch to the angiogenic phenotype. It implies a change in the local equilibrium between positive and negative regulators of microvessel growth. Usually the up-regulation of an angiogenic inducer is not sufficient by itself for a tumour cell to become angiogenic and therefore certain inhibitors have to be down regulated. Similarly, tumour cells may stimulate stromal and infiltrating leukocytes to produce angiogenic factors. In addition to these well-characterised models of tumour angiogenesis, new hypotheses are arising. Indeed, it has been shown how cancer cells may initially co-opt existing host blood vessels and the growing mass could cause the collapse and the regression of these blood vessels with subsequent necrosis and hypoxia, which in turn may induce neo-angiogenesis [79].

The third model represents a new and provocative concept in cancer biology that has raised some criticisms [80]. Such a model would suggest that tumour cells

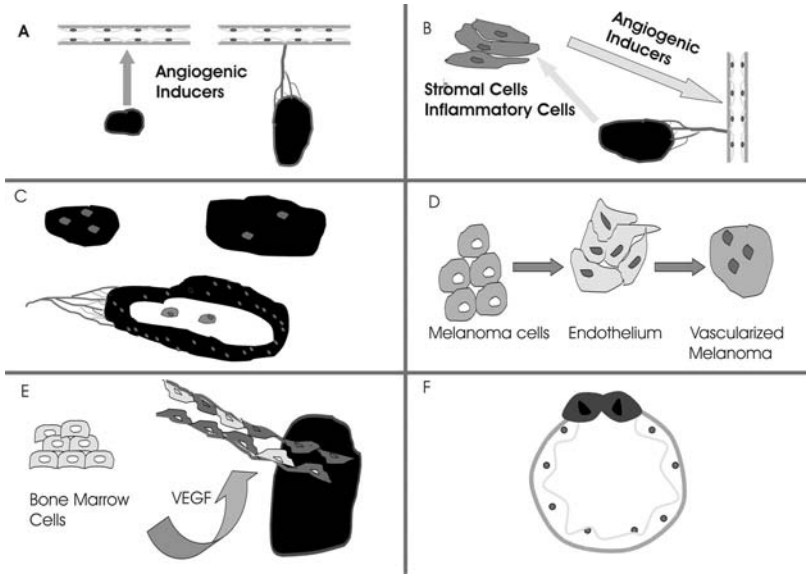

Figure 1.4

Different mechanisms of tumour angiogenesis. Panel A: Tumour produces angiogenic inducers; Panel B: Tumour activates host cells to produce angiogenic inducers; Panel C: Tumour grows around pre-existing vessels, increases in size inducing vessel collapse followed by necrosis. Subsequent hypoxia stimulates angiogenesis from neighbouring capillaries; Panel D: vasculogenic mimicry; Panel E: Mobilisation of EC precursors from bone marrow; Panel F: Mosaicism in tumour capillaries that are constituted by endothelial and cancer cells.

metamorphose into vessels that either carry blood or connect to the host's blood supply. This model has been named vasculogenic mimicry, because it is reminiscent of the differentiation process occurring during vasculogenesis. Highly invasive primary and metastatic melanoma cells may generate vascular channels, lined externally by melanoma cells that facilitate tumour perfusion independent of angiogenesis.

Recently it has been noted the existence of angioblast-like circulating endothelial precursor cell in adult human blood. These precursors may be endowed with the phenotype of embryonic angioblasts, which are migratory EC precursor capable of circulating, proliferating, and differentiating into mature ECs, but which have neither acquired characteristic markers of mature endothelium nor lumenised [81]. Id deficient mice allowed demonstrating the role of these EC precursors in tumour angiogenesis. Adult mice with reduced Id gene dosage cannot support tumour neoangiogenesis. However, mobilisation of bone-marrow EC precursors overcome the genetic defect restoring tumour angiogenic response [82].

The last model may explain the observation that metastasising tumour cells transiting into the vascular lumen may reside temporarily on the microvessel wall and

occupy up to 4% of the total vascular surface area. Approximately 15% of vessels of a human colon carcinoma transplanted in mice contain a subpopulation of tumour cells that in the vessel wall share space with ECs. These blood vessels have been defined as "mosaic" blood vessels [83].

Acknowledgments

This study was supported by Associazione Italiana per la Ricerca sul Cancro, Istituto Superiore di Sanità (IV Programma Nazionale di Ricerca sull'AIDS-2001 and Progetto "Tumour therapy"), Compagnia di San Paolo, Ministero dell'Istruzione, dell'Università e della Ricerca (60% and PRIN: 2000).

1.7 References

[1] Eichmann, A., Corbel, C., Nataf, V., Vaigot, P., Bréant, C., and Le Dourin, N.M., Ligand-dependent development of the endothelial and hemoipoietic lineages from embryonic mesodermal cells expressing vascular endothelial growth factor receptor two, *Proc. Natl. Acad. Sci. USA* 94, 1997.

[2] Cleaver, O. and Krieg, P.A., VEGF mediates angioblast migration during development of the dorsal aorta in Xenopus, *Development* 125, 3905-3914, 1998.

[3] Carmeliet, P., Ferreira, V., Breier, G., Pollefeyt, S., Kieckens, L., Gertsenstein, M., Fahrig, M., Vandenhoeck, A., Harpal, K., Eberhardt, C., Declercq, C., Pawling, J., Moons, L., Collen, D., Risau, W., and Nagy, A., Abnormal blood vessel development and lethality in embryos lacking a single VEGF allele, *Nature* 380, 435-439, 1996.

[4] Ferrara, N., Carver-Moore, K., Chen, H., Dowd, M., Lu, L., O'Shea, K.S., Powell-Braxton, L., Hillan, K.J., and Moore, M.W., Heterozygous embryonic lethality induced by targeted inactivation of the VEGF gene, *Nature* 380, 439-442, 1996.

[5] Risau, W. and Flamme, I., Vasculogenesis, *Annu. Rev. Cell Develop. Biol.* 11, 73-91, 1995.

[6] Roman, B.L. and Weinstein, B.M., Building the vertebrate vasculature: research is going swimmingly, *Bioessays* 22, 882-893, 2000.

[7] Oettgen, P., Transcriptional regulation of vascular development, *Circ. Res.* 89, 380-388, 2001.

[8] Zhong, T.P., Rosenberg, M., Mohideen, M.A., Weinstein, B., and Fishman, M.C., *gridlock*, an HLH gene required for assembly of the aorta in zebrafish, *Science* 287, 1820-1824, 2000.

[9] Yancopoulos, G.D., Klagsbrun, M., and Folkman, J., Vasculogenesis, angiogenesis, and growth factors: ephrins enter the fray at the border, *Cell* 93, 661-664, 1998.

[10] Yancopoulos, G.D., Davis, S., Gale, N.W., Rudge, J.S., Wiegand, S.J., and Holash, J., Vascular-specific growth factors and blood vessel formation, *Nature* 407, 242-248, 2000.

[11] Carmeliet, P., Mechanisms of angiogenesis and arteriogenesis, *Nature Med.* 6, 389-395, 2000.

[12] Djonov, V., Schmid, M., Tschanz, S.A., and Burri, P.H., Intussusceptive angiogenesis: its role in embryonic vascular network formation, *Circ. Res.* 86, 286-292, 2000.

[13] Drake, C.J. and Little, C.D., VEGF and vascular fusion: implications for normal and pathological vessels, *J. Histochem. Cytochem.* 47, 1351-1356, 1999.

[14] Risau, W., Mechanism of angiogenesis, *Nature* 386, 671-674, 1997.

[15] Folkman, J., Angiogenesis in cancer, vascular, rheumatoid, and other disease, *Nature Med.* 1, 27-31, 1995.

[16] Hanahan, D., Signaling vascular morphogenesis and maintenance, *Science* 277, 48-50, 1997.

[17] Bussolino, F., Mantovani, A., and Persico, G., Molecular mechanisms of blood vessel formation, *Trends Biochem. Sci.* 22, 251-256, 1997.

[18] He, Z., Wang, K.C., Koprivica, V., Ming, G., and Song, H.J., Knowing how to navigate: mechanisms of semaphorin signaling in the nervous system, *Science's STKE.* 2002, RE1., 2002.

[19] Murayama, T. and Asahara, T., Bone marrow-derived endothelial progenitor cells for vascular regeneration, *Curr. Opin. Mol. Ther.* 4, 395-402, 2002.

[20] Scholz, D., Cai, W., and Schaper, W., Arteriogenesis, a new concept of vascular adaptation in occlusive disease, *Angiogenesis* 4, 247-257, 2001.

[21] Schaper, W. and Buschmann, I., Collateral circulation and diabetes, *Circulation* 99, 2224-2226, 1999.

[22] Buschmann, I.R., Hoefer, I.E., van Royen, N., Katzer, E., Braun-Dulleaus, R., Heil, M., Kostin, S., Bode, C., and Schaper, W., GM-CSF: a strong arteriogenic factor acting by amplification of monocyte function, *Atherosclerosis* 159, 343-356, 2001.

[23] Schaper, W., Therapeutic arteriogenesis has arrived, *Circulation* 104, 1994-1995, 2001.

[24] Arras, M., Ito, W.D., Scholz, D., Winkler, B., Schaper, J., and Schaper, W., Monocyte activation in angiogenesis and collateral growth in the rabbit hindlimb, *J. Clin. Invest.* 101, 40-50, 1998.

[25] Gospodarowicz, D., Ferrara, N., Schweigerer, L., and Neufeld, G., Structural characterization and biological functions of fibroblast growth factor, *Endocr. Rev.* 8, 95-114, 1987.

[26] Ferrara, N. and Davis-Smyth, T., The biology of vascular endothelial growth factor, *Endocrinol. Rev.* 18, 4-25, 1997.

[27] Neufeld, G., Cohen, T., Gengrinovitch, S., and Poltorak, Z., Vascular endothelial growth factor (VEGF) and its receptors, *Faseb J.* 13, 9-22, 1999.

[28] Matsumoto, T. and Claesson-Welsh, L., VEGF Receptor Signal Transduction, *Science's STKE* www.stke.org/cgi/content/full/OC-sigtrans; 2001/112/re21, 2001.

[29] Gerber, H., Malik, A.K., Solar, P.G., Sherman, D., Liang, X.H., Meng, G., Hong, K., Marsters, J.C., and Ferrara, N., VEGF regulates hematopoietic stem cell survival by an internal autocrine loop mechanism, *Nature* 417, 954-958, 2002.

[30] Mitola, S., Sozzani, S., Luini, W., Arese, M., Borstatti, A., Weich, H.A., and Bussolino, F., Tat-HIV-1 induces human monocyte chemotaxis by activation of vascular endothelial growth factor receptor-1, *Blood* 90, 1365-1372, 1997.

[31] Street, J., Bao, M., deGuzman, L., Bunting, S., Peale, F.V., Ferrara, N., Steinmetz, H., Hoeffel, J., Cleland, L.J., Daugherty, A., van Bruggen, N., Redmond, H.P., Carano, R.A.D., and Filvaroff, E.H., Vascular endothelial growth factor stimulates bone repair by promoting angiogenesis and bone turnover, *Proc. Natl. Acad. Sci. USA* 99, 9656-9661, 2002.

[32] Karkkainen, M.J., Makinen, T., and Alitalo, K., Lymphatic endothelium: a new frontier of metastasis research, *Nature Cell Biol.* 4, E2-E5, 2002.

[33] Luttun, A., Tjwa, M., Moons, L., Wu, Y., Angelillo-Scherrer, L.F., Nagy, J.A., Hooper, A., Priller, J., De Klerck, B., Compernolle, V., Daci, E., Bohlen, P., Dewerchin, M., Herbert, J., Fava, R., Matthys, P., Carmeliet, G., Collen, D., Dvorak, H.F., Hicklin, J.D., and Carmeliet, P., Revascularization of ischemic tissues by PlGF treatment, and inhibition of tumor angiogenesis, arthritis, and atherosclerosis by anti-Flt1, *Nature Med.* 8, 831-840, 2002.

[34] Stone, J., Itin, A., Alon, T., Pe'er, J., Gnessin, H., Chan-Ling, T., and Keshet, E., Development of retinal vasculature is mediated by hypoxia-induced vascular endothelial growth factor (VEGF) expression by neuroglia, *J. Neurosci.* 15, 4738-4747, 1995.

[35] Harris, A.L., Hypoxia - a key regulatory factor in tumor growth, *Nature Rev. Cancer.* 2, 38-47, 2002.

[36] Arbiser, J.L., Moses, M.A., Fernandez, C.A., Ghiso, N., Cao, Y., Klauber, N., Frank, D., Brownlee, M., Flynn, E., Parangi, S., Byers, H.R., and Folkman, J., Oncogenic H-ras stimulates angiogenesis by two distinct pathways, *Proc. Natl. Acad. Sci. USA*, 861-866, 1997.

[37] Grugel, S., Finkenzeller, G., Weindel, K., Barleon, B., and Marme, D., Both v-Ha-Ras and v-Raf stimulate expression of the vascular endothelial growth factor in NIH 3T3 cells, *J. Biol. Chem.* 270, 25915-25919, 1995.

[38] Soldi, R., Mitola, S., Strasly, S., Defilippi, P., Tarone, G., and Bussolino, F., Role of $\alpha v\beta 3$ integrin in the activation of vascular endothelial growth factor receptor-2, *EMBO J.* 18, 734-740, 1999.

[39] Bussolino, F., Serini, G., Mitola, S., Bazzoni, G., and Dejana, E., Dynamic modules and heterogeneity of function: a lesson from tyrosine kinase receptors in endothelial cells, *EMBO Rep.* 2, 763-767, 2001.

[40] Kawasaki, T., Kitsukawa, T., Bekku, Y., Matsuda, Y., Sanbo, M., Yagi, T., and Fujisawa, H., A requirement for neuropilin-1 in embryonic vessel formation, *Development* 126, 4895-4902, 1999.

[41] Kitsukawa, T., Shimono, A., Kawakami, A., Kondoh, H., and Fujisawa, H., Overexpression of a membrane protein, neuropilin, in chimeric mice causes anomalies in the cardiovascular system, nervous system, and limbs, *Development* 121, 4309-4318, 1995.

[42] Miao, H.Q., Soker, S., Feiner, L., Alonso, J.L., Raper, J.A., and Klagsbrun, M., Neuropilin-1 mediates collapsin-1/semaphorin III inhibition of endothelial cell motility: functional competition of collapsin-1 and vascular endothelial growth factor-165, *J. Cell Biol.* 146, 233-242, 1999.

[43] Gagnon, M.L., Bielenberg, D.R., Gechtman, Z., Miao, H.Q., Takashima, S., Soker, S., and Klagsbrun, M., Identification of a natural soluble neuropilin-1 that binds vascular endothelial growth factor: *in vivo* expression and antitumor activity, *Proc. Natl. Acad. Sci. USA* 97, 2573-2578, 2000.

[44] Soker, S., Takashima, S., Miao, H.Q., Neufeld, G., and Klagsbrun, M., Neuropilin-1 is expressed by endothelial and tumor cells as an isoform-specific receptor for vascular endothelial growth factor, *Cell* 92, 735-745, 1998.

[45] Hunter, T., Signaling-2000 and beyond, *Cell* 100, 113-127, 2000.

[46] Fong, G.H., Rossant, J., Gertsenstein, M., and Breitman, M.L., Role of the Flt-1 receptor tyrosine kinase in regulating the assembly of vascular endothelium, *Nature* 376, 66-70, 1995.

[47] Shalaby, F., Rossant, J., Yamaguchi, T.P., Gertsenstein, M., Wu, X.F., Breitman, M.L., and Schuh, A.C., Failure of blood-island formation and vasculogenesis in Flk-1-deficient mice, *Nature* 376, 62-66, 1996.

[48] Ruoslahti, E. and Rajotte, D., An address system in the vasculature of normal tissues and tumors, *Annu. Rev. Immunol.* 18, 813-827, 2000.

[49] St. Croix, B., Rago, C., Velculescu, V., Traverso, G., Romans, K.E., Montgomery, E., Lal, A., Riggins, G.J., Lengauer, C., Vogelstein, B., and Kinzler, K.W., Genes expressed in human tumor endothelium, *Science* 289, 1197-1202, 2000.

[50] Palade, G.E., Simionescu, M., and Simionescu, N., Structural aspects of the permeability of the microvascular endothelium, *Acta Physiol. Scand. Suppl.* 463, 11-32, 1979.

[51] Stewart, P.A. and Wiley, M.J., Developing nervous tissue induces formation of blood-brain barrier characteristics in invading endothelial cells: A study using quail-chick transplantation chimeras, *Dev. Biol.* 84, 183-192, 1981.

[52] Le Couter, J., Lin, R., and Ferrara, N., Endocrine gland-derived VEGF and the emerging hypothesis of organ-specific regulation of angiogenesis, *Nature Med.* 8, 913-917, 2002.

[53] Corbacho, A.M., De La Escalera, G., and Clapp, C., Roles of prolactin and related members of the prolactin/growth hormone/placental lactogen family in angiogenesis, *J. Endocrinol.* 173, 219-238, 2002.

[54] Brooks, P.C., Role of integrins in angiogenesis, *Eur. J. Cancer* 32A, 2423-2429, 1996.

[55] Hynes, R.O., A reevaluation of integrins as regulators of angiogenesis, *Nature Med.* 8, 918-921, 2002.

[56] McAllister, K.A., Grogg, K.M., Johnoson, D.W., Gallione, C.J., Baldwin, M.A., Jackson, C.E., Helmbold, E.A., Markel, D.S., McKinnon, W.C., and Murrel, J., Endoglin, a TGF-β binding protein of endothelial cells, is the gene for hereditary haemorrhagic telangiectasia type-1, *Nature Genet.* 8, 345-351, 1991.

[57] Sato, T.N., Tozawa, Y., Deutsch, U., Wolburg-Buchholz, K., Fujiwara, Y., Gendron-Maguire, M., Gridley, T., Wolburg, H., Risau, W., and Qin, Y., Distinct roles of the receptor tyrosine kinases Tie-1 and Tie-2 in blood vessel formation, *Nature* 376, 70-74, 1995.

[58] Suri, C., Jones, P.F., Patan, S., Bartunkova, S., Maisonpierre, P.C., Davis, S., Sato, T.N., and Yancopoulos, G.D., Requisite role of angiopoietin-1, a ligand for the Tie2 receptor, during embryonic angiogenesis, *Cell* 87, 1171-1180, 1996.

[59] Suri, C., McClain, J., Thurston, G., McDonald, D.M., Zhou, H., Oldmixon, E.H., Sato, T.N., and Yancopoulos, G.D., Increased vascularization in mice overexpressing angiopoietin-1, *Science* 282, 468-471, 1998.

[60] Maisonpierre, P.C., Suri, C., Jones, P.F., Bartunkova, S., Wiegand, S.J., Radziejewski, C., Compton, N., McClain, J., Aldrich, T.H., Papadopoulos, N., Daly, T.J., Davis, S., Sato, T.N., and Yancopoulos, G.D., Angiopoietin-2, a natural antagonist for Tie2 that disupts in angiogenesis, *Science* 277, 55-60, 1997.

[61] Thurston, G., Angiopoietin-1 protects the adult vasculature against plasma leakage, *Nature Med.* 6, 460-463, 2000.

[62] Thurston, G., Rudge, J.S., Ioffe, E., Zhou, H., Ross, L., Croll, S.D., Glazer, N., Holash, J., McDonald, D.M., and Yancopoulos, G.D., Angiopoietin-1 protects the adult vasculature against plasma leakage, *Nature Med.* 6, 460-463, 2000.

[63] Larcher, F., Murillas, R., Bolontrade, M., Conti, C.J., Jorcano, J.L., Detmar, M., Brown, L.F., Schon, M.P., Elicker, B.M., Velasco, P., Richard, L., Fukumura, D., Monsky, W., Claffey, K.P., Jain, R.K., Lakatos, L., Okamoto, N., Tobe, T., Hackett, S.F., Ozaki, H., Vinores, M.A., LaRochelle, W., Zack, D.J., and Campochiaro, P.A., VEGF/VPF overexpression in skin of transgenic mice induces angiogenesis, vascular hyperpermeability, and accelerated tumor development. Increased microvascular density and enhanced leukocyte rolling and adhesion in the skin of VEGF transgenic mice. Transgenic mice model of ocular neovascularization driven by vascular endothelial growth factor (VEGF) overexpression [letter; comment] Transgenic mice with increased expression of vascular endothelial growth factor in the retina: a new model of intraretinal and subretinal neovascularization [see comments], *Oncogene* 17, 303-311, 1998.

[64] Adams, J.C., Thrombospondins: multifunctional regulators of cell interactions, *Annu. Rev. Cell Dev. Biol.* 17, 21-25, 2001.

[65] O'Reilly, M.S., Holmgren, L., Shing, Y., Chen, C., Rosenthal, R.A., Moses, M., Lane, W.S., Cao, Y., Sage, E.H., and Folkman, J., Angiostatin: a novel angiogenesis inhibitor that mediates the suppression of metastases by a Lewis lung carcinoma, *Cell* 79, 315-328, 1994.

[66] O'Reilly, M.S., Boehm, T., Shing, Y., Fukai, N., Vasios, G., Lane, W.S., Flynn, E., Birkhead, J.R., Olsen, B.R., and Folkman, J., Endostatin: an endogenous inhibitor of angiogenesis and tumor growth, *Cell* 88, 277-285, 1997.

[67] Browder, T., Folkman, J., and Pirie-Shepherd, S., The hemostatic system as a regulator of angiogenesis, *J. Biol. Chem.* 275, 1521-1524, 2000.

[68] Szekanecz, Z. and Koch, A.E., Chemokines and angiogenesis, *Curr. Opin. Rheumatol.* 13, 202-208, 2001.

[69] Hanahan, D. and Folkman, J., Patterns and emerging mechanisms of the angiogenic switch during tumorigenesis, *Cell* 86, 353-364, 1996.

[70] Semenza, G.L.I., Angiogenesis in ischemia and cancer, *Annu. Rev. Med.* 54, 17-28, 2003.

[71] Weidner, N., Semple, J.P., Welch, W.R., and Folkman, J., Tumor angiogenesis and metastasis, correlation in invasive breast carcinoma, *N. Engl. J. Med.* 324, 1-8, 1991.

[72] Hanahan, D., A flanking attack on cancer, *Nature Med.* 4, 13-14, 1998.

[73] Mantovani, A., Bottazzi, B., Colotta, F., Sozzani, S., and Ruco, L., The origin and function of tumor-associated macrophages, *Immunol. Today* 13, 265-270, 1992.

[74] Fukumura, D., Xavier, R., Sugiura, T., Chen, Y., Park, E., Lu, N., Selig, M., Nielsen, G., Taksir, T., Jain, R.K., and Seed, B., Tumor induction of VEGF promoter activity in stromal cells, *Cell* 94, 715-725, 1998.

[75] Holash, J., Wiegand, S.J., and Yancopoulos, G.D., New model of tumor angiogenesis: dynamic balance between vessel regression and growth mediated by angiopoietins and VEGF, *Oncogene* 18, 5356-5362, 1999.

[76] Asahara, T., Takahashi, T., Masuda, H., Kalka, C., Chen, D., Iwaguro, H., Inai, Y., Silver, M., and Isner, J.M., VEGF contributes to postnatal vascularization by mobilizing bone marrow-derived endothelial progenitor cells, *EMBO J.* 18, 3964-3972, 1999.

[77] Folberg, R., Hendrix, M.J., and Maniotis, A.J., Vasculogenic mimicry and tumor angiogenesis, *Am. J. Pathol.* 156, 361-381, 2000.

[78] Chang, Y.S., di Tomaso, E., McDonald, D.M., Jones, R., Jain, R.K., and Munn, L.L., Mosaic blood vessels in tumors: frequency of cancer cells in contact with flowing blood, *Proc. Natl. Acad. Sci. USA* 97, 14608-14613, 2000.

[79] Holmgren, L., O'Reilly, M.S., and Folkman, J., Dormancy of micrometastases: balanced proliferation and apoptosis in the presence of angiogenesis suppression, *Nature Med.*, 1996.

[80] MacDonald, D.M., Munn, L., and Jain, R.K., Vasculogenic mimicry: how convincing, how novel, and how significant?, *Am. J. Pathol.* 156, 383-388, 2000.

[81] Rafii, S., Circulating endothelial precursors: mystery, reality, and promise, *J. Clin. Invest.* 105, 17-19, 2000.

[82] Lyden, D., Hattor, I.K., Dias, S., Costa, C., Blaikie, P., Butros, L., Chadburn, A., Heissig, B., Marks, W., Witte, L., Wu, Y., Hicklin, D., Zhu, Z., Hackett, N.R., Crystal, R.G., Moore, M.A., Hajjar, K.A., Manova, K., Benezra, R., and Rafii, S., Impaired recruitment of bone-marrow-derived endothelial and hematopoietic precursor cells blocks tumor angiogenesis and growth, *Nature Med.* 7, 1194-1201, 2001.

[83] Folkman, J., Can mosaic tumor vessels facilitate molecular diagnosis of cancer?, *Proc. Natl. Acad. Sci. USA* 98, 398-400, 2001.

Chapter 2

Novel Directions in Tumour Biology: From Basement Membrane-Directed Polarity to DNA Methylation

Cédric Plachot and Sophie A. Lelièvre
Department of Basic Medical Sciences, Purdue University (U.S.A.)

2.1 Abstract

It is now well established that dynamic interactions between cells and their microenvironment are essential for the regulation of tissue function, cell behaviour, and gene expression. Notably the influence of extracellular matrix proteins on structural and functional epithelial tissue differentiation and normal epithelial cell behaviour has been linked to specific interactions between basement membrane-related extracellular matrix proteins and their cell membrane receptors. The importance of the basement membrane in tissue polarisation, a critical parameter of tissue differentiation and cell survival, was clearly demonstrated using three-dimensional cultures of epithelial cells that mimic physiologically relevant conditions. A major advancement in the understanding of the epigenetic regulation of gene expression has been obtained thanks to the identification of several molecular systems involved in chromatin remodelling. These discoveries have enabled biologists to begin deciphering the mechanisms by which extracellular matrix signalling regulates gene expression. In this chapter, we will review the fundamental processes of basement membrane-directed polarisation and chromatin remodelling and discuss how alterations in these processes may be associated with tumour development. An overview of novel therapeutic strategies targeted to the regulation of cell-extracellular matrix interactions and chromatin remodelling factors in cancer cells will also be presented.

2.2 Introduction

The identification of novel targets for cancer therapy relies on the understanding of the mechanisms that direct tumour behaviour. This review will develop two aspects of tumour biology that have brought considerable potential for understanding tumour development and cancer progression, and discuss their relevance for cancer therapy. The first aspect focuses on the relationship between tumour cells from epithelial origin and their microenvironment and more particularly the basement membrane, a specific type of extracellular matrix (ECM). The basement membrane acts as a signal transducer to epithelial cells, an organiser of cellular compartmentalisation and tissue polarisation, and a physical barrier between epithelial structures and the surrounding stroma. Changes in cell-basement membrane interaction occur early during tumour development and increasing alterations between basement membrane organisation and basement membrane receptors at the surface of tumour cells may account for significant modifications in tumour cell behaviour during cancer progression.

The second feature of tumour biology we are addressing in this chapter is related to epigenetics, which refers to the control of gene expression without alterations in DNA sequence. It has become increasingly evident that beside numerous examples

of mutations and other DNA aberrations found in the genome of tumour cells, a number of unaltered genes coding for key regulatory proteins are simply turned on or off. Most often alterations in the expression of genes are the consequences of chromatin remodelling that switches gene promoters between open and closed conformations. Two mechanisms involved in chromatin remodelling, the ATP-dependent SWI/SNF modulatory complex and post-translational histone modifications, have been deciphered. These mechanisms are influenced by DNA methylation, which chemically modifies DNA and hence regulates the recruitment of the machinery necessary for chromatin remodelling. Understanding how genes are controlled locally has opened new possibilities for the implementation of strategies aimed at altering gene expression, and notably the expression of genes involved in proliferation control, in cancer.

Finally, in a third section of the chapter, we will discuss promising directions in tumour biology research by exploring the connection between basement membrane signalling and chromatin remodelling. In each chapter section a particular aspect of tumour biology will be discussed in comparison with the normal situation, since as it was proposed more than two decades ago [1], the best way to understand how cells go awry is to first understand how cells behave normally.

2.3 Cell-Basement Membrane Interactions during Tumour Progression

More than 80% of cancers originate from epithelial tissue and one of the earliest modifications in the neoplastic epithelium is the alteration of tissue polarity. Tissue polarisation is a characteristic of epithelial differentiation and is accompanied with the compartmentalisation of proteins along the polarisation axis (Figure 2.1).

This phenomenon induces an asymmetrical intracellular organisation in which different subcellular areas are morphologically or functionally distinct. Tissue polarity is responsible for the appropriate function of the epithelial tissue. For instance it influences cell proliferation and directs secretion vectorially into the lumen in breast, salivary, or pancreatic glandular structures [2, 3, 4] and also regulates appropriate cell assembly in the epidermis [5]. Typically polarisation is initiated by the deposition of a continuous basement membrane against what then becomes the basal plasma membrane of epithelial cells. Basement membrane deposition triggers the redistribution of receptors of basement membrane components to the basal cell membrane, while proteins involved in cell-cell junctions redistribute to cell membranes in contact with other cells. The predominant and most studied receptors of the basement membrane are the integrins that belong to a superfamily of proteins capable of heterodimerization. Unravelling alterations in both basement membrane and integrin organisation in tumours has considerably improved our understanding of the mechanisms involved in tumour progression and resistance to treatment.

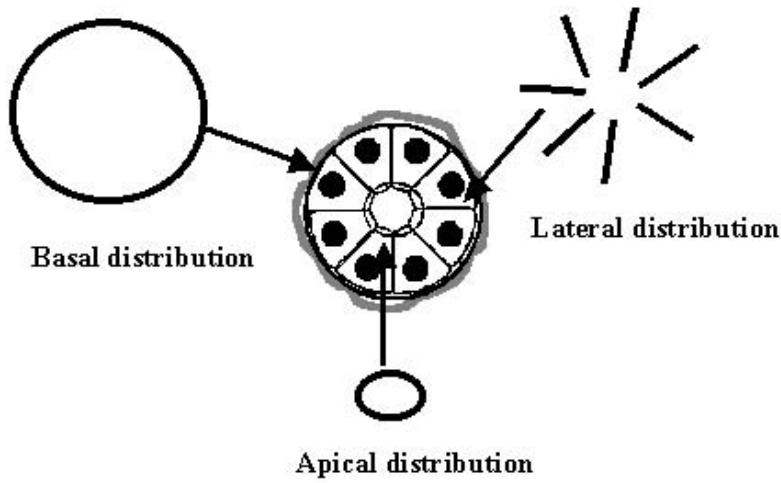

Figure 2.1

Compartmentalisation of proteins along the polarisation axis. The centre of the figure represents a polarised glandular structure, in which one layer of epithelial cells is organised around a lumen (cell nuclei are drawn as black filled-circles). Polarisation is induced by the deposition of a continuous basement membrane (in grey) that delineates the external side of the glandular structure. Upon basement membrane deposition, cell membrane proteins redistribute to different compartments: certain proteins are only found at basal cell membranes (basal distribution), others relocalise to cell-cell contacts (lateral distribution), while certain types of proteins concentrate to the cell membranes that delineate the internal lumen (apical distribution).

2.3.1 The Roles of Basement Membrane-Integrin Interaction in Normal Tissue

The basement membrane is composed of an organised lattice of fibrous proteins, including nidogens, laminins and collagen IV, and proteoglycans that make contact with the cell membrane via specific receptors [6, 7]. Laminins are among the main constituents of basement membranes. These heterotrimeric glycoproteins are composed of heavy α, light β, and light γ chains held together by disulphite bonds (Figure 2.2). To date 11 different chain isoforms have been identified [7] and have been described to be expressed in a tissue-specific and developmentally regulated

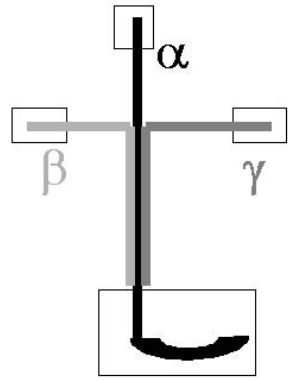

Figure 2.2

Structure of laminin. Three types of chains (α, β, and γ) organised cruciformly are involved in laminin formation. Binding sites for major laminin receptors (integrins) are indicated by a box.

manner. All major types of basement membranes contain at least one of the laminin variants. For instance, in the mammary gland laminin 1, 5, 9, and 10 are present and are mainly in contact with myoepithelial cells that surround luminal epithelial cells. Laminins are also in contact with a portion of the luminal cell surface [8]. In the epidermis, keratinocytes are in continuous contact with laminin 5 and 1 [9]. It was recently shown using lung organotypic cultures that in order to mediate polarisation laminin must be polymerised and that polymerisation is mediated by the outer globular region of its β chain [10].

The major receptors of fibrous basement membrane molecules belong to the integrin family of proteins. The term integrin was chosen because these molecules are integral membrane proteins (Figure 2.3) and play a major role in the integration of functions between the ECM and the cytoskeleton [11]. They act as noncovalently associated α/β heterodimers that were originally thought to mediate exclusively cell-ECM interactions in multicellular organisms. Integrins possess a cytoplasmic domain that participates in cellular signalling via its ability to associate with and activate signal transduction pathways, and to connect with the cytoskeletal network. The extracellular domain of integrins binds to ECM proteins including fibronectin, collagen, nidogen, and laminin [12]. The interaction between integrins and laminin seems to be largely determined by the α chain of laminin. However, integrins can also bind counter receptors on adjacent cells. This is illustrated by the localisation of $\beta 1$ and αv integrins to cell-cell boundaries. Such a localisation has been proposed to participate in the maintenance of polarity by integrating or supporting the role of other cell-cell adhesion molecules [13, 14].

To date 18 α-integrin chains and 8 β-integrin chains have been identified in

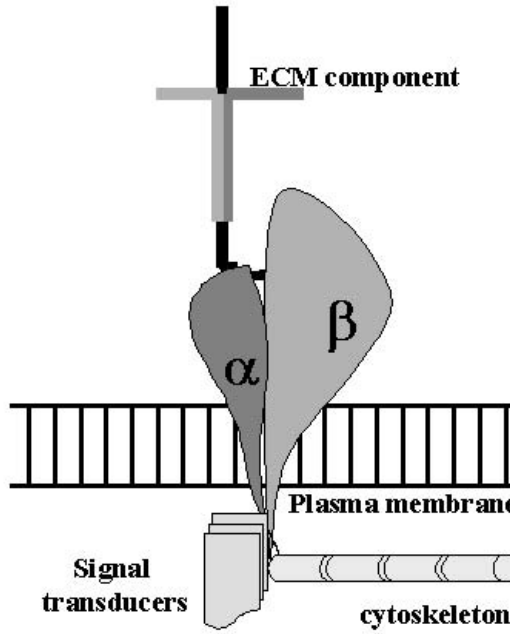

Figure 2.3

Integrin heterodimers and signal transduction. Upon the binding of their extracellular domains to specific ECM components (e.g., a cruciform laminin is represented in this image) α and β integrin heterodimers interact, via their intracellular domains, with signal transducers and elements of the cytoskeleton.

vertebrates. In addition, for most chain types, several isoforms can be generated by alternative mRNA splicing. Binding specificity is determined by both the conformation of individual α and β chains and the cellular context [15, 16]. $\alpha 1/\beta 1$, $\alpha 2/\beta 1$, $\alpha 3/\beta 1$, $\alpha 6/\beta 1$, $\alpha 7/\beta 1$, $\alpha 9/\beta 1$, $\alpha v/\beta 3$, $\alpha v/\beta 5$, $\alpha v/\beta 8$, and $\alpha 6/\beta 4$ have all been reported to bind laminin. Among those, $\alpha 6/\beta 1$, $\alpha 7/\beta 1$, and $\alpha 6/\beta 4$ are viewed almost exclusively as laminin receptors. The $\beta 4$ subunit is unique among integrins because it possesses a distinctively large cytoplasmic domain (1000 amino-acids instead of 50 amino-acids) and encompasses fibronectin type III repeats that bring elasticity and allow resistance to mechanical forces [17]. The first pair of repeats has been shown to mediate $\beta 4$-integrin unique association with intermediate filaments via an interaction with plectin [18]; other integrins are mainly connected to the actin network.

$\alpha 6/\beta 4$-integrins are localised to the basal plasma membrane of polarised epithelial cells where they preferentially interact with laminin 5. Their role in polarisation is exemplified by their specific localisation to hemidesmosomes, the ultrastructures that maintain adhesion of the epithelium to the underlying basement membrane

and are critical for the induction and maintenance of tissue polarity [19]. The role of $\alpha 6/\beta 4$ integrins in tissue polarity has been well demonstrated thanks to the use of three-dimensional (3D) culture systems that reproduce glandular differentiation [2, 20–23] and epidermis formation [5] of normal and nonmalignant cells placed in contact with a reconstituted basement membrane. Human primary mammary luminal epithelial cells cultured within collagen-I gels instead of reconstituted basement membrane arrested growth and formed 3D cell clusters; however, they did not polarise, as shown by the deposition of milk precursors at the basal rather than the apical pole of the cell clusters and the absence of $\beta 4$-integrin [8]. Subsequent addition of laminin 1 was sufficient to restore polarity and $\beta 4$-integrin localisation at basal cell membranes. In another study, $\beta 4$-integrin blocking antibodies were able to suppress polarity in breast glandular structures and induce cells to proliferate [24].

$\beta 1$-integrins have been involved in polarity by acting directly on the assembly of the basement membrane. They mainly localise to regions of cell-cell interaction; however, certain dimers, like $\alpha 3/\beta 1$ are also located to the basement membrane area. Expression of $\beta 1$-integrin lacking its extracellular domain induced poor lactation performances in transgenic mice. Alterations in the function of the mammary gland were accompanied with an abnormal accumulation of laminin and $\beta 4$-integrin at the lateral surface of luminal epithelial cells [25].

Another important function of integrin-mediated polarity is the maintenance of cell survival in a growth-arrested state. This function was demonstrated by interrupting $\beta 1$-integrin binding using function-blocking antibodies in 3D mammary cultures [26] and expressing truncated $\beta 1$-integrin in mice [25]. Both manipulations induced apoptosis in mammary luminal epithelial cells. Furthermore, adhesion-mediated activation of $\beta 4$-integrin was shown to trigger phosphorylation of Akt and Bad, two transducers involved in the inhibition of apoptotic pathways [27]. However, the authors suggested that cell survival might result from integrin involvement in the maintenance of cell adhesion rather than from a direct interaction between a particular integrin and mediators of apoptotic pathways.

2.3.2 Alteration of Polarity in Cancer

Originally, reports described that tumour progression was paralleled by changes in basement membrane organisation and hence might be accompanied by alterations in polarity. Discontinuous laminin has been observed in pancreatic acinar carcinoma [28] and other reports have indicated that well-differentiated gastric adenocarcinomas have a discontinuous but thick basement membrane, while increasing loss of differentiation is associated with the production of thinner and fragmentary, or even totally disorganised, basement membranes [29]. Similarly, organotypical cultures of mouse epidermal invasive tumour cells revealed that classical basement membrane components are expressed but there is no formation of a structured basement membrane, except in some areas of well differentiated tumours [30]. The presence of intact basement membrane in certain tumour regions was intriguing since it sug-

gested that tumour cells in these areas might maintain polarity. The consequence of the presence of polarised tumour cells for tumour behaviour was recently unravelled. Indeed maintenance of β4-integrin-mediated polarity may drive resistance to apoptosis normally induced by cytotoxic drugs. This possibility is illustrated by recent work showing that the expression of altered β4-integrin in nonmalignant human breast epithelial cells is accompanied with impaired polarisation and increased sensitivity to cytotoxic drugs. Whereas, ligation of β4-integrins in tumour cells and induction of hemidesmosome formation initiate resistance to apoptosis induction via NFkB activation [31].

The loss of polarity usually seen in many tumours can easily be linked to the presence of an incomplete basement membrane. In mammary cancer, this hypothesis is based on the fact that mesenchymal cells that usually produce a lot of a laminin rapidly disappear during tumour progression. Although tumour cells can produce a number of basement membrane components, they make minimal amounts of a laminin, which results in the formation of incomplete laminin [32]. In addition the increase in matrix metalloprotease (MMP) activity [33], and notably gelatinase activity, in the vicinity of tumour cells may be responsible for the cleavage of basement membrane components and thus contribute to the alteration of polarity, as suggested by MMP2-mediated cleavage of the γ2 chain of laminin 5 in certain tumours [34].

Alterations in basement membrane receptors also contribute to the loss of polarity in tumours. Malignant development is often associated with defective hemidesmosomal structures [35]. α6/β4 integrins may still be expressed but they are not localised to hemidesmosomes. Depending on the type of neoplastic lesion, the alteration of polarity may be accompanied by either an increase in α6/β4 integrin expression (e.g., squamous cell carcinoma) or a decrease in α6/β4 integrin expression (e.g., basal cell carcinoma) [36]. Alterations in α2/β1 and α3/β1 integrins are also observed, as shown by their pericellular distribution instead of typical cell-cell localisation in epidermal carcinoma [5]. A change in the ratio between β4 and β1-integrins have been reported between malignant, nonpolarised HMT-3522 mammary epithelial cells and their compared to their nonmalignant counterpart. Interestingly polarity and glandular differentiation could be reinduced in these tumour cells using function blocking β1-integrin antibodies, indicating that modifications in the dominant integrin pathway may also be involved in the loss of polarity associated with tumour development [24].

Interestingly, once released from their participation in tissue polarity, integrins become involved in tumour behaviour. α6/β4-integrins may redistribute to actin-rich cell protrusions during migration of carcinoma cells [37] and may promote invasion via activation of phosphoinositide 3-kinase [38]. The same integrin dimer has also been shown to stimulate chemotactic migration, a key component of invasion [39]. Similarly α6/β1 integrins may promote adhesion, migration, and survival of tumour cells [24, 40, 41]. These cancer-related functions may be mediated either by the appearance of a splice variant, as reported for the α6-integrin subunit [42], the binding of truncated laminin (e.g., peptides derived from the laminin α chain) [43], or abnormal clustering, as shown for α6/β1-integrins [44]. In addition, the formation of integrin clusters in invadopodia may serve as docking sites for MMPs and hence

allow focal proteolysis of the surrounding matrix [45].

Alterations in basement membrane deposition and integrins are obvious illustrations of the loss of polarity. However, more subtle alterations in cell and tissue polarity appear very early during tumour development. In carcinoma *in situ*, a basement membrane still delineates the basal surface of the external cell layer, but the central lumen has been completely filled by tumour cells that are not in contact with the basement membrane (Figure 2.4). This phenomenon was reproduced in culture by activating erb2 receptor, a member of the epidermal growth factor (EGF) signalling pathway, in preformed mammary glandular structures [46]. This study suggests that constitutive activation of EGF-related signalling pathways may contribute to tumour cell survival upon the loss of basement membrane contact. In addition, this survival could be mediated by the loss of function of proteins involved in positioning control, that normally direct the requirement for basement membrane attachment. For instance expression of the tumour suppressor protein Dab2 is frequently lost in ovarian and breast cancers. Reexpression of Dab2 in ovarian and breast tumour cells was shown to induce cell death. However, cell death could be prevented by the attachment of tumour cells to a basement membrane [47].

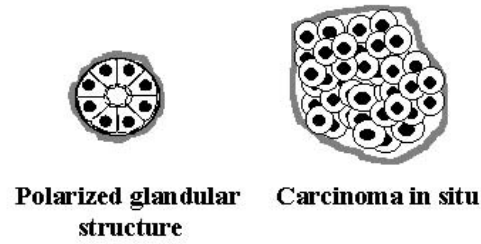

Figure 2.4

Epithelial cell organisation in normal glandular structures and carcinoma *in situ*. A section through a normal and fully polarised (baso-apical polarisation) glandular structure shows the central lumen (left image), while a section through a carcinoma *in situ* surrounded by a continuous basement membrane shows a mass of tumour cells; the basement membrane is in light grey.

2.3.3 Novel Anti-Cancer Strategies Based on Cell-ECM Interaction

The better understanding of the role of the basement membrane and its receptors in the regulation of normal and tumour cell behaviours has led to the development of both general and specific anti-cancer strategies. A strategy currently tested in clinical trials is to prevent the expression of MMPs that degrade the basement membrane and stromal ECM and are found activated in most tumour types investigated so far. Broad-spectrum MMP inhibitors produced initially have a structure that imitates collagen structure. They act by chelating the zinc ion present at the active site of MMPs. These broad range inhibitors have shown promising results in clinical trials and have been proposed to be used in adjuvant treatment or maintenance therapy following response to usual cytotoxic drugs [48]. They are also being investigated for use in refractory cancers [49]. It would certainly be an advantage, in order to reduce the extent of side effects and get a higher response rate in certain types of cancer, to use inhibitors targeted to specific MMPs. For instance, inhibitors specific of basement membrane proteases MMP-2 and MMP-9 have been recently developed and have been shown to prevent tumour growth and invasion in xenograft-bearing animals [50]. Other possibilities for more specific targeting of defined MMPs could include the use of ribozymes that block MMP expression. Such a system has been under investigation *in vitro* for MMP-9 [51]. Neverthless, caution should be used with inhibitors of MMP activity that act principally in the cell's microenvironment. Tumour cells may not be directly targeted (with the exception of the use of ribozymes) and might easily develop counter-actions that would still permit tumour progression. Therefore MMP inhibitors may only be useful in combined therapy with agents that directly act on tumour cells. Novel approaches have also been developed to inhibit tumour invasion by blocking or down-regulating integrins involved in tumour cell adhesion. FTY720, an immunosuppressive agent, significantly prevents tumour cells adhesion and migration on ECM by inducing a decrease in integrin expression via an unknown mechanism [52]. Another compound, Contortrostatin, a homodimeric disintegrin (a soluble integrin ligand capable of disrupting cell-matrix interactions), has been shown to prevent cell invasion through an artificial basement membrane and significantly inhibit ovarian cancer dissemination in a nude mice model [53].

None of these therapeutic approaches have yet been developed to modulate basement membrane-related cellular polarity. However, in light of the results reported above and showing that tumour cells may resist apoptosis induction by cytotoxic drugs via β4-integrin-mediated polarity, a promising strategy may be to block this pathway in certain tumours. A possible approach could be to use recombinant human antibodies specific for laminin. Such antibodies have been recently developed and shown to reduce tumour cell attachment to laminin [54]. The authors have proposed that these antibodies might have a potential application in cancer therapy. Nevertheless, like for many therapeutic tools, the difficulty will be to intervene only at the tumour cell level and not the normal tissue level.

2.4 Chromatin Remodelling and Cancer

Chromatin is defined as the organised assembly of DNA, histone and nonhistone proteins. The basic repeating units of chromatin, referred to as nucleosomes, are composed of 147 base pair DNA sequences wrapped around an octamer of four different histone proteins (H2A, H2B, H3, and H4). This nucleosomal configuration can be further condensed (e.g., by histone H1) to form "heterochromatin." Chromatin condensation prevents DNA accessibility to transcription factors and the transcriptional machinery, and ultimately leads to the repression of gene transcription. In contrast, decondensed chromatin fibres form an open chromatin or "euchromatin" that may be associated with active gene expression. The reorganisation of chromatin between open and closed conformations is referred to as "chromatin remodelling" [55].

Different systems are involved in the control of chromatin structure:

- the ATP-dependent chromatin remodelling complex switching/sucrose nonfermenting (SWI/SNF) which mediates the sliding of nucleosomes along DNA [56],
- protein complexes that induce covalent histone modifications, including acetylation, phosphorylation, and methylation [57].

In addition, there is growing evidence to show that the recruitment of chromatin remodelling complexes is influenced by DNA methylation, an important epigenetic mechanism of gene silencing [58]. Alterations in the function or the recruitment of chromatin remodelling complexes are associated with improper chromatin conformation and subsequent dysregulation of gene expression that seem to play a critical role in tumour development and progression [59].

2.4.1 The SWI/SNF ATP-Dependent Chromatin Remodelling Complex

The SWI/SNF complex is a multiprotein assembly (8-12 proteins) that remodels chromatin structure in an ATP-dependent manner [56].

Mechanisms by which SWI/SNF influence chromatin conformation are intricate and not yet fully understood. On one hand, SWI/SNF activity can mediate the formation of an open chromatin by altering individual nucleosomal structures or acting in concert with other chromatin remodelling factors to decondense higher-order chromatin fibres [56] (Figure 2.5). On the other hand, when associated with other chromatin remodelling factors such as the histone deacetylase Sin3, SWI/SNF activity may also be involved in inactive chromatin conformation and subsequent gene silencing, [60] (Figure 2.5). Therefore the molecular context at the level of a specific

gene promoter is likely to play a critical role in determining whether SWI/SNF will participate in closing or opening chromatin.

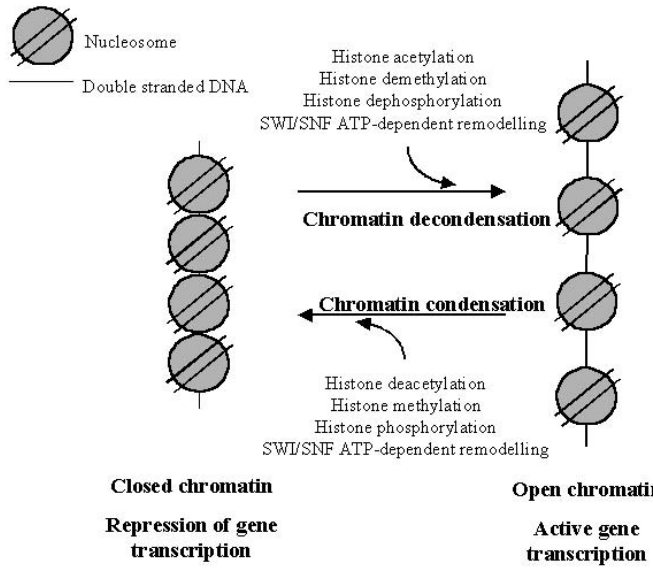

Figure 2.5

Regulation of chromatin conformation. Compaction of nucleosomes and formation of higher order chromatin folding is associated with the repression of gene transcription. Histone deacetylation induced by HDACs and SWI/SNF activity may act separately or in concert to mediate chromatin compaction. Histone methylation and phosphorylation may also provide chromatin condensation. Histone acetylation induced by HATs, histone dephosphorylation, and histone demethylation lead to open chromatin conformation, which may be associated with active gene transcription. Depending on the composition of the multiprotein complex, SWI/SNF activity may also be involved in the formation of an open chromatin.

2.4.2 Histone Modifying Enzymes

Covalent posttranslational modifications of histones are critical for nucleosome stability, and thus chromatin organisation. Acetylation/deacetylation is the most studied covalent modification of histones that participates in the control of chromatin structure. Other histone modifications may be induced by phosphorylation and methylation; although less understood these posttranslational modifications also seem to play a role in chromatin conformation. Finally, histones may also undergo ubiquitination, but the influence of such a modification on chromatin remodelling remains to be clarified.

The interaction between DNA and histones is principally mediated by the attraction between negative charges of DNA and positive charges of the lysine residues located on histone tails. The addition of an acetyl group (C_2H_3O) onto lysines is mediated by histone acetyltransferases (HATs) and neutralises the positive charges of histones, and hence may disrupt histone-DNA interactions and induce the formation of open chromatin (Figure 2.5). The reverse reaction catalysed by histone deacetylases (HDACs), increases the affinity of histones for DNA, which, in turn, triggers chromatin compaction and subsequent gene silencing [61] (Figure 2.5). HATs and HDACs are organised as multiprotein assemblies and may cooperate with ATP-dependent chromatin remodelling complexes to regulate gene transcription. This co-operation has been observed for the multi-protein assembly that forms the nucleosome remodelling and deacetylation (NuRD) complex [60].

Supplementation of histones with phosphate ion PO_4^{3-} (i.e., phosphorylation) is principally mediated by the histone H1 kinase cyclin E Cdk2 and the family of histone H3 kinases Msk/Rsk. Several studies have shown that histone phosphorylation (notably on the serine-10 residue of histone H3) may have opposite effects by promoting chromatin condensation as well as activation of gene expression. This is well illustrated for histone H3, the phosphorylation of which correlates with chromosome compaction during mitosis [62], while it is also associated with the transcription of the early-response genes c-fos and c-jun [63, 64].

Histone methylation is catalysed by histone methyl transferases (HMTs) and consists of the addition of methyl (CH3) groups onto either arginine or lysine residues mainly located on histones H3 and H4. In contrast to acetylation, histone methylation does not change the overall charge of histone tails, but rather increases histone basicity and hydrophobicity that, in turn, enhances histone affinity for anionic molecules like DNA. Recent data suggest that histone methylation might be involved in heterochromatin assembly. Indeed, the heterochromatin-associated protein Suvar3-9 has been shown to methylate histone H3 *in vitro* [65]. Interestingly, histone methylation may also be associated with active gene transcription when preferentially targeted to acetylated histones H3 and H4 [61]. Additional support for a role of histone methylation in promoting gene expression arises from the findings of a direct interaction between HATs (e.g., CBP) and HMTs [61]. To complicate the matter further, an interplay between histone methylation and phosphorylation has also been observed.

Site-specific histone methylation on the lysine 9 residue of histone H3 prevents histone phosphorylation on serine 10. Whereas, when histone methylation is prevented upon Suvar3-9 deletion, histone H3 phosphorylation is induced and abnormal chromosome condensation follows [55]. Altogether reports suggest that one type of post-translational alteration occurring on histone probably influences the effect that additional histone alterations will have on chromatin structure.

2.4.3 Dysregulation of Chromatin Remodelling in Cancer

Cancer is characterised by dramatic changes in the pattern of gene expression. Consequently it is not surprising to find alterations in chromatin structure in tumour cells. According to the literature, these alterations are mainly due to the retargeting of chromatin modifiers to different sets of genes. However, it is unclear whether the retargeting of chromatin modifiers is a consequence of alterations in the molecules they interact with or whether initial alterations in chromatin modifiers may be sufficient to trigger the abnormal expression of specific genes.

Accumulating data strongly suggest that SWI/SNF acts as a tumour suppressor in mammalian cells. Mutations within the SNF5/INI1 components of the SWI/SNF complex have been found in several cases of rhabdoid tumour and leukaemia [66, 67], and mutations in Brg1, the ATPase subunit of the SWI/SNF complex, have been observed in prostate, lung, and breast cancer cell lines [68]. In addition, SNF5 or Brg1 knock out mice display a cancer-prone phenotype [69, 70]. A possible explanation for the tumour suppressor role of the SWI/SNF complex arose from data showing that SWI/SNF subunits interact with tumour suppressors, including Rb, BRCA1, and Myc. For example, Rb can act in concert with Brg1 to assist in gene silencing and induce growth arrest [71]. In addition, several lines of evidence suggest that functions of BRCA1 and Myc are partially dependent on the presence of SWI/SNF [72, 73]. Thus abnormal SWI/SNF may prevent proper functions of these key regulators of cell behaviour. Conversely, we cannot rule out that proteins like Rb, BRCA1, or Myc may control gene expression by directing the SWI/SNF complex to distinct promoters and hence induce chromatin remodelling. Since Rb, BRCA1, and Myc are mutated or silenced in certain cancers, alterations in their function or expression may also have repercussions on the targeting of SWI/SNF to specific DNA sequences.

Similarly to SWI/SNF, the impairment of HATs function has been linked to cancer. A well-described example is the chromosomal translocation affecting the CREB binding protein (CBP) gene, a HAT, which is associated with leukaemia [59]. This chromosomal translocation may lead to the fusion of CBP with other proteins that, in turn, modify CBP targeting to DNA or CBP activity. Fusions with the mixed lineage leukaemia/trithorax protein (MLL), monocytic leukaemia zinc finger (MOZ), MOZ related factor (MORF), and transcriptional intermediary factor (TIF) have all been shown to alter the HAT function of CBP [59].

There are many reasons to believe that dysregulation of HDAC functions is also involved in tumorigenesis. For example, HDACs may be recruited by certain

oncoproteins that subsequently modify HDACs subnuclear distribution and may ultimately lead to improper chromatin remodelling and gene expression. This possibility is illustrated by the fact that mutations or chromosomal translocations affecting the retinoic acid receptor dimers RAR/RXR may induce a persistent interaction between RAR/RXR and the SIN3-HDAC complex and hence promote leukaemia [59]. Additional support for a role of HDACs in tumorigenesis is demonstrated by the ability of HDAC inhibitors (including suberoyl anilide hydroxamic acid: SAHA, or trichostatine A: TSA) to induce growth arrest, differentiation, or apoptosis in a wide variety of human malignant cell lines *in vitro*, including bladder, breast, prostate, lung, ovary and colon cancer cells [74]. Cell growth arrest may be mediated by de novo expression of the cyclin dependent kinase inhibitor p21, as observed in the T24 human bladder carcinoma cells treated with SAHA [75]. HDAC inhibitors are also efficient to reduce tumour growth in chemically-induced animal models of mammary carcinoma, or following transplantation of prostate tumours or melanoma into nude mice [76, 77, 78].

2.4.4 DNA Methylation and Chromatin Remodelling in Normal and Cancerous Tissues

Another attractive aspect of the regulation of chromatin remodelling comes from recent data showing that SWI/SNF and HDACs interact with the DNA methylation machinery, and more particularly, that HDACs are involved in methylation-mediated aberrant gene silencing in cancer.

DNA methylation corresponds to the addition of a methyl group to DNA, most often onto a cytosine (Cp) followed by a guanosine (G). In promoter sequences of genes, CpG dinucleotides are clustered to form CpG islands. When methylated, CpG islands may trigger gene silencing. One of the most accepted explanations for promoter methylation-induced gene silencing is the recruitment of histone deacetylases by methyl-CpG binding proteins (MBPs) to methylated DNA that, in turn, causes deacetylation of adjacent histones and subsequent chromatin condensation [79]. Almost all MBPs interact with HDACs and require deacetylase activity to repress gene transcription (Figure 2.6). Methyl binding domain 2 (MBD2) related-protein is part of the histone deacetylase complex MeCP1 [80], while the presence of MBD1 in MeCP1 is still discussed [81, 82]. MBD3 is a component of the NuRD multisubunit assembly containing both ATP-dependent nucleosome remodelling activities, because of the presence of the SWI2/SNF2 ATPase Mi2, and histone deacetylase properties mediated by Sin3A, HDAC1, and HDAC2 [83]. MBD2 is not part of NuRD but can direct the complex to methylated DNA [83]. Transcriptional repression mediated by the methyl CpG-binding protein 2 (MeCP2) is partially dependent on histone deacetylase activity (mainly via Sin3A) [84]. In addition, interactions between HDAC1, HDAC2, and proteins responsible for DNA methylation, the DNA methyltransferases 1 (DNMT1) [85] and 3a [86] have been demonstrated to play a role in gene silencing. DNMT1 is usually located to replication foci where it methy-

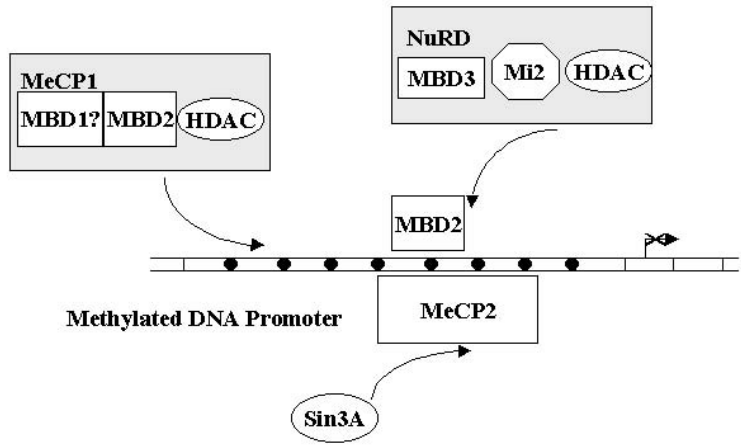

Figure 2.6

Methyl CpG binding proteins, chromatin remodelling factors, and methylated gene silencing. MBD2 is part of the histone deacetylase complex MeCP1 and binds to methylated DNA (black-filled circles), while the presence of MBD1 in MeCP1 is still being discussed. NuRD is composed of MBD3, Mi2-an ATP-dependent nucleosome remodelling factor- and histone deacetylases Sin3A, HDAC1, and HDAC2. MBD2 is not part of NuRD but directs the complex to methylated genes. MeCP2 binds to methylated DNA promoter sequences and can repress gene expression via HDAC (Sin3A) dependent or independent pathways.

lates newly synthesised DNA. The interaction between DNMT1 and HDAC2 at the level of replicating DNA during late S phase may further explain how a repressive heterochromatin state is maintained throughout cell generations [85]. Altogether, these observations connect chromatin remodelling, HDAC activity, and DNA methylation.

Aberrant DNA methylation is a hallmark of malignant cells. It may act upstream of histone modifications responsible for abnormal chromatin remodelling and improper gene expression by recruiting HDACs to sets of genes different from the ones targeted in a normal situation. In cancer, aberrant methylation associated with HDAC-mediated gene silencing has been shown for cell cycle genes (e.g., CDK2A and 2B) [87], genes involved in DNA repair (e.g., MLH1) [87], tumour suppressor genes (e.g., BRCA1) [88], inhibitors of invasion and metastasis (e.g., TIMP3) [87], and other key regulatory genes including the human telomerase reverse transcriptase [89] and RARβ [90].

2.4.5 Anti-Cancer Strategies Based on Chromatin Remodelling

The development of drugs targeting epigenetic mechanisms is relevant for cancer treatment because these drugs could influence the pattern of gene expression and thus cell behaviour. An approach based on the inhibition of HDACs is currently under investigation. The goal is to reinduce genes aberrantly silenced during tumorigenesis by acetylating histones. Inhibitors of HDACs have been shown to promote growth arrest and even differentiation or apoptosis in many tumour cell lines and in tumour bearing animals [74, 91]. The most studied HDAC inhibitors with potential therapeutic use are hydroxamic-acid-based hybrid polar compounds like SAHA; they act by blocking the catalytic site of HDACs. Several HDACs inhibitors are currently in phase I or II clinical trials and some objective tumour regressions have been observed [91, 92]. The biologic activity of HDAC inhibitors is monitored by measuring the increase in the level of acetylated histones in tumours. However, since these inhibitors are not specific of a particular deacetylase, we do not know whether the effect observed with tumour cells is solely due to histone hyperacetylation or whether treatment-induced acetylation of transcription factors, such as p53, might also regulate gene transcription and hence influence cell cycle and cell proliferation [93]. In addition, treatment-induced acetylation has also been detected in normal tissues, and we do not know the long-term consequences of hyperacetylation for these tissues. Results presented on chromatin remodelling during differentiation in part III of this chapter suggest caution should be taken when using HDAC inhibitors.

The regulation of gene expression by HDACs seems to be selective. Only about 2% of genes are affected upon treatment of normal and transformed cells with SAHA or TSA [74, 94]. For a number of genes this phenomenon may be due to the upstream regulation of gene expression resulting from DNA methylation. Indeed treatment with the HDACs inhibitor TSA is not sufficient to restore gene expression at certain loci, whereas treatment with the global demethylating agent 5 Aza 2'-deoxycytidine (5Aza) leads to a substantial reinduction of the expression of these genes, and additional treatment with TSA enhances the effect on 5Aza-mediated gene expression [87–90]. 5Aza has been used in clinical trials with various results; there were undesirable secondary effects (high toxicity, mucositis, diarrhoea, nausea, vomiting, and skin rash) and no significant antitumour activity could be measured for most types of cancer tested, including breast carcinoma [95, 96]. Additionally, preliminary results obtained in our laboratory showed that treatment of preformed breast tumour-like clusters with 5Aza did not alter malignant cell proliferation and did not induce glandular differentiation (unpublished results). Although combined treatment with 5Aza and HDACs inhibitors may be more efficient to restore the expression of methylated genes in cancer, it seems very dangerous to use such broad range inhibitors in patients. Therefore, knowing whether a specific type of acetylase and methyltransferase or MBP can be associated with the regulation of distinct subclasses of genes may be extremely useful for designing more specific, less toxic, and more efficient therapies.

2.5 Extracellular Matrix Signalling to the Cell Nucleus, Chromatin Remodelling, and Cell Behaviour

As we discussed in the first part of this chapter, the basement membrane plays a critical role in the induction and maintenance of epithelial cell differentiation. The formation of differentiated structures is accompanied by changes in gene expression and, according to recent data on chromatin remodelling reported in the second part of the chapter, it is expected that as a consequence of cell-basement membrane interaction, there will be significant alterations in the organisation of chromatin. Therefore understanding how basement membrane signalling regulates chromatin will be invaluable to identify intracellular pathways that may be modulated in future therapeutic strategies.

2.5.1 Chromatin Remodelling during Differentiation

A common feature for the study of the role of chromatin rearrangement in the differentiation process is to use TSA, a reversible inhibitor of HDACs. TSA treatment should maintain the expression of genes that would have been turned off normally by hypoacetylation during the differentiation process. Prevention of global histone hypoacetylation using HDAC inhibitors has various effects on cell differentiation according to the cell type. For instance, TSA treatment prevents the differentiation of nonmalignant rat stellate cells into myofibroblasts because, while TSA treatment hyperacetylates histones and should induce de novo gene expression, it also induces the inhibition of collagen I and III synthesis, as well as smooth muscle α-actin, a marker of differentiation [97]. Thus histone hypoacetylation somehow plays a role in differentiation. A possible explanation for the repressive effect on gene expression observed in the example described above is that TSA maintains the expression of certain genes, the products of which act as transcriptional repressors for other genes involved in the differentiation process.

As discussed in section 1.4, HDAC inhibitors may induce differentiation of tumour cells [91]. SAHA triggers differentiation in several transformed cell lines including the T24 human bladder carcinoma and MCF-7 human breast adenocarcinoma [74], indicating that hypoacetylation is involved in tumorigenesis. The differentiated phenotype was assessed according to morphological and proliferation parameters, as well as the expression of markers such as milk proteins in MCF-7 cells and gelsolin in T24 cells. However, it should be noted that the expression of differentiation markers is not necessary indicative of true phenotypic reversion since this pattern of expression may also occur naturally in a number of tumours. Moreover, the effect of drug treatments on cell proliferation may be quite different between cells cultured as a monolayer (technique most often used) and cells cultured in conditions

that promote the formation of more physiologically relevant, tumour-like 3D multicellular structures. If indeed hypoacetylation plays a role in both differentiation and tumorigenesis, it is likely that the pattern of genes affected by this epigenetic modulation is different in each case. We do not know at this point if the genes affected by HDAC inhibitors in the examples described above are subject to methylation-mediated hypoacetylation or only methylation-free-hypoacetylation.

The use of 3D cultures in which cells are in contact with a reconstituted basement membrane has provided evidence that HDAC activity is involved in basement membrane-mediated mammary glandular differentiation [98, 99]. In the 3D culture system, mouse mammary epithelial cells differentiate into polarised glandular structures and express functional markers of milk production such as β-casein. Interestingly, glandular differentiation was accompanied by histone hypoacetylation, as shown for histone H4. When mammary epithelial cells were treated with TSA during the differentiation process, β-casein expression was prevented [99], indicating that shutting down certain genes is necessary for functional differentiation. Similarly in a human model of breast glandular differentiation, TSA-induced hyperacetylation triggered the loss of polarity, as shown by the fragmentation of the basement membrane, and pushed the cells back into the cell cycle [98]. Thus, chromatin remodelling mediated by histone deacetylation participates in basement membrane regulated events. At this time, there is no direct evidence showing that specific chromatin remodelling complexes are recruited by ECM-mediated differentiation. However, the potential connection between integrin signalling and HATs (e.g., CBP, SRC-1, and SRC-3), histone H3 kinases Rsk2 and Msk1, and histone H1 kinase cyclin E-cdk2 [58] described in the next paragraph, suggests that some of these chromatin remodelling factors might be involved in basement membrane-directed tissue differentiation.

2.5.2 Extracellular Matrix Signalling to Chromatin

A direct connection between basement membrane signalling and gene regulation was first described several years ago upon the discovery of ECM-responsive elements in several gene promoter sequences. A laminin responsive element was identified in the enhancer region of the β-casein gene [100] and, more recently, it was shown that the activation of this enhancer is modulated by the state of histone acetylation [101]. These results were obtained using mouse mammary epithelial cells stably transfected with the bovine β-casein promoter and subsequently treated with sodium butyrate, an inhibitor of HDACs. Sodium butyrate treatment was able to induce the transcription of β-casein controlled by the exogenous promoter, regardless of the presence of ECM. In another study, the expression of the α5-integrin subunit was shown to be positively regulated by the ECM component fibronectin in rabbit corneal epithelial cells. Transcription factor Sp1 that binds to the fibronectin responsive element was involved in this regulation [102].

Conversely, the ECM may have a repressive action on gene transcription. This effect was demonstrated for the TGF-β gene promoter in mammary epithelial cells

[103]. When grown on plastic, mammary epithelial cells displayed a high level of TGF-β1, while it was strongly downregulated in cells grown in the presence of reconstituted basement membrane. This observation was further confirmed using the chloramphenicol acetyl transferase (CAT) gene as reporter gene under the control of the TGF-β1 promoter. CAT transcription was inhibited by the presence of the basement membrane.

Integrins are among the main transducers of signals induced by the ECM. Integrin binding to laminin activates a cascade of biochemical reactions as well as the reorganisation of the cytoskeleton and nuclear structure. Biochemical pathways include principally the tyrosine kinase cascade Ras/MAPK [104]. Interestingly Ras/MAPK signalling has been directly connected to chromatin remodelling complexes. Following a cascade of sequential activations by phosphorylation/dephosphorylation of Ras/Raf/MAPKK/MAPK, Erk MAPK is translocated into the nucleus where it interacts with chromatin remodelling factors. For instance, histone acetylases CBP, SRC-1, and SRC-3 are activated upon phosphorylation by Erk1 and Erk2. In addition, Erk can also activate histone H3 kinases, Rsk2 and Msk1, and histone H1 kinase cyclin E-cdk2 [58]. Therefore, interactions between integrins and basement membrane components may be able to direct chromatin remodelling, thereby controlling gene expression and cell phenotype.

Other proteins that may be involved in ECM or, more specifically, basement membrane signalling to chromatin could be found among proteins, other than histones, that contain a histone-fold sequence [105, 106]. These proteins can interact with other histone-fold bearing proteins and thus may regulate chromatin structure. Our laboratory is currently investigating this possibility with the example of the nuclear mitotic apparatus protein, NuMA. The nuclear distribution of NuMA is regulated by basement membrane-induced differentiation in mammary epithelial cells and seems to play a role in the control of MMP activity as well as basement membrane-mediated survival in these cells; NuMA distribution and function are altered in cancer [98, and unpublished results].

2.6 Conclusion

In this chapter, we have presented and discussed aspects of tumour biology research that have led scientists and clinicians to envision the development of novel anti-cancer strategies. These strategies illustrate an emerging view of cancer therapy, which aims at monitoring the illness chronically by influencing, and even reprogramming, tumour cell behaviour rather than killing tumour cells. The goals are to prevent invasion and dissemination as well as restrain tumour cell proliferation. Unfortunately, the drugs that are currently being tested have a broad range of action and thus may also have effects on normal tissues. A better drug design will require at least,

- understanding the pathways that lead to the regulation of the expression of genes involved in the control of proliferation and differentiation from the cell membrane to the chromatin for each type of tissue, and
- undertaking pharmacological tests not only on tumours but also on nonmalignant and differentiated tissues.

The success of such difficult investigations will require thorough mathematical modelling of the different signalling networks and the dynamics of the multiprotein complexes involved.

Acknowledgments

We thank Patricia Abad for critical reading of the manuscript. This work was supported by grants from the Department of Defense/Breast Cancer Research Program (DAMD-17-00-1-0226) and the Walther Cancer Institute (WCI-110-114) to Sophie A. Lelièvre, and a postdoctoral fellowship from the Joyce Fox Jordan/Purdue Cancer Centre program to Cédric Plachot.

2.7 References

[1] Bissell, M.J., The differentiated state of normal and malignant cells or how to define a "normal" cell in culture, *Int. Rev. Cytol.* 70, 27, 1981.

[2] Barcellos-Hoff, M.H. et al., Functional differentiation and alveolar morphogenesis of primary mammary cultures on reconstituted basement membrane, *Development* 105, 223, 1989.

[3] Laoide, B.M. et al., Immortalised mouse submandibular epithelial cell lines retain polarised structural and functional properties, *J. Cell Sci.* 109, 2789, 1996.

[4] Bendayan, M., Duhr, M.A., and Gingras, D., Studies on pancreatic acinar cells in tissue culture: basal lamina (basement membrane matrix promotes three-dimensional reorganisation, *Eur. J. Cell Biol.* 42, 60, 1986.

[5] Marchisio, P.C., Trusolino, L., and De Luca, M., Topography and biological role of integrins in human skin, *Microsc. Res. Tech.* 38, 353, 1997.

[6] Erickson, A.C. and Couchman, J.R., Still more complexity in mammalian basement membranes, *J. Histochem. Cytochem.* 48, 1291, 2000.

[7] Miosge, N., The ultrastructural composition of basement membranes *in vivo*, *Histol. Histopathol.* 16, 1239, 2001.

[8] Gudjonsson, T. et al., Isolation, immortalization, and characterization of a human breast epithelial cell line with stem cell properties, *Genes Dev.* 16, 693, 2002.

[9] Marchisio, P.C. et al., The basement membrane protein BM-600/nicein codistributes with kalinin and the integrin $\alpha 6\beta 4$ in human cultured keratinocytes, *Exp. Cell Res.* 205, 205, 1993.

[10] Schuger, L. et al., Laminin fragment E4 inhibition studies: basement membrane assembly and embryonic lung epithelial cell polarisation requires laminin polymerization, *Int. J. Dev. Biol.* 42, 217, 1998.

[11] DeSimone, D.W. et al., The integrin family of cell surface receptors, *Biochem. Soc. Trans.* 15, 789, 1987.

[12] Belkin, A.M. and Stepp, M.A., Integrins as receptors for laminins, *Microsc. Res. Tech.* 51, 280, 2000.

[13] Ekblom, P., Vestweber, D., and Kemler, R., Cell-matrix interactions and cell adhesion during development, *Annu. Rev. Cell Biol.* 2, 27, 1986.

[14] Raghavan, S. et al., Conditional ablation of $\beta 1$ integrin in skin. Severe defects in epidermal proliferation, basement membrane formation, and hair follicle invagination, *J. Cell Biol.* 150, 1149, 2000.

[15] Sethi, T. et al., The small GTP-binding protein R-Ras can influence integrin activation by antagonizing a Ras/Raf-initiated integrin suppression pathway, *Mol. Biol. Cell.* 10, 1799, 1999.

[16] Shattil, S.J. and Ginsberg, M.H., Perspectives series: cell adhesion in vascular biology. Integrin signaling in vascular biology, *J. Clin. Invest.* 100, 1, 1997.

[17] Nievers, M.G. et al., Ligand-independent role of the $\beta 4$ integrin subunit in the formation of hemidesmosomes, *J. Cell Sci.* 111, 1659, 1998.

[18] Geerts, D. et al., Binding of integrin $\alpha 6\beta 4$ to plectin prevents plectin association with F-actin but does not interfere with intermediate filament binding, *J. Cell Biol.* 147, 417, 1999.

[19] Jones, J.C., Hopkinson, S.B., and Goldfinger, L.E., Structure and assembly of hemidesmosomes, *Bioessays* 20, 488, 1998.

[20] Blau, H. et al., Fetal type 2 pneumocytes form alveolar-like structures and maintain long-term differentiation on extracellular matrix, *J. Cell Physiol.* 136, 203, 1988.

[21] Petersen, O.W. et al., Interaction with basement membrane serves to rapidly distinguish growth and differentiation pattern of normal and malignant human breast epithelial cells, *Proc. Natl. Acad. Sci. USA* 89, 9064, 1992.

[22] Yamanari, H. et al., Extracellular matrix components regulating glandular differentiation and the formation of basal lamina of a human pancreatic cancer cell line *in vitro*, *Exp. Cell Res.* 211, 175, 1994.

[23] Webber, M.M. et al., Acinar differentiation by non-malignant immortalized human prostatic epithelial cells and its loss by malignant cells, *Carcinogenesis* 18, 1225, 1997.

[24] Weaver, V.M. et al., Reversion of the malignant phenotype of human breast cells in three-dimensional culture and *in vivo* by integrin blocking antibodies, *J. Cell Biol.* 137, 231, 1997.

[25] Faraldo, M.M. et al., Perturbation of β1-integrin function alters the development of murine mammary gland, *EMBO J.* 17, 2139, 1998.

[26] Boudreau, N. et al., Suppression of ICE and apoptosis in mammary epithelial cells by extracellular matrix, *Science* 267, 891, 1995.

[27] Tang, K. et al., The β4 integrin subunit rescues A431 cells from apoptosis through a PI3K/Akt kinase signaling pathway, *Biochem. Biophys. Res. Commun.* 264, 127, 1999.

[28] Ingber, D.E., Madri, J.A., and Jamieson, J.D., Neoplastic disorganization of pancreatic epithelial cell-cell relations. Role of basement membrane, *Am. J. Pathol.* 121, 248, 1985.

[29] Nakamura, K., Mori, M., and Enjoji, M., Distribution of basement membrane antigens in clinical gastric adenocarcinomas: an immunohistochemical study, *J. Clin. Pathol.* 40, 1418, 1987.

[30] Hornung, J. et al., Basement membrane formation by malignant mouse keratinocyte cell lines in organotypic culture and transplants: correlation with degree of morphologic differentiation, *J. Cancer Res. Clin. Oncol.* 113, 325, 1987.

[31] Weaver, V. et al., β4 integrin-dependent formation of polarised three-dimensional architecture confers resistance to apoptosis in normal and malignant mammary epithelium, *Cancer Cell* 2, 205, 2002.

[32] Slade, M.J. et al., The human mammary gland basement membrane is integral to the polarity of luminal epithelial cells, *Exp. Cell Res.* 247, 267, 1999.

[33] Curran, S. and Murray, G.I., Matrix metalloproteinases: molecular aspects of their roles in tumour invasion and metastasis, *Eur. J. Cancer* 36, 621, 2000.

[34] Giannelli, G. et al., Induction of cell migration by matrix metalloprotease-2 cleavage of laminin-5, *Science* 277, 225, 1997.

[35] Tomakidi, P. et al., Defects of basement membrane and hemidesmosome structure correlate with malignant phenotype and stromal interactions in HaCaT-Ras xenografts, *Differentiation* 64, 263, 1999.

[36] Rossen, K. et al., Expression of the $\alpha 6\beta 4$ integrin by squamous cell carcinomas and basal cell carcinomas: possible relation to invasive potential?, *Acta Derm. Venereol.* 74, 101, 1994.

[37] Rabinovitz, I., Toker, A., and Mercurio, A.M., Protein kinase C-dependent mobilization of the $\alpha 6\beta 4$ integrin from hemidesmosomes and its association with actin-rich cell protrusions drive the chemotactic migration of carcinoma cells, *J. Cell Biol.* 146, 1147, 1999.

[38] Shaw, L.M. et al., Activation of phosphoinositide 3-OH kinase by the $\alpha 6\beta 4$ integrin promotes carcinoma invasion, *Cell* 91, 949, 1997.

[39] O'Connor, K.L., Shaw, L.M., and Mercurio, A.M., Release of cAMP gating by the $\alpha 6\beta 4$ integrin stimulates lamellae formation and the chemotactic migration of invasive carcinoma cells, *J. Cell Biol.* 143, 1749, 1998.

[40] Shaw, L.M. et al., Function of the integrin α 6 β 1 in metastatic breast carcinoma cells assessed by expression of a dominant-negative receptor, *Cancer Res.* 56, 959, 1996.

[41] Nejjari, M. et al., $\alpha 6\beta 1$ integrin expression in hepatocarcinoma cells: regulation and role in cell adhesion and migration, *Int. J. Cancer* 83, 518, 1999.

[42] Tennenbaum, T. et al., A splice variant of α 6 integrin is associated with malignant conversion in mouse skin tumorigenesis, *Proc. Natl. Acad. Sci. USA* 92, 7041, 1995.

[43] Nakahara, H. et al., A mechanism for regulation of melanoma invasion. Ligation of $\alpha 6\beta 1$ integrin by laminin G peptides, *J. Biol. Chem.* 271, 27221, 1996.

[44] Nakahara, H. et al., Activation of $\beta 1$ integrin signaling stimulates tyrosine phosphorylation of p190RhoGAP and membrane-protrusive activities at invadopodia, *J. Biol. Chem.* 273, 9, 1998.

[45] Mueller, S.C. et al., A novel protease-docking function of integrin at invadopodia, *J. Biol. Chem.* 274, 24947, 1999.

[46] Muthuswamy, S.K. et al., ErbB2, but not ErbB1, reinitiates proliferation and induces luminal repopulation in epithelial acini, *Nat. Cell Biol.* 3, 785, 2001.

[47] Sheng, Z. et al., Restoration of positioning control following disabled-2 expression in ovarian and breast tumor cells, *Oncogene* 19, 4847, 2000.

[48] Steward, W.P. and Thomas, A.L., Marimastat: the clinical development of a matrix metalloproteinase inhibitor, *Expert Opin. Investig. Drugs* 9, 2913, 2000.

[49] Scatena, R., Prinomastat, a hydroxamate-based matrix metalloproteinase inhibitor. A novel pharmacological approach for tissue remodelling-related diseases, *Expert Opin. Investig. Drugs* 9, 2159, 2000.

[50] Oba, K. et al., Prevention of liver metastasis of human colon cancer by selective matrix metalloproteinase inhibitor MMI-166, *Cancer Lett.* 175, 45, 2002.

[51] Hua, J. and Muschel, R.J., Inhibition of matrix metalloproteinase 9 expression by a ribozyme blocks metastasis in a rat sarcoma model system, *Cancer Res.* 56, 5279, 1996.

[52] Azuma, H. et al., Marked prevention of tumor growth and metastasis by a novel immunosuppressive agent, FTY720, in mouse breast cancer models, *Cancer Res.* 62, 1410, 2002.

[53] Markland, F.S. et al., A novel snake venom disintegrin that inhibits human ovarian cancer dissemination and angiogenesis in an orthotopic nude mouse model, *Haemostasis.* 31, 183, 2001.

[54] Sanz, L. et al., Generation and characterization of recombinant human antibodies specific for native laminin epitopes: potential application in cancer therapy, *Cancer Immunol. Immunother.* 50, 557, 2001.

[55] Wu, J. and Grunstein, M., 25 years after the nucleosome model: chromatin modifications, *Trends Biochem. Sci.* 25, 619, 2000.

[56] Flaus, A. and Owen-Hughes, T., Mechanisms for ATP-dependent chromatin remodeling, *Curr. Opin. Genet. Dev.* 11, 148, 2001.

[57] Berger, S.L., Histone modifications in transcriptional regulation, *Curr. Opin. Genet. Dev.* 12, 142, 2002.

[58] Spencer, V.A. and Davie, J.R., Signal transduction pathways and chromatin structure in cancer cells, *J. Cell. Biochem. Suppl.* 35, 27, 2000.

[59] Cairns, B.R., Emerging roles for chromatin remodeling in cancer biology, *Trends Cell Biol.* 11, S15, 2001.

[60] Tong, J.K. et al., Chromatin deacetylation by an ATP-dependent nucleosome remodelling complex, *Nature* 395, 917, 1998.

[61] Rice, J.C. and Allis, C.D., Histone methylation versus histone acetylation: new insights into epigenetic regulation, *Curr. Opin. Cell Biol.* 13, 263, 2001.

[62] Cheung, P., Allis, C.D., and Sassone-Corsi, P., Signaling to chromatin through histone modifications, *Cell* 103, 263, 2000.

[63] Mahadevan, L.C., Willis, A.C., and Barratt, M.J., Rapid histone H3 phosphorylation in response to growth factors, phorbol esters, okadaic acid, and protein synthesis inhibitors, *Cell* 31, 775, 1991.

[64] Chadee, D.N. et al., Increased Ser-10 phosphorylation of histone H3 in mitogen-stimulated and oncogene- transformed mouse fibroblasts, *J. Biol. Chem.* 274, 24914, 1999.

[65] Rea, S. et al., Regulation of chromatin structure by site-specific histone H3 methyltransferases, *Nature* 406, 593, 2000.

[66] Versteege, I. et al., Truncating mutations of hSNF5/INI1 in aggressive paediatric cancer, *Nature* 394, 203, 1998.

[67] Grand, F. et al., Frequent deletion of hSNF5/INI1, a component of the SWI/SNF complex, in chronic myeloid leukemia, *Cancer Res.* 59, 3870, 1999.

[68] Wong, A.K. et al., BRG1, a component of the SWI-SNF complex, is mutated in multiple human tumor cell lines, *Cancer Res.* 60, 6171, 2000.

[69] Klochendler-Yeivin, A. et al., The murine SNF5/INI1 chromatin remodeling factor is essential for embryonic development and tumor suppression, *EMBO Rep.* 1, 500, 2000.

[70] Bultman, S. et al., A Brg1 null mutation in the mouse reveals functional differences among mammalian SWI/SNF complexes, *Mol. Cell.* 6, 1287, 2000.

[71] Dunaief, J.L. et al., The retinoblastoma protein and BRG1 form a complex and cooperate to induce cell cycle arrest, *Cell*, 79, 119, 1994.

[72] Cheng, S.W. et al., c-MYC interacts with INI1/hSNF5 and requires the SWI/SNF complex for transactivation function, *Nat. Genet.* 22, 102, 1999.

[73] Bochar, D.A. et al., BRCA1 is associated with a human SWI/SNF-related complex: linking chromatin remodeling to breast cancer, *Cell* 102, 257, 2000.

[74] Marks, P.A., Richon, V.M., and Rifkind, R.A., Histone deacetylase inhibitors: inducers of differentiation or apoptosis of transformed cells, *J. Natl. Cancer Inst.* 92, 1210, 2000.

[75] Richon, V.M. et al., Histone deacetylase inhibitor selectively induces p21WAF1 expression and gene-associated histone acetylation, *Proc. Natl. Acad. Sci. USA* 97, 10014, 2000.

[76] Cohen, L.A. et al., Chemoprevention of carcinogen-induced mammary tumorigenesis by the hybrid polar cytodifferentiation agent, suberanilohydroxamic acid (SAHA), *Anticancer Res.* 19, 4999, 1999.

[77] Qiu, L. et al., Anti-tumour activity *in vitro* and *in vivo* of selective differentiating agents containing hydroxamate, *Br. J. Cancer* 80, 1252, 1999.

[78] Butler, L.M. et al., Hybrid polar inhibitors of histone deacetylase suppress the growth of the CWR22 human prostate cancer xenograft, *Proc. Am. Assoc. Cancer Res.* 41, abstract 289, 2000.

[79] Leonhardt, H. and Cardoso, M.C., DNA methylation, nuclear structure, gene expression, and cancer, *J. Cell Biochem.* 35, 78, 2000.

[80] Ng, H.H. et al., MBD2 is a transcriptional repressor belonging to the MeCP1 histone deacetylase complex, *Nat. Genet.* 23, 58, 1999.

[81] Cross, S.H. et al., A component of the transcriptional repressor MeCP1 shares a motif with DNA methyltransferase and HRX proteins, *Nat. Genet.* 16, 256, 1997.

[82] Ng, H.H., Jeppesen, P., and Bird, A., Active repression of methylated genes by the chromosomal protein MBD1, *Mol. Cell Biol.* 20, 1394, 2000.

[83] Zhang, Y. et al., Analysis of the NuRD subunits reveals a histone deacetylase core complex and a connection with DNA methylation, *Genes Dev.* 13, 1924, 1999.

[84] Nan, X. et al., Transcriptional repression by the methyl-CpG-binding protein MeCP2 involves a histone deacetylase complex, *Nature* 393, 386, 1998.

[85] Rountree, M.R., Bachman, K.E., and Baylin, S.B., DNMT1 binds HDAC2 and a new co-repressor, DMAP1, to form a complex at replication foci, *Nat. Genet.* 25, 269, 2000.

[86] Fuks, F. et al., Dnmt3a binds deacetylases and is recruited by a sequence-specific repressor to silence transcription, *EMBO J.* 20, 2536, 2001.

[87] Cameron, E.E. et al., Synergy of demethylation and histone deacetylase inhibition in the re-expression of genes silenced in cancer, *Nat. Genet.* 21, 103, 1999.

[88] Magdinier, F. et al., Regional methylation of the 5' end CpG island of BRCA1 is associated with reduced gene expression in human somatic cells, *FASEB J.* 14, 1585, 2000.

[89] Devereux, T.R. et al., DNA methylation analysis of the promoter region of the human telomerase reverse transcriptase (hTERT) gene, *Cancer Res.* 59, 6087, 1999.

[90] Bovenzi, V. and Momparler, R.L., Antineoplastic action of 5-aza-2'-deoxycytidine and histone deacetylase inhibitor and their effect on the expression of retinoic acid receptor β and estrogen receptor α genes in breast carcinoma cells, *Cancer Chemother. Pharmacol.* 48, 71, 2001.

[91] Marks, P.A. et al., Histone deacetylase inhibitors as new cancer drugs, *Curr. Opin. Oncol.* 13, 477, 2001.

[92] Marks, P. et al., Histone deacetylases and cancer: causes and therapies, *Nat. Rev. Cancer* 1, 194, 2001.

[93] Marks, P.A. et al., Inhibitors of histone deacetylase are potentially effective anticancer agents, *Clin. Cancer Res.* 7, 759, 2001.

[94] Van Lint, C., Emiliani, S., and Verdin, E., The expression of a small fraction of cellular genes is changed in response to histone hyperacetylation, *Gene Expr.* 5, 245, 1996.

[95] Weiss, A.J. et al., Phase II study of 5-azacytidine in solid tumors, *Cancer Treat. Rep.* 61, 55, 1977.

[96] Abele, R. et al., The EORTC Early Clinical Trials Cooperative Group experience with 5-aza-2'-deoxycytidine (NSC 127716) in patients with colo-rectal, head and neck, renal carcinomas, and malignant melanomas, *Eur. J. Cancer Clin. Oncol.* 23, 1921, 1987.

[97] Niki, T. et al., A histone deacetylase inhibitor, trichostatin A, suppresses myofibroblastic differentiation of rat hepatic stellate cells in primary culture, *Hepatology* 29, 858, 1999.

[98] Lelievre, S.A. et al., Tissue phenotype depends on reciprocal interactions between the extracellular matrix and the structural organisation of the nucleus, *Proc. Natl. Acad. Sci. USA* 95, 14711, 1998.

[99] Pujuguet, P. et al., Trichostatin A inhibits β-casein expression in mammary epithelial cells, *J. Cell Biochem.* 83, 660, 2001.

[100] Schmidhauser, C. et al., A novel transcriptional enhancer is involved in the prolactin- and extracellular matrix- dependent regulation of β-casein gene expression, *Mol. Biol. Cell* 3, 699, 1992.

[101] Myers, C.A. et al., Characterization of BCE-1, a transcriptional enhancer regulated by prolactin and extracellular matrix and modulated by the state of histone acetylation, *Mol. Cell Biol.* 18, 2184, 1998.

[102] Larouche, K. et al., Expression of the α 5 integrin subunit gene promoter is positively regulated by the extracellular matrix component fibronectin through the transcription factor Sp1 in corneal epithelial cells *in vitro*, *J. Biol. Chem.* 275, 39182, 2000.

[103] Streuli, C.H. et al., Extracellular matrix regulates expression of the TGF-β1 gene, *J. Cell Biol.* 120, 253, 1993.

[104] Schwartz, M.A., Integrin signaling revisited, *Trends Cell Biol.* 11, 466, 2001.

[105] Ramakrishnan, V., The histone fold: evolutionary questions, *Proc. Natl. Acad. Sci. USA* 92, 11328, 1995.

[106] Wolffe, A.P., Transcriptional regulation in the context of chromatin structure, *Essays Biochem.* 37, 45, 2001.

Chapter 3

Interstitial Transport in Solid Tumours

Paolo A. Netti[1] **and Rakesh K. Jain**[2]

[1] *Department of Materials and Production Engineering, University of Naples 'Federico II', Naples (Italy),*

[2] *Edwin Steele Laboratory, Department of Radiation Oncology, Massachusetts General Hospital and Harvar d Medical School, Boston (U.S.A.)*

3.1 Introduction

The movement of fluids, molecules, and particles within tumour interstitium has countless biophysical and clinical implications. Since the proliferation of cancer cells and their response to treatment are determined by the distribution and clearance of nutrients, metabolites, and bioactive agents, transport of these molecules plays a crucial role in tumour growth, angiogenesis, metastasis, and therapy. Trafficking of small and large molecular weight agents in solid tumours may occur both by diffusion and convection and depends on the physiochemical properties of both the diffusing molecule and the medium [34], [54], [67], [75], [89]. Diffusion is the dominant mode of interstitial transport for small molecular weight agents, and when the driving force for convection is reduced, it may be the dominant or at least a significant mechanism of transport of large molecules as well [42]. Therefore the understanding of the biological and physical factors that regulate interstitial transport in tumour interstitium has important implication in the control of tumour development and in the developing strategies to improve drug penetration in tumour masses.

Tumour interstitium is a complex network structure composed of elastic fibres and collagen interdispersed with hydrophilic macromolecular constituents to form a fluid saturated gel-like medium. Similar to polymer gels, interstitial movement of molecules occurs mainly within the accessible fluid phase of the network driven by concentration gradient (diffusion) or by interstitial fluid movement (convection) [35]. Interstitial diffusion rate depends upon size, charge, and shape of the diffusion molecule as well as on specific or nonspecific binding between the molecule and tissue component [36]. For a given molecule, diffusion rate is strictly controlled by the amount and type of constituents forming the extracellular matrix (ECM), such as collagens, proteoglycans, hyaluronic acid, and elastin as well as on their microstructural assembly. The extracellular matrix acts as a dispersive filter, controlling fluid composition and the rate of molecular trafficking. This control is mediated by a synergistic interaction among ECM constituents. In mature tissues, resistance to diffusion is generally attributed to the amount of hydrophilic ground substance, predominately glycosaminoglycans [1], [19], [55], [63], [71], [89]. The highly hydrophilic proteoglycan chains are noncovalently bound to the more rigid structural fibres to form a hydrated gel [51], [61]. However, it is now appreciated that GAG content alone does not fully account for the high transport resistance presented by many soft tissues [32], [55], [89]. Tumour tissue may possess unique characteristics due in part to an embryonic-like stage of development with extensive remodelling of the extracellular matrix [29], [30], [31], which leads to substantial differences in the composition and assembly [22], [29], [80], [82] and therefore in the transport properties [67]. Interstitial rate of diffusion varies with tumour type [67] and within the same tumour it may change both in time and space [36], [37].

Molecules may also move through the interstitial space dragged by fluid flow. Interstitial fluid flow involves a complex equilibrium between the fluid pressure and tissue stresses, which are influenced by tissue properties such as hydraulic con-

ductivity and tissue elasticity [65], [66], [86]. Besides the capillary-lymphatic exchange [33], interstitial fluid movement may also occur as consequence of tissue deformation. Indeed, tumour interstium can be envisaged as a poroelastic material in which fluid transport may take place as a result of tissue deformation [65], [66]. Fluid percolation, on the other hand, induces deformation of the solid matrix [12], [60], [68]. Although the coupling between tissue mechanics and fluid flow is well established in the field of biomechanics [63], only recently these concepts have been used to describe fluid flow in solid tumours (see chapter 4 of this volume and [65], [66], [67], [69]). The tissue parameters that control fluid transport also depend on the composition and assembly of the extracellular matrix and vary significantly between tumour type and for a given tumour may change both in space and in time.

Since many new and promising therapeutic strategies rely on delivery of large agents such as genes, viruses, immunomodulators, and monoclonal antibodies, hindered interstitial transport may pose a strong limitation to their effectiveness [35], [39], [43]. In this chapter we will discuss the experimental techniques used to quantify the interstitial transport in solid tumours along with the most recent experimental data and their implication for cancer therapy.

3.2 Interstitial Transport Parameters

Transport of macromolecules in tumour interstitum may occur both by convection and diffusion and can be described by the following constitutive equation [36]

$$\mathbf{J} = -D\nabla c + cR_F\mathbf{u} = -D\nabla c + cR_F K\nabla p\,, \tag{3.1}$$

where $\mathbf{J}$ is the mass flux, D is the diffusion coefficient of the molecule in the interstitium, c is the interstitial concentration, R_F is the drag coefficient (= solute velocity/fluid velocity), $\mathbf{u}$ is the interstitial fluid velocity, K is the interstitial hydraulic conductivity, and p is the interstitial fluid pressure. The drag coefficient measures the ratio between the solute and the fluid and may vary from 0 to values higher than unity [25], [56].

In normal tissues, it is assumed that convection is the dominant mechanism of transport for large molecules [34], [79]. Interstitial fluid movement occurs from the capillary to lymphatics driven by interstitial fluid pressure gradients. However, most tumours do not have anatomically well-defined lymphatic vessels and this leads to an increase in interstitial fluid pressure and a consequent reduction of the driving force for fluid flow [11], [13], [72]. Therefore convective transport is strongly hindered in tumour interstitium ([2], [3], [4], [5], [42]) and diffusion, although highly inefficient, becomes the relevant mechanism of transport for macromolecules. The combination of reduced interstitial fluid flow and the slow diffusion rate of macromolecules in the tumour interstitium are possible causes of the therapeutic inefficiency of large

molecular drugs [38]. Strategies to overcome these transport limitations are aimed at the enhancement of the interstitial convective transport [10], [68].

Experimental evaluation of transport parameters of molecules within tumour interstitium is useful to assess the accessibility of a given drug to tumour tissue. Ideally, knowing the transport parameters of the tissue as function of both time and space, one could develop precise mathematical models which would be able to accurately describe the evolution of concentration of a variety of drugs in the interstitial space of a tumour. Since the selective tumour cell kill depends on the concentration-time history of a drug, such models would be extremely useful in developing optimal dose schedules of anticancer agents. Furthermore, since diffusion rate depends upon the structural assembly of the medium, an experimentally evaluated diffusion coefficient serves as probe of tissue structure. Measurements of diffusion coefficient *in vivo* require specific techniques and animal models since it should be carried in a non-invasive manner over distances of less than 1 mm with a high spatial resolution. In the following sections the most relevant experimental techniques to measure interstitial transport parameters along with the relevant animal models will be described.

3.3 Experimental Models

3.3.1 Multicellular Spheroids

Multicellular spheroids have been often used as *in vitro* model to evaluate the interstitial transport resistance [84]. In these studies spheroids are exposed to the culture medium at a known drug concentration. The diffusion coefficient is evaluated by measuring the drug concentration profile within the spheroids at several times. The methods used to measure the concentration profile include microelectrode, autoradiography, quantitative fluorescence microscopy, and fractional disaggregation of various spheroids layer to measure cellular concentration in each layer. Although this model has been widely used in the past it is now appreciated that it has severe limitation in reproducing data relevant for an *in vivo* comparison [20]. The extracellular matrix composition and assembly produced by tumour spheroids is significantly different from when the same cells are grown *in vivo*. Therefore the interstitial transport parameters in spheroids are significantly different from those measured in the tumour tissue when the same cells are grown in an animal model [20].

3.3.2 Animal Models

The most relevant experimental models to measure diffusion coefficient within tumour interstitium are those involving a direct measurement in a tumour implanted *in vivo*. Several models can be used to measure interstitial transport parameters and

these can be divided in two classes: macroscopic and microscopic models. The first are used for an overall evaluation of the transport properties of the tumour interstitium (i.e., tissue-level) while the latter provides information about transport on a local microscopic scale.

3.3.2.1 Macroscopic Model

These studies involve an intravenous injection of the drug into an animal-bearing tumour, measurement of drug concentration within the tumour as function of time by sequential sacrifice of animals, and estimation of the interstitial transport parameter by using specific mathematical models [6], [7]. Depending on the type of drug, interstitial concentration can be measured by radioassay, chemical assay, bioassay, or immunoassay. A very useful experimental model for interstitial transport studies, known as isolated tumour, was introduced by Gullino [28]. In this model the tumour is fed by a single artery and the blood flow leaves from a single vein and is isolated by surrounding host. This model allows one to cannulate the tumour artery and vein and, thus, study directly the blood flow rate and transport in tumours [50].

3.3.2.2 Microscopic Model

Over the past years several techniques have been developed to visualise the microvasculature and the microcirculation *in vivo*. Among those the transparent chamber techniques have proved to be a very useful tool to study tumour interstitial transport [41], [43]. Originally developed by Sandison in 1924 for rabbit ear [83], the transparent chamber has been continuously developed and adapted to cranium, skin, and even to the upper-arm skin fold in man [14], [15], [43]. With the use of various optical and electronic devices and quantitative fluorescence techniques, these chambers permit noninvasive, continuous, and quantitative measurements of interstitial transport [8], [9], [15], [16], [17], [18], [67], [70], [75].

3.4 Experimental Techniques to Quantify Interstitial Transport

3.4.1 Diffusion Coefficient

Most of the experimental techniques used to quantify interstitial transport parameters have limited capability for noninvasive measurements of diffusion in a small sample. Results obtained with invasive methods [59] must be interpreted with caution since these techniques may alter the fluid balance and damage the structure of the tissue by causing oedema that may strongly affect the diffusion characteristics of the tissue. Intravital microscopy coupled with quantitative fluorescence has

been shown to be a more appropriate technique to measure the diffusion coefficient of fluorescently labelled molecules since it strongly reduces the perturbation of the tissue [8], [9], [15], [17], [18], [24], [64], [67], [70], [75], [76]. The diffusion coefficient can be calculated based on the spatial distribution of fluorescence as the labelled material spreads through the tissue (relaxation of fluorescence gradient) [18], [24], [70], [64], or by adapting the method of fluorescence recovery after photobleaching (FRAP) based on the recovery of fluorescence pattern in a small region of the tissue ($< 40\,\mu m$) [8], [9], [67], [76], [75]. The latter method has a high spatial resolution allowing multiple diffusion measurements within the same tissue and also allows discrimination between diffusive and convective transport [17].

3.4.2 Hydraulic Conductivity

The experimental measurements of tissue hydraulic conductivity (K) have been made mostly under *in vitro* conditions ([52], [55], [85]) and in a few studies *in vivo* ([12], [21], [85]). *In vitro*, K is generally estimated by measuring the flow after applying pressure across a tissue slice of known area and thickness. Recently K has been measured *ex-vivo* by the confined compression test, which couples measurement of fluid transport, tissue mechanics, and hydration [67]. The advantage of these preparations is the well defined geometry of the sample such as cross-sectional area and thickness of the specimen. The major drawback of these techniques is the poor control and maintenance of *in vivo* tissue characteristics such as tissue integrity, pressure, hydration, and strain. *In vivo* estimations of K are also not straightforward, since the characterisation of tissue dimensions can be difficult. Several approaches have been used to perform these measurements. Swabb et al. [85] evaluated K by measuring the unsteady fluid flow oozing out from a tumour grown around a porous capsule. DiResta et al. [21] evaluated K by direct measurements of pressure and velocity profiles within a solid tumour xenograft. Boucher et al. [12] evaluated K by measuring the pressure profile generated in a solid tumour during intratumoural fluid infusion. However, there is a significant discrepancy among the *in vivo* K values reported using different techniques that may be ascribed to the experimental uncertainty associated with these procedures and to capillary fluid filtration that may influence the estimation of this transport parameter. The *in vivo* K values reported by Boucher et al. [12] are in good agreement with the *ex-vivo* data obtained on the same tumour type suggesting that the procedure used by these authors may be seen as the most reliable.

3.5 Role of Solute Dimension and Charge

Diffusion of small molecular weight molecules, such as oxygen and small molecular weight drugs, within interstitial space is scarcely hindered since the molecular

size is very small compared to the matrix pore size [87]. Transport of small molecular weight molecules may therefore be envisaged as occurring in the free fluid phase within the extracellular matrix with a negligible steric obstruction resulting from the solid matrix network. A wide range of novel cancer therapies seek to utilise macromolecular agents such as proteins, gene vectors, liposomes, or polymers that are intended to recognise cancer cells and exert a selectively toxic effect. However, due to their large size the transport of these agents within the interstitial space may be significantly hindered [39]. Compared to conventional chemotherapeutic agents, which are small molecules less than 1 nm in diameter, these novel agents have dimensions that span between 10 to 1000 nm in diameter and therefore their interstitial movement is strongly reduced by steric obstruction. Diffusion of probe macromolecules within tumour and normal tissues have been measured by several investigators (for a review see [36]). The diffusion coefficient data for different molecular weight molecules diffusing in water solution, normal and tumour tissues are shown in Figure 3.1.

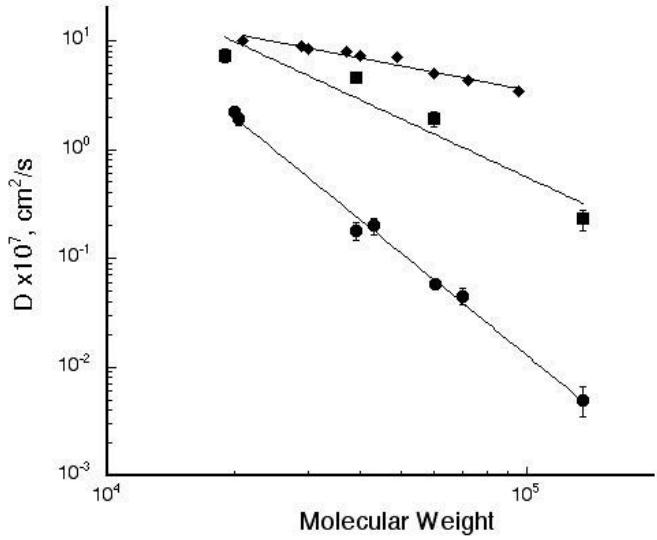

Figure 3.1

Dependence of diffusion coefficient on molecular weight in normal and tumour tissues. Data are obtained at room temperature and corrected to 37^{o}C. Symbols are:
(diamond) diffusion of dextran in aqueous solution, data from [27],
(square) diffusion of dextran in mature granulation tissue, and
(circle) in VX2 carcinoma implanted in rabbit, data from [26] and [70].
Lines are fit of the data with the relationship $D = a(MW)^{-b}$.

The dependence of diffusion coefficient upon the molecular weight of the diffusing molecule can be described by a power law

$$D = a(MW)^{-b}, \tag{3.2}$$

where MW is the molecular weight of the diffusing molecule, and a and b are two experimental constants. In Table 3.1, the coefficients a and b are reported for various molecular weight dextrans in water solutions, normal and tumour tissues. The coefficient b is 0.5 for water solution, according to the Stokes-Einstein relationship, and ranges from 0.75 to 3 for tissues. The increase of the coefficient b indicates that there is an additive hindrance to the movement of macromolecules within the interstitium that may depend on several factors such as steric obstruction, nonspecific interaction, and configurational dynamics of the molecule [76].

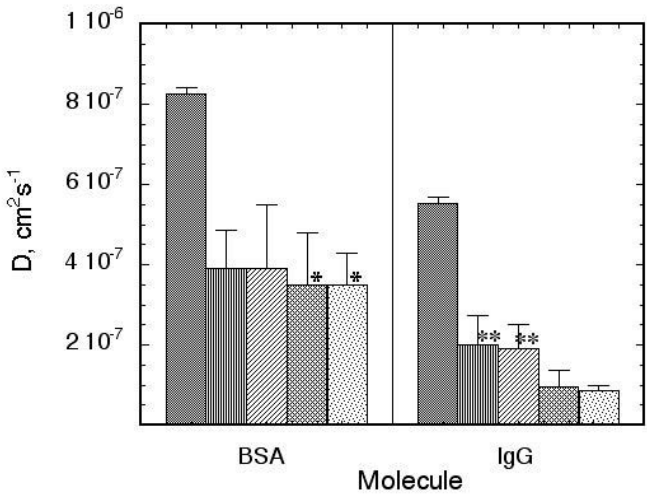

Figure 3.2

Interstitial mobility of BSA (68 kDa) and IgG (150 kDa) in four tumour types and in solution. Diffusion coefficient measured *in vivo* in dorsal skin-fold chamber on mice-bearing tumour xenograft by FRAP. From left to right the columns refer to aqueous solutions, colon carcinoma LS174T, mammary carcinoma MCaIV, osteblastoma HSTS26, and gliobastoma U87. Data from Netti et al. [67].

It has been often reported in the past that diffusion coefficient of a given macromolecule in a tumour is higher than the diffusion coefficient of the same molecule

Table 3.1 Dependence on the molecular weight of the diffusion coefficient of several macromolecules in solution and tissues ($D = a(MW)^{-b}\, cm^2/s$).

Tissue	Diffusant (MW range)	a	b	Ref.
Human articular cartilage (*in vitro*)	Dextran (5–40 kDa)	6×10^{-2}	1.34	[59]
Mesentery cat	Dextran (3.4–393 kDa)	2.75×10^{-3}	0.758	[64]
Mesentery rat	Dextran (3.45–41.2 kDa)	5.5×10^{-3}	1.09	[24]
Rabbit ear granulation tissue	Dextran (19.4–150 kDa)	1×10^{-6}	2.96	[70]
VX2 carcinoma	Dextran (19.4–150 kDa)	2.51×10^{-2}	1.14	[26]
Colon carcinoma LS174T Dorsal chamber	Proteins (68–155 kDa)	3.2×10^{-2}	0.81	[67]
Mammary carcinoma McaIV Dorsal chamber	Proteins (68–155 kDa)	6.4×10^{-2}	0.87	[67]
Osteosarcoma HST26T Dorsal chamber	Proteins (68–155 kDa)	13.5	1.57	[67]
Glioblastoma U87 Dorsal chamber	Proteins (68–155 kDa)	51.1	1.69	[67]
Glioblastoma U87 Dorsal chamber	Various solutes (68–2000 kDa)	0.76	1.4	[75]
Glioblastoma U87 Cranial window	Various solutes (68–2000 kDa)	3.9×10^{-4}	0.68	[75]
Melanoma Mu89 Dorsal chamber	Various solutes (68–2000 kDa)	8×10^{-3}	0.95	[75]
Melanoma Mu89 Cranial window	Various solutes (68–2000 kDa)	3.9×10^{-4}	0.68	[75]

in normal host tissue [34], [85]. However, it has been recently shown that the difference between the diffusion coefficient in tumour and in host normal tissue depend upon the tumour and the host tissue type [67], [75]. Figure 3.2 shows the diffusion coefficient of BSA (68 kDa) and IgG (150 kDa) in four different tumour types and in buffered saline solution alone. The coefficient b for glioblastoma and sarcoma ($b \approx 1.6$) is much higher than the two carcinomas group ($b \approx 0.8$) indicating a much stronger dependence of diffusion coefficient upon the molecular weight for the glioblastoma and sarcoma tissues compared to the carcinoma. As a consequence, the difference in diffusion coefficient among tumour types becomes more evident at high molecular weight. Indeed, BSA diffuses at a modestly hindered rate that does not differ significantly among tumour types. Although the mean BSA mobility in the mammary carcinoma (MCaIV) and colon carcinoma (LS174T) are approximately 10% greater than in the glioblastoma (U87) and sarcoma (HSTS 26T), the difference is not significant. However, the diffusion coefficient of the larger IgG molecule is significantly greater in the two carcinomas (MCaIV and LS174T) compared to the glioblastoma (U87) and sarcoma (HSTS 26T).

The molecular weight is not the only factor influencing the interstitial mobility of a macromolecule. Parameters such as charge and configuration may also affect the rate of diffusion of a macromolecule in the tumour interstitium [44], [46]. Charge may influence both steric partition and diffusion coefficient. Comparing the diffusion coefficient of a globular protein (BSA) and a linear macromolecule (Dextran) within the same tissue it has been reported that BSA diffuses at a slower rate compared to Dextran of equivalent size [24], [70]. Molecular charge regulates the nonspecific binding (stickiness) between the diffusing molecule and the interstitial space. Binding is a very important parameter in the interstitial transport since it may affect the effective diffusion rate by lowering the molecular mobility [47]. This parameter has been experimentally evaluated *in vivo* by using FRAP (see Figure 3.3, [9]).

3.6 Hydraulic Conductivity

There is a paucity of data in the literature regarding the hydraulic conductivity (K) of tissue, in particular tumour, due to the experimental difficulties to evaluate this parameter. In Table 3.2, a summary of the experimental evaluation of K *in vitro* and *in vivo* is reported. The data reported depend on the technique used to evaluate the parameter since the different experimental techniques may modify tissue condition and hydration. The value of K depends upon the tumour type and within the same tissue depends on tissue hydration or deformation. Figure 3.4 shows the tissue hydraulic conductivity for the four tumours as a function of tissue deformation (i.e., hydration).

Tumour hydraulic conductivity is a strong function of tissue hydration according to data reported for other soft tissues [55]. The dependence of K on tissue

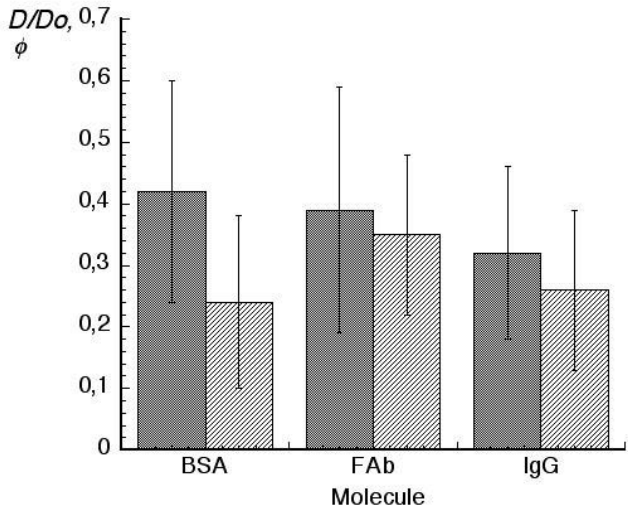

Figure 3.3

Dependence of interstitial diffusion coefficient and nonspecific binding on molecule size and charge. Diffusion coefficient (left column) and immobile fraction (right column) of BSA (68 kDa), antibody fragment (Fab'), and nonspecific antibody IgG (150 kDa). Data from Berk et al. [9].

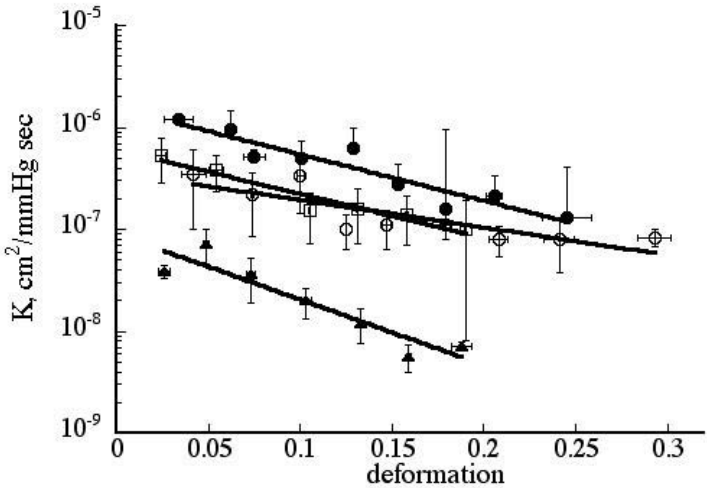

Figure 3.4

Dependence of hydraulic conductivity on tissue deformation. Tissue hydraulic conductivity as a function of tissue deformation evaluated by confined compression experiments on freshly sliced tumour tissue [67]. Solid lines are the fit of the experimental data with the equation $K = K_0 \exp(-bE)$ where K_0 and β are empirical parameters, and E is the tissue deformation.

hydration is well described by an exponential law, in agreement with that suggested in the literature for other soft tissues [63] and hydrogels [45]

$$K = K_0 e^{\beta E},$$

where β is an experimental parameter, E is the tissue deformation (i.e., the trace of the matrix deformation tensor), and K_0 is the hydraulic conductivity at zero tissue deformation. The hydraulic conductivity of the unstrained tissue (K_0) can be estimated by extrapolating to zero the data reported in Figure 3.3 (see Table 3.1). By comparing the hydraulic conductivity values for tumour and normal tissues, it can be concluded that in general the resistance to water flow is lower in tumour than in normal tissues.

Hydraulic conductivity regulates the interstitial fluid velocity that along with the retardation factor R_F determine the interstitial convective rate of a solute. The retardation coefficient is a phenomenological parameter and depends on tissue hydration and structure, and molecular properties of solutes. It has been poorly quantified in the literature [56] and there are no direct evaluations of this parameter for tumour tissue. Parameswaran and co-workers have examined R_F of albumin in membrane-like structures, such as pig mediastinal pleura [73] and rabbit mesentery [74] during tissue perfusion and found that RF depends on the perfusion rate. This finding is consistent with another report in the literature that indicates an inverse relationship between RF and infusion rate in tumour tissue [60]. The retardation of convective transport is likely due to deformation of the tissue due to solid stress generated by the fluid flow. A more systematic experimental approach is necessary to gather more information about the retardation factor in tumour tissues and its dependence on the physiochemical and structural properties of the tissue and the solutes.

3.7 Role of Extracellular Matrix Composition and Assembly

In mature normal tissues, interstitial resistance to water and solute transport is generally attributed to the amount of proteoglycans [1], [19], [63], [71]. Indeed, there is a general correlation between fluid and solute transport resistance with the amount of glycosaminoglycans (GAG) in the tissue (Figure 3.5). However, the same conclusion cannot be drawn for tumour tissues [67].

Tumour tissue may possess unique characteristics due in part to an embryonic-like stage of development with extensive synthesis of extracellular matrix ([29], [80], [82]), which leads to substantial differences in composition and assembly compared to the host tissue ([22], [51], [57], [58]). These differences have important consequences in regulating the transport parameters of tumour tissues. Anomalous assembly of the fibrillar component and its interaction with the proteoglycan component of the tumour ECM greatly influence the physiological barrier to macromolecule

Table 3.2 Interstitial hydraulic conductivity of tumor and normal tissues. Hydraulic conductivity was determined by different methods: in confined compression ($^+$), K is evaluated from the time constant for stress relaxation by fitting the data with a poroviscoleastic model [67]; *in vivo* ($^-$), K is calculated based on pressure gradients measured by micropipet pressure probes during infusion of saline [12]; in *ex-vivo* or *in vitro* (^{o*}) excised tissue is placed in a flow cell in which a pressure gradient is imposed on the tissue and water flow through the sample measured [55], [89].

Hydraulic conductivity ($10^{-8}\, cm^2/mmHg - s$)

Tissue type	K *in vitro* (confined compression)	K *in vitro* (flow chamber)	K *in vivo* (intratumoral infusion)
Colon carcinoma LS174T	$45 \pm 27^+$	24 ± 11^o	$17 \pm 10^-$
Mammary carcinoma Mca IV	$250 \pm 100^+$	–	–
Glioma U87	$65 \pm 30^+$	–	–
Osteosarcoma HSTS-26T	$9.2 \pm 7.1^+$	0.73 ± 0.17^o	–
vitrous body	–	$420 \pm 140^*$	–
Hepatoma	–	2.80^*	–
Subcutaneous tissue	–	0.65^*	–
Sclera	–	0.19^*	–
Aorta	–	$0.12 \pm 0.08^*$	–
corneal stroma	–	$0.11 \pm 0.04^*$	–
cartilage surface layer	–	0.07^*	–
cartilage deep layer	–	0.026^*	–
femoral head cartilage	–	$0.02 \pm 0.006^*$	–

motion posed by healthy tissue ECM. In a series of recent studies ([20], [67], [75]) it has been shown that contrary to what occurs in normal tissues, transport resistance to fluid and macromolecules in tumour tissues does not correlate with the amount of GAG but rather to the amount of fibrillar collagen. Figure 3.5 shows that the hydraulic conductivity of four different type of tumour tissues changes by almost two orders of magnitude with virtually no change in GAG content. Analogously, Figure 3.6a shows that the diffusion coefficient of a 155 kDa molecule (IgG) does not correlate with the GAG content. On the other hand, Figure 3.6b shows that diffusion coefficient of macromolecules within tumour interstitium correlates well with the amount of collagen in the tissue. The influence of fibrillar collagen has been definitely proven by showing that enzymatic digestion of collagen network leads to a substantial increase of diffusion coefficient [67]. The dependence of transport resistance of tumour interstitium on the fibrillar collagen content of the tissues, is corroborated by recent data by Pluen et al. [75] and by Ramanujan et al. [78], and

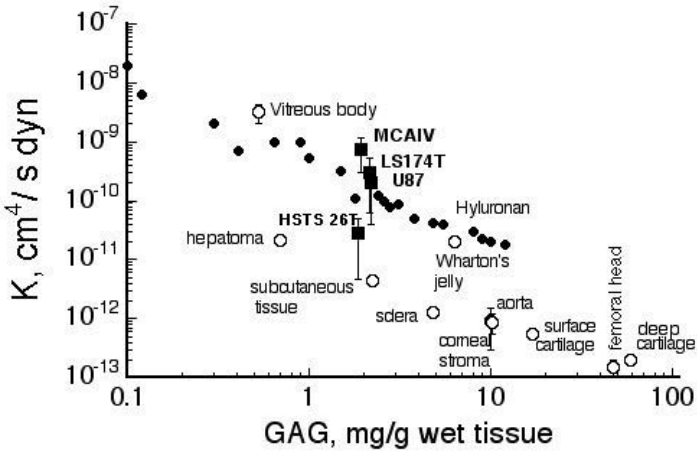

Figure 3.5

Hydraulic conductivity of various tissue and hyaluronic acid aqueous solutions as a function of glycosaminoglycan (GAG) composition. The symbols are: (full circle) hyluronan solutions [89]; (circle) various tumour and normal tissues [55]; (square) carcinomas, sarcoma, and glioblastoma tissues [67].

also by the data obtained by direct intratumoural infusion of macromolecular solutions by Boucher et al. [12]. Furthermore, recently Brown et al. [15] have loosened tumour collagen by chronic treatment with the hormone relaxin and demonstrated an increase in diffusive transport. Taken together these findings can be generalised by concluding that tumours with a well defined collagen network are more resistant to macromolecular drugs compared to tumours that exhibit a loose collagen network. Degeneration of the fibrillar network and a resulting compromised physiological function may be a general feature of tumours. Indeed, ECM organisation is often abnormal in tumours ([22], [57], [58]) and this may explain the discrepancy reported in the fluid and macromolecular transport resistance in tumours compared to normal tissues.

Since the extracellular matrix assembly and composition of a given tumour is determined by tumour-host tissues interaction, it suggests that also the transport properties of a tumour are controlled by the host. Therefore, in determining the transport resistance of a solid tumour particular attention should be paid to the choice of the relevant experimental model. It has been recently shown that interstitial transport properties of a given tumour depend upon the anatomical location of the implants [75]. Along the same line, it has also been shown that tumour spheroids, as *in vitro* models for interstitial transport, fail to reproduce the *in vivo* tissue characteristics and therefore interstitial transport data obtained with *in vitro* models should be interpreted with caution [20].

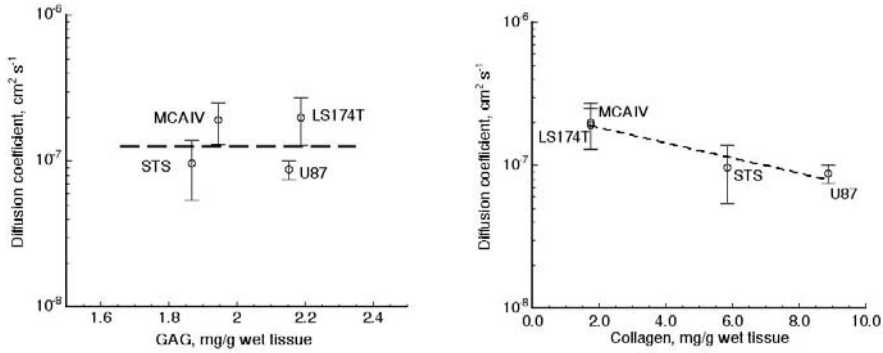

(a) (b)

Figure 3.6

Dependence of interstitial diffusion coefficient of a 155 kDa molecule (IgG) on tissue GAG (a) and collagen (b) content. Data are adapted from Netti et al. [67]. Dashed lines are the best fit of the data with the exponential equation $D = D_1 \exp(-\alpha[M1])$, where α and D_1 are empirical parameters and [M1] is the composition of the ECM component (i.e., GAG or collagen).

The micro-structural assembly of the ECM may lead to microporous structure with complex interconnectivity. The interconnection of micropores, or effective available volume, within the tissue controls both the partition coefficient and apparent diffusion rate of macromolecular drugs. It has been recently shown that pore-matrix connectedness and shape strongly regulates the dependence of diffusion coefficient upon molecular weight [90].

3.8 Relevance for Delivery of Molecular Medicine

A wide range of novel cancer therapies seek to utilise macromolecular agents such as proteins, monoclonal antibodies, gene vectors, viruses, liposomes, or polymers. Since the size of these agents are significantly larger compared to that of conventional therapies, the success of "molecular medicine" may ultimately depend on how well the agent can penetrate the tumour interstitial matrix. Therefore, a better understanding of the physiochemical parameters that control tumour interstitial transport, along with appropriate mathematical modelling of the processes involved, may be helpful in proposing and designing novel strategies to improve the delivery of macromolecular agents to solid tumours.

Studies on the role of the extracellular matrix assembly and composition on interstitial transport have lead to the identification of measurable tumour characteristics

that could be useful in predicting penetration by therapeutic macromolecules. For instance, the results obtained suggest that the feasibility of therapeutic approaches requiring macromolecule penetration could be assessed by histological staining of tumour tissue biopsies or by optical imaging [14], [15], [67], [75]. Delivery of high-molecular-weight agents should be facilitated in tumours with poorly organised and loosely interconnected collagen networks. However, further studies are needed along these lines since the assembly of the interstitial network is probably determined by the interaction of both neoplastic and host cells. Particularly in tumours of epithelial origin, host stromal cells are involved in the production and organisation of matrix molecules [48]. Hence, the transport properties of the tumour interstitial matrix likely depends on the site of tumour growth as well as on the tumour type [75].

Besides the size and charge, the transport of a molecule depends on the flexibility of the diffusing molecule. Comparing the diffusive regimes in polymer gels of several molecules with different molecular rigidity it has been shown that configurational change of diffusing macromolecule may control the transport regime [76]. Not only flexible macromolecules exhibit greater mobility in the gel than comparable-size rigid spherical particles, but also flexible macromolecules can undergo to mechanisms of transport not possible for rigid ones. In particular, flexible macromolecules move via reptation through the polymer network even when their radius of gyration exceed the gel mesh size.

Mathematical modelling of coupled fluid and macromolecular transport in tumour interstitium has helped elucidate the role of extracellular matrix compliance, hydraulic conductivity, and diffusion coefficient in macromolecular drug distribution within tumour tissues [2], [3], [4], [5], [23], [62], [65], [66], [67], [69], [77], [78]. These basic models provided new insight for understanding the physiological barrier to fluid and macromolecular transport in solid tumours and represent a valuable tool for determining the relevant transport parameters both *in vitro* and *in vivo* [12]. Further studies are needed along these directions to integrate in the basic theory spatial and temporal effect on transport parameters, dependence of the parameters on the tissue hydration and include finite volume analysis to take into account complex geometry.

3.9 Conclusion and Challenge

Interstitial movement of macromolecules is controlled by chemical-physical properties and configurational dynamics of the transported molecule as well as the microstructure and composition of the extracellular matrix. The macroscopic parameters that control the rate of interstitial transport are the tissue hydraulic conductivity (K) and the diffusion coefficient (D), which define the intrinsic convective and diffusive rate of the transport, respectively. These parameters are related to molecular properties of the solute, such as molecular size, charge and configuration, and molec-

ular and structural parameters of the interstitium such as composition, charge, and assembly. Albeit some of these relationships have been established, at least empirically, most of them remain still fundamentally unknown. The acquisition of these basic relationships through a heuristic approach is urgently needed.

There is a paucity of quantitative data on the penetration of large agents in tumour interstitum and in particular on the role of charge, shape, and configuration on their transport parameters. This deficiency is significant considering the vast array of different agents currently under development or in use for cancer therapy; there is no consensus on the best chemical-physical characteristics an agent should have [49], [81], [88]. The need for measuring the relevant transport parameters for the novel agents developed by molecular medicine is urgent to assess the feasibility of the approaches and to design appropriate time-dose schedule to enhance their efficacy.

The tumour interstitium is not a passive fibre-matrix gel but rather a living material undergoing dynamic remodelling of cell shape, matrix structure, and cell-matrix connections. As a consequence interstitial transport parameters change both in time and space leading to gradients in drug concentration within tumour tissue [35], [53]. To address the important issue of space and time heterogeneity of tumour tissues, novel techniques with the ability to monitor pharmacokinetics and physiological parameters simultaneously and continuously with a high spatial resolutions (1–10 μm) are needed. One of the most promising novel noninvasive method that meets these requirements is the multiphoton *in vivo* microscopy associated with transparent chamber preparations [15]. With this technique it will be possible to investigate tissue in three dimension with the adequate spatial resolution. The use of this technique should permit in the future to investigate and exploit the mechanisms that underline the heterogeneous distribution of drugs within tumour interstitium.

Acknowledgments

The authors wish to thank Drs. Yves Boucher and Edward Brown for their comments and careful review of the manuscript. Financial support from Italian Minister of Research (CLUSTER) to Paolo A. Netti and from the National Institutes of Health (P01CA80124) to Rakesh K. Jain are also acknowledged.

3.10 References

[1] Auckland, K. and Nicolaysen, G., Interstitial fluid volume: local regulatory mechanisms, *Physiol. Rev.* 61, 556-643, 1981.

[2] Baxter, L.T. and Jain, R.K., Transport of fluid and macromolecules in tumors. I. Role of interstitial pressure and convection, *Microvasc. Res.* 37, 77-104, 1989.

[3] Baxter, L.T. and Jain, R.K., Transport of fluid and macromolecules in tumors. II. Role of heterogeneous perfusion and lymphatics, *Microvasc. Res.* 40, 246-263, 1990.

[4] Baxter, L.T. and Jain, R.K., Transport of fluid and macromolecules in tumors. III. Role of binding and metabolism, *Microvasc. Res.* 41, 5-23, 1991.

[5] Baxter, L.T. and Jain, R.K., Transport of fluid and macromolecules in tumors. IV. A microscopic model of the perivascular distribution, *Microvasc. Res.* 41, 252-272, 1991.

[6] Baxter, L.T., Yuan, F., and Jain, R.K., Pharmacokinetics analysis of the perivascular distribution of bifunctional antibodies and haptens: comparison with experimental data, *Cancer Res.* 52, 5838-5844, 1992.

[7] Baxter, L.T., Zhu, H., Mackensen, D.G., Butler, W.F., and Jain, R.K., Biodistribution of monoclonal nntibodies: Scale up from mouse to man using a physiologically based pharmacokinetic model, *Cancer Res.* 55, 4511-4522, 1995.

[8] Berk, D.A., Yuan, F., Leunig, M., and Jain, R.K., Fluorescence photobleaching with spatial Fourier analysis: Measurement of diffusion in light-scattering media, *Biophys. J.* 62, 2428-2436, 1993.

[9] Berk, D., Yuan, F., Leunig, M., and Jain, R.K., Direct *in vivo* measurement of targeted binding in a human tumor xenograft, *Proc. Natl. Acad. Sci. USA* 94, 1785-1790, 1997.

[10] Bobo, H.R., Laske, D.W., Akbasac, A., Morrison, P.F., Dedrick, R.L., and Oldfield, E.H., Convection enhanced delivery of macromolecules in the brain, *Proc. Natl. Acad. Sci. USA* 91, 2076-2080, 1994.

[11] Boucher, Y., Baxter, L.T., and Jain, R.K., Interstitial pressure gradients in tissue-isolated and subcutaneous tumors: Implications for therapy, *Cancer Res.* 50, 4478-4484, 1990.

[12] Boucher, Y., Brekken, C., Netti, P.A., Baxter, L.T., and Jain, R.K., Intratumoral infusion of fluid: estimation of hydraulic conductivity and implications for the delivery of therapeutic agents, *Brit. J. Cancer* 78, 1442-1448, 1998.

[13] Boucher, Y. and Jain, R.K., Microvascular pressure is the principal driving force for interstitial hypertension in solid tumors: implication for vascular collapse, *Cancer Res.* 52, 5110-5114, 1992.

[14] Brown, E.B., Campbell, R.B., Tsuzuki, Y., Xu, L., Carmeliet, P., Fukumura, D., and Jain, R.K., *In vivo* measurement of gene expression, angiogenesis, and physiological function in tumors using multiphoton laser scanning microscopy, *Nature Medicine* 7, 864-868, 2001.

[15] Brown, E., McKee, T., diTomaso, E., Pluen, A., Boucher, Y., and Jain, R.K., Dynamic imaging of collagen and its modulation in tumors *in vivo* using second harmonic generation, submitted, 2003.

[16] Chary, S.R. and Jain, R.K., Analysis of diffusive and convective recovery of fluorescence after photobleaching. Effect of uniform flow field, *Chem. Engng. Commun.* 55, 235-241, 1987.

[17] Chary, S.R. and Jain, R.K., Direct measurement of interstitial convection and diffusion of albumin in normal and neoplastic tissue by fluorescence photobleaching, *Proc. Natl. Acad. Sci. USA* 86, 5385-5389, 1989.

[18] Clauss, M.A. and Jain, R.K., Interstitial transport of rabbit and sheep antibodies in normal and neoplastic tissues, *Cancer Res.* 50, 3487-3492, 1990.

[19] Comper, W.D. and Laurent, T.C., Physiological function of connective tissue polysaccharides, *Physiol. Rev.* 58, 255-315, 1978.

[20] Davies, C.L., Berk, D.A., Pluen, A., and Jain, R.K., Comparison of IgG diffusion and extracellular matrix composition in rhabdomyosarcomas grown in mice versus *in vitro* as spheroids reveals the role of host stromal cells, *Brit. J. Cancer* 86, 1639-1644, 2002.

[21] DiResta, G.R., Lee, J., Larson, S.M., and Arbit, E., Characterization of neuroblastoma xenograft in rat flank. 1. Growth, interstitial fluid pressure and interstitial fluid velocity profiles, *Microvasc. Res.* 46, 158-177, 1993.

[22] Dvorak, H.F., Tumors: Wounds that do not heal, *New Engl. J. Med.* 315, 1650-1659, 1986.

[23] el-Kareh, A.W. and Secomb, T.W., Theoretical models for drug delivery to solid tumors, *Critical Reviews in Biomedical Engineering* 25, 503-571, 1997.

[24] Fox, J.R. and Wayland, H., Interstitial diffusion of macromolecules in the rat mesentery, *Microvasc. Res.* 18, 255-276, 1979.

[25] Fry, D.L., Cornhill, J.F., Sharma, H., Pap, J.M., and Mitschelen, J., Uptake of low density lipoprotein, albumin, and water by deendothelialized *in vitro* minipig aorta, *Arteriosclerosis* 6, 475-490, 1986.

[26] Gerlowski, L.E. and Jain, R.K., Microvascular permeability of normal and neoplastic tissues, *Microvasc. Res.* 31, 288-305, 1986.

[27] Granath, K.A. and Kvist, B.E., Molecular weight distribution analysis by gel chromatography on Sephadex, *J. Chromatography A* 28, 69-81, 1967.

[28] Gullino, P. and Grantham, F., Studies on the exchange of fluids between host and tumor I. A method for growing 'tissue isolated' tumors in laboratory animals, *J. Natl. Cancer Inst.* 27, 679-693, 1961.

[29] Iozzo, R.V., Biology of a disease - proteoglycans: structure, function, and role in neoplasia, *Laboratory Investigation* 53, 373-396, 1985.

[30] Iozzo R.V., Bolender R.P., and Wight, T.N., Proteoglycan changes in the intercellular matrix of human colon carcinoma, *Laboratory Investigation* 47, 124-138, 1982.

[31] Iozzo, R.V. and Wight, T.N., Isolation and characterization of proteglycan synthesis by human colon and colon carcinoma, *J. Biol. Chem.* 257, 11135-11144, 1982.

[32] Jackson, R.L., Bush, S.J., and Cardin, A.D., Glycosaminoglycans: molecular properties, protein interactions, and role in neoplasia, *Physiol. Rev.* 71, 481-539, 1991.

[33] Jain, R.K., Transport of molecules across tumor vasculature, *Cancer Metastasis Reviews* 6, 559-594, 1987.

[34] Jain, R.K., Transport of molecules in the tumor interstitium: a review, *Cancer Res.* 47, 3039-3051. 1987.

[35] Jain, R.K., Barrier to drug delivery in solid tumors, *Scientific American* 271, 58-65, 1994.

[36] Jain, R.K., Transport phenomena in tumors, *Adv. Chem. Engng.* 19, 129-194, 1994.

[37] Jain, R.K., Delivery of molecular medicine to solid tumors, *Science* 271, 1079-1080, 1996.

[38] Jain, R.K., Whitaker Lecture: Delivery of molecules, particles, and cells to solid tumors, *Annals of Biomedical Engineering* 24, 457-473, 1996.

[39] Jain, R.K., The next frontier of molecular medicine: Delivery of therapeutics, *Nature Medicine* 4, 655-657, 1998.

[40] Jain, R.K., Delivery of molecular and cellular medicine to solid tumors, *Advanced Drug Delivery Reviews* 46, 149-168, 2001.

[41] Jain, R.K., Delivery of molecular medicine to solid tumors: lessons from *in vivo* imaging of gene expression and function, *J. Controlled Release* 74, 7-25, 2001.

[42] Jain, R.K. and Baxter, L.T., Mechanism of heterogeneous distribution of monoclonal antibodies and other macromolecules in tumors: significance of elevated interstitial pressure, *Cancer Res.* 48, 7022-7032, 1988.

[43] Jain, R.K., Munn, L.L., and Fukumura, D., Dissecting tumour pathophysiology using intravital microscopy, *Nature Reviews Cancer* 2, 266-276, 2002.

[44] Johnson, E.M., Berk, D.A., Jain, R.K., and Deen, W.M., Diffusion and partitioning in charged agarose gels, *Biophys. J.* 68, 1561-1568, 1994.

[45] Johnson, E.M. and Deen, W.M., Hydraulic permeability of agarose gels, *AIChE J.* 42, 1220-1224, 1996.

[46] Johnson, E., Berk, D.A., Jain, R.K., and Deen, W., Hindered diffusion in agarose gels: Test of effective medium model, *Biophys. J.* 70, 1017-1026, 1996.

[47] Juweid, M., Neumann, R., Paik, C., Perez-Bacete, M.J., Sato, J., VanOsdol, W., and Weinstein, J.N., Micropharmacology of monoclonan antibodies in solid tumor: direct experimental evidence for a binding site barrier, *Cancer Res.* 52, 5144-5149, 1992.

[48] Knudson, W., Biswas, C., and Toole, B.P., Interactions between human tumor cells and fibroblasts stimulate hyaluronate synthesis, *Proc. Natl. Acad. Sci. USA* 81, 6767-6771, 1984.

[49] Kramm, C.M., Sena-Esteves, M., Barnett, F.H., Rainov, N.G., Schuback, D.E., Yu, J.S., Pechan, P.A., Paulus, W., Chiocca, E.A., and Breakefield, X.O., Gene therapy for brain tumors, *Brain Pathol.* 5, 345-381, 1995.

[50] Kristjansen, P.E.G., Roberge, S., Lee, I., and Jain, R.K., Tissue-isolated human tumor xenograft in athymic nude mice, *Microvasc. Res.* 48, 389-402, 1994.

[51] Labat-Robert, J. and Robert, L., Interaction between structrural glycoproteins and collagens, in *Collagen*, M.E. Nimmi, Ed., CRC Press, Boca Raton, FL, 173-186, 1988.

[52] Lai Fook, S.J., Rochester, N.L., and Brown, L.V., Effects of albumin, dextran, and hyluronidase on pulmonary interstitial conductivity, *J. Appl. Physiol.* 67, 606-613, 1989.

[53] Lankelma, J., Dekker, H., Luque, R.F., Luykx, S., Hoekman, K., van der Valk, P., van Diest P.J., and Pinedo, H.M., Doxorubicin gradients in human breast cancer, *Clin. Cancer Research* 5, 1703-1707, 1999.

[54] Laurent, T.C., Björk, I., Pietruszkiewicz, A., and Persson, H., On the interaction between polysaccharides and other macromolecules: II. The transport of globular particles through hyaluronic acid solutions, *Biochim. Biophys. Acta* 78, 351-359, 1963.

[55] Levick, J.R., Flow trough interstitium and other fibrous matrices, *Quart. J. Exp. Physiol.* 72, 409-437, 1987.

[56] Levick, J.R., An analysis of the interaction between interstitial plasma protein, interstitial flow, and fenestral filtration and its application to synovium, *Microvasc. Res.* 47, 90-125, 1994.

[57] Line, S.R., Torloni, H., and Junqueira, L.C., Diversity of collagen expression in the pleomorphic adenoma of paroid gland, *Virchows Archiv. A, Pathological Anatomy & Histopathology* 414, 477-483, 1989.

[58] Liotta, L.A. and Rao C.N., Role of extracellular matrix in cancer, *Ann. N.Y. Acad. Sci.* 460, 333-344, 1985.

[59] Maroundas, A., Physical chemistry of articular cartilage and the intervertebral disc, in *The Joint and Synovial Fluid* Vol.2, L. Sokoloff, Ed., Academic Press, New York, 240-293, 1980.

[60] McGuire, S. and Yuan, F., Quantitative analysis of intratumoral infusion of color molecules, *Am. J. Physiol. - Heart & Circulatory Physiology* 281, H715-H721, 2001.

[61] Montes, G.S. and Junqueira, L.C.U., Histochemical localizzation of collagen and of proteoglycans in tissues, in *Collagen* vol. 1, M.E. Nimmi, Ed., CRC Press, Boca Raton, FL, 173-186, 1988.

[62] Morrison, P.F., Laske, D.W., Bobo, H., Oldfield, E.H., and Dedrick, R.L., High-flow microinfusion: tissue penetration and pharmacodynamics, *Am. J. Physiol.* 266, R292-R305, 1994.

[63] Mow, V.C., Holmes, M.H., and Lai, W.M., Fluid transport and mechanical properties of articular cartilage: a review, *J. Biomech.* 17, 377-394, 1984.

[64] Nakamura, Y. and Wayland, H., Macromolecular transport in the cat mesentery, *Microvasc. Res.* 9, 1-21, 1975.

[65] Netti, P.A., Baxter, L.T., Boucher, Y., Skalak, R., and Jain, R.K., Time-dependent behavior of interstitial fluid pressure in solid tumors: Implication for drug delivery, *Cancer Res.* 55, 5451-5458, 1995.

[66] Netti, P.A., Baxter, L.T., Boucher, Y., Skalak, R., and Jain, R.K., Macro and microscopic fluid transport in living tissues: Application to solid tumors, *AIChE J.* 43, 818-834, 1997.

[67] Netti, P.A., Berk, D.A., Swartz, M.A., Grodzinsky, A.J., and Jain, R.K., Role of extracellular matrix assembly in interstitial transport in solid tumors, *Cancer Res.* 60, 2497-2503, 2000.

[68] Netti, P.A., Hamberg, L.M., Babich, J.W., Roberge, S., Kierstead, D., Graham, W., Hunter, G.J., Wolf, G.L., Boucher, Y., Fischman, A., and Jain, R.K., Enhancement of fluid filtration across tumor vessels: Implication for delivery of macromolecules, *Proc. Natl. Acad. Sci. USA* 96, 3137-3142, 1999.

[69] Netti, P.A., Travascio, F., and Jain, R.K., Coupled macromolecular transport and gel mechanics: a poroviscoelastic approach, submitted to *AIChE J.*, 2003.

[70] Nugent, L.J. and Jain, R.K., Extravascular diffusion in normal and neoplastic tissues, *Cancer Res.* 44, 238-244, 1984.

[71] Ogston, A.G. and Sherman, T.F., Effect of hyaluronic acid upon diffusion of solutes and flow of solvent, *J. Physiology* 156, 67-74, 1961.

[72] Padera, T.P., Kadambi, A., di Tomaso, E., Carreira, C.M., Brown, E.B., Boucher, Y., Choi, N.C., Mathisen, D., Wain, J., Mark, E.J., Munn, L.L., and Jain, R.K., Lymphatic metastasis in the absence of functional intratumor lymphatics, *Science* 296, 1883-1886, 2002.

[73] Parameswaran, S., Brown, L.V., Ibbott, G.S., and Lai-Fook, S.J., Hydraulic conductivity, albumin reflection and diffusion coefficients of pig mediastinal pleura, *Microvasc. Res.* 58, 114-127, 1999.

[74] Parameswaran, S., Brown, L.V., and Lai-Fook, S.J., Effect of flow on hydraulic conductivity and reflection coefficient of rabbit mesentery, *Microcirculation* 5, 265-274, 1998.

[75] Pluen, A., Boucher, Y., Ramanujan, S., McKee, T.D., Gohongi, T., di Tomaso, E., Brown, E.B., Izumi, Y., Campbell, R.B., Berk, D.A., and Jain, R.K., Role of tumor-host interactions in interstitial diffusion of macromolecules: Cranial vs. subcutaneous tumors, *Proc. Natl. Acad. Sci. USA* 98, 4628-4633, 2001.

[76] Pluen, A., Netti, P.A., Jain, R.K., and Berk, D.A, Diffusion of macromolecules in agarose gels: Comparison of linear and globular configurations, *Biophysical Journal* 77, 542-552, 1999.

[77] Ramanujan, S., Koenig, G.C., Padera, T.P., Stoll, B.R., and Jain, R.K., Local imbalance of proangiogenic and antiangiogenic factors: a potential mechanism of focal necrosis and dormancy intumors, *Cancer Res.* 60, 1442-1448, 2000.

[78] Ramanujan, S., Pluen, A., McKee, R.D., Brown, E.B., Boucher, Y., Jain, R.K., Diffusion and convection in collagen gels: Implications for transport in the tumor interstitium, *Biophys. J.* 83, 1650-1660, 2002.

[79] Rippe, B., Kamiya, A., and Folkow, B., Simultaneous measurements of capillary diffusion and filtration exchange during shifts in filtration-absorption and at graded alterations in the capillary permeability surface area product (PS), *Acta Physiol Scand.* 104, 318-336, 1978.

[80] Ronnov-Jessen, L., Petersen, O.W., and Bissel, M.J., Cellular changes involved in conversion of normal to malignant breast: importance of the stromal reaction, *Physiological Rev.* 76, 69-125, 1996.

[81] Rosenfeld, M.E. and Curiel, D.T., Gene therapy strategies for novel cancer therapeutics, *Current Opinion in Oncol.* 8, 72-77, 1996.

[82] Sakamoto, S. and Sakamoto, M., Degratative processes of connective tissue proteins with special emphasis on collagenolysis and bone resorption, *Molecular Aspects of Medicine* 10, 301-428, 1988.

[83] Sandison, J.C., A new method for microscopy study of living growing tissues by introduction of a transparent chamber in the rabbit's ear, *Anat. Rec.* 28, 281-287, 1924.

[84] Sutherland, R., Buchegger, F., Schreyer, M., Vacca, A., and Mach, J.P., Penetration and binding of radiolabeled anti-carcinoembryonic antigen monoclonal antibodies and their antigen binding fragments in human colon multicellular tumor spheroids, *Cancer Res.* 47, 1627-1633, 1987.

[85] Swabb, E.A., Wei, J., and Gullino, P.M., Diffusion and convection in normal and neoplastic tissues, *Cancer Res.* 34, 2814-2822, 1974.

[86] Swartz, M.A., Kaipainen, A., Netti, P.A., Brekken, C., Boucher, Y., Grodzinsky, A.J., and Jain, R.K., Mechanics of interstitial-lymphatic fluid transport: Theoretical foundation and experimental validation, *J. Biomech.* 32, 1297-1307, 1999.

[87] Vaupel, P., Effect of percentual water content in tissues and liquids on the diffusion coefficients of O_2, CO_2, N_2, and H_2, *Pfugers Arch.* 361, 201-204, 1976.

[88] Verma, I.M. and Somia, N., Gene therapy - promises, problems, and prospects, *Nature* 389, 239-242. 1997.

[89] Winlove, C.P. and Parker, K.H., The physiological function of the extracellular matrix, in *Interstitium, Connective Tissue, and Lymphatics*, R.K. Reed, G.A. Laine, J.L. Bert, C.P. Winlove, and N. McHale, Eds., Portland Press, London, 137-165, 1995.

[90] Yuan, F., Krol, A., and Tong, S., Available space and extracellular transport of macromolecules: effects of pore size and connectedness, *Ann. Biomed. Engng.* 29, 1150-1158, 2001.

Chapter 4

Modelling Avascular Tumour Growth

Helen M. Byrne
Centre for Mathematical Medicine School of Mathematical Sciences, University of Nottingham (U.K.)

4.1 Introduction

When setting out to model new phenomena, it is natural to focus initially on simple, well-defined systems. Thus, before using the Navier-Stokes' equations to study turbulent fluid flow, one might first consider steady laminar flow. Looking through the mathematical literature on solid tumour growth a similar pattern emerges: the earliest models focused on avascular tumour growth; then models of angiogenesis were developed; and, now, models of vascular tumour growth are starting to emerge. The improvements in biomedical techniques such as imaging and gene-sequencing that have occurred over the past thirty years provide an alternative explanation for this development: as experimental procedures became more sophisticated and knowledge about solid tumour growth increased, the deficiencies of the earlier mathematical models became apparent and pointed the direction for new modelling approaches.

Given the large, and ever increasing, number of mathematicians who are now studying different aspects of solid tumour growth, it would be impossible to review the entire modelling literature here. Instead, in this chapter we will focus on mathematical models of avascular tumour growth. In so doing, we hope to explain how the field has developed and matured in line with new biological insights.

We start our review, in section 4.2, by considering models in which details of the tumour's spatial structure are neglected and attention focused on, for example, the tumour's overall volume or the total number of cells present within the tumour. The resulting models are formulated as systems of differential equations and have been widely used by clinicians to estimate kinetic parameters associated with tumour growth *in vivo* and *in vitro* and to assess the efficacy of different therapeutic strategies.

For the next class of models that we study, in section 4.3, the role of a single, rate-limiting, diffusible growth factor on the tumour's development is investigated. Since the concentration and hence potency of the chemical will vary as if diffuses through the tumour, spatially nonuniform growth will emerge naturally from such models. The chemical of interest may promote cell division (e.g., glucose or oxygen) or promote cell death (e.g., chemotherapeutic drugs, tumour necrosis factor, or other biproducts of cell degradation). Equally, it may be supplied externally (e.g., oxygen and drugs) or be produced by the cells themselves (e.g., tumour necrosis factor). By specialising the model appropriately and assuming one-dimensional growth, each of these cases may be investigated. The resulting models typically comprise a reaction-diffusion equation for the growth factor and an integro-differential equation for the tumour radius. Additional equations may be used to determine the tumour's spatial structure. For example, if the chemical of interest is oxygen, the transition from rapid proliferation to quiescence and from quiescence to necrosis may be assumed to coincide with the oxygen concentration passing through experimentally determined threshold values. As we show, these models can be used to identify conditions under which a tumour will evolve to an equilibrium configuration and to show how its size,

structure, and stability to time-dependent perturbations depend on physically relevant parameters such as the concentration of oxygen being supplied to the tumour.

In section 4.4 we turn our attention to tumour invasion. We show how the spatially-structured models of section 4.3 can be adapted to study the impact of symmetry-breaking perturbations on tumours undergoing one-dimensional (usually radially-symmetric) growth. We explain how linear stability analysis may be used to identify those asymmetric perturbations to which the tumour is unstable and how the range of instability varies with parameters such as the concentration of oxygen outside the tumour and the strength of surface tension effects. In this way, it is possible to predict conditions under which an avascular tumour will maintain an approximately radially-symmetric structure and those for which its outer boundary will become highly irregular, the latter case corresponding to a highly invasive and aggressive tumour.

The chapter concludes in section 4.5 with a summary of the earlier sections and a brief discussion of directions for future mathematical research in modelling solid tumour growth.

4.2 Spatially-Uniform Models of Avascular Tumour Growth

4.2.1 Introduction

In this section we present a number of mathematical models that have been used to describe the growth dynamics of solid tumours when spatial effects are neglected. The models are amongst the earliest that were used to describe solid tumour growth and are formulated as systems of differential equations. As we show, models of this type may be used to describe how the numbers of proliferating, quiescent, and dead cells contained within a tumour change over time. Equally, differential equation models may be used to compare the response of a tumour to different chemotherapeutic protocols (continuous drug infusion or periodic pulsing).

The remainder of this section is organised in the following way. In section 4.2.2 we present models in which the tumour is assumed to be homogeneous, containing only one type of cell. In section 4.2.3 we investigate the response of such homogeneous tumours to different chemotherapeutic strategies. In section 4.2.4 we generalise the earlier models so that heterogeneous tumours containing different cell types may be studied. The section concludes with a discussion of the spatially-uniform models.

4.2.2 Growth of Homogeneous Solid Tumours

One of the simplest models that can be used to describe the way in which the number of cells $N(t)$ within a solid tumour changes over time is the exponential growth law which states

$$\frac{dN}{dt} = kN, \quad \text{with } N(t=0) = N_0, \tag{4.1}$$

$$\Rightarrow N(t) = N_0 e^{kt}.$$

In Equation (4.1) $k > 0$ represents the net rate at which the cells proliferate, and N_0 denotes the number of cells initially present within the tumour. In this model, there are no constraints on cell growth: all nutrients and other vital growth factors are assumed to be available in abundance. In consequence, the model predicts that the population will increase, without limit.

Whilst an exponential growth law may provide an accurate description of the early stages of a tumour's development, it is clearly unable to capture the periods of reduced growth and eventual saturation that are observed when avascular tumours are grown *in vitro* or when vascular tumours develop *in vivo*. This discrepancy arises because as the tumour increases in size competition for nutrients and other vital resources, such as space, can no longer be neglected. A simple modification of (4.1) which takes account of competition for resources (without specifying what those resources are) is the logistic growth law

$$\frac{dN}{dt} = kN\left(1 - \frac{N}{\theta}\right), \quad \text{with } N(t=0) = N_0 > 0, \tag{4.2}$$

$$\Rightarrow N(t) = \frac{\theta N_0}{N_0 + (\theta - N_0)e^{-kt}} \to \theta \text{ as } t \to \infty.$$

In (4.2), $\theta > 0$ represents the carrying capacity of the population.

Whilst the logistic growth law predicts almost exponential growth of small tumours and growth saturation when the tumour reaches its carrying capacity ($N = \theta$), the symmetry of $N(t)$ about its point of inflection (where $\frac{d^2N}{dt^2} = 0$ and $N = \theta/2$) means that it is not particularly flexible when it is used to fit (or describe) experimental data. A more general family of curves, which, depending on the choice of α, can saturate more or less rapidly than (4.2), is given by

$$\frac{dN}{dt} = \frac{k}{\alpha}N\left[1 - \left(\frac{N}{\theta}\right)^{\alpha}\right], \quad \text{with } N(t=0) = N_0, \tag{4.3}$$

$$\Rightarrow N(t) = \theta\left(\frac{N_0^{\alpha}}{N_0^{\alpha} + (\theta^{\alpha} - N_0^{\alpha})e^{-kt}}\right)^{1/\alpha}.$$

We remark that the logistic growth law is a special case of (4.3) (set $\alpha = 1$) and that the Gompertzian growth law is recovered in the limit as $\alpha \to 0^+$.

In order to compare the three models presented above, we plot in Figure 4.1 growth curves for each model for fixed values of the proliferation rate k and the carrying capacity θ.

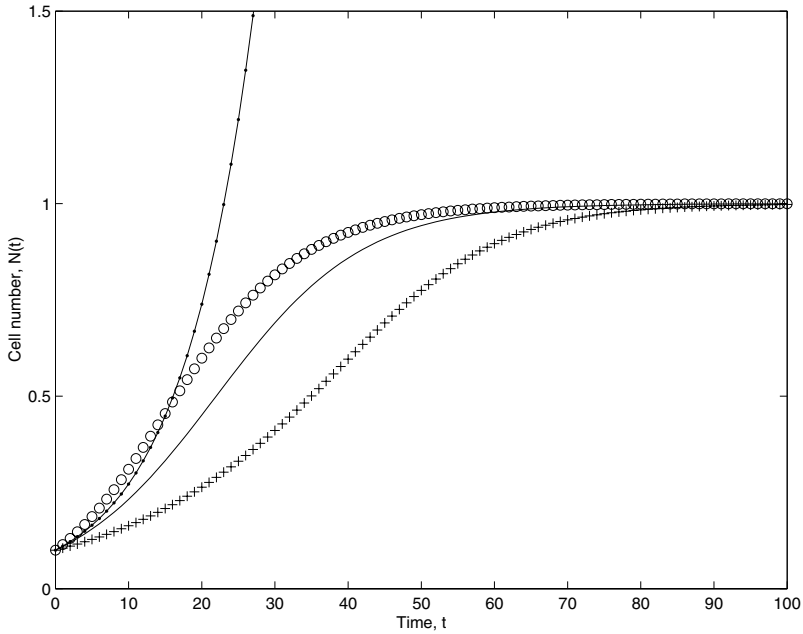

Figure 4.1

Diagram showing how the tumour's evolution depends on the choice of growth law. Key: exponential growth law (dot-dashed line); logistic growth law (solid line); general growth law ($\alpha = 0.5$, circles and $\alpha = 2.0$, crosses). Parameter values: $k = 0.1, \theta = 1.0, N_0 = 0.1, \alpha = 0.5$, or $\alpha = 2.0$.

Many alternative growth laws have been proposed to describe the development of solid tumours (for details, see, for example [24,25]). The different models have enjoyed varying degrees of success when applied to experimental data. A common weakness of models of this type (i.e., models in which a single differential equation describes the tumour's growth rate and the effects of any other external factors, such as nutrient availability or tumour cell heterogeneity, are neglected) is the difficulty in relating the model parameters (e.g., k and θ for the logistic growth law) to the behaviour of individual cells. We will return to this issue in section 4.3 where we present spatially-structured models of avascular tumours. Before that, we discuss

two possible modifications of Equations (4.1) to (4.3) which lead to models that provide preliminary insight into the impact that cellular heterogeneity and chemotherapy may have on solid tumour growth. In the first case we consider the response of a tumour to a cytotoxic (poisonous) chemotherapeutic agent which is administered either as a continuous infusion or via a series of pulses. In the second case, we suppose that the tumour contains different cell types and investigate how the proportion of each cell type changes over time.

4.2.3 Treatment of Homogeneous Solid Tumours

We now consider a tumour growing *in vivo* which, in the absence of therapeutic intervention, undergoes logistic growth. A chemotherapeutic drug, which kills tumour cells when it comes into contact with them, is injected into the patient. Following section 4.2.2, we denote by $N(t)$ the number of tumour cells at time t and by $A(t)$ the (average) drug concentration within the tumour and assume that

$$\frac{dN}{dt} = kN\left(1 - \frac{N}{\theta}\right) - \mu AN \equiv f(N, A), \tag{4.4}$$

$$\frac{dA}{dt} = a(t) - \lambda A - \gamma AN \equiv g(N, A), \tag{4.5}$$

with

$$N(t = 0) = N_0 \quad \text{and} \quad A(t = 0) = A_0. \tag{4.6}$$

In Equations (4.4) and (4.5) μ denotes the rate at which the drug kills tumour cells, λ represents the drug's half-life (or decay rate), γ represents the rate at which the drug becomes ineffective as a result of cell kill, and $a(t)$ represents the rate at which the drug is delivered to the tumour. We will consider two alternative delivery protocols:

$$\textbf{Continuous Infusion:} \quad a(t) = a_\infty \; \forall \; t \geq 0.$$

$$\textbf{Periodic Infusion:} \quad a(t) = \begin{cases} a_\infty & n < t < n + \tau \\ 0 & n + \tau < t < n + 1. \end{cases}$$

4.2.3.1 Continuous Infusion

When $a_\infty = 0$ (i.e., no drug is administered), Equation (4.4) reduces to (4.2) and, hence, $N(t) \to \theta$ as $t \to \infty$. It seems reasonable to expect that when the tumour is continuously exposed to a cytotoxic drug, both the tumour and the drug concentration will evolve to equilibrium values. In order to study the impact of continuous drug infusion, we now identify and classify the equilibrium solutions of Equations (4.4) and (4.5), paying particular attention to how they depend on a_∞ (and, hence, the amount of drug that is administered).

When $\frac{d}{dt} = 0$, Equations (4.4) and (4.5) reduce to give

$$0 = kN\left(1 - \frac{N}{\theta} - \frac{\mu}{k}A\right) \quad \text{and} \quad 0 = a_\infty - \lambda A - \gamma N A\,,$$

so that either

$$N = 0 \quad \text{and} \quad A = \frac{a_\infty}{\lambda}\,,$$

or

$$0 = N^2 + \frac{\lambda}{\gamma}\left(1 - \frac{\gamma\theta}{\lambda}\right)N + \frac{\lambda\theta}{\gamma}\left(\frac{a_\infty\mu}{\lambda k} - 1\right) \quad \text{and} \quad A = \frac{k}{\mu}\left(1 - \frac{N}{\theta}\right). \quad (4.7)$$

Now, for a particular tumour and a specific drug, the parameters k, θ, μ, λ, and γ will be fixed: the only parameter over which there will be some degree of control is a_∞, which we take as our bifurcation parameter.

Elementary analysis indicates that (4.7) possesses no real roots if

$$a_\infty > a_\infty^{max} \equiv \frac{\lambda k}{\mu}\left[1 + \frac{\lambda}{4\gamma\theta}\left(1 - \frac{\gamma\theta}{\lambda}\right)^2\right].$$

Thus, if the administered dose is such that $a_\infty > a_\infty^{max}$ then the only physically realistic steady solution is the trivial, tumour-free solution for which $N = 0$.

Further analysis of (4.7) indicates that for intermediate values of a_∞ ($0 < a_\infty \leq a_\infty^{max}$) the nontrivial steady state solutions depend on the parameter grouping $\gamma\theta/\lambda$. Referring to Figure 4.2, we note that if $\gamma\theta/\lambda > 1$ then there is a finite range of a_∞ ($\lambda k/\mu < a_\infty < a_\infty^{max}$) for which (4.7) possesses two, physically realistic solutions: for smaller values of a_∞ ($0 \leq a_\infty < \lambda k/\mu$) there is a single, nontrivial solution. We note also that if $\gamma\theta/\lambda \quad 1$ then for moderate values of a_∞ ($0 \leq a_\infty < \lambda k/\mu$) there is a single, nontrivial solution: for larger values of a_∞ ($\lambda k/\mu < a_\infty < a_\infty^{max}$) there are no physically realistic, nontrivial equilibrium solutions.

Whilst the above analysis and the results presented in Figure 4.2 show how the equilibrium solutions depend on the system parameters, they do not enable us to determine which solution would be realised in regions of parameter space where more than one equilibrium occurs. One method that can be used to address such questions involves using linear stability analysis to determine the local stability of the equilibrium solutions to time-dependent perturbations. We now describe this technique, and use it to assess the stability of the trivial, tumour-free solution $(N, A) = (0, a_\infty/\lambda)$ which exists for all parameter values.

We linearise about $(N, A) = (0, a_\infty/\lambda)$ by introducing the small parameter $\epsilon \ll 1$ and writing

$$N(t) = \epsilon\bar{N}(t) \quad \text{and} \quad A(t) = \frac{a_\infty}{\lambda} + \epsilon\bar{A}(t). \quad (4.8)$$

We substitute with (4.8) in Equations (4.4) and (4.5), and equate coefficients of $O(\epsilon)$ to obtain

$$\frac{d\bar{N}}{dt} = \left(k - \frac{\mu a_\infty}{\lambda}\right)\bar{N},$$

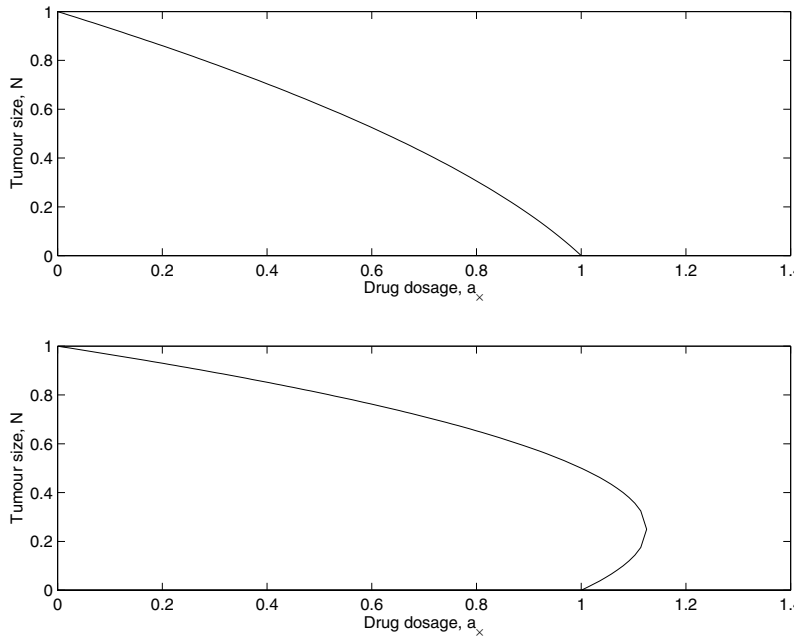

Figure 4.2

Bifurcation diagrams showing how the tumour's equilibrium size varies with the drug dosage, a_∞ for the cases (a) $\gamma\theta/\lambda < 1$ and (b) $\gamma\theta/\lambda > 1$. Parameter values: (a) $\theta = \lambda = \mu = k = 1, \gamma = 0.5$ and (b) $\theta = \lambda = \mu = k = 1, \gamma = 2$.

$$\frac{d\bar{A}}{dt} = \lambda\bar{A} - \frac{\gamma a_\infty}{\lambda}\bar{N}.$$

Therefore

$$\bar{N}(t) = \bar{N}(0)e^{(k-\mu a_\infty/\lambda)t}$$

and

$$\bar{A}(t) = \left(\bar{A}(0) + \frac{\gamma a_\infty \bar{N}(0)}{\lambda^2 + k\lambda - \mu a_\infty}\right) e^{-\lambda t} - \frac{\gamma a_\infty \bar{N}(0)}{\lambda^2 + k\lambda - \mu a_\infty} e^{(k-\mu a_\infty/\lambda)t}.$$

We deduce that if $a_\infty > \lambda k/\mu$ then $\bar{N}(t), \bar{A}(t) \to 0$ as $t \to \infty$, i.e., the tumour evolves to the trivial, tumour-free solution. Therefore, if $a_\infty > \lambda k/\mu$ then the trivial solution (with $(N, A) = (0, a_\infty)$) is said to be linearly stable whereas if $a_\infty < \lambda k/\mu$ it is said to be linearly unstable. Given that a_∞ denotes the concentration of drug administered to the tumour, we deduce from the above analysis that if the drug concentration exceeds the threshold value $\lambda k/\mu$ then the tumour will be eradicated.

The same technique can be used to assess the linear stability of the nontrivial equilibrium solutions of (4.4) and (4.5), although the algebra is more involved. To

determine the stability of a nontrivial solution $(N, A) = (N_\infty, A_\infty)$, where N_∞ and A_∞ solve (4.7), we seek solutions of the form

$$N(t) = N_\infty + \epsilon \bar{N}(t) \quad \text{and} \quad A(t) = A_\infty + \epsilon \bar{A}(t) \quad \text{where } \epsilon \ll 1.$$

Substituting with these trial solutions in Equations (4.4) and (4.5) and equating to zero coefficients of $O(\epsilon)$ we deduce that

$$\frac{d\bar{N}}{dt} = \frac{\partial f}{\partial N}\bar{N} + \frac{\partial f}{\partial A}\bar{A} \equiv k\left(1 - \frac{2N_\infty}{\theta} - \frac{\mu a_\infty}{k}\right)\bar{N} - \mu N_\infty \bar{A},$$

$$\frac{d\bar{A}}{dt} = \frac{\partial g}{\partial N}\bar{N} + \frac{\partial g}{\partial A}\bar{A} \equiv -\gamma A_\infty \bar{N} - (\lambda + \gamma N_\infty)\bar{A},$$

where

$$\frac{\partial f}{\partial N} \equiv \frac{\partial f}{\partial N}(N_\infty, A_\infty),$$

and so on. This pair of linear differential equations possesses solutions of the form

$$(\bar{N}, \bar{A}) = (\tilde{N}, \tilde{A})e^{\sigma t}$$

where, for nontrivial solutions (i.e., $(\tilde{N}, \tilde{A}) \neq 0$), σ satisfies the dispersion relation

$$0 = \sigma^2 - \left(\frac{\partial f}{\partial N} + \frac{\partial g}{\partial A}\right)\sigma + \left(\frac{\partial f}{\partial N}\frac{\partial g}{\partial A} - \frac{\partial f}{\partial A}\frac{\partial g}{\partial N}\right),$$

and we have linear stability if $\Re(\sigma) < 0$. Using the dispersion relation it is straightforward to show that this will be the case if

$$\frac{\partial f}{\partial N} + \frac{\partial g}{\partial A} < 0 < \frac{\partial f}{\partial N}\frac{\partial g}{\partial A} - \frac{\partial f}{\partial A}\frac{\partial g}{\partial N}.$$

Example
We apply the above techniques to our model of continuous drug infusion with

$$\theta = \lambda = \mu = k = 1, \quad \gamma = 1/2, \quad \text{and} \quad a_\infty \in (0, 1).$$

The nontrivial equilibrium solutions (N_∞, A_∞) satisfy

$$0 = N_\infty^2 + N_\infty - 2(a_\infty - 1) \quad \text{or} \quad 2N_\infty = -1 \pm \sqrt{9 - 8a_\infty}$$

$$A_\infty = 1 - N_\infty,$$

and there is a single, physically-realistic (i.e., positive) solution for $a_\infty \in (0, 1)$.

Using elementary calculus, it is possible to show that

$$\begin{pmatrix} \frac{\partial f}{\partial N} & \frac{\partial f}{\partial A} \\ \frac{\partial g}{\partial N} & \frac{\partial g}{\partial A} \end{pmatrix}_{(N_\infty, A_\infty)} = \begin{pmatrix} 1 - 2N_\infty - A_\infty & -N_\infty \\ -\frac{A_\infty}{2} & -1 - \frac{N_\infty}{2} \end{pmatrix}$$

$$\Rightarrow \frac{\partial f}{\partial N} + \frac{\partial g}{\partial A} = -\left(\frac{3N_\infty}{2} + A_\infty\right) < 0$$

and

$$\frac{\partial f}{\partial N}\frac{\partial g}{\partial A} - \frac{\partial f}{\partial A}\frac{\partial g}{\partial N} = N_\infty^2 + \frac{N_\infty}{2} > 0.$$

Hence we deduce that, where it exists, the physically-realistic equilibrium solution is stable to time-dependent perturbations.

In Figure 4.3 we use the above approach to show how the local stability of the steady state solutions presented in Figure 4.2 change as the drug concentration, a_∞, varies. As predicted above, when $\gamma\theta/\lambda < 1$, the nontrivial solution is stable where it exists and the trivial solution unstable. For values of a_∞ for which there are no nontrivial steady states the tumour-free steady state is stable. The case when $\gamma\theta/\lambda > 1$ is slightly different. Here where multiple, nontrivial steady state solutions exist, the smaller steady state is unstable while both the larger solution and the trivial, tumour-free solution are stable. Indeed, the smaller steady state acts as a boundary, separating the basins of attraction of the two stable solutions.

4.2.3.2 Periodic Infusion

The analysis of the continuous infusion model presented above suggests that if the drug dosage is sufficiently large ($a_\infty > k/\mu$) then the tumour will be eliminated. In real situations, side-effects mean that continuous infusion is not usually a viable drug delivery protocol: if delivered systemically, the drug may have an adverse effect on vital organs such as the liver where there is a rapid cell turnover rate. As a result, chemotherapeutic drugs are often delivered as a series of continuous infusions, so that the patient's healthy organs (and, unfortunately, the tumour) can recover between successive treatments.

We now investigate the impact of periodic infusion on our solid tumour growth model. For simplicity we study the following simple model

$$\frac{dN}{dt} = kN\left(1 - \frac{N}{\theta} - \mu A\right), \quad \text{with } N(0) = N_0, \tag{4.9}$$

$$\text{and} \quad A(t) = \begin{cases} a_\infty & n < t < n + \tau \\ 0 & n + \tau < t < n + 1. \end{cases} \tag{4.10}$$

(**Note:** this model can be derived from (4.4) and (4.5) by assuming $a_\infty = \lambda \hat{a}_\infty$ and $\hat{a}_\infty \sim O(1) \ll \lambda$.)

Since $A(t)$ is piecewise constant, Equation (4.9) is simply a logistic equation, whose carrying capacity switches between $\theta(1 - \mu a_\infty/k)$ and θ as $A(t)$ switches between a_∞ and 0 at times $t = n, n + \tau$ $(n = 0, 1, 2, \ldots)$. By assuming continuity of $N(t)$ at these switching times, it is possible to construct the following analytical

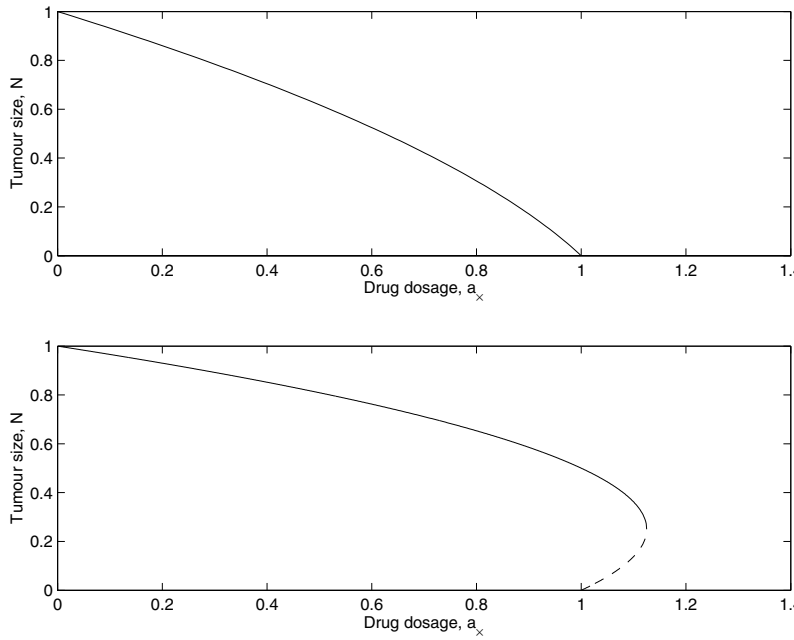

Figure 4.3

Diagrams showing how the stability of the equilibrium solutions presented in Figure 4.2 change as a_∞ varies for the cases (a) $\gamma\theta/\lambda < 1$ and (b) $\gamma\theta/\lambda > 1$. Parameter values: (a) $\theta = \lambda = \mu = k = 1, \gamma = 0.5$ and (b) $\theta = \lambda = \mu = k = 1, \gamma = 2$. Stable solutions are represented by solid lines and unstable solutions by dashed lines.

solution for $N(t)$:

$$N(t) = \begin{cases} \dfrac{\theta\Lambda N_n}{N_n + [\theta\Lambda - N_n]\exp\left[-k\Lambda(t-n)\right]} & n < t < n+\tau \\ \dfrac{\theta N_{n+\tau}}{N_{n+\tau} + (\theta - N_{n+\tau})\exp[-k(t-n-\tau)]} & n+\tau < t < n+1 \end{cases} \tag{4.11}$$

where

$$\Lambda = 1 - \frac{\mu a_\infty}{k},$$

$N(0) = N_0$ is prescribed, $N_n = N(t = n)$ $(n \geq 1)$,

$$N_{n+\tau} = N(t = n+\tau) = \frac{\theta\Lambda N_n}{N_n + [\theta\Lambda - N_n]\exp[-k\Lambda\tau]}$$

and, by continuity of $N(t)$ at $t = n+1$, the coefficients N_n satisfy the following

recurrence relation:

$$N_{n+1} = \frac{\theta\Lambda N_n}{\Lambda N_n + [(1-\Lambda)N_n + (\theta\Lambda - N_n)\exp[-k\Lambda\tau]]\exp[-k(1-\tau)]}. \quad (4.12)$$

In Figure 4.4 we show how the sequence $\{N_n\}_{n=0}^{\infty}$ evolves and how the limiting behaviour depends on the drug dosage applied. In all cases, the sequence eventually settles to an equilibrium which decreases in magnitude as a_∞ increases.[1] Indeed, if the drug dosage is sufficiently large, then eradication of the tumour occurs. Obviously, with periodic infusion the dosage required to achieve eradication is greater than that required for continuous infusion (this is because with periodic infusion the tumour cells are exposed to the drug for less time).

Recall that when we studied the tumour's response to continuous drug infusion, the tumour eventually settled to a time-independent equilibrium solution. By contrast, as the results of Figure 4.4 indicate, when there is periodic infusion, the system may also evolve to a (nontrivial) periodic solution for which $N(t) = N(1+t)$ and hence $N_n = N_{n+1} \equiv N_\infty > 0$, say. Using Equation (4.12) it is possible to show that nontrivial periodic solutions will arise if

$$N_\infty = \frac{\theta\Lambda(1 - e^{-k(1-\tau)}e^{-k\Lambda\tau})}{\Lambda + (1-\Lambda)e^{-k(1-\tau)} - e^{-k(1-\tau)}e^{-k\Lambda\tau}}.$$

In Figure 4.5 we show how N_∞ decreases as the drug dosage a_∞ increases.

4.2.4 Heterogeneous Growth of Solid Tumours

In the models that we have studied thus far all tumour cells were assumed to be identical. In practice solid tumours consist of many different types of cells. For example, vascular tumours growing *in vivo* may contain blood vessels that supply nutrients to the tumour, extracellular matrix and immune cells such as macrophages (macrophages are white blood cells that are usually associated with wound-healing but which are now believed to play an important role in solid tumour growth [22]).

In addition, the tumour cell population may contain functionally distinct sub-populations. These sub-populations, which are often caused by genetic mutations, may be characterised by different proliferation and death rates and different responses to environmental conditions (for example, cells with mutant p53 are believed to be able to survive longer periods of oxygen deprivation than cells with normal

[1] Note that even though the sequence $\{N_n\}_{n=0}^{\infty}$ evolves to an equilibrium, the system does not settle to a time-independent steady state: rather it settles to a periodic solution, with $N = N(t)$ during the interval $n < t < n+1$.

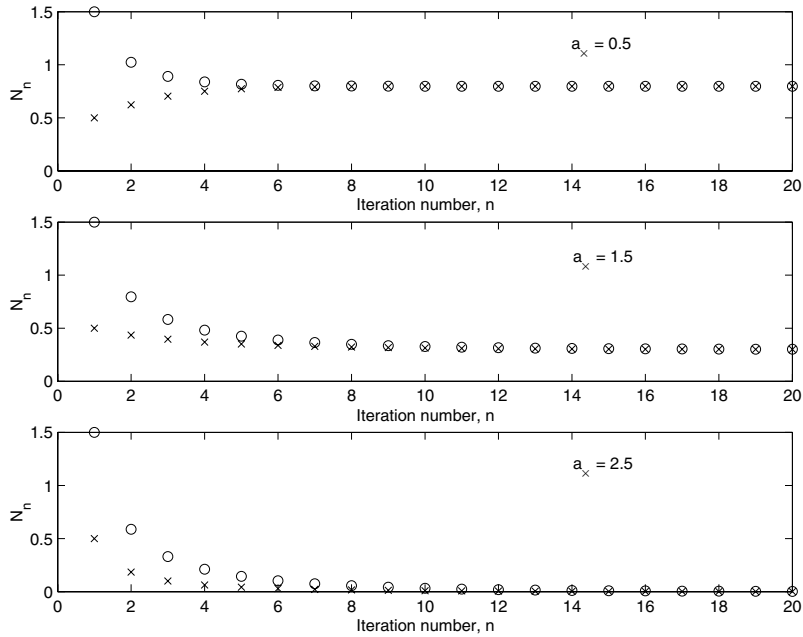

Figure 4.4

Series of diagrams showing the tumour's response to periodic infusion at different drug dosages for different initial conditions. Key: top panel, $a_\infty = 0.5$**; middle panel,** $a_\infty = 1.5$**; bottom panel,** $a_\infty = 2.5$**. Parameter values:** $\theta = 1 = \mu = k, \tau = 0.5$**. Circles correspond to** $N(0) = N_0 = 1.5$**, crosses to** $N(0) = N_0 = 0.5$**.**

p53 [15]). These functional variations can also mean that certain sub-populations are less responsive to chemotherapeutic intervention.

By considering the proliferation rates of tumour cells at increasing distances from a blood vessel, we can appreciate a different type of heterogeneity within solid tumours which is based upon local environmental conditions. Cells adjacent to the blood vessel have an abundant supply of nutrient and, hence, proliferate freely. As the distance from the vessel increases the local nutrient concentration falls since it is being progressively consumed as it diffuses away from the blood vessel. Eventually a point is reached at which the nutrient concentration becomes so low that the tumour cells there are unable to proliferate, although they have sufficient nutrient to remain alive. These cells are termed quiescent. At greater distances from the vessel, the nutrient concentration may become so low that the quiescent cells are unable to stay alive: they die due to nutrient deprivation, forming a region of necrotic cellular debris. Thus we may characterise tumour cells as (a) proliferating, (b) quiescent, and (c) necrotic or dead. Typically, all three cell types will be present within a vascular

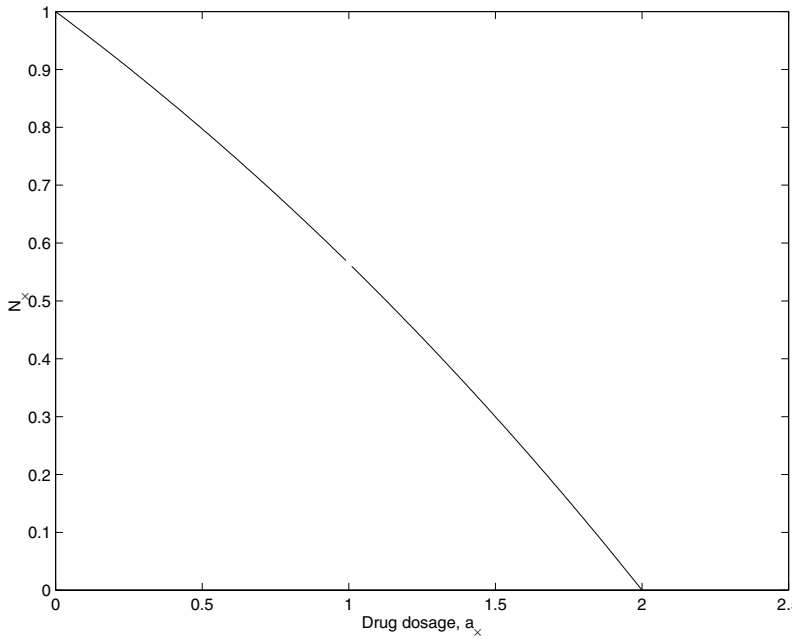

Figure 4.5

Diagram showing how N_∞ varies with a_∞ when periodic solutions emerge. Parameter values: $\theta = 1 = \mu = k, \tau = 0.5$.

tumour and a well-developed avascular tumour [13,26].

In section 4.3 the spatially-structured models that we study enable us to distinguish between these different cell types on the basis of the local nutrient concentration. However, in order to gain some insight into the proportion of each cell type within a tumour (and how this changes as the tumour evolves), we now present a mathematical model in which the three cell types are considered separately.

We denote by $P(t)$ the number of proliferating cells at time t, $Q(t)$ the number of quiescent cells, $D(t)$ the number of dead or necrotic cells, and $N(t) = P(t) + Q(t) + D(t)$ the total number of tumour cells. The schematic diagram presented in Figure 4.6, on which our model is based, illustrates how cells may change from one state to another, how new cells are produced (proliferation) and how dead cells are degraded.

Guided by Figure 4.6, we deduce that our mathematical model may be written as follows

$$\frac{dP}{dt} = (k_{PP} - k_{PQ} - k_{PD})P + k_{QP}Q, \tag{4.13}$$

$$\frac{dQ}{dt} = k_{PQ}P - (k_{QP} + k_{QD})Q, \tag{4.14}$$

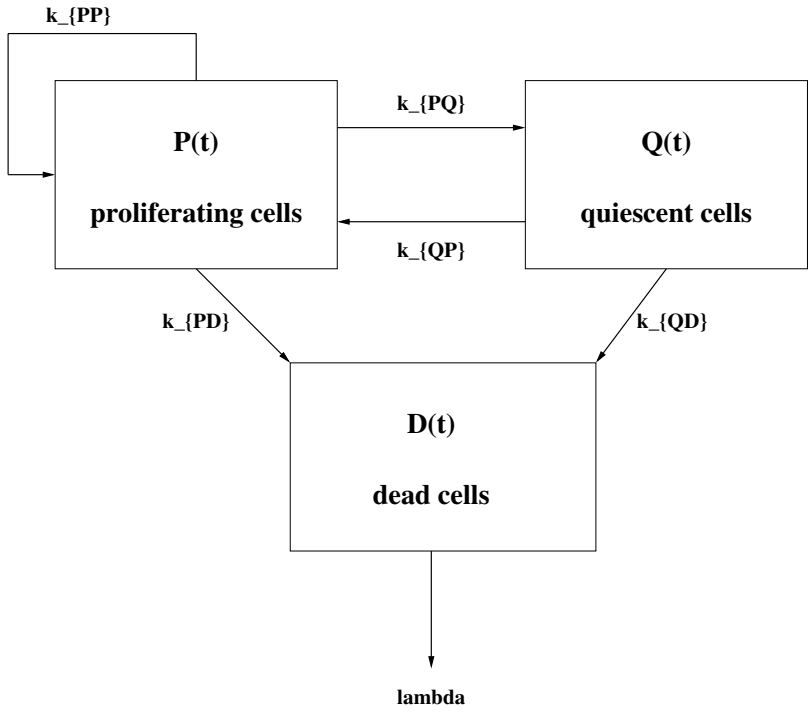

Figure 4.6
Schematic diagram of model of heterogeneous tumour growth.

$$\frac{dD}{dt} = k_{PD}P + k_{QD}Q - \lambda D, \tag{4.15}$$

with

$$P(0) = P_0, \quad Q(0) = Q_0, \quad D(0) = D_0. \tag{4.16}$$

In Equations (4.13) to (4.15), the functions k_{PP} and k_{PQ} represent, respectively, the rate at which proliferating cells produce new cells (these daughter cells are assumed to enter the proliferating state) and the rate at which cells stop proliferating and become quiescent. The interpretation of the other functions follows similarly.

In order to fully specify our model it remains to choose the functions $k_{IJ}(I, J = P, Q, N)$. In practice the rates k_{IJ} depend on the local nutrient level within the tumour. Rather than introducing nutrient as an additional model variable, for simplicity, and by analogy with the competition term that appears in the logistic growth law (see Equation (4.2)), we assume that the transition rates between the proliferating, quiescent, and dead states depend on the total number of cells in the tumour mass and the number of cells in each state. One possible choice of the transition rates is

as follows

$$k_{PP} = \frac{\hat{k}_{PP}}{\hat{N}+N}, \quad k_{PQ} = \frac{\hat{k}_{PQ}P}{\hat{N}+N},$$

$$k_{PD} = \hat{k}_{PD}, \quad k_{QP} = \frac{\hat{k}_{QP}Q}{\hat{N}+N}, \quad k_{QD} = \frac{\hat{k}_{QD}(P+Q)}{\hat{N}+N}, \tag{4.17}$$

with λ, the decay rate of the necrotic cellular material, assumed constant. When these kinetic terms are substituted into Equations (4.13) to (4.15) we observe that our mathematical model comprises a system of coupled differential equations. This system may be studied using the same analytical techniques as those used to investigate the models of sections 4.2.2 and 4.2.3. For example, it is possible to show that if $k_{PD} = 0$ (i.e., if natural cell death is neglected) then Equations (4.13) to (4.15) admit the following equilibrium solutions

$$P = Q = D = 0,$$

or

$$0 = \left(\frac{\hat{k}_{PQ}}{\hat{k}_{QP}} - 1\right) P^2 + \left(\frac{\hat{k}_{QD}^2}{\hat{k}_{PP}\hat{k}_{QP}}\right) \left(1 - \frac{\hat{k}_{PQ}}{\hat{k}_{QP}} - \frac{\hat{k}_{PQ}}{\hat{k}_{QD}}\right) P + \left(1 + \frac{\hat{k}_{QD}}{\hat{k}_{QP}}\right)^2$$

with

$$Q^2 = \frac{(\hat{k}_{PQ}P - \hat{k}_{PP})P}{\hat{k}_{QP}},$$

and

$$0 = D^2 + (\hat{N} + P + Q)D - \frac{\hat{k}_{QD}}{\lambda}(P+Q)Q.$$

We remark that there are at most two nontrivial equilibrium solutions. In practice it is necessary to determine whether the solutions are physically realistic (i.e., P, Q, and D are nonnegative). For example, the expression relating Q to P indicates that physically realistic equilibrium solutions must satisfy $P > \hat{k}_{PP}/\hat{k}_{PQ}$.

As an exercise, the reader is encouraged to determine the linear stability of the different equilibrium solutions.

4.2.5 Discussion

In this section we have presented a range of mathematical models of increasing complexity that may be used to provide insight into the overall growth dynamics of solid tumours. Whilst the models neglect any spatial effects that may be present within the tumour, they can be used to estimate the kinetic parameters from experimental data and to predict or estimate the response to therapy.

There are many ways in which the models that we have studied could be extended. For example, in section 4.3 we present a class of well-studied spatio-temporal

models that reproduce the layered spatial structure that characterises avascular tumours and multicellular spheroids growth *in vitro*.

Another possible extension which enables the action of cell-cycle specific drugs, such as doxorubicin, to be investigated involves introducing a second independent variable $0 < a < T$, say. Then $n(t, a)$ denotes the number of cells at time t which are in position a of their cycle and $N(t)$, the total number of cells at time t, is related to $n(t, a)$ in the following way

$$N(t) = \int_0^T n(t, a)da$$

where, in the absence of therapy, $n(t, a)$ may satisfy the following partial differential equation

$$\frac{\partial n}{\partial t} + \frac{\partial n}{\partial a} = -\mu_0 n - \mu_1 nN,$$

with

$$n(0, a) = n_0(a)$$

and

$$n(t, 0) = \int_0^T \beta(a)n(t, a)da.$$

In the above equations, the constants μ_0 and μ_1 represent rates of natural cell death and cell death due to overcrowding respectively, and $\beta(a)$ denotes the proliferation rate of cells at position a of their cell cycle. Models of this type are termed age-structured models, and their analysis may be quite involved. Further details about models of this form can be found in [19] whereas a more general discussion of age-structured models is presented in [20].

4.3 One-Dimensional Spatial Models of Avascular Tumour Growth

4.3.1 Introduction

The earliest spatially-structured models of avascular tumour growth are due to Burton and Greenspan [3,16]. At this time, biologists were focusing on the effect that changes in the composition of the medium surrounding the tumours had on their growth [13,26]. They recorded the radii of the (approximately radially-symmetric) tumours over time, supplementing their measurements, where possible, with information about the oxygen distribution within the tumours and the proportion of the tumours that were necrotic and hypoxic. Faced with such data, it is not surprising

that the key variables in the corresponding mathematical models are: $R(t)$, the position of the outer tumour radius of the assumed radially-symmetric tumour; $c(r,t)$, the concentration within the tumour of a particular diffusible chemical (this may be a growth factor such as oxygen or glucose or a new anti-cancer drug that is being tested prior to clinical trials); $R_H(t)$, the locus of the boundary separating proliferating and quiescent cells; and $R_N(t)$, the locus of the boundary separating the quiescent and necrotic cells. Since the tumours change in size over time, the domains on which the resulting models are formulated also vary and must be determined as part of the solution process. Consequently, the models that we now study fall within the wider class of moving boundary problems [12].

The outline of this section is as follows. In section 4.3.2 we present in general form the class of moving boundary problems that we use to study avascular tumour growth. In section 4.3.3 we show how, under certain conditions, the models may be reduced to systems of differential equations similar in form to those studied in section 4.2. We indicate the sort of insight that these spatially-structured models can provide by presenting some analytical results in section 4.3.4. The section then concludes with a discussion of the merits and weaknesses of these models.

4.3.2 The Mathematical Model

The simplest models that describe the growth of a radially-symmetric, avascular tumour comprise equations governing the evolution of a single, growth rate limiting, diffusible chemical $c(r,t)$, the outer tumour radius $R(t)$, and the hypoxic and necrotic radii $R_H(t)$ and $R_N(t)$. The principle of mass balance is used to derive equations for $c(r,t)$ and $R(t)$ whereas $R_H(t)$ and $R_N(t)$ are defined implicitly, occurring when the chemical concentration passes through known threshold values. We state the model equations both in words and in mathematics, in order to highlight the connection between the underlying physical assumptions and the mathematical formulation.

The chemical concentration, $c(r,t)$.

$$\begin{pmatrix}\text{rate of change of}\\ \text{chemical concentration}\end{pmatrix} = \begin{pmatrix}\text{flux due to}\\ \text{diffusion}\end{pmatrix} - \begin{pmatrix}\text{rate of chemical}\\ \text{consumption}\end{pmatrix},$$

$$\frac{\partial c}{\partial t} = \frac{D}{r^2}\frac{\partial}{\partial r}\left(r^2\frac{\partial c}{\partial r}\right) - \Gamma(c,R,R_H,R_N). \quad (4.18)$$

In Equation (4.18) D denotes the assumed constant diffusion coefficient of the chemical and $\Gamma(c,R,R_H,R_N)$ its rate of consumption. In practice $\Gamma(c,R,R_H,R_N)$ will be a nonlinear function which depends on the tumour cell line being studied and the chemical of interest. In order to demonstrate the qualitative behaviour of the model we suppose that the chemical is a vital nutrient (e.g., oxygen or glucose) and assume

that it is consumed at a constant rate Γ by proliferating and quiescent cells. Thus we write

$$\Gamma(c, R, , R_H, R_N) = \Gamma H(r - R_N),$$

where $H(.)$ denotes the Heaviside step function ($H(x) = 1$ if $x > 0$ and $H(x) = 0$ otherwise).

The outer tumour radius, $R(t)$.

$$\begin{pmatrix} \text{rate of change of} \\ \text{tumour volume} \end{pmatrix} = \begin{pmatrix} \text{total rate of cell} \\ \text{proliferation} \end{pmatrix} - \begin{pmatrix} \text{total rate of} \\ \text{cell death} \end{pmatrix}, \tag{4.19}$$

$$\frac{1}{3}\frac{d}{dt}(R^3) = R^2\frac{dR}{dt} = \int_0^R S(c, R, R_H, R_N)r^2 dr \; - \; \int_0^R N(c, R, R_H, R_N)r^2 dr.$$

In Equation (4.19), $S(c, R, R_H, R_N)$ and $N(c, R, R_H, R_N)$ denote respectively the rates of cell proliferation and cell death within the tumour. Cell proliferation is assumed to be localised in nutrient-rich regions (where $c_H < c$ or $R_H < r < R$) where it occurs at a rate which is proportional to the local nutrient concentration c. We assume that apoptosis and necrosis contribute to the overall cell death rate, with apoptosis occurring at a constant rate throughout the tumour and necrosis being initiated in nutrient-poor regions (where $c < c_N$ or $r < R_N$). Thus, as simple representative examples, we write

$$S(c, R, R_H, R_N) = scH(r - R_H) \text{ and } N(c, R, R_H, R_N) = s\lambda_A + s\lambda_N H(R_N - r),$$

where s, λ_A and λ_N are positive constants. Substituting with S and N in Equation (4.19) yields

$$\frac{1}{s}R^2\frac{dR}{dt} = \int_{R_H}^R cr^2 dr - \frac{1}{3}(\lambda_A R^3 + \lambda_N R_N^3). \tag{4.20}$$

The hypoxic and necrotic boundaries, $R_H(t)$ *and* $R_N(t)$.

$$\left.\begin{array}{ll} c(r,t) > c_H & \forall\ r \in (0, R) \Rightarrow R_N = R_H = 0, \\ \exists\ r \in (0, R(t)) & \text{such that } c_N < c(r,t) \le c_H \Rightarrow R_N = 0 < R_H < R \\ & \text{with } c(R_H, t) = c_H, \\ \exists\ r \in (0, R(t)) & \text{such that } c(r,t) \le c_N < c_H \Rightarrow 0 < R_N < R_H < R \\ & \text{with } c(R_N, t) = c_N \text{ and } c(R_H, t) = c_H. \end{array}\right\} \tag{4.21}$$

In Equations (4.21), the internal free boundaries $R_H(t)$ and $R_N(t)$ are defined implicitly in terms of threshold nutrient concentrations c_H and c_N. These constants

denote respectively the minimum nutrient concentration at which cell proliferation can occur and the maximum nutrient concentration at which necrosis occurs. In Figure 4.7 we provide a schematic diagram to illustrate the structure of a well-developed avascular tumour which possesses a central necrotic core and a hypoxic region.

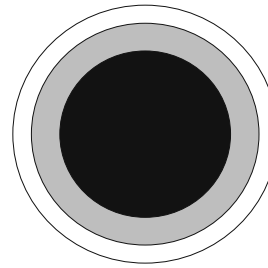

Figure 4.7

Schematic diagram of a fully-developed avascular tumour. The central region represents the necrotic core (where $c(r,t) \leq c_N$), the middle annulus represents the hypoxic region (where $c_N < c(r,t) \leq c_H$), and the outer rim represents the proliferating region (where $c_H < c(r,t)$).

We close the model equations by prescribing the following boundary and initial conditions

$$\left.\begin{array}{c} \dfrac{\partial c}{\partial r} = 0 \quad \text{at } r = 0, \\ c = c_\infty \quad \text{on } r = R(t), \\ c,\ \dfrac{\partial c}{\partial r} \text{ continuous across } r = R_H(t) \text{ and } r = R_N(t), \\ c(r,0) = c_0(r),\ R(t=0) = R_0. \end{array}\right\} \tag{4.22}$$

In Equations (4.22) c_∞ is the assumed constant nutrient concentration external to the tumour, $c_0(r)$ is the initial nutrient distribution within the tumour when $R = R_0$. Thus we impose symmetry of the nutrient profile about $r = 0$, we fix the nutrient concentration on the outer tumour boundary and prescribe the initial nutrient concentration and tumour radius.

Nondimensionalisation

Before continuing with an analysis of the model equations, it is appropriate to recast them in terms of dimensionless variables. Denoting by C, X, and T typical nutrient concentrations, lengthscales and timescales respectively, we introduce the following dimensionless variables

$$c^* = \frac{c}{C}, \quad r^* = \frac{r}{X}, \quad t^* = \frac{t}{T}, \quad R^* = \frac{R}{X}, \quad R_H^* = \frac{R_H}{X}, \quad R_N = \frac{R_N}{X}.$$

When written in terms of c^*, r^*, etc., our model equations become

$$\frac{\partial c^*}{\partial t^*} = \left(\frac{DT}{X^2}\right)\frac{1}{r^{*^2}}\frac{\partial}{\partial r^*}\left(r^{*^2}\frac{\partial c^*}{\partial r^*}\right) - \Gamma T H(r^* - R_N^*),$$

$$R^{*^2}\frac{dR^*}{dt^*} = \int_0^{R^*}\left\{sTCc^*H(r^* - R_N^*) - sT\lambda_A - sT\lambda_N H(R_N^* - r^*)\right\} r^{*^2}\, dr^*.$$

At this stage, our choice of the scalings (C, X, T) remains unspecified. We base our choice of C and X on typical experimental measurements. For example, if oxygen is the nutrient of interest then $C \sim 10\%$ and, for an avascular tumour, $X \sim 1$mm. We remark that there are several timescales implicit in the model equations. These include:

- The nutrient diffusion timescale, X^2/D
- The tumour doubling timescale, $1/sC$
- The nutrient consumption timescale, $1/\Gamma$

In practice, experimental parameter estimates indicate that

$$\begin{pmatrix}\text{nutrient diffusion timescale, } X^2/D\\ \sim \text{ mins or hours}\end{pmatrix} \ll \begin{pmatrix}\text{tumour doubling timescale, } 1/sC\\ \sim \text{ weeks}\end{pmatrix}.$$

Since we wish to simulate changes in the tumour's spatial structure, we focus on the longer timescale, choosing

$$T = \frac{1}{sC}.$$

In addition, we make the following quasi-steady assumption in the nutrient equation

$$O(\Gamma) = O(\frac{D}{X^2}) \gg O(T^{-1}).$$

This equation then reduces to give

$$0 = \frac{1}{r^{*^2}}\frac{\partial}{\partial r^*}\left(r^{*^2}\frac{\partial c^*}{\partial r^*}\right) - \Gamma^* H(r^* - R_N^*),$$

$$\text{where} \quad \Gamma^* = \frac{\Gamma X^2}{D} \sim O(1).$$

We now state, in full, our nondimensionalised model equations

$$0 = \frac{1}{r^{*^2}}\frac{\partial}{\partial r^*}\left(r^{*^2}\frac{\partial c^*}{\partial r^*}\right) - \Gamma^* H(r^* - R_N^*),$$

$$R^{*^2}\frac{dR^*}{dt^*} = \int_0^{R^*}\left\{c^*H(r^* - R_N^*) - \lambda_A^* - \lambda_N^* H(R_N^* - r^*)\right\} r^{*^2}\, dr^*,$$

$$R_H^* = 0 \text{ if } c^* > c_H^* \ \forall\ r \text{ and otherwise } c^*(R_H^*, t^*) = c_H^*,$$
$$R_N^* = 0 \text{ if } c^* > c_N^* \ \forall\ r \text{ and otherwise } c^*(R_N^*, t^*) = c_N^*,$$
$$\frac{\partial c^*}{\partial r^*} = 0 \quad \text{at } r^* = 0,$$
$$c^* = c_\infty^* \quad \text{on } r^* = R^*,$$
$$R^*(0) = R_0^*, \text{ prescribed,}$$

$$\text{where} \quad \Gamma^* = \frac{\Gamma X^2}{D}, \quad \lambda_A^* = \frac{\lambda_A}{C}, \quad \lambda_N^* = \frac{\lambda_N}{C},$$
$$c_\infty^* = \frac{c_\infty}{C}, \quad c_H^* = \frac{c_H}{C}, \quad c_N^* = \frac{c_N}{C}.$$

Henceforth, we omit the $*$s for clarity.

We remark that, by choosing $C = c_\infty$, we could have eliminated c_∞ from the model equations. Since we want to investigate the effect of varying c_∞, we choose to retain c_∞ as an explicit model parameter. For similar reasons, we choose not to scale lengths with R_0.

4.3.3 Model Simplification

Using the simple functional forms that appear in our model equations, we may construct analytical expressions for c in terms of R, R_H, and R_N and algebraic equations that define the free boundaries R_H and R_N in terms of R. The evolution of $R(t)$ is, in turn, governed by a nonlinear differential equation. At any given time, the form of these relations depends on the current value of $R(t)$, this value indicating whether the tumour contains regions of hypoxia or necrosis.

When $0 < R^2(t) < 6(c_\infty - c_H)/\Gamma$, it is possible to show that

$$c(r,t) = c_\infty - \frac{\Gamma}{6}(R^2 - r^2),$$
$$\frac{dR}{dt} = \frac{R}{3}\left(c_\infty - \frac{\Gamma R^2}{15} - \lambda_A\right), \tag{4.23}$$
$$\text{with} \quad R_N = 0 = R_H.$$

Thus, for this range of R, the tumour contains only proliferating cells.

When $6(c_\infty - c_H)/\Gamma < R^2(t) < 6(c_\infty - c_N)/\Gamma$, we have

$$c(r,t) = c_\infty - \frac{\Gamma}{6}(R^2 - r^2),$$
$$\frac{dR}{dt} = \frac{R}{3}\left[\left(c_\infty - \frac{\Gamma R^2}{6}\right)\left(1 - \frac{R_H^3}{R^3}\right) + \frac{\Gamma R^2}{10}\left(1 - \frac{R_H^5}{R^5}\right) - \lambda_A\right], \tag{4.24}$$

$$\text{with} \quad R_N = 0 \quad \text{and} \quad R_H^2 = R^2 - \frac{6}{\Gamma}(c_\infty - c_H). \tag{4.25}$$

Hence, for this range of R, the tumour contains a central quiescent or hypoxic region which is surrounded by an outer proliferating rim.

When $6(c_\infty - c_N)/\Gamma < R^2$, it is possible to show that

$$c(r,t) = \begin{cases} c_N & 0 < r < R_N \\ c_N + \Gamma(r - R_N)^2(r + 2R_N)/6r & R_N < r < R \end{cases},$$

$$\frac{dR}{dt} = \frac{R}{3}\left[c_N\left(1 - \frac{R_H^3}{R^3}\right) - \left(\lambda_A + \lambda_N \frac{R_N^3}{R^3}\right)\right] \tag{4.26}$$

$$+ \frac{\Gamma R^3}{6}\left[\frac{1}{5}\left(1 - \frac{R_H^5}{R^5}\right) - \frac{R_N^2}{R^2}\left(1 - \frac{R_H^3}{R^3}\right) + \frac{R_N^3}{R^3}\left(1 - \frac{R_H^2}{R^2}\right)\right], \tag{4.27}$$

$$\text{with} \quad \left(1 - \frac{R_N}{R}\right)^2\left(1 + \frac{2R_N}{R}\right) = \frac{6}{\Gamma R^2}(c_\infty - c_N), \tag{4.28}$$

$$\text{and} \quad \left(1 - \frac{R_N}{R_H}\right)^2\left(1 + \frac{2R_N}{R_H}\right) = \frac{6}{\Gamma R_H^2}(c_H - c_N). \tag{4.29}$$

In this case, the tumour is fully developed, containing a central necrotic core, an intermediate hypoxic annulus and an outer proliferating rim.

In the next section we use the above results to make a number of predictions about the tumour's growth. In particular, we investigate how the tumour's spatial structure is affected by model parameters such as the rate at which the tumour cells consume nutrient and the threshold concentrations at which quiescence and necrosis are initiated.

Before continuing we remark that by differentiating with respect to time the algebraic expressions for R_H and R_N our model may be reduced to systems of coupled differential equations which are similar in form to those studied in section 4.2. For example, if $6(c_\infty - c_H)/\Gamma < R^2 < 6(c_\infty - c_H)/\Gamma$ then we obtain the following differential equations for $R(t)$ and $R_H(t)$

$$\frac{dR}{dt} = \frac{R}{3}\left[\left(c_\infty - \frac{\Gamma R^2}{6}\right)\left(1 - \frac{R_H^3}{R^3}\right) + \frac{\Gamma R^2}{10}\left(1 - \frac{R_H^5}{R^5}\right) - \lambda_A\right],$$

$$\frac{dR_H}{dt} = \frac{R}{R_H}\frac{dR}{dt}.$$

Since $0 < R_H < R$ we deduce that $|\frac{dR_H}{dt}| > |\frac{dR}{dt}|$ i.e., if the tumour contains a quiescent region $R_H(t)$ evolves more rapidly than $R(t)$. We note also that when the outer tumour radius is expanding (i.e., $\frac{dR}{dt} > 0$) so is the quiescent boundary.

4.3.4 Model Predictions

Setting $d/dt = 0$ in Equation (4.23) we deduce that the tumour will evolve to a steady state that is devoid of quiescent and necrotic cells and has $R^2 = 15(c_\infty - \lambda_A)/\Gamma$ provided that this is a valid solution i.e., quiescence has not been initiated. This will be the case if, at equilibrium, $c > c_H \ \forall r \in (0, R)$. Using the expression for the nutrient concentration it is possible to show that this will be the case provided that

$$c_\infty - c_H > \frac{5}{2}(c_\infty - \lambda_A).$$

This inequality shows how the rates of proliferation and apoptosis of the tumour cells must be inter-related in a tumour which, at equilibrium, has no quiescence or necrosis.

Using Equation (4.23) it is also possible to show that the tumour volume $V(t) = 4\pi R^3(t)/3$ satisfies the following growth law

$$\frac{dV}{dt} = V\left[c_\infty - \lambda_A - \frac{\Gamma}{15}\left(\frac{3V}{4\pi}\right)^{2/3}\right]$$

or, equivalently,

$$\frac{dV}{dt} = \frac{kV}{\alpha}\left[1 - \left(\frac{V}{\theta}\right)^{\alpha}\right],$$

$$\text{where} \quad \alpha = \frac{2}{3}, \quad k = \frac{2}{3}(c_\infty - \lambda_A), \quad \theta = \frac{4\pi}{3}\left[\frac{15}{\Gamma}(c_\infty - \lambda_A)\right]^{3/2}.$$

This result shows how the spatially-structured models that we are studying relate to the spatially-averaged models of section 4.2 and, in particular, how the growth of a uniformly proliferating tumour may be described by model 3 of section 4.2. By making this comparison between the two models we can also see how local parameters associated with the spatially-structured model relate to the spatially-averaged parameters that appear in the spatially-uniform models.

We commented above that the kinetic terms that we employ are overly simplistic and should be replaced by experimentally-determined functions. In general, these functions will be nonlinear and the resulting models will not admit analytical solutions: they must be solved numerically. Whilst numerical simulations are of tremendous value, they may obscure the manner in which the various mechanisms interact. Complementary insight into the system's behaviour can be gained by studying special cases for which the model equations simplify greatly [7]. We sketch below how this may be achieved by focusing on three, physically-relevant cases:

1. Small tumour analysis ($0 < R \ll 1$);
2. Tumour behaviour near the onset of necrosis ($0 < R_N \ll R \sim O(1)$); and
3. Well-developed tumours, with thin proliferating rims ($0 < R - R_N \ll 1$).

In order to simplify the analysis, we assume further that the transition from quiescence to necrosis is very rapid and hence that $c_H = c_N$ and $R_H = R_N$.

4.3.4.1 Small Tumour Analysis, $0 < R \ll 1$

If $R_N = 0$ and $0 < R \ll 1$ then $c \sim c_\infty \ \forall \ r \in (0, R)$ and, by solving Equation (4.23) to leading order in R, we deduce that $R(t)$ satisfies

$$R(t) \sim R(0) \exp\left(\frac{(c_\infty - \lambda_A)t}{3}\right).$$

Thus, when the tumour is small, the nutrient is uniformly distributed within the tumour volume and its growth rate depends on the balance between the rate of cell loss due to apoptosis and the rate of cell proliferation, the latter effect being regulated by the external nutrient concentration, c_∞. In particular, if $c_\infty < \lambda_A$ then the tumour is not being supplied with enough nutrient to grow, and it will regress to the tumour-free solution $R = 0$ which is linearly stable (see section 4.2). Similarly, if $c_\infty > \lambda_A$ then sufficient nutrient is being supplied for tumour growth to occur: in this case the trivial solution $R = 0$ is unstable.

4.3.4.2 Tumour Behaviour near the Onset of Necrosis, $0 < R_N \ll R \sim O(1)$

In order to study this behaviour we assume that

$$R \sim R_0 + \epsilon R_1 + \epsilon^2 R_2 \quad \text{and} \quad R_N \sim \epsilon R_{N1} \qquad (\epsilon \ll 1).$$

Substituting with the expressions above in Equation (4.28) and equating coefficients of $O(\epsilon)$ we deduce that

$$R_0^2 = \frac{6(c_\infty - c_N)}{\Gamma}, \quad R_1 = 0, \quad R_2 = \frac{3R_{N1}^2}{2R_0},$$

where $R = R_0$ when necrosis is initiated. These results indicate that when the necrotic core is small, temporal variations in $R(t)$ are smaller than variations in $R_N(t)$. Substituting for R_2 and R_N in Equation (4.26) yields a differential equation for R_2 which is singular in the limit as $\epsilon \to 0$. We regularise this equation by introducing a short timescale $\tau = t/\epsilon^2$ and obtain

$$R_2(\tau) = R_2(\tau = 0) + R_0 \left(\frac{1}{5}(c_\infty - c_N) - \frac{1}{3}(\lambda_A - c_N)\right)\tau.$$

Using the above expression for $R_2(\tau)$ we deduce that the necrotic core persists if $c_\infty > c_N + 5(\lambda_A - c_N)/3$ and otherwise it will disappear at time $\tau = \tau^*$ where

$$\tau^* = R_2(\tau = 0) / \left\{ R_0 \left[\frac{1}{5}(c_\infty - c_N) - \frac{1}{3}(\lambda_A - c_N)\right] \right\}.$$

For a particular set of experiments, involving a particular tumour cell line and for which c_∞ is known, we can use these results to relate some of the parameters governing the tumour cells' proliferation and death rates. For example, if the spheroids contain a necrotic core then we deduce that $c_\infty > c_N + 5(\lambda_A - c_N)/3$.

The above analysis also provides some insight into the way in which the tumour's volume and spatial structure change when the necrotic core is very small. Since temporal variations in $R(t)$ are much smaller than variations in $R_N(t)$ ($O(\epsilon^2)$ rather than $O(\epsilon)$), we deduce that the necrotic core evolves rapidly while the overall tumour volume remains approximately constant. These predictions are consistent with independent experimental observations of multicell spheroids grown *in vitro* [18].

4.3.4.3 Well-Developed Tumours, with Thin Proliferating Rims, $R - R_N \ll 1$

We assume that R_N is related to R in the following way

$$R - R_N = \delta R_{N1} + O(\delta^2),$$

where the small parameter $0 < \delta \ll 1$ characterises the width of the proliferating rim. Substituting with these expression in Equation (4.28) and equating to zero coefficients of $O(\delta)$ we deduce that

$$c_\infty - c_N \sim \frac{\Gamma}{2}(\delta R_{N1})^2 = \frac{\Gamma}{2}(R - R_N)^2$$

and

$$\frac{dR}{dt} = -\frac{1}{3}(\lambda_A + \lambda_N)R + \delta(c_N + \lambda_N)R_{N1} + O(\delta^2).$$

Solving for $R(t)$, we deduce that

$$R(t) \to R_\infty \equiv \frac{3\delta(c_N + \lambda_N)R_{N1}}{(\lambda_A + \lambda_N)} \quad \text{as} \quad t \to \infty.$$

Assuming that $c_N, R_{N1} \sim O(1)$, we deduce further that $R_\infty \sim O(\delta/(\lambda_A + \lambda_N))$. In particular, if experimental measurements of the tumour radius at equilibrium indicate that $R_\infty \sim O(1)$ we deduce that $\lambda_A + \lambda_N \sim O(\delta)$. Combining the above results, we deduce that there are two necessary conditions for realising growth-saturated avascular tumours which possess thin proliferating rims and have

$$R_\infty \sim O(1), \qquad c_\infty = c_N + O(\delta), \quad \text{and} \quad \lambda_A + \lambda_N \sim O(\delta).$$

The constraints on λ_A and λ_N are tumour-cell specific whereas the constraint on c_∞ can be realised by choosing the external nutrient concentration appropriately.

4.3.5 Discussion

Before developing more complex models, we reflect upon the insight gained from the simple, radially-symmetric models studied in this section. The models can be used to identify conditions under which a tumour will grow to an equilibrium configuration and to show how its size, spatial structure, and stability to time-dependent

perturbations depend upon physically relevant parameters such as the externally-supplied nutrient concentration c_∞. The model can be used to predict conditions under which certain equilibrium configurations will be realised e.g., a necessary condition for obtaining a tumour with a thin proliferating rim is that the external nutrient concentration be approximately equal to that at which necrosis is initiated (i.e., $c_\infty \approx c_N$).

There are many ways in which the model presented above could be extended. For example, we could use experimentally-determined functions for the rates of cell proliferation, apoptosis, and necrosis. Equally, we could include additional diffusion equations to describe the action of other diffusible growth factors which may be present in the tumour environment. These chemicals, which may be supplied externally or expressed by the tumour cells themselves, may promote or inhibit the tumour's growth. For example, by-products of the cell degradation process that accompanies necrosis are believed to inhibit cell proliferation. Models of this type are studied in [6]. A further model extension which provides a simplistic description of vascular tumour growth involves including a distributed source of nutrient (or a distributed sink of waste products) in the outer portion of the tumour: the distributed source means that nutrients may be supplied to the tumour either by exchange with its vasculature or by diffusion across the tumour's outer boundary. For details of models of this type refer to [21].

Given that avascular tumours are usually radially-symmetric and vascular tumours possess highly irregular boundaries, it is natural to ask whether this change in morphology is due to the nonuniform distribution of blood vessels that accompanies vascularisation or whether the radially symmetric avascular tumours are themselves unstable to asymmetric perturbations. Although the spatially-structured models presented in this section are not amenable to such analysis, in the next section we show how they can be extended to address this important question.

4.4 Asymmetric Growth of Avascular Tumours

4.4.1 Introduction

In this section we show how the one-dimensional models of avascular tumour growth presented in section 4.3 may be modified in order to study growth in two and three dimensions. The approach we adopt was originally developed by Greenspan [17] and involves the introduction of new variables that describe the local cell velocity and pressure within the tumour. We motivate the inclusion of pressure and velocity into the model in the following way. Suppose that the tumour is incompressible and contains no voids or holes. Then cell proliferation and death will generate spatial variations in the pressure within the tumour and these will drive cell motion, with

cells moving away from regions of high pressure (i.e., net cell proliferation) towards regions of lower pressure (i.e., net cell death). We also introduce surface tension effects into the model: such restraining forces maintain the tumour's compactness and counteract the expansive force caused by net cell proliferation.

The remainder of this section is organised in the following way. The model that we study is presented in section 4.4.2. In section 4.4.3 we show how the model reduces to the one-dimensional models of section 4.3 when growth is assumed to be one-dimensional. The stability of steady, radially-symmetric solutions to symmetry-breaking perturbations is investigated in section 4.4.4 using linear stability analysis. The section concludes in section 4.4.5 with a brief discussion of the strengths and weaknesses of the models.

4.4.2 The Model Equations

The mathematical model that we study is presented below in dimensionless form (for details of the nondimensionalisation process, refer to [6]). For simplicity we assume that there is no central necrosis within the tumour volume (i.e., the tumour is small enough that all cells are nutrient-rich and proliferating). The key physical variables are assumed to be the nutrient concentration $c(\boldsymbol{r}, t)$, the cell velocity $\boldsymbol{v}(\boldsymbol{r}, t)$, and the pressure $p(\boldsymbol{r}, t)$. The locus of the tumour boundary is represented by the surface $\Gamma(\boldsymbol{r}, t) = 0$ (the precise details of this surface depend on the geometry under consideration). The evolution of $c, \boldsymbol{v}$, and p is determined by the following system of partial differential equations

$$0 = \nabla^2 c - \Gamma, \tag{4.30}$$

$$\nabla \cdot \boldsymbol{v} = S(c) - N(c) \equiv c - \lambda_A, \tag{4.31}$$

$$\boldsymbol{v} = -\mu \nabla p. \tag{4.32}$$

Equation (4.30) is the natural extension in higher spatial dimensions of the diffusion equation that was used in section 4.3. Equation (4.31) expresses mass balance within the tumour when it is viewed as an incompressible fluid. To reinforce the similarity with the models discussed in section 4.3, we use the same proliferation and death rates as adopted there. We view the tumour as a porous medium and, hence, use Darcy's law to relate the velocity of the cells moving throughout the tumour to the pressure, the constant of proportionality μ denoting the sensitivity of the tumour cells to pressure gradients. More details on porous media models for growing tumours are given in Chapter 5.

We remark that Equations (4.31) and (4.32) may be combined to eliminate $\boldsymbol{v}$ from the model equations, giving

$$0 = \mu \nabla^2 p + (c - \lambda_A). \tag{4.33}$$

We append to Equations (4.30) and (4.33) the following boundary and initial conditions

$$c = c_\infty, \quad p = \gamma \kappa \quad \text{on} \quad \Gamma(\boldsymbol{r}, t) = 0, \tag{4.34}$$

$$\frac{\partial c}{\partial r} = \frac{\partial p}{\partial r} = 0 \quad \text{at} \quad \boldsymbol{r} = 0. \tag{4.35}$$

In (4.34) c_∞ and $p_\infty = 0$ are the assumed constant nutrient concentration and pressure outside the tumour, $\gamma \geq 0$ is the surface tension coefficient, and κ the mean curvature of the tumour boundary. Thus Equations (4.34) state that the nutrient concentration is continuous across the tumour boundary and that there is a jump discontinuity in the pressure, this jump being proportional to the curvature of the boundary (and playing the role of a surface tension force which maintains the tumour's compactness). Equation (4.35) guarantees that the nutrient and pressure profiles are bounded at the origin.

In order to complete our model, it remains to determine how the tumour boundary $\Gamma(\boldsymbol{r}, t) = 0$ evolves. Since in this section we focus on spherical geometry, we write $\boldsymbol{r} = (r, \theta)$ and parameterise the tumour boundary in the following way

$$\Gamma(\boldsymbol{r}, t) = 0 = r - R(\theta, t).$$

We assume further that the boundary moves with the local cell velocity so that

$$\frac{\partial R}{\partial t} = \boldsymbol{v} \cdot \boldsymbol{n} = -\mu \nabla p \cdot \boldsymbol{n}, \qquad \text{with} \quad R(\theta, 0) = R_0(\theta). \tag{4.36}$$

In Equation (4.36), $\boldsymbol{n}$ represents the unit outward normal to the tumour boundary, and we have prescribed $\Gamma(\boldsymbol{r}, 0) = 0$, the initial locus of the tumour boundary.

In summary, our model of solid tumour growth comprises Equations (4.30), (4.33), and (4.36) which we solve subject to (4.34) and (4.35).

4.4.3 Radially-Symmetric Model Solutions

Under radial symmetry, $c = c(r, t), p = p(r, t)$, and $r = R(t)$ on the tumour boundary, and the model equations reduce to give

$$0 = \frac{1}{r^2}\frac{\partial}{\partial r}\left(r^2 \frac{\partial c}{\partial r}\right) - \Gamma,$$

$$0 = \frac{\mu}{r^2}\frac{\partial}{\partial r}\left(r^2 \frac{\partial p}{\partial r}\right) + (c - \lambda_A),$$

$$\frac{dR}{dt} = -\mu \frac{\partial p}{\partial r}\bigg|_{r=R(t)}.$$

Integrating the equation for p once with respect to r and imposing (4.35), we deduce that

$$-\mu \frac{\partial p}{\partial r} = \frac{1}{r^2}\int_0^r (c - \lambda_A)\rho^2 d\rho \;\Rightarrow R^2 \frac{dR}{dt} = \int_0^R (c - \lambda_A) r^2 dr\,.$$

This expression for $R(t)$ is equivalent to Equation (4.19) of section 4.3 when $R_N = 0$ and shows how the current model reduces to the original model under radial symmetry.

As in section 4.3, we can integrate the equations for c and p to obtain the following expressions for the nutrient concentration and pressure distribution in terms of $R(t)$

$$c(r,t) = c_\infty - \frac{\Gamma}{6}(R^2 - r^2),$$

$$p(r,t) = \frac{\gamma}{R} - \frac{\Gamma}{120\mu}(R^2 - r^2)^2 + \frac{1}{6\mu}\left(c_\infty - \lambda_A - \frac{\Gamma R^2}{15}\right)(R^2 - r^2).$$

Further

$$\frac{dR}{dt} = \frac{R}{3}\left(c_\infty - \lambda_A - \frac{\Gamma R^2}{15}\right).$$

In the next section, we investigate what happens when these radially-symmetric solutions are subjected to small, symmetry-breaking perturbations, so that, for example,

$$c \sim c_0(r,t) + \epsilon c_1(r,\theta,t), \qquad \text{where } \epsilon \ll 1.$$

As with the linear stability analysis of section 4.3, our aim is to identify conditions under which the perturbations grow over time and conditions under which they regress. In the former case the underlying, radially-symmetric solution is said to be unstable to symmetry-breaking perturbations and in the latter it is stable.

4.4.4 Linear Stability Analysis

To minimise the complexity of the analysis, we assume that the underlying radially-symmetric solution has reached its steady-state configuration, so that

$$(c_0, p_0, R_0) = (c_0(r), p_0(r), R_0)$$

where, from section 4.4.3,

$$c_0 = c_\infty - \frac{\Gamma}{6}(R_0^2 - r^2), \quad p_0 = \frac{\gamma}{R_0} - \frac{s\Gamma}{120\mu}(R_0^2 - r^2)^2,$$

$$\text{and} \qquad R_0^2 = \frac{15}{\Gamma}(c_\infty - \lambda_A). \tag{4.37}$$

We determine the response to symmetry-breaking perturbations by introducing the small parameter $\epsilon \ll 1$ and seeking solutions to Equations (4.30), (4.33), (4.36), (4.34), and (4.35) of the form

$$\left.\begin{aligned} c &\sim c_0(r) + \epsilon c_1(r,\theta,t), \\ p &\sim p_0(r) + \epsilon p_1(r,\theta,t), \\ R &\sim R_0 + \epsilon R_1(\theta,t). \end{aligned}\right\}$$

Substituting with the above trial solutions in the governing equations and equating coefficients of $O(\epsilon)$ we deduce that (c_1, p_1, R_1) solve

$$0 = \nabla^2 c_1 = \nabla^2 p_1 + c_1, \tag{4.38}$$

$$\frac{\partial R_1}{\partial t} = -\mu \left[\frac{\partial p_1}{\partial r} + R_1 \frac{d^2 p_0}{dr^2} \right]_{r=R_0}, \tag{4.39}$$

$$\text{with} \quad \frac{\partial c_1}{\partial r} = \frac{\partial p_1}{\partial r} = 0 \quad \text{at} \ \ r = 0, \tag{4.40}$$

$$c_1 = -R_1 \left. \frac{dc_0}{dr} \right|_{r=R_0}, \tag{4.41}$$

$$p_1 = -R_1 \left. \frac{dp_0}{dr} \right|_{r=R_0} - \frac{\gamma}{R_0^2} (2R_1 + \mathcal{L}(R_1))_{r=R_0}, \tag{4.42}$$

$$R_1(\theta, 0) = R_{10}(\theta), \quad \text{prescribed.} \tag{4.43}$$

In (4.42), we denote by $\mathcal{L}(\cdot)$ the θ-dependent component of the Laplacian operator

$$\nabla^2 f(r,\theta) = \frac{1}{r^2}\frac{\partial}{\partial r}\left(r^2 \frac{\partial f}{\partial r}\right) + \frac{\mathcal{L}(f)}{r^2} \quad \text{where} \quad \mathcal{L}(f) = \frac{1}{\sin\theta}\frac{\partial}{\partial \theta}\left(\sin\theta \frac{\partial f}{\partial \theta}\right).$$

We have used results presented in section 4.6.3 to determine the $O(\epsilon)$ contributions to the curvature on the tumour boundary and the normal derivative of the pressure there (see Equations (4.47) and (4.50)). We seek separable solutions to Equations (4.38) to (4.43) of the form

$$\begin{aligned} c_1(r,\theta,t) &= \chi_k(t) r^k P_k(\cos\theta), \\ p_1(r,\theta,t) &= \left(\pi_k(t) - \frac{\chi_k r^2}{2\mu(2k+3)}\right) r^k P_k(\cos\theta), \\ R_1(\theta,t) &= \rho_k(t) P_k(\cos\theta), \end{aligned} \tag{4.44}$$

where the Legendre polynomials $P_k(\cos\theta)$ satisfy $\mathcal{L}(P_k) = -k(k+1)P_k$ so that $\nabla^2(r^k P_k) = 0$. We remark that Equation (4.40) is automatically satisfied by our choice of c_1 and p_1.

Expressions relating the coefficients χ_k and π_k to ρ_k are obtained by imposing conditions (4.42) and exploiting the orthogonality of the Legendre polynomials. In this way we deduce that

$$\chi_k R_0^k = -\frac{\Gamma R_0}{3}\rho_k$$

and

$$\pi_k R_0^k = \frac{\gamma \rho_k}{2R_0^2}(k-1)(k+2) + \frac{\chi_k R_0^{k+2}}{2\mu(2k+3)}.$$

Substituting with these results in (4.39) we deduce that

$$\frac{1}{\rho_k}\frac{d\rho_k}{dt} = (k-1)\left(\frac{2\Gamma R_0^2}{15(2k+3)} - \frac{\gamma\mu}{2R_0^3}k(k+2)\right). \tag{4.45}$$

From (4.45) we note that all modes evolve independently i.e., there is no coupling between the modes. Also, the system is insensitive to perturbations involving

$P_1(\cos\theta)$. This is to be expected since the Legendre polynomial $P_1(\cos\theta)$ corresponds simply to a translation of the coordinate axes. We note also that when surface tension effects are neglected ($\gamma = 0$) then the radially-symmetric steady state is unstable to all modes for which $k \geq 2$. More generally, if $\gamma > 0$ then the steady state is unstable to only a finite number of modes, those for which

$$k(k+2)(2k+3) < \frac{4\Gamma R_0^5}{15\mu\gamma}.$$

Since the steady state radius R_0 is defined in terms of the system parameters (see Equation (4.37)), this result shows how the choice of parameter values influences the modes to which the steady state is unstable. We note also that as γ increases the number of unstable modes declines. In particular, if $2\Gamma R_0^5/15\mu\gamma < 15$ there are no integers which satisfy the above inequality and, consequently, that the radially symmetric steady state is stable to perturbations involving Legendre polynomials of arbitrary order. Recalling that $\Gamma R_0^2 = 15(c_\infty - \lambda_A)$, we deduce that this will be the case if the external nutrient concentration c_∞ satisfies

$$c_\infty < \lambda + \frac{\Gamma}{15}\left(\frac{225\mu\gamma}{4\Gamma}\right)^{2/5}.$$

By differentiating (4.45) with respect to k we may determine the fastest growing mode for a given set of parameter values (and, hence, for a given value of R_0). After some manipulation, we deduce that the fastest growing mode satisfies

$$(2k+3)^2(3k^2+2k-2) = \frac{4\Gamma R_0^5}{3\mu\gamma}.$$

4.4.5 Discussion

The analysis presented above provides a mechanism which may explain how the irregular morphology that characterises certain solid tumours may be initiated. To understand this, consider a uniform cluster of tumour cells for which the surface tension coefficient γ is sufficiently large that the underlying radially symmetric solution is stable to all Legendre polynomials. Our analysis predicts that such a cluster will remain radially symmetric throughout the tumour's development. Suppose that there is a mutation which leads to a reduction in γ i.e., the surface tension forces holding the tumour cells together are weakened. If the reduction in γ is large enough then the tumour will become unstable to a finite range of asymmetric modes and will develop an asymmetric morphology.

We stress that the above mechanism is only one possible explanation for why solid tumours develop irregular, fractal-like morphologies. In practice, the acquisition of a blood supply, as a result of angiogenesis, may also destroy the tumour's radial symmetry, by making the nutrient supply rate spatially heterogeneous, and

hence stimulating nonuniform growth. Whilst there are now a number of realistic models of angiogenesis and vascular tumour growth, the development of mathematical models with the power to investigate the potential for vascularisation to stimulate asymmetric tumour growth remains to be developed.

There are, of course, many alternative model modifications that may be studied. The exercises at the end of this section are designed to introduce the reader to some of the extensions which have been documented in the literature. These include a consideration of more general perturbations involving spherical harmonics $Y_{km}(\theta, \phi)$, other geometries and a study of the stability of radially-symmetric avascular tumours that contain a necrotic core to asymmetric perturbations.

The model that we have studied assumes that there is a single rate-limiting nutrient or chemical within the tumour environment. In practice, the tumour will be bathed in a variety of chemicals, some of which promote cell proliferation (e.g., oxygen and glucose) and others which inhibit mitosis (e.g., tumour necrosis factor, anti-cancer drugs). These growth factors may be supplied to the tumour (e.g., oxygen, drugs) or they may be produced as a by-product of the cells' normal functions (e.g., tumour necrosis factor is a by-product of cell degradation). By extending our mathematical model to include additional diffusible chemicals, it should be possible to study the impact that the presence of multiple chemicals has on the tumour's development [10].

An important assumption of the tumour growth model studied in this section concerns the validity of Darcy's law to describe cell motion within the tumour. This issue is discussed in detail in Chapter 5 of this volume and in [1,2,8,9,23], where the tumour cell migration if the tumour is modelled as a two-phase material (the two phases represent the cells and the extracellular water in which they are bathed). In addition to providing some justification for the use of Darcy's law to describe cell motion, the multiphase models provide a more general theoretical framework with which to study alternative constitutive laws (e.g., the tumour cells may be viewed as visco-elastic materials) and for incorporating cellular heterogeneity into the models. Whereas the spatially-structured models that we have discussed thus far assume that the tumour contains a single population of cells, in practice, solid tumours may contain many cell types e.g., mutant subpopulations of the primary tumour cells, extracellular matrix and immune response cells. The models also pave the way for studies in which mechanical interactions with the tissue surrounding the tumour may be studied [11].

4.5 Conclusions

In this chapter, we have presented three complementary modelling approaches that have been used to study the growth of avascular tumours. These range from spatially-averaged models, which may be formulated as systems of coupled differen-

tial equations, to moving boundary problems involving systems of partial differential equations. As each new modelling approach was presented we explained how it is related to the previous models. In this way we aimed to emphasise the inter-relations between the different models and to show how the newer models can be viewed as natural extensions of their predecessors, the demand for such modifications being driven, in part, by new biological insights.

Obviously there remain many ways in which the models we have studied could be further modified or improved. Where appropriate, these extensions have been discussed in the text. For example, in order to distinguish more accurately between a tumour's response to a chemotherapeutic drug which is noncell cycle specific and another drug which acts only during a specific portion of the cell cycle, it is necessary to consider age- or cell-cycle structured models [19]. While it is relatively straightforward to develop and study such models when spatial effects are neglected, the extension of the spatially-structured models of sections 4.3 and 4.4 to include cell-cycle effects remains an open problem.

A related issue which we have ignored concerns the relative impact of therapy on cancerous and normal tissue, the main problems here being toxicity and excessive destruction of healthy tissue. There are several models which compare chemotherapeutic cell kill in cancerous and normal tissue. However these models neglect cell cycle and spatial effects and assume highly simplistic couplings between the different cell populations.

Another important area of investigation that emerges from the models with spatial structure presented in sections 4.3 and 4.4 concerns the validity of Darcy's law as a description of tumour cell motion. Further, given that solid tumours are highly heterogeneous, containing, for example, several clonal populations, extracellular matrix, extracellular fluid, endothelial cells, macrophages, and multiple growth factors, it is natural to want to develop models in which the evolution of each cell population and growth factor is faithfully described. Since the different cellular species may be subject to different 'forces' (e.g., macrophages migrate via chemotaxis to hypoxic regions and the extracellular matrix is relatively immotile, although it may be deformed by cells that crawl across it), these models will need to be fairly general in nature. One promising avenue for further study involves the application of multiphase models to describe the more complex and realistic scenarios [1,2,8,9,23]. The idea is to identify a finite number of volume-occupying species or phases (e.g., tumour cells, extracellular matrix, and extracellular fluid) which together comprise the tumour volume. Mass and momentum balance equations are developed for each phase. The models are then closed by making appropriate choices of constitutive laws to describe, for example, the stress tensor in each phase and introducing additional reaction diffusion equations to describe the chemical species of interest (for details of this approach, see Chapter 5 and [1,2,9]). In addition to providing a framework for studying complex tumour structures, the multiphase approach also represents a natural way in which to investigate interactions between the tumour cells and the surrounding tissue.

Since the multiphase models described above and many of the models described in this chapter may seem rather general in nature, it is interesting to note the appear-

ance in the literature of mathematical models that are focused on specific tumours. For example, Swanson et al. [27] have combined reaction diffusion models of cell migration with accurate three-dimensional geometry taken from medical atlases to simulate the spread of gliomas through the brain. Also, Franks et al. [14] are developing models that describe the development of avascular tumours constrained within compliant cylindrical tubes in order to simulate the early stages of breast cancer, when the tumour cells are still localised within the breast ducts.

In conclusion, while existing models have provided valuable insight into certain aspects of avascular tumour growth and also raised a number of interesting mathematical challenges, there remain a vast array of open problems whose resolution has the potential to make a significant contribution to the efforts being made by clinicians to find better treatments for cancer.

4.6 Problems

Before proposing some problems to the reader, we show how the $O(\epsilon)$ contributions to the normal derivative of the pressure and the curvature on the tumour boundary may be determined.

Mean Curvature
The mean curvature κ of the surface $r = F(\theta)$ is given by

$$\kappa = -\frac{1}{2(F^2 + F_\theta^2)^{3/2}} \left\{ F F_{\theta\theta} - 3F_\theta^2 - 2F^2 + \frac{F_\theta}{F}(F^2 + F_\theta^2)\frac{\cos\theta}{\sin\theta} \right\}, \quad (4.46)$$

where subscripts denote differentiation with respect to θ.

Now, on the perturbed tumour boundary we have

$$\Gamma(\boldsymbol{r}, t) = r - R_0 - \epsilon R_1(\theta, t).$$

Setting $F(\theta) = R_0 + \epsilon R_1(\theta, t)$ in (4.46) and equating coefficients of $O(\epsilon^n)$ it is possible to show that

$$\kappa = \frac{1}{R_0} - \frac{\epsilon}{2R_0^2} \left\{ 2R_1 + \frac{1}{\sin\theta}\frac{\partial}{\partial\theta}\left(\sin\theta \frac{\partial R_1}{\partial\theta} \right) \right\} + O(\epsilon^2). \quad (4.47)$$

Normal Derivatives
The unit outward normal $\boldsymbol{n}$ to the surface $\Gamma(\boldsymbol{r}, t) = 0 = r - R(\theta, t)$ is defined as follows

$$\boldsymbol{n} = \frac{\nabla\Gamma}{|\nabla\Gamma|}.$$

Thus, on the perturbed tumour boundary, where $R(\theta, t) = R_0 + \epsilon R_1(\theta, t)$,

$$\boldsymbol{n} = \left(1 + \frac{\epsilon^2 R_{1\theta}^2}{R_0^2 + \epsilon^2 R_{1\theta}^2} \right)^{-1/2} \left(\hat{\boldsymbol{r}} - \frac{\epsilon R_{1\theta}}{R_0 + \epsilon R_{1\theta}} \hat{\boldsymbol{\theta}} \right), \quad (4.48)$$

where $\hat{\boldsymbol{r}}$ and $\hat{\boldsymbol{\theta}}$ are unit vectors.

Now

$$\nabla p = \left(\frac{\partial p}{\partial r}, \frac{1}{r}\frac{\partial p}{\partial \theta}\right) = \left(\frac{dp_0}{dr} + \epsilon\frac{\partial p_1}{\partial r}, \frac{\epsilon}{r}\frac{\partial p_1}{\partial \theta}\right) + O(\epsilon^2),$$

where $p(r,\theta,t) = p_0(r) + \epsilon p_1(r,\theta,t) + O(\epsilon^2)$. Evaluating ∇p on the perturbed tumour boundary $\Gamma(\boldsymbol{r},t) = 0$ where $r = R_0 + \epsilon R_1(\theta,t)$ we deduce

$$\nabla p|_{r=R_0+\epsilon R_1} = \left(\frac{dp_0}{dr} + \epsilon R_1\frac{d^2p_0}{dr^2} + \epsilon\frac{\partial p_1}{\partial r}\right)_{r=R_0} + O(\epsilon^2). \tag{4.49}$$

Combining (4.48) and (4.49) we deduce finally that on $\Gamma(\boldsymbol{r},t) = 0$

$$\nabla p \cdot \boldsymbol{n} = \left.\frac{dp_0}{dr}\right|_{r=R_0} + \epsilon\left(R_1\frac{d^2p_0}{dr^2} + \frac{\partial p_1}{\partial r}\right)_{r=R_0} + O(\epsilon^2). \tag{4.50}$$

4.6.1 Problems Related to Section 4.2

1. Consider a tumour which contains $N(t)$ cells at time t where

$$\frac{dN}{dt} = kN\left(1 - \frac{N}{\theta}\right).$$

Suppose that the tumour is a spherically symmetric mass of radius $R(t)$ and volume $4\pi R^3/3$. By equating the tumour volume at time t to $N(t)$, the total number of cells at time t, show that $R(t)$ satisfies

$$\frac{dR}{dt} = \hat{k}R\left(1 - \frac{R^3}{\hat{\theta}}\right).$$

How are the parameters $\hat{k}$ and $\hat{\theta}$ related to k and θ?

[**Remark:** It would be difficult to derive the above differential equation for $R(t)$ from first principles.]

2. Consider a tumour which is being treated with a continuous infusion of a chemotherapeutic drug. At time t the tumour contains $N(t)$ cells and the local drug concentration is $A(t)$ where

$$\frac{dN}{dt} = kN\left(1 - \frac{N}{\theta}\right) - \mu NA, \tag{4.51}$$

$$\frac{dA}{dt} = a_\infty - \lambda A. \tag{4.52}$$

In Equation (4.51) the constants k and θ denote the proliferation rate and carrying capacity of the tumour cells when no drug is present, and μ represents the rate at which the drug kills the tumour cells. In Equation (4.52), a_∞ represents the amount of drug being infused and λ its decay rate (note: we are assuming that the rate at which the drug is degraded when it kills tumour cells may be neglected).

Taking a_∞ as a bifurcation parameter, show how the steady states of Equations (4.51) and (4.52) (and their stability) vary with a_∞. Use your results to predict the minimum value of a_∞ that guarantees tumour eradication.

Note: By fixing a_∞ and varying the tumour cell proliferation rate k, we can also use the model compare the effectiveness of the drug when it is used to treat tumours whose proliferation rates vary.

3. The following pair of differential equations model the way in which a tumour containing $N(t)$ cells responds to a drug $A(t)$ which is administered as a series of pulses:

$$\frac{dN}{dt} = kN - \mu NA, \tag{4.53}$$

$$\frac{dA}{dt} = a(t) - \lambda A, \tag{4.54}$$

where

$$a(t) = \begin{cases} a_\infty & n < t < n + \tau \\ 0 & n + \tau < t < n + 1, \end{cases} \tag{4.55}$$

$$A(0) = A_0 \quad \text{and} \quad N(0) = N_0.$$

In Equation (4.55) τ denotes the duration of each period of treatment, a_∞ the amount of drug administered, and λ the assumed constant decay rate of the drug.

By assuming that $A(t)$ is continuous as the drug is switched on and off, show that

$$A(t) = \begin{cases} \dfrac{a_\infty}{\lambda} + \left(A_j - \dfrac{a_\infty}{\lambda}\right) e^{-\lambda(t-n-\tau)} & j < t < j + \tau \\ \left(\dfrac{a_\infty}{\lambda} + \left(A_j - \dfrac{a_\infty}{\lambda}\right) e^{-\lambda\tau}\right) e^{-\lambda(t-n-\tau)} & j + \tau < t < j + 1 \end{cases}$$

where $A_j = A(t = j)$ $(j = 0, 1, \ldots)$ and

$$A_{j+1} = A_j e^{-\lambda\tau} + \frac{a_\infty}{\lambda} e^{-\lambda}(e^{\lambda\tau} - 1). \tag{4.56}$$

By using the above expression for $A(t)$ and assuming continuity of $N(t)$ at the switching times, show further that

$$N(t) = \begin{cases} N_j e^{k(t-j)} \exp\left\{-\frac{\mu}{\lambda}\left(a_\infty(t-j) + \left[A_j - \frac{a_\infty}{\lambda}\right](1-e^{-\lambda(t-j)})\right)\right\} \\ j < t < j+\tau \\ N_{j+\tau} e^{k(t-j-\tau)} \exp\left\{-\frac{\mu}{\lambda}\left(\frac{a_\infty}{\lambda} + \left[A_j - \frac{a_\infty}{\lambda}\right](1-e^{-\lambda(t-j-\tau)})\right)\right\} \\ j+\tau < t < j+1. \end{cases}$$

where $N_j = N(t=j)$, $N_{j+\tau} = N(t=j+\tau)$,

$$N_{j+\tau} = N_j e^{k\tau} \exp\left\{-\frac{\mu}{\lambda}\left(a_\infty \tau + \left[A_j - \frac{a_\infty}{\lambda}\right](1-e^{-\lambda\tau})\right)\right\}$$

and

$$\frac{N_{j+1}}{N_j} = \exp\left\{-\frac{\mu}{\lambda}\left(f_j + a_\infty \tau - \frac{\lambda k}{\mu}\right)\right\} \tag{4.57}$$

where

$$f_j = \frac{a_\infty}{\lambda} + \left(A_j - \frac{a_\infty}{\lambda}\right)(2 - e^{-\lambda\tau} - e^{-\lambda(1-\tau)}).$$

Note: By fixing $A_j = A_{j+1} \equiv A_\infty$ in Equation (4.56), we deduce that, as $t \to \infty$, the drug concentration settles to a periodic solution for which

$$A_\infty = \frac{a_\infty}{\lambda} e^{-\lambda(1-\tau)}.$$

From (4.57) we note that if $N_{j+1} > N_j$ then the tumour continues to grow, if $N_{j+1} < N_j$ then the drug is reducing the tumour's size and that if $N_{j+1} = N_j$ then the tumour settles to a periodic solution. Determine the conditions for which $N_{j+1} = N_j$.

4. The following system of differential equations describes how a tumour that contains a drug-sensitive and a drug-resistant population of cells responds to continuous infusion with a drug

$$\frac{dN_1}{dt} = k_1 N_1 \left(1 - \frac{N_1 + N_2}{\theta}\right) - \mu N_1 A, \tag{4.58}$$

$$\frac{dN_2}{dt} = k_2 N_2 \left(1 - \frac{N_1 + N_2}{\theta}\right), \tag{4.59}$$

$$\frac{dA}{dt} = a_\infty - \lambda A, \tag{4.60}$$

$$\text{with} \quad N_1(0) = N_{10},\ N_2(0) = N_{20},\ A(0) = A_0.$$

In the above equations, N_1 and N_2 denote the number of drug-sensitive and drug-resistant cells respectively, k_1 and k_2 their proliferation rates, and θ their

carrying capacity, when no drug is present. We denote by $A(t)$ the drug concentration at time t, λ its decay rate, and a_∞ the rate at which it is delivered to the tumour.

Identify the equilibrium solutions of the above differential equations focusing on the cases $k_1 > k_2$ and $k_1 < k_2$. In each case, determine whether it is possible to eliminate the tumour by infusing the system with sufficiently large drug concentrations.

4.6.2 Problems Related to Section 4.3

1. The following equations describe the growth of a one-dimensional tumour in response to an externally supplied nutrient

$$0 = \frac{\partial^2 c}{\partial x^2} - \lambda H(c - c_N),$$

$$\frac{dR}{dt} = \int_0^R s(c)dx,$$

$$\text{where} \quad s(c) = \begin{cases} s(c - c^*) & c > c_N \\ -\mu & c \leq c_N \end{cases}$$

$$\text{with} \quad c = c_\infty \text{ at } x = R(t),$$

$$\frac{\partial c}{\partial x} = 0 \text{ at } x = 0,$$

$$c = c_N \text{ when } x = R_N(t),$$

$$c, \ \frac{\partial c}{\partial x} \text{ continuous across } x = R_N(t)$$

$$R = R_0 \text{ at } t = 0,$$

where $\lambda, c_N, c^*, c_\infty, s, \mu$, and R_0 are positive constants and $c_\infty > c_N$.

Assuming that $R_N = 0$, (i.e., the tumour does not possess a necrotic region), solve for $c(x, t)$ in terms of $R(t)$. Use this expression to derive an expand $O\Delta E$ for the tumour radius, $R(t)$. Identify the steady state solutions of this $O\Delta E$ and, hence, deduce that if

$$c_\infty - c_N > \frac{3}{2}(c_\infty - c^*) > 0$$

then the tumour will evolve to a nontrivial steady state which does not possess a necrotic region.

Suppose now that $3(c_\infty - c^*)/2 > c_\infty - c_N > 0$ and that $R_N(t = 0) > 0$. Determine the nutrient concentration in terms of $R(t)$ and $R_N(t)$ and derive an

expression relating $R_N(t)$ to $R(t)$. By substituting with $c(x,t)$ in the equation for $R(t)$, obtain the following $O\Delta E$ for $R(t)$

$$\frac{dR}{dt} = s(R - R_N)\left[c_N - c^* + \frac{\lambda}{6}(R^2 - 4RR_N + 5R_N^2)\right] - \mu R_N.$$

Determine the steady state solutions for which $0 < R_N < R$. What parameters govern the width of the proliferating rim?

2. The following equations describe the effect of an externally supplied poison β on the growth of a radially-symmetric cluster of mold

$$0 = \frac{1}{r^2}\frac{\partial}{\partial r}\left(r^2\frac{\partial \beta}{\partial r}\right) - \beta_\infty,$$

$$R^2\frac{dR}{dt} = \int_0^R (s - \beta)r^2 dr,$$

$$\text{with} \qquad \frac{\partial \beta}{\partial r} = h(\beta - \beta_\infty) \text{ on } r = R(t), \quad \frac{\partial \beta}{\partial r} = 0 \text{ at } r = 0,$$

$$\text{and } R = R_0 \text{ at } t = 0.$$

For what size clusters does the model generate biologically realistic solutions?

For the case $h = 2$, draw a bifurcation diagram, showing how the number and size of the steady state solutions change with s/β_∞. What concentration of poison would you recommend to be confident of eradicating the mold?

3. The following equations describe the growth of a radially-symmetric tumour in response to an externally-supplied nutrient such as oxygen

$$\frac{\partial n}{\partial t} + \frac{1}{r^2}\frac{\partial}{\partial r}(r^2 v n) = k(c)n \tag{4.61}$$

$$0 = \frac{1}{r^2}\frac{\partial}{\partial r}\left(r^2\frac{\partial c}{\partial r}\right) - \lambda n H(c - c_N),$$

$$\text{where} \quad k(c) = \begin{cases} k_+ & \text{if } c > c_N \\ -k_- & \text{if } c \le c_N \end{cases}$$

$$\frac{dR}{dt} = v(R,t), \tag{4.62}$$

$$c(R,t) = c_\infty,$$

$$\frac{\partial c}{\partial r}(0,t) = v(0,t) = 0,$$

$$c, \ \frac{\partial c}{\partial r} \text{ continuous across } r = R_N(t),$$

$$\text{and } R(0) = R_0.$$

In the equations, $n(r,t)$ denotes the tumour cell density, $v(r,t)$ the cell velocity, $c(r,t)$ the local oxygen concentration, $R(t)$ the position of the outer tumour radius, and $R_N(t)$ the interface between proliferating and dead cells. The parameters $\lambda, c_N, c_\infty, R_0$, and $k_\pm$ are positive constants.

By assuming that the tumour is fully occupied by tumour cells, so that $n \equiv 1$ for $0 \leq r \leq R(t)$, use Equation (4.61) to obtain an expression for the cell velocity $v(r,t)$ in terms of $k(c)$. Use this result in Equation (4.62) to show that

$$R^2 \frac{dR}{dt} = \int_0^{R(t)} k(c) r^2 dr\,.$$

By solving for $c(r,t)$ and assuming that $R_0 < R^* = \sqrt{6(c_\infty - c_N)/\lambda}$, explain briefly how the tumour evolves. In particular, show that, since $k_- > 0$, the tumour eventually achieves a steady state, which you should determine. (Note: you do NOT need to solve the ODEs for $R(t)$ – you simply need to derive ODE for $R(t)$ and the corresponding algebraic equation for $R_N(t) = R_N(R(t))$.)

4.6.3 Problems Related to Section 4.4

1. Consider the following mathematical model which may be used to describe the three-dimensional growth of an avascular tumour

$$0 = \nabla^2 c - \Gamma,$$

$$\boldsymbol{v} = -\nabla p, \quad \nabla . \boldsymbol{v} = s(c - \tilde{c}),$$

$$\frac{\partial R}{\partial t} = \boldsymbol{v}.\boldsymbol{n} \quad \text{on } \Gamma(\boldsymbol{r},t) = r - R(\theta,\phi,t) = 0,$$

$$\text{with} \quad c = 1, \quad p = \alpha\kappa \quad \text{on } \Gamma(\boldsymbol{r},t) = 0,$$

$$\frac{\partial c}{\partial r} = \frac{\partial p}{\partial r} = 0 \quad \text{at } \boldsymbol{r} = 0,$$

$$\text{and} \quad c \geq 0 \text{ throughout the tumour.}$$

Eliminate $\boldsymbol{v}$ from the governing equations and suppose that the model admits solutions of the form

$$c = c_0(r) + \epsilon \chi_{lm}(t) r^l Y_{lm}(\theta,\phi),$$

$$p = p_0(r) + \epsilon \left(\pi_{lm}(t) - \frac{s\chi_{lm} r^2}{2(2l+3)} \right) r^l Y_{lm}(\theta,\phi),$$

$$R = R_0 + \epsilon \rho_{lm}(t) Y_{lm}(\theta,\phi),$$

where $\epsilon \ll 1$ and $Y_{lm}(\theta, \phi)$ $(-l \leq m \leq l)$ denote the spherical harmonics of order $l \geq 1$ for which $\nabla^2 Y_{lm} = -l(l+1)Y_{lm}$. Construct the leading order, radially-symmetric equilibrium solutions (c_0, p_0, R_0). Use linear stability analysis to derive a differential equation that governs $\rho_{lm}(t)$, the growth rate of the asymmetric perturbation to the tumour boundary. Does your result vary for the $(2l+1)$ spherical harmonics of order l?

Note: In order to distinguish between the growth rates of the $(2l+1)$ spherical harmonics of order l, we must continue the expansions for c, p, and R to $O(\epsilon^2)$ and use weakly nonlinear analysis. The special case $l = 2$ is discussed in [5].

2. The following system of equations has been proposed to describe the two-dimensional growth of a nonnecrotic avascular tumour in response to an externally-supplied nutrient

$$0 = \nabla^2 c - \Gamma = \mu \nabla^2 p + s(c - \lambda_A),$$

$$\frac{dR}{dt} = -\mu \nabla p \cdot \boldsymbol{n} \quad \text{on } \Gamma(\boldsymbol{r}, t) = 0,$$

$$\text{with} \quad \frac{\partial c}{\partial r} = \frac{\partial p}{\partial r} = 0 \quad \text{on } \boldsymbol{r} = 0,$$

$$c = c_\infty - \alpha\kappa, \quad p = 0 \quad \text{on } \Gamma(\boldsymbol{r}, t) = r - R(\theta, t) = 0,$$

with $c \geq 0$ throughout the tumour volume. In the above equations, κ denotes the mean curvature, and $\boldsymbol{n}$ denotes the unit outward normal to the tumour boundary $\Gamma(\boldsymbol{r}, t) = 0$.

We may determine the stability of steady, radially-symmetric model solutions to asymmetric perturbations by seeking trial solutions of the form

$$\left.\begin{array}{l} c \sim c_0(r) + \epsilon c_1(r, \theta, t), \\ p \sim p_0(r) + \epsilon p_1(r, \theta, t), \\ R \sim R_0 + \epsilon R_1(\theta, t). \end{array}\right\} \qquad (\epsilon \ll 1).$$

Construct the leading order, radially-symmetric equilibrium solution (c_0, p_0, R_0).

Assume that (c_1, p_1, R_1) can be decomposed as follows

$$c_1 = \chi_k(t) r^k P_k(\cos\theta),$$

$$p_1 = \left(\pi_k(t) - \frac{s\chi_k r^2}{2\mu(2l+3)}\right) r^k P_k(\cos\theta),$$

$$R_1 = \rho_k P_k(\cos\theta),$$

where $P_k(\cos\theta)$ denotes a Legendre polynomial of order k for which

$$\frac{1}{\sin\theta}\frac{\partial}{\partial\theta}\left(\sin\theta \frac{\partial P_k}{\partial\theta}\right) = -k(k+1)P_k.$$

Use linear stability analysis to determine the growth rate of the asymmetric perturbations $P_k(\cos\theta)$. Show that if $\alpha > 0$ then only a finite number of modes are unstable. Compare your results with those obtained for Greenspan's model which were presented in section 4.4.4.

Note: Details of the above analysis are described in [4,6].

3. The following partial differential equations may be used to describe the nutrient-limited growth of a necrotic avascular tumour

$$\nabla^2 c - \Gamma H(c - c_N) = 0$$

$$\mu\nabla^2 p + s(c - \lambda_A)H(c - c_N) - s(\lambda_A + \lambda_N)H(c_N - c) = 0,$$

$$\frac{dR}{dt} = -\mu\nabla p \cdot \boldsymbol{n} \quad \text{on} \quad \Gamma(\boldsymbol{r}, t) = 0,$$

$$\text{with} \quad \frac{\partial c}{\partial r} = 0 = \frac{\partial p}{\partial r} \quad \text{at} \quad \boldsymbol{r} = 0,$$

$$c = c_\infty, \quad p = \alpha\kappa \quad \text{on} \quad \Gamma(\boldsymbol{r}, t) = r - R(\theta, t) = 0,$$

$$c = c_N \quad \text{on} \quad \Gamma_N(\boldsymbol{r}, t) = r - R_N(\theta, t) = 0,$$

$$c,\ p,\ \frac{\partial c}{\partial r},\ \frac{\partial p}{\partial r} \quad \text{continuous across} \quad \Gamma_N(\boldsymbol{r}, t) = 0.$$

Use linear stability analysis to extend the analysis of section 4.4.4 and to investigate the stability with respect to asymmetric perturbations (involving Legendre polynomials $P_k(\cos\theta)$) of radially-symmetric equilibrium solutions for which the tumour possesses a necrotic core.

Note: Details of this analysis are discussed in [4,6].

4. The following mathematical model may be used to describe the development of a nonnecrotic spheroid in response to two chemicals σ and β

$$\nabla^2\sigma - \Gamma_\sigma = 0,$$

$$\nabla^2\beta - \Gamma_\beta = 0,$$

$$\mu\nabla^2 p + s(\sigma - \beta) = 0,$$

$$\frac{dR}{dt} = -\mu\nabla p \cdot \boldsymbol{n} \quad \text{on} \quad \Gamma(\boldsymbol{r}, t) = 0$$

$$\text{with} \quad \frac{\partial\sigma}{\partial r} = 0 = \frac{\partial\beta}{\partial r} = \frac{\partial p}{\partial r} \quad \text{at} \quad \boldsymbol{r} = 0,$$

$$\sigma = \sigma_\infty, \quad \beta = \beta_\infty, \quad p = \alpha\kappa \quad \text{on} \quad \Gamma(\boldsymbol{r}, t) = 0 = r - R(\theta, t),$$

$$\text{and} \quad \sigma, \beta \geq 0 \quad \text{throughout the tumour volume.}$$

What roles do σ and β play in the tumour's development?

Determine the steady, radially-symmetric solutions, and investigate how they depend on the constants σ_∞ and β_∞.

Use linear stability analysis to determine the stability of the steady, radially-symmetric solutions to asymmetric perturbations for which the dependent variables have the following form

$$\left.\begin{array}{c}\sigma(r,\theta,t) \sim \sigma_0(r) + \epsilon\Sigma_k \pi_k(t) P_k(\cos\theta), \\ R(\theta,t) \sim R_0 + \epsilon\Sigma_k \rho_k(t) P_k(\cos\theta),\end{array}\right\} \quad \text{where } \epsilon \ll 1.$$

Note: Details of this analysis are discussed in [6].

5. Consider a nonnecrotic avascular tumour which is growing in a two-dimensional Cartesian domain in response to a growth inhibitor β.

   The governing equations may be written in the following form

$$\frac{\partial^2\beta}{\partial x^2} + \frac{\partial^2\beta}{\partial y^2} - \Gamma = 0,$$

$$\frac{\partial^2 p}{\partial x^2} + \frac{\partial^2 p}{\partial y^2} + \frac{s}{\mu}(1-\beta) = 0,$$

$$\frac{dX}{dt} = -\mu\left(\frac{\partial p}{\partial x} + \frac{\partial p}{\partial y}\right)\cdot \boldsymbol{n} \quad \text{on } \Gamma(\boldsymbol{x},t) = 0,$$

$$\text{with} \quad \frac{\partial\beta}{\partial x} = \frac{\partial p}{\partial x} = 0 \quad \text{on } x = 0,$$

$$\frac{\partial\beta}{\partial y} = \frac{\partial p}{\partial y} = 0 \quad \text{on } y = 0, h,$$

$$\beta = \beta_\infty, \quad p = \alpha\kappa \quad \text{on } \Gamma(\boldsymbol{x},t) = x - X(y,t) = 0,$$

$$\text{and} \quad \beta \geq 0 \quad \text{throughout the tumour.}$$

   Assume that, to leading order, the tumour grows uniformly in the x-direction and seek trial solutions of the form

$$\left.\begin{array}{c}\beta(x,y,t) \sim \beta_0(x,t) + \epsilon\beta_1(x,t)\cos(k\pi y/h) \\ p(x,y,t) \sim p_0(x,t) + \epsilon p_1(x,t)\cos(k\pi y/h) \\ X(y,t) \sim X_0(t) + \epsilon X_1(t)\cos(k\pi y/h)\end{array}\right\} \quad (\epsilon \ll 1, \;\; k = 0,1,2,\ldots).$$

   By substituting with these expressions in the model equations and equating coefficients of $O(1)$ and $O(\epsilon)$, determine (β_0, p_0, X_0) and state the partial differential equations that govern (β_1, p_1, X_1). Determine (β_1, p_1, X_1) for the special case when $X_0(t) = X_0$, constant.

4.7 References

[1] Ambrosi, D. and Preziosi, L., On the closure of mass balance models for tumor growth, *Math. Models Methods Appl. Sci.* 12, 737-754, 2002.

[2] Breward, C.J.W., Byrne, H.M., and Lewis, C.E., The role of cell-cell interactions in a two-phase of solid tumor growth, *J. Math. Biol.* 45, 125-152, 2002.

[3] Burton, A.C., Rate of growth of solid tumours as a problem of diffusion, *Growth* 30, 157-176, 1966.

[4] Byrne, H.M., The importance of intercellular adhesion in the development of carcinomas, *IMA J. Math. Appl. Med. Biol.* 14, 305-323, 1997.

[5] Byrne, H.M., A weakly nonlinear analysis of a model of avascular solid tumour growth, *J. Math. Biol.* 33, 59-89, 1999.

[6] Byrne, H.M. and Chaplain, M.A.J., Free boundary value problem associated with the growth and development of multicellular spheroids, *Eur. J. Appl. Math.* 8, 639-658, 1997.

[7] Byrne, H.M. and Chaplain, M.A.J., Necrosis and apoptosis: distinct cell loss mechanisms in a mathematical model of solid tumour growth, *J. Theor. Med.* 1, 223-236, 1998.

[8] Byrne, H.M., King, J.R., McElwain, D.L.S., and Preziosi, L., A two-phase model of solid tumor growth, *Appl. Math. Lett.*, 2003.

[9] Byrne, H.M. and Preziosi, L., Modelling solid tumor growth using the theory of mixtures, *IMA J. Math. Appl. Med. Biol.* Submitted.

[10] Chaplain, M.A.J., Ganesh, M., and Graham, I., Spatio-temporal pattern formation on spherical surfaces: numerical simulation and application to solid tumour growth, *J. Math. Biol.* 42, 387-423, 2001.

[11] Chen, C.Y., Byrne, H.M., and King, J.R., The influence of growth-induced stress from the surrounding medium on the development of multicell spheroids, *J. Math. Biol.* 43, 191-220, 2001.

[12] Crank, J., *Free and Moving Boundary Problems*. Clarendon Press, Oxford, 1984.

[13] Folkman, J. and Hochberg, M., Self-regulation of growth in three-dimensions, *J. Exp. Med.* 138, 745-753, 1973.

[14] Franks, S.J., Byrne, H.M., King, J.R., and Lewis, C.E., Modelling the growth of ductal carcinoma in situ. *J. Math. Biol.* Submitted.

[15] Gammack, D., Byrne, H.M., and Lewis, C.E., Estimating the selective advantage of mutant p53 tumour cells to repeated rounds of hypoxia, *Bull. Math. Biol.* 63, 135-166, 2001.

[16] Greenspan, H.P., Models for the growth of a solid tumour by diffusion, *Stud. Appl. Math.* 52, 317-340, 1972.

[17] Greenspan, H.P., On the growth and stability of cell cultures and solid tumours, *J. Theor. Biol.* 56, 229-242, 1976.

[18] Groebe, K. and Mueller-Klieser, W., On the relation between size of necrosis and diameter of tumour-spheroids, *Intl. J. Rad. Oncol. Biol. Phys.* 34, 395-401, 1996.

[19] Gyllenberg, M. and Webb, G., A nonlinear structured population model of tumour growth with quiescence, *J. Math. Biol.* 28, 671-684, 1990.

[20] Hoppensteadt, F., *Mathematical Theories of Populations: Demographics, Genetics, and Epidemics*, SIAM, Philadelphia, 1975.

[21] Jackson, T.L. and Byrne, H.M., A mathematical model to study the effects of drug resistance and vasculature on the response of solid tumours to chemotherapy, *Math. Biosci.* 164, 17-38, 2000.

[22] Kelly, C.E., Leek, R.D., Byrne, H.M., Cox, S.M., Harris A.L., and Lewis, C.E., Modelling macrophage infiltration into avascular tumours, *J. Theor. Med.* 4, 21-38, 2002.

[23] Landman, K.A. and Please, C.P., Tumour dynamics and necrosis: Surface tension and stability, *IMA. J. Math. Appl. Med.* 18, 131-158, 2001.

[24] Marusic, M., Bajzer, Z., Freyer, J.P., and Vukpavlovic, S., Analysis of growth of multicellular tumour spheroids by mathematical models, *Cell Prolif.* 27, 73-94, 1994.

[25] Marusic, M., Bajzer, Z., Vukpavlovic, S., and Freyer, J.P., Tumour-growth *in-vivo* and as multicellular spheroids compared by mathematical models, *Bull. Math. Biol.* 56, 617-631, 1994.

[26] Sutherland, R.M. and Durand, R.E., Growth and cellular characteristics of multicell spheroids, *Recent Results in Cancer Research* 95, 24-49, 1984.

[27] Swanson, K.R., Alvord, E.C., and Murray, J.D., A quantitative model for differential motility of gliomas in grey and white matter, *Cell. Prolif.* 33, 317-329, 2000.

Chapter 5

Mechanical Models in Tumour Growth

Davide Ambrosi[1] **and Francesco Mollica**[2]
[1] *Dipartimento di Matematica, Politecnico di Torino, Torino (Italy),*
[2] *Istituto CNR per la Tecnologia dei Materiali Compositi, Napoli (Italy)*

5.1 Introduction

When looking at a tumour at a macroscopic scale, one does not consider the single cells and their mutual and external interaction, but attempts to describe the body as a continuum. Roughly speaking, one looks at a tumour mass staying at a sufficiently long distance so that single cells are indistinguishable. Under such a point of view, the biological system is to be described by a system of partial differential equations, where the unknowns are the mass density of the species and their velocity, concentration of soluble factors and so on. The mathematical model accounting for the growth of a tumour should then read (according to someone *must be*) a set of balance laws: balance of mass of the several components of the tissue, balance of momentum, and balance of energy. However, a soft tissue is a continuum with two peculiar characteristics that do not allow application of the classical methods of single-continuum mechanics in a straightforward manner in its description:

- the mass of a living tissue increases (growth) or diminishes (resorption) in time and energy is irreversibly spent in this process,
- a soft tissue is made of several components (cells, extracellular matrix), mixed at a small spatial scale, exchanging mass with each other.

The subject of this chapter is the mathematical modelling of tumour growth by the formalism of continuum mechanics, addressing in a specific way the two items listed above.

The first item, the mechanics of a growing body, is related to the importance of keeping into account mechanical loadings in studying tumour growth, a rather recent experimental achievement. In 1997 Helmlinger et al. [13] have measured the growth of a tumour spheroid embedded in a gel of suitably variable rigidity. They have demonstrated that when the rigidity of the external gel is increased, so that the loading at the boundary of the grown spheroid and the stress field inside it become larger, the spheroid modifies its growth rate in a nontrivial fashion. Namely, the volume of the tumour grows more slowly for increasing rigidity of the external gel and, at a cellular level, the stress yields decreased apoptosis, no significant changes in proliferation, and increasing cellular packing. From a macroscopic point of view such a complex behaviour depends on the stress field in the tumour spheroid. In this chapter we outline a mechanical framework in which the concept of stress has an exact meaning: the framework of the mechanics of a growing continuum medium. We believe that this is the correct setting to try to understand and reproduce the experimental results.

The second item listed above suggests to approach the modelling problem with the mixture theory: one does not consider the components of a soft tissue (cells of different type, extracellular matrix, liquid, etc.) separately, in their real spatial distribution but components co-exist at any point of the body under consideration. This approach can be intuitively justified by taking averages of the state variables

of the system (for instance, mass) into elementary volumes that are small enough to contain many representatives of the species under consideration and, at the same time, are small with respect to the macroscale.

5.2 Single Constituent Framework

The description of tumour growth requires taking quite a large number of biological effects into account. This is probably the reason why people have concentrated their effort on modelling the complex response of cell populations to chemical factors and nutrients rather than on the mechanics of the ensemble of tumour cells, i.e., the multicell spheroid. In fact, the approach usually encountered in the literature is to write down a balance equation for the cell population and a set of reaction diffusion equations for those nutrients and chemical factors which are thought to influence growth and motion. The main challenges involved in developing such models are then in describing how cells migrate, reproduce, and die, and how various chemicals diffuse, how they are produced, and taken up by the cells. However, the displacement of the species occurring in the modelization is often introduced in a rather crude way, without introducing any balance of forces.

This aspect is particularly relevant when the material exhibits mechanical properties that characterise solids (at least to some extent); in his case the knowledge of its deformation is required to define a mechanical response. The question in this case is: Deformation with respect to what?

Here we model the growing material as a single phase continuum, in which growth is seen not as an increase of the number of particles, but as an *increase of the mass of the already existing particles*. In the specific case of biological tissues, a particle can be thought of as a small region of space, for example the visual field of a microscope containing a sufficiently large number of cells. In such a case, at any configuration of the body there can be exactly the same particles that were there in the original configuration, so that it is possible to define a motion that connects all of these configurations. The total mass of the body in going from the original to the current configuration may change because the mass of the particles may have changed.

The modelling of growth of soft tissues within a continuum mechanics framework for a single constituent has been discussed in the past by Rodriguez et al. [21] and an excellent review article on the subject is due to Taber [22]. In these papers the basics of growth kinematics are laid down and also the influence of stress on growth is taken into account.

In this chapter we will use the notion of multiple natural configurations [14], [16] and the concept of growth mentioned above to study the volumetric growth of a continuous medium in a general way, having in mind tumour growth as a specific application. In particular, we discuss a description of the mechanical properties of

a growing medium that splits growth and mechanical response into two separate contributions. The biological mechanism that growth takes place depending upon the availability of nutrients, particularly relevant for tumour growth, is also taken into account.

5.3 Kinematics of Growth

Let a body be in the configuration κ_0 at time $t = 0$. Suppose that the body has undergone growth or resorption together with the possible application of loads, so that at current time t the configuration is κ_t (see Figure 5.1).

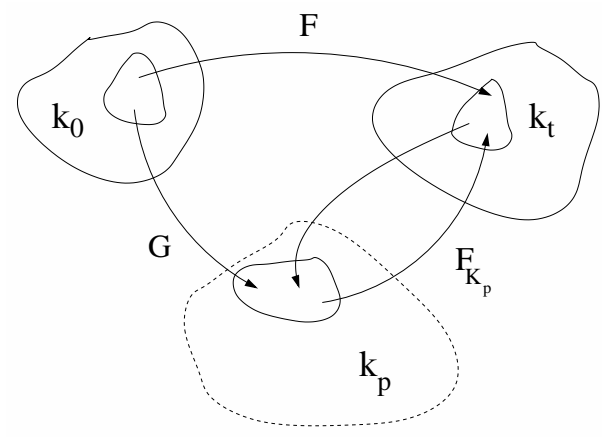

Figure 5.1

Diagram of the motion from the original unstressed configuration κ_0 to the current configuration κ_t. If we cut a generic particle out of the body and relieve its state of stress while keeping its mass constant, it will reach its *natural state* at time t. The *natural configuration* of the body at time t is the collection of all the particles in their natural states at time t.

Let $\mathbf{X}$ be the position of a given particle at time $t = 0$, and let $\mathbf{x}$ be the position of the same particle in the current configuration κ_t. Since the same particles are present in both the original and current configuration we can define the motion of the body [23]:

$$\mathbf{x} = \boldsymbol{\chi}(\mathbf{X}, t), \tag{5.1}$$

and the corresponding deformation gradient, supposed to be invertible:

$$\mathbf{F} = \frac{\partial \boldsymbol{\chi}}{\partial \mathbf{X}}. \tag{5.2}$$

The velocity is given by

$$\mathbf{v} = \frac{\partial \boldsymbol{\chi}}{\partial t}, \tag{5.3}$$

while

$$\varrho = \varrho(\mathbf{x}, t), \tag{5.4}$$

is the density field at time t so that $\varrho_0(\mathbf{X}) = \varrho(\mathbf{x}(\mathbf{X}, 0), 0)$ is the density field at time $t = 0$.

Consider the motion from the original unstressed configuration κ_0 to the current configuration κ_t as depicted in Figure 5.1. Each particle of the body may have grown or been resorbed and the state of stress may be different from zero. If we cut a generic particle out of the body and relieve its state of stress while keeping its mass constant, it will reach a state that is in general different from the one it had in κ_0 and also from the one achieved in κ_t. This is the *natural state* of that particle at time t, while the *natural configuration* of the body at time t is the collection of all the particles in their natural states at time t. As indicated in Figure 5.1, we can measure the deformation from the natural configuration κ_p through the tensor $\mathbf{F}_{\kappa_p}$, while the path from κ_0 to the natural configuration κ_p, which can be seen as a path of unconstrained growth, will be described by the tensor $\mathbf{G}$. The following decomposition giving the splitting holds:

$$\mathbf{F} = \mathbf{F}_{\kappa_p}\mathbf{G}. \tag{5.5}$$

Notice that, since mass is preserved along the path from κ_p to κ_t, the tensor $\mathbf{F}_{\kappa_p}$ is not directly related to growth. Hence we will assume that $\mathbf{F}_{\kappa_p}$ is connected to the stress response of the material while the tensor $\mathbf{G}$ is the one that is directly connected to growth and will be therefore named *growth tensor*. In this way we have separated the contribution of pure growth from the stress-inducing deformation. The tensors $\mathbf{F}_{\kappa_p}$ and $\mathbf{G}$ behave in the same way as the deformation gradient $\mathbf{F}$: the deformation gradient $\mathbf{F}$ is a mapping from a tangent space onto another tangent space, and therefore it indicates how the body is deforming locally in going from κ_0 to κ_t. In a completely analogous way $\mathbf{F}_{\kappa_p}$ tells how the body is deforming locally in going from the natural configuration κ_p to κ_t, while $\mathbf{G}$ tells how the body is growing locally. As the deformation gradient $\mathbf{F}$ is invertible, from Equation (5.5) follows that $\mathbf{F}_{\kappa_p}$ and $\mathbf{G}$ are invertible too.

5.4 Balance Laws

The motion from κ_0 to κ_t obeys the usual equation of balance of mass with a source term; in Eulerian form

$$\frac{\partial \varrho}{\partial t} + \operatorname{div}(\varrho \mathbf{v}) \equiv \dot{\varrho} + \varrho \operatorname{div} \mathbf{v} = \Gamma\rho, \tag{5.6}$$

where Γ is the growth rate (possibly dependent on the state variables of the problem). The divergence operator applies to quantities calculated in a fixed position of the space and a superscript dot $\dot{(\ )}$ denotes the material time derivative.

In a Lagrangian frame of reference, thanks to Reynolds' theorem, Equation (5.6) rewrites

$$\dot{(\varrho J)} = \Gamma \rho J \,, \tag{5.7}$$

where

$$J := \det \mathbf{F} = \det \mathbf{G} \det \mathbf{F}_{\kappa_p} := J_G J_{\kappa_p} \,.$$

Expanding the time derivative at the left hand side of Equation (5.7) one gets

$$\varrho J_{\kappa_p} \dot{J}_G + J_G (\varrho \dot{J}_{\kappa_p}) = \Gamma \rho J_G J_{\kappa_p} . \tag{5.8}$$

At this stage we characterise the tensor $\mathbf{G}$ which arises from the splitting (5.5). We stipulate that two of the terms appearing in Equation (5.8) satisfy the following relationships:

$$\dot{J_G} = \Gamma J_G . \tag{5.9}$$

Then it follows that

$$(\varrho \dot{J}_{\kappa_p}) = 0. \tag{5.10}$$

The continuity equation (5.8) is then replaced by Equation (5.10) whereas Equation (5.9) provides the form of Γ in terms of the growth tensor. Equation (5.10) resembles the usual Lagrangian version of conservation of mass in the absence of mass sources. The simplicity of this last equation is a consequence of our assumption that mass is conserved from κ_p to κ_t. By simple calculations Equation (5.9) can be rewritten as follows:

$$\mathrm{t}r\, \mathbf{D}_G = \Gamma \tag{5.11}$$

where $\mathbf{D}_g := \mathrm{sym}\, (\dot{\mathbf{G}} \mathbf{G}^{-1})$.

The knowledge of the tensor $\mathbf{G}$ allows us to tell whether a certain particle is growing or being resorbed. In fact, from Equation (5.9) we have

$$\begin{aligned} &J_G < 1 \Rightarrow \text{resorption}, \\ &J_G > 1 \Rightarrow \text{growth}. \end{aligned} \tag{5.12}$$

It might be noticed, though, that for isotropic growth, i.e., $\mathbf{G} = g\mathbf{I}$ where g is a scalar, Equation (5.9) rewrites

$$\frac{3\dot{g}}{g} = \Gamma \tag{5.13}$$

so that in this case the knowledge of Γ determines $\mathbf{G}$ completely.

The balance of linear momentum reads:

$$\frac{\partial}{\partial t}(\varrho \mathbf{v}) + \mathrm{div}(\varrho \mathbf{v} \otimes \mathbf{v}) - \mathrm{div}\, \mathbf{T} = \varrho \mathbf{b} + \Gamma \varrho \mathbf{v}, \tag{5.14}$$

where $\mathbf{T}$ is the Cauchy stress tensor, $\mathbf{b}$ is the body force, and the last term at the r.h.s. represents the contribution to the momentum due to the mass source. Using the mass balance Equation (5.6) the momentum equation rewrites

$$\varrho\dot{\mathbf{v}} = \text{div}\,\mathbf{T} + \varrho\mathbf{b}. \tag{5.15}$$

In the case of biological tissues, the characteristic velocities are so small that we can neglect the inertial terms in Equation (5.15) and the system can be conveniently described as quasi-static so that the local form reduces to:

$$\text{div}\,\mathbf{T} = \rho\mathbf{b}. \tag{5.16}$$

The volumetric external force is usually negligible; when this is no case, it can account for a chemotactic force inducing attraction between the cells. Sometimes a Lagrangian approach is more convenient, in particular when the final configuration of the body is unknown and there are traction boundary conditions. For these cases it is useful to introduce a Lagrangian measure of the stress defined in the original reference configuration κ_0, such as the first Piola-Kirchoff stress tensor defined as

$$\mathbf{P} = J\mathbf{T}\mathbf{F}^{-T}. \tag{5.17}$$

The equation for the balance of linear momentum in terms of the first Piola-Kirchoff stress tensor simply reads:

$$\text{Div}\,\mathbf{P} = 0, \tag{5.18}$$

where the operator Div stands for the divergence with respect to the reference configuration.

5.5 Nutrient Factors

As a matter of fact, the growth of biological tissues is strongly dictated by the availability of nutrient and by the influence of several chemical signals, e.g., growth factors. In particular, a tumour mass in its early stages is fed by the environment thanks to the nutrient diffusing in the interstitial liquid. When a tumour mass has become so big that this mechanism does not provide sufficient nutrient anymore, the internal region becomes hypoxic. At this time the tumour stimulates the creation of a vascular structure, a stage called *angiogenesis*. In this paper we just focus on the first part of tumour growth, when the availability of nutrients is essentially dictated by its diffusion; the angiogenesis process is in fact a complex mechanism of self organisation, discussed in other chapters of this book.

Nutrient factors are dissolved in the interstitial liquid, which in our single component model is indistinguishable from the tumour body. Therefore we assume that

the concentration of nutrient $n(\mathbf{x}, t)$ obeys the following reaction-diffusion equation [17]

$$\frac{\partial n}{\partial t} + \text{div}(n\mathbf{v}) - \text{div}\,(D(n)\text{grad}\; n) = -\gamma n\rho. \tag{5.19}$$

Equation (5.19) is a mass balance law for the nutrient: its concentration at a fixed point changes in time because of the transport due to the velocity field $\mathbf{v}$, because of the diffusion due to Brownian motion and because of the uptake by the tumour appearing at the r.h.s., where γ is the absorption rate.

We assume that the concentration of n is constant at the boundary of the tumour, so that the boundary condition reads:

$$n\Big|_{\partial\mathcal{P}} = n_0. \tag{5.20}$$

The equations that describe the motion of the nutrient are coupled to the mass and momentum balance equations by the r.h.s. of Equation (5.19) and are conveniently rewritten in Lagrangian coordinates using Reynolds' transport theorem (see for instance [12]). For a reference system fixed on the body by standard calculations we obtain:

$$\frac{\partial}{\partial t}(nJ) - \text{ Div}\left[D(n)\,\mathbf{F}^{-1}\,\text{Div}\,\left(J\mathbf{F}^{-T}n\right)\right] = -\gamma\, n\rho J. \tag{5.21}$$

The equation can be further simplified observing that the time needed to get a steady state for chemical quantities is usually much smaller than the typical time needed for growth. In this respect, we can assume that diffusion and production always balance in Equation (5.21):

$$\text{Div}\left[D\mathbf{F}^{-1}\,\text{Div}\,\left(J\mathbf{F}^{-T}n\right)\right] = \gamma n\rho J. \tag{5.22}$$

5.6 Constitutive Equations

To close the equation of motion (5.16) or (5.18), together with the balance of mass Equation (5.11), we need to prescribe the constitutive equations that account for the behaviour of the material as a function of the applied loads and of the available nutrient diffusing through the interior. In particular, we need to prescribe a constitutive equation for the response of the material from the natural configuration, i.e., for the path κ_p to κ_t, and independently, an evolution equation for the natural configuration itself, i.e., for the path κ_0 to κ_p.

In analogy with [2] we assume that the mechanical response is hyperelastic from the natural configuration, so that the tumour will be modelled as a hyperelastic material that is capable of growing. Of course, this is a simplification of the behaviour of the material, which, in principle, would be better approximated using a viscoelastic constitutive equation. Nevertheless, since in the case of tumour spheroids the characteristic times of the rate dependent response of the material are much less than

the characteristic times of growth and of mechanical loading, the material can be thought of as a hyperelastic material without introducing a significant error. We can then introduce an energy function W_{κ_p} such as [23]

$$W = W_{\kappa_p}(\mathbf{F}_{\kappa_p}), \tag{5.23}$$

from which we can derive the Cauchy stress tensor:

$$\mathbf{T} = \varrho \mathbf{F}_{\kappa_p} \left(\frac{\partial W_{\kappa_p}}{\partial \mathbf{F}_{\kappa_p}} \right)^T, \tag{5.24}$$

where the subscript κ_p at W denotes the dependence of the functional on the natural configuration. In this way the material is always elastic from the natural configuration, but it might not exhibit *the same* elastic properties.

Once it is known how the material behaves from each natural configuration, we need to describe how the natural configurations evolve. In general, this can be simply done by prescribing a suitable evolution equation for the growth tensor $\mathbf{G}$, which may depend on a variety of quantities.

$$\dot{\mathbf{G}} = \mathcal{G}(\mathbf{X}, t, \mathbf{G}, \mathbf{S}, n), \tag{5.25}$$

where

$$\mathbf{S} = J\mathbf{F}^{-1}\mathbf{T}\mathbf{F}^{-T}, \tag{5.26}$$

is the second Piola-Kirchoff stress tensor. The evolution equation can depend on the applied stress, as is well known in the case of bones, in which growth is regulated by Wolff's law. Other cases of stress dependent growth have also been observed [11].

Given an observer measuring a material vector $\mathbf{x}$, an observer* rotated by $\mathbf{Q}(t)$ will measure the position $\mathbf{Q}\mathbf{x}$. Therefore the following relations hold between the gradient of deformation measured by the two observers:

$$\mathbf{F}^* = \frac{\partial}{\partial \mathbf{X}}(\mathbf{Q}\mathbf{x}) = \mathbf{Q}\frac{\partial \mathbf{x}}{\partial \mathbf{X}} = \mathbf{Q}\mathbf{F}. \tag{5.27}$$

Given the splitting in Equation (5.5), the simplest transformation law for the tensors $\mathbf{G}$ and $\mathbf{F}_{\kappa_p}$ ensuring that the relationship (5.27) is satisfied is

$$\mathbf{F}^*_{\kappa_p} = \mathbf{Q}\mathbf{F}_{\kappa_p}, \qquad \mathbf{G}^* = \mathbf{G}. \tag{5.28}$$

The growth tensor $\mathbf{G}$ is therefore an invariant tensor, i.e., its form does not change upon frame changes and therefore it can be differentiated directly with respect to time [12]. Analogously, the second Piola-Kirchoff stress tensor $\mathbf{S}$ is an invariant measure of stress and this is the reason why it has been adopted in the right hand side of Equation (5.25).

Notice that the evolution Equation (5.25) for $\mathbf{G}$ involves the nutrient and the stress, thus coupling the growth tensor with other relevant quantities of the behaviour of the material. Therefore, in general, one cannot look at growth as being separated from the overall mechanical response, and actually Equation (5.25) has to be solved simultaneously with the other equations of motion. In this sense, the diagram in Figure 5.1 means that at each time the two paths leading to κ_t are to be considered jointly.

5.7 Specific Constitutive Assumptions

In this section the general theory illustrated above is applied via specific constitutive assumptions. Generally speaking, we are conscious that anisotropy is a crucial characteristic of biological tissues. However, in the case of tumour spheroids, the assumption of isotropy is definitely very reasonable. On the other hand, there is experimental evidence [13] that tumour spheroids are compressible, thus we model the response from the natural configurations as an isotropic compressible nonlinearly elastic material. For simplicity we assume that the type of material response is the same for each natural configuration. The specific model we refer to is a material of Blatz-Ko type [4], one of the most widely used compressible hyperelastic materials.

The Cauchy stress tensor takes the form

$$\mathbf{T} = \frac{\mu}{J_{\kappa_p}}[-(J_{\kappa_p})^q\mathbf{I} + \mathbf{B}_{\kappa_p}], \tag{5.29}$$

where $\mathbf{B}_{\kappa_p} = \mathbf{F}_{\kappa_p}\mathbf{F}_{\kappa_p}^T$, μ and q are material constants ($\mu > 0$,$q \leq 0$). Substituting Equation (5.29) into Equation (5.17) we obtain the first Piola-Kirchoff stress tensor:

$$\mathbf{P} = \mu J_G[-(J_{\kappa_p})^q\mathbf{F}_{\kappa_p}^{-T} + \mathbf{F}_{\kappa_p}]\mathbf{G}^{-T}. \tag{5.30}$$

The simplest form of the growth tensor is

$$\mathbf{G}(\mathbf{X}, t, n) = g(\mathbf{X}, t, n)\mathbf{I}, \tag{5.31}$$

where the scalar function g is the growth function. Equation (5.31) implies that growth develops in the same way in all directions, therefore it is isotropic. Growth can be then prescribed through an evolution equation of the form

$$\dot{g} = \mathcal{G}(\mathbf{X}, t, g, n). \tag{5.32}$$

If $g = g(t)$, then growth is said to be homogeneous.

Summarising, we specialise the growth model to the following governing equations:

$$\varrho_0 = \varrho J_{\kappa_p}, \tag{5.33}$$

$$\text{div}\,(D\ \text{grad}\, n) = \gamma\, n\rho, \tag{5.34}$$

$$\text{div}\,\mathbf{T} = 0, \tag{5.35}$$

supplemented by the specific constitutive equations

$$\dot{g} = \tfrac{g}{3}\Gamma(\mathbf{X}, t, n, g), \tag{5.36}$$

$$\mathbf{T} = \tfrac{\mu}{J_{\kappa_p}}[-(J_{\kappa_p})^q\mathbf{I} + \mathbf{B}_{\kappa_p}]. \tag{5.37}$$

Here the unknowns are the density ϱ, the growth function g, the nutrient n, and the three components of the motion $\boldsymbol{\chi}$, which appear in Equations (5.33) indirectly through Equations (5.1) and (5.5).

5.8 Simple Applications

In order to show how the general theory illustrated above can be applied, in this section we solve some simple problems, namely the homogeneous growth inside a rigid cylinder and the inhomogeneous growth of a sphere under no applied external loads. The following procedure is adopted: the motion is assumed to have some symmetry, and the function g is assumed to have a certain simple form. Then we seek a deformation of the material that satisfies the equilibrium equation and appropriate boundary conditions. In the first problem, the deformation is homogeneous, so that the equilibrium equation is automatically satisfied. In the second problem the assumed form of the growth function gives rise to inhomogeneous deformations. In such a case growth is accompanied by residual stresses, as described in [19]: the stress in the material is different from zero even though there are no external forces applied.

5.8.1 Isotropic and Homogeneous Growth Inside a Rigid Cylinder

Suppose that the body occupies the space inside a rigid cylinder, a configuration resembling the growth of a tumour in a vessel. This representation recalls a type of breast cancer named ductal carcinoma, in which tumour cells grow inside a breast duct for nearly 10 cm, receiving nutrients through the walls.

Since the cylinder walls are supposed to be rigid, the motion is

$$x = X, \qquad y = Y, \qquad z = \lambda\, Z, \tag{5.38}$$

so that the deformation gradient is

$$\mathbf{F} = \begin{bmatrix} 1 & 0 & 0 \\ 0 & 1 & 0 \\ 0 & 0 & \lambda \end{bmatrix} = \text{Diag}\,\{1, \quad 1, \quad \lambda\}\,. \tag{5.39}$$

As an example we assume that growth is homogeneous

$$g = g(t). \tag{5.40}$$

This can occur when growth is triggered only if the level of nutrients is above a threshold value $\hat{n}$; for instance, suppose that the growth rate is piecewise constant

$$\Gamma = \hat{\Gamma} H(n - \hat{n}), \tag{5.41}$$

where H is the Heaviside function, which is unity when the concentration of nutrient is above $\hat{n}$ and zero otherwise. In this case Equation (5.36) can be integrated to give

$$g = \exp(\hat{\Gamma} t/3). \tag{5.42}$$

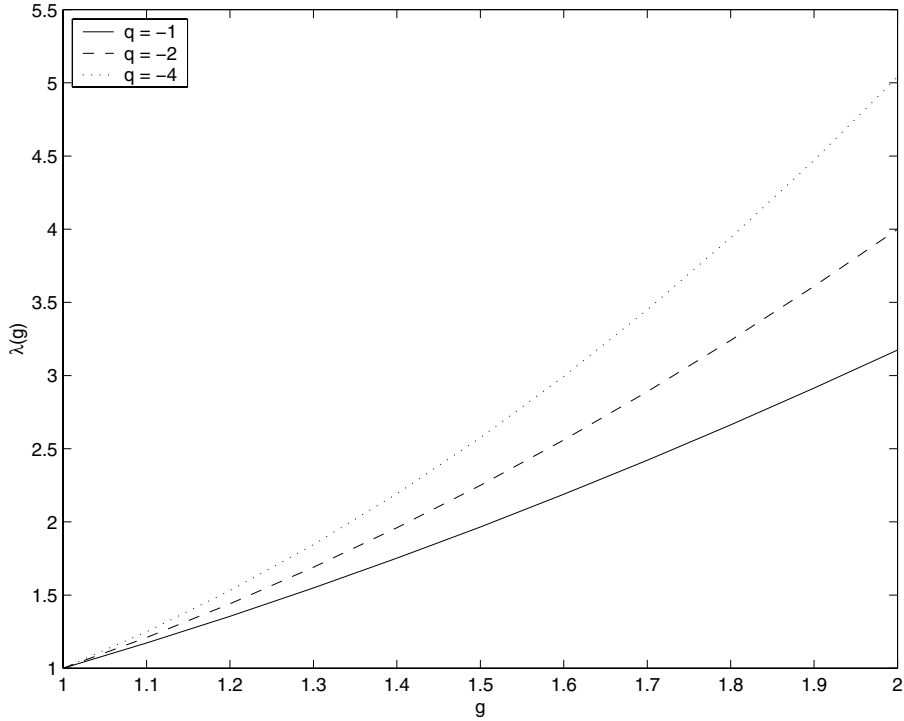

Figure 5.2

Growth inside a rigid cylinder: axial displacement of the material as a function of g for different values of q.

From Equations (5.40), (5.39), and (5.5), it immediately follows that

$$\mathbf{F}_{\kappa_p} = \text{Diag}\left\{\frac{1}{g}, \quad \frac{1}{g}, \quad \frac{\lambda}{g}\right\}. \tag{5.43}$$

Substituting it into Equation (5.29) we can write the Cauchy stress tensor:

$$\mathbf{T} = \mu\ \frac{g^3}{\lambda}\text{Diag}\left\{\frac{1}{g^2} - \left(\frac{\lambda}{g^3}\right)^q, \quad \frac{1}{g^2} - \left(\frac{\lambda}{g^3}\right)^q, \quad \frac{\lambda^2}{g^2} - \left(\frac{\lambda}{g^3}\right)^q\right\}. \tag{5.44}$$

The relationship between g and λ can be obtained by enforcing the boundary conditions on the top and bottom surface of the cylinder. For simplicity we will assume that these surfaces are stress free, so that $T_{zz} = 0$, and this in turn implies that

$$\lambda = g^{\frac{2-3q}{2-q}}. \tag{5.45}$$

Equation (5.45) gives the axial displacement of the material as a function of growth. The plot is given in Figure 5.2 for different values of q. Of course the displacement is an increasing function of g, and through Equation (5.42) is an exponentially increasing function of time.

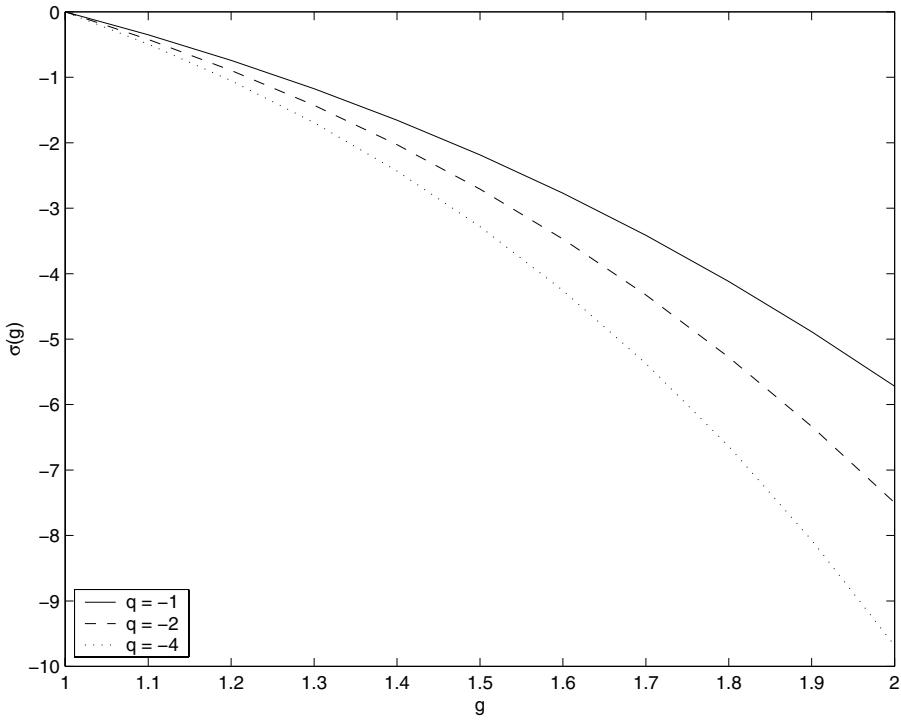

Figure 5.3
Growth inside a rigid cylinder: wall stress versus g.

Another important quantity that can be calculated is the stress exerted by the growing tumour on the wall. By substituting Equation (5.45) into the first components of the r.h.s. of Equation (5.44) we obtain

$$\sigma_w = \mu \left(g^{\frac{2q}{2-q}} - g^{\frac{4-4q}{2-q}} \right). \tag{5.46}$$

The wall stress as a function of the growth function g is shown in Figure 5.3. As we can see, the pressure of the tumour on the duct walls increases with growth and with the axial expansion.

5.8.2 Isotropic and Nonhomogeneous Growth of a Sphere: Residual Stresses

In this problem we look for the deformation of a sphere of initial radius $\bar{R}$ growing freely. Any steady radially symmetric distribution of nutrient will give rise

to a growth tensor of the following form

$$\mathbf{G} = g(R)\ \mathbf{I}. \tag{5.47}$$

This form of growth is incompatible in the sense of Skalak et al. [20] and residual stresses will arise as a consequence. The determination of these residual stresses is the goal of this problem.

The total deformation will be assumed to be an isotropic volume expansion. In spherical polar coordinates the deformation will be

$$r = \lambda(R), \qquad \theta = \Theta, \qquad \phi = \Phi. \tag{5.48}$$

The deformation gradient will be

$$\mathbf{F} = \text{Diag}\ \left\{\lambda', \quad \frac{\lambda}{R}, \quad \frac{\lambda}{R}\right\}, \tag{5.49}$$

where a superscript $(\cdot)'$ denotes differentiation with respect to R. Analogously as before we can calculate $\mathbf{F}_{\kappa_p}$ from the expressions of $\mathbf{F}$ and $\mathbf{G}$:

$$\mathbf{F}_{\kappa_p} = \text{Diag}\ \left\{\frac{\lambda'}{g}, \quad \frac{\lambda}{gR}, \quad \frac{\lambda}{gR}\right\}, \tag{5.50}$$

and plug it into the constitutive equation (5.29). For this problem it is more convenient to use the first Piola-Kirchoff stress tensor (5.17) instead of the Cauchy stress tensor:

$$\mathbf{P} = \text{Diag}\ \{P_{RR}, \quad P_{\Theta\Theta}, \quad P_{\Phi\Phi}\}, \tag{5.51}$$

where

$$\begin{cases} P_{RR} = \mu\, g \left[\lambda' - \Delta^q\, \dfrac{g^2}{\lambda'}\right], \\ P_{\Theta\Theta} = P_{\Phi\Phi} = \mu\, g \left[\dfrac{\lambda}{R} - \Delta^q\, \dfrac{g^2 R}{\lambda}\right], \\ \Delta = J_{\kappa_p} = \dfrac{\lambda'\lambda^2}{g^3 R^2}. \end{cases} \tag{5.52}$$

In order to find the relationship between the growth function g and the volume expansion λ we need to satisfy the conservation of linear momentum and the boundary conditions. The only nontrivial equation is

$$\frac{\mathrm{d}}{\mathrm{d}R} P_{RR} + \frac{2}{R}(P_{RR} - P_{\Theta\Theta}) = 0. \tag{5.53}$$

Plugging the components (5.52) into Equation (5.53) we obtain an ordinary differential equation of the second order in λ:

$$\lambda'' = \frac{\frac{2}{R}\left[\frac{1}{R} + \frac{g^2\Delta^q(1-q)}{\lambda\lambda'}\right](\lambda - \lambda' R) - \left[\lambda' - \frac{3g^2\Delta^q(1-q)}{\lambda'}\right]\frac{g'}{g}}{1 + \frac{g^2\Delta^q(1-q)}{(\lambda')^2}}. \tag{5.54}$$

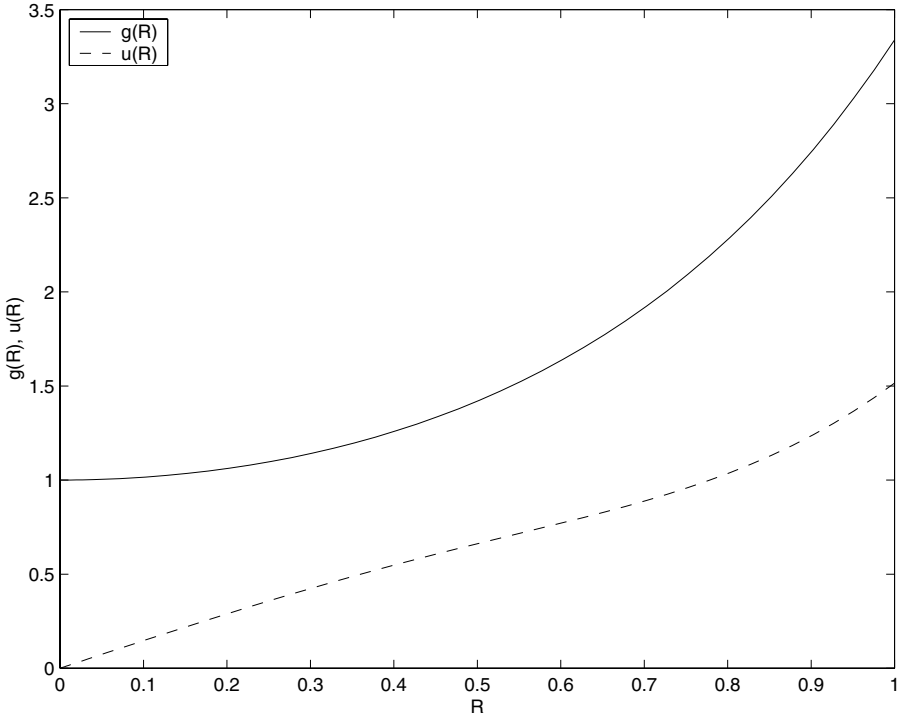

Figure 5.4

Isotropic and inhomogeneous growth of a sphere: growth function g and radial displacement $u = r - R$ versus radius.

Equation (5.54) has to be supplemented by a specific form of the growth function $g(R)$. Typically in tumour growth g is an increasing function of R: the outer shell of the tumour spheroid receives more nutrient than the inner one and is thus able to grow more. A particularly simple form is

$$g(R) = \alpha \frac{\sinh(kR)}{R}, \tag{5.55}$$

where α and k are constants.

Equation (5.54) has to be integrated with the following boundary conditions

$$P_{RR}|_{R=\bar{R}} = 0, \tag{5.56}$$

$$\lambda|_{R=0} = 0. \tag{5.57}$$

The differential equation (5.56) has been numerically integrated by the fourth order Runge-Kutta scheme, the boundary conditions being satisfied by a shooting method.

The results in terms of radial displacement, radial stress, hoop stress are depicted in Figures 5.4 and 5.5. The stress $P_{\Theta\Theta}$ of the outer layers, which grow more,

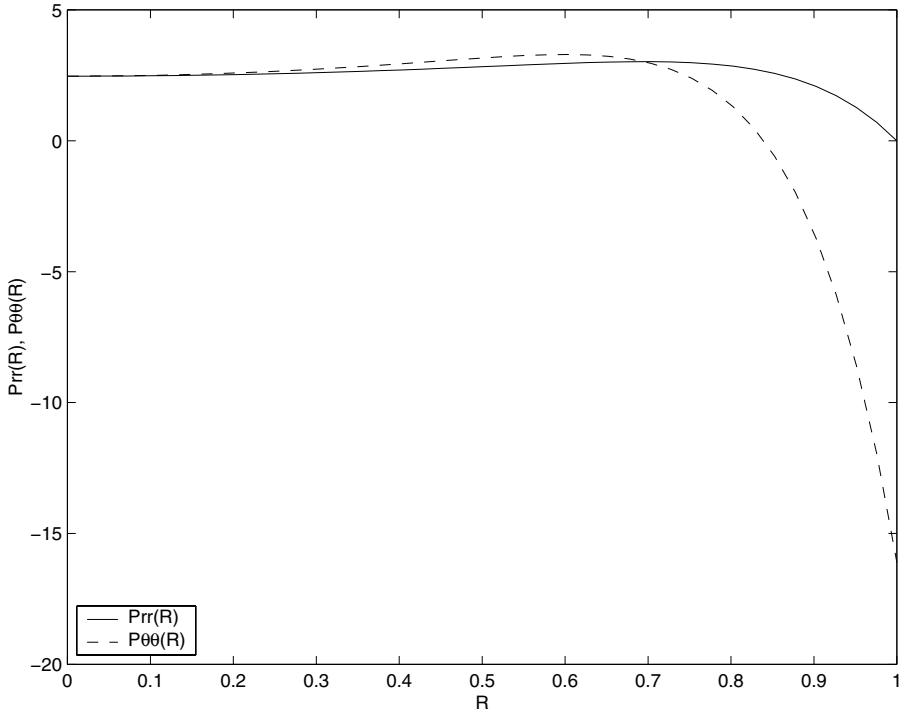

Figure 5.5

Isotropic and inhomogeneous growth of a sphere: radial stress and hoop stress

is in compression, while the inner layers, which grow less, are kept in tension. The radial stress P_{RR} is in tension. The radial displacement and the density are increasing functions of the undeformed radius.

5.9 A Multicellular Spheroid as a Mixture

Recently a mathematical description of avascular tumour as a multiphase system, namely a saturated porous material, has been proposed [3], [7], [18]. This approach starts from the observation that multicell spheroids are basically made of two constituents: a solid skeleton constituted by an ensemble of sticky cells and by an organic liquid filling the extra-cellular space, which is used by the cells to grow. The introduction of such a mechanical framework allows one to deal with stresses and with their influence on the evolution of the system. However, these models are based on the constitutive assumption that an ensemble of cells behaves as a "viscous

growing fluid," so that one does not need to describe the deformations of the material with respect to some reference configuration, but only to deal with their rates. In this respect, it is possible to use an Eulerian framework and the mathematical description of the "growing fluid" just involves an additional source of mass. This is the subject of the second part of this chapter.

The determination of the movement due to the macroscopic growth of the tumour mass can be addressed on the basis of the deformable porous media theory (see for instance Bowen [6]), suitably adapted to the present biological framework. The ensemble of cells is assumed to live in a liquid environment in which some chemical factors diffuse. The multicell spheroid is then modelled as a living material characterised (as all organic tissues) by a porous structure permeated by an organic fluid. In addition, the porous structure is deformable: its constituent (the cells) move, duplicate and die, originating deformation and volumetric growth of the tumour.

We will assume that the multicell spheroid is constituted by a single type of cells with constant density ρ_T, exchanging mass and momentum with the extracellular liquid that surrounds them, having constant density ρ_ℓ. At any point of the cells-liquid mixture both components are co-present, each one with its own volumetric fraction ϕ_T and ϕ_ℓ, respectively. Focusing on the evolution of tumour cells and of the extracellular liquid one can write the following system of equations

$$\frac{\partial(\rho_T\phi_T)}{\partial t} + \nabla\cdot(\rho_T\phi_T\mathbf{v}_T) = \rho_T\Gamma_T\,, \tag{5.58}$$

$$\frac{\partial(\rho_\ell\phi_\ell)}{\partial t} + \nabla\cdot(\rho_\ell\phi_\ell\mathbf{v}_\ell) = \rho_\ell\Gamma_\ell\,, \tag{5.59}$$

$$\rho_T\phi_T\left(\frac{\partial\mathbf{v}_T}{\partial t} + \mathbf{v}_T\cdot\nabla\mathbf{v}_T\right) - \nabla\cdot\mathbf{T}_T = \mathbf{m}_T\,, \tag{5.60}$$

$$\rho_\ell\phi_\ell\left(\frac{\partial\mathbf{v}_\ell}{\partial t} + \mathbf{v}_\ell\cdot\nabla\mathbf{v}_\ell\right) - \nabla\cdot\mathbf{T}_\ell = \mathbf{m}_\ell\,, \tag{5.61}$$

where Γ_T, Γ_ℓ are the production rates of cells and liquid, respectively, and $\mathbf{T}_T, \mathbf{T}_\ell$ are the partial stress tensor of the tumour and liquid, respectively. The momentum supply $\mathbf{m}_\ell, \mathbf{m}_T$ typically account for the drag due to the local interaction between the components and for the Fickian diffusion of the single constituent. The saturation assumption states that at any point the space is occupied by a tumour cell or by the extracellular liquid and reads

$$\phi_T + \phi_\ell = 1\,. \tag{5.62}$$

As there are no external sources, the following conservation conditions for mass and momentum are to be satisfied:

$$\rho_T\Gamma_T + \rho_\ell\Gamma_\ell = 0\,, \tag{5.63}$$

$$\mathbf{m}_T + \mathbf{m}_\ell + \rho_T\Gamma_T\mathbf{v}_T + \rho_\ell\Gamma_\ell\mathbf{v}_\ell = 0\,. \tag{5.64}$$

Summing up the mass balance equations (5.58) and (5.59), and taking Equation (5.62) into account gives

$$\nabla\cdot(\phi_T\mathbf{v}_T + \phi_\ell\mathbf{v}_\ell) = \Gamma_T + \Gamma_\ell\,. \tag{5.65}$$

It can be noticed that, because of Equation (5.63), the r.h.s. of Equation (5.65) vanishes if $\rho_T = \rho_\ell$.

Performing experimental measures to provide a constitutive equation for the partial stresses $\mathbf{T}_T$ and $\mathbf{T}_\ell$ is not an easy task. In fact the partial stresses are defined *in* the mixture, and their properties sometimes cannot be obtained from information on the mechanical properties of the single components by themselves. This problem suggests to write down a momentum equation for the whole mixture. Adding up the two momentum equations in (5.60) and (5.61), after some algebra gives the momentum equation for the multicellular spheroid, i.e., the mixture composed by the extracellular liquid and the cells

$$\rho_m \left(\frac{\partial \mathbf{v}_m}{\partial t} + \mathbf{v}_m \cdot \nabla \mathbf{v}_m \right) = \nabla \cdot \mathbf{T}_m \ , \tag{5.66}$$

where

$$\rho_m := \rho_T \phi_T + \rho_\ell \phi_\ell \ , \tag{5.67}$$

is the density of the mixture, and

$$\mathbf{v}_m := \frac{\rho_T \phi_T \mathbf{v}_T + \rho_\ell \phi_\ell \mathbf{v}_\ell}{\rho_m} \ , \tag{5.68}$$

is the mass average velocity, and $\mathbf{T}_m$ is the stress tensor of the mixture. The latter contains convective contributions that are not included in the barycentric momentum appearing at the left hand side of Equation (5.66).

Equations (5.65) and (5.66) can be conveniently considered instead of the mass balance for the liquid and the momentum balance for the solid. In addition, as the motion of cells and of the intercellular fluid is very slow, inertial terms can be neglected when compared to the stress terms. The system of evolution equations then rewrites as

$$\frac{\partial \phi_T}{\partial t} + \nabla \cdot (\phi_T \mathbf{v}_T) = \quad \Gamma_T \, , \tag{5.69}$$

$$\nabla \cdot (\phi_T \mathbf{v}_T + \phi_\ell \mathbf{v}_\ell) = \Gamma_T + \Gamma_\ell, \tag{5.70}$$

$$-\nabla \cdot \mathbf{T}_m = \quad 0 \, , \tag{5.71}$$

$$-\nabla \cdot \mathbf{T}_\ell = \quad \mathbf{m}_\ell \, . \tag{5.72}$$

Equation (5.70) reads as a saturation constraint on the space of the possible solutions and therefore calls for a Lagrange multiplier P, the reaction of the mixture that ensures the accomplishment of the constraint [5]. On the basis of thermodynamics arguments, it can be seen that P must contribute to each partial stress proportionally to the volume fraction, so that

$$\mathbf{T}_T = \tilde{\mathbf{T}}_T - \phi_T P, \qquad \mathbf{T}_\ell = \tilde{\mathbf{T}}_\ell - \phi_\ell P. \tag{5.73}$$

At this point one needs to deduce constitutive equations relating stresses ($\mathbf{T}_m$ and $\mathbf{T}_\ell$) and interaction forces ($\mathbf{m}_\ell$) to a suitable set of constitutive variables. The

term Γ_T has to be determined on the basis of phenomenological observation on the duplication and death of tumour cells and Γ_ℓ follows from (5.63).

We model the mixture as composed by two fluids: an ideal one (the intercellular fluid) and a fluid of cells that interact with each other by elastic repulsion and viscous drag. Regarding the constitutive equation for $\mathbf{T}_\ell$, we assume that it is an ideal fluid. This means that, for instance, if two cells switch place they do not tend to return to their original position, (as is the case of an elastic solid) and the stress field is unmodified. It is however known that cells are subject to strong short range cell-cell interactions, which represent a resistance to their relative motion. Assuming also isotropy and absence of memory effects, a possible constitutive equation for the stress of the mixture accounting for the qualitative behaviour outlined above is the following:

$$\mathbf{T}_m = -\Sigma(\phi_T)\mathbf{I} + \lambda_T(\phi_T)\nabla\cdot\mathbf{v}_T\mathbf{I} + \mu_T(\phi_T)\left(\nabla\mathbf{v}_T + (\nabla\mathbf{v}_T)^T\right) - P\mathbf{I}, \quad (5.74)$$

where Σ accounts for the elastic interaction of the cells, and μ_T measures the resistance of the multicell spheroid to shear, which depends on the density of cells. This constitutive equation corresponds to an elastic viscous fluid subject to the kinematical constraint (5.65).

The momentum equation for the mixture then writes

$$\nabla P + \Sigma'(\phi_T)\nabla\phi_T = \nabla\left[\lambda_T(\phi_T)\nabla\cdot\mathbf{v}_T\right] + \nabla\cdot\left[\mu_T(\phi_T)(\nabla\mathbf{v}_T + (\nabla\mathbf{v}_T)^T)\right], \quad (5.75)$$

where $\Sigma' = d\Sigma/d\phi_T$.

Assuming that $\tilde{\mathbf{T}}_\ell = 0$ and that the interaction force $\mathbf{m}_\ell$ has the form

$$\mathbf{m}_\ell = (1-\phi)^2 K^{-1}(\mathbf{v}_\ell - \mathbf{v}_s) + P\nabla\phi, \quad (5.76)$$

one gets Darcy's law

$$\phi_\ell(\mathbf{v}_\ell - \mathbf{v}_T) = -K\nabla P\,. \quad (5.77)$$

Remark In the one-dimensional case Equation (5.65) can be integrated to give (in Cartesian coordinates)

$$\phi_T v_T + \phi_\ell v_\ell = \text{const}\,. \quad (5.78)$$

For symmetry reasons in the centre of the tumour both liquid and cell velocity vanish, so that the integration constant is zero. This allows to write an explicit expression for $\mathbf{v}_\ell$ which can be back substituted in Equation (5.77) to get,

$$v_T = K_\ell \frac{\partial P}{\partial x}\,. \quad (5.79)$$

It is known that at the steady state the interstitial pressure is higher in the kernel of the tumour. If P can be identified with the interstitial pressure, according to Equation (5.79) the cells move toward the centre of the tumour while the extracellular liquid flows toward its border (see Figure 5.6). The experiments discussed in Dorie et al. [9,10] show that a recirculation then forms: tumour cells starve near the centre generating reusable materials which flow to the border to feed new-born cells. This phenomenon is reproduced in the simulation presented in the following section.

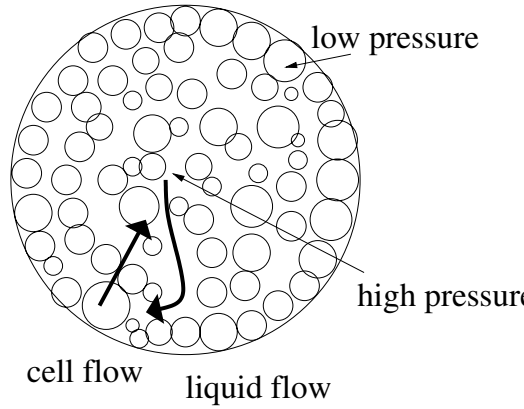

Figure 5.6
Relative motion of cells and extracellular liquid in a tumour.

5.10 A Numerical Simulation

The aim of this section is to demonstrate the ability of the model to account in a qualitatively correct way for the growth, the nonuniform character of compression, the flow of the interstitial liquid, the process of internalisation of cells described in the last section, and the existence of a steady state. The simulation is performed for a single nutrient species, characterised by the concentration $n(\mathbf{x}, t)$, filtrating through the border of the tumour and consumed by tumour cells according to Equation (5.19). In addition, we consider the viscosity terms negligible ($\lambda_T = \mu_T = 0$), equal density ($\rho_T = \rho_\ell$), and use

$$K_\ell = K_0(1 - \phi_T)^{0.1}, \tag{5.80}$$

$$\Sigma = \begin{cases} \alpha \dfrac{(\phi_T - \phi_0)^2(\phi_T - \overline{\phi})}{\sqrt{1 - \phi_T}} & \text{if } \phi_T > \phi_0, \\ 0 & \text{otherwise.} \end{cases} \tag{5.81}$$

Finally

$$\Gamma_T = \left[\gamma \left(n - \overline{n}\right)_+ - \delta\right] \phi_T \,, \tag{5.82}$$

where f_+ is the positive part of f, and it is assumed that the tumour boundary is stress free.

Focusing on the evolution between the tumour midline and the border, three phases can be recognised during the evolution (see Figure 5.7).

- At the initial stage the tumour is so small ($R \approx 0.6$) that all cells are able to duplicate because the level of nutrient is everywhere larger than $\hat{n}$. The

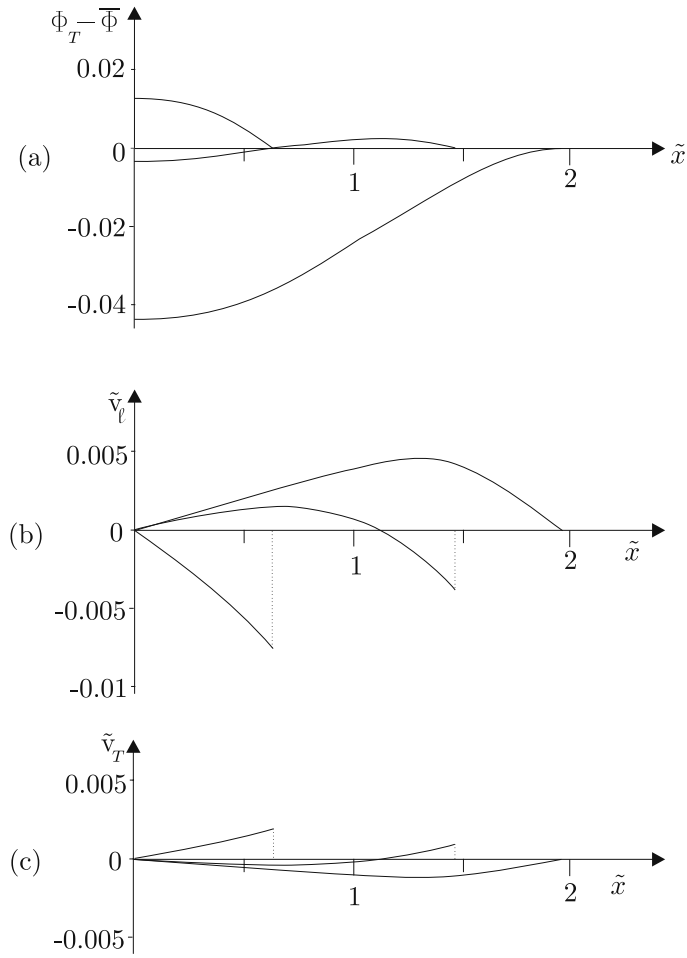

Figure 5.7

Volume ratio (a) and velocity of liquid phase (b) and of the tumour cells (c) at $\tilde{t} = 500, 1000$, and in the stationary configuration. The dotted vertical line shows the position of the tumour border while the axis on the left is the tumour centerline. The numerical simulation has been performed for equations written in nondimensional form: the tumour has initial dimensionless radius 0.1 and dimensionless parameters are $\tilde{D} = K_0\alpha/Q = 0.1$, $\tilde{\gamma} = \gamma n_0/\delta_n = 0.01$, $\tilde{\delta} = \delta/\delta_n = 0.001$, $\phi_0 = 1/2$, $\overline{\phi} = 2/3$, and $\hat{n} = \overline{n}/n_0 = 0.5$.

maximum value of the volume ratio, and therefore the maximum stress, is in the centre of the tumour. Tumour cells move from the centre to the border of the tumour ($v_T \geq 0$ everywhere), while the liquid moves in the opposite direction ($v_\ell \leq 0$ everywhere).

- In an intermediate stage ($R \approx 1.45$) the tumour can be divided into three regions: a central one where the volume ratio of tumour cells is below the stress-free value $\overline{\phi}$ with a minimum in the centre; an intermediate region where the volume ratio of tumour cells is above the stress-free value and increases till it reaches a maximum; and a border region in which the volume ratio of tumour cells decreases. In the first two regions tumour cells move toward the centre, while in the third one they move toward the boundary ($v_T \geq 0$), pushing forward the border of the tumour. The velocity of the fluid and cells vanishes where the volume ratio reaches its maximum. The last two regions can be identified with the proliferating region characterised by cells moving away from the point of maximum and organic liquid sucked toward it.

- When the tumour reaches the stationary configuration (in the present simulation $R \approx 1.95$), the maximum volume ratio is reached at the border, that does not move any more. Tumour cells, which are created in the outer region, move toward the centre ($v_T \leq 0$ everywhere) where they do not find enough nutrient and die, the organic liquid moves in the opposite direction ($v_\ell \geq 0$ everywhere). This is in agreement with the phenomenon of internalisation of cells mentioned in Dorie et al. [9,10]: tumour cells starve near the centre generating reusable materials which flow to the border to feed new-born cells.

5.11 Concluding Remarks

In the first part of this chapter we illustrated a possible way to model growth using the theory of materials with multiple natural configurations. Growth is seen as a mass increase determined by an increase in volume at constant density and without introduction of new particles. The same particles constituting the body at the initial time change their mass according to whether there is growth or resorption. In the second part of the chapter we introduced a multiphase description of the growth process. We started from the idea that multicell spheroids are made of at least two constituents: a component of sticky cells each (elastic membranes filled by organic fluid) and an organic liquid filling the extra-cellular space, which is used by the cells to grow.

In this framework one can give a precise meaning to the concept of stress. This is essential for describing several phenomena involving the stress evolution inside the growing spheroid, at the interface with the external tissues, and the mechanical

coupling between what happens inside and outside the growing tumour. This description allows in principle to determine how the tumour uncontrolled growth may cause compression, collapse, or rupture of the surrounding tissues and, in particular, collapse of immature blood vessels and infiltration and rupture of ducts and capsules. In turn, the model allows to determine how the stresses inside the tumour related to the compression of the external tissues can interfere with tumour growth.

The careful reader might wonder which is the link between the framework of *single constituent* mechanics and *mixture* theory, if any. In mixture theory [6] growth reads as a *mass exchange* between phases, a physically more correct position. As an example, in a tumour spheroid the growth of cells actually occurs at the expense of the extracellular fluid. However, the theory of mixtures, while clarifying the real nature of the mass source, yields two well known difficulties: the definition in the form of the partial stresses, that is the stress that acts on the components in the mixture, and the imposition of boundary conditions, that typically involve continuity of physical quantities (mass flow, stress) that have a different meaning on the two sides of the boundary [1].

The point to be answered experimentally is whether a tumour spheroid or some tumours *in vivo* exhibit mechanical properties that characterise solids. If this is the case, modelling a tumour as a viscous fluid is not sufficient and the intermediate stress-free configurations discussed in the first part of the chapter must be introduced. Conversely, the multiphase description is much more realistic than the single-constituent one and it accounts for mass growth in its physically correct fashion: not a mass source but a mass exchange. Therefore the next natural step seems to be the statement of a theory of *growing mixtures* in which the exchange of mass between species with elastic properties is accounted for in the same way as discussed here for the single-constituent case.

From a mathematical point of view, the key point is the characterisation of the constitutive equation for $\mathbf{G}$ (5.25), a problem that has to be properly addressed in a thermodynamical framework, not introduced in this review. We just mention two very recent papers on this subject by DiCarlo and Quiligotti [8] and Klisch et al. [15].

5.12 References

[1] Ambrosi, D., Infiltration through deformable porous media, *ZAMM* 82, 115-124, 2002.

[2] Ambrosi, D. and Mollica, F., On the mechanics of tumour growth, *Int. J. Eng. Sci.* 40, 1297-1316, 2002.

[3] Ambrosi, D. and Preziosi, L., On the closure of mass balance models of tumour growth, *Math. Models Methods Appl. Sciences* 12, 737-754, 2002.

[4] Blatz, P.J. and Ko, W.L., Application of finite elasticity theory to the deformation of rubbery materials, *Trans. Soc. Rheology* 6, 223-251, 1962.

[5] Bluhm, J., de Boer, R., and Wilmanski, K., The thermodynamic structure of the two-component model of porous incompressible materials with true mass densities, *Mech. Res. Commun.* 22, 171-180, 1995.

[6] Bowen, R.M., *The Theory of Mixtures*, in *Continuum Physics*, Vol. 3, A.C. Eringen, ed., Academic Press, New York, 1976.

[7] Byrne, H.M. and Preziosi, L., Modelling solid tumour growth using the theory of mixtures, *IMA J. Math. Appl. Med. Biol.*, submitted.

[8] DiCarlo, A. and Quiligotti, S., Growth and balance, *Mech. Res. Comm.* 29, 449-456, 2002.

[9] Dorie, M.J., Kallman, R.F., and Coyne, M.A., Effect of cytochalasin B nocodazole on migration and internalisation of cells and microspheres in tumour cells, *Exp. Cell. Res.* 166, 370-378, 1986.

[10] Dorie, M.J., Kallman, R.F., Rapacchietta, D.F., van Antwerp, D., and Huang, Y.R., Migration and internalisation of cells and polystyrene microspheres in tumour cell spheroids, *Exp. Cell. Res.* 141, 201-209, 1982.

[11] Fung, Y.C., *Biomechanics: Mechanical Properties of Living Tissues*, Springer-Verlag, Heidelberg, 1993.

[12] Gurtin, M.E., *An Introduction to Continuum Mechanics*, Academic Press, New York, 1981.

[13] Helmlinger, G., Netti, P.A., Lichtenbeld, H.C., Melder, R.J., and Jain, R.K., Solid stress inhibits the growth of multicellular tumour spheroids, *Nature Biotech.* 15, 778-783, 1997.

[14] Humphrey, J.D. and Rajagopal, K.R., A constrained mixture model for growth and remodeling of soft tissues, *Math. Models Methods Appl. Sci.* 12, 407-430, 2002.

[15] Klisch, S.M., Van Dyke, T.J., and Hoger, A., A theory of volumetric growth for compressible elastic biological materials, *Math. Mech. Solids* 6, 551-575, 2001.

[16] Mollica, F., Rajagopal, K.R., and Srinivasa, A.R., The inelastic behavior of metals subject to loading reversal, *Int. J. Plasticity* 17, 1119-1146, 2001.

[17] Murray, J.D., *Mathematical Biology*, 3rd Edition, Springer-Verlag, Heidelberg, 1993.

[18] Netti, P.A., Baxter, L.T., Boucher, Y., Skalak, R., and Jain, R.K., Macro- and microscopic fluid transport in living tissues: application to solid tumours, *AIChE J.* 43, 818-834, 1997.

[19] Skalak, R., Dasgupta, G., and Moss, M., Analytical description of growth, *J. Theor. Biol.* 94, 555-577, 1982.

[20] Skalak, R., Zargaryan, S., Jain, R.K., Netti, P.A., and Hoger, A., Compatibility and genesis of residual stress by volumetric growth, *J. Math. Biol.* 34, 889-914, 1996.

[21] Rodriguez, E.K., Hoger, A., and McCulloch, A., Stress dependent finite growth in soft elastic tissues, *J. Biomech.* 27, 455-467, 1994.

[22] Taber, L., Biomechanics of growth, remodeling, and morphogenesis, *Appl. Mech. Rev.* 48, 487-545, 1995.

[23] Truesdell, C.A. and Noll, W., *The Non-linear Field Theories of Mechanics*, 2^{nd} Edition, Springer-Verlag, Heidelberg, 1992.

Chapter 6

Modelling Tumour-Induced Angiogenesis

H.A. Levine[1] **and B.D. Sleeman**[2]
[1]*Department of Mathematics, Iowa State University (U.S.A)*
[2]*School of Mathematics, University of Leeds (U.K.)*

6.1 Abstract

As discussed in Chapters 4 and 5, avascular tumour nodules consist structurally of an inner necrotic core of dead cells as a result of nutrient starvation, an intermediate layer of quiescent cells and an outer layer of live proliferating cells. At this stage the nodule is limited to a size of at most a few millimetres in diameter. In this state of "dynamic equilibrium" there is a balance between mitosis and apoptosis and disintegration of tumour cells into waste products. For any further development to occur the tumour must initiate the process of angiogenesis — the recruitment of new blood vessels from a pre-existing vasculature (see Chapter 1). In order to achieve this the tumour cells first secrete angiogenic growth factors which in turn induce endothelial cells lining a neighbouring blood vessel to express a proteolytic enzyme which degrades the blood vessels basement lamina. The endothelial cells then migrate towards the tumour. As they migrate the endothelial cells proliferate and form sprouts which develop into loops and branches allowing for a micro-circulation of blood. From these branches more sprouts form and the process continues resulting in a capillary network. Interactions between the endothelial cells and the extracellular matrix are fundamental to the developing network. The growing capillary network eventually penetrates the tumour thus completing the angiogenic process and supplying the tumour with the nutrients it requires for further development. This in turn enables the tumour to rapidly grow and invade surrounding tissue. This chapter explains how to develop continuum (macroscopic) models of angiogenesis. In particular it concentrates on the evolution of four very important ingredients involved in tumour induced angiogenesis; namely endothelial cells, tumour angiogenic factors, proteolytic enzyme, and fibronectin, (here used as a generic term for matrix proteins) each of which has a crucial role to play. Using the idea of reinforced random walks and Michaelis Menten kinetics we will derive a system of coupled

nonlinear ordinary and partial differential equations modelling the initiation of tumour angiogenesis. We then develop the ideas further in order to model endothelial cell migration and proliferation into the extra-cellular matrix leading to angiogenesis. The main focus here is to model possible antiangiogenic strategies. The final part of the chapter discusses various methods of mathematical analysis which underpin and provide a deeper understanding of the qualitative properties of angiogenesis models. Mathematical modelling of angiogenesis has been discussed by a number of authors (Balding and McElwain [1], Orme and Chaplain [15], Sleeman [20], Chaplain and Anderson [4], Sherrat et al. [19]). These works have been mainly devoted to modelling the macroscopic events of endothelial cell evolution and migration characteristics within the ECM. The modelling ideas are based on the principles of mass conservation and chemical kinetics. While there are some formal similarities with the modelling strategies developed in this chapter there are several significant differences.

In the excellent review paper [2] Bellomo and Preziosi provide a survey of the mathematical models and methods associated with the analysis and simulation of tumour dynamic interaction with the immune system. The aim is to develop a general framework for the expression of immuno-mathematical theories and to develop research strategies.

6.2 Introduction

An understanding of the mechanisms of capillary sprout formation as a result of cell migration is fundamental to the understanding of vascularisation in many physiological and pathological situations. In the development of tumours, capillary growth through angiogenesis leads to vascularisation of the tumour, providing it with its own blood supply and consequently allowing for rapid growth and metastasis. It is important to distinguish between vasculogenesis and angiogenesis. Vasculogenesis is defined as the formation of new vessels in sites from pluripotent mesenchymal cells (e.g., angioblasts). Angiogenesis (our concern here) is defined as the outgrowth of new vessels from a pre-existing network. It is fundamental to the formation of blood vessels during placental growth, wound healing, and in tumour growth. In tumour growth angiogenesis is initiated by the release of certain growth factors from the tumour. This observation is the outcome of the fundamental work of Judah Folkman (see his article in [6] for an elegant overview). The most often cited growth factors are fibroblast growth factors (FGFs), vascular endothelial cell growth factor (VEGF), transforming growth factor alpha (TGFα), and related epidermal growth factor (EGF). VEGF is highly specific for endothelial cells and may be induced by hypoxia. We now discuss the major morphological components of the stable vessel that are involved in the angiogenic process. Endothelial cells (EC) which make up the linings of capillaries and other vessels [17] form a monolayer of flattened

and extended cells inside capillaries. The surface of the capillaries is covered with a collagenous network intermingled with laminin. This is called the basal lamina (BL). This layer is continuous and serves as a scaffold (or exocytoskeleton) upon which the EC rest. The BL is mainly formed by the EC while layers of EC and BL are sheathed by fibroblasts and possibly smooth muscle cells. In response to one or more angiogenic stimuli (we concentrate on VEGF) the EC in nearby capillaries appear to thicken and produce proteolytic enzymes (es) which in turn degrade the BL. In further response to the angiogenic factor, the cell surface begins to develop pseudo-podia that penetrate the weakened BL into the extra cellular matrix (ECM). The EC subsequently begin to accumulate in regions where the concentration of VEGF reaches a threshold value. The vessel dilates as the EC aggregate and the proteases degrade the BL and the ECM, thus allowing the EC to migrate and grow toward the VEGF source by chemotaxis. The EC proliferate as they move and other cells (e.g., pericytes) move towards the migrating EC to initiate the building of a primitive BL. In this way capillary sprouts are formed.

6.3 Biochemical Kinetics

In order to better understand how the angiogenic factor acts on the ECs we consider that each cell has a certain number of receptors to which the angiogenic factors (ligands) bind. The receptor-ligand complexes (intermediates) in turn stimulate the cell to produce proteolytic enzymes and form new receptors. We propose to model this process in the following manner: If V denotes a molecule (dimer) of angiogenic factor and R denotes some receptor (also a dimer) on the endothelial cell surface to which it binds, the activated complex so formed, RV, signals a cascade of intracellular signalling events which results in the transcription of RNAs which in turn are translated by the ribosomes into proteolytic enzyme, C. The receptor complex RV is subsequently invaginated into the cell cytoplasm from the cell surface where it is degraded. In the cell nucleus, the cell signal cascade activated by the receptor activate transcription factors which leads to the translation of a new receptor R which then moves to the cell surface. The proteolytic enzyme C degrades the basal laminar wall leaving a product F' by acting as a catalyst for fibronectin degradation. We use classical Michaelis-Menten kinetics for this standard catalytic reaction. In symbols

$$
\begin{aligned}
V + R &\underset{k_{-1}}{\overset{k_1}{\rightleftharpoons}} RV, \\
RV &\overset{k_2}{\to} C + R, \\
C + F &\overset{k_3}{\to} [CF], \\
[CF] &\overset{k_4}{\to} F' + C.
\end{aligned}
\tag{6.1}
$$

The point of view adopted here is that the receptor dimers at the surface of the cell function the same way an enzyme functions in classical enzymatic catalysis. This is a first step in modelling a much more complicated process. It is known that an endothelial cell will produce, in response to a single molecule of growth factor, several, n_v say, molecules of protease. The number n_v will in general be quite large and will depend on the concentrations of growth factor the cell encounters at its cell surface [18]. This means that the mechanism (6.1) should strictly be modified to read

$$V + R \underset{k_{-1}}{\overset{k_1}{\rightleftharpoons}} RV,$$

$$S + RV \overset{k_2}{\rightarrow} C + R.$$

Here S is an overall molecular resource term which reflects the resources used in the translation of protein from the messenger RNA.

That is, a single molecule of growth factor, by binding to an EC receptor, initiates a cascade of signalling and amplification events involving G-proteins, transcription factors, and DNA which lead to the synthesis of several molecules of protease and a receptor cell of the initial type. Once this cascade has been initiated, the growth factor is rendered inert along a second pathway. The sequence of kinetic events is very long and the rate constants for each step are not known.

The overall mechanism is known as the Map-kinase signalling cascade. The precise details have been recorded in the appendix to [12].

Let x denote position along the capillary vessel wall and t denote time. With concentrations expressed in micro moles per litre, we define the following quantities:

v = concentration of angiogenic factor V.

c = concentration of proteolytic enzyme C.

r = density of receptors R on the cell directed into the basement lamina.

l = concentration of intermediate receptor complex RV.

η = concentration of endothelial cells.

f = concentration of fibronectin.

Applying the law of mass action to the first two equations in (6.1) we obtain

$$\frac{\partial r}{\partial t} = -k_1 r v + (k_{-1} + k_2) l, \tag{6.2}$$

$$\frac{\partial l}{\partial t} = k_1 r v - (k_{-1} + k_2) l, \tag{6.3}$$

$$\frac{\partial v}{\partial t} = -k_1 r v + k_{-1} l, \tag{6.4}$$

$$\frac{\partial c}{\partial t} = k_2 l. \tag{6.5}$$

The upshot of the remarks above concerning the Map-kinase signalling cascade would result in Equation (6.5) being replaced by

$$\frac{\partial c}{\partial t} = n_v k_2 l,$$

where now the constant k_2 includes a resource factor involving the concentration $[S]$ which is assumed to be in excess so that its time variation may be neglected. We take $n_v = 1$ for illustrative purposes. Applying standard Michaelis-Menten kinetics to the third and fourth equations in (6.1) there results

$$\frac{\partial f}{\partial t} = -\frac{\lambda_2 c f}{1 + \nu_2 f}, \tag{6.6}$$

where λ_2=k_4 and $\nu_2 = k_4/k_3$. The rate equations for protease and fibronectin are not complete as they stand. For example, it is known that protease decays at a rate proportional to its concentration. It is also known that the ECs produce fibronectin. To account for these we modify Equations (6.5) and (6.6) to

$$\frac{\partial c}{\partial t} = k_2 l - \mu c, \tag{6.7}$$

$$\frac{\partial f}{\partial t} = \beta(f_m - f) f \eta - \frac{\lambda_2 c f}{1 + \nu_2 f}, \tag{6.8}$$

where $\beta > 0$, $\mu > 0$, and f_m is the density of fibronectin in the normal capillary. The five rate equations require initial conditions for r, l, v, c, and f. Although the number of receptors per EC is not known precisely, it is known to be of the order of $10^5 \pm 10^3$. The next step in modelling the kinetics is to relate the receptor density r to the endothelial cell density η. In order to do this we need to consider the underlying reasoning which supports the Michaelis-Menten mechanism. We do not go into this here but refer to the arguments, based on the pseudo steady state hypothesis, set out in [11], [10]. The upshot of these arguments is that the kinetic equations for c and v can be written as

$$\frac{\partial c}{\partial t} = \frac{\lambda_1 v \eta}{1 + \nu_1 v} - \mu c, \tag{6.9}$$

$$\frac{\partial v}{\partial t} = -\frac{\lambda_1 v \eta}{1 + \nu_1 v}. \tag{6.10}$$

6.4 Reinforced Random Walks and Cell Movement

To model the dynamics of the EC we employ the ideas of reinforced random walks [5] as described in [11], [10], and [16]. In order to understand the idea behind the notion of reinforced random walks we consider the parent capillary wall to be a one dimensional lattice with endothelial cells equally spaced and in nonoverlapping contact located at reference points nh along the x-axis. Let $\hat{\tau}_n^{\pm}(\mathrm{W})$ depending on the control substances W, be the transition probability rate per unit time for a one

step move of an EC at site n to site $n+1$ or site $n-1$ respectively. Then the time rate of change of $\eta_n(t)$ is governed by the equation

$$\frac{\partial \eta_n}{\partial t} = \hat{\tau}^+_{n-1}(W)\eta_{n-1} + \hat{\tau}^-_{n+1}(W)\eta_{n+1} - (\hat{\tau}^+_n(W) + \hat{\tau}^-_n(W))\eta_n. \tag{6.11}$$

That is, $\eta_n(t)$ will be augmented by cells moving from the positions $(n\pm1)h$ to nh and diminished by cells moving from nh to either $(n+1)h$ or $(n-1)h$. The quantity $(\hat{\tau}^+_n(W) + \hat{\tau}^-_n(W))^{-1}$ is the mean waiting time at site n. It is convenient to think of this conditional probability density as the density of endothelial cells. The transition probability rates $\hat{\tau}^{\pm}_n(\cdot)$ depend on the control substances we have denoted by W and are defined on the lattice at $\frac{1}{2}-$step size. For our modelling W will include the proteolytic enzyme c and fibronectin f. Now suppose that the decision of "when to move" is independent of the decision "where to move." Then the mean waiting time across the lattice is constant. Hence the transitions $\hat{\tau}^{\pm}_n$ must be suitably scaled and normalised so that

$$\hat{\tau}^+_n(W) + \hat{\tau}^-_n(W) = 2\lambda \tag{6.12}$$

where λ is a scaling parameter. Let the transition rates depend on W only at the nearest neighbours $W_{(n+1/2)}$. Define the new jump process τ by

$$\hat{\tau}^{\pm}_n(W) = 2\lambda \frac{\tau(W_{(n\pm1/2)})}{\tau(W_{(n+1/2)}) + \tau(W_{(n-1/2)})} \equiv 2\lambda N^{\pm}(W). \tag{6.13}$$

The master equation (6.11) now reads

$$\begin{aligned}\frac{1}{2\lambda}\frac{\partial \eta_n}{\partial t} = {} & N^+(W_{n-1/2}, W_{n-3/2})\eta_{n-1} + N^-(W_{n+1/2}, W_{n+3/2})\eta_{n+1} \\ & - [N^+(W_{n+1/2}, W_{n-1/2}) + N^-(W_{n-1/2}, W_{n+1/2})]\eta_n. \end{aligned} \tag{6.14}$$

We now proceed to the continuous limit using Taylor's expansion and by letting $h\to0$ and $\lambda\to\infty$ in such a way that

$$D \equiv 1/2 \lim_{h\to0,\lambda\to\infty} \lambda h^2 < \infty. \tag{6.15}$$

This results in the continuum limit of the master equation, viz;

$$\frac{\partial \eta}{\partial t} = D\frac{\partial}{\partial x}((\eta\frac{\partial}{\partial x}(\ln\frac{\eta}{\tau})) \tag{6.16}$$

where $\eta(x,t)$ now denotes endothelial cell density and $\tau = \tau(W) = \tau(W(f,c))$. To complete the model we need to impose appropriate initial and boundary conditions. These are

$$\begin{aligned} c(x,0) &= c_0(x) \geq 0, \\ f(x,0) &= f_m(x) > 0, \\ v(x,0) &= v_0(x) > 0. \end{aligned} \tag{6.17}$$

The system is closed by taking the "no-flux" boundary condition

$$\eta \frac{\partial}{\partial x}(\ln \frac{\eta}{\tau}) = 0, \quad x = 0, 1. \tag{6.18}$$

It is important to appreciate that when we compare Equations (6.11) and (6.16), the connection between angiogenesis at the cell level and at the cell density level is via modelling of the transition rate $\tau(W)$. It is a challenging and open problem of how one should model $\tau(W)$ at the individual cell level. Nevertheless at the cell density level experimentation is easier and this fact coupled with a qualitative knowledge of the properties of the solutions of (6.11) facilitates the modelling of $\tau(W)$ considerably. To begin with we shall suppose the transition probability rate function τ to be factored as

$$\tau(W(f, c)) = \tau_1(c)\tau_2(f). \tag{6.19}$$

These factors are chosen in order to provide a measure of how responsive ECs are to protease and to fibronectin. It is known that proteases stimulate the movement of endothelial cells. Here we choose

$$\tau_1(c)\tau_2(f) = \left(\frac{\alpha_1 + c}{\alpha_2 + c}\right)^{\gamma_1} \left(\frac{\beta_1 + f}{\beta_2 + f}\right)^{\gamma_2}. \tag{6.20}$$

where $0 < \alpha_1 \ll 1 < \alpha_2$ and $\beta_1 > 1 \gg \beta_2 > 0$. The idea here is that ECs move in response to fibronectin degradation by moving to lower levels of f concentration and in response to protease by moving to higher levels of c concentration. That is, the greater the degree of protease production the greater the degree of fibronectin degradation. It is this mechanism that allows for the breakdown of the capillary wall. Choosing $\tau_1(c)\tau_2(f)$ as a rational function of c and f is to avoid singularities in the coefficients of η_x, η, which would otherwise arise in Equation (6.16) when f and c are small. Other choices for these factors which avoid this and still preserve the qualitative properties above are given in [12].

6.5 Numerical Experiments

In the numerical computations we choose

$$\begin{aligned} \eta(x, 0) &= 1, \\ v(x, 0) &= v_0 k_m (1 - cos(2\pi x))^m, \\ c(x, 0) &= 0, \\ f(x, 0) &= 1, \end{aligned} \tag{6.21}$$

where v_0, k_m, and m are positive constants. The constant k_m is chosen so that

$$\int_0^1 v(x, 0)dx = v_0.$$

Table 6.1 Value of parameters.

$\eta(x,t)$ (EC movement)	$D = 3.6 \times 10^{-5}$	$\alpha_1 = 0.001$	$\alpha_2 = 1.0$	$\gamma_1 = 1.2$
$\eta(x,t)$ (EC movement)	$\beta_1 = 1.0$	$\beta_2 = 0.001$	$\gamma_2 = 1.2$	
v (VEGF kinetics)	$\lambda_1 = 73.0$	$\nu_1 = 0.007$	$m = 100$	$v_0 = 15$
c (enzyme kinetics)	$\lambda_1 = 73.0$	$\nu_1 = 0.007$		
f (fibronectin)	$\beta = 0.222$	$\lambda_2 = 19.0$	$\nu_2 = 1.28$	

The constant m is to be thought of as a measure of how concentrated or localised the angiogenic factor is. This is the type of problem one might consider if a small amount of growth factor were supplied to the rest state suddenly, or over a very short time scale.

Good biological constants for events occurring *in vivo* are notoriously hard to find. This is further complicated by the fact that under the general rubric "fibronectin," for example, are a whole host of ECM proteins including the family of collagens. Also, there are many different growth factors. Further complicating these issues is the fact that much of the data available is *in vitro* data. In living systems, the situation may be quite different. We have carried out an extensive literature search and have chosen parameter values which are representative of the mechanisms proposed here, (see Table 6.1, the units are given in detail in [11]).

Figures 6.1 to 6.4 present the results of numerical experimentation with the system (6.8) to (6.10), (6.16), (6.20), and (6.21). With $m = 100$ we observe that the fibronectin density rapidly degrades in the interval $0.44 < x < 0.56$ which has a length of about 6 to 10 microns. It is in this interval that the growth factor is initially most highly concentrated. The channel width is in the range of a typical capillary diameter.

In Figure 6.2 the response of the EC to the angiogenic stimulus is shown to form a bimodal structure of aggregation. It is suggestive of a primitive lining to the emerging capillary sprout. Figure 6.3 illustrates the rapid uptake of growth factor by the EC while Figure 6.4 shows the convergence of proteolytic enzyme to a steady state.

6.6 Antiangiogenesis Models

In the previous section we developed a model for the initiation of sprouting of capillaries from a nearby blood vessel. Here we discuss the modelling of angiogenesis in the ECM. We also propose two mechanisms whereby protease expressed by ECs in the presence of growth factor may be inhibited by angiostatin, a general antiangiogenesis agent. Several antiangiogenic agents alone or in combination with conventional therapies are now in clinical trials [7]. These trials are based on strategies that

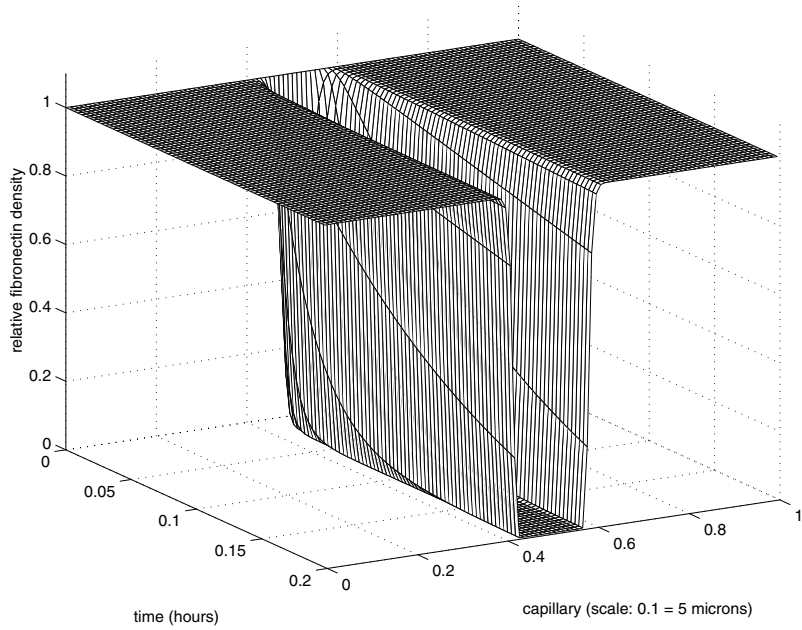

Figure 6.1
Time evolution of fibronectin degradation.

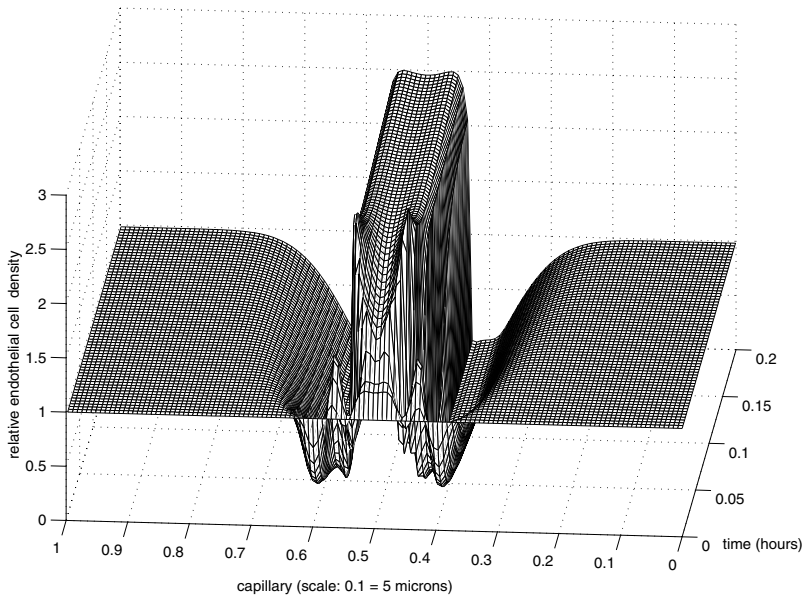

Figure 6.2
Time evolution of EC distribution illustrating bimodality.

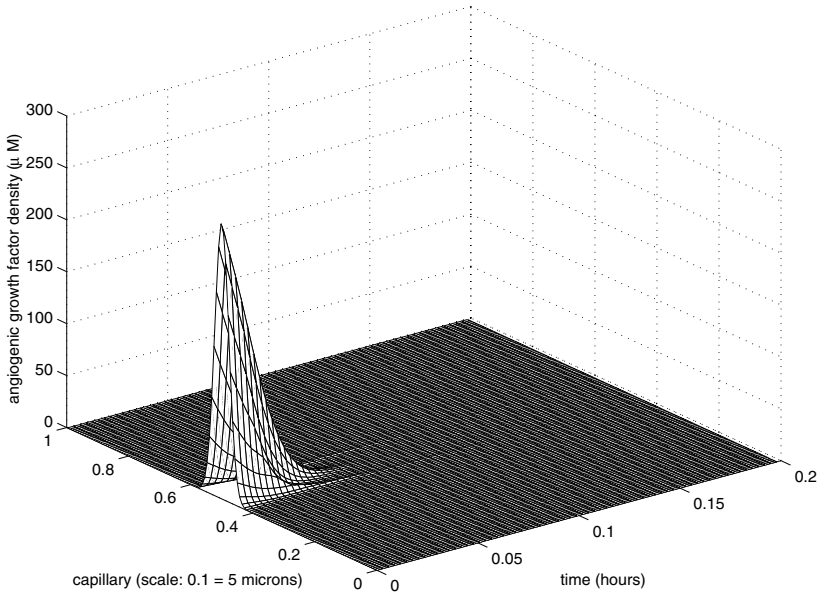

Figure 6.3
Time evolution of growth factor.

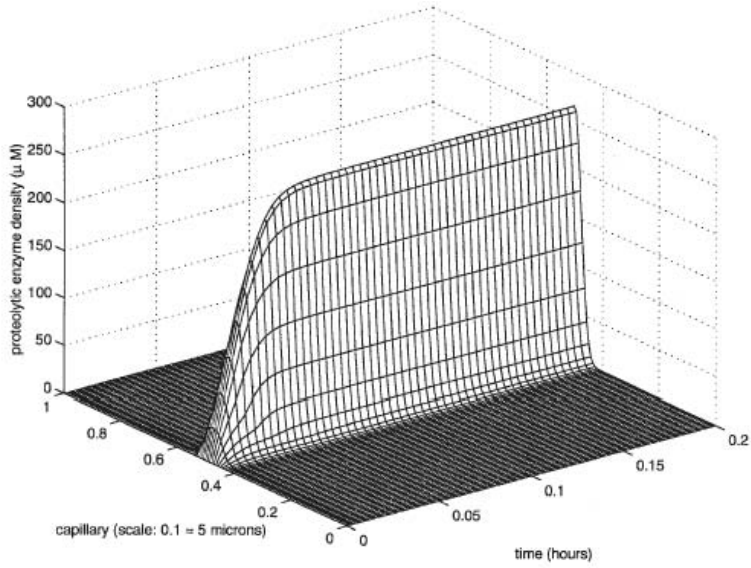

Figure 6.4
Time evolution of protease.

(i) interfere with angiogenic ligands;

(ii) upregulate or deliver endogenous inhibitors; or

(iii) directly target the vasculature.

However there are a number of potential problems as discussed by Carmeliet and Jain [3] that warrant caution in clinical trials in humans. We shall concentrate on strategies (i) and (ii).

In order to proceed we first describe the geometry of the problem and then outline the biochemistry of angiogenesis and its inhibition. A fundamental aspect of this is to develop the appropriate chemical considerations and then to describe a model for the penetration of capillary sprouts into the ECM.

6.6.1 The Geometry of the Problem

Throughout we shall use Figure 6.5 as a basis for the modelling process.

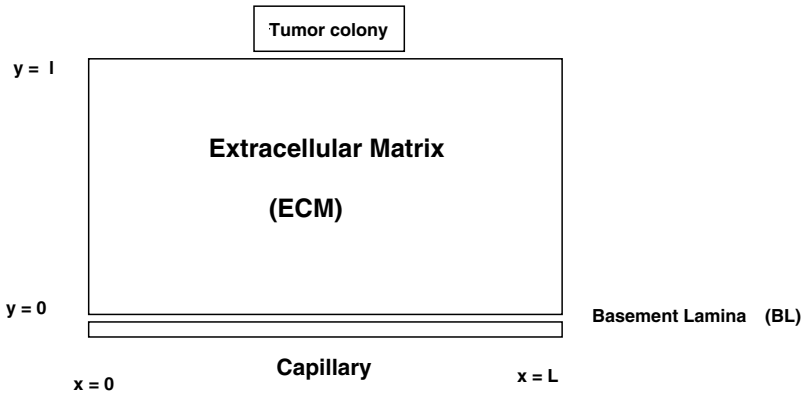

Figure 6.5
The geometry for the mathematical model.

In the $x - y$ plane we envisage a capillary segment of L microns located along the x-axis on the interval $[0, L]$ with a tumour colony located l microns above the x-axis.

A time dependent function defined on $[0, L] \times [0, l]$ will be denoted by upper case letters $G(x, y, t)$. A function defined inside the capillary wall will be denoted by lower case letters $g(x, t)$. Note that in general $g(x, t) \neq G(x, 0, t)$. Although we imagine the capillary wall to be negligibly thin we take as a measure of its penetrability, the density of fibronectin $f(x, t)$.

6.6.2 The Biochemistry of Angiogenesis and Its Inhibition

As above let V denote a molecule of angiogenic factor and R a receptor on the EC surface. These combine to produce an intermediate complex RV which is an activated state of the receptor that results in the production and expression of proteolytic enzyme, C and a modified intermediate receptor R'. The receptor R' is subsequently removed from the cell surface after which it is either regarded to form R or a new R is then synthesised by the cell. It then moves to the cell surface.

$$V + R \underset{k_{-1}}{\overset{k_1}{\rightleftharpoons}} RV, \tag{6.22}$$

$$RV \overset{k_2}{\rightarrow} C + R. \tag{6.23}$$

6.6.3 Mechanism for the Production of Protease Inhibitors

There are several ways in which angiostatic agents might inhibit angiogenesis [14]. Here we restrict attention to two such mechanisms:

(1) **Angiostatin as a direct inhibitor of protease [22]**

$$A + C_A \rightleftharpoons C_I, \tag{6.24}$$

where C_I denotes proteolytic enzyme molecules which are inhibited by the angiostatin A from functioning as a catalyst for fibronectin degradation. C_A denotes those molecules which degrade fibronectin.

In terms of concentrations;

$$[C] = [C_A] + [C_I] + [C_A F]. \tag{6.25}$$

Assuming Equation (6.22) is in equilibrium we have

$$[C_I] = \nu_e [A][C_A], \tag{6.26}$$

where ν_e is the equilibrium constant for this step and $(\nu_e \gg 1)$.

(2) **Angiostatin stimulates ECs to produce inhibitor**

Another possibility is to involve the endothelial cells once more. In this more complex mechanism the angiostatin stimulates ECs to express an inhibitor I according to the mechanism;

$$A + R_A \underset{k_{-3}}{\overset{k_3}{\rightleftharpoons}} AR_A, \tag{6.27}$$

$$[AR_A] \stackrel{k_4}{\rightarrow} I + R_A, \tag{6.28}$$

$$C_A + I \rightleftharpoons C_I. \tag{6.29}$$

Here R_A is a receptor protein on the EC, $[AR_A]$ is the intermediate complex and I is a protease inhibitor produced by the ECs in response to the angiostatic agent by an overall mechanism which we assume to be of Michaelis-Menten type. C_I denotes the proteolytic enzyme molecules that are inhibited by I from functioning as a catalyst for fibronectin degradation. Assuming the step (6.27) to be in equilibrium we have

$$[C_I] = \nu_e [I][C_A]. \tag{6.30}$$

6.6.4 Mechanism for the Degradation of Fibronectin

$$C_A + F \underset{k_{-5}}{\overset{k_5}{\rightleftharpoons}} [C_A F], \tag{6.31}$$

$$[C_A F] \stackrel{k_6}{\rightarrow} C_A + F'. \tag{6.32}$$

6.7 Equations of Mass Action

Consider the case for which A is converted by the ECs into a protease inhibitor I. The law of mass action applied to Equations (6.22) to (6.32) gives

$$\frac{\partial [V]}{\partial t} = -k_1 [R][V] + k_{-1}[RV], \tag{6.33}$$

$$\frac{\partial [R]}{\partial t} = -k_1 [R][V] + (k_{-1} + k_2)[RV], \tag{6.34}$$

$$\frac{\partial [RV]}{\partial t} = k_1 [R][V] - (k_{-1} + k_2)[RV], \tag{6.35}$$

$$\frac{\partial [C]}{\partial t} = k_2 [RV] - \mu [C], \tag{6.36}$$

$$\frac{\partial [A]}{\partial t} = -k_3 [A][R_A] + k_{-3}[R_A A], \tag{6.37}$$

$$\frac{\partial [R_A]}{\partial t} = -k_3 [R_A][A] + (k_{-3} + k_4)[R_A A], \tag{6.38}$$

$$\frac{\partial [R_A A]}{\partial t} = k_3 [A][R_A] - (k_{-3} + k_4)[R_A A], \tag{6.39}$$

$$\frac{\partial [I]}{\partial t} = k_4 [R_A A]. \tag{6.40}$$

When angiostatin acts directly as an inhibitor, the last four equations (6.37) to (6.40) may be deleted.

The enzyme kinetics for fibronectin decay leads to three additional ordinary differential equations.

It is reasonable to assume that the kinetics for degradation of fibronectin by protease is of Michaelis-Menten type. The treble then reduces to the form

$$\frac{\partial[F]}{\partial t} = -\lambda_3 \frac{[C_A][F]}{1+\nu_3[F]}. \tag{6.41}$$

In order to develop the model in terms of measurable quantities, e.g., relating receptor densities to EC densities, we employ a number of techniques and observations, namely,

- conservation laws,
- the idea of pseudo steady states [13], and
- inner and outer singular perturbations.

For a full discussion of these arguments we refer to [11]. These ideas used in conjunction with the following conservation equation for protease and the equilibrium equation of active protease

$$[C] = [C_A] + [C_I] + [C_A F],$$

$$[C_I] = \nu_e [I][C_A], \tag{6.42}$$

leads to the set

$$\frac{\partial[V]}{\partial t} = \frac{-\lambda_1[V](t)[EC](t)}{1+\nu_1[V](t)}, \tag{6.43}$$

$$\frac{\partial[C]}{\partial t} = \frac{\lambda_1[V](t)[EC](t)}{1+\nu_1[V](t)} - \mu[C](t), \tag{6.44}$$

$$\frac{\partial[A]}{\partial t} = \frac{-\lambda_2[A](t)[EC](t)}{1+\nu_2[A](t)}, \tag{6.45}$$

$$\frac{\partial[I]}{\partial t} = \frac{\lambda_2[A](t)[EC](t)}{1+\nu_2[A](t)}. \tag{6.46}$$

6.8 Chemical Transport in the Capillary and in the ECM

We introduce the notation

Table 6.2 Notation for quantities used in the text

In the Capillary	Definition	In the ECM
$c(x,t)$	proteolytic enzyme C	$C(x,y,t)$
$c_a(x,t)$	active protease C_A	$C_a(x,y,t)$
$c_i(x,t)$	inhibited enzyme C_I	$C(x,y,t)$
$i_a(x,t)$	protease inhibitor I	$I_a(x,y,t)$
$f(x,t)$	fibronectin F	$F(x,y,t)$
$a(x,t)$	angiostatin A	$A(x,y,t)$
$\eta(x,t)$	EC density	$N(x,y,t)$
$v(x,t)$	angiogenic factor	$V(x,y,t)$

6.8.1 Chemical Transport in the Capillary

(i) **Angiostatin stimulates EC to produce inhibitor**

$$\frac{\partial v}{\partial t} = \frac{-\lambda_1 v}{1+\nu_1 v}\frac{\eta}{\eta_0} + v_r(x,t), \tag{6.47}$$

$$\frac{\partial c}{\partial t} = \frac{\lambda_1 v}{1+\nu_1 v}\frac{\eta}{\eta_0} - \mu c, \tag{6.48}$$

$$\frac{\partial f}{\partial t} = \frac{4}{T_f} f\left(1-\frac{f}{f_0}\right)\frac{\eta}{\eta_0} - \frac{\lambda_3 c_a f}{1+\nu_3 f}, \tag{6.49}$$

$$\frac{\partial a}{\partial t} = \frac{-\lambda_2 a}{1+\nu_2 a}\frac{\eta}{\eta_0} + a_r(x,t), \tag{6.50}$$

$$\frac{\partial i_a}{\partial t} = \frac{\lambda_2 a}{1+\nu_2 a}\frac{\eta}{\eta_0} - \frac{i_a(x,t)}{T_{rel}}, \tag{6.51}$$

$$c = c_a + c_i + \nu_3 c_a f, \tag{6.52}$$

$$c_i = \nu_e i_a c_a. \tag{6.53}$$

(ii) **Angiostatin acts directly as an inhibitor**

$$\frac{\partial v}{\partial t} = \frac{-\lambda_1 v}{1+\nu_1 v}\frac{\eta}{\eta_0} + v_r(x,t), \tag{6.54}$$

$$\frac{\partial c}{\partial t} = \frac{\lambda_1 v}{1+\nu_1 v}\frac{\eta}{\eta_0} - \mu c, \tag{6.55}$$

$$\frac{\partial f}{\partial t} = \frac{4}{T_f} f\left(1 - \frac{f}{f_0}\right)\frac{\eta}{\eta_0} - \frac{\lambda_3 c_a f}{1+\nu_3 f}, \tag{6.56}$$

$$\frac{\partial a}{\partial t} = a_r(x,t) - \frac{a(x,t)}{T_{rel}}, \tag{6.57}$$

$$c = c_a + c_i + \nu_3 c_a f, \tag{6.58}$$

$$c_i = \nu_e i_a c_a. \tag{6.59}$$

6.8.2 Chemical Transport in the ECM

Here we set down the model equations governing cell transport in the ECM. We follow this with an important commentary.

(i) **Angiostatin stimulates EC to produce inhibitor**

$$\frac{\partial V}{\partial t} = \nabla\cdot[D_V(x,y)\nabla(V^m)] - \frac{-\lambda_1 V}{1+\nu_1 V}\frac{N}{\eta_0} + v_r(x,t), \tag{6.60}$$

$$\frac{\partial C}{\partial t} = \frac{\lambda_1 V}{1+\nu_1 V}\frac{N}{\mu_0} - \mu C, \tag{6.61}$$

$$\frac{\partial F}{\partial t} = D_F K(x,y)|\nabla F| + \frac{4}{T_F} F\left(1 - \frac{F}{F_0}\right) - \frac{\lambda_3 C_a F}{1+\nu_3 F}, \tag{6.62}$$

$$\frac{\partial A}{\partial t} = \nabla\cdot[D_A(x,y)\nabla(A^m)] - \frac{-\lambda_2 A}{1+\nu_2 A}\frac{N}{\mu_0} + a_r(x,t)(1 - \frac{F}{F_0}), \tag{6.63}$$

$$\frac{\partial I_a}{\partial t} = \frac{\lambda_2 A}{1+\nu_2 A}\frac{N}{\eta_0} - \frac{I_a(x,t)}{T_{rel}}, \tag{6.64}$$

$$C = C_a + C_i + \nu_3 C_a F, \tag{6.65}$$

$$C_i = \nu_e I_a C_a. \tag{6.66}$$

(ii) **Angiostatin as direct inhibitor**

$$\frac{\partial V}{\partial t} = \nabla\cdot[D_V(x,y)\nabla(V^m)] - \frac{-\lambda_1 v}{1+\nu_1 v}\frac{\eta}{\eta_0} + v_r(x,t), \tag{6.67}$$

$$\frac{\partial C}{\partial t} = \frac{\lambda_1 V}{1+\nu_1 V}\frac{N}{\mu_0} - \mu C, \tag{6.68}$$

$$\frac{\partial F}{\partial t} = D_F K(x,y)|\nabla F| + \frac{4}{T_F} F\left(1 - \frac{F}{F_0}\right) - \frac{\lambda_3 C_a F}{1+\nu_3 F}, \tag{6.69}$$

$$\frac{\partial A}{\partial t} = \nabla\cdot[D_A(x,y)\nabla(A^m)] + a_r(x,t)(1 - \frac{F}{F_0}) - \frac{A}{T_{rel}}, \tag{6.70}$$

$$\frac{\partial I_a}{\partial t} = \frac{\lambda_2 A}{1+\nu_2 A}\frac{N}{\eta_0} - \frac{I_a(x,t)}{T_{rel}}, \tag{6.71}$$

$$C = C_a + C_i + \nu_3 C_a F, \tag{6.72}$$

$$C_i = \nu_e A C_a. \tag{6.73}$$

Remarks

(1) We assume that background fibronectin production is in much greater excess than that of the EC. So the logistic term is independent of N.

(2) We assume the ECM is a porous medium.

(3) We allow for the inhomogeneous diffusion of growth factor and for angiostatin.

(4) We need to account for the diffusion of fibronectin in the ECM.

Generally diffusion is based on Fick's law which states that the flux of particles is proportional to the gradient of concentration. The assumption being that the surrounding medium is homogeneous, the local concentration of the diffusing particle is small, and the particles themselves are small. Fibronectin is a high molecular weight protein in a highly heterogeneous region which is held in the ECM by noncovalent linkages with other proteins. To model this we use diffusion by mean curvature (see [8]).

6.9 Cell Movement

6.9.1 Cell Movement in the Capillary

Here we recall the transport of an EC

$$\frac{\partial \eta}{\partial t} = D\frac{\partial}{\partial x}(\eta \frac{\partial}{\partial x}(\ln \frac{\eta}{\tau})), \tag{6.74}$$

$$\tau_1(c)\tau_2(f) = \left(\frac{\alpha_1 + c}{\alpha_2 + c}\right)^{\gamma_1} \left(\frac{\beta_1 + f}{\beta_2 + f}\right)^{\gamma_2}, \tag{6.75}$$

where $0 < \alpha_1 \ll 1 < \alpha_2$ and $\beta_1 > 1 \gg \beta_2 > 0$.

6.9.2 Cell Movement in the ECM

This time we use a $2 - D$ form of the reinforced random walk master equation and write

$$\begin{aligned}\frac{\partial N}{\partial t} &= D_N \nabla \cdot [N \nabla \ln(\frac{N}{T(C_a, F)})] \\ &+ Q(\kappa)\left(N[\theta(1 - \frac{N}{\eta_0}) + G(C_a)\frac{\partial C_a}{\partial t}]H(C_a - C_{a,0}) - \mu_1 N\right).\end{aligned} \tag{6.76}$$

We take the transition rate function T to be of the same form (although with different parameters) as τ.

$Q(\kappa)$ is a curvature sensitivity factor.

$H(C_a - C_{a,0})$ is a switch.

The second term on the right hand side of 6.76 is composed of a logistic growth term together with a term which represents growth in response to active protease.

6.10 Transmission, Boundary, and Initial Conditions

6.10.1 Transmission Conditions

$$v_r(x,t) = B_1 V(x,0,t), \tag{6.77}$$

$$a_r = A_r H(t - T_{iv}) \tag{6.78}$$

where A_r is the rate at which angiostatin is supplied.

$$N(x,0,t) - \psi_1 H(f_1 - f(x,t))\eta(x,t) = 0, \tag{6.79}$$

$$-D_V(x,0,t)\frac{\partial V^m}{\partial y} + \psi(V(x,0,t) - v(x,t)) = 0, \tag{6.80}$$

$$-D_A(x,0,t)\frac{\partial A^m}{\partial y} + \psi^1(A(x,0,t) - a(x,t)) = 0, \tag{6.81}$$

$$-D_F(x,0,t)\frac{\partial F(x,0,t)}{\partial y} = 0, \tag{6.82}$$

together with standard transport conditions.

6.10.2 Boundary Conditions

$$D_V(x,l,t)\frac{\partial V^m(x,l,t)}{\partial y} - V_l(x,t) = 0, \tag{6.83}$$

$$D_A(x,l,t)\frac{\partial A^m(x,l,t)}{\partial y} = 0, \tag{6.84}$$

$$D_F(x,l,t)\frac{\partial F(x,l,t)}{\partial y} = 0, \tag{6.85}$$

$$D_N N \frac{\partial(\ln \frac{N}{T})}{\partial y}(x,l,t) + \theta^1 N = 0 \tag{6.86}$$

where, for example

$$V_l(x,t) = v_0 \frac{\sigma}{L}[1 - \cos(\left(\frac{2\pi x}{L}\right)]^{m_0} e^{-\delta t}.$$

We also apply "no-flux" type boundary conditions at $x = 0, L$.

6.10.3 Initial Conditions

$$\begin{array}{lll} \eta(x,0) = 1, & v(x,0) = 0, & f(x,0) = 1, \\ c(x,0) = 0, & a(x,0) = 0, & i_a(x,0) = 0, \\ N(x,y,0) = 0, & V(x,y,0) = 0, & F(x,y,0) = 1, \\ C(x,y,0) = 0, & A(x,y,0) = 0, & I_a(x,y,0) = 0. \end{array}$$

6.11 Numerical Experiments

In the first set of experiments a tumour was implanted 25 microns from an existing capillary. In Figure 6.6 we see the advance of EC across the ECM while in Figure 6.7 we see the degradation of fibronectin creating a channel in the ECM.

During the computations travel times at various points in the ECM were calculated. For example it was found that it takes 3.49 hours for growth factor to diffuse across the ECM from a tumour 25 microns away from the parent capillary. It then takes another 0.25 hours for the emerging capillary sprout to move 2.5 microns towards the tumour. The mean tip speed is 0.242 mm/day. The sprout advances a further 2.5 microns at a mean tip speed of 0.436 mm/day and so on. On extrapolating these times to a tumour implanted at 2 mm from the parent capillary obtain travel times of the order of 16 days which is in good agreement with travel times observed in corneal rabbit eye experiments.

In Figures 6.8 and 6.9 we give time courses for EC density and fibronectin degradation when angiostatin allows for the expression of protease inhibitor. Angiostatin is activated in the capillary system when the sprout has developed over 4.45 hours. Notice that the maximum EC density decreases while the fibronectin channel narrows and shrinks. Similar phenomena are observed in numerical experiments in which angiostatin acts directly as an inhibitor. For full details of these results and of further experiments we refer to [8].

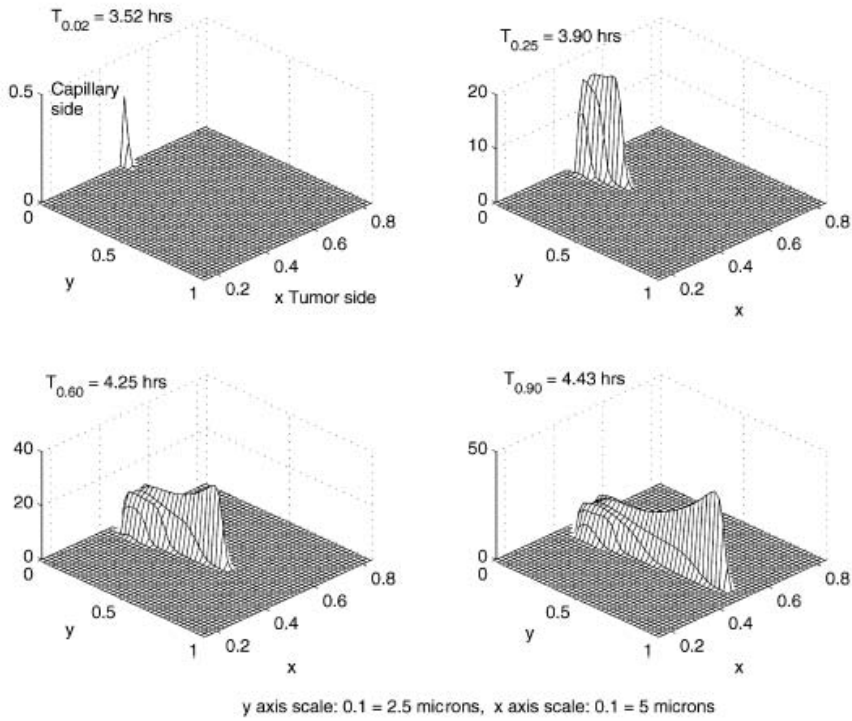

Figure 6.6

Time course for EC propagation in the ECM.

Our numerical investigations suggest the more efficaciously one can tie up the protease the more rapidly can one inhibit angiogenesis.

Several antiangiogenesis agents alone or in combination with conventional therapies are now in clinical trials. These trials are based on strategies that

(1) interfere with angiogenic ligands;

(2) upregulate or deliver endogenous inhibitors; or

(3) directly target the vasculature.

However there are a number of potential problems as discussed by Carmeliet and Jain [3] that warrant caution in clinical trials in humans. anticancer therapy is currently a subject of considerable controversy. While it offers new hope for the successful treatment of cancer, a degree of caution is necessary. It is hoped that the work described here will make a positive contribution to the debate by putting the possible mechanisms on a quantitative footing.

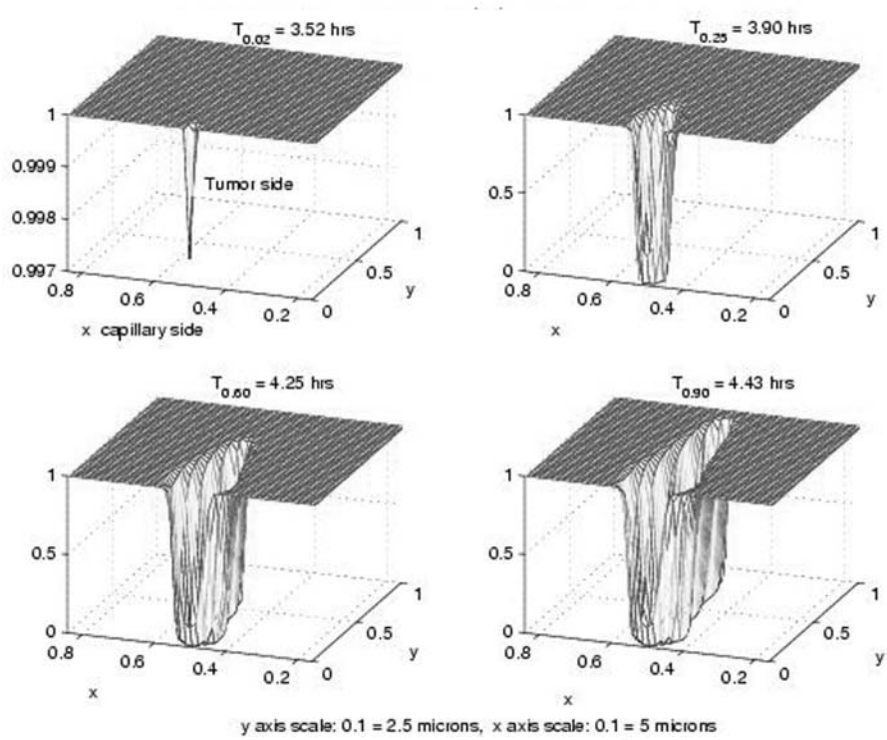

Figure 6.7

Time course for fibronectin degradation in the ECM.

6.12 Mathematical Analysis

We shall be concerned with an investigation of the qualitative properties of solutions to the following problem. Let $\Omega \subset I\!R^n$ be a bounded domain with boundary $\partial\Omega$. We seek solutions $P,\ \omega \in I\!R^{m+1}$ of the system

$$\begin{aligned} \frac{\partial P}{\partial t} &= D\nabla\cdot\left[P\nabla\ln(\frac{P}{\Phi(\omega)})\right] \\ \frac{\partial \omega}{\partial t} &= \mathbf{F}(P,\omega),\quad (x,t)\in\Omega\times(0,T), \end{aligned} \tag{6.87}$$

subject to the "no-flux" boundary condition

$$P\nabla\ln(\frac{P}{\Phi(\omega)})\cdot\mathbf{n} = 0,\quad (x,t)\in\partial\Omega\times(0,T), \tag{6.88}$$

where $\mathbf{n}$ is the inward pointing normal to $\partial\Omega$.

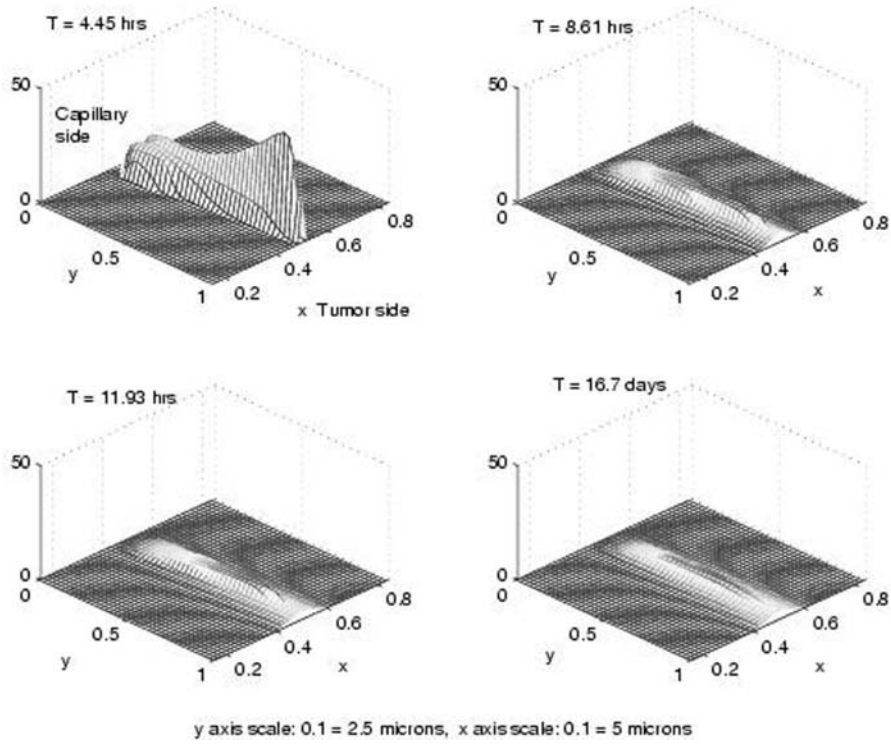

Figure 6.8
Time course for EC propagation in the ECM after introduction of angiostatin.

We prescribe the initial conditions

$$P(x,0) = P_0(x) > 0, \ x \in \bar{\Omega} \tag{6.89}$$

$$\omega(x,0) = \omega_0(x) \geq 0, \tag{6.90}$$

where $D \geq 0$ is a constant diffusion coefficient, P is population density (e.g., endothelial cell density), and ω is a vector of growth factors, growth inhibitors, fibronectin, protease, etc. The study of the above problem is central to understanding tumour angiogenesis models and also the processes of aggregation and dispersal of cells or other organisms. Key references are [9] and [21]. These papers deal almost exclusively with qualitative properties of the system of Equations (6.88) to (6.90). Questions of local and global existence are discussed in [23]. To begin with we consider some remarkable exact solutions for one space dimension systems.

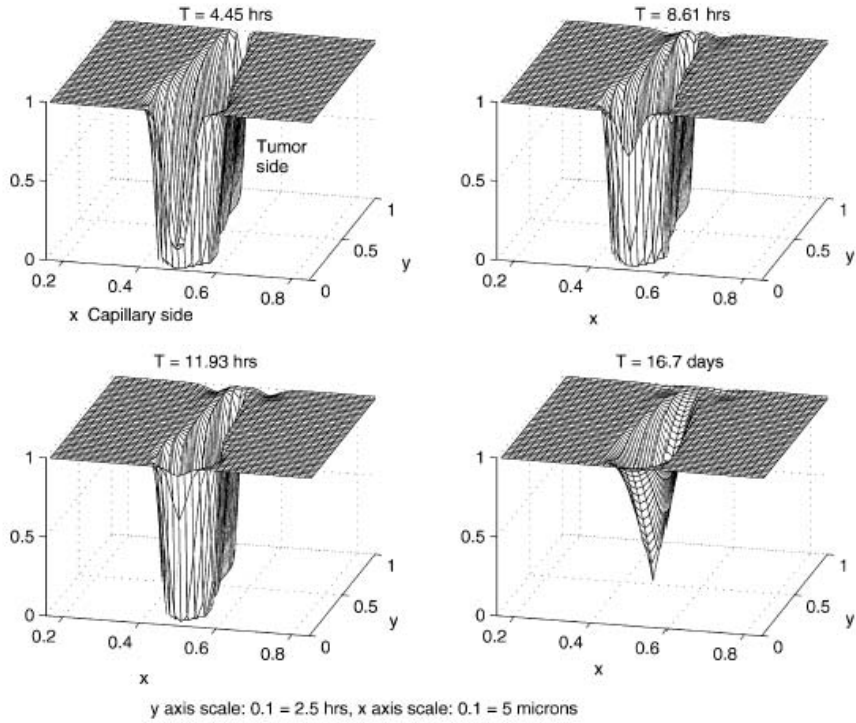

Figure 6.9

Time course for fibronectin degradation in the ECM after introduction of angiostatin.

6.13 Exact Solutions

Consider

$$\frac{\partial P}{\partial t} = D\frac{\partial}{\partial x}((P\frac{\partial}{\partial x}(\ln\frac{P}{\Phi(\omega)})), \tag{6.91}$$

$$\frac{\partial \omega}{\partial t} = \lambda P\omega - \mu\omega, \quad (x,t)\in\partial\Omega\times(0,T), \tag{6.92}$$

$$P\frac{\partial}{\partial x}\ln(\frac{P}{\Phi(\omega)}) = 0, \quad (x,t)\in\partial\Omega\times(0,T), \tag{6.93}$$

$$P(x,0) = P_0(x) > 0, \quad x\in\bar{\Omega}, \tag{6.94}$$

$$\omega(x,0) = \omega_0(x)\geq 0. \tag{6.95}$$

For $\Phi(\omega)$ we take

$$\Phi(\omega) = \omega^a, a = \pm 1. \tag{6.96}$$

Without loss of generality we scale and normalise the system of Equations (6.91) to (6.96) and consider the problem;

$$\frac{\partial P}{\partial t} = D\frac{\partial}{\partial x}((P\frac{\partial}{\partial x}(\ln\frac{P}{\Phi(\omega)})), \tag{6.97}$$

$$\frac{\partial \omega}{\partial t} = P\omega, \quad (x,t)\in\partial\Omega\times(0,T), \tag{6.98}$$

$$\frac{P_x}{P} - a\frac{\omega_x}{\omega} = 0, \quad x = 0,\pi, \tag{6.99}$$

$$P(x,0) = P_0(x) > 0, \tag{6.100}$$

$$\omega(x,0) = \omega_0(x)\geq 0. \tag{6.101}$$

6.13.1 Method 1

Set

$$\psi = \ln W \tag{6.102}$$

then Equations (6.97) and (6.98) are equivalent to the problem

$$\psi_{tt} = \psi_{xxt} - a(\psi_x\psi_t)_x, \tag{6.103}$$

or

$$\mathcal{L}\psi\equiv\psi_{tt} + a(\psi_x\psi_t)_x, = \psi_{xxt}, \quad 0 < x < \pi,\ t > 0 \tag{6.104}$$

$$\psi_{xt} - a\psi_x\psi_t = 0, \quad x = 0,\pi, \tag{6.105}$$

$$\psi(x,0) = \ln\omega(x,0) = \psi_0(x), \quad 0\leq x\leq\pi, \tag{6.106}$$

$$\psi_t(x,0) = P(x,0) = P_0(x). \tag{6.107}$$

$\mathcal{L}$ is a quasi-linear operator of the second order. It allows for a discussion of the system (6.103) in the hodograph plane (ψ_x, ψ_t). Now $\mathcal{L}$ is
HYPERBOLIC at (x,t) if and only if

$$(\psi_x)^2 - 4a\psi_t > 0, \tag{6.108}$$

ELLIPTIC if

$$(\psi_x)^2 - 4a\psi_t < 0, \tag{6.109}$$

PARABOLIC if

$$(\psi_x)^2 - 4a\psi_t = 0. \tag{6.110}$$

Since $P(x,t) = \psi_t(x,t) > 0$ we see that L is HYPERBOLIC if $a = -1$. However if $a = 1$ then $(\psi_x)^2 - 4a\psi_t$ can change sign even though $\psi_t > 0$. We call this the mixed type case. Now set

$$\psi(x,t) = \phi(t) + u(x,t), \text{ where } \phi(t) = \alpha t + \beta \tag{6.111}$$

where $\phi(t) = \alpha t + \beta$ and $u(x,t)$ satisfies

$$u_{tt} + a\alpha u_{xx} + a(u_x u_t)_x = u_{xxt}, \tag{6.112}$$

$$u_{xt} - a u_x(\alpha + u_t) = 0, \quad x = 0, \pi, \tag{6.113}$$

$$u(x,0) = \psi_0(x) - \beta, \quad 0 \leq x \leq \pi, \tag{6.114}$$

$$u_t(x,0) = P_0(x) - \alpha. \tag{6.115}$$

The idea now is to look for a solution of the form

$$u(x,t) = \sum_{n=1}^{\infty} A_n \exp(cNnt)\cos(Nnx), \tag{6.116}$$

where A_n, c, and N are parameters to be determined. As an example take $a = 1$, (mixed case), $\alpha = 1, \beta = 0$. Then we can show that

$$P(x,t) = \psi_t = 1 + u_t = 1 + 2Nc \sum_{n=1}^{\infty} \epsilon^n \exp(cNnt)\cos(Nnx), \tag{6.117}$$

where ϵ is an arbitrary parameter, and N and c satisfy the indicial equation

$$c^2 + Nc - 1 = 0. \tag{6.118}$$

If we take c to be the positive root, this solution exists as long as

$$t < T(\epsilon, N) = -\ln|\epsilon|/Nc. \tag{6.119}$$

For then the series converges absolutely and uniformly on compact sets of $[0,\pi]\times[0,T]$. When it exists the series (6.117) can be summed to give

$$P(x,t) = 1 - 2Nc + 2Nc\left(\frac{1 - \epsilon\exp(Nct)\cos(Nx)}{1 - 2\epsilon\exp(Nct)\cos(Nx) + \epsilon^2\exp 2(Nct)}\right) \tag{6.120}$$

which "blows up" at the single point $(x,t) = (x_0, T)$, where $\cos Nx_0 = \pm 1$ and $0 < x_0 < \pi$. When we take c to be the negative root, then the solution will exist for all $t > 0$ and decay to a spatially homogeneous solution. Now consider the case when $a = -1$ (the hyperbolic case). The same method leads to the solution

$$P(x,t) = 1 + 2Nc\epsilon\exp(Nct)\left(\frac{\epsilon\exp(Nct) + \cos(Nx)}{1 + 2\epsilon\exp(Nct)\cos(Nx) + \epsilon^2\exp 2(Nct)}\right) \tag{6.121}$$

where $c^2 + Nc + 1 = 0$. Both roots of this equation have negative real part. This solution decays exponentially to $P = 1$ as $t \to \infty$.

6.13.2 Method 2

Set $a = 1$ and let

$$\psi = \alpha t + \phi. \tag{6.122}$$

Then

$$\phi_{tt} + \alpha\phi_{xx} - \phi_{xxt} + (\phi_x\phi_t)_x = 0. \tag{6.123}$$

Now set

$$\phi = -\ln(c - u),$$

where c is a parameter, and seek $u(x,t)$ in the separated form

$$u(x,t) = T(t)\cos nx + g(t).$$

This idea is due to Yin Yang, Hua Chen, and Weian Liu [23]. After considerable manipulations it is found that;

(i) $g(t)$ satisfies a second order ordinary differential equation with constant coefficients.

(ii) $T(t)$ is an exponential function of t.

(iii) $g(t)$ and $T(t)$ involve parameters which must satisfy certain compatibility conditions.

The upshot of these ideas is

$$P(x,t) = \alpha - \frac{Ak_1\exp(k_1t) + Bk_2\exp(k_2t) \pm 2c_1\sqrt{AB}\cos nx \exp c_1 t}{A\exp(k_1t) + B\exp(k_2t) \pm 2c_1\sqrt{AB}\cos nx \exp c_1 t}, \tag{6.124}$$

$$\omega(x,t) = \frac{\exp\alpha t}{A\exp(k_1t) + B\exp(k_2t) \pm 2c_1\sqrt{AB}\cos nx \exp c_1 t}, \tag{6.125}$$

where c_1, A, and B are arbitrary constants and $k_{1,2} = c_1 \pm n\sqrt{n - c_1}$.

We conclude the following:

(a) If $A > B > 0, c_1 < \alpha - n^2(\sqrt{A} + \sqrt{B}/\sqrt{A} - \sqrt{B})^2$, then P, ω exist globally.

(b) If $0 < A < B, c_1 < \alpha$, there exists a $T > 0$ such that P, ω exists on $0 < t < T$ and blows up in finite time T at some point $x_0 \in [0, \pi]$.

Note: The solutions obtained here are precisely the same as those obtained in the first method when $a = 1$ after a shift in the time axis. Case (a) corresponds to taking the positive root of $c^2 + Nc - 1 = 0$ while case (b) corresponds to the choice of the negative root. The second type cannot be observed in numerical simulations since the problem is very unstable and any component of the solution in a direction tangent to the unstable manifold leads to blow up in finite time.

6.13.3 Method 3

This method was suggested by H.F. Weinberger. Set

$$a\alpha = 1$$

then from Equation (6.112)

$$u_{tt} + u_{xx} + a(u_x u_t)_x = u_{xxt}, 0 \leq x \leq \pi, t > 0 \tag{6.126}$$

$$u_{xt} - a u_x (1/a + u_t) = 0, x = 0, \pi, \tag{6.127}$$

$$u(x,0) = \psi_0(x) - \beta, 0 \leq x \leq \pi, \tag{6.128}$$

$$u_t(x,0) = P_0(x) - 1/a. \tag{6.129}$$

This time we look for solutions which are harmonic in x and t, i.e.,

$$u_{tt} + u_{xx} = 0,$$

and also satisfy

$$u_{xxt} = a(u_x u_t)_x. \tag{6.130}$$

Integrate Equation (6.130) to get

$$[u_{xt} - a(u_x u_t)]_0^\pi = 0,$$

which implies that

$$u_x(0,t) = u_x(\pi,t).$$

Now write

$$z = x + it, \bar{z} = x - it = w$$

to see that $u(x,t)$ can be expressed in the separated form

$$u = F(z) + G(w) \tag{6.131}$$

$$u_{zzz} - u_{www} = a\left(\frac{\partial}{\partial z} + \frac{\partial}{\partial w}\right)(u_z^2 - u_w^2). \tag{6.132}$$

We find that F and G satisfy

$$F_{zzz} - 2aF_z F_{zz} = \theta,$$

$$G_{www} - 2aG_w G_{ww} = \theta \tag{6.133}$$

where θ is a separation constant. For θ=0, $G(w) = \bar{F(z)}$ and we get

$$u(x,t) = \frac{1}{a}\ln[\cos^2(\theta_1 x - \alpha) + \sinh^2(\theta_1 t + \beta)], \tag{6.134}$$

for further arbitrary constants θ_1, α, and β. Set $\theta_1 = N$ (an integer) then;

$$P(x,t) = \frac{1}{a} + \frac{1}{a}\frac{N\sinh 2(Nt+\beta)}{\cos^2(Nx-\alpha) + \sinh^2(Nt+\beta)}$$

$$\omega(x,t) = \exp(t/\alpha + \beta)[\cos^2(Nx-\alpha) + \sinh^2(Nt+\beta)]^{1/\alpha}. \tag{6.135}$$

(i) If $a = 1, \beta \leq 0$, then $P(x,t)$ blows up in finite time $T = -\beta/N$ at the point $x_0 = 2\alpha + (2m+1)\pi/2N$, where m is an integer such that $x_0 \in (0,\pi)$. Furthermore, at the blow-up point $(x-0,T),\ \omega(x_0,T) = 0$.

(ii) If $\beta > 0$, then $P(x,t), \omega(x,t)$ exists globally. Again we see that there is sensitive dependence on initial conditions as β passes through $\beta = 0$. The solution set is a subset of the solution set obtained in method 1. (These solutions do not always satisfy the boundary conditions.)

6.14 Aggregation

An important question, which is again motivated by the need to understand how new capillaries sprout via angiogenesis from a pre-existing vasculature, is: Can we expect solutions to the system (6.87) to possess spatially nonconstant, piecewise constant aggregating solutions?

Definiton: $P(x,t)$ aggregates if it converges to a nonconstant steady state in finite or infinite time.

Numerical experiments of Othmer and Stevens [16] show that $P(x,t)$ can evolve to an aggregating solution through the formation of a 'shock.' Their experiments were based on the system (6.87) with

$$\begin{aligned} \Phi(\omega) &= \frac{\beta+\omega}{\gamma+\omega}, \\ \mathbf{F}(P,\omega) &= \frac{P\omega}{1+\nu\omega} - \mu\omega + \gamma_r \frac{P}{1+P}. \end{aligned} \tag{6.136}$$

We argue that the seeds of such shock formation are already present in the simple hyperbolic case of Equations (6.97) and (6.98) $(a < 0)$ in the zero-diffusion limit if $a \to \infty$, $D \to 0$ in such a way that $aD =$ constant. Before doing so, let us see how Equation (6.87) can be manipulated to exploit the idea of the hodograph plane further and the forms of F, Φ above.

One has to understand that the mass transport, i.e., the transport of P is always along characteristics. For example the solution of $u_t + u_x = 0$ has the form $u = f(x-t)$ so that the solution is propagated along the characteristic lines $x - t = const.$

We set $\gamma_r = 0$, solve the equation $\omega_t = F(P,\omega)$ for P and set $\psi = \mu t + K + \ln\omega$. There results, after a long and somewhat tedious calculation, a single equation of the form

$$\mathcal{L}\psi = \psi_t t + D(M_2(\omega) - 2)\psi_x\psi_{xt} + D(M_1(\omega) - 1)\psi_t\psi_{xx} = \psi_{xxt} + \mathcal{F}(\omega, \psi_x, \psi_t) \tag{6.137}$$

where

$$M_i(\omega) = \omega \frac{d}{d\omega}[i \ln A(\omega) + \text{nl } (\Phi(\omega))], \tag{6.138}$$

and where $A(\omega) = \omega/(1 + \nu\omega)$ and $i = 1, 2$. The form of $\mathcal{F}$ need not concern us here.

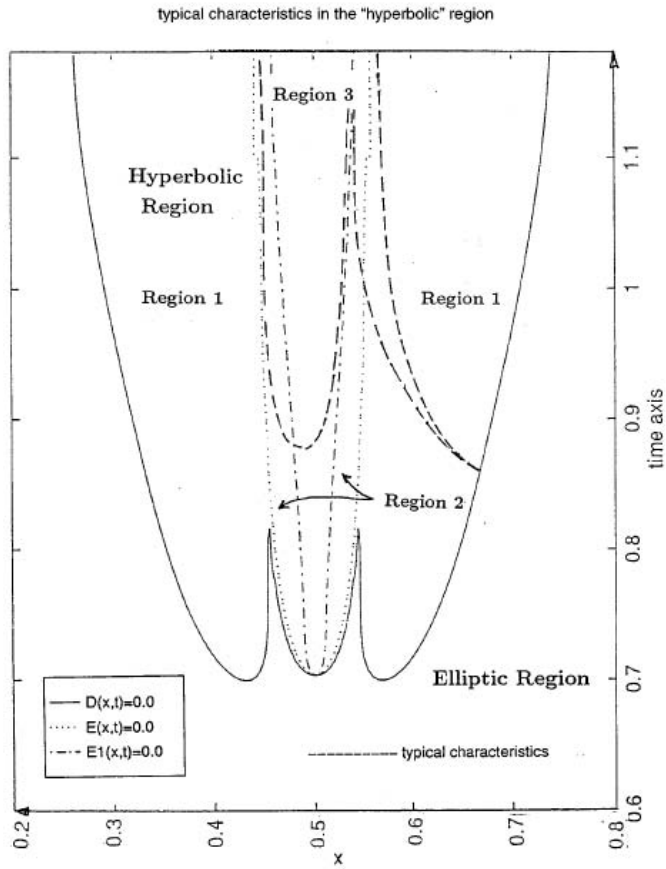

Figure 6.10
Schematic sketch of the characteristics in the generic case.

Now one sees that the discriminant condition is ω dependent and that the "type" of the operator $\mathcal{L}$ will depend not only on the gradient of ψ but also upon the magnitude of ω. Typically what is found in the physical plane is illustrated in Figure 6.10. The general situation is as follows. For a fixed value of ω one has an elliptic region, R_0 and a hyperbolic region which possesses three possible subre-

gions, R_1, R_2, and R_3 say. In R_1, the slopes of characteristics emanating from the parabolic boundary have the same sign so that the mass transport is into region R_2. (The boundary, the curve $E(x,t) = 0$ is the curve where the slopes change from having the same sign to having opposite sign. It is a caustic curve.) For some ω the region R_3 may appear. It too is a hyperbolic region with a boundary given by $E_1(x,t) = 0$ which is also a second caustic asymptotic to the first, where $E_1(x,t) = -3D^2(M_2(\omega)-2)^2\psi_x^2 + 4D\psi_t(M_1(\omega)-1)$. Mass trapped in R_3 cannot escape.

A detailed discussion of just how these regions appear as one increases constant initial data $\omega(x,0) = \omega_0$ with $P(x,0) = 1 + \epsilon\cos(2\pi x)$ is beyond the scope of these notes. The situation is roughly as follows: when ω_0 is small and positive, there are only the two regions R_0, R_1 as shown in Figure 6.11. Finite time blow-up will occur on the boundary at the cusp point shown in the figure.

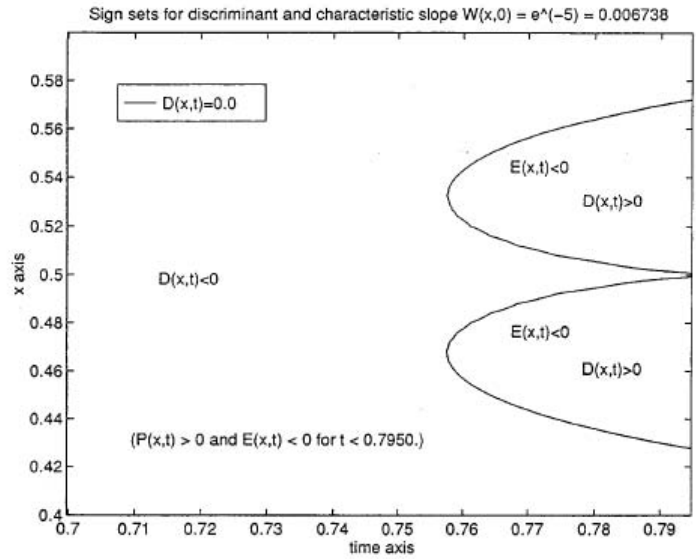

Figure 6.11
Schematic sketch of the characteristics when ω_0 is small.

For larger values of ω_0, the regions R_2, R_3 appear as time evolves (Figure 6.10). R_2 is quite narrow, while a second caustic appears to be very nearly a straight line although it is in fact a thin parabola with R_3 as its interior. Further increase of ω_0 leads to a widening of R_2 and R_3 with the two caustics pushing together more closely in time (see Figures 6.12 to 6.15).

For example, in the numerical simulations by Othmer and Stevens [16] (Figure 6.16) what happens is the following. The data starts in the elliptic region and

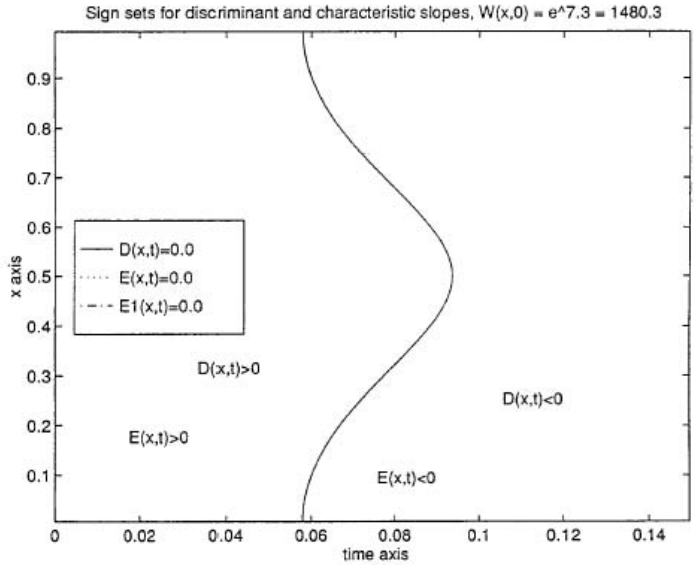

Figure 6.12
Regions of "ellipticity" and "hyperbolicity" for small times.

aggregates toward the centre illustrated by the evolving peak at $t \approx 10$. Then the solution $P(x,t)$ is so large at the centre as to cause a change in type so that it begins to collapse leading to the plateau-like region. It cannot collapse back to a constant because the caustic regions have since formed and the mass cannot be transported all the way back to the ends of the interval.

Consider Equation (6.112) with $\alpha = 1$ and where we have restored the diffusion coefficient D, i.e.,

$$u_{tt} + Dau_{xx} + Da(u_x u_t)_x = Du_{xxt}. \tag{6.139}$$

Let $D \to 0, a \to -\infty$ so that $aD = -1$ and consider the initial value problem

$$\begin{aligned} u_{tt} - u_{xx} &= (u_x u_t)_x, -\infty < x < \infty, \\ u(x,0) &= u_0(x), \\ u_t(x,0) &= u_1(x). \end{aligned} \tag{6.140}$$

Set $p = u_x, q = u_t$ then

$$\begin{aligned} q_t &= (pq)_x + p_x, \\ p_t &= q_x. \end{aligned} \tag{6.141}$$

Now look for a solution of the form

$$q = F(p) - 1, \tag{6.142}$$

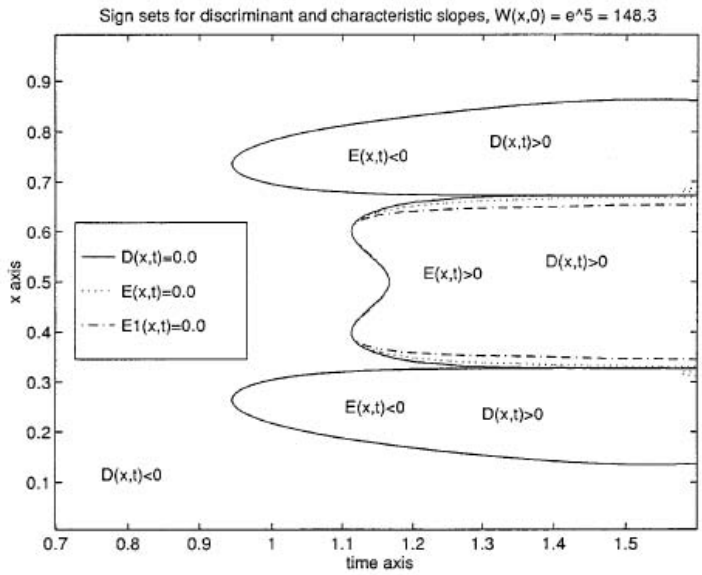

Figure 6.13
The separation of caustics more pronounced.

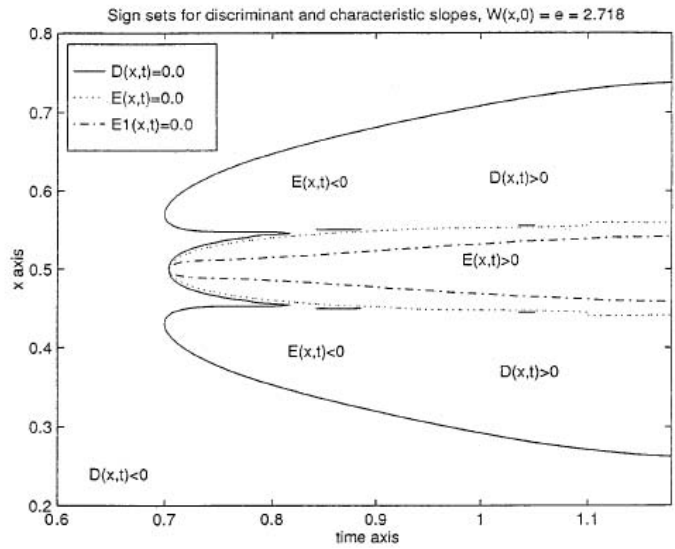

Figure 6.14
Further separation of caustics.

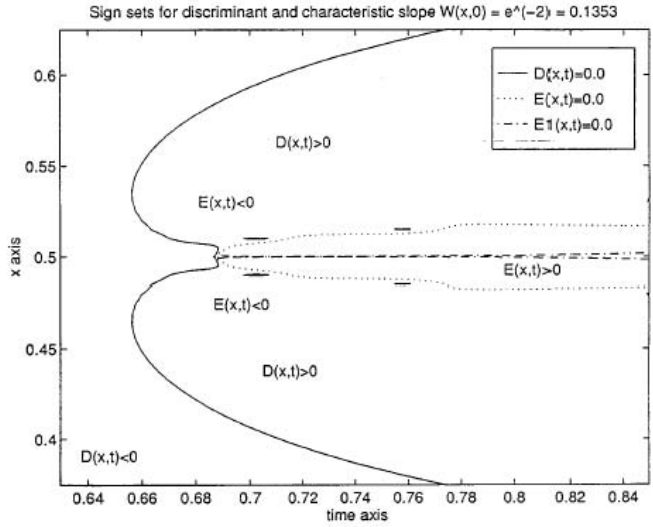

Figure 6.15
An attempt towards blow-up in finite time.

where

$$u_1(x) = F(u_0(x)) - 1. \tag{6.143}$$

For consistency we must have

$$\begin{aligned} q_t &= (pF(q))_x, \\ p_t &= F'(p)p_x = q_x, \end{aligned} \tag{6.144}$$

and so

$$(F'(p))^2 - pF'(p) - F(p) = 0. \tag{6.145}$$

Equation (6.145) is the characteristic equation for $\psi_{tt} = (\psi_x \psi_t)_x$. We have

$$F'(p) = \frac{1}{2}\left(p \pm \sqrt{p^2 + 4F(p)}\right). \tag{6.146}$$

By the method of characteristics we obtain the implicit solution

$$\begin{aligned} p(x,t) &= p_0(x + F'(p(x,t)), \\ &= u_0'(x + F'(p(x,t))t), \end{aligned} \tag{6.147}$$

where $F(p)$ is a nonconstant solution of (6.145). If we set

$$\sigma = x + F'(p)t, \tag{6.148}$$

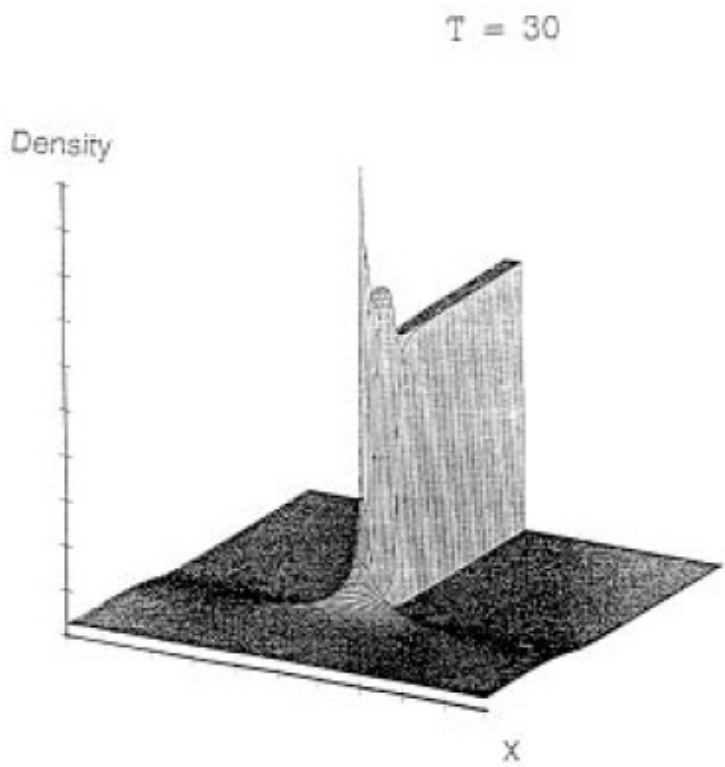

Figure 6.16

Shock formation and aggregation for the Othmer-Stevens systems taken from *SIAM J. Appl. Math.* 57, 1044-1081, 1997.

then implicit differentiation leads to

$$p_x(x,t) = \frac{p_0'(\sigma)}{1 - tp_0'(\sigma)F''(p)}. \tag{6.149}$$

Thus if no damping is present shocks in p will form in positive finite time along those characteristics which are strictly convex, $(F'' > 0)$ if and only if $p' = u_0'' > 0$ somewhere or along concave characteristics if $p_0' = u_0'' < 0$ somewhere. We can also construct simple "wave-type" shocks under the scaling $\tau = \epsilon t, \epsilon x$, [9]. These are embedded in the travelling waves which we construct below.

6.15 Travelling Waves

Write the partial differential equation (6.97) as a quasi-linear first-order system and consider the Cauchy problem

$$\begin{pmatrix} p \\ q \end{pmatrix}_t + \begin{pmatrix} Daq & Dap \\ -1 & 0 \end{pmatrix} \begin{pmatrix} p \\ q \end{pmatrix}_x = \begin{pmatrix} D & 0 \\ 0 & 0 \end{pmatrix} \begin{pmatrix} p \\ q \end{pmatrix}_{xx}, \tag{6.150}$$

where $q = (\ln\omega)_x$. Set

$$\begin{aligned} p(x,t) &= u(x,t) + v(x,t), \\ q(x,t) &= u(x,t) - v(x,t). \end{aligned} \tag{6.151}$$

We then find that $u(x,t)$, $v(x,t)$ must satisfy the pair of equations

$$\begin{aligned} u_t + 2Dauu_x - Du_{xx} &= -(v_t - 2Davv_x - Dv_{xx}), \\ u_t - u_x &= v_t + v_x, \\ u(x,0) &= u_0(x), \\ v(x,0) &= v_0(x). \end{aligned} \tag{6.152}$$

This system has extremely rich dynamics which are currently under investigation.

Suppose we look for travelling waves of the form

$$\begin{aligned} u(x,t) &= u(x+t), \\ v(x,t) &= v(x-t), \end{aligned} \tag{6.153}$$

then

$$\begin{aligned} u_t + 2Dauu_x - Du_{xx} &= 0, \\ v_t - 2Davv_x - Dv_{xx} &= 0. \end{aligned} \tag{6.154}$$

These are "Burger's equations" which can be integrated to give the solutions $u(x+t)$, $v(x-t)$ where

$$u(x+t) = \frac{c_1 + c_2 \exp a(c_1 - c_2)\xi}{1 + \exp a(c_1 - c_2)\xi}, \ \xi = x + t, \tag{6.155}$$

where $c_1 + c_2 = -1/Da, c_1 > c_2, c_1 c_2 = -A/Da$ with $A > 0$, arbitrary.

Note that $u \to c_1$ as $\xi \to \infty$ and to c_2 as $\xi \to -\infty$. Similarly

$$v(x-t) = \frac{c_1' + c_2' \exp - a(c_1' - c_2')\eta}{1 + \exp - a(c_1' - c_2')\eta}, \ \eta = x - t. \tag{6.156}$$

So our problem has solutions which are the sum of two travelling waves. This may also be used to provide support for the existence of aggregating solutions.

6.16 References

[1] Balding, D. and McElwain, D.L., A mathematical model of tumour-induced capillary growth, *J. Theor. Biol.* 114, 53-73, 1985.

[2] Bellomo, N. and Preziosi, L., Modelling and mathematical problems related to tumour evolution and its interaction with the immune system, *Math. Comp. Mod.* 32, 413-452, 2000.

[3] Carmeliet, P. and Jain, R.K., Angiogenesis in cancer and other diseases, *Nature* 407, 249-257, 2000.

[4] Chaplain, M.A.J. and Anderson, A.R.A., Modelling the growth and form of capillary networks, in *On Growth and Form: Spatio-Temporal Pattern Formation in Biology*, Wiley, New York, 225-249, 1999.

[5] Davis, B., Reinforced random walks, *Prob. Theory Rel. Fields* 84, 203-229, 1990.

[6] Folkman, J., Angiogenesis-retrospect and outlook, in *Angiogenesis: Key Principles - Science - Technology - Medicine*, R. Steiner, P.B. Weisz, and R. Langer, Eds., Birkhäuser, Boston, 1992.

[7] Folkman, J., in *Cancer Medicine*, J.F. Holland et al., Eds., Decker, New York, 132-152, 2000.

[8] Levine, H.A., Pamuk, S., Sleeman, B.D., and Nilsen-Hamilton, M., Mathematical modeling of capillary formation and development in tumor angiogenesis: penetration into the stroma, *Bull. Math. Biol.* 63, 801-863, 2001.

[9] Levine, H.A. and Sleeman, B.D., A system of reaction diffusion equations arising in the theory of reinforced random walks, *SIAM J. Appl. Math.* 57, 683-730, 1997.

[10] Levine, H.A., Sleeman, B.D., and Nilsen-Hamilton, M., A mathematical model for the roles of pericytes and macrophages in the initiation of angiogenesis. I. the role of protease inhibitors in preventing angiogenesis, *Math. Biosci.* 168, 77-115, 2000.

[11] Levine, H.A., Sleeman, B.D., and Nilsen-Hamilton, M., Mathematical modeling of the onset of capillary formation initiating angiogenesis, *J. Math. Biol.* 42, 195-238, 2001.

[12] Levine, H.A., Tucker, A.L., and Nilsen-Hamilton, M., A mathematical model for the role of cell signal transduction in the initiation and inhibition of angiogenesis, *Growth Factors* (in press).

[13] Murray, J.D., *Mathematical Biology*, Springer-Verlag, Heidelberg, 1989.

[14] Nelsen, N.J., Inhibitors of angiogenesis enter phase III testing, *J. Natl. Cancer Inst.* 90, 960-962, 1998.

[15] Orme, M.E. and Chaplain, M.A.J., Two-dimensional models of tumour angiogenesis and anti-angiogenesis strategies, *IMA J. Math. Appl. Med. Biol.* 14, 73-98, 1997.

[16] Othmer, H.G. and Stevens, A., Aggregation, blow-up and collapse: the ABC's of taxis and reinforced random walks, *SIAM J. Appl. Math.* 57, 1044-1081, 1997.

[17] Paweletz, N. and Knierim, M., Tumor-related angiogenesis, *Crit. Rev. Oncol. Hematol.* 9, 197-242, 1989.

[18] Ramanujan, S., Koenig, G.C., Padera, T.P., Stoll, B.R., and Jain, R.K., Local imbalance of proangiogenic and antiangiogenic factors: a potential mechanism of focal necrosis and dormancy in tumors, *Cancer Res.* 60, 1442-1448, 2000.

[19] Sherrat, J.A., Perumpanani, A.J., and Owen, M.R., Pattern formation in cancer, in *On Growth and Form: Spatio-Temporal Pattern Formation in Biology*, Wiley, New York, 47-73, 1999.

[20] Sleeman, B.D., Solid tumour growth: a case study in mathematical biology, in *Nonlinear Mathematics and Applications*, Cambridge University Press, Cambridge, 237-256, 1996.

[21] Sleeman, B.D. and Levine, H.A., Partial differential equations of chemotaxis and angiogenesis, *Math. Models Methods Appl. Sci.* 24, 405-426, 2001.

[22] Stack, M.S., Gately, S., Bafetti, L.M., Enghild, J., Soff, J., and Soff, G.A., Angiostatin inhibits endothelial and melanoma cellular invasion by blocking matrix-enhanced plasminogen activation, *Biochem. J.* 340, 77-84, 1999.

[23] Yang, Y., Chen, H., and Liu, W., On existence of global solutions and blow-up to a system of reaction-diffussion equations modelling chemotaxis, *SIAM J. Math. Anal.* 33, 763-785, 2001.

Chapter 7

Multi-Scale Analysis of Angiogenic Dynamics and Therapy

Levon Arakelyan, Yifat Merbl, Peteris Daugulis, Yuval Ginosar, Vladimir Vainstein, Vera Selitser, Yuri Kogan, Hila Harpak, and Zvia Agur
Institute for Medical Biomathematics (IMBM), Bene Ataroth (Israel)

7.1 Introduction

Growth of malignant tumours beyond the diameter of 1 to 2 mm critically depends on their neovascularization, which provides vital nutrients and growth factors,

and also clears toxic waste products of cellular metabolism [1]. Indeed angiogenesis — the formation of new blood vessels by budding from existing ones — has been proven to have a widespread significance in clinical oncology. Its role as a target for cancer therapy, first recognised by Folkman in 1971 [2], has received wide acceptance in the early 1990s following the discovery of the first specific antiangiogenic substances by O'Reilly et al. [3,4]. This therapeutic approach seems advantageous in being universal for different solid tumours and in lacking prominent side effects.

Intensive research during the last 15 years has led to a better understanding of this process and to a recognition of its complexity [5–12]. Major determinants of new vasculature formation are genetic features as well as nutrient availability. Moreover, vascular endothelial growth factor (VEGF) and other stimulatory factors are involved in the regulation of endothelial cell (EC) proliferation and migration [13–20]. The dynamics of the tumour vasculature are not merely the consequence of newly formed vessels, but also of immature vessels transformation into mature ones and the reverse process of destabilisation. Immature vessels may also regress in response to certain stimuli.

In order to establish successful antiangiogenic treatment protocols, the dynamics of angiogenesis must be better understood [21]. But, as was mentioned above and will be further demonstrated, the comprehensive angiogenesis dynamics are too complex to be captured by intuition alone, since they involve several interacting oscillatory processes, which operate on several scales of time and space.

Theory of population dynamics in perturbed environments suggests that oscillatory disease processes can be efficiently controlled when the natural temporal process of the disease is antagonised by an additional, externally imposed, temporal process. The latter can be either a natural process, e.g. the host immune system response in the control of African trypanosomiasis parasitaemia [22], or an artificial one, e.g., a well controlled periodicity of vaccination or chemotherapy efforts, as in the case of measles "pulse vaccination strategies" [23,24], HIV chemotherapy [25,26], or cancer chemotherapy [27–29].

In the present chapter we show how mathematical theory can contribute to the understanding of antiangiogenic therapy. We do so by briefly describing how mathematical models for the angiogenic dynamics are constructed, and subsequently calculated numerically. We begin by elaborating on the complexity of angiogenesis and analysing some empirical results which relate to tumour growth and its vasculature development, thus illustrating this complexity. Then we move to discuss the importance of modelling angiogenesis and present some alternatives for such modelling. These alternatives are tested for their ability to demonstrate and explain phenomena observed empirically. Using these models we test the potential effects of various drugs and drug schedules on the biological system. We then close by introducing some already accomplished applications of such models, along with suggesting further potential applications.

7.2 Defining the Challenge

As mentioned above, intensive research has led to recognition of this complex process [5–12]. Fundamentally, the genetic features of the tumour and the availability of the nutrients are the major determinants of new vasculature formation. Those determinants affect through mediators in the form of growth factors. Under conditions of nutrient deprivation, tumour cells secrete stimulatory factors such as VEGF, a potent stimulator of EC proliferation and migration [13–20]. Consequently, additional blood vessels are formed and the signal for increased VEGF production disappears. VEGF expression will now return to its basic, genetically determined level. The fate of the newly formed blood vessels will depend on this basic VEGF level. If lower than a certain given survival threshold, they will undergo regression [30–32]. This negative feedback can produce successive cycles of growth and regression of blood vessels [33].

Direct *in vivo* experiments show that newly formed blood vessels are dynamic structures, continuously undergoing growth and regression [34,35]. This dynamic instability can come to an end by vessel maturation, a process where immature vessels are covered by pericytes [34,35], which is governed by platelet derived growth factor (PDGF) and the angiopoietin system [36–40]. The significance of the angiopoietin system in vessel maturation has recently become clear [38–40]. This system includes Tie-2, the endothelium-specific receptor tyrosine kinase, its agonist, angiopoietin-1 (Ang1), and its natural antagonist angiopoietin-2 (Ang2). Ang1 promotes vessel maturation, while Ang2 antagonises its action and can destabilise mature vessels [36,37]. Ang1 and Ang2 can be expressed variably in EC or in human tumour cells, depending on the individual tumour type [36,37,41,42]. Hence, the expression of VEGF, Ang1, Ang2, as well as PDGF, can be influenced by both genetic and micro-environmental factors.

From the description above, it is clear that the angiogenesis process involves several interactive sub-processes, namely tumour growth and regression, nutrient-dependent production of angiogenic factors, vascular growth and regression, vessel maturation, and destabilisation of mature vessels. Several angiogenic factors should be taken into account, including VEGF, PDGF, Ang1, Ang2, and possibly more. Moreover, the system is comprised of three scales (levels) to be considered; the molecular level, the cellular level, and the tissue level. Hence, its modelling is a multi-scale modelling. To demonstrate the complexity of the issue, we bring some experimental data, of which analysis was performed. The analysis shows the need for modelling tools in order to fully understand empirical results, all the more so if one wishes to predict or even manipulate treatment results.

7.2.1 Analysis of Experimental Results

In order to better understand the dynamics of vascular development and tumour growth, analysis was conducted on experimental results, using mathematical and statistical tools.

7.2.1.1 Description of the experiment

The data given were of an experiment performed in M. Neeman's laboratory at the Weizmann Institute, Israel [33,43]. The experiment was conducted on 11 mice, and included subcutaneous implantation of a tumour spheroid in a specific location in the mouse's body and following its growth and angiogenesis, including vessel maturation and functionality [44].

In essence, the data supplied contained:

1. Tumour volume
2. Vessel density – total
3. An estimate of the fraction of functional (perfused) vessels
4. An estimate of the degree of maturation of the vessels

Magnetic resonance imaging (MRI) was used for measuring tumour growth and blood vessel density. The functionality of vessels was assessed by MRI signal intensity changes in response to an elevated oxygen level, while the maturation of vessels was assessed by MRI signal intensity changes in response to an elevated carbon dioxide level. These tests were performed in several measurement points inside the tumour and in certain locations in the body, relative to the tumour. These measurement points (see Figure 7.1 for the definition of reference points in the mouse's body (left) and in the tumour (right)), are specified herein by order from inside the tumour to the furthest point checked:
In – Inside the tumour spheroid
Rim – Any point located within the 1 mm wide rim around the tumour spheroid
Cn – A close reference site, within 7 mm distance from the tumour spheroid
Cf – A further distant reference site yet in the same tissue

7.2.1.2 Data processing

The above data were processed and prepared for analysis, in the following way:

- Tumour volume was measured in mm^3.
- Total vessel density was presented as the average vessel density (AVD). Signal intensities (S) were measured within the 1 mm diameter vicinity (Rim) of the implanted tumour as well as in a control region about 7 mm away from

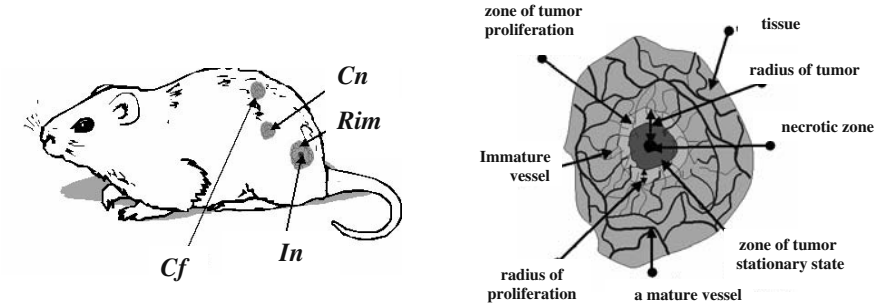

Figure 7.1

Left- The nomenclature of locations in the mouse's body. Right- schematisation of the tumour and its close vicinity, demonstrating the radius measured for tumour volume calculations and mature and immature vessels in its immediate vicinity.

the tumour (Cn), serving as a reference point. AVD was calculated as $1 - ln(S_{Rim}/S_{Cn})$. The outcome of this processing reflects in percentage the degree by which AVD is higher or lower than the normal level measured in the healthy tissue (at Cn).

- F (functionality) reflects the density of perfused (mature + immature) vessels in a certain tested area. The calculation of parameter F is performed using MRI measurements. As mentioned above, these measurements were performed separately for each of the four location points defined. Under the "calculating parameter values" section will be further demonstration of the application of readings in different locations within the same mouse.

- Similarly, M (maturation) reflects the maturation level of the vessels in the area tested. The calculation of parameter M is performed using MRI measurements. Also in common with F, maturation measurements were performed separately for each of the four location points defined above. The use of which will be explained below.

7.2.1.3 Calculating parameter values

We defined several parameters, for later use, characterising the tumour and representing interrelations between the selected aspects of its growth and vascularity. For example, the rate of tumour growth was defined as:

$$\text{Tumour growth rate } = \left(\frac{Vtum(X)}{Vtum(X-1)}\right)^{\frac{1}{Time(X)-Time(X-1)}},$$

where X represents the measurement day.

In addition, the reference points Cn and Cf were checked in order to serve as control over changes in readings that are immaterial to the progress of the disease. In order to apply this, several parameters were calculated. This was carried out firstly by calibrating the readings in points Rim or In, using the same day and mouse readings of one of the two reference points. Two parameter examples are:

1. $M_{\frac{Rim}{Cn}}$ – denotes the calibration of a result reflecting density of mature vessels in Rim using the reading in Cn as a reference point.
2. $F_{\frac{In}{Cf}}$ – denotes the calibration of a result reflecting density of functional (perfused) vessels in *In* using the matching reading in Cf as a reference point.

Secondly, a calibration was performed over maturation test results in comparison with functionality results. This is in order to render the numerical results equivalent. The source of this necessity was that maturation and functionality values are retrieved using different procedures and may elicit numerically incomparable results, though in normal tissue they reflect identical amounts of vessels. This was solved by calculating the ratio between matching readings of both maturation and function, performed in the normal tissue (either Cn or Cf) since these two values are expected to be practically equal. After such a ratio was defined (marked as K), it served as a correction factor for these above mentioned values, for example: $K = M_{Cf}/F_{Cf}$.

7.2.1.4 Data analysis

While observing *in vivo* tumour sizes depending on time (Figure 7.2), three growth behaviours are apparent, differing in growth rate. Thus, mice were assigned to three groups, according to differences in growth rates and growth patterns:

- Fast growing group: The mice in this group show continuous, rapid tumour growth with no fluctuations observed in tumour size. These mice died first, around 20 days from implantation.
- Medium growing group: The mice in this group started a relatively slow tumour growth, which increased past some point. The growth was characterised by occasional mild fluctuations. Their survival was intermediate, in most cases (19 to 36 days).
- Slow growing group: These mice showed a slow tumour growth rate. In addition, many fluctuations in size were apparent during their growth. These mice survived the longest, over 70 days.

7.2.1.5 Interconnecting tumour growth rate with AVD

Further analysis was performed, by observing the relations between tumour growth rates and AVD. This was done separately for each of the three growth pattern groups. Figure 7.3 relates to the fast, medium, and slow groups in the upper, middle,

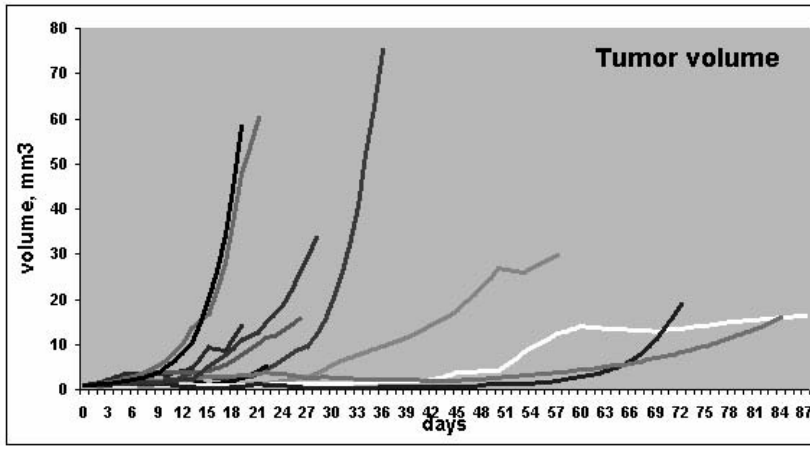

Figure 7.2

Course of *in vivo* tumour growth. Tumour volume designated in mm^3 depending on time in days. Each curve describes growth of one tumour, implanted in one mouse.

and lower parts, respectively. In the left part of Figure 7.3 are the layouts of tumour growth rate and AVD results, per each reading performed, per each of the mice in the group. There is no indication of the time point in the experiment at which these readings were performed. This is because we are here interested in researching the relation between AVD and tumour growth rate, independent of time. In each of the groups, three to four mice are presented, each marked by a different shape. After the layout was complete, the boundaries within which these points distributed were marked by dashed lines. Per each of the three groups, an additional graph is presented on the right side of Figure 7.3, showing the course of growth, i.e., tumour volume depending on time, of one mouse of that group. Note that the scales of these three graphs (upper, middle, and lower Figure 7.3, on the right) are different, a result of the vast differences in the growth rates.

The values of all readings of all three mice of the first group (the upper graphs) had a minimal tumour growth rate value of one, as appears from the marked inclusive range. Hence, there was no measurement where the tumour was found to have regressed in size, rather it grew constantly from one measurement to the next.

In the example of a specific mouse of this group (upper-right) it is seen that the volume increased rapidly and indeed, continuously, reaching a maximum of 60 mm^3 in about 20 days.

As for the reading range of AVD values, it was between 0.665 to 1.2. This relatively dense appearance (in comparison with the other groups) corresponds to a constant growth without the fluctuations observed in other groups.

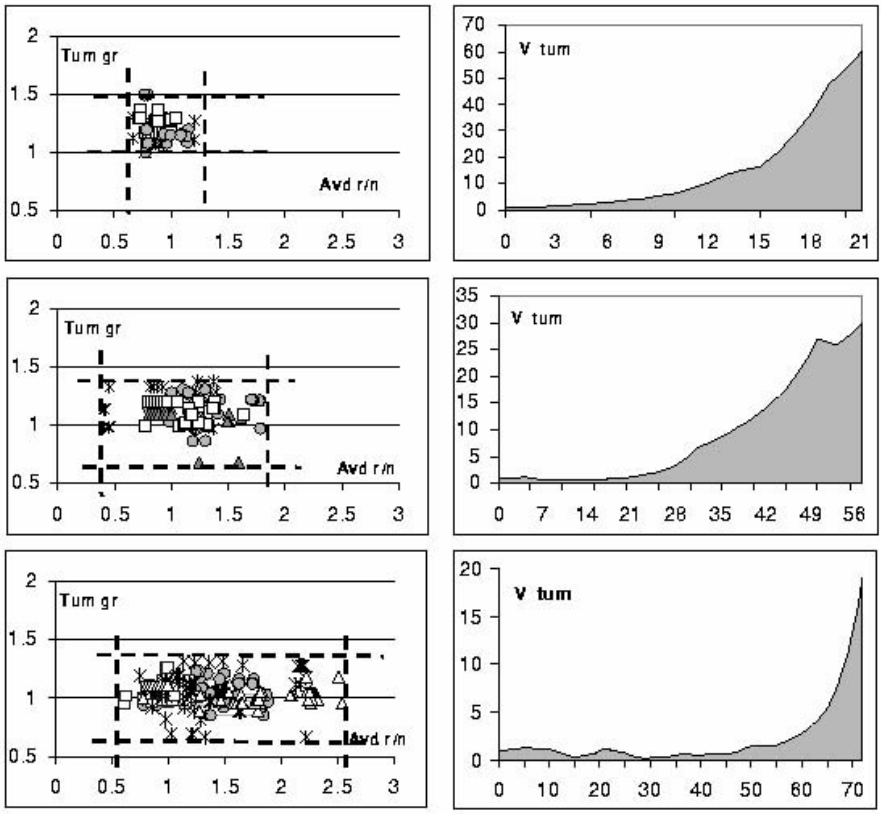

Figure 7.3

The left column, upper, middle, and lower, contains coordinates of all readings performed in the fast, medium, and slow growing groups, respectively. The points depict the values of growth rate coinciding with AVD. In these figures, the results of each individual mouse are marked by a different shape. The boundaries within which all points of a group are distributed, are marked by dashed lines. The right column, upper, middle and lower graphs, show the tumour volume (mm^3) depending on time (days), i.e., the course of growth, of a single individual mouse in the corresponding group. Note that the scales of these three graphs are different, a result of the vast differences in the growth rates.

Both the second and the third groups had a wider range of tumour growth rates, with some of their values lower than one, indicating a decrease in tumour volume. The AVD ranges were also wider in these two groups, with the third group having the widest range of both growth rate and AVD, as well as the most intense fluctuations in the tumour development. Note that in these two groups, one may find, on both ends of the AVD range, readings of growth rate either over or under unity. This indicates that there is no clear association between AVD value and the tumour growth trend (rate over one, indicating increase or rate under one, indicating decrease). Below we introduce the concept of using a time delay assumption in the analysis of these data. This might enable establishing a relation between the two factors: tumour growth and vessel density.

When observing the individual examples of mice from the second and third groups, a slower growth rate compared with that of the first group is apparent. While in the mouse of the first group a maximum of 60 mm^3 was reached in 21 days, in the mouse of the second group the tumour size was about 1 mm^3 after 20 days and reached a maximum of about 30 mm^3 within 55 days. As for the individual mouse of the third group, tumour size was kept at a minimum around 1 mm^3 for about 50 days, and grew to only 20 mm^3 after 70 days. While some fluctuations are observed in the individual reading of the second group (some regression around the day five), much more prominent fluctuations are demonstrated in the mouse from the third group.

From these observations, it seems that fluctuating and slow growth typically is associated with drastic changes of AVD, within a relatively wide range. Clearly, AVD is a crucial factor influencing tumour growth, and there is a mutual effect between the two processes. Hence, it biologically makes sense that when a phenomenon of fluctuation in size is observed, drastic changes are also apparent in AVD measurements, playing both roles of effector and consequence. It would be interesting to find a correlation between any of the relevant values measured here.

7.2.1.6 Correlation tests

The correlations between tumour growth rate and variants of vessel density were calculated (Microsoft Excel, see Table 7.1), as well as between tumour size and the same variants of vessels density (data not shown). As demonstrated in the previous section regarding calculating parameter values, density relates to either mature vessels or to functional vessels (i.e., those that were estimated *in vivo* to be perfused by blood). These density readings, performed in a choice of locations in the tumour, are then calibrated using different options for reference points (see Figure 7.1). Hence, there is a variety of measurement results for "vessel density" depending on the type of vessels tested, the location of the testing point in the tumour, and the choice of its reference point. A result of 0.4 to 0.6 indicated an intermediate correlation while a result of 0.6 and higher represented a strong correlation. As apparent in Table 7.1, no correlation was found without time delay, while after introducing time delay into the calculations, either an intermediate correlation ($M_{I/f}, M_{o/f}$) or a strong one ($F_{I/f}, F_{o/f}$), was found (see below for elaboration on the concept of time delay). One may notice that in the case of mature vessels ($M_{I/f}, M_{o/f}$) the correlation was

Table 7.1 The correlation between the tumour growth rates (Ktg) and vessel density parameters ($M_{i/f}, M_{o/f}, F_{i/f}, F_{o/f}$) of all readings of a specific mouse, "P." $M_{I/f}$: Mature vessel density in point In vs. point Cf. $M_{o/f}$: Mature vessel density in point Rim vs. point Cf. $F_{I/f}$: Functioning vessel density in point In vs. point Cf. $F_{o/f}$: Functioning vessel density in point Rim vs. point Cf. These correlations were calculated both with and without time delay. The time delay of 3 days was found to be optimal for some of the parameters while time delay of 4 days was found optimal for the others.

Mouse "P"				
	K tg ~ M i/f	K tg ~ M o/f	K tg ~F i/f	K tg ~ F o/f
without time delay	-0.174706611	0.059830672	0.305976706	0.095252136
time delay of 3-4 days	-0.493741611	-0.460786427	0.644311185	0.670577493

negative, reflecting destabilisation of the vessels in response to tumour growth.

7.2.1.7 The concept of time delay

Both the correlation table (7.1) and the previous observation that large changes in AVD seem to correlate with slow and typically fluctuating growth (Figure 7.3), appear to point to a physiologically expected relation between growth behaviour and vasculature. Nevertheless, it is clear that a change in AVD cannot immediately affect the tumour size and neither will changes in tumour size immediately affect the vessel number. Rather, there must be a genetically and environmentally determined kinetics dictating the characteristic time by which tumour growth will respond to changes in AVD, and vice versa. Hence, the next step in our analysis was to investigate the role of different putative time-delays between changes in vessel density and tumour growth rate. This will serve the purpose of disentangling the above described intricate dynamics, and will enable the unification of the different angiogenesis sub-processes into one picture. This means that instead of observing the relations between AVD and tumour growth rate of the same reading, on the same day, the growth rate was checked to correlate with the vessel density reading of some specific time earlier or later. At this phase, the search concentrated on finding the time delay at which results were to be observed, so that the relation between vessel density and growth rate was best established.

The method used for testing the effect of time delays was a mathematical calculation using a correlation function (again, Microsoft Excel). Since the experiment performed consisted of implanting an avascular tumour, which further developed vasculature, we chose to test the dependence of vessel densities (whether functional or mature) upon tumour growth. Hence, per each mouse, different time delay options were checked by testing the correlation function (data not shown), between AVD/F/M readings of certain days and the tumour growth on the suggested preceding day. We then searched for the best time delay for each mouse, which were not identical among all mice (data not shown).

7.2.1.8 Testing the effects of time delay on the analysis outcomes

Vascular densities of different categories of vessels, mature or functional, were calibrated for each individual mouse, according to the described in "calculating parameter values" above, similarly to the process preceding the correlation tests. For example, $M_{I/f}$, stands for density of mature vessels in area In calibrated according to readings in area Cf. In addition to vascular density readings, tumour volume was measured as well ($Vtum$). To demonstrate the relation between vascular density measurements and $Vtum$, we bring the diagrams in Figure 7.4, relating to the previously mentioned mouse. Measurements for each of the different vascular density categories are represented by a curve. Entries whose coordinates are vascular density (y axis) and $Vtum$ (x axis) of each measurement, were connected according to the chronological order in which the measurements were taken, yielding a curve which unfolds with time. This type of representation is denoted "phase plane." In upper Figure 7.4, the diagram was constructed without any time delay. This means that the entries represent measurements of the same day for both vascular density and $Vtum$. In lower Figure 7.4, on the other hand, the optimal time delay found for this specific mouse (as mentioned in the previous section) was applied into the diagram. Hence, each entry represents a vascular density reading of a given day and a $Vtum$ reading of a day preceding it, by the constant time delay chosen. Please note that the axes are now principally switched compared with Figure 7.3, i.e., here the x axis relates to $Vtum$, and the y axis is AVD.

7.2.1.9 Conclusions from the analysis of the experiments

In both upper and lower parts of Figure 7.4, once $Vtum$ is over a certain size, there appears to be a state of constant growth and no change in any of the vascular density measurements. This is indicated by the lines being rather straight, horizontal, and overlapping in that range of $Vtum$. Nevertheless, as it appears in Figure 7.4 (upper), there is an area of intensive occurrences in the lower range of $Vtum$ i.e., per certain tumour sizes within that range, many different values of vessel densities (y axis) were observed. All the more so, the directions of the lines with time indicate that per the same value of vascular density measurement, one may find the tumour to be either shrinking or in the process of growing. This shows that under the same vascular density conditions, it is not yet determined whether the growth trend shall be negative or positive.

In Figure 7.4 (lower), time delay was introduced into the system; specifically in this case, it was 3 days (optimal time delay found according to the techniques described above). Once applying the time delay into the results, one can appreciate the change in the appearance of the graph, in that the areas of intensive occurrences have cleared up. Instead, oscillations emerge (depicted as a limit cycle behaviour in these phase planes), indicating an interdependent growth behaviour of the two processes.

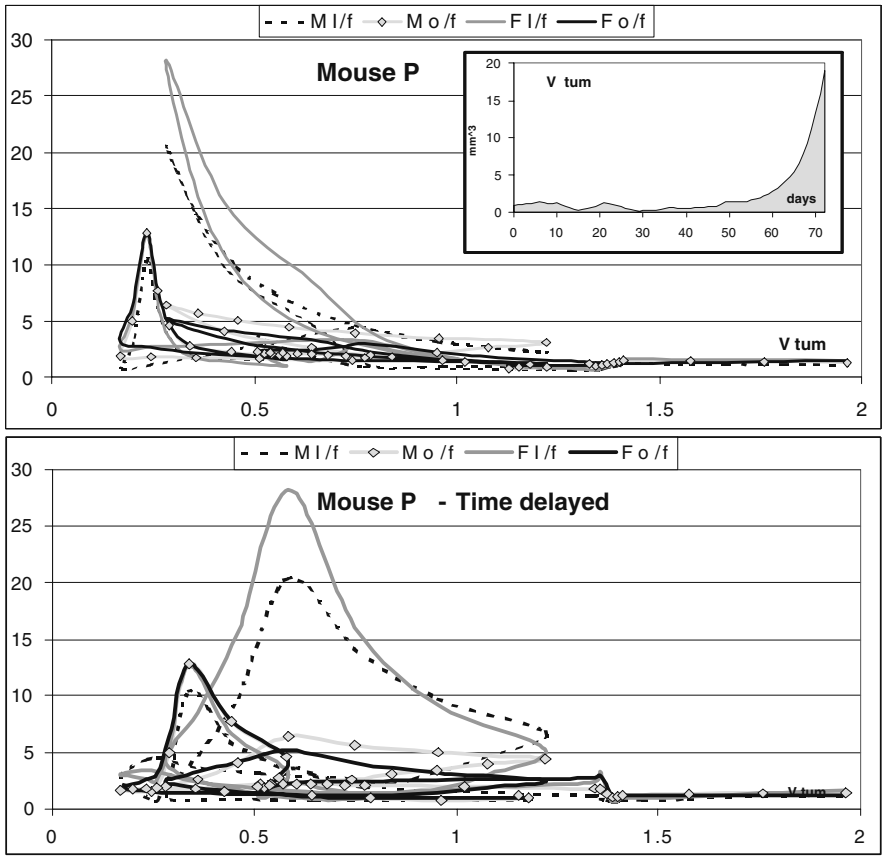

Figure 7.4

Analysis of experimental results of mouse "P," relating vessel density to tumour growth. Vessel density of four different calculated parameters presented as a function of tumour volume ($Vtum$) measurements. $M_{I/f}$: Mature vessel density in point In vs. point Cf. $M_{o/f}$: Mature vessel density in point Rim vs. point Cf. $F_{I/f}$: Functioning vessel density in point In vs. point Cf. $F_{o/f}$: Functioning vessel density in point Rim vs. point Cf. The entries are connected according to their chronological order. Upper: The entries are density and $Vtum$ measured at the same day. Lower: A time delay of 3 days was applied, hence, the entries are created by the measurement of density at a given day and $Vtum$ measured 3 days earlier.

Analysing tumour growth, contrasting growth trends are observed under the same vessel density, as reflected by the lines in Figure 7.4 (lower part, dotted line). In the major loop of $Vtum$ corresponding with $M_{I/f}$ (density of mature vessels inside the tumour, calibrated by their density in reference point Cf) there are two entries where $M_{I/f}$ equals about 7.5. However, in the first entry ($Vtum$ 0.4) the tumour is in the process of increasing, while the second entry ($Vtum$ 1.2) is a bifurcation point, where a switch occurs from a phase of growth to a phase of regression in size. This means that a single vessel density entry cannot reflect the trend of tumour growth, which is not monotonic. It is to be expected that more complete analysis of the system can be obtained by separating the involved elements (such as mature vs. immature vessels, or functional vessels etc.) and checking the role of each one of them in dictating the growth status, possibly through regression analysis.

Both maturation and functionality of vessels were separately analysed here, and found to each have the oscillatory behaviour described above. This actually means, that, through the process of tumour growth, both mature vessels category and the functioning vessels category, may transiently undergo regression. The regression of functional vessels is a decrease in the total amount of mature vessels (which are clearly functioning) and of functioning immature vessels. The regression of mature vessels is in essence the process of destabilisation. Hence, our results infer to the fact that immature vessels may undergo regression and mature vessels may undergo destabilisation into immaturity (possibly later leading to regression), even in the course of tumour growth.

Our analysis results (data not shown) suggest that there might be a different time delay between mature and immature blood vessels in correlation with the tumour growth, and this will be further investigated.

7.3 Mathematical Models of Tumour Growth and Angiogenesis

Vascular tumour growth, including dynamics of both vasculature and malignant cells, have been described in mathematical models by Hahnfeldt et al. [45], who propose a macroscopic model, assuming logistic tumour growth. However, this model neither takes into account vessel maturation nor does it allow for the nutrient-dependency secretion of proangiogenic factors. Bellomo and Preziosi [46] and De Angelis and Preziosi [47] describe the vascular tumour system on three scales: molecules, cells, and macroscopic entities (such as tumour volume). The latter model is much more detailed than the previous one [45], however it also does not include maturation of new blood vessels.

In this section, we present two classes of angiogenesis models: continuous models and a discrete model. The continuous models have been fully analysed in [48]. These models generally define three major processes: tumour growth, growth factor

production, and vessel growth. Each model defines the interrelations between the three, with several complexity levels being analysed. The analysis of the different continuous models relates to the empirical findings presented in the previous part. Hence, we are attempting to identify within each of the models the observed phenomenon of tumour size fluctuations accompanied by slow growth. In addition, the importance of including a time delay into the system is being demonstrated.

The *a priori* advantage of the continuous models is their analytic tractability, that is, their solution holds universally, no matter what the precise parameter values are. However, once these models become too complex, we find ourselves lacking the tools for solving them. This trade-off is a constraint, which makes us choose the suitable balance between complexity and applicability. Nevertheless, since our ultimate aim is to provide methods for improving drug treatment of vascular tumours, we must take into account events both on the molecular and the organic levels, without compromising our ability to analyse the global dynamics. This delicate balance is achieved here by using both the analytically tractable models and the more complex discrete models. The former are used for deciphering the universal behaviour of angiogenesis, while the latter are used for making realistic, practical, and empirically testable predictions.

Below we present and analyse several continuous models, which differ in complexity. Subsequently, we present the discrete model, which is complex enough to mimic real life, yet simple enough to enable simulation under many parameter sets. This model implements an algorithm of vascular tumour growth. The algorithm further addresses the complexity described and demonstrated above. This is performed by taking into account all the aforementioned sub-processes constituting the modelled process, along with the effects of several critical growth factors. Modelling is carried out on three scales; the molecular level, the cellular level and the tissue level. As we shall see in the next section, the algorithm used here enables the induction of drug therapy as well.

7.3.1 Continuous Models

In this part we consider angiogenesis models presented by order of increased complexity, which originates from adding dimensions to the system. In addition, time delay is also introduced into the system. Time delay was introduced into the analysis of empirical results in the previous section, and was shown to have a major impact. Similarly, mathematical analysis of these models shows here that in a sense this time delay is mandatory if one wishes to demonstrate the fluctuations observed in experimental results.

7.3.1.1 General assumptions of the models

Each of the models described herein involves the following time dependent variables:

- the number of tumour cells or tumour size (denoted by N)

- the amounts of growth factors known to be involved in angiogenesis supplying the tumour defined as P. For more accurate description, P may be broken down into several growth factors (proteins) which may differ in their effects and/or kinetics

- the effective volume of blood vessels supplying the tumour, which again may either be defined separately for immature and mature vessels or as the total of both, denoted by V

All modelling alternatives are systems of ordinary differential equations with or without time delay. In all of these models we use "sigmoid like" functions — smooth monotonous functions having a horizontal asymptote, e.g., $1/[1 + e^{k(x+s)}]$. These functions describe a response of the system to the relevant biological stimuli affecting it. The reasons for such a choice of the response function are the experimental observations which show that below and above certain thresholds, changes in the intensity of the stimuli have minor effects on the response. Between the threshold values (in the sensitivity region), the process rate depends monotonously on the stimuli value. In our analysis we use only the basic properties of sigmoidal functions, and we do not expect their exact shape to be easily determined from experiments or otherwise.

We assume that the tumour size dynamics is determined by availability of oxygen and nutrients. The amount of nutrients delivered and the oxygen supplied to the tumour is proportional to the volume of blood vessels supplying the tumour, whether inside the tumour or in its close vicinity. To take this into account we use effective vessel density (EVD) which may relate to immature vessels, mature vessels, or the total of both, denoted by E_1, E_2, or E, respectively. EVD is calculated by dividing the corresponding vessel volume by the tumour size $E = \frac{V}{N}$. To simplify our models we assume that vessel wall permeability (perfusion) is the same for immature and mature vessels. For the tumour size dynamics in all our models we assume the Malthusian law determined by

$$\dot{N} = f_1(E)N(t), \tag{7.1}$$

where f_1 is an increasing sigmoid function capturing the processes of cell proliferation and death:

$$f_1(E = 0) < 0, \qquad \lim_{E\to\infty} f_1(E) > 0. \tag{7.2}$$

For dynamics of protein (growth factor) compartments we assume that proteins are produced by tumour cells or immature vessels, and degraded by an intrinsic clearance process. Elaboration of the clearance process will be discussed later, suggesting the introduction of additional consuming elements, such as the forming vessels, into the model.

For dynamics of vessel compartments we assume that it is a superposition of four processes, some are contrasting some of the others: formation of immature vessels, regression of immature vessels, maturation of immature vessels, and destabilisation of mature vessels into immature vessels. We assume that these four processes are driven by sigmoid like responses, as described above, depending on specified proteins. These proteins are the stimuli mentioned earlier as the effectors of these functions.

7.3.1.2 A three-dimensional model with no time delay

The simplest modelling option presented merely captures the three independent variables mentioned earlier: tumour size N, total vessel volume V, and the amount of protein P. The only thing that we assume about the protein is that it drives the vessel formation or regression in a sigmoidal way. The rate of change of N is determined by a Malthusian law sigmoidally depending on E (representing EVD, as defined earlier). The protein P is produced by the tumour at a rate sigmoidally dependent on E and is decaying, by some clearance process as mentioned above, at a constant positive rate δ. The rate of change of the vessel volume V is sigmoidally driven by the protein. Thus we have the system

$$\begin{cases} \dot{N} = f_1(E)N, \\ \dot{P} = f_2(E)N - \delta P, \\ \dot{V} = f_3(P)V, \end{cases} \tag{7.3}$$

where

- f_1 is the tumour cells proliferation rate, it is an increasing function of E and satisfies Equation (7.2).
- f_2 is the protein production rate, it is a decreasing function of E and satisfies

$$f_2(E) > 0\,, \qquad \lim_{E\to\infty} f_2(E) = 0. \tag{7.4}$$

- f_3 is the vessel growth rate, it is an increasing function of P and satisfies

$$f_3(P = 0) < 0\,, \qquad \lim_{P\to\infty} f_3(P) > 0. \tag{7.5}$$

To simplify the analysis we make a substitution of variables $V \to E$ and get a system

$$\begin{cases} \dot{N} = f_1(E)N, \\ \dot{P} = f_2(E)N - \delta P, \\ \dot{E} = f_3(P)E - f_1(E)E. \end{cases} \tag{7.6}$$

The next step towards the purpose of mathematically demonstrating the phenomena observed empirically, is the analysis of Hopf bifurcation points. For mathematical background on Hopf points we refer the reader to [49]. To this end, we shall

only clarify, that Hopf points are specific cases of fixed points essentially admitting small oscillations in their vicinity. Their biological equivalent are steady states in which the biological system is expected to demonstrate oscillatory behaviour. Since such a behaviour was observed in the empirical results, it was of high interest to research the existence of such points in each of the systems suggested.

For each set of parameters which determine f_1, f_2, and f_3, the model has one fixed point $Q^{(1)} = (N^{(1)}, P^{(1)}, E^{(1)})$ with $N^{(1)} > 0$, given by

$$f_1(E^{(1)}) = 0\,, \qquad f_3(P^{(1)}) = 0\,, \qquad N^{(1)} = \frac{\delta P^{(1)}}{f_2(E^{(1)})}\,.$$

We claim that there are no Hopf bifurcation points among this family of steady states.

Here is an explanation: the matrix of the system linearised at such a point is

$$M = \begin{pmatrix} 0 & 0 & f_1'(E^{(1)})N^{(1)} \\ f_2(E^{(1)}) & -\delta & f_2'(E^{(1)})N^{(1)} \\ 0 & f_3'(P^{(1)})E^{(1)} & -f_1'(E^{(1)})E^{(1)} \end{pmatrix} = \begin{pmatrix} 0 & 0 & a'N^{(1)} \\ b & -\delta & -b'N^{(1)} \\ 0 & c'E^{(1)} & -a'E^{(1)} \end{pmatrix}, \tag{7.7}$$

where all the new parameters $a' = f_1'(E^{(1)})$, $b = f_2(E^{(1)})$, $b' = -f_2'(E^{(1)})$, and $c' = f_3'(P^{(1)})$ are positive.

We calculate the characteristic equation

$$\det(M - \lambda I) = -\lambda^3 - \lambda^2(a'E^{(1)} + \delta) - \lambda(a'\delta E^{(1)} + b'c'N^{(1)}E^{(1)}) + a'bc'N^{(1)}E^{(1)} \tag{7.8}$$

Hopf points arise when the characteristic polynomial at the fixed point admits a pair of pure imaginary roots. If a cubic polynomial admits such a pair $\pm Ai, A \in \mathbf{R}$ then it has the form

$$-(\lambda^2 + A^2)(\lambda + B) = -(\lambda^3 + B\lambda^2 + A^2\lambda + A^2B), \tag{7.9}$$

for some $B \in \mathbf{R}$. Since the coefficients of $\det(M - \lambda I)$ satisfy $-(a'bc'N^{(1)}E^{(1)}) < 0$ and $a'E^{(1)} + \delta > 0, a'\delta E^{(1)} + b'c'N^{(1)}E^{(1)} > 0$, we have that the characteristic polynomial cannot have pure imaginary roots and thus there are no Hopf points with $N \neq 0$ in Equation (7.6).

7.3.1.3 Introducing time delays into the three-dimensional model

While analysing empirical results (see the above section "analysis of experimental results"), the introduction of time delay elicited the appearance of oscillatory behaviour, as well as improved by far the correlation between two major processes, namely the dynamics of vessel density and tumour growth. This correlation may indicate that the correct way for describing the mutual dependence between the processes must involve time delay. The oscillatory behaviour might also indicate that Hopf points would be found if time delay is introduced into the analytical system. Thus, the next step was to apply time delay and analyse its effect.

Two time delays were introduced: τ_1 in the proliferation/death response to stimuli and τ_2, in the vessel formation/regression response to stimuli.

Let $E_{\tau_1} = E(t-\tau_1), P_{\tau_2} = P(t-\tau_2)$, then system (7.3) is modified, yielding:

$$\begin{cases} \dot{N} = f_1(E_{\tau_1})N, \\ \dot{P} = f_2(E)N - \delta P, \\ \dot{E} = f_3(P_{\tau_2})E - f_1(E_{\tau_1}))E. \end{cases} \tag{7.10}$$

This system has the same fixed points as (7.6). Again we are only interested in the family of fixed points $Q^{(1)}$. The analysis of the behaviour of 7.10 near $Q^{(1)}$ gives rise to the following transcendental analogue of Equation (7.8):

$$\lambda^3 + c_1\lambda^2 e^{-\lambda\tau_1} + \delta\lambda^2 + (c_1\delta)\lambda e^{-\lambda\tau_1} + c_2\lambda e^{-\lambda\tau_2} - c_3 e^{-\lambda(\tau_1+\tau_2)} = 0, \tag{7.11}$$

where $c_1 = a'E^{(1)}, c_2 = b'c'E^{(1)}N^{(1)}, c_3 = a'bc'N^{(1)}E^{(1)}$ are independent positive parameters.

The rigidity of the algebraic equation (7.8) is relaxed in Equation (7.11) by the time delays which appear in the exponential factors. This enables us to find appropriate positive parameters for f_1, f_2, and f_3 such that there are pure imaginary solutions to Equation (7.11). (The computation is not given here and appears in [48].) As already mentioned, existence of Hopf bifurcation points is conditioned by pure imaginary solutions, therefore we deduce that for every $(\tau_1, \tau_2) \neq (0,0)$ the family $Q^{(1)}$ contains Hopf points.

7.3.1.4 A five-dimensional model with time delays

To make our models more elaborate and realistic, we introduce more compartments representing vessels and proteins. First, the inclusive representation of vessels effective volume V, is replaced by separate descriptions of the effective immature and mature vessel volumes denoted by V_1 and V_2, respectively. The values of either vessel subpopulation will be separately analysed. Hence, the model allows both maturation of immature vessels and destabilisation of mature vessels. Secondly, the general term protein, denoted P, is now replaced by two specific proteins namely $VEGF$, denoted P_1 and $Ang1$, denoted P_2. We assume that $VEGF$ is produced by the tumour at a rate sigmoidally dependent on the effective vessel density and decays at a constant rate δ_1, and that $Ang1$ is produced by the tumour at a constant rate α and decays at a constant rate δ_2. Note that another growth factor, $Ang2$, is not modelled here as an additional dimension, rather it is assumed to exist in a constant amount. Hence, it is represented as one of the constant parameters wherever relevant in the functions f_1, f_2, and f_3. Let us also introduce time delays τ_1, τ_2, and τ_3 for tumour proliferation/death, immature vessel formation/regression and destabilisation,

respectively. We get the system:

$$\begin{cases} \dot{N} = f_1(E_{\tau_1})N, \\ \dot{P}_1 = f_2(E)N - \delta_1 P_1, \\ \dot{P}_2 = \alpha N - \delta_2 P_2, \\ \dot{V}_1 = f_3(P_{1\tau_2})V_1 - f_4(P_2)V_1 + f_5(P_{2\tau_3})V_2, \\ \dot{V}_2 = f_4(P_2)V_1 - f_5(P_{2\tau_3})V_2, \end{cases} \tag{7.12}$$

where f_1, f_2, and f_3 satisfy (7.2), (7.4), and (7.5), respectively and

- f_4 is the maturation rate, it is a positive increasing function of P_2.
- f_5 is the destabilisation rate, it is a positive decreasing function of P_2 and satisfies

$$\lim_{P_2 \to \infty} f_5(P_2) = 0. \tag{7.13}$$

After making the substitutions $V_i \to E_i = V_i/N$ and $E_2 \to E = E_1 + E_2$ we get the system

$$\begin{cases} \dot{N} = f_1(E_{\tau_1})N, \\ \dot{P}_1 = f_2(E)N - \delta_1 P_1, \\ \dot{P}_2 = \alpha N - \delta_2 P_2, \\ \dot{E}_1 = f_3(P_{1\tau_2})E_1 - f_4(P_2)E_1 + f_5(P_{2\tau_3})(E - E_1) - f_1(E_{\tau_1})E_1, \\ \dot{E} = f_3(P_{1\tau_2})E_1 - f_1(E_{\tau_1})E. \end{cases} \tag{7.14}$$

For each set of parameters which determine f_1, f_2, f_3, f_4, and f_5, the model has one fixed point $Q^{(2)} = (N^{(2)}, P_1^{(2)}, P_2^{(2)}, E_1^{(2)}, E^{(2)})$ with $N^{(2)} > 0$ given by the conditions

$$\begin{aligned} &f_1(E^{(2)}) = 0\,, \qquad f_3(P_1^{(2)}) = 0\,, \qquad N^{(2)} = \frac{\delta_1 P_1^{(2)}}{f_2(E^{(2)})}, \\ &P_2^{(2)} = \frac{\alpha\delta_1 P_1^{(2)}}{\delta_2 f_2(E^{(2)})}\,, \qquad E_1^{(2)} = \frac{f_5(P_2^{(2)})E^{(2)}}{f_4(P_2^{(2)}) + f_5(P_2^{(2)})} \end{aligned} \tag{7.15}$$

while exercising on the system the same analysis (full analysis appears in [48]), we find that for every pair $(\tau_1, \tau_2) \neq (0, 0)$, there always exist parameter sets such that $Q^{(2)}$ is a Hopf bifurcation point of the system (7.14).

We summarise the results about $3 - D$ and $5 - D$ models in the following proposition:

Proposition 7.3.1 *The ODE systems (7.10) and (7.14) admit a Hopf bifurcation point if and only if at least one of the time delays is nonzero.*

7.3.1.5 Further extension of the model

We further extended the model, by allowing $Ang2$ not to be constant, but rather to be produced by immature vessels, thus being a function of their quantity. Hence, we introduced an additional dimension to the model. In this case, the maturation/destabilisation process depends both on $Ang1$ and on $Ang2$. Here too, time delays were implemented. The analysis of this last system (not shown), demonstrated again the existence of Hopf points when at least one of the time delays is nonzero.

Another possibility for extension that was exercised, was the addition of protein consumption by growing vessels, rather than assuming it is merely constantly cleared by entities outside the modelled system. This was performed on the $3 - D$ model without time delay and had no Hopf points, similarly to other systems with no time delay.

7.3.1.6 Interpreting the results

A biological observed phenomenon is a given, for which we seek an explanation or at least a description. In the case of the empirical results presented above, a major apparent phenomenon is an oscillatory behaviour. One of the means for analytically describing oscillatory behaviour is a system of equations with Hopf bifurcation points. Introduced above were several modelling suggestions describing angiogenesis, with or without time delays. As demonstrated, whenever time delay was introduced into the system, Hopf points were found, leading to oscillatory behaviour. This might mean that the more appropriate candidate for describing the biological system in question is the alternative that includes time delays. While it is recognised that time delay will often elicit Hopf points, here it was shown that the latter were to be found for any angiogenesis model with time delay. Note that the introduction of time delay was also mandatory for the analysis of the empirical results. These conclusions underline the possible significance of time delays in tumour dynamics.

7.3.2 A Discrete Model

7.3.2.1 Description of the algorithm

The algorithm of the discrete mathematical model includes six major processes simultaneously, namely tumour cell proliferation and death, immature vessel formation and regression, immature vessel maturation, and mature vessel destabilisation (the complete algorithm is described in detail in [50,51]). A simplified scheme of the algorithm (Figure 7.5) presents three interconnected modules, within which these six subprocesses are included: tumour growth (proliferation and death), angiogenesis (immature vessel growth and regression), and maturation (formation and destabilisation of mature vessels). Each of these modules operates on three scales: molecular,

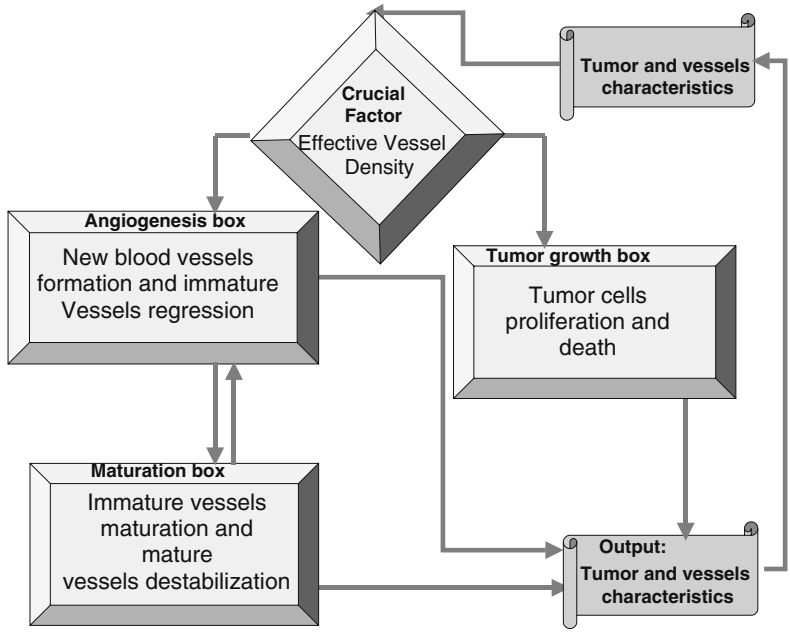

Figure 7.5

The simplified algorithm describing the principal interactions affecting a vascular tumour growth. It defines three major entities indicated as "boxes;" tumour growth, immature vessels (angiogenesis), and mature vessels, and conveys the interrelationships between them. These interactions occur across three organisation scales: molecular, cellular, and organ level (for a full description of this algorithm, we refer to [50,51]).

cellular and macroscopic (tissue level).

The tumour module consists of tumour cell proliferation and death, further subdividing into:

- a genetically determined block, which is cell type-specific and does not vary in time, and
- a block which is time-variant and nutrient-dependent.

A crucial factor in the tumour module is the density of the total perfused vasculature (to be denoted effective vascular density, EVD). Proliferation rate is directly proportional to EVD and death rate is inversely proportional to it. In addition, proliferation and death rates are both nutrient-dependent [52]. Two additional quantities are calculated in this module, namely VEGF and PDGF production. They are both

inversely related to EVD so that aggravation of nutrient depletion results in increasing secretion of proangiogenic factors [7–9]. The tumour growth module interacts with the angiogenesis and the maturation modules via the relevant regulatory proteins.

In the angiogenesis module we calculate immature vessel volume. Immature vessel volume increases proportionally to VEGF concentration, once above a given threshold level, and regresses if VEGF is below a given, possibly different, threshold level. The latter threshold is generally referred to as "survival level" [30] to [33].

In the maturation module, we calculate mature vessels volume according to pericyte concentration [52,53] and according to Ang1/Ang2 ratio [54]. Pericytes proliferate proportionally to PDGF concentration [34,35]. Ang1 and Ang2 are continuously secreted by tumour cells and immature vessels, respectively [36,37,41,42,52, 53,55]. Additionally, Ang2 can be secreted by tumour cells, if the latter are nutrient-depleted [37]. We assume that maturation of immature vessels occurs if pericytes concentration and Ang1/Ang2 ratio are above their respective threshold levels, otherwise, if under these thresholds, immature vessels do not undergo maturation, while mature vessels undergo destabilisation and become immature [38] to [42].

7.3.2.2 Numerical calculations

The above algorithm is precisely described mathematically by a large set of formulas underlying each and every interaction in Figure 7.5 and more. This full mathematical model has been studied by numerical simulations only, as it is much too complex to be tractable to mathematical analysis (but see the analysis of less complex forms of the model in the previous section, "continuous models"). Some simulation results of the full model are presented in section 7.4.1.

Recursive numerical simulations of the model have been performed. Note that at this point, we needed to define the parameter space within which simulations will be conducted. Owing to the relative novelty of the field of angiogenesis, and hence, the scarcity of experimentally evaluated parameters, we used arbitrary dimensionless units for all model parameters. Initial conditions were 100 tumour units and zero vascular densities. Calculation step duration is equivalent to generation time of tumour cells, that is, to one cell cycle.

At every time step the model calculates the tumour size, which is determined as a function of tumour cell number, the number of free endothelial cells and pericytes, the concentrations of the regulatory factors (VEGF, PDGF, Ang1, and Ang2), and the volume of immature and of mature vessels.

In addition, immature and mature vessel densities (the volumes of corresponding vessels divided by tumour size) are calculated and summed into EVD. EVD is defined as the sum of the densities of any perfused vessels, whether immature or mature. For simplicity we assume here that perfusion efficiency is the same in immature and mature vessels. However, this constraint can be easily alleviated.

The model assumes several threshold-dependent and ratio-dependent effects of regulatory factors, as follows:

- A threshold of VEGF concentration above which endothelial cell proliferation takes place
- A threshold of VEGF concentration under which endothelial cells, either incorporated into immature blood vessels or unattached, undergo apoptosis
- A threshold concentration of free unattached pericytes above which immature vessels can mature
- Ang1/Ang2 ratio above which immature vessels mature and below which mature vessels are destabilised

7.4 Applying the Models: From Theory to the Clinic

One can utilise angiogenesis mathematical modelling to serve several purposes. As we saw above, empirical data may reflect very intriguing phenomena, the analysis of which is enabled using such tools. The better understanding of such phenomena will lead to novel ideas for research and therapy. In addition, this work gives new options for the evaluation of novel antiangiogenic therapies. This will be demonstrated in the results section below. Clearly, if one wishes to apply such models for pharmaceutical or clinical uses, an additional module will have to be added to them, addressing the question of the pharmacodynamics and pharmacokinetics of the modelled drugs. This will be addressed towards the end of this section.

7.4.1 Simulation Results

The computer simulation of the tumour growth and angiogenesis discrete model described above, was represented as time series of the measured quantities: the effective vascular density, the tumour size, the concentrations of VEGF, Ang1 and Ang2, Ang1/Ang2 ratio, the immature and mature vessel volume, and more. Time is measured in cell cycles, while values on the y-axes in all graphs are expressed in arbitrary units.

7.4.1.1 Simulation of antiangiogenic and antimaturation therapies

One interesting application of this model may be the simulation of "prototypical" antiangiogenic and antimaturation therapies. Continuous administration was simulated, of two different hypothetical drugs affecting vascular dynamics, namely a VEGF-production inhibitor (drug A) and an Ang1 production inhibitor (drug B).

Monotherapy by drug A only, drug B only, or combination of both drugs, were simulated and compared with disease progression with no intervention. The different therapies were applied under similar conditions in terms of initial tumour size, reaction coefficients, and initial total vessel volume. For each of the initial sets, the simulated aspects of tumour growth were vascular volume, concentrations of Ang1 and Ang2, and tumour size. Those are presented in Figures 7.6 and 7.7 as a function of time in the upper, middle, and lower graphs, respectively.

However, for some of these therapies, three different sets of initial proportions of immature vessels were applied, being 50%, 95%, or 5%, as will be indicated in each of the examples herein.

Figure 7.6 shows simulation results of tumor growth characteristics under no therapy (left), drug A monotherapy (middle), and drug B monotherapy (right). The therapies were applied under the same initial conditions for the disease and under the assumption that initial volumes of immature and mature vessels were equal. One may notice in these simulations that drug A therapy (middle) slows down tumour growth without eliminating it. Rather, tumour size continues to increase nonlinearly, even under a prolonged treatment period and increased drug dose (not shown). As for drug B, (right) its application seems to cause a substantial deceleration in tumour growth, yet when observed under a smaller scale (inserts of Figure 7.6, right), one may appreciate that the trend of nonlinear growth still exists.

Figure 7.7 presents the simulation results of the combination therapy of drugs A and B with 50%, 95%, and 5% initial immature vessel percentage (left, middle, and right, respectively). All combination treatments simulated appear to cause prolonged suppression of tumour growth and a significant linear decrease in average tumour size. In the case of the immature vessel density being 95% (Figure 7.7, middle), the suppression was much more remarkable. Hence, in addition to having an advantage over the monotherapies simulated (Figure 7.6), it is demonstrated that the relative deceleration in tumour growth caused by this particular combination therapy is a function of the initial relative proportion of immature/mature vessel volume. Thus, the suggested combination therapy seems to yield an even better result when the proportion of immature vessels is relatively large (Figure 7.7, middle). Note that this general result is independent of initial conditions, other than immature vessel proportion.

In order to check whether the phenomenon of oscillatory growth behaviour, is also apparent in simulation results, two simulations were performed, the results of which are brought in Figure 7.8. The difference in the setting of the system between the two simulations, is in the intrinsic level of Ang1 which is defined as genetically determined. This Ang1 level was assumed to be 1 unit (upper Figure 7.8) or 35 units (lower Figure 7.8). All other simulation conditions (parameters) were set as equal in both cases. On the right side of Figure 7.8, simulated tumour growth is presented (size as a function of time in days). Observing the left part of Figure 7.8, one may appreciate that this simulated tumour growth is characterized by fluctuations, in both upper and lower parts (Ang1 equals 1 and 35 respectively). This is coherent with the findings presented in section “defining the challenge” where such fluctuations were demonstrated in the experimental results.

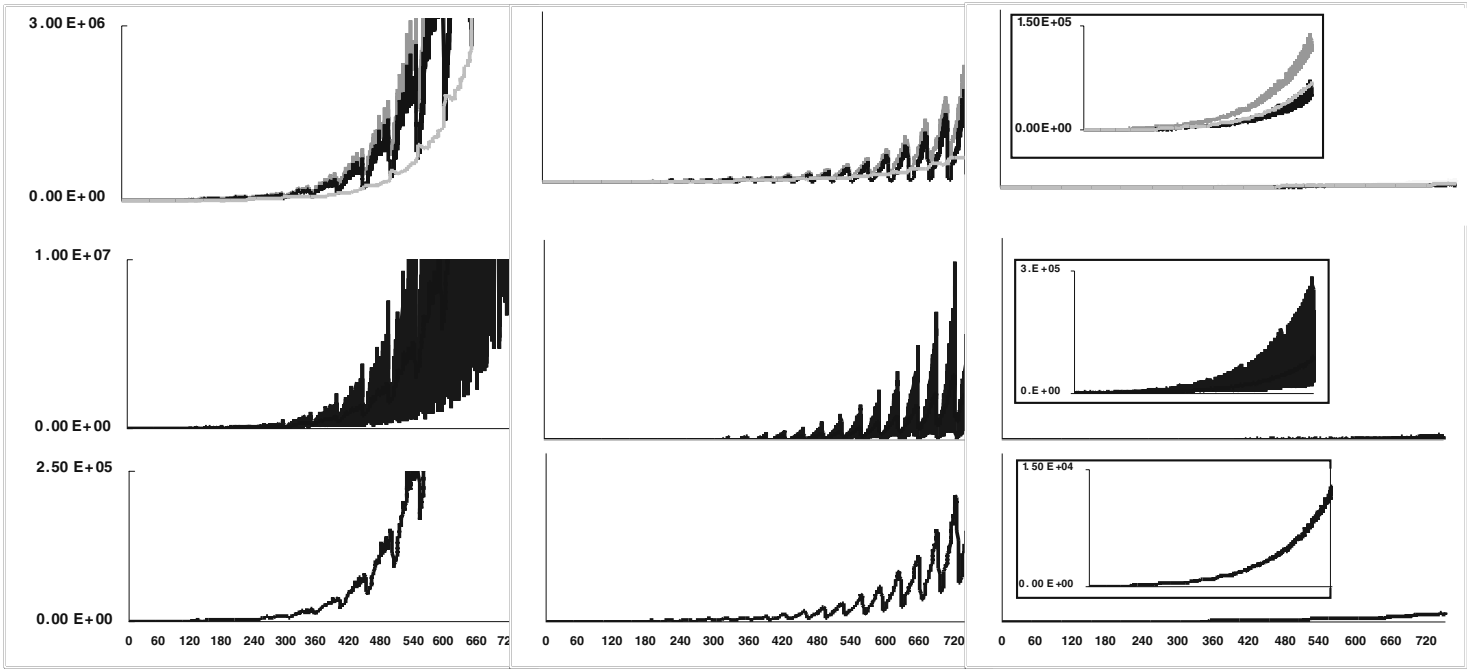

Figure 7.6
Simulation results of tumour growth under no therapy (left), drug A monotherapy (middle) and drug B monotherapy (right), where initial immature and mature vessel volume are assumed to be equal. Vascular volume, concentrations of Ang1 and Ang2 and tumour size are displayed in upper, middle and lower graphs, respectively. Inserted in the right column graphs are smaller scale magnifications of the larger scale results.

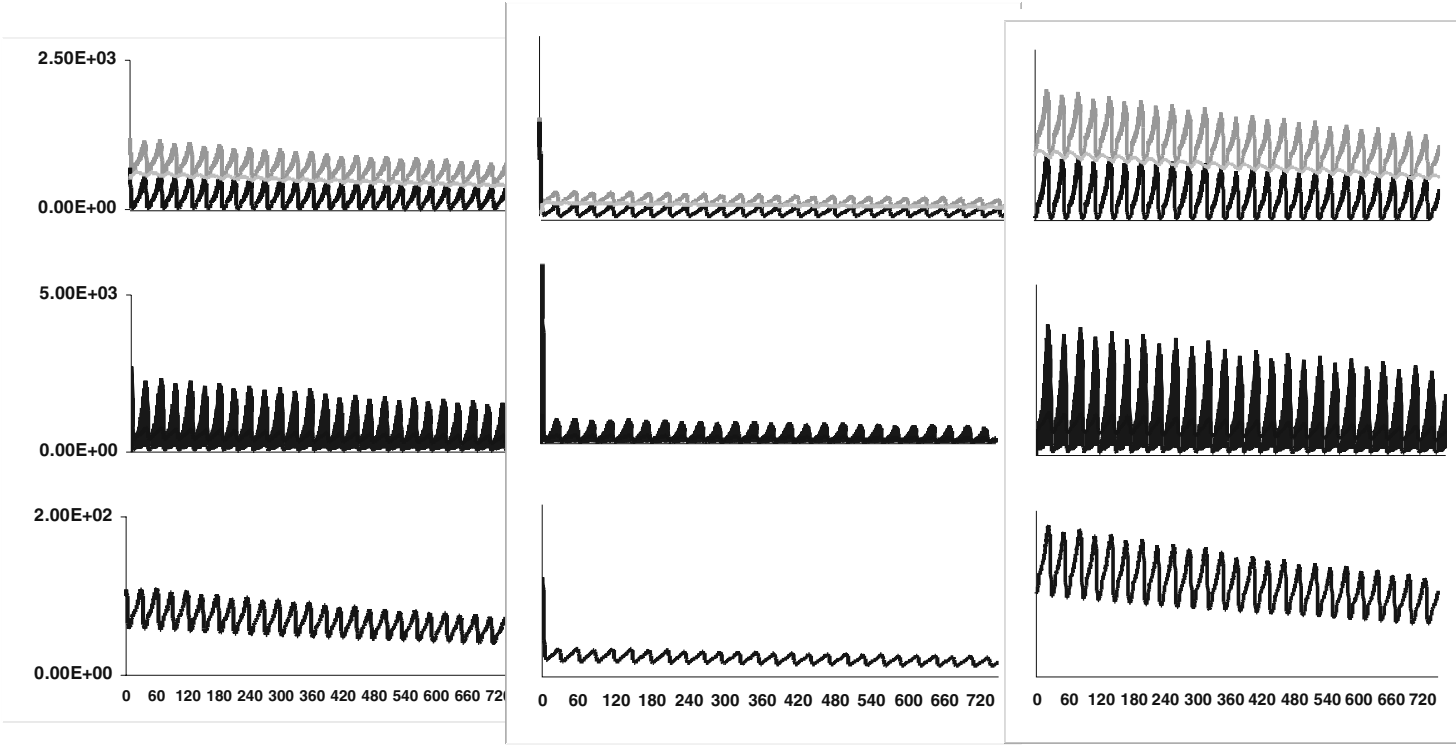

Figure 7.7
Simulation results of tumour growth under combination therapy of drug A and drug B. Initial conditions were equal except for immature vessel percentage, being 50%, 95% and 5% (left, middle, and right, respectively). Vascular volume, concentrations of Ang1 and Ang2 and tumour size are presented in upper, middle, and lower graphs, respectively.

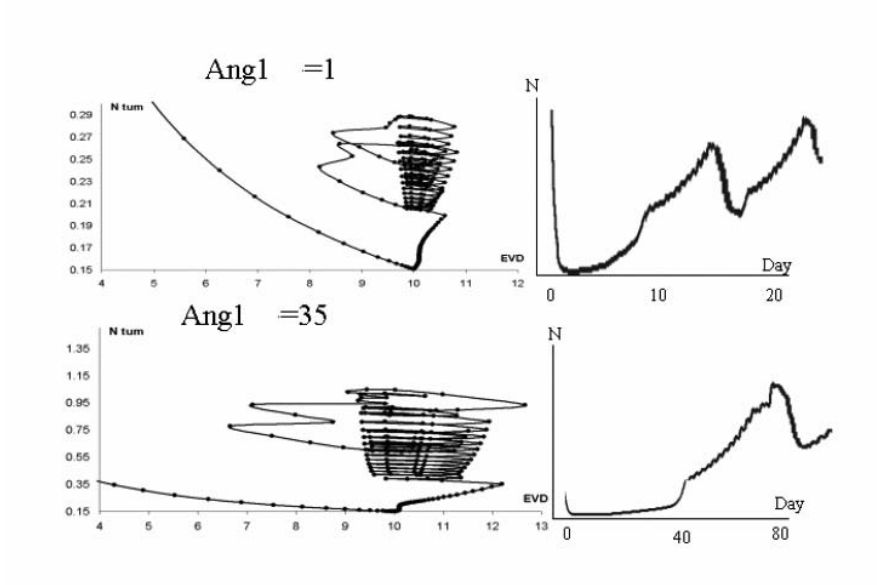

Figure 7.8

Results of two simulated situations, where the difference in the setting of the system is in the intrinsic level of Ang1. It was assumed to be 1 unit (upper) or 35 units (lower). Left: Phase plane representation of simulation results, showing EVD (x axis) as a function of tumour size ($Ntum$, y axis). (See phase plane representation of the experimental results in Figure 7.4). Right: Simulation results of tumour growth as a function of time in days.

In the first example above one may see how the utilization of the discrete mathematical model may help exploring therapy options and coming across new ideas to be further empirically tested. In the latter example, we have demonstrated the appearance of oscillatory growth phenomena in simulations of the discrete model. Similar phenomena were observed in the preceding section "analysis of experimental results."

7.4.2 Devising Drug Pharmacokinetic and Pharmacodynamic Models for Angiogenesis Simulations

One of the purposes in modeling angiogenesis is to predict the outcomes of a treatment, using a known drug and a well defined schedule. Once this is achieved, the model could be used for more sophisticated tasks, e.g., exploring new drugs or novel treatment protocol options for existing drugs.

7.4.2.1 The general structure

In order to make all these applications possible, we have to implement drug pharmacokinetics (PK) and pharmacodynamics (PD) as a part of the selected angiogenesis model. The PK model enables calculating drug concentration in the tissues where the drug effect occurs or in any other modeled compartments. The drug PD model accounts for the interaction between the drug and the modeled disease. The PD model interacts with the drug PK model, correlating the drug effect on the system to its concentration.

The drug PK can be modeled by one of the classical PK models [56], chosen according to the properties of the drug. The drug PK model includes a description of drug delivery and absorption, drug distribution in the body (both in the central compartment and in the peripheral compartments) and drug elimination from the body. The design of the PK model is adapted to the specific properties of the modeled drug. Thus, delivery method, absorption characteristics, number and nature of distribution compartments, the exchange between the compartments, and the metabolism and elimination patterns are chosen according to the information we have on the drug.

The drug PD model applies the drug effects to all the components of the mathematical models which simulate the biological processes of the target tissues. The effect of the drug is a function of the drug concentration in the target tissue or in the central compartment. In terms of the model, this effect can be expressed as a change in values of certain variables (e.g., the inhibition of production of a substance can be represented as a reduction of its production rate). Practically any drug effect can be described within this framework, given that the affected cell population or substance is represented in the disease model. Consequently, the same model can serve for describing the side-effects of the drug, which might require implementation of additional compartments simulating the tissues where the side effects take place.

7.4.2.2 Implementing PK/PD in the cancer model

Below we describe an example of drug PK and PD implementation in our angiogenesis model. The drug administration device in this example is a tablet. The drug is absorbed from the device by a first-order kinetics process, and enters the central compartment, which represents the blood. The volume of distribution of the drug (Vd) is not constant. Rather, it is elevating as a function of the drug amount. This represents the effect of a concentration-dependent drug binding by tissue proteins. In addition to the central compartment (blood), the model includes two peripheral compartments. One of the two represents the target tissue (in our case the tumour), where the drug concentration defines the effect of the drug on the disease. The drug concentration in the target tissue can differ from that in the blood. The rate of exchange between the blood (central compartment) and the tumour (target peripheral compartment), and so the resulting target tissue drug concentration, depends on the tumour tissue perfusion. The second peripheral compartment represents an additional distribution compartment for the drug. While differing from the central compartment in its drug distribution properties, it is implemented in order to complete the simulation of the drug pharmacokinetics and plays no role in the effect of the drug on the dis-

ease (pharmacodynamics). The clearance of the drug from the body is described by elimination from the central compartment by a first order kinetics process.

The drug effect is a function of the drug concentration in the target compartment. This function is of a sigmoid type: an increase in drug concentration leads to an increase in the effect, with saturation. In our example, the drug has three independent effects: (i) reducing the proliferation rate of the tumour cells, (ii) increasing the apoptotic rate of the tumour cells, and (iii) inhibiting VEGF production by the tumour cells. All these effects are expressed as sigmoid-like concentration-dependant functions, altogether yielding the resulting effect of the treatment.

7.5 Discussion

The complexity of angiogenesis and its significance in potential cancer therapy are well recognised. In experimental data brought here, several growth behaviours have been observed. Rapid tumour growth seems to have coincided with large ranges of vessel densities. In addition, growth seemed to be either in progress or in regress with no apparent direct relation with vessel density at the time of measurements. We have identified an oscillatory behaviour of tumour size in the periods in which growth rate was mild. This oscillatory behaviour may represent a limit-cycle fixed point, where both tumour size and vessel density fluctuate with a relatively fixed amplitude. Since there is a mutual effect of these two processes, it would be difficult to pinpoint cause and effect relationships. Still, one should expect to find some cyclic behaviour in the interaction of these two processes. The graphics of the relation between vessel density measurements and tumour size measurements, as it unfolds with time, are presented in Figure 7.4. In Figure 7.4 (lower), where an assumption of time delay was implemented, an oscillatory behaviour was observed, suggesting an interdependent path of development for these two processes. The concept of time delay falls into place with the biological intuition that there is a time gap between the appearance of the stimulus and the response to it. It also falls to reason that the duration of such a time gap would be variable between individuals, a function of genetic or environmental variability.

In addition, the fact that contrasting growth trends were observed under the same vessel density indicates that tumour growth is not a simple function of vessel density. Rather, growth rate is a function of several coexisting effects. This stresses the significance of separating the analysis of the involved processes, such as the dynamics of mature vs. immature vessels, or functional vessels, and checking the role of each one of them in controlling tumour growth status. Also, it is very likely that different time delays should be considered when checking the correlation with the tumour growth of each of the separate processes (e.g., the influence on growth of immature vs. mature vessels, may be kinetically different). The comparison of

time delays between individual cases and between different effectors, is a substantial issue to be addressed in future work.

Tumour growth and angiogenesis were modelled both in an analytical continuous way and in a discrete way, later implemented into a computer simulation.

As discussed already, the analytical model can aid in understanding the phenomena under research, but carries with it an inherent limit on complexity. Analysing the continuous models, we have shown that only if time delay is implemented into the models, is it possible to identify Hopf points. Hopf points are stable fixed points, which potentially can account for situations in which tumour size does not progress, rather it fluctuates between maxima and minima that are relatively similar. The latter result underlies the global properties of angiogenic dynamics, and supports the significance of time delay in the description of this process. It is also important for showing how connected the mathematical description brought herein is to the biological reality.

The discrete modelling proves to be an apparatus enabling the interactive integration of many different processes which occur on different biological organisation levels. We showed here that such an apparatus is essential for incorporating the high level of complexity in the description of the relevant processes. Hence, this provides an opportunity to study empirical phenomena, novel antiangiogenic drugs, new drug combinations, new drug schedules, etc. Some of the results are summarised herein (see [51] for complete results) and suggest that the combination of antiVEGF and antiAng1 therapies may be advantageous over the possibility of adopting a regime applying just one of them.

Looking into future work, we suggest that mathematical modelling can be highly instrumental in unravelling the complexity of cancer growth and therapy. Modelling tools may be used both for reaching a better understanding of the causality of the processes in question, and for easily testing new drugs. Our discrete mathematical algorithm suggests that there are many points in this complex dynamics, where suppression or stimulation by new drugs can be examined. This would require the addition of pharmacokinetics and pharmacodynamics modelling to the work already presented here.

7.6 Conclusions

Angiogenesis dynamics is highly complex, including several processes which operate on different levels of the biological system. Fragile new vessels form and regress, and at the same time can be covered by pericytes and mature into more resilient forms which, subsequently, may still be destabilised. The rates of these dynamics are determined by a plurality of factors, such as the genetic characteristics of the organism, the availability of nutrients at certain moments, and of proteins like VEGF and other stimulatory factors, affecting endothelial cell proliferation and

migration during other moments. Moreover, the different dynamical processes are interconnected by several feed-back loops, which can accelerate some of them while decelerating others. In order to concurrently account for the interactive dynamics of the relevant nutrients and growth factors, the different cell types, tumour mass, and the various blood vessel types, the model of angiogenesis should necessarily be a multi-scale one. Several continuous models with increasing complexity were discussed here. They were all shown to require the inclusion of time delays in order to identify Hopf points, which possibly represent the oscillatory phenomena observed empirically. The discrete model discussed here, included a highly complex description of the relevant processes. This description served as a basis for constructing a simulation apparatus which offers further research opportunities. One such application was presented here, suggesting a major advantage to the combination of antiVEGF and antiAng1 therapy over a monotherapy, which uses just one of such drugs. It is our hope that cancer therapy will be aided by using modelling tools such as those presented here, both for reaching a better understanding of the processes in question and for easily testing new therapies.

Acknowledgments

We are much obliged to Prof. Michal Neeman for providing the experimental data analysed in this work and for a very useful discussion. We are also indebted to Assaf Gilead for aiding in data analysis. The work was supported by the Chai Foundation, and the European Union Commission through the Human Potential Programme, Contract No HPRN-CT-2000-00105. Dr. Arakelyan is a recipient of the Shapira Scholarship from the Center of Absorption in Science of the Israeli Ministry of Absorption.

7.7 References

[1] Folkman, J., Angiogenesis in cancer, vascular, rheumatoid, and other disease, *Nat. Med.* 1, 27, 1995.

[2] Folkman, J., Tumour angiogenesis: therapeutic implications, *N. Engl. J. Med.* 285, 1182, 1971.

[3] O'Reilly, M.S. et al., Angiostatin: a novel angiogenesis inhibitor that mediates the suppression of metastases by a Lewis lung carcinoma, *Cell* 79, 315, 1994.

[4] O'Reilly, M.S. et al., Endostatin: an endogenous inhibitor of angiogenesis and tumour growth, *Cell* 88, 277, 1997.

[5] Carmeliet, P. and Jain, R.K., Angiogenesis in cancer and other diseases, *Nature* 407, 249, 2000.

[6] Yangopoulos, G.D. et al., Vascular-specific growth factors and blood vessel formation, *Nature* 407, 242, 2000.

[7] Kerbel, R.S., Tumour angiogenesis: past, present, and the near future, *Carcinogenesis* 21, 505, 2000.

[8] Danielsen, T. and Rofstad, E.K., The constitutive level of vascular endothelial growth factor (VEGF) is more important than hypoxia-induced VEGF upregulation in the angiogenesis of human melanoma xenografts, *Brit. J. Cancer* 82(9), 1528, 2000.

[9] Dor, Y., Porat, R., and Keshet, E., Vascular endothelial growth factor and vascular adjustments to perturbations in oxygen homeostasis, *AJP-Cell Physiology* 280, 1367, 2001.

[10] Ikeda, E. et al., Hypoxia-induced transcriptional activation and increased mRNA stability of vascular endothelial growth factor in C6 glioma cells, *J. Biol. Chem.* 270, 19761, 1995.

[11] Lin, P. et al., Anti-angiogenic gene therapy targeting the endothelium-specific receptor tyrosine kinase Tie-2, *Proc. Natl. Acad. Sci.* 95, 8829, 1998.

[12] Diaz Flores, L. et al., Microvascular pericytes: a review of their morphological and functional characteristics, *Histol. Histopathol.* 6, 269, 1991.

[13] Breier, G. et al., Expression of vascular endothelial growth factor during embryonic angiogenesis and endothelial cell differentiation, *Development* 114, 521, 1992.

[14] Shweiki, D. et al., Vascular endothelial growth factor induced by hypoxia may mediate hypoxia-initiated angiogenesis, *Nature* 359, 843, 1992.

[15] Ferrara, N. and Henzel, W.J., Pituitary follicular cells secrete a novel heparin-binding growth factor specific for vascular endothelial cells, *Biochem. Biophys. Res. Commun.* 161, 851, 1989.

[16] Ferrara, N. et al., Molecular and biological properties of the vascular endothelial growth factor family of proteins, *Endocr. Rev.* 13, 18, 1992.

[17] Ferrara, N. et al., Heterozygous embryonic lethality induced by targeted inactivation of the VEGF gene, *Nature* 380, 439, 1996.

[18] Carmeliet, P. et al., Abnormal blood vessel development and lethality in embryos lacking a single VEGF allele, *Nature* 380, 435, 1996.

[19] Barleon, B. et al., Migration of human monocytes in response to vascular endothelial growth factor (VEGF) is mediated via the VEGF receptor flt-1, *Blood* 87, 3336, 1996.

[20] Neufeld, G. et al., Vascular endothelial growth factor (VEGF) and its receptors, *FASEB* 13, 9, 1999.

[21] Jain, R.K., Normalizing tumour vasculature with anti-angiogenic therapy: a new paradigm for combination therapy, *Nat. Med.* 7, 987, 2001.

[22] Agur, Z., Abiri, D., and Van der Ploeg, L.H.T., Ordered appearance of antigenic variants of African trypanosomes, explained in a mathematical model based on a stochastic process and immune-selection against putative switch intermediates, *Proc. Natl. Acad. Sci. USA* 86, 9626, 1989.

[23] Agur, Z. et al., Pulse mass measles vaccination across age cohorts, *Proc. Nat. Acad. Sci. USA* 90, 11698, 1993.

[24] Shulgin, B., Stone, L., and Agur, Z., Pulse vaccination strategy in the SIR endemic model, *Bull. Math. Biol.* 60, 1123, 1998.

[25] Agur, Z., Clinical trials of Zidovudine in HIV infection, *Lancet* 2, 734, 1989.

[26] Agur, Z. et al., Zidovudine toxicity to murine bone marrow may be affected by the exact frequency of drug administration, *Exp. Hematol.* 19, 364, 1991.

[27] Agur, Z., Arnon, R., and Schechter, B., Effect of the dosing interval on survival and myelotoxicity in mice treated by Cytosine arabinoside, *Eur. J. Cancer* 28A, 1085, 1992.

[28] Ubezio, P. et al., Increasing 1-b-D-arabinofuranosylcytosine efficacy by scheduled dosing intervals based on direct measurement of bone marrow cell kinetics, *Cancer Res.* 54, 6446, 1994.

[29] Agur, Z., Resonance and anti-resonance in the design of chemotherapeutic protocols, *J. Theor. Medicine* 1, 237, 1998.

[30] Benjamin, L.E. and Keshet, E., Conditional switching of vascular endothelial growth factor (VEGF) expression in tumours: induction of endothelial cell shedding and regression of hemangioblastoma-like vessels by VEGF withdrawal, *Proc. Natl. Acad. Sci.* 94, 8761, 1997.

[31] Jain, R.K. et al., Endothelial cell death, angiogenesis, and microvascular function after castration in an androgen-dependent tumour: role of vascular endothelial growth factor, *Proc. Natl. Acad. Sci.* 95, 10820, 1998.

[32] Holash, S.J., Wiegandand, G.D., and Yancopoulos, G.D., New model of tumour angiogenesis: dynamic balance between vessel regression and growth mediated by angiopoietins and VEGF, *Oncogene* 18, 5356, 1999.

[33] Gilead, A. and Neeman, M., Dynamic remodeling of the vascular bed precedes tumour growth: MLS ovarian carcinoma spheroids implanted in nude mice, *Neoplasia* 1, 226, 1999.

[34] Benjamin, L.E. et al., Selective ablation of immature blood vessels in established human tumours follows vascular endothelial growth factor withdrawal, *J. Clin. Invest.* 103, 159, 1999.

[35] Benjamin, L.E. et al., A plasticity window for blood vessel remodeling is defined by pericyte coverage of the preformed endothelial network and is regulated by PDGF-B and VEGF, *Development* 125, 1591, 1998.

[36] Currie, M.J. et al., Angiopoietin-1 is inversely related to thymidine phosphorylase expression in human breast cancer, indicating a role in vascular remodeling, *Clin. Cancer Res.* 7, 918, 2001.

[37] Koga, K. et al., Expression of angiopoietin-2 in human glioma cells and its role for angiogenesis, *Cancer Res.* 61, 6248, 2001.

[38] Davis, S. et al., Isolation of angiopoietin-1, a ligand for the Tie2 receptor, by secretion-trap expression cloning, *Cell* 87, 1161, 1996.

[39] Suri, C. et al., Requisite role of angiopoietin-1, a ligand for the TIE2 receptor, during embryonic angiogenesis, *Cell* 87, 1171, 1996.

[40] Maisonpierre, P.C. et al., Angiopoietin-2, a natural antagonist for Tie2 that disrupts *in vivo* angiogenesis, *Science* 277, 55, 1997.

[41] Audero, E. et al., Expression of angiopoietin-1 in human glioblastoma regulates tumour-induced angiogenesis, *Arterioscl. Thromb. Vasc. Biol.* 21, 536, 2001.

[42] Stratmann, A., Cell type-specific expression of angiopoietin-1 and angiopoietin-2 suggests a role in glioblastoma angiogenesis, *Am. J. Pathol.* 153, 1459, 1998.

[43] Abramovitch, R. et al., *In vivo* prediction of vascular susceptibility to vascular endothelial growth factor withdrawal: magnetic resonance imaging of C rat glioma in nude mice, *Cancer Res.* 59, 5012, 1999.

[44] Merbl, Y. et al., Analysis of murine experimental data describing tumour development, angiogenesis, and microvessel maturation, *in preparation.*

[45] Hahnfeldt, P. et al., Tumour development under angiogenic signaling: a dynamic theory of tumour growth, treatment response, and postvascular dormancy, *Cancer Res.* 59, 4770, 1999.

[46] Bellomo, N. and Preziosi, L., Modeling and mathematical problems related to tumour evolution and its interaction with the immune system, *Math. Comp. Modeling* 32, 413, 2000.

[47] De Angelis, E. and Preziosi, L., Advection-diffusion models for solid tumour evolution *in vivo* and related free boundary problem, *Math. Models Methods Appl. Sci.* 10, 379, 2000.

[48] Daugulis, P. et al., Hopf bifurcation analysis for angiogenesis models, *Discrete and Continuous Dynamical Systems* in press.

[49] Chicone, C., *Ordinary Differential Equations with Applications*, Springer-Verlag, Heidelberg, 1998.

[50] Arakelyan, L., Vainstain, V., and Agur, Z., Optimizing anti-angiogenic therapy using mathematical tools. *Proceedings of the American Society of Clinical Oncology (ASCO)* 21, 440a, 2002.

[51] Arakelyan, L., Vainstain, V., and Agur, Z., A computer algorithm describing the process of vessel formation and maturation, and its use for predicting the effects of anti-angiogenic and anti-maturation therapy on vascular tumour growth, *Angiogenesis*, in press.

[52] Darland, D.C. and D'Amore, P.A., Blood vessel maturation: vascular development comes of age, *J. Clin. Invest.* 103, 157, 1999.

[53] Ahmad, S.A. et al., Differential expression of angiopoietin-1 and angiopoietin-2 in colon carcinoma, *Cancer* 92, 1138, 2001.

[54] Goede, V. et al., Analysis of blood vessel maturation processes during cyclic ovarian angiogenesis, *Lab. Invest.* 78, 1385, 1998.

[55] Kakolyris, S. et al., Relationship of vascular maturation in breast cancer blood vessels to vascular density and metastasis, assessed by expression of a novel basement membrane component LH39, *Brit. J. Cancer* 82, 844, 2000.

[56] Gabrielsson, J. and Weiner, D., *Pharmacokinetics and Pharmacodynamics Data Analysis: Concepts and Applications*, 3rd Edition, Swedish Pharmaceutical Press, Stockholm, 2000.

Chapter 8

Adhesion Mechanisms in Cancer Metastasis

Anne Leyrat[1], **Alain Duperray**[2], **and Claude Verdier**[1]

[1] *Laboratoire de Rhéologie, UJF-INPG, CNRS (UMR 5520), BP 53, Grenoble cedex 9 (France),*
[2] *Laboratoire de Migration Cellulaire et Infiltration Tumorale (EA2942 INSERM), Institut Albert Bonniot, La Tronche cedex (France)*

8.1 Introduction

Cell adhesion plays a crucial role in every aspects of a cell's life, from embryogenesis, to morphogenesis, to wound healing or to the progression of cancer. Adhesive interactions between a cell and its surrounding neighbours or extracellular matrix[1] are mediated by transmembrane proteins named cell adhesion molecules (CAMs). These proteins usually span the entire phospholipid bilayer, which isolates the interior of the cell (cytoplasm) from the exterior. They also contain domains extending into the aqueous medium on each side of the bilayer. They are therefore exposed on both the external and internal surface of the cell. On the external side, they can interact with ligands exposed either by other cells or by the components of their extracellular matrix. On the internal side, they can interact both mechanically (attachment) and "biochemically" with components of the cell cytoskeleton (essential for cell motility) and of the cell signalling machinery (control of cell fate). These interactions are regulated by interconnected pathways which may arise from the cell itself (autocrine), from a distant origin (paracrine signals from neighbouring cells or endocrine signals mediated by molecules transported by the blood) or from very close (juxtacrine signals going through cell junction channels, or signals due to membrane attached proteins of one cell interacting with receptors on an adjacent cell). CAMs are usually classified in four families: integrins, cadherins, immunoglobulins and selectins. They are involved in the control of key mechanisms such as proliferation,[2] differentiation,[3] and migration.[4] This control arises from two main functions of the CAMs, the "mechanical" gluing function, and the signal transduction function. The aim of this chapter is to introduce these key notions on cellular adhesion mechanisms and to show that (why and how) adhesion mechanisms should be taken into account in models dealing with the development of cancer and metastasis.

8.2 Cell-Cell Interactions and Signalling

Cells communicate with each other through different means, in order to coordinate growth, differentiation, and metabolism. Soluble signalling molecules (growth factors, cytokines, etc.) released by cells and targeting receptors on target cells allow

[1] Extracellular matrix refers to the environment filling the spaces between cells. The extracellular matrix is a complex three dimensional network of proteins and carbohydrates secreted and remodelled by the cell. It helps bind the cells together in tissues and also provides a lattice through which cells can move.

[2] Refers to the process through which cells multiply to form new tissues or colonies.

[3] Process though which cells gain specific functions and thereby loose their pluripotency.

[4] Cells can leave their original place and move through adjacent tissues through the process called migration.

distant communication. Cell adhesion molecules, which constitute the cement stabilising the structure of tissues through their mechanical gluing function, also provide a means to promote local communications between adjacent cells. The picture is even more complicated, since soluble signalling molecules can interfere with the function of, or cooperate with, cell adhesion molecules.

8.2.1 Extracellular Signalling and Signal Transduction

Extracellular signalling molecules synthesised and released by signalling cells produce a specific response only in target cells that have receptors for these signalling molecules. Whatever the origin and the route through which a signalling molecule reaches its target, the extracellular signals must be converted into cellular responses, a process which is known as signal transduction. Signal transduction pathways can promote changes in gene expression,[5] cell morphology, and cell movement by modulating the activity of specific transcription[6] factors, by affecting the adhesive contacts between cells and between the cells and the extracellular matrix. The complexity of these events lies in the fact that the different pathways are interconnected and form meshes, rather than linear paths.

The interaction of cell surface receptors, with water-soluble ligands, rely on conformational matches between the receptor and the ligand molecules. There are four major classes of such receptors, each one possessing a specific way to trigger signalling pathways:

- G-protein-coupled receptors: upon activation by ligand binding, they activate or inhibit enzymes that can generate specific second messenger;[7]
- ion-channel receptor: change their conformation upon ligand binding so that ions can flow through the receptor;
- tyrosine-kinase-linked receptors or cytokine receptors: stimulation upon binding induces formation of a dimeric receptor which interacts with and activates one or more cytosolic protein-tyrosine kinases. The receptors for many cytokines, interferon, human growth factor, are of this type;
- receptors with intrinsic enzymatic activity, which are activated upon ligand binding. Some catalyse conversion from GTP to cyclic GMP (second messenger), others work as protein phosphatases, removing phosphate groups from

[5]Gene expression is the process in which the information encoded in a particular gene is decoded in a particular protein.

[6]Transcription is the process in which DNA is copied into RNA. RNA has a central role in protein synthesis: messenger RNA carries instruction from DNA that specify the correct order of amino acids during protein synthesis. Translation of mRNA, which is controlled by transfer RNA, results in the stepwise assembly of amino acids into proteins, ribosomal RNA also helps in this process.

[7]Second messengers are intercellular signalling molecules which regulate various metabolic functions.

phosphotyrosine residues in substrate proteins, thereby modifying their activity. Many growth factor receptors are ligand-triggered protein kinases (also called receptor serine/threonine kinases or receptor tyrosine kinases). They can phosphorylate certain residues in their own cytosolic domain, as well as certain substrate proteins.

8.2.2 Cell Adhesion Molecules as Biochemical and Mechanical Transducers

Cell adhesion molecules are yet another type of cell surface receptors, since these molecules can interfere with, or even trigger, signalling pathways, in a manner which is as efficient as growth factor receptors or cytokine receptors. Only two main classes of cell adhesion molecules involved in the process of cancer metastases, namely cadherins and integrins, are described in details in this chapter, along with the signalling pathways which either control them or are triggered by them. But all adhesion molecules share the common features of involving specific receptor-ligand interactions. These interactions rely on conformational matches between the receptor and the ligand molecules. Van der Waals forces, hydrophobic and electrostatic interactions are all important, but it is the local 3D geometry of the binding pocket of the receptor, where the ligand penetrates, that determines the characteristics of the bond. Good conformational matches lead to strong and long-lasting bonds, whereas poor conformational matches do the contrary [1]. The reason is that receptor-ligand binding relies on noncovalent bonds such as hydrogen bonds, which are weak individually, but can be strong collectively. Since hydrogen bonding operates effectively within narrow geometric ranges, a large number of hydrogen bonds is needed for a good conformational match between the receptor and the ligand at the binding pocket.

It is well established that biochemical signals arising from different origins and transiting through cells can lead to protein phosphorylation or dephosphorylation[8] which can induce protein conformational changes. These conformational changes can modify the specificity of a receptor for ligands (binding to ligand B instead of ligand A upon deformation). Mechanical forces applied to an adhesive receptor (pulling on the receptor on one side, while an attachment to the cytoskeleton resists the traction force on the other side) may also deform the receptor and therefore modify the conformational match between the receptor and the ligand. These mechanical effects could then transduce the mechanical signal into biochemical signals that result in biological responses. For instance, Bierbaum et al. [2] and Schmidt et al. [3] showed that tyrosine phosphorylation (a biochemical response which may trigger signalling cascades) was altered by stressing integrins, but not by stressing nonadhesive receptors (showing the necessity for a transduction of forces). Other

[8] Addition of removal of a phosphate group.

cell adhesion molecules have also been suggested to be able to transmit forces across the cell surface to the cytoskeleton (platelet-endothelial cell adhesion molecule [4], E-selectin [5], and E-cadherin [6]).

A review of the literature shows that adhesive receptor-ligand interactions are usually described in biochemical terms. Nevertheless, physical analyses and measurements should be performed in order to determine not only which, but also how these molecular links transmit mechanical forces.

8.2.3 Force Measurements for Estimating Adhesive Interactions

In order to have access to the mechanical forces, new instruments have been developed during the past fifteen years. The range of forces is wide and depends on the nature of the bonds or forces in presence. Van der Waals, electrostatic, steric repulsion forces, hydrophobic interactions, as well as hydrogen bondings or covalent bonds are present in biological systems, and these can combine to create receptor-ligand interactions. The latter interactions have been shown to reach energies of about 30 kT, as compared to a few kT [7] (k being the Boltzmann constant and T the temperature). Salts (Ca2+), pH, and temperature can affect the nature of the bonds, by changing conformations of binding pockets (i.e., with integrins), and since forces in cellular systems are dynamic ones, the treatment of this information is rather difficult and may lead to significant differences in the levels of forces found in the literature. Nevertheless, there exists a few interesting methods for measuring such interactions. The AFM apparatus [8], also called SFM (scanning force microscope) when used for surface scanning, allows the determination of forces in the range of 0.01 to 100 nN and has been used intensively for the investigation of immunoglobulins, fibrinogen, and fibronectin. It can be used either in the contact, noncontact, or tapping mode. Different tips (cone, pyramid, sphere) can also be used. In particular, the use of a sphere makes it possible to couple it with the JKR test [9,10]. The surface force apparatus or SFA (10 to 1000 nN) can be used also for investigating biological molecules [11] and consists of two crossed-cylinders coated with such molecules. It provides a unique way to have access to force versus separation distance (or energy-distance) curves. The accuracy is about a few Angstroms. Micropipettes have also been developed [12] in the range (0.01 to 1000 pN) and proved to be efficient for example when studying red blood cell aggregation. The optical tweezer [13] uses a laser beam focused through a microscope objective to move a bead attached to a cell. It allows to measure the force exerted on the bead. This recent technique covers the range of forces (0 to 200 pN). Finally flowing devices (microchannels, see chapter 9 of this book) are also of interest since they can monitor forces using the flow pressure [14]. Thus one can have access to the shear stress required to detach cells from a wall for example, which is related to the bonding force.

The use of such techniques is guided by the numbers of effective bonds. Some studies deal with one single receptor-ligand interaction, whereas others concentrate on several ones. Indeed, an additional mode of regulation of the adhesive properties

of cell adhesion molecules lies in the cooperation of several receptor-bond interactions. This is a common feature of cadherins which are found in high concentration in adherence plaques or junctions, and of integrins, which form clusters known as focal adhesion plaques. This cooperation is also under the control of biochemical signals, but it may as well depend on mechanical stimuli.

8.3 Key Steps of Cancer Metastasis

The leading cause of death among cancer patients is the occurrence of metastases, which are secondary tumours arising at a distant site from the primary tumour. Tumours of comparable size and histology can have widely divergent metastatic potential, depending on their genotype and their local environmental influences, such as angiogenesis, stroma-tumour interactions, and production of cytokines by the local tissue. Metastasis is a cascade of linked sequential steps involving multiple host-tumour interactions mediated by cell adhesion molecules. Six steps can be defined:

1. **Detachment:** Tumour cells can detach from the primary tumour probably due to a decrease in their adhesive interactions with their neighbours. It is largely admitted that a loss of function of E-cadherins is related to this first step. It is also known that cell acquisition of motile properties correlates with a loss of its ability to recognise and adhere to its neighbours [15]. Cadherins are also involved in these events, as their function can be regulated by intracellular proteins called catenins. A detailed description of cadherin molecules and of their mode of action and regulation, in the framework of cancer metastasis, is given in section 8.4 of this chapter.

2. **Invasion:** The detached cells may then break through the supporting basal lamina[9] by using degradative enzymes, e.g., matrix metalloproteases (MMPs). A review on these crucial actors of cancer cell progression is beyond the scope of this chapter and is covered by the article of Kleiner and Stetler-Stevenson [16]. Using appropriate adhesion molecules (mainly of the integrin family) and degradative enzymes, cancer cells may then be able to attach and detach from the extracellular matrix and turn on the modifications of cell shape and microrheological properties necessary to migrate through the surrounding tissues, until they eventually reach a blood or a lymphatic vessel.

3. **Intravasation:** Intravasation occurs in blood or lymphatic circulation either directly in the tumour neo-vessels or indirectly in lymphatic channels. Metastasis is more likely to occur in vascularised tumours because of the leaky nature

[9]Basal lamina are flexible thin mats of specialised extracellular matrix that underlie all epithelial cell sheets and tubes. They separate cells from the underlying or surrounding connective tissue.

of neo-vasculature produced by angiogenesis, which facilitates the penetration of tumour cells in the blood circulation. If tumour cells reach a vessel and are able to cross the basal lamina and the endothelium lying on it, they will be able to enter the circulation.

4. **Transport and arrest:** As they travel though the blood stream, invasive cancer cells may encounter immunocompetent cells which hopefully may put an end to their journey through the body. Some cancer cells are nevertheless able to survive in the circulation by disguising themselves (they would express native leukocyte membrane molecules), and therefore escape immunological attacks. Circulating cancer cells can also interact with blood components such as platelets [17], leukocytes or other tumour cells [18] and form aggregates whose size help tumour cell retention and arrest in the circulation (immobilisation). This type of arrest and the biochemical reactions triggered by the release of cytokines from the platelets are believed to induce the expression of adhesion molecules by the endothelial cells (E-selectins) which help the extravasation of the cancer cells. The role of another kind of selectin, known as P-selectin, has been hypothesised (reviewed by Krause et al. [19]). Given that, on one hand, P-selectin is expressed on human pancreatic cell lines which are highly metastatic in lungs of mice and that, on the other hand, the ligand of P-selectin (sialyl Lewis-a) is also expressed on the same tumour cells, a homotypic[10] adhesion between cancer cells mediated by this receptor-ligand interaction might therefore lead to the production of cancer cell aggregates. The role of P-selectin in the formation of aggregates of tumour cells with platelets is more controversial, it appears to depend on the cell lines tested.

5. **Extravasation:** The migration of tumour cells through the endothelial lining towards the surrounding tissues can be facilitated by different cell interactions described in 4), which lead to tumour cell arrest in the circulation. But another mechanism showing cooperation between cancer cells and blood components in the process of extravasation has been enlightened in a recent *in vitro* study [20]. These authors demonstrated that polymorphonuclear neutrophils (leukocytes) incubated with tumour conditioned medium (TCM) show an ability to help cancer cells in the process of extravasation through different endothelial cell monolayers. TCM downregulated PMNs cytocidal function, delayed PMN apoptosis[11] and upregulated PMN adhesion molecule expression. The TMC treated PMNs were shown to attach to tumour cells and to play a role in transporting these cells through endothelial monolayers. Tumour cells are therefore able to exploit PMNs and alter their function to facilitate their extravasation. The more classical form of tumour cell extravasation process, similar to that followed by leukocytes during inflammation is described in details in Chapter 9 of this book. In this process, individual cancer cells first

[10] Homotypic interactions involve cells of the same type.

[11] Apoptosis refers to a programmed cell death.

stop in the circulation, by developing adhesive interactions with the endothelial cell lining, then develop strong adhesive interactions to spread on it and migrate towards an endothelial cell junction through which they migrate.

6. **Invasion of the target organ:** This step requires the same type of properties as those described in step 2, i.e., action of MMPs and acquisition of motility.

   This description of the metastasis cascade shows the importance of cell-cell and cell-stroma adhesive interactions in the development of secondary tumours. Cadherins and integrins might stabilise tissue integrity, whereas the loss or alteration of these cell surface proteins has been shown to be associated with increased metastatic potential. The picture is nevertheless far more complicated, due to the fact that activation of these cell surface receptors transmits signals from the outside into the cell and thus directs cell behaviour. The signalling pathways involved can suffer from crosstalks with other pathways, resulting in the acquisition of an invasive phenotype. The signals passing from the inside of the cell to the outside, which can result in the emergence of paracrine or juxtacrine signals addressed to neighbouring cells, can also suffer from crosstalks with other pathways, or "short-circuits" due to oncogenes. The crucial role of cadherins and integrins are reviewed in sections 8.4 and 8.5.

8.4 Cadherin-Catenin Complex and Cancer Metastasis

Cadherins have been proven to play a very important role in the pathogenesis of different types of cancer such as prostate cancer [21] or lung cancer [15].

8.4.1 Structure and Regulation of Function

Cadherins belong to a family of transmembrane glycoproteins that mediate cell-cell adhesion in the presence of extracellular calcium. There are more than 20 different kinds of cadherins currently classified. The most extensively studied are E- (epithelial), N- (neuronal), and P- (placental) cadherins. Cadherins are mainly tissue type specific, but they can be expressed in various other tissues during development.

Cell-cell adhesion is mainly mediated by homophilic[12] interactions, but heterophilic interactions are also possible between different cadherin molecules. Classical cadherins (Figure 8.1) are composed of five cadherin repeats in the N-terminal

[12]Homophilic interactions = interactions between molecules of the same type (different type = heterotypic).

extracellular domain, and a single transmembrane segment containing a carboxy terminal in the intracellular domain. This latter mediates the anchorage of cadherins to the cytoskeleton via a group of cytoplasmic proteins known as catenins. β/γ-catenin along with α-catenin form the cytoplasmic cell adhesion complex through which cadherin molecules are linked to the cytoskeleton, but they also regulate the function of cadherins. The assembly and turnover of the adhesion structures involving cadherins are regulated by complex biochemistry, which involves cadherin synthesis, degradation and the generation of external and internal signals.

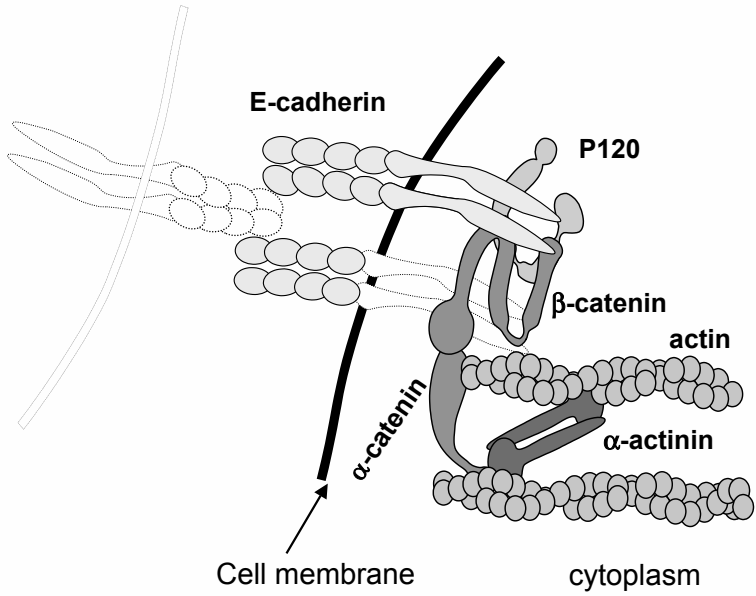

Figure 8.1

Structure of classical cadherins showing the proteins involved in the cytoplasmic cell adhesion complex.

Since most, if not all cancers, arise from epithelial dysfunction, it is not surprising that one of the best characterised cadherin molecules is E-cadherin, which is the key component for adherence junctions between epithelial cells. When epithelial cells contact each other, in the presence of extracellular calcium, they use

E-cadherin molecules to rapidly form adhesion structures in a zipper like fashion. The E-cadherin-catenin complex begins to form during the passage of E-cadherin to the cell membrane. The first catenin to interact with cadherin is either β-catenin or γ-catenin (plakoglobin) which can be substituted for each other in the cadherin-catenin complex. This is followed by the recruitment of α-catenin from the cytosol, and its binding to a short region close to the NH2 terminal of β-catenin or γ-catenin. This would result in the formation of stable bonds between the complex and the actin cytoskeleton. Spectrin would also bind to the complex in the NH2 terminal domain of α-catenin [22].

The role of p120, a fourth catenin-like molecule, in the regulation and stabilisation of adhesion is more controversial. It would have a role in the modulation of cadherin clustering and thus the stabilisation of adhesion. Indeed, cadherin-catenin complexes would set off a signalling pathway that results in the attraction of E-cadherin. Freely diffusing cadherins would become trapped by the immobilised cadherin-catenin complexes, and the local increase in the concentration of E-cadherin could then strengthen cell-cell adhesion through the formation of lateral bonds. But other studies report on the negative regulatory role of p120 on adhesion. A recent model proposes that transbinding of cadherins result in the activation of p120 and the strengthening of adhesion, whereas intracellular signalling induces the inhibitory effects of p120 on intercellular adhesion [23]. Recent studies also suggest that p120 promotes cell migration by recruiting and activating Rho-family GTPases [25,26] (cf. section 8.4.2).

It has been suggested that the loss of adhesive function of E-cadherins is a prerequisite for tumour cell invasion and metastasis formation [24,25]. Multiple mechanisms are found to underlie the loss of E-cadherin function in cancer:

- Mutation or deletion of the E-cadherin gene itself
- Mutation of the β-catenin gene
- Transcriptional repression of the E-cadherin gene
- Aberrant tyrosine phosphorylation of the components of the cytoplasmic cell adhesion complex

The loss of E-cadherin mediated cell-cell adhesion, leading to a detachment of tumour cells from the primary tumour, is probably not sufficient to confer an invasive phenotype to tumour cells. It seems more likely that E-cadherin downregulation results in the activation or alteration of specific signalling pathways, which in turn, trigger tumour cell invasion and tumour cell growth (E-cadherin could induce cell cycle arrest via upregulation of cyclin-dependent kinase p27, [27]). Only a few studies investigated the role of the cytoskeleton upon the loss of E-cadherin mediated cell-cell adhesion and the induction of tumour malignancy. Since cadherin based adhesion complexes are functionally linked to the dynamics of actin and microtubule cytoskeletal structures, the loss of E-cadherin mediated cell adhesion might therefore probably lead to dramatic cytoskeletal rearrangements. This is why the role of

small GTPases of the Rho family, which not only modulate cadherin activity, but also control the actin cytoskeleton, should also be considered.

Recent studies have shown that mesenchymal cadherins, in particular N-cadherin, have an opposite effect as compared to E-cadherins: they enhance tumour cell motility and migration [25,28]. N-cadherin deleterious effect can even overcome E-cadherin mediated cell-cell interactions. Studies also show a conversion of E-cadherins to N-cadherins in human tumours [25,29], a well characterised phenomenon in normal development. A novel concept of 'cadherin switch' from epithelial to mesenchymal cadherins supports the transition from a benign, to an invasive malignant tumour phenotype. Unlike E-cadherin, N-cadherin would promote a dynamic adhesive state in tumours, allowing not only a dissociation of tumour cells from the tumour mass, but also their interaction with stromal and endothelial components. The fact that N-cadherin expressing breast carcinoma cells were specifically sensitised to fibroblast growth factor (FGF-2)-induced invasion and upregulation of the proteolytic enzyme MMP-9 seems to show that MMP can mediate the pro-invasive effect of N-cadherins. It also shows that FGF receptor signalling has a functional interaction with N-cadherins. E-cadherin has also been shown to associate with FGFR in tumour cells of the exocrine pancreas, and in this case, FGF stimulation enhances cell-cell adhesion. Although it seems to contradict many reports showing that FGFR signalling decreases cell adhesion and triggers tumour cell invasion, it brings up the possibility that FGFR can associate with different cadherins in a cell type or tumour specific manner. So far, the cadherin switch has been described *in vivo*, only during the development of malignant melanoma and prostate carcinoma and *in vitro* observations only suggest that it might also occur in other cancer types. What regulates the cadherin switch is therefore a very crucial question since it may probably prove to apply to many different types of cadherins, in a tumour specific manner.

8.4.2 Upstream and Downstream Signalling by the Cadherin-Catenin Complex

8.4.2.1 Catenins

β-catenin, γ-catenin, and armadillo share partial homology with the protein product of the tumour suppressor gene APC. APC can stabilise the level of these catenins by complexing with glycogen-synthetase kinase-3β. Such complexes are involved in the signalling pathway driven by the secreted glycoprotein wingless (Wg/Wnt). This Wnt signalling pathway is an important feature in cell-cell adhesion since it regulates the degradation of β-catenins. When the Wnt signal is off, a pathway involving GSK-3β and APC leads to the degradation of β-catenin. When it is on, degradation of β-catenin is prevented (by inhibition of GSK-3, which normally marks for its degradation). This "on" signal then allows β-catenin to accumulate in the cytoplasm, eventually to translocate to the nucleus and to participate in the regulation of gene expression (TCF-LEF-1 target genes). The target genes of

translocated β-catenin are considered involved in apoptosis inhibition and promotion of cellular proliferation and migration. Future investigation will probably address the relationship between E-cadherin downregulation and β-catenin signalling during tumour progression and the question of whether the loss of E-cadherin results in the activation of the Wnt pathway, which is known to produce an invasive phenotype. The well known ability of E-cadherin overexpression to effectively block proliferation and invasiveness of cancer cells might therefore be a consequence not directly of cell adhesion, but instead of the ability of E-cadherin to sequester β-catenin and effectively shut off the expression of LEF/TCF/β-catenin-responsive genes [30]. Nevertheless, how a cell responds to the downregulation of E-cadherin is likely to depend on whether or not it is receiving a Wnt signal. Although catenins perform distinct functions in E-cadherin mediated cell-cell adhesion and in Wnt signalling pathway, there might be some crosstalk between the adhesive and signalling pathways. The complete mechanism of action of β-catenin has not been elucidated yet. It should be noted that tyrosine phosphorylation of β-catenin may also play a role in the acquisition of metastatic properties.

Recently, a negative signalling function of α-catenin has been discovered [30, 31]. The loss of α-catenin in the epidermis resulted in the sustained activation of the Ras-MAP kinase pathway and the association of E-cadherin-catenin complexes with downstream members of tyrosine kinase growth factor receptor pathways.

8.4.2.2 RhoGTPases

The Rho subfamily of GTPases, which includes Rho, Rac, and Cdc42, is involved in various aspects of cytoskeletal organisation, cell polarity, and motility. For example, Rho is involved in the regulation of stress fibers and focal adhesion formation, Rac is involved in the formation of lamellipodia and membrane ruffling, and Cdc42 is necessary for actin microspikes/filopodia to form. These proteins cycle between two guanine-nucleotide bound states, the GTP-bound form, which is active, and the inactive GDP-bound form. Small GTPases of the Rho-familly are known to modulate cadherin activity. The inactivation of Rac or Rho results in the dislocation of E-cadherin and its complex members from adherens junctions leading to the loss of cell-cell adhesion [32,33]. Their activation leads to the converse: overexpression of constitutively active Rac induces a greater accumulation of E-cadherin, β-catenin, and actin at the regions of contact between epithelial cells, whereas dominant negative Rac has the opposite effect. This is due to a protein termed IQGAP, which can only interact with Cdc42 and Rac in their GTP form. IQGAP can also associate with α-catenin, inducing its dissociation from the cadherin-catenin complex. When Cdc42 and Rac are in the GDP-bound inactive forms, Cdc42 and Rac cannot interact with IQGAP, and IQGAP interacts with β-catenin, thereby dissociating α-catenin from the cadherin-catenin complex. This state confers the weak adhesive activity. When Cdc42 and Rac are in the GTP-bound active forms at sites of cell-cell contact, Cdc42 and Rac1 interact with IQGAP. Then, IQGAP is unable to interact with β-catenin, resulting in the stabilisation of the cadherin-catenin complex. Thus, Cdc42 and Rac positively regulate cell-cell adhesion by the suppression of the activity of

IQGAP to perturb the cadherin-catenin complex. Therefore, Cdc42, Rac, and IQGAP can cyclically regulate cell-cell adhesion by remodelling the cadherin-catenin complex. The dysregulation of IQGAP has been proposed to correlate with malignancy in gastric cancers [34]. On the other hand, activated Rac also promotes cell mobility when adherens junctions are rare or absent.

In some other cells, activation of Rho proteins can contribute to the loss of adherens junctions. In fact the ability of TGF-β to promote the loss of adherens junctions is dependent on Rho and ROCK function. In keratinocytes, active Rac1 causes the dis-assembly of adherens junctions, and Rac function is required for the loss of adherens junctions caused by oncogenic Ras. The effect of Rac1 is nevertheless dependent on the composition of the ECM with which the cells are in contact (going from promoting to antagonising cell-cell adhesion) [35].

The regulation goes also the other way around: cell-cell adhesive interactions through cadherins seem to regulate Rho family GTPases. Indeed, cadherin engagement depresses RhoA and elevates Rac1 activity. Cell-cell interactions mediated by E-cadherins also seem to result in Cdc42 activation. A potential pathway to Rac1 activation is suggested by the finding that adherens junction formation stimulates PI(3)-kinase activity [36], which may have an influence on the localisation of active Rac at adherens junctions. This is another way, in addition to PI(3)k activation, for E-cadherin to promote actin polymerisation. Betzon et al. [37] also reported that Rac is activated upon induction of intercellular adhesion in epithelial cells, but this occurs even if actin polymerisation is prevented, showing that actin polymerisation is not required for initial Rac activation. This activation is dependent on functional cadherins, but inhibition of epidermal growth factor receptor signalling efficiently blocks the increased Rac-GTP levels observed after adhesive interactions. Cadherin dependent adhesion might therefore activate Rac via epidermal growth factor receptor signalling.

8.5 Integrins and Metastasis

8.5.1 Structure and Regulation of Function

Integrins are receptor proteins which are of crucial importance for the interaction of cells with their environment [38,39]. Functional integrins (Figure 8.2) consist of two transmembrane glycoprotein subunits that are noncovalently bound. Those subunits are called α and β. The α-subunits all have some homology to each other, as do the β-subunits. The receptors always contain one α-chain and one β-chain and are thus called heterodimeric. Both of the subunits contribute to the binding of ligand. Until now 18 α- and 8 β-subunits have been identified. From these subunits some 24 integrins are formed in the nature, which implies that not all possible

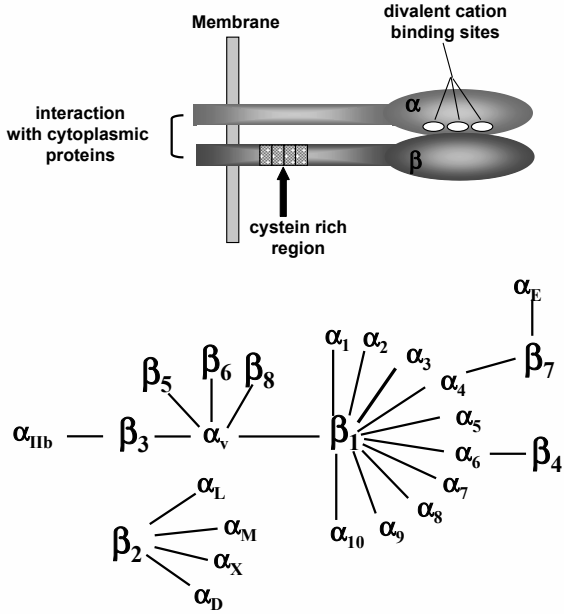

Figure 8.2
Structure of integrins and combinations of subunits.

combinations exist. The $\beta 4$-subunit, for instance, can only form a heterodimer with the $\alpha 6$-subunit. On the other hand the $\beta 1$-subunit can form heterodimers with ten different α-subunits. Because not all the $\beta_1\alpha$-heterodimers have the same ligand specificities, it is believed that the α-chain is at least partly involved in the ligand specificity.

Integrins differ from other cell-surface receptors (like growth factor receptors) in that they bind their ligands with a low affinity[13] (10^6 to 10^9 litres/mole) and that they are usually present at 10 to 100-fold higher concentration on the cell surface. When integrins are diffusely distributed over the cell surface, no adhesion can occur. The integrins can only bind their ligands when they exceed a certain minimal number of integrins at certain places, called focal contacts and hemidesmosomes. During the process of cell adhesion, integrins therefore have to cluster for their combined

[13]Affinity of a receptor for its ligand is related to the rate of reaction of binding of a single copy of the ligand to a single receptor site, it is independent of the number of sites.

weak affinities to give rise to a spot on the cell surface, which has enough adhesive (sticking) capacity to adhere to the extracellular matrix. In this way, cells can bind simultaneously but weakly to large numbers of matrix molecules and still have the opportunity to explore their environment without losing all attachment to it, by building or breaking down focal contacts. If the receptors were to bind strongly to their ligands, cells would probably be irreversibly bound to the matrix, depriving it from motility. This problem does not arise when attachment depends on multiple weak adhesions.

Integrins are composed of long extracellular domains which adhere to their ligands, and short cytoplasmic domains, devoid of enzymatic features, that link the receptors to the cytoskeleton of the cell. There is, however, one exception to this rule, which is the $\beta 4$-subunit, which contains a very large cytoplasmic domain of some 1000 amino acids, while the other integrins only have cytoplasmic domains of up to 60 amino acids. The structure of different α-subunits is very similar. All contain seven homologous repeats of 30 to 40 amino acids in their extracellular domain, spaced by stretches of 20 to 30 amino acids. The three or four repeats that are most extracellular, contain sequences with cation-binding properties. Since the interaction of integrins with their ligand is cation-dependent, these sequences are thought to be involved in binding. Common integrin ligands are fibronectin and laminin, which are both part of the extracellular matrix or basal lamina. Both of the ligands mentioned above are recognised by multiple integrins. The capacity of many integrins to bind their ligand is regulated by cellular signalling mechanisms through a process called integrin activation or inside out signal transduction. The clustering of integrins is regulated by signalling enzymes like PI(3)K, PKCs, and the Ras and Rap GTPases, as well as adaptor proteins, and seems to involve changes in the cytoskeletal structures that allow the lateral movement of integrins. These intimate interactions between signalling proteins and the cytoskeleton therefore appear to be very important for regulating integrin avidity[14] by inside-out signalling.

8.5.2 Upstream and Downstream Signalling by Integrins

Integrins are genuine signalling receptors. They transduce signals by associating with adapter proteins that connect them to the cytoskeleton, with cytoplasmic kinases and with transmembrane growth factor receptors. Integrins activate various protein tyrosine kinases, such as focal adhesion kinase, Src-family kinases, and a serine threonine kinase named Abl.

Integrin clustering and association with cytoskeleton appear to give rise to integrin growth-factor receptor complexes. Integrins therefore appear not only to signal on their own, but are also necessary for optimal activation of growth factor receptors. The mitogen activated protein kinase pathway (MAP-kinase pathway) provides

[14]Here, avidity refers to the total binding capacity of a cluster of receptors to multiple or multivalent ligands.

a very good example of this principle. Integrins play an important role in the control of cell cycle. Normal cells require anchorage to ECM to proliferate. This is because integrins activate growth promoting signalling pathways that are responsible for anchorage dependence. This is thought to provide another mechanism for matrix-specific growth regulation. Cell attachment through integrins may also facilitate exit from cell cycle and provide signal for differentiation. However, integrin signal alone is probably only permissive for differentiation.

Integrins also play an important role in the control of cell life and death. The loss of attachment to the ECM causes apoptosis in many normal cell types. This is likely to be important in the maintenance of tissue architecture and in the destruction of cells that have attached to an inappropriate tissue location. But the ability of integrins to protect from cell death is both integrin and cell-specific. Protection against death correlates with the ability of the integrin to induce Bcl-2 expression. Tumour cells are usually anchorage independent, this may explain their tendency to leave their original site and metastasise.

Integrins are also one of the main actors for the control of cell shape, growth, and survival. Indeed, integrins and receptors for soluble mitogens such as growth factors, regulate cell spreading and migration through activation of the Rho-family of GTPases. Among those, Cdc42 induces filipodia, Rac induces lamelipodia, and Rho induces focal adhesions and associated stress fibres. The binding of integrins to their ligands of the ECM therefore induces an interdependence between the ECM and the cytoskeleton.

8.6 Introducing the Adhesive Properties in Models of Cell Migration

In this section a few models are reviewed, which attempt to include the influence of the adhesive properties in modelling cell migration. First, cell migration is described, then two models are presented, and finally the application of such models to predict cancer cell migration is considered.

8.6.1 Cell Migration

Cell migration is a sophisticated mechanism which is driven by chemotaxis or haptotaxis for example. The cell becomes polarised and develops lamellipodia which extends far to the front [40]. This is the case for a fibroblast moving onto a rigid surface. Behind the cell, the uropod appears, such as a tail. The nucleus of the cell forms a bump which makes the whole cell look like a snail. Inside the cell, subtle changes in the viscoelasticity of the cell are achieved, which preserve the total actin concentration: actin filaments reticulate (in a gel-like manner) at the front whereas

they become less densely packed (as in a solution, or sol) at the back or close to the nucleus [41]. The actin-myosin complex plays a fundamental role here. In order for the cell to move, it is required to generate traction forces to pull itself forward. These forces are generated by focal adhesion plaques, usually consisting of integrin clusters. Some cells can migrate very fast like the neutrophils of the immune systems (about 1 mm/h) whereas cancer cells are more cautious and can reach velocities up to only 0.1 mm/h. In order for the actin units (rigid helical proteins) to form a gel, myosin molecules are required which act together with actin binding proteins (ABP) activated at the front. Fimbrin or the α-actinin combine with myosin-II to form respectively tight or loose bundling networks, whereas filamin is responsible for the formation of gel-like structures. Disassembly proteins (gelsolin, CapZ, ADF, cofilin) are also necessary for breaking this architecture away from the leading edge. The result is that the cell develops this (these) filopodium(a)/microspike(s) consisting of tight bundles at the front, and behind are regions where the cell is made of gels, followed by loose bundles of actin networks further away.

The role of adhesion is important because of interactions between the cell proteins involved (integrins mainly) and the ECM. Integrins bind to the cytoskeleton which consists (at the front) of tight parallel bundles of actin filaments and this confers an increased rigidity to this biological assembly which will allow the cell to generate traction forces. As a result of these interactions with the ECM, signalling by tyrosine kinases generates new receptors which will allow the creation of new focal sites. Such traction forces have been indeed measured on deformable substrates with tiny beads included, the motion of which gives access to the forces generated by a migrating fibroblast [42]. Other methods following wrinkle patterns on deformable substrates also give interesting data in the case of keratocyte locomotion [43].

8.6.2 Modelling Cell Migration Using Adhesion Receptors

To make migration more effective, the cell needs to develop strong traction forces, but on the other hand, these forces cannot be too large, otherwise it would also be difficult to break the bonds at the rear of the cell. This is indeed what is observed experimentally [44], as revealed by the evolution of the migration speed as a function of the force exerted on the bonds. A maximum migration speed is obtained at a typical level of force or affinity.

One way to model adhesion through this multi-step process is to use a distribution of bonds located underneath the cell. Such an idea is motivated by the observations (RICM) of adhering cells, which show that not every part of it is in contact with the substrate. In the model of Dickinson and Tranquillo [45], distributions of receptor-ligand bonds are assumed. In particular, one can also assume an adhesion gradient, which may influence the directional motility of a cell. They use a stochastic model to show how migration is affected by the magnitude of the force and the distribution of ligands on the cell. Adhesion receptors undergo rapid binding, and this results in a time-dependent motion, and levels of forces are also time-dependent.

Mean distributions can then be obtained which lead to the determination of mean speed, persistence time, and random motility coefficient. Note that one of the results is a bell-shape curve for the velocity of migration as a function of the so-called adhesion concentration factor, in agreement with Palecek et al. [44].

Another former approach, by DiMilla et al. [46], is also of interest, as they include cell polarisation, cytoskeleton force generation, and dynamic adhesion to create cell movement. Two models for adhesion are presented, one including a spatial distribution of receptor-ligand pairs due to the cell polarity, or one presenting a spatial variation in strength. In addition, a viscoelastic model is used for the cell. Assuming that a quasistatic motion is obtained, results are presented for the velocity of migration. The biphasic shape of the curve speed (force) can be found also in this case, but further results can be obtained, such as the effect of force, cell rheology as well as the effects of receptor-ligand dynamics and the number of such pairs. The maximum in migration speed, a parameter-dependent factor, is correlated to the balance between contractile force and adhesiveness.

8.6.3 Cancer Cell Migration

Finally, combining the different approaches above, it may be concluded that migration speed is somehow related to the level of affinity between cell receptors and ligands. Also it is the short-term adhesion which seems to control this migration. On the other hand, it seems like cancer cell migration is different from model cells which are usually studied (fibroblasts, keratocytes mainly). In particular [47], it has been shown that tumour cells develop migrating cell clusters, therefore single cell models might not apply. They also seem to develop stronger cell-cell interactions and have a high cell polarity. Some cancer cells (melanoma, for example) are larger and are less dynamic (more cautious) compared to migrating leukocytes. Another aspect is the strong pulling forces that they seem to develop at attachment sites, combined with the fact that they reorganise the matrix and seem to be more independent of it. Finally, focal contact receptors are not necessarily associated with integrins. Furthermore, cytoskeleton components seem to link efficiently with collagen fibres. Therefore, cancer cell migration modelling is still a challenge and may require further assessments.

8.7 Conclusion

Cell adhesion is omnipresent in the process of physiological, as well as pathological life events. Its control over the progress of cancer metastasis is only starting to be uncovered. It proves to go far beyond the well admitted mechanical role of cell adhesion molecules as a cement of tissues (normal or pathologic). Interconnected

signalling pathways, involving not only cell adhesion molecules, but also growth factor receptors and other types of cell surface receptors, are at play in the control of cell fate. These meshes of pathways offer many possibilities of cross talks and short-circuits, which may in particular be induced by oncogenes. For example, it is well known that short-circuiting of integrin signalling pathways by Src oncoproteins may result in an increased phosphorylation of focal adhesion kinase, thereby giving a false anchorage signal to cells, and leading to abnormal adhesion independent cell survival and growth. In addition to this first and foremost anchorage independency, invasive cancer cells must acquire specific properties in order to detach from the primary tumour, to migrate through the tissues surrounding the primary tumour, to escape attacks of the immune system, to migrate again, through endothelial linings, or through the target organ. These properties are all related to the expression, or activation, of specific adhesion molecules. The hypothesis first proposed by Fidler [48], in 1990, according to which, cells capable of forming metastasis may belong to a subpopulation differing from mean properties of cells from the initial tumour, stresses the importance of accounting for the specificity of cells, when designing experiments aimed at measuring cell adhesive properties. Classical experimental assays, such as those described in Chapter 9, may only give mean properties of cell populations, and might hide the relevant individualities. The way, in the future, to develop efficient and precise targeting, may therefore rely on exploring cell, as well as patient's individual properties. New approaches emerging in the postgenomic era, such as the toponomic[15] approach, will undoubtedly accelerate our understanding of the relationship between the structures, which are involved in adhesive interactions, and the functions carried out by such structures. Knowing how linking, as well as signalling proteins interact, to make the cell able to exhibit a given adhesive property, will probably help in developing treatments, which will be specific enough so as to preserve normal cells or to prevent cancer cells from becoming more invasive.

8.8 References

[1] Zhu, C., Bao, G., and Wang, N., Cell mechanics: mechanical response, cell adhesion, and molecular deformation, *Annu. Rev. Biomed. Eng.* 2, 189, 2000.

[2] Bierbaum, S. and Notbohm, H., Tyrosine phosphorylation of 40 kDa proteins in osteoblastic cells after mechanical stimulation of β1-integrins, *Eur. J. Cell Biol.* 77, 60, 1998.

[15] Toponome refers to the rules (nomos) presiding the spatial arrangement (topos) of proteins at the surface and in the cytoplasm of a cell.

[3] Schmidt, C. et al., Mechanical stressing of integrin receptors induces enhanced tyrosine phosphorylation of cytoskeletally anchored proteins, *J. Biol. Chem.* 273, 5081, 1998.

[4] Wang, N. and Ingber, D.E., Probing transmembrane mechanical coupling and cytomechanics using magnetic twisting cytometry, *Biochem. Cell Biol.* 73, 327, 1995.

[5] Yoshida, M. et al., Leukocyte adhesion to vascular endothelium induces E-selectin linkage to the actin cytoskeleton, *J. Cell Biol.* 133, 445, 1996.

[6] Potard, U.S., Butler, J.P., and Wang, N., Cytoskeletal mechanics in confluent epithelial cells probed through integrins and E-cadherins, *Am. J. Physiol.* 272, 1654, 1997.

[7] Israelachvili, J. et al., Direct measurements of specific ligand-receptor interactions between model membrane surfaces, in *Studying Cell Adhesion*, P. Bongrand, P.M. Claesson, and A.S.G. Curtis, Eds., Springer, Heidelberg, 38, 1994.

[8] Binnig, G., Quate, C., and Gerber, C., Atomic force microscope, *Phys. Rev. Letters* 56, 930, 1986.

[9] Johnson, K.L., Kendall, K., and Roberts, A.D., Surface energy and the contact of elastic solids, *Proc. R. Soc. Lond.* A324, 301, 1971.

[10] Canetta, E., Leyrat, A., and Verdier, C., A physical model for predicting the adhesion between a functionalised microsphere and a living cell, *Math. Comp. Modelling*, in press, 2003.

[11] Israelachvili, J., *Intermolecular and Surface Forces*, Academic Press, New York, 1991.

[12] Evans, E. et al., Detachment of agglutinin-bonded red blood cells, I, II, *Biophys. J.* 59, 849, 1991.

[13] Ashkin, A. and Dziedzic, J.M., Internal cell manipulation using infrared laser traps, *Proc. Natl. Acad. Sci. USA* 86, 7914, 1989.

[14] Bongrand, P. et al., Use of hydrodynamic flows to study cell adhesion, in *Physical Basis of Cell-Cell Adhesion*, P. Bongrand, Ed., CRC Press, Boca Raton, FL, 125, 1978.

[15] Bremnes, R.M. et al., The E-cadherin cell-cell adhesion complex and lung cancer invasion, metastasis, and prognosis, *Lung Cancer* 36, 115, 2002.

[16] Kleiner, D.E. and Stetler-Stevenson, W.G., Matrix metalloproteinases and metastasis, *Cancer Chemother. Pharmacol.* 43, 51, 1999.

[17] Gasic, G. et al., Platelet tumor interactions in mice. The role of platelets in the spread of malignant disease, *Int. J. Cancer* 11, 704, 1973.

[18] Saiki, I., Cell adhesion molecules and cancer metastasis, *Jpn. J. Pharmacol.* 75, 215, 1997.

[19] Krause, T. and Turner, G.A., Are selectins involved in metastasis?, *Clin. Exp. Metastasis* 17, 183, 1999.

[20] Wu, Q.D. et al., Human neutrophils facilitate tumor cell transendothelial migration, *Am. J. Physiol. Cell Physiol.* 280, C814, 2001.

[21] Mason, M.D., Davies, G., and Jiang, W.G., Cell adhesion molecules and adhesion abnormalities in prostate cancer, *Crit. Rev. Oncol. Hematol.* 41, 11, 2002.

[22] Beavon, I.R.G., The cadherin-catenin complex in tumour metastasis: structure, function, and regulation, *Eur. J. Cancer* 36, 1607, 2000.

[23] Anastasiadis, P.Z. and Reynolds, A.B., Regulation of Rho GTPases by p120-catenin, *Curr. Opin. Cell Biol.* 13, 604, 2001.

[24] Cano, A. et al., The transcription factor snail controls epithelial-mesenchymal transitions by repressing E-cadherin expression, *Nat. Cell Biol.* 2, 76, 2000.

[25] Cavallaro, U., Schaffhauser, B., and Christofori, G., Cadherins and the tumour progression: is it all in a switch?, *Cancer Lett.* 176, 123, 2002.

[26] Noren, N.K. et al., p120 catenin regulates the actin cytoskeleton via Rho family GTPases, *J. Cell Biol.* 150, 567, 2000.

[27] St-Croix, B. et al., E-cadherin-dependent growth suppression is mediated by the cyclin-dependent kinase inhibitor p27(KIP1), *J. Cell Biol.* 142, 557, 1998.

[28] Hazan, R.B. et al., Exogenous expression of N-cadherin in breast cancer cells induces cell migration, invasion, and metastasis, *J. Cell Biol.* 148, 779, 2000.

[29] Tomita, K. et al., Cadherin switching in human prostate cancer progression, *Cancer Res.* 60, 3650, 2000.

[30] Jamora, C. and Fuchs, E., Intercellular adhesion, signalling and the cytoskeleton, *Nat. Cell Biol.* 4, E101, 2002.

[31] Vasioukhin, V. et al., Hyperproliferation and defects in epithelial polarity upon conditional ablation of α-catenin in skin, *Cell* 104, 605, 2001.

[32] Evers, E.E. et al., Rho family proteins in cell adhesion and cell migration, *Eur. J. Cancer* 36, 1269, 2000.

[33] Braga, V.M. et al., The small GTPases Rho and Rac are required for the establishment of cadherin-dependent cell-cell contacts, *J. Cell Biol.* 137, 142, 1997.

[34] Takemoto, H. et al., Localization of IQGAP1 is inversely correlated with intercellular adhesion mediated by E-cadherin in gastric cancers, *Int. J. Cancer* 91, 783, 2001.

[35] Sahai, E. and Marshall, C.J., ROCK and Dia have opposing effects on adherens junctions downstream of Rho, *Nat. Cell Biol.* 4, 408, 2002.

[36] Noren, N.K. et al., Cadherin engagement regulates Rho family GTPases, *J. Biol. Chem.* 276, 33305, 2001.

[37] Betson, M. et al., Rac activation upon cell-cell contact formation is dependent on signaling from the epidermal growth factor receptor, *J. Biol. Chem.* 277, 36962, 2002.

[38] Hynes, R.O., Integrins: versatility, modulation, and signaling in cell adhesion, *Cell* 69, 11, 1992.

[39] Hynes, R.O., Cell adhesion: old and new questions, *Trends Cell. Biol.* 9, M33, 1999.

[40] Condeelis, J., Life at the leading edge: the formation of cell protrusions, *Ann. Rev. Cell Biol.* 9, 411, 1993.

[41] Stossel, T., On the crawling of animal cells, *Science* 260, 1086, 1993.

[42] Dembo, M. and Wang, Y.-L., Stresses at the cell-to-substrate interface during locomotion of fibroblasts, *Biophys. J.* 76, 2307, 1999.

[43] Burton, K., Park, J.H., and Taylor, D.L., Keratocytes generate traction forces in two phases, *Molecular Biology of the Cell* 10, 3745, 1999.

[44] Palecek, S.P. et al., Integrin-ligand binding properties govern cell migration speed through cell-substratum adhesiveness, *Nature* 385, 537, 1997.

[45] Dickinson, R.B. and Tranquillo, R.T., A stochastic model for adhesion-mediated cell random motility and haptotaxis, *J. Math. Biol.* 31, 563, 1993.

[46] DiMilla, P.A., Barbee, K., and Lauffenburger, D.A., Mathematical model for the effects of adhesion and mechanics on cell migration speed, *Biophys. J.* 60, 15, 1991.

[47] Friedl, P., Brocker, E.B., and Zanker, K.S., Integrins, cell matrix interactions and cell migration strategies: fundamental differences in leukocytes and tumor cells, *Cell Adhesion and Communication* 6, 225, 1998.

[48] Fidler, I.J., Critical factors in the biology of human cancer metastasis: twenty-eighth G.H.A. Clowes memorial award lecture, *Cancer Res.* 50, 6130, 1990.

Chapter 9

Static and Dynamic Interactions between Endothelium and Circulating Cells in Cancer

Roxana Chotard-Ghodsnia[1,3], Agnès Drochon[1], Alain Duperray[2], Anne Leyrat[3], and Claude Verdier[3]

[1]*Biomécanique et Génie Biomédical, CNRS (UMR 6600), UTC, Compiègne (France),* [2]*Laboratoire de Migration Cellulaire et Infiltration Tumorale (EA2942 INSERM), Institut Albert Bonniot, La Tronche cedex (France),* [3]*Laboratoire de Rhéologie, UJF-INPG, CNRS (UMR 5520), BP 53, Grenoble cedex 9 (France)*

9.1 Introduction

Cellular adhesion to vascular endothelium in the fluid dynamic environment of the circulation is an important aspect of many physiological and pathological processes. Examples include leukocyte adhesion during recruitment to a site of tissue injury and cancer cell adhesion during metastasis.

Circulating leukocyte emigration from vasculature into tissues (leukocyte extravasation) is the central event in inflammation. Through extensive studies in recent years, it has become clear that at least four distinct steps act in sequence to regulate leukocyte extravasation [1]:

- selectin-carbohydrate mediated initial leukocyte tethering and rolling;
- activation of integrins on leukocyte surfaces;
- transition from rolling to firm adhesion of leukocytes on endothelial cells; and
- migration of leukocytes through interendothelial junctions (transendothelial migration or diapedesis) to extravascular tissue space, following the guidance of chemo-attractants.

To metastasise, tumour cells must shed into the blood stream (intravasation) directly by invasion into the tumour-derived vasculature or indirectly by lymphatic drainage, survive in the circulation, and finally migrate through normal vascular endothelium (extravasation) and proliferate in the target organs. Tumour cell extravasation plays a key role in tumour metastasis. It has been proposed in the literature that adhesion of circulating tumour cells to the endothelium, mediated by specific ligand-receptor interactions, is an essential prerequisite step for extravasation to occur. However, the precise mechanisms by which tumour cells penetrate the endothelial cell junction remains one of the least understood aspects of extravasation [2].

Inside the body, the endothelium is continuously subjected to flow induced mechanical stress. These forces induce biochemical signals which can alter the surface expression of adhesion molecules and, therefore, influence the endothelial monolayer's ability to bind circulating cells. These cells contact the endothelium at a rate dependent upon the fluid dynamics and adhere through receptor-ligand bonds with a probability that varies with the flow rate. Thus, mechanical stresses and strains play important roles in interactions between endothelium and circulating cells.

Due to difficulties in characterising both hemodynamic forces acting on circulating cells and expression level of adhesion molecules on vascular endothelium *in vivo*, different flow devices have been widely used to study such interactions under controlled flow conditions. These include *in vitro* flow devices such as cone-and-plate rheometers and parallel-plate flow chambers.

In this chapter, we first describe adhesion molecules involved in interactions between endothelium and leukocytes or tumour cells. We then discuss the *in vitro* devices to study cell-endothelium interactions with particular emphasis on *in vitro* flow

devices used to simulate flow conditions in blood vessels. Finally, we describe experimental and mathematical modelling of circulating cell-endothelium interactions under flow. Understanding the complex interplay among blood flow, cell adhesion, and vascular biology at the molecular level is crucial for developing new therapeutic approaches against pathological inflammation and tumour metastasis.

9.2 Receptors Involved in Interactions between Endothelium and Leukocytes or Tumour Cells

Cell-cell interactions and cell-matrix interactions are mediated by cellular adhesion molecules (CAMs), a diverse group of glycoproteins expressed at the surface of every cell in the body. These CAMs selectively bind to one another, and play a critical role in various functions of cellular organisms, such as tissue development and cohesion, wound healing, cell migration, inflammation, and cancer metastasis. The recruitment of leukocytes into sites of inflammation involves a cascade of sequential events controlled by the interaction between adhesion molecules expressed by leukocytes and by the endothelium. Cell migration across endothelial monolayers involves leukocyte adherence to the endothelium, crawling on the endothelial surface and penetration between endothelial clefts. This process of leukocyte diapedesis has been extensively studied and may serve as a paradigm for the mechanisms involved in tumour cell arrest and extravasation. Several adhesion receptors belonging to different families including integrins, selectins, immunoglobulin-like molecules, and cadherins (Figure 9.1) have been shown to participate in this mechanism [3]. In the current model, selectins are implicated in the initial rolling, while adhesion receptors from the integrin family and the immunoglobulin superfamily are involved in the firm attachment, flattening, and extravasation of leukocytes; cadherins, and more specifically the endothelial specific VE-cadherin, are involved in the control of endothelial cell junctions.

9.2.1 Selectins

The selectin family comprises three proteins [4]: E-selectin (CD62E), L-selectin (CD62L), and P-selectin (CD62P). They all contain a lectin domain, an epidermal growth factor domain, and a variable number of short consensus repeats of 60 amino acids present in the complement regulatory proteins. E- and P-selectins are expressed on endothelial cells, while L-selectin expression is restricted to leukocytes. Selectins bind to carbohydrate ligands via their lectin domain. It has been shown that tetrasaccharides sialyl-Lewis^x and sialyl-Lewis^a (sLe^x, sLe^a) are ligands for all the three selectins [5].

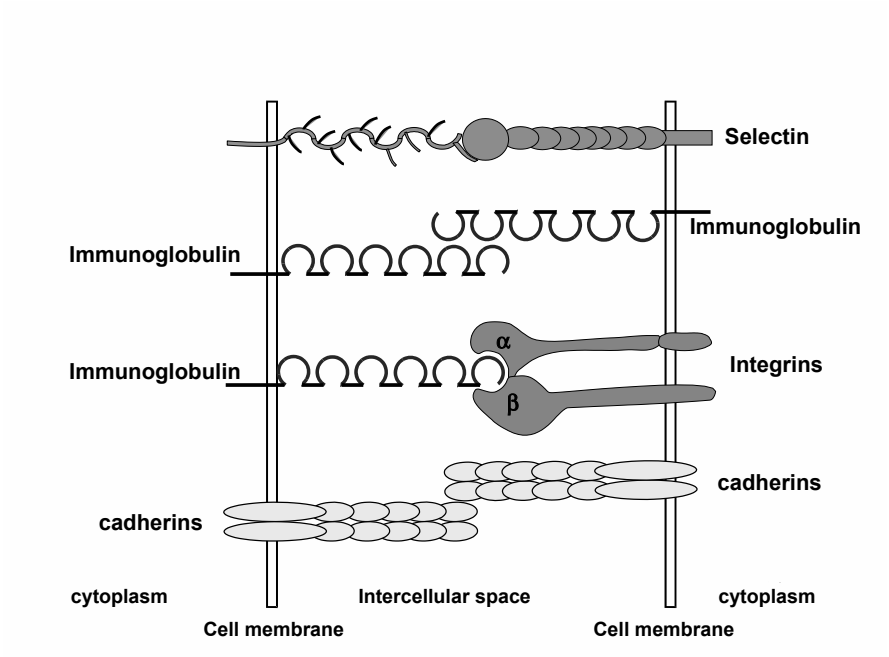

Figure 9.1

Adhesion molecules involved in leukocyte diapedesis. Selectins, expressed by leukocytes or endothelial cells, interact with glycosylated ligands. Members of the immunoglobulin superfamily, like PECAM-1, can bind to another molecule of PECAM-1 at cell-cell junctions. ICAM-1, which is also a member of the immunoglobulin superfamily expressed by endothelial cells, is a ligand for $\beta 2$ leukocyte integrins. VE-cadherin, expressed at interendothelial junction participates in the regulation of vascular permeability.

9.2.1.1 E-selectin

E-selectin (CD62E) is a 115 kD glycoprotein, only expressed on endothelial cells after activation by interleukin-1 (IL-1), tumour necrosis factor-α (TNF-α), or bacterial endotoxin such as lipopolysaccharides (LPS). After endothelial cell stimulation, newly synthesised E-selectin is rapidly detected with a maximal surface expression after 3 to 6 hours and a return to basal levels within 24 hours. This rapid downregulation, has been explained by the release of a soluble form of E-selectin, and internalisation of the molecule. This regulation of E-selectin expression might be crucial to control leukocyte accumulation in inflammatory responses. Monoclonal antibodies specific for E-selectin have been shown to inhibit leukocyte transmigration. It has been suggested that binding of leukocytes to E-selectin on activated en-

dothelium upregulates CD11b (Mac-1) on the leukocytes, and induces an increased adhesion through an ICAM-1/Mac-1 interaction (see also Sections 9.2.2 and 9.2.3).

9.2.1.2 P-selectin

P-selectin (CD62P) is a single chain glycoprotein of 140 kD, expressed in platelets and endothelial cells and stored in intracellular organelles. After activation, P-selectin is mobilised to the external plasma membrane within minutes. This increase in P-selectin expression is transient, and the protein is rapidly internalised inside the cell, where it is degraded or recycled. P-selectin is also upregulated transcriptionnally by TNF-α. The principal ligand for P-selectin is PSGL-1 (P-selectin glycoprotein ligand-1), expressed on all leukocytes.

9.2.1.3 L-selectin

L-selectin (CD62L), a 80-100 kD protein, is expressed specifically by a majority of leukocytes, and interacts with glycosylated endothelial counter-receptors.

Inhibitory experiments with antibodies as well as knock out mice have demonstrated that these selectins are important for the initiation of rolling and adhesion of leukocytes. Evidence that selectins are involved in metastasis comes from the fact that sialyl-Lewis^x and its isoform sialyl-Lewis^a have been found on different types of carcinomas, and that cells expressing these molecules can bind to activated endothelium [6].

9.2.2 Integrins

Integrins are transmembrane glycoproteins composed of two chains named α and β, which are noncovalently linked to each other and form an extracellular binding pocket specific to a given ligand. Both chains are needed for ligand binding. The α chain family is composed of 18 different members, and the β family consists of 8 members, but only 24 different types of integrins have been identified. The intracellular domain of integrins binds to the cell cytoskeleton. Integrins are characterised by low affinity constants for their ligands. This supposes that they must cooperate with each other in order to produce strong adhesion forces. This cooperation lies on the formation of clusters at the surface of the cell membrane, where a high concentration of intracellular proteins involved in linking the integrins to the cytoskeleton is also found. These clusters, known as focal adhesion points, allow the cells to attach tightly to their substrate. A more detailed description of integrins is provided in Chapter 8.

Integrins expressed by leukocytes and tumours cells are involved in the interaction with endothelial cells. $\beta 2$ integrins are exclusively expressed on leukocytes. $\beta 2$ integrins include four different heterodimers CD11a/CD18 (LFA-1 for lymphocyte function-associated antigen-1), CD11b/CD18 (Mac-1), CD11c/CD18 (p150,95), and CD11d/CD18. A mutation in the gene encoding the $\beta 2$ (CD18) molecule results in

a genetic disorder: leukocyte adhesion deficiency (LAD). LAD patients show recurrent bacterial infections due to a defect in the effective recruitment of leukocytes in response to infections, demonstrating the importance of $\beta 2$ integrins in the inflammation process.

LFA-1 and Mac-1 are strongly involved in leukocyte adhesion to endothelium by binding to ICAM (see Section 9.2.3) expressed by endothelial cells. Functional analysis has demonstrated that CD11a/CD18 (LFA-1) is critical in neutrophil transmigration, and important in transmigration of other leukocyte subtypes. CD11b (Mac-1) antibodies alone are not as potent an inhibitor of neutrophil transmigration *in vitro* but they add significantly to the effect of CD11a antibodies *in vitro*. *In vivo* both CD11a and CD11b monoclonal antibodies can reduce inflammation, suggesting both redundancy and a dependence on the inflammatory stimulus and organ involved. This redundancy is also suggested by the fact that CD11b knock out mice show no defect in leukocyte transmigration [7].

The most important member of the $\beta 1$ integrin subfamily on leukocytes is VLA-4 (Very Late Antigen-4, CD49d/CD29). VLA-4 is expressed by most leukocytes and binds to fibronectin and the immunoglobulin superfamily member VCAM-1 (Vascular Cell Adhesion Molecule-1). VCAM-1 binding occurs with approximately four times greater affinity than binding to fibronectin.

On tumour cells, the expression panel of integrins is often modified when compared to normal cells, but their specific involvement in cell extravasation is not clear at the moment. However, over-expression of $\alpha \mathrm{v} \beta 3$ [8] which interacts with PECAM-1 (Platelet Endothelial Cell Adhesion Molecule-1, see Section 9.2.3), and $\alpha 4 \beta 1$ [9] which interacts with VCAM-1, on invasive tumour cell participate in adhesion to endothelium.

9.2.3 Immunoglobulin Superfamily

Many cell adhesion molecules contain one or more immunoglobulin-like domains and have been classified into the immunoglobulin superfamily. These receptors are involved in both homophilic and heterophilic interactions, and play a major role in the interactions of circulating cells with endothelial cells. Three immunoglobulins which are particularly important in the cascade are intercellular adhesion molecule-1 (ICAM-1) or CD54, vascular cell adhesion molecule-1 (VCAM-1) and platelet endothelial cell adhesion molecule-1 (PECAM-1).

ICAM-1 (CD54) is a single chain membrane glycoprotein of 80-115 kD, with five immunoglobulin-like repeats in its extracellular domain [10]. ICAM-1 is moderately expressed on resting endothelial cells, but release of cytokines at sites of inflammation and immune response such as TNF-α, IL-1 or IFN-γ results in augmented cellular expression of ICAM-1. ICAM-1 is a ligand for leukocyte integrins CD11a/CD18 (LFA-1) and CD11b/CD18 (Mac-1). The interaction between Mac-1/LFA-1 (CD11a b/CD18) and endothelial ICAM-1 is a well documented adhesion pathway, which plays an important role in the adhesion and extravasation of leuko-

cytes. ICAM-1 is also a receptor for the major group of rhinoviruses and the malaria trophozoite plasmodium falciparum. It has been recently shown that fibrinogen is a ligand for ICAM-1, and that fibrinogen binding to ICAM-1 results in an enhanced adhesion of leukocytes to HUVEC monolayers, and an increase in transendothelial migration [11].

VCAM-1 (CD106) is a transmembrane glycoprotein of 110 kD expressed only on cytokine-activated endothelium. VCAM-1 is a ligand for $\alpha 4\beta 1$ (VLA-4) and $\alpha 4\beta 7$ integrins. VLA-4 binds VCAM-1 through the first and the fourth immunoglobulin domain. Using monoclonal antibodies, several studies have shown that VCAM-1 is involved in the transmigration of monocytes and eosinophils, but its involvement in lymphocyte transendothelial migration remains to be clarified.

PECAM-1 (CD31) is a 130 kD glycoprotein expressed on endothelial cells, platelets and some leukocytes. CD31 is constitutively expressed on endothelial cells, and its expression is not modified by cytokines. PECAM-1 can interact both with itself in a homophilic interaction and with other molecules in a heterophilic interaction. Molecular cloning studies have shown that CD31 is composed of six extracellular immunoglobulin-like domains, a short transmembrane region, and a relatively long cytoplasmic tail of 118 amino-acid containing potential sites for post-translational modifications. In endothelial cells, CD31 is localised at intercellular junctions, and thus plays a role in the control of vascular permeability. The high level of constitutive expression of PECAM-1 in endothelial cells suggests that its function might be regulated, and phosphorylation of the cytoplasmic domain has been demonstrated. PECAM-1 is directly involved in the process of leukocyte diapedesis between endothelial cells, as demonstrated by inhibition studies using anti-PECAM-1 monoclonal antibodies and soluble recombinant PECAM-1. Leukocytes blocked in transmigration by anti-PECAM-1 antibodies remain attached to the endothelium, clearly implicating PECAM-1 in diapedesis rather than in adhesion. PECAM-1 may participate in tumour cell intravasation by controlling inter-endothelial junctions. In addition, PECAM can interact with the integrin $\alpha v\beta 3$ [12] which, as already mentioned, is over-expressed at the surface of invasive cancer cells. This interaction could contribute to their adhesion to endothelial cells.

9.2.4 Cadherins

The calcium dependent cell adhesion molecules (cadherins) are so called because they have both adhesion and calcium binding sites. This family is described in detail in Chapter 8. Evidence for a role of this family of adhesion receptors in tumour cell extravasation is scant. However, the endothelial specific VE-cadherin, which has been involved in the control of the intercellular endothelial junctions [13] and thus the control of leukocyte diapedesis, may also play a role in controlling tumour cell extravasation [14].

9.3 Leukocyte or Tumour Cell Adhesion under Flow Conditions

9.3.1 Multistep Process of Leukocyte Adhesion

One of the most important aspects of leukocyte extravasation is that it is a multistep process (Figure 9.2): initial contact, primary adhesion (rolling), activation, secondary adhesion, and transendothelial migration (diapedesis) [1].

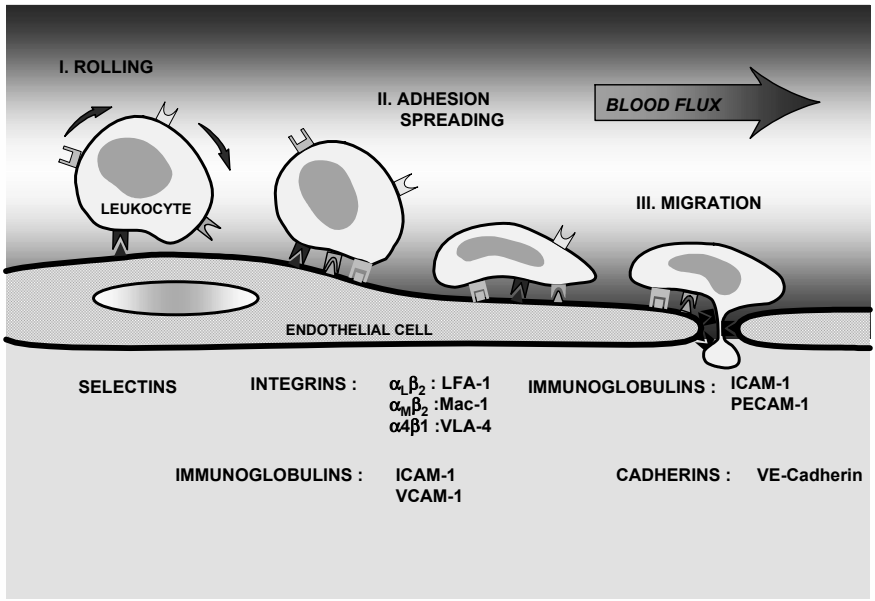

Figure 9.2
Leukocyte diapedesis: a multistep adhesion cascade.

Initial contact with endothelium is aided by the size of postcapillary venules, which are the main sites of selective leukocyte extravasation [15]. The diameter

of these venules (approximately 20 to 60 μm) is small enough to make frequent contacts between leukocytes and endothelium, but large enough to make brief contacts. The initial contact is also supported by increased vascular permeability in an inflammatory situation. This leads to plasma leakage and an increase in local hematocrit which changes the flow characteristics and thus allows more frequent contact between leukocytes and the vessel wall [16]. Following this initial contact, leukocytes roll slowly along the endothelium for some distance before establishing firm adhesion. This rolling keeps the cells in close contact with the endothelium, and is mediated by selectins and their ligands. They can then be activated by substances in the local environment, by factors bound to the endothelium, or by adhesion receptors themselves. Activation of leukocytes alters their adhesion characteristics and allows the establishment of firm adhesion (secondary adhesion). Flattening of leukocytes upon activation greatly increases the leukocyte-endothelial cell contact area which allows a large number of bonds to form and decreases fluid forces on the cell. This permits a highly shear-resistant adhesion. This strong adhesion of leukocytes on endothelium involves leukocyte integrins (Mac-1, LFA-1, $\alpha 4\beta 1$) and their ligands on endothelial cells (ICAM-1, VCAM-1). Then, leukocytes can migrate to interendothelial junctions and transmigrate (diapedesis) [3]. This last step is not completely understood, but it has been shown that ICAM-1, and adhesive proteins expressed at the interendothelial junctions (VE-cadherin, PECAM-1) are involved.

9.3.2 Adhesive Interactions between Cancer Cells and Endothelium

Despite the striking similarities between the process of leukocyte diapedesis and tumour cell extravasation, there are differences between leukocytes and circulating tumour cells. Leukocytes are very motile small cells whereas tumour cells are larger, with a far less ability to migrate. However, these bigger cells can be arrested easily by size constraints in the microcirculation. In addition, these cells can form multicellular aggregate, by interacting with themselves or with leukocytes and platelets, and it has been shown that multicellular emboli generate metastases more efficiently. Morphological evidence indicates that only single cancer cells can enter and be arrested in the capillaries, whereas multicellular emboli tend to arrest in larger vessels [17]. In the case of single cancer cells, adhesive macromolecules such as selectins, integrins, cadherins, and immunoglobulins govern the adhesive interactions between cancer cells and the endothelium. Initial contacts between cancer cells and the endothelium are weak and transient and likely to be mediated by carbohydrate-carbohydrate recognition. This initiates activation of both the endothelium and cancer cells through cytokines, free radicals, bioactive lipids, and growth factors. These mediators cause the expression of new adhesion molecules which will reinforce the initial adhesive bonds. Then humoral mediators or integrin-related signalling pathways lead to endothelial cell retraction, cancer cell locomotion, and transendothelial migration of cancer cells [18].

9.4 In Vitro Devices to Study Circulating Cell-Endothelial Cell Adhesion

9.4.1 Static Assays

Circulating cell-endothelium adhesion is generally studied using three types of assays: static assays, *in vitro* flow assays, and *in vivo* flow assays. Static assays are the most straightforward and inexpensive systems available for adhesion studies. In these systems, the substrate, which can be a cultured endothelial cell monolayer or a purified ligand, is covered with a cell (leukocyte or cancer cell) suspension for some period of time. Nonadherent cells are then rinced or centrifuged away, and adherent cells are quantified. These systems allow controlled stimulation of cells. They also allow quantification of cells which transmigrate through the monolayer onto the substrate (or through it, in case of a porous substrate), and can give a measure of the strength of adhesion (with centrifugation) [19]. Variants utilise a multilayered artificial blood vessel wall into which cells can migrate following diapedesis to examine transmigration and chemotactic stimuli [20]. The common disadvantage of all static assay systems is the lack of shear forces associated with blood flow. With static assays, it is impossible to distinguish primary and secondary adhesion events.

9.4.2 In Vitro Flow Assays

Since circulating cell-endothelium interactions take place in the fluid dynamic environment of blood circulation, one of the obvious questions about these adhesive interactions is whether they are capable of arresting circulating cells under the conditions of fluid flow. *In vitro* flow devices were designed to address this problem under controlled flow conditions. Flow assays provide more realistic information than static assays by allowing discrimination of primary adhesion events (such as rolling) from secondary adhesion events (like firm adhesion and transmigration). They are also useful to examine the activation of cells under flow induced mechanical forces. We will present three major *in vitro* devices for subjecting cultured cells to laminar flow, i.e., the cone-and-plate system, the radial flow chamber, and the parallel-plate flow chamber. Some specific configurations of the parallel-plate flow chamber will be described in details.

9.4.2.1 Cone-and-Plate System

The cone-and-plate system consists of a stationary plate and a rotating cone (Figure 9.3). The volume separating the two surfaces is filled with a liquid. The cells are either cultured adherent to the stationary plate or suspended in the medium.

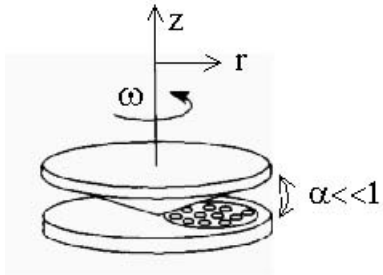

Figure 9.3
Cone-and-plate system.

The rotation of the upper cone, with an angular velocity ω, causes the fluid to move in a circumferential direction. The gap h between the cone and the plate increases with the radial position r ($h = r \tan \alpha$). As the angle α between the cone and the plate is small, typically less than one degree, the flow in any local region can be approximated as the flow between two parallel surfaces. The modified Reynolds number ($\tilde{R}e = \rho r^2 \omega \alpha^2 / 12\mu$) should be less than one to ensure a laminar flow with negligible secondary flows. The azimutal velocity varies as a function of z (the distance from the stationary disk):

$$v_\theta = \frac{\omega z}{\alpha} \tag{9.1}$$

Thus, for a given angular velocity and conic taper, the shear stress exerted by the moving fluid is constant regardless of the position and described as:

$$\tau = \frac{\mu \omega}{\alpha} \tag{9.2}$$

With such a device, Dewey et al. studied the effect of shear stress on endothelial cell shape and orientation. They showed that cultured endothelial cells aligned in the direction of flow and that this cell shape change and orientation is quite sensitive to the magnitude of the applied shear stress and to the time of application [21]. More recently, Blackman et al. [22] transformed a traditional cone-and-plate device in order to simulate physiological and pathological loading regimes (e.g., arterial wave forms, repetitive load cycling) experienced by cells *in vivo*.

9.4.2.2 Radial Flow Chamber

In a radial flow chamber (Figure 9.4), fluid is introduced in the centre, moves out radially and exits at the edge. So the radial flow apparatus provides an axisymmetric laminar flow field between two parallel disks. In this geometry, the cross-sectional area for flow between the two disks increases radially and the radial velocity decreases. Thus the wall shear stress decreases radially and this produces a continuous range of shear stress values within a given experiment. The wall shear stress can be

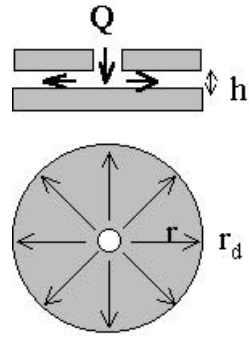

Figure 9.4
Radial flow chamber.

estimated by the following formula:

$$\tau_w = \frac{3\mu Q}{\pi h^2 r} \tag{9.3}$$

where Q is the flow rate, μ the fluid viscosity, h the height of the radial flow channel, and r the radial position. The typical geometric values are: 140 to 300 μm gap height and 2 to 3 cm disk radius. The local Reynolds number must be less than 2000 to ensure laminar flow field. Typical wall shear stresses range from 0 to 4 Pa.

The radial flow chamber has been used in general studies of receptor-mediated cell adhesion. For instance, Cozen-Roberts et al. [23] used this device to study the detachment of receptor-coated latex beads from ligand-coated glass surfaces. This device could be easily adapted to study cell-cell interactions under a range of shear stresses. To do so, endothelial cells should be cultured on the lower disk and leukocytes or cancer cells suspended in the circulating medium. However, a potential problem is that many adhesion events are dependent on both shear stress magnitude and suspended cell activation. Thus, increased cell adhesion near the periphery could be due either to the lower shear stress there or to longer exposure of suspended cells to activating substances derived from the endothelial monolayer.

9.4.2.3 Parallel-Plate Flow Chamber

The most commonly used flow device is the parallel-plate flow chamber [24–26]. It consists of a channel with a rectangular cross section of height h, width b, and length L. In this device a pressure gradient is created between either end of the rectangular chamber, causing the fluid to flow inside the channel. The pressure gradients can be established by either a hydrostatic pressure head or by active pumps. For the flow to be two-dimensional, the channel height must be much smaller than its width. For the velocity profile to be fully developed and parabolic over nearly the entire length of the channel, the entrance length must be small compared to the channel length. In this type of flow chamber, assuming Newtonian fluid behaviour,

the wall shear stress τ_w is independent of position and is predicted by the following formula:

$$\tau_w = \frac{6\mu Q}{bh^2} \tag{9.4}$$

where Q is the flow rate and μ the fluid viscosity. The typical geometric values are 100 to 200 μm gap height, 2 to 3 cm width, and 5 to 7 cm length. The Reynolds number ($Re = \rho Q / \mu b$) is generally less than 100 to ensure a laminar flow. The wall shear stress can be varied from 0.5 to 5 Pa by changing the flow rate or the gap height of the flow channel.

9.4.2.4 Linear Shear Stress Parallel-Plate Flow Chamber

In commonly used parallel-plate flow chambers, the shear stress in the whole field is constant and dependent upon the flow rate and the gap between the two plates. Whenever one wants to change the shear stress in the field, the flow rate has to be altered or the gap height has to be changed. These procedures, however, will affect cell-cell interactions after the cells and the surface are exposed to a different shear stress in the previous shear flow. The properties of the two-dimensional stagnation flow permit the design of a flow channel such that the wall shear stress is linearly distributed along the centre line of the channel.

Usami et al. [27] realised this set up by letting the sides of a flow channel be coincident with streamlines corresponding to a stagnation flow. The wall shear stress depends on the axial position x and is described by:

$$\tau_w = \frac{6\mu Q}{b_1 h^2}\left(1 - \frac{x}{L}\right) \tag{9.5}$$

where b_1 is the entrance width of the flow channel. Thus, the wall shear stress decreases from the maximum at the entrance ($x = 0$) to zero at the exit ($x = L$). With this design, cell-cell interactions can be studied efficiently over a wide range of shear stresses using a single flow rate.

9.4.2.5 Side-View Parallel-Plate Flow Chamber

One of the limitations of the parallel-plate flow chamber is that it can only provide top views of cells that are in contact with the substrate. Some important adhesion and deformation parameters that are related to cell-surface contact under flow are hard to obtain quantitatively from a top-view chamber. Cao et al. [28] developed an *in vitro* side-view flow chamber that permits observations from the side of the cells in contact with various adhesive surfaces under dynamic flow conditions. This flow chamber consists of two precision rectangular glass tubes called microslides. A smaller microslide is inserted into a larger one to create a flow channel with a flat surface on which either cultured vascular endothelium can be grown or purified adhesion molecules can be coated. Two optical prisms with a 45^o chromium-coated surface are used along the flow channel to generate light illumination and observation pathways. The side-view image of cell-substrate contact can be obtained using a light microscope. The characteristic data of this flow channel are: 550 μm height,

700 μm width, and 5 cm long. The wall shear stress can be estimated by the following formula:

$$\tau_w = \frac{6\mu Q}{bh^2} F \tag{9.6}$$

where F is the correction factor for a rectangular channel with a finite aspect ratio. Here for a $b/h = 1.27$, F varies from 1.4 to 1.5 in the central regions ($F_{mean} = 1.45$). For shear stresses ranging from 0 to 3 Pa, the corresponding Reynolds number is less than 80, and the entrance length less than 2 mm. This design allows to measure the effects of flow on cell-surface adhesion strength. Moreover, it permits a close observation of cell deformation and adhesive contact to various surfaces under flow conditions.

9.4.2.6 Parallel-Plate Flow Chamber with a Porous Bottom Wall

Another configuration of a parallel-plate flow chamber is the one with a porous bottom wall designed by Chotard-Ghodsnia et al. [29]. It consists of two stainless steel parts which enclose a pair of parallel glass plates to allow for microscope visualisation. A porous material is held on a nylon screen positioned on the bottom plate, as shown in the assembled view of this chamber (Figure 9.5). Thus, the circulating medium can flow both along and across the porous bottom wall. The inlet fluid (P_{in}, Q_{in}) is evacuated through a tangential outlet (P_{out}, Q_{out}) and a filtrate outlet (P_f, Q_f). With this flow chamber, cells adhering to the porous material can be exposed to both a transmural pressure (TMP) and a shear stress (τ_w). This *in vitro* system thus allows a more realistic reproduction of flow conditions near the vessels' wall *in vivo*. Indeed, the transmural pressure might tend to favour cell attachment to the endothelium whereas the fluid shear stress tends to detach cells from the vessel wall. This might also affect the signal mechanotransduction.

The hydraulic permeability, L_p, of the porous bottom wall (1.0×10^{-10}m/(Pa s)) is similar to that of a blood vessel wall (1.5×10^{-10}m/(Pa s) [30]). Thus, the filtrate flow rate Q_f is very small as compared to input flow rate Q_{in}, and the tangential

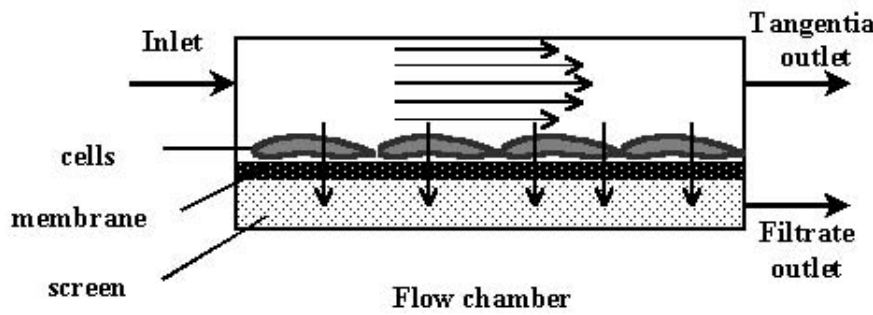

Figure 9.5
Flow chamber with a porous bottom wall.

flow can still be approximated by the plane Poiseuille law. This is confirmed by our experimental and theoretical analysis and, consequently, the wall shear stress can be considered as a constant along the flow channel, given by:

$$\tau_w = \frac{6\mu Q_{in}}{bh^2} \tag{9.7}$$

Besides, the transmural flow is governed by Darcy's law:

$$Q_f = L_p\,(bL)\,TMP_m \tag{9.8}$$

where TMP_m, the mean transmural pressure, writes: $TMP_m = (P_{in} + P_{out})/2 - P_f$, since the pressure profile is linear. We first used this flow chamber to study morphological and biochemical responses of fibroblasts when submitted to tangential and normal stresses [31]. Our results constitute evidence that transmural pressure is at least as important as shear stress in regulating cell morphology mediated by the cAMP pathway (cyclic adenosine monophosphate: an intracellular signal transducer). Further studies should be carried out to study the influence of the transmural pressure on circulating cell/endothelium interactions.

9.5 In Vitro Flow Studies of Circulating Cell-Endothelium Adhesion

The rolling of leukocytes on activated endothelium is a critical step in the inflammatory cascade and has received considerable attention in the literature [32]. Leukocytes rolling occurs via the following steps:

1. a receptor-ligand bond forms, exerting an adhesive stress which slows cell velocity;
2. the slower motion of the cell promotes additional bonding;
3. bonds dissociate at the back edge of contact, causing the cell to tumble forward in the direction of flow.

These receptor-ligand bonds between the leukocyte and the endothelium exert a friction on the leukocyte, such that its velocity drops well below the hydrodynamic velocity for an unencumbered leukocyte at the same separation distance and wall shear rate. In the cell biology literature, rolling is often defined as a significant decrease in velocity to perhaps 50% or less of the hydrodynamic velocity for an unencumbered cell [33].

Although static assays may detect possible receptor-ligand pairs, they do not provide information on how ligands interact with receptors under more physiological, dynamic conditions. For cells to adhere under flow, the potential receptor-ligand

pair must quickly react. Once a bond is formed, it must be able to overcome the drag force exerted by the fluid. Thus, dynamic adhesion studies are better to detect receptor-ligand pairs that can mediate rolling as compared to static experiments [34].

The most commonly used device for dynamic adhesion experiments is the parallel-plate flow chamber. The endothelial monolayer is cultured on the bottom plate of the flow channel and leukocytes or tumour cells are perfused to the flow channel at a rate that produces the desired wall shear stress. A typical observation of leukocytes rolling over an endothelial monolayer, obtained in our experimental set up, is shown in Figure 9.6. Some leukocytes are rolling whereas some others are firmly adherent in a TNF-α-stimulated endothelial monolayer.

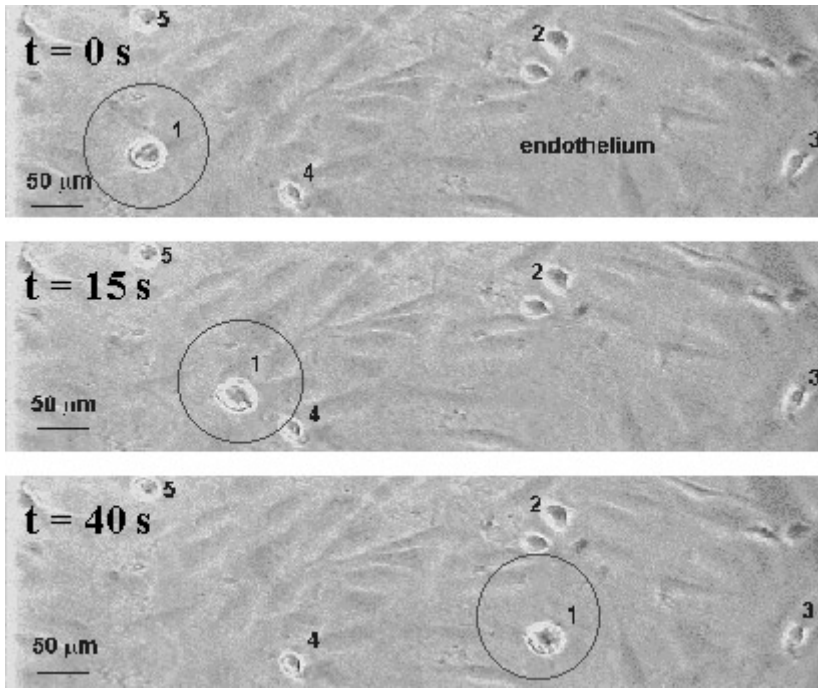

Figure 9.6

Leukocyte rolling on endothelial monolayer: one cell (1) is rolling while others (2 to 5) are adhering.

Such *in vitro* flow studies showed that distinct sets of adhesion molecules mediate leukocyte rolling and firm adhesion, as widely discussed in a recent review article [35]: (1) L-, E-, or P-selectins are capable of tethering free flowing leukocytes. Shear stress levels in excess of $0.05Pa$ are required for optimal selectin-dependent tethering and rolling of leukocytes; (2) α_4-integrins are capable of supporting leukocyte adhesion to activated endothelium under flow; (3) β_2-integrins cannot initiate

leukocyte adhesion under flow conditions, except possibly at wall shear stresses less that $0.05Pa$, but can support activation-dependent firm adhesion and subsequent migration. Moreover, it has been observed that leukocyte rolling velocity varies with wall shear stress [24,26,36–38] and that the velocity of rolling cells varies considerably with time [37,39]. Kaplanski et al. [39] observed multiple short term arrests (of 2 s duration) of neutrophils on endothelial monolayer under $5s^{-1}$ shear rate. Dong et al. [40] used a side-view parallel-plate flow chamber to study the influence of cell deformation on leukocyte rolling adhesion in shear flow. They showed that changes in shear flow and cell deformability resulted in significant changes in characteristic adhesion binding time, cell-surface contact, and cell rolling velocity. Recently, the influence of shear stress on leukocyte migration behaviour was also studied in a parallel-plate flow chamber. Shear flow significantly increases the kinetics of leukocyte transmigration as compared to static conditions [41].

In contrast to leukocytes, the effect of shear stress on cancer cell adhesion to endothelium has received much less attention in the literature, although cancer cells and leukocytes have been shown to share some adhesion mechanisms [42]. Several authors have reported E-selectin-dependent rolling of varied cancer cell types on the endothelial monolayer under flow conditions [43,44]. A recent work of Moss et al. [45] showed the importance of studying cancer cell adhesion under flow conditions. Using a parallel-plate flow chamber, they compared the adhesion of cancer cells with different metastatic potential and showed that highly metastatic cells were more adhesive to shear stimulated endothelial cells while nonmetastatic cells were more adhesive to endothelial monolayer not stimulated. More recent experiments carried out by Dong et al. [46] with a modified parallel-plate flow chamber, suggested that shear flow plays a significant role in tumour cell extravasation.

9.6 Modelling of Circulating Cell-Endothelium Interactions

Although *in vitro* flow experiments can be more easily controlled than *in vivo* studies, there remains a large number of confounding cellular features such as: endothelial cell surface heterogeneity, adhesion molecule expression, cell activation, and cell deformability. Experimental models were developed to make it easier to understand the biophysical basis of circulating cell/endothelium interactions. Then mathematical models could be developed to interpret these experimental results.

9.6.1 Experimental Modelling

Springer and coworkers simplified leukocyte endothelium systems by replacing the cultured endothelial cells with purified P-selectin reconstituted in lipid bilayers [47,48] and purified E-selectin absorbed to polystyrene slides [49]. Neutrophils rolled over both substrata with a velocity proportional to the selectin surface density. Kitayama and coworkers [50] compared the adhesion pattern of colon cancer cells to that of leukocytes over an E-selectin coated substratum. Adhesive interactions to E-selectin in laminar flow were weaker for colon cancer cells than for leukocytes. Cancer cells showed a "stop and roll" movement with variable rolling velocities whereas leukocytes rolled with a relatively stable speed.

Although these experiments removed the variability of the endothelial monolayer, circulating cell activation and deformability was still present and caused complications.

Cell-free systems were then developed to study specific molecular (receptor-ligand) interactions without the confounding influence of rheology, roughness, signalling, and complex molecular display involved when using cells. In these systems, coated microspheres are used to model leukocytes and coated substratum to model endothelial surface.

Brunk and coworkers [51,52] used sLe^x-coated polystyrene microspheres over E-selectin-coated glass substratum in a parallel-plate flow chamber to model leukocyte rolling over endothelium. They showed that these microspheres rolled on the coated substratum with dynamics similar to those of leukocytes rolling over stimulated endothelial cells. The particle rolling velocity was found to be a function of wall shear stress and selectin or sLe^x surface densities. Moreover, the rolling velocity varied with time, as also seen in leukocyte/endothelium systems [37,39]. These cell-free studies allowed to understand how the rolling velocity depends quantitatively on receptor number, ligand density, and shear rate.

Bongrand and coworkers used cell-free systems to measure the lifetime of individual ligand-receptor bonds with a flow chamber [53,54]. To observe the formation and dissociation of single bonds, they operated with microspheres (2.8 μm diameter) much smaller than cells under low shear rates (of the order of a few seconds^{-1}). They determined the velocity, attachment frequency, and duration of binding arrests of each microsphere and found that microspheres exhibited frequent arrests of fairly constant duration (approximately 1 s). Their results suggest that the arrests observed with low receptor densities involved single molecular bonds and the duration of these bonds was not affected by shear forces [53]. They also showed that the rate of bond formation is a function of microsphere-substratum distance [54,55].

9.6.2 Mathematical Modelling

Analysis of the forces involved in leukocyte-endothelium adhesion at the equilibrium state was pioneered by Bell [56]. Evans [57] established a theoretical framework of a one-dimensional tape peeling model to compute the adhesion force between a biomembrane and a substrate with constant adhesive strength. To study the receptor-mediated cell adhesion to a ligand-coated surface, Hammer and collaborators [58] took steps from Bell's theory and developed a cell adhesion model taking receptor-ligand bond kinetics into consideration. This model, called "adhesive dynamics," allows to interpret experimental results on rolling cells and to understand the molecular basis of cell-free rolling systems. We now describe this mathematical model in more details.

"Adhesive dynamics" is a computational technique that combines the fluid mechanics analysis of particle motion and the Monte Carlo simulation of bond formation and breakage between receptors and ligands [58]. The adhesive dynamic method has been extensively described [58–60]. Briefly, sLe^x-coated microspheres are modelled as hard spheres with receptors distributed randomly over the surface. The planar surface coated with E-selectin is assumed to be uniformly reactive (E-selectin density is always larger than sLe^x density on the microspheres). Receptors and ligands are modelled as adhesive springs with spring constant σ and equilibrium length λ. Each adhesive molecule reacts with the substrate with an overall association rate k_f (forward reaction) and dissociation rate k_r (reverse reaction). k_f is a function of ligand density, relative velocity between the particle and the surface (slip velocity V_s) and the intrinsic forward rate constant k_{in}. The model proposed by Bell [56] was used to describe k_r of a bond under applied force F:

$$k_r = k_r^0 \exp\left(\gamma F / k_b T\right) \tag{9.9}$$

where k_r^0 is the unstressed dissociation constant rate, k_b is the Boltzmann's constant, T is the temperature, and γ is the bond interaction length (also called reactive compliance, it represents the sensitivity of the dissociation to the applied force). Flow-induced forces tend to alter the rate of dissociation compared to cases where no force acts on receptor-ligand bonds. The Bell model takes into account the influence of these dislodging forces on the dissociation rate.

Each free receptor can become tethered in the time interval dt with a probability:

$$P_f = 1 - \exp(-k_f dt) \tag{9.10}$$

and each tethered receptor can become free in a time interval dt with a probability:

$$P_r = 1 - \exp(-k_r dt) \tag{9.11}$$

During each time step, bond formation and breakage are simulated by a Monte Carlo sampling of these probability distributions. The Monte Carlo approach simulates the fate of each individual bond to generate an ensemble of realisations. Each simulation represents an experimental measurement and can be directly compared to it.

At any instant, the forces, f, exerted by the tethers on the particle can be calculated from the distance between the end points of the attachment, l, and using the Hooke's law: $f = \sigma (l - \lambda)$. To obtain the net force and torque acting on the particle, the total force and torque exerted by the bonds on the cell are added to interfacial forces and to the force and torque exerted by the fluid shear on the cell. The motion of the particle can be fully described by the following relation:

$$\mathbf{U} = \mathbf{MF} \tag{9.12}$$

where **M** is the mobility matrix (known for a sphere near a plane wall in a viscous fluid [59]), **U** is a vector with three components of linear velocity and three components of angular velocity, and **F** is a vector with three components of total force and three components of the net torque acting on the particle. Thus, once the net force and torque are known, the velocity of the particle can be calculated.

The simulation begins with a freely moving particle at a constant velocity and a separation distance (40 nm) greater than the receptor-ligand bond. The position of the free receptors and tethers, the velocity of the particle, and the net force and torque exerted on it are known. According to the position of free receptors at time t, tethers are formed at $t + dt$ following the probability of Equation (9.10). Tethers are broken at $t + dt$ following Equation (9.11). Then, new positions of free receptors and tethers are calculated (from velocity and position at t), as well as new net force at $t + dt$. Finally, the velocity of the particle at $t + dt$ is obtained using Equation (9.12). The process is repeated until the particle travels across the field of view or a predefined time is reached. After each simulation, the trajectory of the particle is recorded and the instantaneous velocity and the average velocity (total displacement divided by time of interactions) are calculated.

This model can recreate different adhesive behaviours ranging from unencumbered motion of particles to rolling and to firm adhesion [58]. It can simulate the effect of many parameters on cell rolling and adhesion, such as the density of receptors and ligands, the rates of reaction between receptor and ligand (association and dissociation rates), the receptor-ligand bond elasticity and the shear rate [61]. To elucidate the relationship between receptor-ligand functional properties and the dynamics of adhesion, Chang et al. [32] expressed the state diagram for cell adhesion under flow. This state diagram describes how biophysical properties of adhesion molecules induce different states of adhesion in flow. These authors showed that the unstressed dissociation rate, k_r^0, and the bond interaction length, γ, are the most important molecular properties that control the dynamics of adhesion. Their results suggest that adhesive behaviour is primarily determined by the biophysical properties of adhesion molecules [32] however, it can be modulated by cell deformability, morphology, and signalling.

More recently, Dong and collaborators [40] developed a 2D model that demonstrates the influence of leukocytes rheological properties in regulating rolling on vascular endothelium. This model incorporates both mechanical aspects of cell deformation and biophysical aspects of adhesion bond kinetics. It was based on the assumption that the fluid energy input to a rolling cell would essentially be distributed

into two parts: cytoplasmic viscous dissipation and energy needed to break adhesion bonds between the rolling cell and its substratum. Both extracellular and intracellular flow fields were solved using finite element methods with a deformable cell membrane represented by an elastic ring. The adhesion energy loss was calculated based on the receptor-ligand kinetics equations. They found that the cell-substrate contact area under high wall shear stress ($2Pa$) could be nearly twice that under low stress ($0.05Pa$) as a result of shear flow-induced cell deformation. An increase in contact area resulted in more energy dissipation to both adhesion bonds and viscous cytoplasm, whereas the fluid energy that is transmitted to a cell decreased due to flattened cell shape. Their results suggest that leukocyte deformability is an essential component that aids in the adhesion process to balance the hemodynamic and leukocyte-endothelium adhesive forces.

9.7 Conclusion

Metastasis is the growth of secondary tumours at sites distant from a primary tumour, and is responsible for the majority of failures in cancer treatment. Cells from a metastatic tumour are able to escape in the surrounding tissues and intravasate into blood, where they can disseminate through the body. Endothelial cells line every blood vessel in the organism and regulate the extravasation of blood cells. This extravasation involves specific junctional proteins and membrane-bound receptors that control cell-cell interactions. Leukocyte interactions with endothelial cells have been extensively studied and serve as a model for interactions of circulating cancer cells with the vasculature. The molecular mechanisms involved in the extravasation of cancer cells through the endothelial monolayer is not fully understood, and better experimental approaches are needed to understand this phenomenon. The use of *in vitro* flow assays, associated with modern microscopic techniques and mathematical modelling, will help identifying the different molecules mediating the process of metastasis. A better understanding of the metastasis mechanisms is crucial for the development of new therapies. The implication of adhesion molecules in the arrest of cancer cells in the vasculature strongly suggests that inhibition of these adhesive interactions could be helpful to inhibit metastasis at the step of extravasation.

9.8 References

[1] Springer, T.A., Traffic signals for lymphocyte recirculation and leukocyte emigration: the multistep paradigm, *Cell* 76, 301, 1994.

[2] Voura, E.B., Sandig, M., and Siu, C.-H., Cell-cell interactions during transendothelial migration of tumor cells, *Microsc. Res. Tech.* 43, 265, 1998.

[3] Johnson-Leger, C., Aurrand-Lions, M., and Imhof, B.A., The parting of endothelium: miracle, or simply a junctional affair?, *J. Cell Science* 113, 921, 2000.

[4] Ebnet, K. and Vestweber, D., Molecular mechanisms that control leukocyte extravasation: the selectins and the chemokines, *Histochem. Cell Biol.* 112, 1, 1999.

[5] Kansas, G.S., Selectins and their ligands: current concepts and controversies, *Blood* 88, 3259, 1996.

[6] Takada, A. et al., Adhesion of human cancer cells to vascular endothelium mediated by a carbohydrate antigen, sialyl Lewis A, *Biochem. Biophys. Res. Commun.* 179, 713, 1991.

[7] Lu, H.F. et al., LFA-1 is sufficient in mediating neutrophil emigration in Mac-1-deficient mice, *J. Clin. Invest.* 99, 1340, 1997.

[8] Albelda, S.M. et al., Integrin distribution in malignant melanoma: association of the β 3 subunit with tumor progression, *Cancer Res.* 50, 6757, 1990.

[9] Tomita, Y. et al., Possible significance of VLA-4 ($\alpha 4\beta 1$) for hematogenous metastasis of renal-cell cancer, *Int. J. Cancer* 60, 753, 1995.

[10] Hubbard, A.K. and Rothlein, R., Intercellular adhesion molecule-1 (ICAM-1) expression and cell signaling cascades, *Free Radic. Biol. Med.* 28, 1379, 2000.

[11] Sans, E. et al., Analysis of the roles of ICAM-1 in neutrophil transmigration using a reconstituted mammalian cell expression model: implication of ICAM-1 cytoplasmic domain and Rho-dependent signaling pathway, *J. Immunol.* 166, 544, 2001.

[12] Buckley, C.D. et al., Identification of $\alpha \mathrm{v} \beta 3$ as a heterotypic ligand for CD31/PECAM-1, *J. Cell Sci.* 109, 437, 1996.

[13] Dejana, E. et al., Vascular endothelial (VE)-cadherin: only an intercellular glue?, *Exp. Cell Res.* 252, 13, 1999.

[14] Liao, F. et al., Monoclonal antibody to vascular endothelial-cadherin is a potent inhibitor of angiogenesis, tumor growth, and metastasis, *Cancer Res.* 60, 6805, 2000.

[15] Fiebig, E., Ley, K., and Arfors, K.E., Rapid leukocyte accumulation by spontaneous rolling and adhesion in the exteriorized rabbit mesentery, *Int. J. Microcirc. Clin. Exp.* 10, 127, 1991.

[16] Tangelder, G.J. et al., Velocity profiles of blood platelets and red blood cells flowing in arterioles of the rabbit mesentery, *Circ. Res.* 59, 505, 1986.

[17] Starkey, R. et al., Influence of migratory blood cells on the attachment of tumour cells to vascular endothelium, *Int. J. Cancer* 34, 535, 1984.

[18] Orr, F.W. et al., Interactions between cancer cells and the endothelium in metastasis, *J. Pathol.* 190, 310, 2000.

[19] Charo, I.F., Yuen, C., and Goldstein, I.M., Adherence of human polymorphonuclear leukocytes to endothelial monolayers: effects of temperature, divalent cations, and chemotactic factors on the strength of adherence measured with a new centrifugation assay, *Blood* 65, 473, 1985.

[20] Hakkert, B.C. et al., A three-dimensional model system to study the interactions between human leukocytes and endothelial cells, *Eur. J. Immunol.* 20, 2775, 1990.

[21] Dewey, C.F. et al., The dynamic response of vascular endothelial cells to fluid shear stress, *ASME J. Biomech. Eng.* 103, 177, 1981.

[22] Blackman, B.R. et al., *In vitro* cell shearing device to investigate the dynamic response of cells in a controlled hydrodynamic environment, *Annals Biomed. Eng.* 28, 363, 2000.

[23] Cozen-Roberts, C., Quinn, J.A., and Lauffenburger, D.A., Receptor-mediated adhesion phenomena: model studies with the radial-flow detachment assay, *Biophys. J.* 58, 107, 1990.

[24] Lawrence, M.B., McIntire, L.V., and Eskin, L.V., Effect of flow on polymorphonuclear leukocyte/endothelial cell adhesion, *Blood* 70, 1284, 1987.

[25] Gallik, S. et al., Shear stress-induced detachment of human polymorphonuclear leukocytes from endothelial cell monolayers, *Biorheology* 26, 823, 1989.

[26] Jones, D.A. et al., P-selectin supports neutrophil rolling on histamine-stimulated endothelial cells, *Biophys. J.* 65, 1560, 1993.

[27] Usami, S. et al., Design and construction of linear shear stress flow chamber, *Annals Biomed. Eng.* 21, 77, 1993.

[28] Cao, J., Usami, S., and Dong, C., Development of a side-view chamber for studying cell-surface adhesion under flow conditions, *Annals Biomed. Eng.* 25, 573, 1997.

[29] Chotard-Ghodsnia, R., Drochon, A., and Grebe, R., A new flow chamber for the study of shear stress and transmural pressure upon cells adhering to a porous biomaterial, *ASME J. Biomech. Eng.* 124, 258, 2002.

[30] Smaje, L.H. and Swayne, G.T.G., The effects of compliance on measurement of hydraulic conductivity in microvessels, *Biorheology* 21, 171, 1984.

[31] Chotard-Ghodsnia, R. et al., Effect of shear stress and of transmural pressure on cAMP-dependent responses of cells adhering to a biomaterial, *Eur. Phys. J.-Applied Phys.* 17, 155, 2002.

[32] Chang, K.C., Tees, D.F.J., and Hammer, D.A., The state diagram for cell adhesion under flow: leukocyte rolling and firm adhesion, *Proc. Natl. Acad. Sci. USA* 87, 11262, 2000.

[33] Chen, S. and Springer, T.A., An automatic braking system that stabilizes leukocyte rolling by an increase in selectin bond number with shear, *J. Cell Biol.* 144, 185, 1999.

[34] Varki, A.J., Selectin ligands, *Proc. Natl. Acad. Sci. USA* 91, 7390, 1994.

[35] Konstantopoulos, K., Kukreti, S., and McIntire, L.V., Biomechanics of cell interactions in shear fields, *Advanced Drug Delivery Reviews* 33, 141, 1998.

[36] Lawrence, M.B. et al., Effect of venous shear stress on CD18-mediated neutrophil adhesion, *Blood* 75, 227, 1990.

[37] Goetz, D.J. et al., Dynamics of neutrophil rolling over stimulated endothelium *in vitro*, *Biophys. J.* 66, 2202, 1994.

[38] Rinker, K.D., Prabhakar, V., and Truskey, G.A., Effect of contact time and force on monocyte adhesion to vascular endothelium, *Biophys. J.* 80, 1722, 2001.

[39] Kaplanski, G. et al., Granulocyte endothelium initial adhesion, *Biophys. J.* 64, 1922, 1993.

[40] Dong, C. and Lei, X.X., Biomechanics of cell rolling: shear flow, cell-surface adhesion, and cell deformability, *J. Biomech.* 33, 35, 2000.

[41] Kitayama, J. et al., Shear stress affects migration behaviour of polymorphonuclear cells arrested on endothelium, *Cellular Immunology* 203, 39, 2000.

[42] Takada, A. et al., Contribution of carbohydrate antigens sialyl Lewis A and sialyl Lewis X to adhesion of cancer cells to endothelium, *Cancer Res.* 53, 354, 1993.

[43] Giavazzi, R. et al., Rolling and adhesion of human tumor cells on vascular endothelium under physiological flow conditions, *J. Clin. Invest.* 92, 3038, 1993.

[44] Tozeren, A. et al., E-selectin-mediated dynamic interactions of breast- and colon-cancer cells with endothelial-cell monolayers, *Int. J. Cancer* 60, 426, 1995.

[45] Moss, M.A., Zimmer, S., and Anderson, K.W., Role of metastatic potential in the adhesion of human breast cancer cells to endothelial monolayers, *Anticancer Research* 20, 1425, 2000.

[46] Dong, C. et al., *In vitro* characterization and micromechanics of tumor cell chemotactic protrusion, locomotion, and extravasation, *Annals Biomed. Eng.* 30, 344, 2002.

[47] Lawrence, M.B. and Springer, T.A., Leukocytes roll on a selectin at physiologic flow rates: distinction from and prerequisite for adhesion through integrins, *Cell* 65, 859, 1991.

[48] Alon, R., Hammer, D.A., and Springer, T.A., Lifetime of the P-selectin-carbohydrate bond and its response to tensile force in hydrodynamic flow, *Nature* 374, 539, 1995.

[49] Lawrence, M.B. and Springer, T.A., Neutrophils roll over E-selectin, *J. Immunol.* 151, 6338, 1993.

[50] Kitayama, J. et al., E-selectin can mediate the arrest type of adhesion of colon cancer cells under physiological shear flow, *Eur. J. Cancer* 36, 121, 2000.

[51] Brunk, D.K., Goetz, D.J., and Hammer, D.A., Sialyl Lewis^x/ E-selectin mediated rolling in a cell free system, *Biophys. J.* 71, 2902, 1996.

[52] Brunk, D.K. and Hammer, D.A., Quantifying rolling adhesion with a cell-free assay: E-selectin and its carbohydrate ligands, *Biophys. J.* 72, 2820, 1997.

[53] Pierres, A., Benoliel, A.-M., and Bongrand, P., Measuring the lifetime of bonds made between surface-linked molecules, *J. Biol. Chem.* 270, 26586, 1995.

[54] Pierres, A., Benoliel, A.-M., and Bongrand, P., Measuring bonds between surface-associated molecules, *J. Immunol. Methods* 196, 105, 1996.

[55] Pierres, A. et al., The dependence of the association rate of surface-attached adhesion molecules CD2 and CD48 on separation distance, *FEBS Letters* 403, 239, 1997.

[56] Bell, G.I., Models for the specific adhesion of cells to cells, *Science* 200, 618, 1978.

[57] Evans, E., Detailed mechanics of membrane-membrane adhesion and separation, I. continuum of molecular cross-bridges, *Biophys. J.* 48, 175, 1985.

[58] Hammer, D.A. and Apte, S.M., Simulation of cell rolling and adhesion on surfaces in shear flow: general results and analysis of selectin-mediated neutrophil adhesion, *Biophys. J.* 63, 35, 1992.

[59] Chang, K.-C. and Hammer, D.A., Influence of direction and type of applied force on the detachment of macromolecularly-bound particles from surfaces, *Langmuir* 12, 2271, 1996.

[60] Kuo, S.C., Hammer, D.A., and Lauffenburger, D.A., Simulation of detachment of specifically bound particles from surfaces under shear flow, *Biophys. J.* 73, 517, 1997.

[61] Chang, K.C. and Hammer, D.A., Adhesive dynamics simulations of sialyl-Lewis^x / E-selectin-mediated rolling in a cell-free system, *Biophys. J.* 79, 1891, 2000.

Chapter 10

Mathematical Modelling of Tissue Invasion

Mark A.J. Chaplain and Alexander R.A. Anderson
The SIMBIOS Centre, Department of Mathematics, University of Dundee, Dundee (Scotland)

10.1 Introduction

The development of a primary solid tumour (e.g., a carcinoma) begins with a single normal cell becoming transformed as a result of mutations in certain key genes. This transformed cell differs from a normal one in several ways, one of the most notable being its escape from the body's homeostatic mechanisms, leading to

inappropriate proliferation. An individual tumour cell has the potential, over successive divisions, to develop into a cluster (or nodule) of tumour cells. Further growth and proliferation leads to the development of an avascular tumour consisting of approximately 10^6 cells. The avascular tumour cannot grow any further, owing to its dependence on diffusion as the only means of receiving nutrients and removing waste products. If the development of the solid tumour were to remain in this avascular state, little or no damage would be done to the host since avascular tumours are relatively small and remain localised in the host tissue and do not spread. However two crucial and inter-linked processes permit the avascular tumour to grow further: tumour-induced angiogenesis (the recruitment of blood vessels) and tissue invasion by the tumour cells.

The tumour cells first secrete angiogenic factors which in turn induce endothelial cells in a neighbouring blood vessel to degrade their basal lamina and begin to migrate towards the tumour. Endothelial cell migration through the extracellular matrix is driven by a chemotactic response to the angiogenic factors and a haptotactic response to components in the matrix such as fibronectin and collagen. The migration is facilitated by the local degradation of the tissue by the endothelial cells. As it migrates, the endothelium begins to form sprouts which can then form loops and branches through which blood circulates. From these branches more sprouts form and the whole process repeats forming a capillary network which eventually connects with the tumour, completing angiogenesis and supplying the tumour with the nutrients it needs to grow further. There is now also the possibility of tumour cells finding their way into the circulation and being deposited in distant sites in the body, resulting in metastasis. The complete process of metastasis involves several sequential steps, each of which must be successfully completed by cells of the primary tumour before a secondary tumour (a metastasis) is formed. Referring also to Chapters 8 and 9, a summary of the key stages of the metastatic cascade is as follows:

- growth of the initial avascular primary tumour;
- recruitment of new blood vessels (angiogenesis) and vascularisation of the primary tumour;
- escape of cancer cells from the primary tumour;
- local degradation of the surrounding tissue by cancer cells and continued migration;
- cancer cells enter the lymphatic or blood circulation system (*intravasation*);
- cancer cells must then survive their journey in the circulation system;
- cancer cells must escape from the blood circulation (*extravasation*);
- cancer cells (from the primary tumour) must then establish a new colony in distant organs;

- the new colony of cells must then begin to grow to form a new, secondary tumour in the new organ.

A crucial part of the angiogenic response of the endothelial cells and the invasive/metastatic process is the ability of the cancer cells to degrade the surrounding tissue or *extracellular matrix* (ECM) [31,32,41,52]. The focus of this chapter will be on one key aspect of tissue invasion: the ability of cells to produce and secrete certain factors known as *matrix degrading or degradative enzymes* (MDEs) and then their migratory response to their modified local tissue environment. The modelling will therefore concentrate upon the so-called *"tissue response unit"* (cf. [46] and [15]) which examines how a cell's migratory response and interaction with the extracellular matrix is controlled by soluble cytokines and insoluble matrix macromolecules (see Figure 10.1).

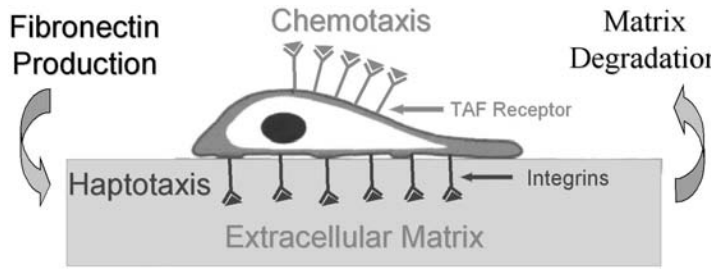

Figure 10.1
Schematic diagram of the tissue response unit.

The extracellular matrix (tissue) itself is a complex mixture of proteins and proteoglycans within and on which the normal cells of solid organs are situated. The matrix is highly dynamic, at any one time being actively secreted and degraded. It has become increasingly clear that the matrix has more than a passive structural role; it can sequester growth factors and indeed be degraded to release fragments which themselves have growth-promoting activity. Thus, while ECM may have to be physically removed in order to allow a tumour to spread or intra- or extra-vasate, its degradation may in addition have biological effects on the tumour cells themselves.

A number of *matrix degradative enzymes* (MDEs) such as the *plasminogen activator* (PA) system and the large family of *matrix metalloproteases* (MMPs) have been described [34,36,55]. Both PAs and the MMPs have been repeatedly implicated in all of the above steps of tumour invasion and metastasis [1,7,9,12,25,26,29,40,47, 53,58]. Regulation of matrix-degradative activity is highly complex. In both these enzyme systems (PAs/MMPs) there exist several endogenous inhibitors [8,28,54], and the enzymes are often secreted as inactive precursors which must themselves be partially degraded to reach full activity. More than one cell type may be involved in

the activation of any one enzyme [28].

Deterministic reaction-diffusion equations have been used to model the spatial spread of tumours both at an early stage in its growth [48] and at the later invasive stage [23,38,42]. Modelling of a related phenomenon, embryonic implantation involving invading trophoblast cells, using a reaction-diffusion approach has also been carried out [10]. Typical solutions observed in all these models [10,23,38,42] appear as invading travelling waves of cancer cells. While these models are able to capture the tumour structure at the tissue level, they fail to describe the tumour at the cellular level and subsequently the subcellular level. On the other hand, cellular automata models provide such a description and allow a more realistic stochastic approach at both the cellular [27,43,51] and subcellular levels [19–22].

The models presented in this chapter are an extension of earlier work by Anderson et al. [5] and consist of two types: a continuum, deterministic model (based on a system of reaction-diffusion-chemotaxis equations) and a discrete, stochastic model (based on a biased random-walk model). Initially, we derive a system of coupled nonlinear partial differential equations, using conservation laws, to model tumour invasion of surrounding tissue. Numerical solutions for this system in both one and two dimensions will be presented, thus allowing the macroscopic dynamics of invasion to be discussed. From a discretised form of these partial differential equations, we derive a discrete biased random-walk model which enables the migration and proliferation of individual cells to be considered.

The models presented here aim to:

(i) investigate the importance of ECM-tumour interactions in governing the migration of tumour cells, and

(ii) make predictions about the metastatic ability of tumour cells.

For example, by considering the cells as discrete individuals we can estimate, for a given initial tumour, how far it will invade and the numbers of cells that migrate outwith the main bulk of the tumour and thus allow for both qualitative and quantitative comparisons with experimental and clinical data. From the clinical perspective, it is the escape of tumour cells beyond the boundary of detectable tumour mass (which may be resected surgically), that gives rise to the serious problems of local and distant recurrence.

The layout of the chapter is therefore as follows: in the next section, we formulate the continuum model of invasion based on a system of partial differential equations. In section 10.3 we present the results of numerical simulations of this model in one and two dimensions. In section 10.4 we derive the discrete biased random walk model (based on the model of section 10.2) and present the results of the discrete simulations in section 10.5. In section 10.6 we discuss some recent extensions of the original model and then finally in section 10.7 we discuss the clinical implications of the results of the model and make some concluding remarks.

10.2 The Continuum Mathematical Model

We will base our mathematical model on generic solid tumour growth, which for simplicity we will assume is at the avascular stage. While most tumours are asymptomatic at this state, it is still possible for cells to escape and migrate to the lymph nodes and for the more aggressive tumours to invade. The model may be extended to incorporate interactions between the tumour cells and blood vessels, thereby modelling angiogenesis and vascular growth. However since one of the aims of the paper is to focus solely on the interactions between the tumour and the surrounding tissue we do not attempt to model interactions between the tumour and the vasculature. In principle, our model can be extended to include such interactions and the general form of our model will be the same for both invading vascular and avascular tumours. In the initial model we consider the following key variables: tumour cell density (denoted by n), MDE concentration (denoted by m), ECM density (denoted by f), and endogeneous inhibitor (e.g., tissue inhibiting metallo-proteases, TIMPs) concentration (denoted by u). Each of the variables (n, m, f, and u) is a function of the spatial variable $\mathbf{x}$ and time t.

As already discussed in the introduction, MDEs are important at many stages of tumour growth, invasion, and metastasis, and the manner in which they interact with endogenous inhibitors, growth factors, and tumour cells is very complex. In our model we assume that the tumour cells produce MDEs which degrade the ECM locally and that the ECM responds by producing endogenous inhibitors (e.g., TIMPs). The ECM degradation, as well as making space into which tumour cells may move by simple diffusion, results in the production of molecules which are actively attractive to tumour cells (e.g., fibronectin) and which then aid in tumour cell motility. We refer to the movement of tumour cells up a gradient of such molecules as haptotaxis. We have therefore chosen to consider tumour cell motion to be driven only by random motility and haptotaxis in response to adhesive or attractive gradients [11,30,31,35,44] created by degradation of the matrix. This approach permits us to investigate cell-matrix interactions in isolation. To describe the random motility of the tumour cells we assume a flux of the form

$$\mathbf{J}_{random} = -D(f, m)\nabla n\,,$$

where $D(f, m)$ may be a constant or a function of either the MDE or ECM concentration, the latter cases representing a chemokinetic response i.e., increased random motility will be observed for regions of high MDE/ECM concentration. We take the haptotactic flux to be

$$\mathbf{J}_{hapto} = \chi n \nabla f\,,$$

where $\chi > 0$ is the (constant) haptotactic coefficient. To enable us to focus entirely on the cell-matrix interactions and how these interactions affect tumour cell *migration*, we do not consider any proliferation of tumour cells in our partial differential equation model. However tumour cell proliferation will be included in the discrete model in section 10.4.

The conservation equation for the tumour cell density n is therefore given by

$$\frac{\partial n}{\partial t} + \nabla \cdot (\mathbf{J}_{rand} + \mathbf{J}_{hapto}) = 0,$$

and hence the partial differential equation governing tumour cell motion (in the absence of cell proliferation) is,

$$\frac{\partial n}{\partial t} = \nabla \cdot (D(f,m)\nabla n) - \chi \nabla \cdot (n \nabla f)\,. \tag{10.1}$$

For the initial simulations given in the next section we chose $D(f,m) = D_n$, a constant, the tumour cell random motility coefficient.

The ECM is known to contain many macromolecules, including fibronectin, laminin, and collagen, which can be degraded by MDEs [12,53]. We assume that the MDEs degrade ECM upon contact and hence the degradation process is modelled by the following simple equation:

$$\frac{\partial f}{\partial t} = -\delta m f, \tag{10.2}$$

where δ is a positive constant.

Active MDEs are produced (or activated) by the tumour cells, diffuse throughout the tissue, and undergo some form of decay (either passive or active). The MDEs are also assumed to be neutralised by the endogenous inhibitors (see below). The equation governing the evolution of MDE concentration is therefore given by:

$$\frac{\partial m}{\partial t} = D_m \nabla^2 m + g(n,m) - h(n,m,f) - k(m,u) \tag{10.3}$$

where D_m is a positive constant, the MDE diffusion coefficient, g is a function modelling the production of active MDEs by the tumour cells, h is a function modelling the MDE decay, and k is a function modelling MDE neutralisation by the endogenous inhibitors. For simplicity we assume that there is a linear relationship between the density of tumour cells and the level of active MDEs in the surrounding tissues (regardless of the amount of enzyme precursors secreted and the presence of endogenous inhibitors) and so these functions are taken to be $g = \mu n$ (MDE production by the tumour cells) and $h = \lambda m$ (natural decay), respectively, although other functional forms have also been tried (cf. [5]). Inhibitors are assumed to neutralise the MDEs in a "one-to-one" reaction, i.e., $k(m,u) = \theta u m$.

Finally, we assume that the ECM produces endogenous inhibitors as a response to the MDEs. These inhibitors produced as a result of tissue degradation, diffuse and decay throughout the tissue and neutralise the MDEs. The equation governing the evolution of inhibitor concentration is therefore given by:

$$\frac{\partial u}{\partial t} = D_u \nabla^2 u + F(m,f) - k(m,u) - \epsilon u \tag{10.4}$$

where D_u is a positive constant, the inhibitor diffusion coefficient, F is a function modelling the inhibitor production, k models neutralisation of the MDEs (as above), and we assume linear decay of the inhibitors.

Hence the complete system of equations describing the interactions of the tumour cells, ECM, MDEs, and endogenous inhibitors as detailed in the previous paragraphs is

$$\begin{aligned}
\frac{\partial n}{\partial t} &= \overbrace{D_n\nabla^2 n}^{random\ motility} - \overbrace{\chi\nabla\cdot(n\nabla f)}^{haptotaxis}, \\
\frac{\partial f}{\partial t} &= -\overbrace{\delta m f}^{degradation}, \\
\frac{\partial m}{\partial t} &= \overbrace{D_m\nabla^2 m}^{diffusion} + \overbrace{\mu n}^{production} - \overbrace{\theta u m}^{neutralisation} - \overbrace{\lambda m}^{decay} \\
\frac{\partial u}{\partial t} &= \overbrace{D_u\nabla^2 u}^{diffusion} + \overbrace{F(m,f)}^{production} - \overbrace{\theta u m}^{neutralisation} - \overbrace{\epsilon u}^{decay}.
\end{aligned} \tag{10.5}$$

This system is considered to hold on some spatial domain Ω (a region of tissue) with appropriate initial conditions for each varaible. We assume that the tumour cells, and consequently the MDEs, and the inhibitors all remain within the domain of tissue under consideration and therefore no-flux boundary conditions are imposed on $\partial\Omega$, the boundary of Ω. We can make a further simplification at this point by assuming that for an actively invading tumour, any negative effect of the endogenous inhibitors has effectively been overcome by the MDEs. Therefore in the remainder of this chapter we focus our attention on the first three equations of the above system (10.5), i.e., we assume that $u = 0$.

In order to solve the system numerically, we first nondimensionalise the equations in the standard way. We rescale distance with an appropriate length scale L (e.g., maximum invasion distance of a cancer cell), time with $\tau = L^2/D$ (where D is a reference chemical diffusion coefficient $\sim 10^{-6}\mathrm{cm}^2\mathrm{s}^{-1}$), tumour cell density with n_0, ECM density with f_0, and MDE concentration with m_0 (where n_0, f_0, and m_0 are appropriate reference variables). Therefore setting

$$\tilde{n} = \frac{n}{n_0}, \quad \tilde{f} = \frac{f}{f_0}, \quad \tilde{m} = \frac{m}{m_0}, \quad \tilde{\mathbf{x}} = \frac{\mathbf{x}}{L}, \quad \tilde{t} = \frac{t}{\tau}$$

in Equation (10.5) and dropping the tildes for notational convenience, we obtain the scaled system of equations:

$$\begin{aligned}
\frac{\partial n}{\partial t} &= \overbrace{d_n\nabla^2 n}^{random\ motility} - \overbrace{\gamma\nabla\cdot(n\nabla f)}^{haptotaxis}, \\
\frac{\partial f}{\partial t} &= -\overbrace{\eta m f}^{degradation}, \\
\frac{\partial m}{\partial t} &= \overbrace{d_m\nabla^2 m}^{diffusion} + \overbrace{\alpha n}^{production} - \overbrace{\beta m}^{decay},
\end{aligned} \tag{10.6}$$

where

$$d_n = \frac{D_n}{D}, \quad \gamma = \frac{\chi f_0}{D}, \quad \eta = \frac{\tau m_0}{\delta}, \quad d_m = \frac{D_m}{D}, \quad \alpha = \frac{\tau \mu n_0}{m_0}, \quad \beta = \tau\lambda.$$

The zero-flux boundary conditions:

$$\mathbf{n} \cdot (-d_n \nabla n + n\chi \nabla f) = 0, \tag{10.7}$$

for the cells and

$$\mathbf{n} \cdot (-d_m \nabla m) = 0, \tag{10.8}$$

for the MDEs are imposed on the boundaries of the domain where $\mathbf{n}$ is an appropriate outward unit normal vector. In one space dimension, the scaled domain is the unit interval $[0, 1]$, while in two space dimensions, the scaled domain is the unit square $[0, 1] \times [0, 1]$.

Initially we assume that there is a nodule of cells already present and in one dimension and that the tumour is centred around $x = 0$ with n having the initial density distribution,

$$n(x, 0) = \exp(-x^2/\epsilon), \quad x \in [0, 1], \tag{10.9}$$

where ϵ is a positive constant. The initial tumour density in two dimensions has a similar form, but is centred on $(0.5, 0.5)$, i.e.,

$$n(x, y, 0) = \exp(-r^2/\epsilon), \quad (x, y) \in [0, 1] \times [0, 1], \tag{10.10}$$

where ϵ is as above and $r^2 = (x - 0.5)^2 + (y - 0.5)^2$.

For both the one and two dimensional results we assume that the tumour has already degraded some of its surrounding tissue and hence we take the initial profile of ECM to be $f(\mathbf{x}, 0) = 1 - 0.5n(\mathbf{x}, 0)$. Finally, we assume that the initial MDE concentration profile is proportional to the initial tumour cell density and take $m(\mathbf{x}, 0) = 0.5n(\mathbf{x}, 0)$. These initial conditions are illustrated graphically at $t = 0$ in each of the figures in the following section.

10.3 Numerical Simulations

10.3.1 One Dimensional Results

The following numerical results were obtained using the NAG routine D03PCF which implements the method of lines and Gear's method. In the following simulations, the parameter values used were as follows: $d_n = 0.001$, $d_m = 0.001$, $\gamma = 0.005$, $\eta = 10$, $\alpha = 0.1$, $\beta = 0$, and $\epsilon = 0.0025$.

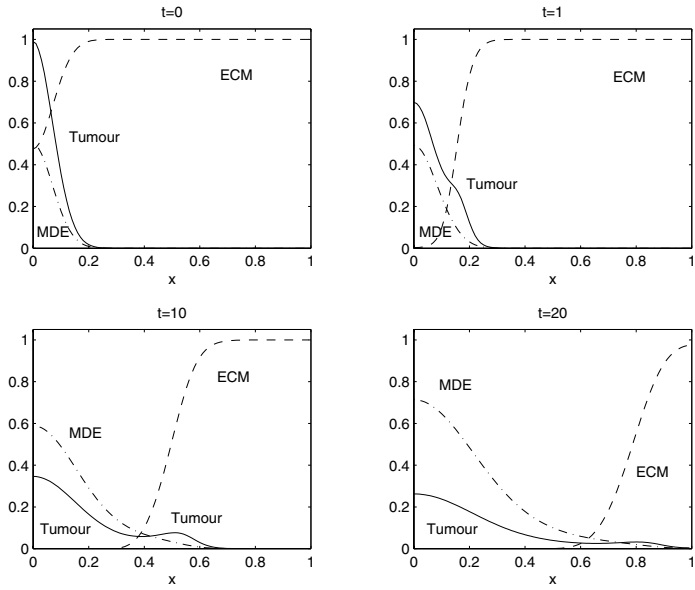

Figure 10.2

One dimensional numerical solution of the system (10.6) with constant tumour cell diffusion showing the cell density, MDE concentration, and ECM density. As the MDEs degrade the ECM the tumour cells invade via a combination of diffusion and haptotaxis. Two distinct, although not completely separated, clusters of cells are seen to form.

Figure 10.2 shows four snapshots in time of the tumour cell density, ECM density, and MDE concentration. The ECM profile shows clearly the degradation by the MDEs. The tumour density distribution at $t = 1$ shows that a small cluster of cells has built up at the leading edge of the tumour due to haptotactic migration. As time evolves this cluster of cells migrates further from the main body of the tumour, which continues to invade the ECM but at a slower rate. These figures indicate that the initial cluster of tumour cells may be able to break into two separate clusters. This becomes even more apparent in subsequent figures.

In the next simulation in Figure 10.3, we consider the effect of *nonlinear diffusion* on the invasion of the tumour cells by taking $D(f, m) = d_n m$. This represents a chemokinetic response of the tumour cells to MDE concentration where we make the simple assumption that the tumour cell random motility is directly proportional to MDE concentration, i.e., where there is a high MDE concentration there is high random cell motility. Using the same parameters as in Figure 10.2, the four snapshots in Figure 10.3 were produced. While the MDE and ECM concentration profiles closely resemble those obtained in Figure 10.2, the tumour density distribution has changed considerably. By $t = 1$ we again see a build up of tumour cells at the leading edge,

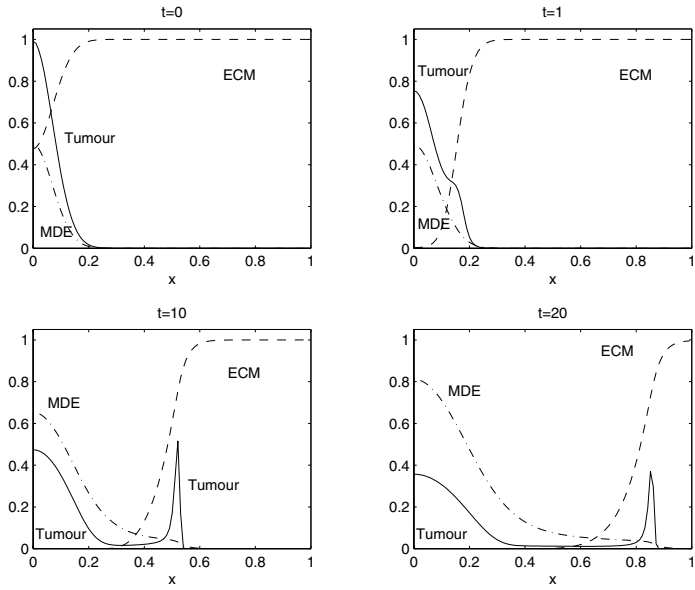

Figure 10.3

One dimensional numerical solution of the system (10.6) with tumour cell diffusion dependent on MDE concentration. As the MDEs degrade the ECM, the tumour cells invade and form two distinct clusters, those mainly driven by diffusion and those driven by haptotaxis.

more pronounced than in Figure 10.2, which then breaks away from the main body of the tumour.

This results in two quite distinct clusters, one of which migrates much further into the ECM. The main body of the tumour however, invades more slowly than was observed in Figure 10.2. If a small cluster of cells breaks away from the main body of the tumour, there is then the potential for these cells to intravasate any neighbouring vessels and start the metastatic cascade. Also if the main body of the tumour were to be surgically removed (resected), the smaller cluster of cells that has invaded further into the ECM may go unnoticed by the surgeon and lead to a possible recurrence. These results indicate the importance of haptotaxis as a mechanism for invasion and implicate its role in the metastatic cascade. We now investigate the effect that changing various parameter values has on the solution.

In Figures 10.4(a) and (b) we have increased γ by a factor of 10 and 100 respectively (all other parameters remain unchanged from Figure 10.1). These figures show the importance of tumour-matrix interactions and haptotaxis. As γ is increased, a larger proportion of the tumour cells invade the tissue, driven forward by haptotaxis and the gradients in the ECM. Indeed from Figure 10.4(b) we can see that almost all the tumour cells are invading in a pulse-like travelling wave.

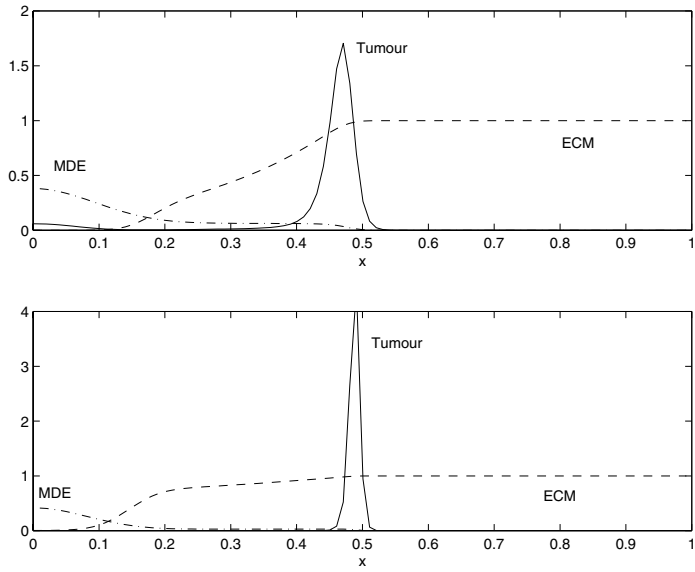

Figure 10.4

One dimensional numerical solutions of the system (10.6), with parameter values as in Figure 10.1 (unless otherwise stated), showing the cell density, MDE concentration, and ECM density. The top panel (a) shows the effect of increasing γ by a factor of 10 ($\gamma = 0.05$) at $t = 2.5$ and the bottom panel (b) shows the effect of increasing γ by a factor of 100 ($\gamma = 0.5$) at $t = 1$.

The importance of haptotaxis as a mechanism of invasion is obvious from these results. This in turn emphasises the importance of gradients which appear in the degraded ECM. Since the ECM is unlikely to be a constant homogeneous mass, in order to make the model more realistic we must consider a spatially heterogeneous ECM. We examine how this affects the tumour cell density distribution by considering such a heterogeneous ECM in two dimensions in the following section.

10.3.2 Two Dimensional Numerical Simulations

The aim of this section is to extend the model to a two dimensional spatial domain and therefore to allow the spatio-temporal dynamics of the model to be explored in more detail. All of the numerical solutions presented in this section were obtained from a finite difference approximation of the system (10.6) with boundary and initial conditions (10.7) to (10.10). Since there are no birth and death terms in the tumour cell equation (10.6) and we impose zero flux boundary conditions (10.7)

then the total cell number is conserved. We used the conservation of cell number as a check on the accuracy of our numerical scheme which was found to be accurate to within 0.01%. The parameter values used in the following simulations (unless specified otherwise) were the same as those used in the one dimensional simulations of Figure 10.2, i.e., $d_n = 0.001$, $d_m = 0.001$, $\gamma = 0.005$, $\eta = 10$, $\alpha = 0.1$, $\beta = 0$, and $\epsilon = 0.0025$.

Initially we assume that we have a circular initial tumour cell distribution given by Equation (10.10) and an ECM distribution given by Figure 10.5. Finally, we assume that the initial MDE concentration profile is proportional to the initial tumour cell density and take $m(\mathbf{x}, 0) = 0.5n(\mathbf{x}, 0)$. The tumour cell initial conditions are illustrated graphically at $t = 0$ in Figure 10.6.

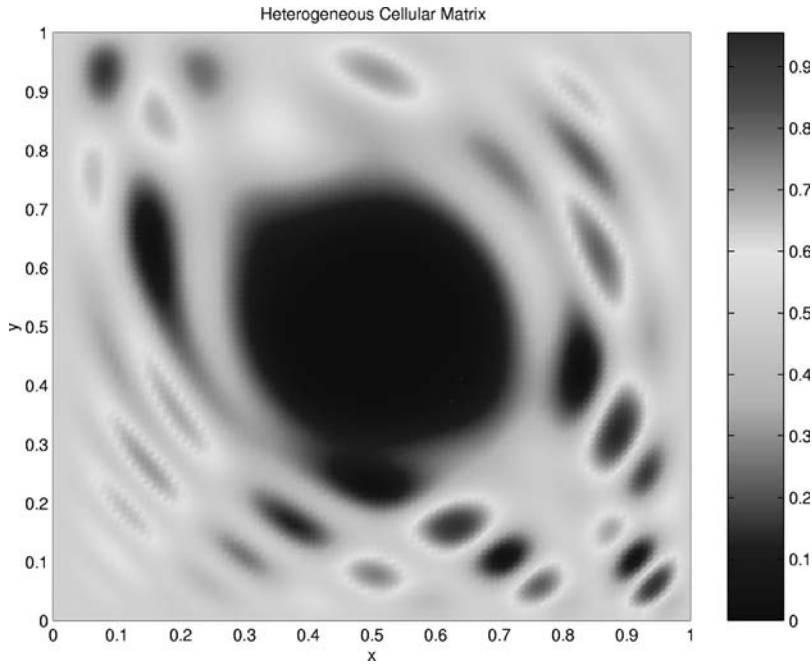

Figure 10.5

Pictorial representation of a hypothetical heterogeneous ECM. Gradation refers to ECM concentration.

To examine the importance of the role of ECM in the invasive process, we consider a hypothetical heterogeneous ECM with an initial distribution given in Figure 10.5, i.e., there are regions of high density of ECM and regions of low density of ECM. Using this initial ECM data, the initial tumour cell distribution, and MDE concentration discussed above, we obtained the results shown in Figures 10.6 and 10.7.

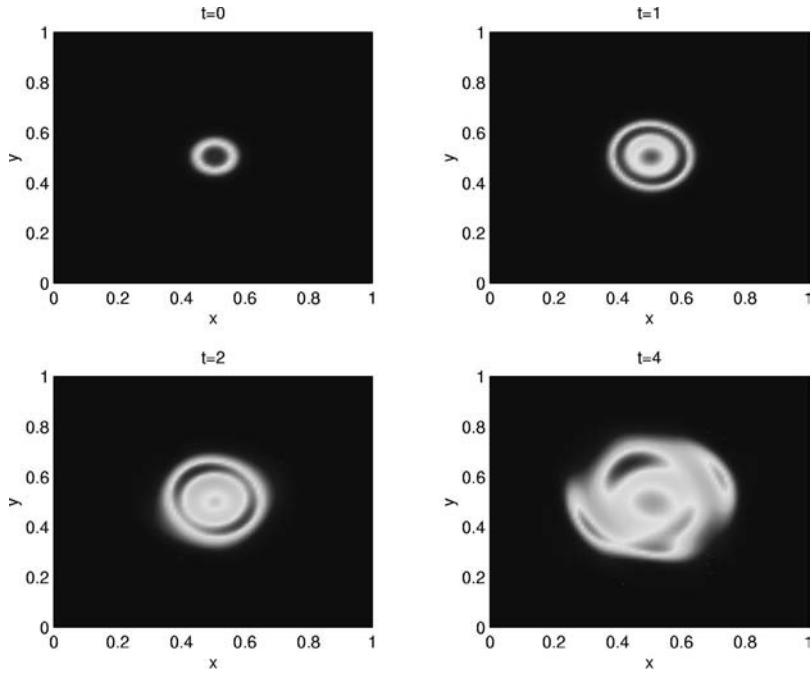

Figure 10.6

Spatio-temporal evolution of the tumour cell density from a numerical simulation of system (10.6) within a heterogeneous ECM (see text for parameter values). The effect of the ECM on the tumour cell density only becomes apparent for the later values of t, where the ring of cells is seen to no longer exist. Gradation as in Figure 10.5.

From Figure 10.6 we note that essentially the same behaviour is observed at the early stages ($t = 1.0, 2.0$) as for the one-dimensional results. However, by $t = 4.0$ the perfect symmetry of the initial tumour cell distribution is broken and there are several regions of higher tumour cell density. At later times, from Figure 10.7, we see that two regions of high cell density form ($t = 7.0$) and continue to invade ($t = 10.0$). The main body of the tumour is approximately bounded by these higher density regions, although by $t = 12.0$ the higher density regions have fragmented and a new 'hotspot' has appeared. The final figure at $t = 15$ shows that the tumour cell density has spread through most of the domain in a somewhat heterogeneous manner with a couple of 'hotspots.' This form of tumour cell density distribution is closer to what is observed in real life and further emphasises the importance of tumour cell/ECM interactions.

The particular choice of initial ECM distribution (Figure 10.5) is perhaps somewhat exaggerated and was selected to emphasise the importance of ECM gradients. However, other forms of initial ECM distribution would produce qualitatively similar

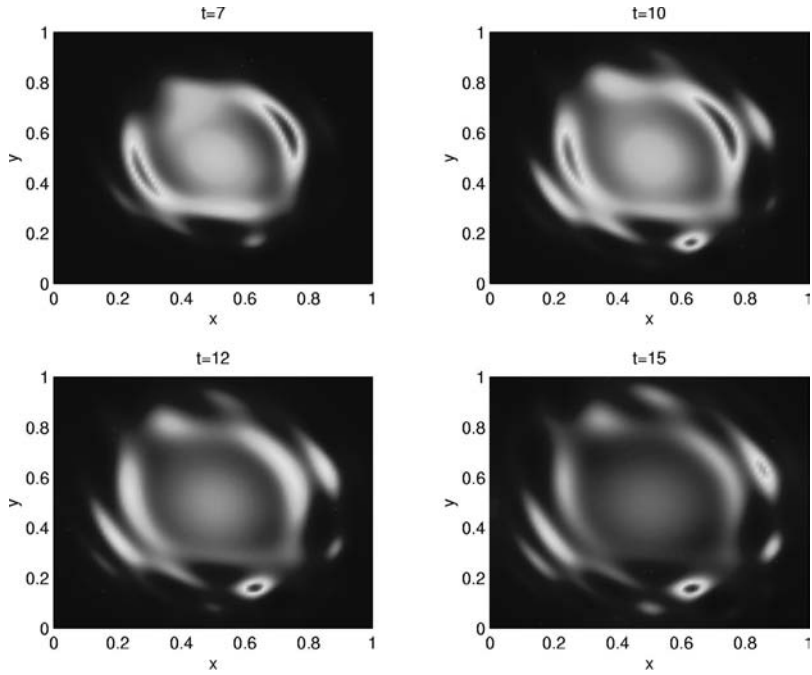

Figure 10.7

Spatio-temporal evolution of the tumour cell density from a numerical simulation of system (10.6) within a heterogeneous ECM, for later values of t (see text for parameter values). The effect of the heterogeneous ECM via haptotaxis on the tumour cells is now apparent, with the cells invading the ECM in a more heterogeneous manner resulting in the appearance of 'hot spots.' Gradation as in Figure 10.5.

final results, i.e., a heterogeneous tumour cell density distribution. The two important factors governing the final tumour cell density distribution are ECM heterogeneity and the haptotactic response of the cells to the gradients created in the degraded matrix. These results are in qualitative agreement with actual clinical observations i.e. it is well-known that small clusters of cells can break away from the central mass of the tumour and invade further leading to possible metastasis.

While the results of sections 10.3.1 and 10.3.2 give an indication of the macroscopic behaviour of our model and produce qualitatively realistic results, they are limited in their quantitative capacity and do not account for other important processes such as cell proliferation, cell mutation, and individual cell-cell interactions. In the following section we present a discrete model that has the capacity to include all of these processes in a realistic manner and produce both spatial and temporal data on individual invading cells.

10.4 The Discrete Mathematical Model

Discrete mathematical models of tumour invasion already exist in the research literature, but these mainly involve the use of cellular automata. For example, the work of Smolle and coworkers [49–51] concerns invasive patterns generated from a cellular automaton which are compared statistically with experimental results in order to detect real invasive patterns. The model allows for an estimation of cell motility and proliferation. Qi [43] developed a cellular automaton model of cancerous growth which was compared with experimental growth curves and shown to agree well. Both of these models included cell proliferation and migration terms. Qi [43] also included the mechanical pressure within the tumour and Smolle and Stettner [51] consider a further level of complexity with the influence of autocrine and paracrine chemicals.

In this section we will develop a discrete mathematical model of tumour invasion which will enable not only a qualitative but also a quantitative comparison with *in vivo* experimental results. The particular technique which we will use to follow the path of an individual tumour cell is a implementation of the method developed in [6] and [4] and first of all involves discretizing (using standard finite-difference methods) the partial differential equation governing the rate of change of tumour cell density, i.e., Equation (10.6). We then use the resulting coefficients of the five-point finite-difference stencil to generate the probabilities of movement of an individual cell in response to its local milieu. This technique differs from previous discrete models such as [51] and [43] in that the movement of individual cells is based on a discrete form of the continuous model. However, like both of these models there is an element of stochasticity (randomness) in the movement rules for the cells. In effect, we will derive a biased random walk governing the motion of a single tumour cell based on the system of partial differential equations (10.6) of section 10.2. In this sense, our discrete model is probably most similar in formulation to the reinforced random walk models of Othmer and Stevens [39], where cell movement is modelled in response to a chemical stimulus by considering an equation (discrete in space and continuous in time) governing the probability that a cell is at a given position at time t. This equation is a function of the transition probabilities for one–step jumps to the orthogonal neighbours. The form of the transition probabilities for the gradient model of [39] is very similar to the probabilities of movement that will be derived from our discrete model (see also [2] and [18]).

We now set about formulating the discrete model and deriving the movement probabilities for an individual tumour cell in response to its surrounding matrix. The implementation of the process of cell proliferation will be described later. We first discretize Equation (10.6) using the Euler finite difference approximation [37]. This involves approximating the continuous two dimensional domain $[0,1] \times [0,1]$ in the usual way as a grid of discrete points (mesh size h), and time (t) by discrete increments (magnitude k). The full discretized system is given in the Appendix. For

clarity we only consider the tumour cell equation,

$$n_{i,j}^{q+1} = n_{i,j}^{q} P_0 + n_{i+1,j}^{q} P_1 + n_{i-1,j}^{q} P_2 + n_{i,j+1}^{q} P_3 + n_{i,j-1}^{q} P_4, \qquad (10.11)$$

where the subscripts specify the location on the grid and the superscripts the time steps. That is $x = ih$, $y = jh$, and $t = qk$ where i, j, k, q, and h are positive parameters.

In a numerical simulation of the continuous model (10.6), the purpose of the discrete equation (10.11) is to determine the tumour cell density at grid position (i, j), and time $q+1$, by averaging the density of the four surrounding neighbours at the previous time q. For our discrete model, we will use the five coefficients P_0 to P_4 from (10.11) to generate the motion of an individual tumour cell. These coefficients can be thought of as being proportional to the probabilities of the tumour cell being stationary (P_0) or moving left (P_1), right (P_2), up (P_3), or down (P_4).

Each of the coefficients P_1 to P_4 consist of two components,

$$P_n = \text{random movement} + \text{haptotaxis} \qquad (10.12)$$

thus showing how the discrete tumour cell equation is linked to the continuous tumour cell equation of system (10.6). The coefficient P_0 has a similar form (see Appendix). Equation (10.12) is very similar to the transition probabilities of the reinforced random walk model of Othmer and Stevens [39]. In particular, their gradient models have a random component and a "taxis" component. Othmer and Stevens [39] used their discrete transition probabilities to then derive a partial differential equation in the continuous limit. It is possible to show this for our model by defining transition probabilities of the form (10.12). The original equation governing the rate of change of tumour cell density (10.6) can then be recovered by following the analysis of [39] in the same rigorous manner.

The exact forms of P_0 to P_4 are functions of the ECM density near an individual tumour cell (see Appendix). Therefore, if there were no ECM the values of P_1 to P_4 would be equal, with P_0 smaller (or larger, depending on the precise values chosen for the space and time steps), i.e., there is no bias in any one direction and the tumour cell is less (more) likely to be stationary, approximating an unbiased random walk. However, if there are gradients in the ECM, haptotaxis dominates and the coefficients P_0 to P_4 will become biased towards the direction of increased ECM density. The motion of an individual cell is therefore governed by its interactions with the matrix macromolecules in its local environment.

Before proceeding to the simulation section, we first of all discuss the manner in which we explicitly incorporate cell proliferation into the discrete model.

10.4.1 Cell Proliferation

In our model we assume that each individual cell has the capacity for proliferation and will produce two daughter cells provided the following two conditions are satisfied:

(i) the parent cell has reached maturity, and

(ii) there is sufficient space surrounding the parent cell for the two new daughter cells to move into.

We defined cell maturity to be 500 discrete time steps. While this timescale is arbitrary, with a precise estimate of parameter values in the original model, this maturity time can be made to correspond with an actual cell cycle time for specific cancer cells. In order to satisfy condition (ii), we assumed that a daughter cell could arise if any one of the parent cell's four orthogonal neighbours was empty. If more than one of the neighbouring grid points is empty then the new cell position is chosen randomly from these points. In order to keep the running time of simulations within reasonable limits we have restricted the maximum number of cells to 3000, with an initial distribution of 500 cells.

10.4.2 Simulation Process for the Discrete Model

Each time step of the simulation process involves solving the discrete form of the system (10.6) numerically to generate the five coefficients P_0 to P_4 (see Appendix). Probability ranges are then computed by summing the coefficients to produce five ranges, $R_0 = 0$ to P_0 and $R_m = \sum_{l=0}^{m-1} P_l$ to $\sum_{l=0}^{m} P_l$, where $m = 1$ to 4. We then generate a random number between 0 and 1, and depending on the range which this number falls in, the current individual tumour cell under consideration will remain stationary (R_0) or move left (R_1), right (R_2), up (R_3), or down (R_4). The larger a particular range, the greater the probability that the corresponding coefficient will be selected. Each tumour cell is therefore restricted to move to one of its four orthogonal neighbouring grid points or remain stationary at each time step.

All the simulations of the discrete model were carried out on a 200×200 grid, which is a discretization of a the unit square, $[0,1] \times [0,1]$, with a space step of $h = 0.005$ and a time step of $k = 0.001$. A discrete form of the no flux boundary condition (10.7) was imposed on the square grid, restricting the tumour cells to within the grid. The initial conditions in all simulations (unless otherwise stated) are given by discrete forms of Equations (10.9) and (10.10) with an initial number of 500 tumour cells centred around $(0.5, 0.5)$.

The parameter values used in the following simulations are the same as those used in the previous two dimensional continuous simulations (unless otherwise stated), i.e., $d_n = 0.001$, $d_m = 0.001$, $\gamma = 0.005$, $\eta = 10$, $\beta = 0$, and $\alpha = 0.1$.

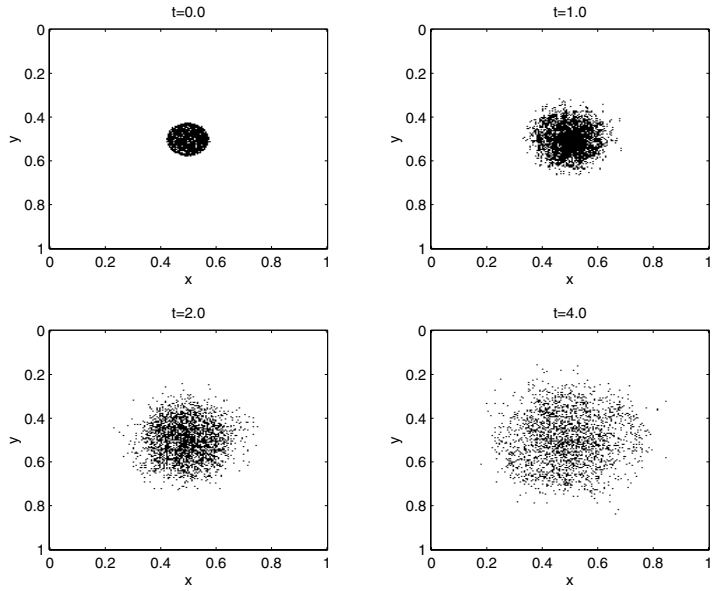

Figure 10.8

Spatio-temporal evolution of tumour cell invasion from a numerical simulation of the discrete model. The figure shows the tumour cells migrating from the centre ($x = 0.5, y = 0.5$) into the heterogeneous ECM as given Figure 10.4 (see text for parameter values). No real structure is apparent but the cell distribution is clearly different from Figure 10.11 and again a few individual cells are seen to invade further into the ECM.

10.5 Discrete Model Simulation Results

We examine the results of invasion by individual cancer cells in a heterogeneous ECM. Using a discrete form of Figure 10.5 for the initial ECM concentration and the same parameters as above, we obtained Figures 10.8 and 10.9. From the initial cluster (at $t = 0.0$) cells begin to migrate outward in a compact, radially symmetric manner. However, by $t = 2.0$ the initial clustering of the cells is not seen and this is further emphasised at $t = 4.0$. We see individual cells migrating out further than the main group. As time evolves we can see from Figure 10.9 (at $t = 7.0$) the two regions of increased cell density that are equivalent to the two regions of higher density seen in Figure 10.7 at $t = 7.0$. As t increases the cells migrate further into the ECM and become more dispersed, although, small clusters can still be observed e.g., just below $x = 0.6$, $y = 0.8$ for $t = 12.0 - 15.0$. This again is in agreement with the continuous results (Figure 10.7). By $t = 15$ quite a few

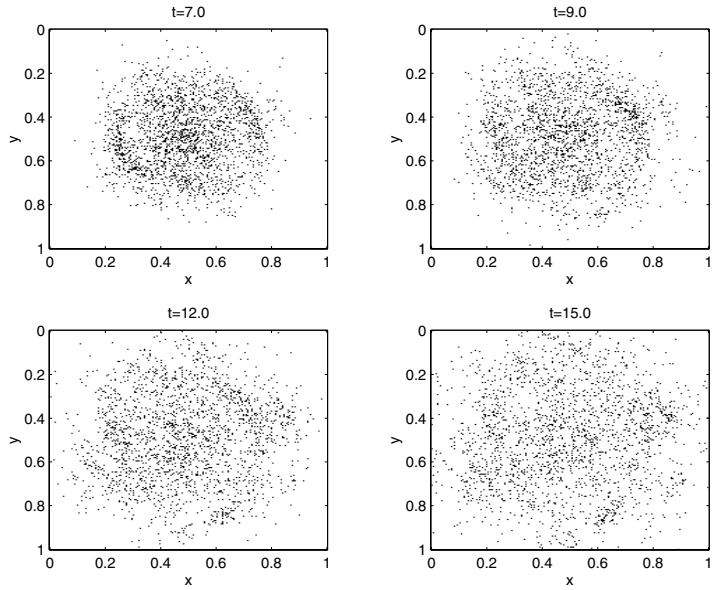

Figure 10.9

Spatio-temporal evolution of tumour cell invasion from a numerical simulation of the discrete model. The figure shows the tumour cells migrating into the heterogeneous ECM as in Figure 10.8 but for later values of t (see text for parameter values). We now observe that the overall distribution of the cells is very similar to the continuous equivalent (Figure 10.10) and a few individual cells have in fact reached the boundaries of the domain.

of the cells have already reached the boundary of the domain, which is something that did not occur in the continuous model simulations. This further illustrates the importance of the ECM structure in aiding or hindering the migration of individual cells that have the potential to metastasise. The most striking feature of these results is to notice that a few individual tumour cells migrate much further into the ECM separated from the main tumour mass. These cells have the greatest potential to metastasise further and are difficult to detect clinically. It should be emphasised that the movements of the individual cells, while governed by the continuous model via the discretisation, do have a genuine stochastic component, and the cell movements can therefore deviate from the continuous results. Also since the discrete model incorporates cell proliferation, whereas the continuous model does not, we expect to see some differences. However, the total cell number is limited to a maximum of 3000 cells and therefore the structures seen in Figure 10.11 are produced mainly by cell migration, i.e., random motility and haptotaxis, rather than cell proliferation.

10.6 Model Extensions

There are several ways in which the model could be extended. At the continuum level explicitly considering the effects of oxygen as a nutrient for the cancer cells is important, and at the discrete level it is crucial to consider more detailed cellular characteristics, in particular the inclusion of cell-cell adhesion. Therefore we shall use the following extended system of partial differential equations as a basis for the discrete model results of this section (as was carried out in section 10.4):

$$\begin{aligned}
\frac{\partial n}{\partial t} &= \overbrace{d_n \nabla^2 n}^{random\ motility} - \overbrace{\gamma \nabla \cdot (n \nabla f)}^{haptotaxis}, \\
\frac{\partial f}{\partial t} &= - \overbrace{\eta m f}^{degradation}, \\
\frac{\partial m}{\partial t} &= \overbrace{d_m \nabla^2 m}^{diffusion} + \overbrace{\alpha n}^{production} - \overbrace{\beta m}^{decay}, \\
\frac{\partial c}{\partial t} &= \overbrace{d_c \nabla^2 c}^{diffusion} + \overbrace{\delta f}^{production} - \overbrace{\mu n}^{uptake} - \overbrace{\nu c}^{decay},
\end{aligned} \tag{10.13}$$

where c denotes oxygen concentration which is assumed to diffuse into the ECM, decay naturally and be consumed by the tumour. For simplicity oxygen production is proportional to the ECM density.

Molecules which facilitate interactions between cells and between cells and the ECM, known as cell adhesion molecules, are now thought to be central to the invasive process [24]. In the above model we already consider cell-ECM adhesion via haptotaxis. In order to include cell-cell adhesion we assume each cell has its own internal adhesion value ($0 \leq \mathrm{A_i} \leq 4$), i.e., the number of neighbouring cells that it will preferentially adhere to. We therefore examine the number of external neighbours each cell has ($\mathrm{A_e}$) and if $\mathrm{A_e} \geq \mathrm{A_i}$ then the cell is allowed to migrate, otherwise it remains stationary.

Since not all cells will have the same level of adhesiveness, some form of heterogeneity needs to be introduced. To take a small step towards including greater detail at the cellular level we shall consider a population of individual cells that have predefined phenotypic traits which specify their behaviour. We define each phenotype to be a set of parameter values that describe the behaviour of the cell expressing it. Therefore a particular phenotype will have a defined proliferation age, O_2 consumption, MDE production, haptotaxis coefficient, and adhesion value. For simplicity we consider four phenotypes (I, II, III, and IV), each progressively more aggressive (in terms of invasiveness) than before. Type I being the least aggressive (having the longest proliferation age, consuming the least oxygen, producing the least MDE, having the smallest haptotaxis coefficient and having the highest adhesion value,

$A_i = 3$), and type IV being the most aggressive (having the shortest proliferation age, consuming the most oxygen, producing the most MDE, having the largest haptotaxis coefficient and having a zero adhesion value i.e. no cell-cell adhesion). For further details on this extended model see [5].

The following simulation was carried out on a 400×400 grid, which is a discretisation of the unit square, $[0,1] \times [0,1]$, with a space step of $h = 0.0025$ and a time step of $k = 0.0005$. No flux boundary conditions were imposed on the square grid, restricting the tumour cells, MDE, ECM, and oxygen to within the grid. Initially, 50 tumour cells were centred around $(0.5, 0.5)$ with a random age, the MDE concentration was zero throughout the domain ($m(x,y) = 0$), and the oxygen concentration was taken to be one ($c(x,y) = 1$). There is no upper limit to the number of cells in the simulation. Each of the initial cells are assigned phenotype I and for each subsequent proliferation there is a small probability of further mutations occurring which will lead to the daughters cells having phenotype II, and so on in a linear fashion. All mutations are assumed to be irreversible.

The distribution of tumour cells, MDE, oxygen, and ECM at $t = 12$ is shown in Figure 10.10. The tumour cell distribution is now radically different geometrically from what was produced in the previous section, showing a more connected tumour with multiple protrusions. The depleted oxygen distribution correlates well with the dead region of the tumour. The MDE distribution produced by the tumour cells shows slightly more symmetry due to diffusion of the MDE, and its impact on the ECM can clearly be seen. The tumour contains two cell types, dead cells and type IV cells, and it is these most aggressive cells that dominate the population, throughout the simulation, and lead the way for invasion at the boundary of the tumour. Since these cells have no cell-cell adhesion dependence, their migration is mainly driven by haptotaxis via the local ECM gradients, and it is these local gradients that ultimately define the tumour geometry.

10.7 Discussion and Conclusions

This work presents a mathematical model for tumour invasion using a novel blend of continuum, deterministic modelling, and discrete, stochastic modelling in one and two space dimensions.

The continuum model consists of a system of nonlinear partial differential equations and examines how tumour cells respond to ECM gradients via haptotaxis, created both by the tumour cells through MDE degradation of the matrix and those already in existence within the matrix. The results from the one dimensional continuum model simulations demonstrate the impact of interactions between tumour cells and the ECM on possible metastasis. In particular if tumour cells move via random migration and haptotaxis and the intensity of the random movements is dependent upon MDE concentration then a small cluster of cells can easily break away from the

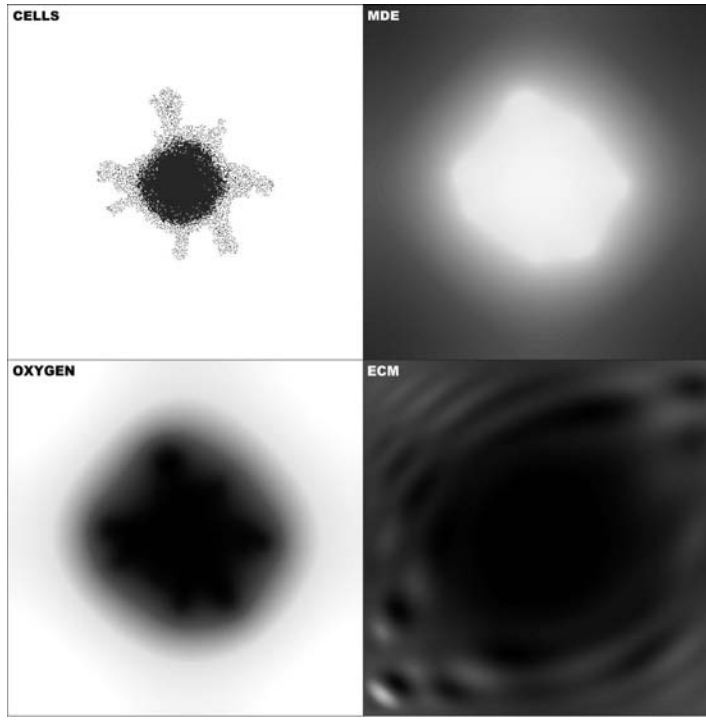

Figure 10.10

Spatial distribution of tumour cells, MDE, ECM, and oxygen (clockwise) at time $t = 12$. Graduation represents phenotype. For the MDE, ECM, and oxygen concentration, white=high concentration, black=low concentration.

main body of the tumour (Figure 10.2). Even without this MDE dependence, it is clear that the tumour cells can split into two groups: those driven by random migration and those driven by haptotaxis (Figure 10.1). However, this result of the model is mainly due to the fact that the only gradients in the ECM are a result of MDE degradation and hence the cells at the leading edge of the tumour are mostly affected by haptotaxis. When ECM heterogeneity is introduced, in the two dimensional simulations, this grouping of cells into those driven mainly by random migration and those driven mainly by haptotaxis is no longer obvious because of the gradients already existing within the ECM. The heterogeneous ECM (Figure 10.5) is more likely to be characteristic of real ECM within the body and the resulting tumour cell density distributions are more realistic (Figures 10.6 and 10.7), i.e., a heterogenous tumour cell density with a few 'hotspots.' Indeed, in Figure 10.11, we present a figure of an actual mammogram of a breast cancer. The contrast arises from the deposition of calcium (microcalcification), which is a common finding in this disease. The central tumour mass can clearly be seen, but also some contrast-bright specks around it,

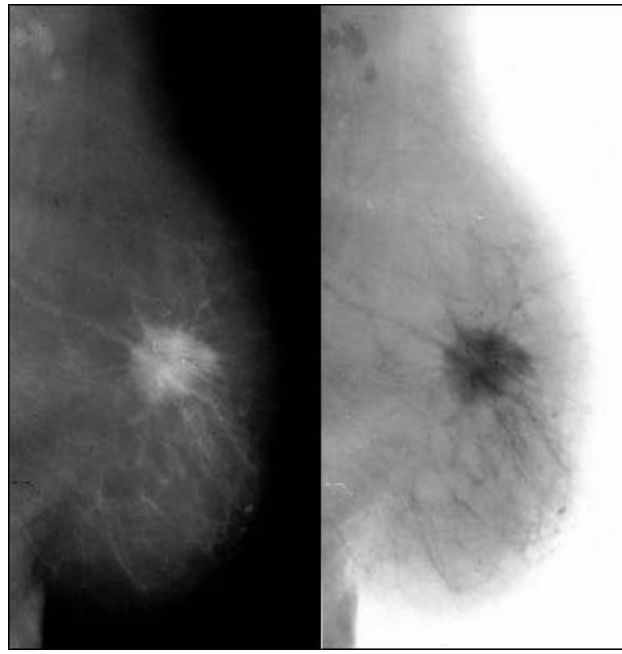

Figure 10.11

Mammogram of a breast cancer. The contrast arises from the deposition of calcium (microcalcification), which is a common finding in this disease. Note the central tumour mass, but also some contrast-bright specks around it, which may represent clusters of tumour cells.

which may represent clusters of tumour cells which have already broken away from the central mass.

The discrete model that we developed was derived from a discretized form of the partial differential equations of the continuum model, and permits the tracking of individual tumour cells and also enables us to explicitly incorporate rules for cell proliferation. With reference to the larger scale, the results from the discrete model confirm the predictions of the continuum model that haptotaxis is important for both invasion and metastasis. On a finer scale, the discrete results show that cell proliferation can aid in invasion as a result of space filling. Also, the ECM structure (via haptotaxis) may aid individual cells in breaking from the main body of the tumour and thus escaping to become possible metastasis (Figures 10.8 and 10.9). The discrete results were also able to show that many cells invade further into the ECM than is predicted from the continuous results — which again has important implications for metastasis.

To some extent the discrete model is still under development and as can be seen from the model extensions in section 10.6 we have included more individual-

based processes such as cell-cell adhesion. However, there is even more potential to include a wider range of cellular characteristics, e.g., genetic information about each cell which can be stored and passed from generation to generation incorporating the possibility of genetic mutations. These may then alter the cell proliferation rate, migration rate, adhesion properties, or apoptotic rate. If exact parameter values were obtained for the discrete model then it would be possible to obtain the physical cell numbers that are falling within a given radius of the main tumour mass and could therefore be used as a predictive tool for estimating how far a surgeon should cut to ensure all of the tumour is removed.

The technique of using partial differential equations as the basis for discrete models is clearly very useful, with the ability to generate movements of individual cells based on a continuum model of a population of cells. Indeed, this technique provides a powerful means of linking micro-scale events to macro-scale events, individual behaviour to population behaviour, with potential application to a wide range of problems in mathematical biology.

From a clinical point of view, these models have enormous potential. Even at this stage, the behaviour of the simulated tumours closely parallels histological observations, especially when a heterogeneous ECM is introduced. It is therefore conceivable that measurement in tumours of some of the parameters used in these models will provide precise information on the invasive behaviour of individual neoplasms. For example, it should then be possible to estimate the likely extent of local infiltration by a tumour, and thereby tailor the radicality of surgical excision for that individual situation. It may also be possible to assess more accurately than at present the likelihood of metastatic disease, which will have important implications for adjuvant systemic therapy.

10.8 Appendix

To discretize the continuous system (10.6) we use Euler finite difference approximations [37], which leads to the system,

$$
\begin{aligned}
n_{i,j}^{q+1} &= n_{i,j}^{q} P_0 + n_{i+1,j}^{q} P_1 + n_{i-1,j}^{q} P_2 + n_{i,j+1}^{q} P_3 + n_{i,j-1}^{q} P_4, \\
f_{i,j}^{q+1} &= f_{i,j}^{q} \left[1 - k\eta n_{i,j}^{q}\right], \\
m_{i,j}^{q+1} &= m_{i,j}^{q} \left[1 - \frac{4kD_m}{h^2} - k\alpha n_{i,j}^{q}(1 - n_{i,j}^{q})\right] \\
&\quad + \frac{kD_m}{h^2}\left[m_{i+1,j}^{q} + m_{i-1,j}^{q} + m_{i,j+1}^{q} + m_{i,j-1}^{q}\right],
\end{aligned}
$$

with $x = ih$, $y = jh$, and $t = pk$.

The coefficient P_0, which is proportional to the probability of no movement,

has the form,

$$P_0 = 1 - \frac{4kD_n}{h^2} - \frac{k\gamma}{h^2}\left(f^q_{i+1,j} + f^q_{i-1,j} - 4f^q_{i,j} + f^q_{i,j+1} + f^q_{i,j-1}\right),$$

and the coefficients P_1, P_2, P_3, and P_4, which are proportional to the probabilities of moving left, right, up, and down respectively, have the forms,

$$P_1 = \frac{kD}{h^2} - \frac{k\gamma}{4h^2}\left[f^q_{i+1,j} - f^q_{i-1,j}\right],$$

$$P_2 = \frac{kD}{h^2} + \frac{k\gamma}{4h^2}\left[f^q_{i+1,j} - f^q_{i-1,j}\right],$$

$$P_3 = \frac{kD}{h^2} - \frac{k\gamma}{4h^2}\left[f^q_{i,j+1} - f^q_{i,j-1}\right],$$

$$P_4 = \frac{kD}{h^2} + \frac{k\gamma}{4h^2}\left[f^q_{i,j+1} - f^q_{i,j-1}\right].$$

When there is no ECM concentration in the same region as a tumour cell, P_1 to P_4 are equal since the values of f are 0. Also when there is an equal amount of ECM on either side of an tumour cell (i.e., no gradient), the values $f_{i,j-1}$ and $f_{i,j+1}$ cancel each other out as do $f_{i-1,j}$ and $f_{i+1,j}$ and thus P_1 to P_4 are equal. Therefore, in both these circumstances unbiased random movements will be produced. However, if there is more ECM on one side of the tumour cell than the other, the probabilities (P_1 to P_4) will no longer be equal and hence directed movement, towards the higher concentration of ECM, will result.

10.9 References

[1] Ahmad, A., Hanby, A., Dublin, E., Poulsom, R., Smith, P., Barnes, D., Rubens, R., Anglard, P., and Hart, I., Stromelysin 3: an independent prognostic factor for relapse-free survival in node-positive breast cancer and demonstration of novel breast carcinoma cell expression, *Am. J. Pathol.* 152, 721-728, 1998.

[2] Alt, W., Biased random walk models for chemotaxis and related diffusion approximations, *J. Math. Biol.* 9, 147-177, 1980.

[3] Anderson, A.R.A., Solid tumour invasion: the importance of cell adhesion, in *Function and Regulation of Cellular Systems: Experiments and Models*, A. Deutsch, M. Falcke, J. Howard, and W. Zimmermann, Eds., Birkhäuser, Boston, 2003.

[4] Anderson, A.R.A. and Chaplain, M.A.J., Continuous and discrete mathematical models of tumour-induced angiogenesis, *Bull. Math. Biol.* 60, 857-899, 1998.

[5] Anderson, A.R.A., Chaplain, M.A.J., Newman, E.L., Steele, R.J.C., and Thompson, A.M., Mathematical modelling of tumour invasion and metastasis, *J. Theor. Med.* 2, 129-154, 2000.

[6] Anderson, A.R.A., Sleeman, B.D., Young, I.M., and Griffiths, B.S., Nematode movement along a chemical gradient in a structurally heterogeneous environment: II. theory, *Fundam. Appl. Nematol.* 20, 165-172, 1997.

[7] Bafetti, L.M., Young, T.N., Itoh, Y., and Stack, M.S., Intact vitronectin induces matrix metalloproteinase-2 and tissue inhibitor of metalloproteinases-2 expression and enhanced cellular invasion by melanoma cells, *J. Biol. Chem.* 273, 143-149, 1998.

[8] Beattie, G.J. and Smyth, J.F., Phase I study of intraperitoneal metalloproteinase inhibitor BB94 in patients with malignant ascites, *Clin. Cancer Res.* 4, 1899-1902, 1998.

[9] Brown, P.D., Matrix metalloproteinases in gastrointestinal cancer, *Gut* 43, 161-163, 1998.

[10] Byrne, H.M., Chaplain, M.A.J., Pettet, G.J., and McElwain, D.L.S., A mathematical model of trophoblast invasion, *J. Theor. Med.* in press, 2002.

[11] Carter, S.B., Principles of cell motility: the direction of cell movement and cancer invasion, *Nature* 208, 1183-1187, 1965.

[12] Chambers, A.F. and Matrisian, L.M., Changing views of the role of matrix metallopoteinases in metastasis, *J. Natl. Cancer Inst.* 89, 1260-1270, 1997.

[13] Chaplain, M.A.J, The mathematical modelling of tumour angiogenesis and invasion, *Acta Biotheor.* 43, 387-402, 1995.

[14] Chaplain, M.A.J, Avascular growth, angiogenesis, and vascular growth in solid tumours: the mathematical modelling of the stages of tumour development, *Math. Comput. Modelling* 23, 47-87, 1996.

[15] Chaplain, M.A.J. and Anderson, A.R.A., Modelling the growth and form of capillary networks, in *On Growth and Form: Spatio-Temporal Pattern Formation in Biology*, M.A.J. Chaplain, G.D. Singh, J. McLachan, Eds., Wiley, New York, 225-250, 1999.

[16] Chaplain, M.A.J. and Sleeman, B.D., Modelling the growth of solid tumours and incorporating a method for their classification using nonlinear elasticity theory, *J. Math. Biol.* 31, 431-479, 1993.

[17] Chaplain, M.A.J. and Stuart, A.M., A model mechanism for the chemotactic response of tumour cells to tumour angiogenesis factor, *IMA J. Math. Appl. Med. Biol.* 10, 149-168, 1993.

[18] Davis, B., Reinforced random walk, *Probab. Th. Rel. Fields* 84, 203-229, 1990.

[19] Düchting, W., Tumor growth simulation, *Comput. & Graphics* 14, 505-508, 1990.

[20] Düchting, W., Computer simulation in cancer research, in *Advanced Simulation in Biomedicine*, D.P.F. Möller, Ed., Springer-Verlag, Heidelberg, 117-139, 1990.

[21] Düchting, W., Simulation of malignant cell growth, in *Fractal Geometry and Computer Graphics*, J.L. Encarnção, H.-O. Peitgen, G. Sakas, and G. Englert, Eds., Springer-Verlag, Heidelberg, 135-143, 1992.

[22] Düchting, W., Ulmer, W., and Ginsberg, T., Cancer: a challenge for control theory and computer modelling, *Euro. J. Cancer* 32A, 1283-1292, 1996.

[23] Gatenby, R.A. and Gawlinski, E.T., A reaction-diffusion model of cancer invasion, *Cancer Research* 56, 5745-5753, 1996.

[24] Hynes, R.O., Integrins: versatility, modulation, and signalling in cell adhesion, *Cell* 69, 11-25, 1992.

[25] Itoh, T., Tanioka, M., Toshida, H., Yoshioka, T., Nishimoto, H., and Itohara, S., Reduced angiogenesis and tumor progression in gelatinase A-deficient mice, *Cancer Res.* 58, 1048-1051, 1998.

[26] Kim, J., Yu, W., Kovalski, K., and Ossowski, L., Requirement for specific proteases in cancer cell intravasation as revealed by a novel semiquantitative PCR-based assay, *Cell* 94, 353-362, 1998.

[27] Kimmel, M. and Axelrod, D.E., Unequal cell division, growth regulation, and colony size of mammalian cells: a mathematical model and analysis of experimental data, *J. Theor. Biol.* 153, 157-180, 1991.

[28] Kleiner, D.E. and Stetler-Stevenson, W.G., Structural biochemistry and activation of matrix metallo-proteases, *Curr. Opin. Cell Biol.* 5, 891-897, 1993.

[29] Koshiba, T., Hosotani, R., Wada, M., Miyamoto, Y., Fujimoto, K., Lee, J.-U., Doi, R., Arii, S., and Inamura, M., Involvement of matrix metalloproteinase-2 activity in invasion and metastasis of pancreatic carcinoma, *Cancer* 82, 642-650, 1998.

[30] Lacovara, J., Cramer, E.B., and Quigley, J.P., Fibronectin enhancement of directed migration of B16 melanoma cells, *Cancer Res.* 44, 1657-1663, 1984.

[31] Lawrence, J.A. and Steeg, P.S., Mechanisms of tumour invasion and metastasis, *World J. Urol.* 14, 124-130, 1996.

[32] Liotta, L.A., Rao, C.N., and Barsky, S.H., Tumour invasion and the extracellular matrix, *Lab. Invest.* 49, 636-649, 1983.

[33] Marusic, M., Bajzer, Z., Freyer, J.P., and Vuk-Pavlovic, S., Analysis of growth of multicellular tumour spheroids by mathematical models, *Cell Prolif.* 27, 73-94, 1994.

[34] Matrisian, L.M, The matrix-degrading metalloproteinases, *Bioessays* 14, 455-463, 1992.

[35] McCarthy, J.B. and Furcht, L.T., Lamini and fibronectin promote the directed migration of B16 melanoma cells *in vitro*, *J. Cell Biol.* 98, 1474-1480, 1984.

[36] Mignatti, P. and Rifkin, D.B., Biology and biochemistry of proteinases in tumor invasion, *Physiol. Rev.* 73, 161-195, 1993.

[37] Mitchell, A.R. and Griffiths, D.F., *The Finite Difference Method in Partial Differential Equations*, Wiley, New York, 1980.

[38] Orme, M.E. and Chaplain, M.A.J., A mathematical model of vascular tumour growth and invasion, *Math. Comp. Modelling* 23, 43-60, 1996.

[39] Othmer, H. and Stevens, A., Aggregation, blowup, and collapse: the ABCs of taxis and reinforced random walks, *SIAM J. Appl. Math.* 57, 1044-1081, 1997.

[40] Parson, S.L., Watson, S.A., Brown, P.D., Collins, H.M., and Steele, R.J.C., Matrix metalloproteinases, *Brit. J. Surg.* 84, 160-166, 1997.

[41] Paweletz, N. and Knierim, M., Tumor-related angiogenesis, *Crit. Rev. Oncol. Hematol.* 9, 197-242, 1989.

[42] Perumpanani, A.J., Sherratt, J.A., Norbury, J., and Byrne, H.M., Biological inferences from a mathematical model of malignant invasion, *Invasion and Metastases* 16, 209-221, 1996.

[43] Qi, A., Zheng, X., Du, C., and An, B., A cellular automaton model of cancerous growth, *J. Theor. Biol.* 161, 1-12. 1993.

[44] Quigley, J.P., Lacovara, J., and Cramer, E.B., The directed migration of B-16 melanoma-cells in response to a haptotactic chemotactic gradient of fibronectin, *J. Cell Biol.* 97, A450-451, 1983.

[45] Retsky, M.W., Swartzendruber, D.E., Wardwell, R.H., and Bame, P.D., Is gompertzian or exponential kinetics a valid description of individual human cancer growth?, *Medical Hypotheses* 33, 95-106, 1990.

[46] Schor, A.M., Schor, S.L., and Baillie, R., Angiogenesis: experimental data relevant to theoretical analysis, in *On Growth and Form: Spatio-Temporal Pattern Formation in Biology*, M.A.J. Chaplain, G.D. Singh, J. McLachan, Eds., Wiley, New York, 210-224, 1999.

[47] Sehgal, G., Hua, J., Bernhard, E.J., Sehgal, I., Thompson, T.C., and Muschel, R.J., Requirement for matrix metalloproteinase-9 (gelatinase B) expression in metastasis by murine prostate carcinoma, *Am. J. Pathol.* 152, 591-596, 1998.

[48] Sherratt, J.A. and Nowak, M.A., Oncogenes, anti-oncogenes, and the immune response to cancer: a mathematical model, *Proc. R. Soc. Lond. B* 248, 261-271, 1992.

[49] Smolle, J. and Grimstad, I.A., Tumor-cell motility and invasion within tumours determined by applying computer simulation to histologic patterns, *Int. J. Cancer* 50, 331-335, 1992.

[50] Smolle, J., Soyer, H.P., Smolle-Juettner, F.M., Stettner, H., and Kerl, H., Computer simulation of tumour cell motility and proliferation, *Path. Res. Pract.* 186, 467-472, 1990.

[51] Smolle, J. and Stettner, H., Computer simulation of tumour cell invasion by a stochastic growth model, *J. Theor. Biol.* 160, 63-72, 1993.

[52] Stetler-Stevenson, W.G., Aznavoorian, S., and Liotta, L.A., Tumor cell interactions with the extracellular matrix during invasion and metastasis, *Ann. Rev. Cell Biol.* 9, 541-573, 1993.

[53] Stetler-Stevenson, W.G., Hewitt, R., and Corcoran, M., Matrix metalloproteinases and tumour invasion: from correlation to causality to the clinic, *Cancer Biol.* 7, 147-154, 1996.

[54] Stetler-Stevenson, W.G., Krutzach, H.L., and Liotta, L.A., Tissue inhibitor of metalloproteinases (TIMP-2), *J. Biol. Chem.* 264, 17372-17378, 1989.

[55] Thorgeirsson, U.P., Lindsay, C.K., Cottam, D.W., and Gomez, D.E., Tumor invasion, proteolysis, and angiogenesis, *J. Neuro-Oncology* 18, 89-103, 1994.

[56] Tracqui, P., From passive diffusion to active cellular migration in mathematical models of tumour invasion, *Acta Biotheor.* 43, 443-464, 1995.

[57] Wheldon, T.E., Mathematical models in experimental and clinical oncology, in *Mathematical Methods in Medicine*, D. Ingram and R.F. Bloch, Eds., J. Wiley & Sons, New York, 1-32, 1986.

[58] Zeng, Z.S. and Guillem, J.G., Unique activation of matrix metalloproteinase-9 within human liver metastasis from colorectal cancer, *Brit. J. Cancer* 78, 349-353, 1998.

Chapter 11

Cancer Immune System Competition: Modelling and Bifurcation Problems

Nicola Bellomo[1], **Maria Letizia Bertotti**[2], **and Santo Motta**[3]

[1] *Dipartimento di Matematica, Politecnico di Torino (Italy);*
[2] *Dipartimento di Matematica, Universit à di Palermo (Italy);*
[3] *Dipartimento di Matematica, Universit à di Catania (Italy),*
Institute of Immunology, Singapore University (Republic of Singapore)

11.1 Introduction

This chapter deals with the modelling and with some mathematical problems related to the interaction and competition between the immune system and cancer cells. It is well understood that the above competition can play a crucial role in the cancer self-organised defence developed by the immune system, but also in connection with therapeutic actions.

The above competition may possibly end up with the elimination of the host, while in some cases the opposite behaviour is observed. Medical treatments may improve the immune response by activating the immune defence and/or specialising the ability of immune cells to identify the presence of the host.

The interested reader is addressed to the specialised literature, e.g., Delves and Roitt [1], Forni, Foa, and Santoni [2], Greller, Tobin, and Poste [3], and Stout and Suttles [4], to recover information on the immune mechanisms from the viewpoint of molecular biology. Moreover, the article by Perelson and Weisbuch [5] provides a review of various mathematical models developed by applied physicists, while some divulgative articles, e.g., Nossal [6], and Kleinstein and Seiden [7], are addressed to a non specialised audience.

The physical system we are dealing with is characterised by a great complexity so that it is very difficult, maybe impossible, developing a detailed mathematical description of all phenomena related to the immune competition. On the other hand, if a certain type of interaction is specialised, one may attempt to develop models suitable to describe specific phenomena at the observation and representation scale which is selected for the modelling process.

As usual in applied mathematics, see Bellomo and Preziosi [8], different scales can be selected toward the mathematical modelling of the same phenomenon. Specifically, one may represent the immune mechanisms referred to cellular and subcellular scales by observing the interaction and competition processes for various cell populations which play the game. On the other hand, pursuing the aim of reducing complexity, one may consider the evolution of the statistical distribution over the biological activities of the cell populations. A further simplification, again of the complexity of the system, consists in looking at the system by considering each cell population as a whole, while its behaviour is observed collectively.

In all cases, the main problem consists in deriving suitable evolution equations toward the description of a complex system which appears to be somehow reluctant to be constrained into a mathematical framework. While complexity is reduced, applied mathematicians have to deal with the problem of identifying the pertinent parameters which may lose biological meaning through the above simplification.

This chapter reports about the state-of-the-art, essentially related to the mathematical literature, on the above outlined topics. Special attention is paid to the proper reference to the above mentioned representation scales. The review will be developed by a selection and critical analysis of research papers which apply different methods to model the immune competition in the presence of neoplastic cells.

The contents will also refer to research perspectives in the field. Hopefully, applied mathematicians will recover in this chapter indications toward future research activity.

The analysis will pay attention to bifurcation phenomena which identify two different asymptotic behaviours of the solution of mathematical models: blow-up of tumour cells related to a progressive deactivation of the immune system; or, conversely, progressive destruction of tumour cells related to immune cells which remain active. Indeed, in order to remain active, tumour cells need both feeding from environmental cells and inhibition of the immune system. On the other hand if the immune system remains active, then it ends up able to destroy tumour cells.

Particularly relevant is the ability of the model to refer the above bifurcation phenomena to specific parameters with well-defined biological meaning. When this is possible, then therapeutic actions can be developed to activate the immune system to prevent its inhibition. On the other hand, when this action is not technically possible, medical action may be addressed to weaken the progression of tumour cells so that the immune competition against the aggressive and invasive host may exhibit the desired asymptotic behaviour.

The contents are organised through five more sections which follow this introduction.

Section 11.2 deals with a concise phenomenological description of the physical system which is the object of the modelling process. The description is based on the viewpoint of mathematicians, while technical aspects of biomolecular theories are left to the specialised literature.

Section 11.3 deals with the modelling at the cellular scale, namely with models at the microscopic scale. Specifically, after providing a concise review of the state-of-the-art, this section mainly refers to generalised shape models. These models are based on the idea that cells can recognise the host by receptors able to recognise certain shapes on the surface of host cells.

Section 11.4 contains a report on the so-called kinetic cellular theory which looks at the statistical distribution over the biological state of the various interacting populations. This type of modelling is based on mathematical methods which are typical of the kinetic theory of gases [9], and develops equations which show a substantial similarity with the Boltzmann or Vlasov equations. This class of model is called generalised kinetic (Boltzmann) models [10]. As shown in the book edited by Bellomo and Pulvirenti [11], these models can be developed to describe a variety of large systems in applied sciences.

Section 11.5 reports about finite models which simplify the real physical system by representing the collective behaviour of each cell population which play the game. This crude simplification generates, as we shall see, models which are stated in terms of ordinary differential equations. The qualitative and quantitative analysis of the solutions may, despite the above simplification, provide useful information on the overall behaviour of the system.

Section 11.6 finally develops a critical analysis on the contents of the chapter, and addresses it to the indication of conceivable research perspectives. Indeed the math-

ematical approach to the modelling and analysis of the complex physical system we are dealing with is the object of a growing interest from the side of applied mathematicians. New mathematical results keep appearing in the literature, and a significant number of interesting results have appeared after the book by Adam and Bellomo [12].

The authors' aim consists not only in offering a survey of the state-of-the-art in the field of the competition between immune and neoplastic cells, but also in developing a critical analysis of the literature with the aim of indicating research perspectives. Hopefully, the contents of this chapter will contribute to a further increase of the attention of applied mathematicians toward the above interesting and stimulating new frontier of applied mathematics.

11.2 Phenomenological Description and Scaling

Immune competition is a complex phenomenon which involves cells or particles of the aggressive hosts and cells of the various populations of the immune system. In order to avoid ambiguities related to a frequent use and, maybe abuse, of the word complexity, it is worth mentioning that here this term is applied to state that interactions are developed at different scales: the cellular dynamics are ruled by subcellular interactions. Moreover different mechanisms operate on the same subject: mechanical for the dynamics and biological for the immune competition. The proliferation ability of the host and the defence ability of the immune system are common features of the competition. In addition, the ability to inhibit the recognition process plays a significant role in the competition against tumour cells, which is contrasted by immune cells operating with different specialised activities.

The interested reader is addressed to the specialised literature, among others, to the already quoted review papers [1] and [2] and divulgative article [6], which can contribute to the understanding of the above phenomena from the side of applied mathematicians and physicists. On the other hand, a careful description of immune competition by means of the language and know-how of medicine and immunology is not an aim of this chapter. Simply we attempt to focus on those features which are useful to develop a mathematical modelling of the above complex system.

The evolution of a cell, as described by various authors, e.g., Forni et al. [2], is regulated by the genes contained in its nucleus. These genes can either be activated or suppressed, when signals stimulate receptors on the cell surface and are then transmitted to the nucleus of the cell. The reception of a particular signal can modify the usual behaviour of a cell. In extreme situations, a particular signal can induce a cell to reproduce itself in the form of identical descendants giving rise to the so-called clone expansion or mitosis, or to die giving rise to the so-called apoptosis or programmed death.

Some theories state that genetic changes, distortion in the cell cycle and loss of

apoptosis are related to DNA corruption, which may even be determined by external actions. Then an interaction and competition at the cellular level is developed, which includes activation, but also inhibition of the immune system. Later, if the number of degenerated cells increases significantly, various phenomena such as condensation of tumour cells into solid forms, macroscopic diffusion, and angiogenesis, can be observed, followed by detachment of metastases and invasion.

The key objective of the mathematical research in the field is the development of a mathematical theory able to describe the interaction and competition between tumours and the immune system, e.g., by means of evolution equations. The dynamics of tumours growth follows. Probably, the above ambitious project will take many years involving a truly multidisciplinary approach. At present research activity simply refers to modelling specific phenomena and to the qualitative analysis and simulations related to their application. However, even at this level challenging mathematical problems are brought to the attention of applied mathematicians.

Referring to the modelling aspects, it is well understood that one has to deal with multiscale modelling and simulations relating to the interaction processes acting on a range of different spatio-temporal scales. Specifically, the characterisation of the system suggests the identification of three natural scales which are also connected to different stages of the disease: processes on the cellular scale are triggered by signals stemming from the sub-cellular level and have an impact on the macroscopic scale, i.e., on the organism, as tumour cells condense and when tumours grow and spread.

At the sub-cellular scale the evolution of a cell is regulated by the genes contained in its nucleus. Receptors on the cell surface can receive signals which are then transmitted to the cell nucleus, where the genes can be activated or suppressed. In extreme situations, particular signals can induce a cell to reproduce itself, or to die. Clone expansion activates a competitive-cooperative interaction between tumour cells and cells of the immune system. If the immune system is active and able to recognise the tumour cells, then it may be able to develop a destruction mechanism; otherwise, tumour growth may develop progressively. The activation and deactivation of immune cells, too, can be regulated by cytokine signals.

At the cellular scale models are proposed to simulate the effects of the failure of programmed cell death and of the loss of cell differentiation. If and when a tumour cell is recognised by immune cells, a competition starts which may end up either with the destruction of tumour cells or with the inhibition and depression of the immune system. Cellular interactions are regulated by signals emitted and received by cells through complex image recognition processes. Therefore, the connection to the sub-cellular scale is evident. On the other hand, the development of tumour cells, if not suppressed by the immune system, tends towards condensation into a solid form so that macroscopic features become important.

At the macroscopic scale, tumour cells start to condense and aggregate into an entity with "quasi fractal surface" which interacts with the outer environment, for example normal host cells and the immune system. These interactions usually occur on the surface and within a layer where angiogenesis (the process of formation of new blood vessels, induced by factor secreted by the tumour, and vital for tumour

growth) takes place. Here, one has the overlap of phenomena at the cellular level with typical macroscopic behaviour such as diffusion or, more generally, phenomena that can be related to the conservation or evolution of macroscopic variables such as the tumour size. In a later stage, as described in Chapter 4 of this volume, the tumour can be characterised by three zones: an external layer in which environmental cells penetrate and determine the detachment of tumour cells; an intermediate layer in which there are clusters of quiescent tumour cells; and an inner zone containing necrotic cells.

Phenomena identified at a certain scale can be related also to the higher or lower scales. For instance, interactions, developed at the cellular level, are ruled by processes which are performed at the sub-cellular scale. Moreover, activation and inhibition of cells belonging to the tumour and to the immune system can also be induced.

Different mathematical methods and structures correspond to the above scales. For instance models at the cellular scale are developed in terms of ordinary differential equations, while multicellular systems are modelled by nonlinear integro-differential equations similar to those of nonlinear kinetic theory (the Boltzmann equation). On the other hand, macroscopic models refer to moving boundary problems for systems of nonlinear partial differential equations. Nonlinearity is an intrinsic feature of all models. The analysis of mathematical problems generated by the above models leads to several sophisticated mathematical problems: some of them will be reported in this chapter.

The above naive description retains some aspects of the way of thinking of an applied mathematician, who has in mind transferring the phenomenological observation into equations. No problem in admitting that an immunologist can be highly disappointed by this attitude. He will deeply look at a certain phenomenon without an immediate aim to transfer this observation into mathematical equations.

When the phenomenological description becomes very detailed, transferring it into mathematical equations may become a very difficult task. On the other hand, accepting that a mathematical model may be based only on a limited amount of phenomenological information, still one may expect from a model the ability to describe phenomena which are not observed experimentally.

Although this chapter is mainly concerned with modelling at the cellular scale, it is worth recalling that the immune competition appears also when cancer cells condense in a solid form while immune cells operate on the outer surface and diffuse inside the solid form. Indeed, immune cells penetrate into tumours and complex interaction phenomena follows. Some perspectives on this interesting topic will be given in the last section.

11.3 Modelling at the Cellular Scale

This section provides a review of models suitable to describe the immune competition at the microscopic scale. Modelling the behaviour of the immune system at the cellular scale is tackled by many authors using a variety of different techniques and with a variety of different aims. The first aim of modelling consists in reproducing the immune response (primary and secondary response). However many other aspects like the auto-immune disease, selection and hyper-mutation of antibodies during an immune reaction auto-immunity, and T-lymphocytes selection in thymus, etc. are studied in the literature and are the object of modelling efforts.

In this general framework modelling the response to known virus-inducing cancer can contribute to the study of cancer vaccines, see e.g., Van der Burg, Offringa, and Melief [13]. Of course, various models are dedicated to study HIV infections, while the activation of the immune response in some cancers has been known since the 1950s. Studies in this area have shown that tumour cells do have an escape-mechanism that prevents the activation of the immune system, see Anichini and Mortarini [14].

The panorama of immune system models is quite large. All models are essentially developed within the framework of the two biological exiting theories, namely the clone selection theory and the idiotypic network theory.

The clone selection theory of the Nobel Prize laureate Frank M. Burnet [15] was developed following the track first highlighted by Paul Ehrlich at the beginning of the 20^{th} century. The theory of the clone selection states that the immune response is the result of a selection of the "right" antibody by the antigen itself, much like the best adapted individual is selected by the environment in the theory of natural selection of Charles Darwin. The selected subset of B cells (and T cells) grows and differentiate; they then turn off when the antigen concentration falls below some threshold. In the framework of this theory, memory B cells will be responsible for acquired immune tolerance.

The idiotypic network theory was formulated by the Nobel Prize laureate Nielse K. Jerne [16]. According to the idiotypic network theory, the immune system is a regulated network of molecules and cells that recognise one another even in the absence of antigens. The idiotypic network hypothesis is based on the concept that lymphocytes are not isolated, but communicate with each other among different species of lymphocytes through interaction among antibodies. Accordingly the identification of antigens is not done by a single recognising set but rather by a system-level recognition of the sets connected by antigen-antibody reaction as a network. Jerne [16] suggested that during an immune response antigen would directly elicit the production of a first set of antibodies, Ab_1. These antibodies would then act as antigens and elicit the production of a second set of "anti-idiotypic" (anti-id) antibodies Ab_2 which recognise idiotopes on Ab_1 antibodies, and so forth.

Nowadays immunologists consider these two theories as independent, nonconflicting, and eventually complementary theories, see [17]. However while clone se-

lection theory is believed to be the fundamental theory for understanding today's knowledge of the immune system, the idiotypic network theory is believed reliable related to the existence of anti-idiotypic reactions, but probably is not relevant in the control of the immune response, see [18].

In what follows we will point out only the main ideas that can guide the reader in the wide literature of the discrete modelling of the immune system. First we will sketch a few leading models based on cellular automata, and then, we will discuss in some detail the Celada-Seiden model [19], which tries to reproduce the behaviour of the immune system at the cellular scale in a sort of *ab initio* computation. Recent extensive reviews on discrete models of the immune system can be found in [5], [17], and [20].

11.3.1 An Overview of Discrete Models

While continuous models have been formulated in the framework of both immunological theories (see [5] and Perelson [21]), discrete models are mostly based on Jerne's theory [16]. Celada-Seiden's [19] model, which may include both theories, rests its foundation on the clone selection theory.

The main task of the immune system is to perform a pattern recognition between cell receptors and antigens. The binding mechanism, mostly unknown in details, is based on different physical effects (short range noncovalent interactions, hydrogen binding, van der Walls interactions, and so on). In order for a receptor and the molecule that it binds, a ligand, to approach each other over an appreciable portion of their surfaces, there must be extensive regions of complementarity. As documented in [7], Oster and Perelson called the constellation of features important in determining binding among molecules the generalised shape of the molecules. Assume that this shape can be described by η parameters; then a point in a η-dimensional space (shape space) specifies the generalised shape of a receptors binding region. On the basis of these considerations Oster and Perelson estimated that in order to be complete the receptor repertoire should satisfy the following conditions:

- Each receptor can recognise a set of related epitopes, each of which differs slightly in shape.
- The repertoire size is of the order of 10^6 or larger.
- At least a subset of the repertoire size is distributed randomly throughout the shape space, see [5].

Later, Farmer, Packard, and Perelson [22] introduced the idea of using binary strings to represent the shape of a receptor. To determine the degree of complementarity between strings many string-matching algorithms are available. These representations have been used in most discrete models.

Discrete models of the immune system have been built up using different techniques. Models based on cellular automata and lattice gas go back to the last two

decades. These model are the most used nowadays and produce interesting results, see [17]. We will shortly describe some of these models in what follows. Models based on spin-glass formalism have been proposed by Parisi, by the end of the 1980s, as documented in [5].

Genetic algorithm-based models have been mainly investigated at the Santa Fe Institute and at the University of New Mexico by Forrest and co-workers, see the review [20] starting in the early 1990s, and [5]. This is a computer science driven approach which brings into the field the experience of computer scientists. The guiding line of this approach is a deeper comprehension of the immune system in order to use the information processing algorithm in applications [20]. Applications can be found in Dasgupta [23].

11.3.2 Automata-Based Models

We now consider in more detail some automata-based models. Since an exhaustive review is beyond the aim of this section we will present only a few of the most representative models. Specifically, the Kaufman, Urbain, and Thomas model (KUT) is one of the first applications of discrete automata to investigate the logic of the normal immune response and introduced in [24].

These authors were interested in the simplest way to describe the logic of interactions among a number of different cell types and their results in terms of immune response. The original model considers five types of cells and molecules: antibodies (Ab), helper cells (Th), suppressor cells (Ts), lymphocytes B (B), and antigens or virus (Ag). Each entity is represented by a boolean variable denoting "spin up" (high concentration) and "spin down" (low concentration). The rules modelling the dynamic evolution of these variables are expressed by logical operations. The application of the rules is iterated over discrete time and the dynamics is observed. The discrete evolution rules are:

$$Ab(t+1) = Ag(t) \quad \text{AND} \quad B(t) \quad \text{AND} \quad Th(t)\,, \tag{11.1}$$

$$Th(t+1) = Th(t) \quad \text{OR} \quad Ag(t) \quad \text{AND NOT} \quad Ts(t)\,, \tag{11.2}$$

$$Ts(t+1) = Th(t) \quad \text{OR} \quad Ts(t)\,, \tag{11.3}$$

$$B(t+1) = Th(t) \quad \text{AND} \quad (Ag(t) \quad \text{OR} \quad B(t))\,, \tag{11.4}$$

$$Ag(t+1) = Ag(t) \quad \text{AND NOT} \quad Ab(t)\,. \tag{11.5}$$

where AND, OR, and NOT are the usual logical operators. There are five fixed points in the state space composed by $2^5 = 32$ points. Fixed points identify the global state of the immune system: naive, vaccinate, immune, paralysed, and paralysed and sick.

Later on, one has to acknowledge the Weisbuch and Atlan model (WA) [25], which was subsequently followed by many other models. Such a model was proposed on the basis of Jerne's theory to study the special case of auto-immune diseases, like multiple sclerosis, in which the immune system attacks the cells of the

nervous system of our own body. As in [24], this model uses five binary variables representing: killer cells (S_1), activated killers (S_2), suppressor cells (S_3), helpers (S_4), and suppressor produced by the helpers (S_5). The binary state of each threshold automaton represents the concentration of the corresponding cell type: 0 corresponds to small concentration, and 1 to high concentration. The different types of cells influence each other with a strength which is 1, 0, or -1. The automaton evolves with the following rule: at the next time step, the concentration of one cell is unity if the sum of the interactions with the various cell types is positive, otherwise the concentration is taken as zero. Let $\mathbf{S} = \{S_1, S_2, S_3, S_4, S_5\}$ be the vector representing the five binary variables and

$$\mathbf{A} = \begin{bmatrix} 1 & 0 & -1 & 1 & 0 \\ 1 & 0 & -1 & 1 & 1 \\ 1 & 0 & 0 & 0 & 0 \\ 1 & 0 & 0 & 0 & 0 \\ 0 & 0 & 0 & 1 & 0 \end{bmatrix} \tag{11.6}$$

the matrix of the synaptic connections; then the evolution of WA network [25] can be described by:

$$\mathbf{S}(t+1) = \text{sgn}\left(\mathbf{A} \cdot \mathbf{S}(t)\right) \ , \tag{11.7}$$

where the function sgn(x) defined on the natural numbers set $\mathbf{N}$ is 1 for $x > 0$ and 0 otherwise.

This model shows the existence of only two basins of attractions over $2^5 = 32$ possible states: the empty state where all the concentrations are zero and the state 10111 where activated killers have small concentration while the other four entities have high concentrations. This corresponds to a healthy carrier state, with killer cells only in the resting state, thus unable to harm the organism by developing an active autoimmune reaction.

Neumann, as documented in [17], studied a different version of KUT model using a boolean and a threshold automata which includes interactions with antigens. Dayan et al., again as documented in [17], extended the WA model using the same dynamics but placing the cells on a two-dimensional lattice to allow simulations in a statistical physics way (Ising-like models). In Dayan et al. the authors use five variables on each lattice site corresponding to five boolean concentrations (0 or 1). The model can be classified as an integer lattice gas with $r = 5$ (five entities) and $K = 2$ (two states per entity). Each site influences itself and its nearest neighbours in the same way as in the WA model. For a square lattice of $L \times L$ sites there are $5 \times L^2$ spins. The main difference is that in this model the evolution of a single site includes the site itself and its nearest neighbours. This lattice-version of the WA model is found to have simpler dynamics than the original model as the number of fixed points is found to be smaller than in [25]. The three dimension extension of the model was done by Wiesner, see the review [17].

Chowdhury et al., as documented in [17] and [23], proposed a unified model of the immune system which recovers, as special cases, the KUT an WA models. The model describes the immune response to HIV and reproduces some features of

experimental results. Extensions of this network approach for modelling HIV and cancer have been discussed, see [17], by Chowdhury and Stauffer.

A majority rule cellular automata was used by Agur [26] to study the signal processing in the IS in a multilayered network. Chowdhury et al., see [17], proposed a model to describe the interaction between various type of immunocomponent cells considering intra- and inter-clone interactions. Many other CA approaches to study different aspects of IS can be found in Perelson [21] and in the book edited by Atlan and Cohen [27].

11.3.3 Shape Space Model Approach

A series of models, see [5], use the shape space approach. Each point of the d-dimensional Euclideian space is associated with a different receptor's generalised shape and, as mentioned before, each coordinate represents one of the main aspects involved in pattern recognition. Most of these models are represented on a two dimensional cellular automata.

The first of these models was proposed by Stewart and Varela [28]. They used a bit-string model in a two dimensional shape space to analyse the metadynamics in which new clones are constantly generated in the bone marrow.

De Boer, Van der Laan, and Hogeweg [29] considered a two dimensional cellular automata model with binary variables and majority rule to describe the concentration of the population with lattice site. This model, as documented in [17], was extended to higher dimensions and very large lattices.

De Boer, Segel, and Perelson (BSP model) proposed a model to describe the time evolution of the immune repertoire. The model, as documented in [30], is the discrete version of a set of population equations.

Each automaton, in this model, describes the time evolution of the concentration of a given clone. The update of the variables associated with the concentration of each clone is based on an activation window driven by a function of a field which depends on the concentration of the populations with complementary shapes of receptors. BSP considered only one and two dimensional lattices and obtained only stable behaviours.

11.3.4 The Celada-Seiden Model

One of the most prominent attempts to reproduce, with the quest for biological fidelity, is the Immune Simulator automaton, also known as the Celada-Seiden model developed in [19] and [31]. The Immune Simulator belongs to the class of immunological cellular automata, but its degree of sophistication sets it apart from simpler CA in the Ising-like class [24].

The Celada-Seiden model explicitly implements the cellular and humoral im-

mune response in one comprehensive set of rules which apply to a variety of cellular and molecular entities. In particular, these include the following cells: lymphocyte B (B), lymphocyte T helper (Th), lymphocyte T killer (cytotoxic) (Tk), macrophage (MA), epithelial cell (as generic target cell) (EP), lymphocyte plasma B (PLB); and the molecules: antigen (bacteria or generic virus) (Ag), antibody (Ab), and immune complexes or Ab-Ag binding (IC). On top of that, some intracellular signals are explicitly represented like for example, interferon-γ (IFN) and danger signal (D), while other cytokines are just "implicitly" taken into account in the interaction rules. The major difference among cellular and molecular entities is that cells may be classified on the basis of a state attribute. The state of a cell is an artificial label introduced by the logical representation of the cell's behaviour.

The model represents a portion of a lymph node of a vertebrate animal as a two-dimensional triangular lattice (six neighbour sites) $L \times L$, with periodic boundary conditions in both directions (up-down, left-right).

The Celada-Seiden model is based on the theory of the clone selection. For this reason, Celada and Seiden [19] had to look for a way to represent the lymphocytes' receptors shape space. The idea of using a bit string to encode the information relative to the specificity to the antigens came from the early work of Farmer et al. [22].

In the Celada-Seiden model a clonotypic set of cells is characterised by the receptor which is represented by a bit-string. The bit-string length l is clearly one of the key parameters in determining both time and space complexity of the algorithm that simulate the behaviour of the whole set of entities as the number of potential repertoire of receptors scales as 2^l (see [32]).

The bonds among the entities are described in terms of matching between binary strings with fixed directional reading frame. Bit strings represent the generic "binding site" of both cells (read the receptor) and molecules (that is peptides, epitopes). Every entity is represented by a certain number of molecules, the receptor being one of these. The repertoire is then defined as the cardinality of the set of possible instances of entities that differ in, at least, one bit of the whole set of binary strings used to represent its attributes.

Indeed, the cells equipped with binding sites and antibodies, have a potential repertoire of $2^{N_e l}$, where N_e indicates the number of binary strings used to represent receptors, MHC-peptide complexes, epitopes and so on, of the entity e. Other entities do not need to be specified by binary strings so their repertoire is just one (i.e., $N_e = 0$). Examples are the interleukin molecules like the interferon$-\gamma$ and the danger signal.

In this model two entities equipped with receptor interact with a probability which is a function of the Hamming distance between the binary strings representing the entities' binding site. This probability is called the affinity potential. For two strings s and s' such probability is max (i.e., equal to 1) when all corresponding bits are complementary ($0 \leftrightarrow 1$), that is, when the Hamming distance between s and s' is equal to the bit string length. A good and widely used analogy is the match between a lock and its key.

If l is the bit string length and m is the Hamming distance between the two

strings, the affinity potential is defined in the range $0, \ldots, l$ as

$$\upsilon(m) = \begin{cases} \upsilon_c^{\frac{m-l}{m_c-l}} & m \geq m_c; \\ 0 & m < m_c; \end{cases} \tag{11.8}$$

where $\upsilon_c \in (0, 1)$ is a free parameter which determines the slope of the function whereas $m_c \in (l/2, l]$ is a cut-off (or threshold) value below which no binding is allowed.

Equipped with their receptors, the cells are free to diffuse on the lattice sites. At each time step, representing 8 hours of real time, cells and molecules residing on the same lattice site take the chance to interact among each other. The rules which implement these reactions are executed in a randomised order. Using immunological terms, they can be grouped as follows [33]:

- Phagocytosis comprise the rules for the activity of antigen processing cells.
- Immune-activation codes for the activity of helper T lymphocytes which recognise the MHC-peptide complex and activate, by releasing cytokines, B cells for antibody production.
- Opsonisation regards the inactivation of the antigen by binding of antibodies.
- Infection is the action of virus.
- Cytotoxicity stays for all those rules which account for the kill of the virus-infected cells by cytotoxic cells.

To complete this very short description of the model we mention the mechanism of hematopoiesis. This takes into account both the generating activity of pluripotent stem cells in the bone marrow which is realised by randomly adding newly formed cells periodically (a mean-reverting process is implemented to assure that in absence of antigenic stimulus, the number of cells is in a steady state), and the selective activity of the thymus for what concerns the positive and negative selection of T lymphocytes to avoid autoimmune reactions.

It is worth noticing that the model, as it is constructed, is modular, in the sense that it allows for the addition or the modification of the cellular and molecular entities together with the set of rules determining their behaviour, to study different phenomena. Indeed this flexibility of the model has been exploited to realise a simulator of the HIV infection, one for the hypersensitive reactions, and the effect of the apoptosis mechanism on the immune response as it will be illustrated later in this section. Moreover, as shown in [30] and [35], the model results to be independent of the computational framework used for the simulator.

The model, with such a degree of detail, has been first used to address different questions revealing its versatility already in the first publication by Celada and Seiden [19]:

- What is the largest self fraction of the total repertoire that is still compatible with reasonable alloreactivity?

- Why is the number of different MHC per individual so small (about four to six)?
- Why is the diversity of MHC molecules in a population so small compared to the possible diversity?

In [35] a modification of the Celada-Seiden model has been used to study the apoptosis mechanism. This work was driven by the *in vitro* experiments performed by Jamin et al. [36]. In this case a subset of B-cell was allowed to present also B-CD5 receptors and the behaviour of these receptors was modelled according to [36]. During the simulation this subset was stimulated, as in the experiment, with two injections of anti-CD5 antibodies. This *naive* model showed good qualitative agreement with experimental results.

Another modification of the Celada-Seiden model which is described in this volume in the chapter by Castiglione and Agur, has been used to study hypersensitivity to a drug during anticancer treatment. In that case a major modification was to introduce the explicit representation for a number of cytokines (IL-4, IL-12, IL-2, and IFN-γ), the subdivision of T helper cells in three classes (Th1, Th2, and Th0 or Th1/2 precursor), the subdivision of the antibodies in immunoglobulins IgE, IgG, and IgM, and the addition of mast cells which are in charge for the release of histamine and other active mediators responsible for the symptoms of type I or IgE mediated allergy.

11.4 Modelling by Generalised Boltzmann Models

The competition between immune cells and aggressive hosts has been modelled also by methods which are typical of nonequilibrium statistical mechanics. The above approach was first proposed by Bellomo and Forni [37] and subsequently developed by various authors as documented in the review papers by Bellomo and De Angelis [38]. The pertinent bibliography is reported in the above cited papers. The various models proposed in the literature may differ for technical aspects, but all refer to the mathematical framework reported in Arlotti, Bellomo, and De Angelis [39].

The substantial difference with respect to the equations of the kinetic theory is that the microscopic state of the cells is defined not only by mechanical variables, say position and velocity, but also by an internal biological microscopic state related to the typical activities of the cells of a certain population.

The above mentioned models are characterised by localised microscopic interactions. This means that cells interact when they are practically in contact. On the other hand, an alternative to the above modelling was proposed by De Angelis and Mesin in [40], where it was assumed that interactions are distributed in space. This paragraph refers specifically to this type of modelling which appears to be able to provide interesting descriptions from the biomolecular point of view.

As stated in the introduction, special attention will be paid to bifurcation phenomena which may define the output of the competition: activation of the immune system with depletion of the tumour cells, or inhibition of the immune system with uncontrolled growth of the tumour cells.

The contents of this section is organised into four subsections. The first one deals with the description of cell populations and their statistical description. The second one with the design of a mathematical framework suitable to generate specific models. The third one with the description of a specific model, while the last one reports some simulations related to the above mentioned bifurcation analysis.

11.4.1 Cell Populations

The immune competition involves several interacting populations each one characterised by a microscopic internal state which may differ from one population to the other. In fact, the dynamics involve at least cells of the immune system and cells of the aggressive host in the presence of environmental cells. However, in some cases, one may even specialise the immune system into various subpopulations characterised by specific activities.

The contents proposed in what follows refers to a system of three interacting populations: cancer, immune, and environmental cells. It is plain that technical generalisations are possible as it will be discussed in the last section. For instance immune cells can be distinguished into a greater number of populations each characterised by specific activities, see Arlotti, Gamba, and Lachowicz [41]. The limitation to only three populations is due here to the choice, of this section, to refer essentially to the model proposed in [40]. Despite a relative simplicity with respect to others, this model provides a detailed description of some interesting biological phenomena.

The so called kinetic (cellular) theory developed as a generalisation either of the Boltzmann or of the Vlasov equation (for large systems of cells) is such that the microscopic state is defined by the vector variable which includes both mechanical and biological microscopic states:

$$\mathbf{w} = \{\mathbf{x}, \mathbf{v}, \mathbf{u}\} \in \mathcal{D} = D_{\mathbf{x}} \times D_{\mathbf{v}} \times D_{\mathbf{u}} \,, \tag{11.9}$$

where the position $\mathbf{x} \in D_{\mathbf{x}}$ and the velocity $\mathbf{v} \in D_{\mathbf{v}}$ are the microscopic mechanical variables, and $\mathbf{u} \in D_{\mathbf{u}}$ characterises the microscopic internal biological state of the cells.

Consider then a system of several interacting populations each labelled with the subscript i. The distribution functions refer to each cell population

$$f_i = f_i(t, \mathbf{w}) \,:\, \mathbb{R}_+ \times \mathcal{D} \to \mathbb{R}_+ \,, \quad i = 1, 2, 3 \,. \tag{11.10}$$

Interactions modify not only position and velocity, but also the above mentioned microscopic internal state. Conversely, such a state may affect mechanical interactions. Generally, not only interactions can modify the microscopic state. They can also generate proliferation or suppression phenomena.

It can be shown how macroscopic observable quantities can be recovered by suitable moments of the above distribution functions. The number density of cells or the size, at time t and position $\mathbf{x}$ is given, under suitable integrability properties, as follows:

$$n_i(t, \mathbf{x}) = \int \int_{D_\mathbf{u} \times D_\mathbf{v}} f_i(t, \mathbf{x}, \mathbf{v}, \mathbf{u})\, d\mathbf{v}\, d\mathbf{u}\ , \tag{11.11}$$

while the total number of cells at time t in a domain $D_\mathbf{x}$ is given by

$$N(t) = \sum_{i=1}^{3} \int_{D_\mathbf{x}} n_i(t, \mathbf{x})\, d\mathbf{x}\ . \tag{11.12}$$

In addition to the above quantities, it is possible to compute mechanical quantities such as local momentum and energy, respectively given by

$$\mathbf{q}_i(t, \mathbf{x}) = \tfrac{1}{n(t,\mathbf{x})} \int \int_{D_\mathbf{u} \times D_\mathbf{v}} \mathbf{v} f_i(t, \mathbf{x}, \mathbf{v}, \mathbf{u})\, d\mathbf{v}\, d\mathbf{u}\ , \tag{11.13}$$

$$e_i(t, \mathbf{x}) = \tfrac{1}{n(t,\mathbf{x})} \int \int_{D_\mathbf{u} \times D_\mathbf{v}} v^2 f_i(t, \mathbf{x}, \mathbf{v}, \mathbf{u})\, d\mathbf{v}\, d\mathbf{u}\ , \tag{11.14}$$

where

$$n(t, \mathbf{x})) = \sum_{i=1}^{3} n_i(t, \mathbf{x})\ . \tag{11.15}$$

Marginal densities such as the number density of the subjects at time t, with position $\mathbf{x}$ and internal state $\mathbf{u}$ is given by the distribution

$$p_i(t, \mathbf{x}, \mathbf{u}) = \int_{D_\mathbf{v}} f_i(t, \mathbf{x}, \mathbf{v}, \mathbf{u})\, d\mathbf{v}\ , \tag{11.16}$$

and the number density at time t and internal state $\mathbf{u}$ in the whole domain $D_\mathbf{x}$ is given by

$$q_i(t, \mathbf{u}) = \int_{D_\mathbf{x}} p_i(t, \mathbf{x}, \mathbf{u})\, d\mathbf{x}\ . \tag{11.17}$$

Similar calculations can be developed for higher order moments. Global quantities are obtained integrating over the space variables.

11.4.2 A Mathematical Framework

As already mentioned, the models described in this section were developed in a framework corresponding to a mean field description which may be considered as a sort of generalisation of the Vlasov equation.

Referring to [40], the evolution equation is derived supposing that it is possible to model the following two quantities:

- The action $\mathcal{P} = \mathcal{P}(\mathbf{w}, \mathbf{w}_*)$ on the subject with microscopic state $\mathbf{w}$ due to the subject with state $\mathbf{w}_*$, so that the resultant action is

$$\mathcal{F}[f](t, \mathbf{w}) = \int_{\mathcal{D}} \mathcal{P}(\mathbf{w}, \mathbf{w}_*)\, f(t, \mathbf{w}_*)\, d\mathbf{w}_* \,. \tag{11.18}$$

- The term describing proliferation/destruction phenomena in the state $\mathbf{w}$ related to pair interactions between cells of the i-th population with microscopic state $\mathbf{w}^*$ with cells of the k-th population with state $\mathbf{w}^{**}$:

$$\mathcal{S}[f](t, \mathbf{w}) = \int_{\mathcal{D}} \int_{\mathcal{D}} \sigma(\mathbf{w}^*, \mathbf{w}^{**}; \mathbf{w})\, f_i(t, \mathbf{w}^*)\, f_k(t, \mathbf{w}^{**})\, d\mathbf{w}^*\, d\mathbf{w}^{**} \,, \tag{11.19}$$

  where σ is a suitable proliferation–destruction function.

Therefore, the mean field equation for a system of three interacting populations neglecting external actions and sources is given by

$$\begin{aligned} &\frac{\partial f_i}{\partial t} + \nabla_{\mathbf{w}} \cdot \Big(\sum_{k=1}^{3} \mathcal{F}_{ik}[f] f_k\Big) \\ &\quad = \sum_{k=1}^{3} \int_{\mathcal{D}} \int_{\mathcal{D}} \sigma_{ik}(\mathbf{w}^*, \mathbf{w}^{**}; \mathbf{w})\, f_i(t, \mathbf{w}^*)\, f_k(t, \mathbf{w}^*)\, d\mathbf{w}^*\, d\mathbf{w}^{**} \,. \end{aligned} \tag{11.20}$$

The above general framework is the one exploited, in a relatively simpler form, in [40]. Such a simplified framework is obtained as follows:

- Interactions between a test cell and a field cell are homogeneously distributed in space. They may change the state of the cells and destroy or create cells.

- The microscopic state is a scalar $u \in [0, \infty)$ and has a different meaning for each population: progression for tumour cells, defence ability for immune cells, and feeding ability for environmental cells.

- The action of the field cells in the state w of the k-th population on the test cells of the i-th population in the state u is modelled by the superposition of two different actions: a conservative action modelled by the function $\varphi_{ik} = \varphi_{ik}(u, w)$ such that its resultant action is

$$\mathcal{F}_i[\mathbf{f}](t, u) = \frac{\partial}{\partial u}\left[f_i(t, u) \sum_{k=1}^{3} \int_0^{\infty} \varphi_{ik}(u, w) f_k(t, w)\, dw \right] , \tag{11.21}$$

  and a nonconservative action assumed to be a delta function over the state v of the interacting test cell: $\psi_{ik}(v, w; u) = p_{ik}(v, w)\delta(u - v)$, such that its resultant action is

$$J_i[\mathbf{f}] = f_i(t, u) \sum_{k=1}^{3} \int_0^{\infty} \int_0^{\infty} p_{ik}(u, w) f_k(t, w)\, dw \,. \tag{11.22}$$

The resultant structure of the evolution model follows:

$$\frac{\partial}{\partial t} f_i(t,u) + \frac{\partial}{\partial u}\left[f_i(t,u) \sum_{j=1}^{3} \int_0^\infty \varphi_{ij}(u,w) f_j(t,w)\, dv \right]$$
$$= f_i(t,u) \sum_{k=1}^{3} \int_0^\infty \psi_{ik}(v,w;u) f_k(t,w)\, dv\, dw\ . \qquad (11.23)$$

Specialisation of the above models may be related, as we shall see, to the analysis of specific phenomena or therapeutic actions.

11.4.3 A Mean Field Model

The mathematical structure described in subsection 11.4.2 can be exploited to derive specific models such as those proposed in the above cited paper. Modelling means providing a detailed description of microscopic interactions. A specific model can be obtained, referring to Equation 11.23, by the following assumptions:

- The progression of neoplastic cells is not modified by interactions with other cells of the same type. On the other hand, it is weakened by interaction with immune cells (linearly depending on their activation state); and it is increased by interactions with environmental cells (linearly depending on their feeding ability). The effect increases with increasing values of the progression: $\varphi_{11} = 0$, $\varphi_{12} = -\alpha_{12} wu$, and $\varphi_{13} = \alpha_{13} wu$.
- The defence ability of immune cells is not modified by interactions with other cells of the same type or with environmental cells. On the other hand, it is weakened by interaction with tumour cells (linearly depending on their activation state) due to their ability to inhibit the immune system: $\varphi_{21} = -\alpha_{21} wu$ and $\varphi_{22} = \varphi_{23} = 0$.
- The feeding ability of environmental cells is not modified by interactions with other cells of the same type or with immune cells. On the other hand, it is weakened by interaction with tumour cells linearly depending on their activation state: $\varphi_{31} = -\alpha_{31} wu$ and $\varphi_{32} = \varphi_{33} = 0$.
- No proliferation of neoplastic cells occurs due to interactions with other cells of the same type. On the other hand, interactions with immune cells generate a destruction linearly depending on their activation state; and a proliferation by interactions with environmental cells depending on their feeding ability and the progression of tumour cells: $p_{11} = 0$, $p_{12} = -\beta_{12} w$, and $p_{13} = \beta_{13} vw$.
- No proliferation of immune cells occurs due to interactions with other cells of the same type and with environmental cells. On the other hand, interactions with tumour cells generate a proliferation linearly depending on their defence

ability and on the progression state of tumour cells: $p_{21} = \beta_{21} vw$ and $p_{22} = p_{23} = 0$.

- No proliferation of environmental cells occurs due to interactions with other cells of the same type and with immune cells. On the other hand, interactions with tumour cells generate a destruction linearly depending on the progression state of tumour cells: $p_{31} = -\beta_{31} w$ and $p_{32} = p_{33} = 0$.

The parameters α correspond to conservative encounters, while the parameters β refer to proliferative and destructive interactions. These parameters have to be regarded as positive, small with respect to 1, constants, to be identified by suitable experiments.

Based on the above modelling of cell interactions, we are now able to derive the evolution equation. Technical calculations yield

$$\frac{\partial f_i}{\partial t}(t,u) = \mathcal{J}_i[\mathbf{f}](t,u) + \mathcal{S}_i(t) f_{is}(u) \tag{11.24}$$

where $i = 1, 2, 3$, while the detailed expression of the interaction terms is given by:

$$\begin{aligned} \mathcal{J}_1 &= \alpha_{12} \frac{\partial}{\partial u} \left[u f_1(t,u) A[f_2](t) - \alpha_{13} u f_1(t,u) A[f_3](t) \right] \\ &\quad + \beta_{13} u f_1(t,u) A[f_3](t) - \beta_{12} f_1(t,u) A[f_2](t) \,, \end{aligned} \tag{11.25}$$

$$\mathcal{J}_2 = \frac{\partial}{\partial u} \left[\alpha_{21} u f_2(t,u) A[f_1](t) \right] + \beta_{21} u f_2(t,u) A[f_1](t) \,, \tag{11.26}$$

and

$$\mathcal{J}_3 = \frac{\partial}{\partial u} \left[\alpha_{31} u f_3(t,u) A[f_1](t) \right] - \beta_{31} f_3(t,u) A[f_1](t) \,, \tag{11.27}$$

where the operator $A[\cdot]$ is defined as follows:

$$A[f_i] = \int_0^{+\infty} w f_i(t,w)\, dw \,. \tag{11.28}$$

11.4.4 Simulations

The application of models, specifically those described above, for the simulation of phenomena of interest in immunology and medicine with particular attention to the immune competition, needs the statement of mathematical problems properly designed with reference to the above competition. Possibly, problems have to be related to specific experiments or therapeutic actions.

Then a qualitative analysis may be developed with reference to existence of solutions and their asymptotic behaviour. In particular, the analysis can be addressed to show the existence of parameters for which a critical value, to be regarded as a bifurcation value, separates two qualitatively different asymptotic behaviours:

- Activation of the immune system and progressive weakening and destruction of tumour cells
- Progressive inhibition of immune cells followed by a blow-up of tumour cells that finally start to condense into a solid form

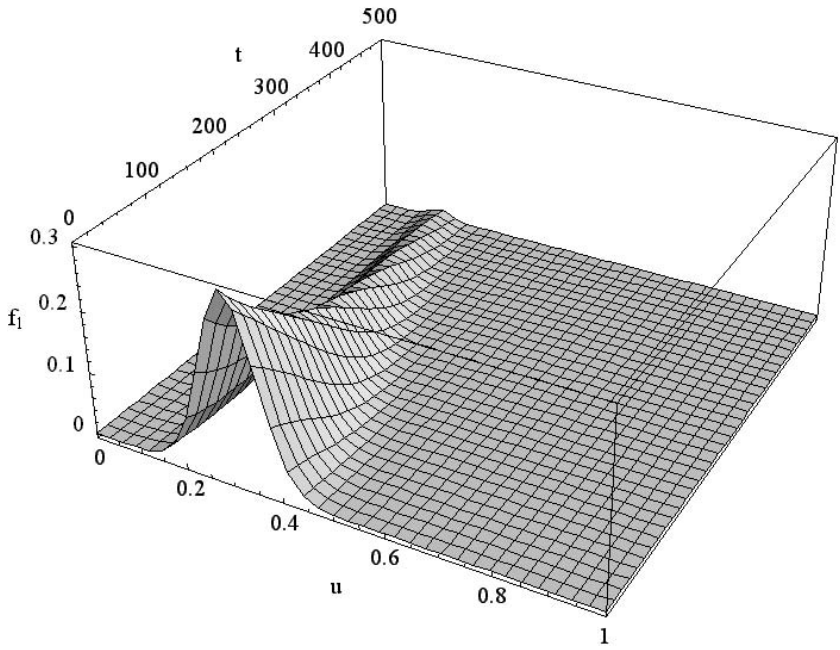

Figure 11.1
Evolution of tumour cells for $\alpha_{21} > \alpha_{21}^c$.

Of course particularly interesting are those cases where the parameter is related to a physical quantity which can be medically modified. Indeed this is the case of the class of models dealt with in this section. Bearing all of the above in mind, we refer to the qualitative analysis developed in the paper by De Angelis and Jabin [42] and to the simulations reported in [43]. Both papers refer to the model reported in subsection 11.4.3.

An example of simulation is reported in Figures 11.1 and 11.2, which analyse the sensitivity of the solutions, with special attention to the asymptotic behaviour, to the parameter α which corresponds to the ability of progressed cells to inhibit the immune system. Accurate simulations, as documented in [43], show how α is a bifurcation parameter which separates two qualitatively different asymptotic behaviours: blow up of progressed cells and progressive inhibition of the immune system, and

the opposite one, regression of progressed cells with effective action of the immune system.

Specifically, Figure 11.1 shows how the evolution has a trend to decrease the number of progressed cells with increasing number and value of the progression. This behaviour occurs when α_{21} is larger than a critical value α_{21}^c. In this case, the immune system is able to contrast the neoplastic growth; tumour cells are able to increase their aggressiveness and to inhibit immune cells. The distribution function of the tumour cells evolves toward larger values of the state u, while the distribution of the immune cells is shifting toward lower values of u.

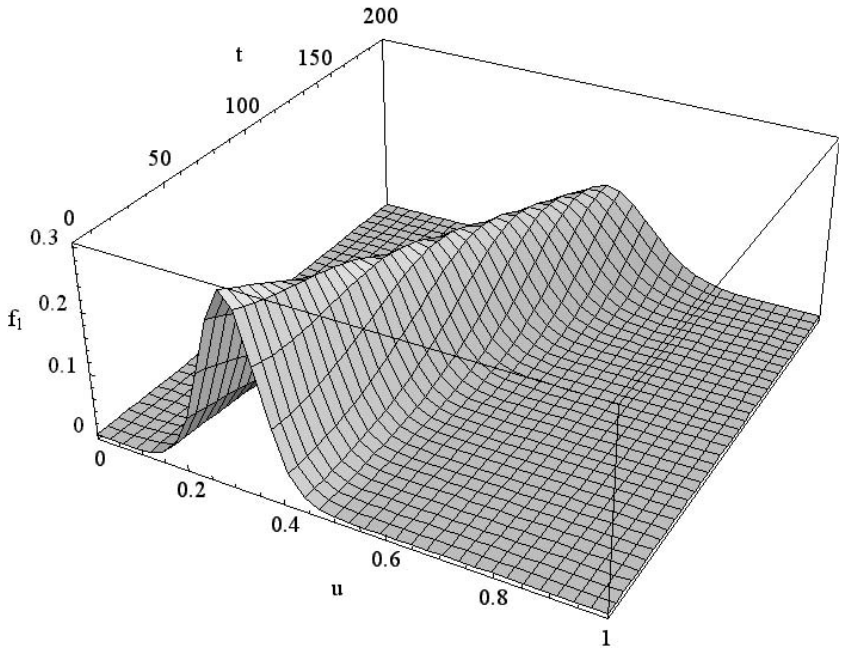

Figure 11.2
Evolution of tumour cells for $\alpha_{21} < \alpha_{21}^c$.

On the other hand the opposite behaviour is observed when α_{21} is below α_{21}^c. This type of evolution is observed in Figure 11.2, where the number of progressed cells, and their activation, shows a trend to increase. Now the immune system is not able to control the growth of tumour cells as shown in Figure 11.3 which shows the evolution of immune cells shifting their activation toward lower values.

It is clear, from the above simulations, the crucial role of the parameter α_{21} among the others parameters. Indeed, α_{21} selects the asymptotic behaviour of the system. Medical therapies can be focused to modify the above parameter.

The behaviour which has been described above is a common feature, as documented in [17], of all kinetic models proposed in the literature, including the ones described in subsection 11.3.2.

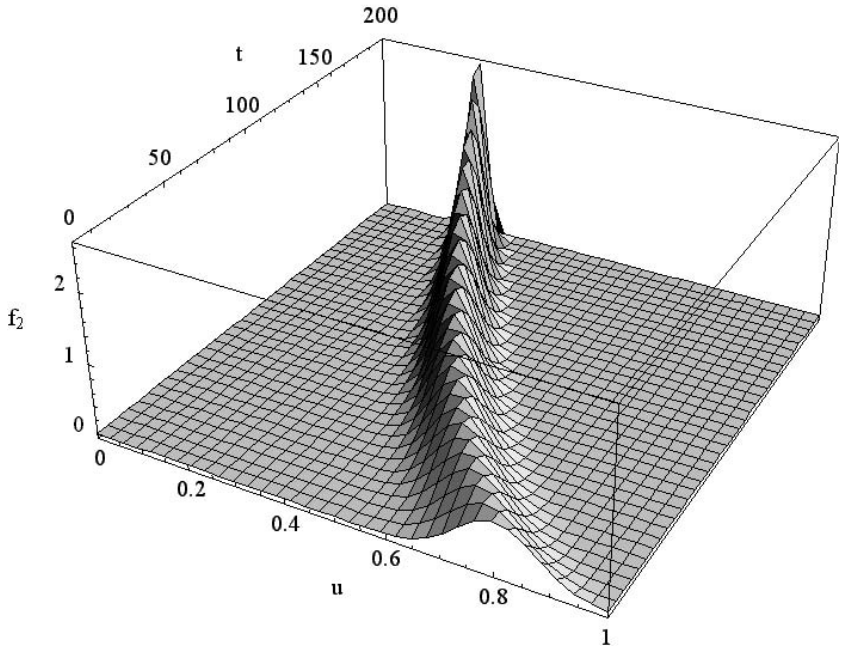

Figure 11.3
Evolution of tumour cells for $\alpha_{21} < \alpha_{21}^c$.

11.5 Finite Models

In the models considered in section 11.4, each cell population is characterised by a typical biological activity, statistically distributed over the cells. Interactions modify the above distribution and may generate proliferation or destruction events. In contrast, in finite models, each population is characterised by a certain fixed activity, while interactions simply modify the number of cells linked to the above activities. Therefore, finite models generally stated in terms of ordinary differential equations, simply refer to the size $n_i = n_i(t)$ of each i-th population.

Definitively the above description has to be regarded as a crude approximation

of physical reality, which may loose relevant features of the system we are dealing with. On the other hand it is worth reporting about this type of modelling, which is able, at least in some cases, to provide an immediate description of the evolution of the immune competition. Rather than providing an overview of the various models available in the literature, already reviewed in [5], a critical analysis of some specific models will be offered in this section with special attention to bifurcation analysis.

An interesting model referring to the populations considered in the previous section was proposed by Kirschner and Panetta [44]. The qualities of this paper are the essential character of the basic assumptions on which it relies, the relatively simple analytical structure of the model (which is expressed by a system of ordinary differential equations) and the phenomenology of conclusions which are drawn by its study. We will devote the main part of the present section reporting on the above paper, with the aim of illustrating the typology of finite models describing tumour cells: immune system dynamics and, in particular, the bifurcation mechanism generally occurring.

After the description of this one, we will mention another significant model of cancer treatment by immunotherapy (also expressed by nonlinear ordinary differential equations) introduced and studied by Nani and Freedman [45], and we will briefly comment on the analogies and the differences between the approaches of the two papers.

11.5.1 A Model by Kirschner and Panetta

The starting point, to motivate this model, is the realisation that, beside surgery, chemotherapy, and radiotherapy, immunotherapy may represent a valid tool in the fight against tumours. Prominence to such a direction has been given by the work of Rosenberg and colleagues at the National Cancer Institute (see Stevenson [46], Rosenberg et al. [47], and Rosenberg [48] and [49]).

Essentially, immunotherapy means a treatment addressed to enhance the immune system capacity to fight tumours. More specifically, immunotherapy contemplates the use of cytokines, proteins which boost the immune response, the most effective of whose appears to be *interleukin*-2 (abbreviated, *IL*-2) eventually combined with the so called adoptive cellular immunotherapy (abbreviated, *ACI*), amounting to injection of cultured immune cells.

The research on modelling immunotherapy relies on a side on an interplay between the clinical and experimental data and on the other side on the construction and exploration of mathematical models, capable of grasping the main features of the phenomena under study and possibly predicting real life observations. It is within such a framework that paper [44] was proposed. Specifically, three interacting populations are taken into account:

- The so called immune effector cells $E(t)$
- The tumour cells $T(t)$

- The concentration $I_L(t)$ of cytokine interleukin-2 in the tumour site compartment under examination

The dynamics of these populations can be modelled by the following system of ordinary differential equations:

$$\begin{cases} \dfrac{dE}{dt} = cT - \mu_2 E + \dfrac{p_1 E I_L}{g_1 + I_L} + s_1 \ , \\ \dfrac{dT}{dt} = r_2(T)T - \dfrac{aET}{g_2 + T} \ , \\ \dfrac{dI_L}{dt} = \dfrac{p_2 ET}{g_3 + T} - \mu_3 I_L + s_2 \ , \end{cases}$$

which are studied together with initial conditions:

$$E(0) = E_0 \ , \qquad T(0) = T_0 \ , \qquad I_L(0) = I_{L_0} \ .$$

Here, $r_2(T) = r_2(1 - bT)$, while s_1 and s_2 represent two treatment terms. Specifically, s_1 represents an external source of effector cells such as *LAK* (*i.e., lymphokine-activated killer cell*) or *TIL* (*i.e., tumour infiltrating lymphocyte*) cells, and s_2 represents an external input of *IL*-2 into the system. The system involves 11 parameters: c, μ_2, p_1, g_1, r_2, b, a, g_2, p_2, g_3, and μ_3. Conceivable values for these parameters, to be chosen on the basis of experimental suggestions, may be found in the literature. We emphasise that, in particular, the value of the parameter c, which represents the antigenicity of the tumour, sensibly varies, depending on the patient and on the cancer.

The model is investigated from a numerical point of view, writing the equations in dimensionless form. This leads to a scaled system.

The case is first analysed when no treatment is present, which corresponds to having $s_1 = 0$ and $s_2 = 0$ in the Equations (11.5.1). Then, the case is studied when some therapy is present. Three subcases are investigated, which contemplate respectively the presence of:

- adoptive cellular immunotherapy (corresponding to $s_1 > 0$ and $s_2 = 0$)
- input of interleukin-2 into the system (corresponding to $s_1 = 0$, $s_2 > 0$)
- immunotherapy with a combination of both *ACI* and *IL*-2 (corresponding to $s_1 > 0$, $s_2 > 0$).

Let us start with the nontreatment case. It turns out that the dynamics associated to the system (11.5.1) depends on the choice of the parameters involved. In particular, it sensibly depends on the parameter c.

Clearly, the interest is for the asymptotic behaviour. So, the individuation of steady states is the first objective, together with informations on their stability/instability character. In this connection, for any equilibrium the eigenvalues of the linearised system are investigated.

The computational investigation performed by the authors indicates that three different qualitative situations for the dynamics can be distinguished when varying c. Accordingly, a bifurcation diagram is provided, which underscores that the trivial equilibrium state $E_0 = (0, 0, 0)$ always exists and is unstable. Indeed, one of the eigenvalues of the Jacobian matrix at E_0 is positive. In addition, up to three nontrivial steady states may exist depending on the value of the parameter c: two bifurcation values c_0 and c_1 are singled out such that:

- If $0 < c < c_0$ three nontrivial steady states exist, one of them (E_1) stable, with a large tumour mass (near the size of its carrying capacity), the other two (E_2 and E_3) unstable.
- If $c_0 < c < c_1$ the steady state E_2 is still present and unstable; in contrast, at $c = c_0$, the equilibria E_1 and E_3 disappear and a stable limit cycle develops.
- If $c_1 < c$ the cycle persists, but its amplitude and period decrease; as for the steady state E_2, when $c = c_1$, it becomes stable. The masses of the tumours in this region are much smaller than for $c < c_1$.

Looking for interpretation and deduction of biological implications of these outcomes, we see that the model contemplates the possibility of a large tumour when the antigenicity c is extremely small. Of particular interest is the detection of stable cycles. One of the outcomes of the numerical investigation is the existence for small c of a cycle of the tumour mass having a period of around 11 years with the tumour spending a portion of the cycle (amounting to 2 or 3 months) near its carrying capacity and the remainder with a mass near zero, say dormant. The interest of such a result is due to the fact that clinical evidence suggests indeed the existence of similar recurrent phenomena.

It is worthwhile noticing that in the nontreatment case, the model does not contemplate a complete clearance of the tumour.

Therefore, let us go to the treatment case. As already anticipated, three subcases are investigated.

1. The case of adoptive cellular immunotherapy ($s_1 > 0$ and $s_2 = 0$).

   The trivial steady state E_0 is lost and substituted by a nontumour equilibrium, again denoted $E_0 = (E_0^*, 0, 0)$. The main purpose is of knowing when the equilibrium E_0 is stable. It turns out that this happens if s_1 is larger than a certain critical value $s_{1_{crit}}$. As for steady states with presence of tumour, investigation leads to a bifurcation diagram distinguishing five different regions in the (c, s_1) parameter space. In particular, worthwhile to be mentioned are the following facts:

   - In one of these five regions a bistability phenomenon occurs: depending on the initial conditions the solution tends to E_0 (so, the immune system succeeds to clear the tumor) or to another equilibrium $E_1 = (E_1^*, T_1^*, 0)$ (implying that the tumor survives).

- In another region of the (c, s_1) parameter space, a stable limit cycle is found.

We point out that the region where E_0 turns out to be stable (correspondingly, where the immune system succeeds in clearing the tumour) is the one with the largest area in the parameter space.

Summarising, according to the model under examination, the effects of *ACI* therapy can yield a tumour-free state if the treatment concentration is above a given critical level. However, for tumours with small antigenicity bistability can occur with the tumour-free state and a near carrying capacity state. A fact which suggests the need of an early treatment, when the tumour is still small.

2. The case of input of interleukin-2 into the system ($s_1 = 0$, $s_2 > 0$).

   Here, the existence of a unique nontumour steady state $E_0 = (0, 0, {I_{L0}}^*)$ which is always unstable seems to suggest that administering *IL*-2 alone without *ACI* cannot clear the tumour.

   Again, a bifurcation diagram results with (four) different regions in the (c, s_2) parameter space. Skipping on a detailed description of the situations occurring in different regions, we point out the existence for s_2 large of a stable "state" $(\infty, 0, s_2/\mu_3)$. This seems to describe a situation where a large amount of administrated *IL*-2 yields (for any value of the antigenicity) to the clearance of the tumour, but at the expenses of an unbounded growth of the immune system. Such a phenomenon may be put into relation with the capillary leak syndrome, which is documented as a side effect of treatments with dose escalation of *IL*-2.

   Summarising, according to the model under examination, for one or another reason, no satisfactory results can be obtained through a treatment with *IL*-2 alone.

3. The case of immunotherapy with a combination of both *ACI* and *IL*-2 ($s_1 > 0$, $s_2 > 0$).

   When both treatment terms are nonzero, the tumour free equilibrium is $E_0 = (E_0^*, 0, {I_{L0}}^*)$, which is stable provided $s_2 < s_{2_{crit}}$ for a certain critical value $s_{2_{crit}}$, and s_1 is larger than a certain function of s_2 and of several parameters, namely

$$s_1 > \frac{g_2 r_2}{a}\left[\frac{s_2(\mu_2 - p_1) + \mu_2\mu_3 g_1}{\mu_3 g_1 + s_2}\right]. \tag{11.29}$$

   Therefore, for concentrations of *IL*-2 administered below $s_{2_{crit}}$, it is the concurrent administering *ACI* which makes the difference for tumour clearance. And, it is important that there are indeed regions in the parameter spaces where the desired clearance may be reached. Moreover, the greater the antigenicity of the tumour, the more likely the treatment will succeed.

   Actually, it turns out that for concentrations of *IL*-2 administered above $s_{2_{crit}}$ the tumour can be cleared too; however an overactivated immune system may

cause problems such as capillary leak syndrome cancelling the benefits of tumour clearance.

Summarising, the model under investigation seems to predict that the effects of combined *ACI* and *IL*-2 treatment may be the best case scenario.

In conclusion, the correlations appearing between the results just discussed and data from clinical and experimental evidence identify the model treated as a significant and interesting one.

It seems worthwhile proceeding with investigation and eventual improvement of this model. First of all, a rigorous analytical study of the bifurcation, which has been numerically evidentiated, is missing.

As for extensions and generalisations, a natural direction could contemplate allowing the terms representing the administration of some therapy to be nonconstant.

11.5.2 A Model by Nani and Freedman

Based on analytical and qualitative rather than computational study, the paper by Nani and Freedman [45] discusses a mathematical model of immunotherapy described by four first order ordinary differential equations. The populations under consideration are:

- The concentration $x_1(t)$ of normal/noncancer cells in a given physiological space or organ of the human anatomy
- The concentration $x_2(t)$ of cancer cells in a given physiological space or organ of the human anatomy
- The concentration $w(t)$ of cancer-killing lymphocyte binding sites such as *LAK* cells in the neighbourhood of the cancer cells and normal cells
- The concentration $z(t)$ of lymphokine (e.g., *IL*-2) in the neighbourhood of the cancer cells and normal cells

If Q_1 [resp., Q_2] denotes the rate of external intravenous reinfusion of lymphocyte (*LAK* cells) [resp., lymphokines (*IL*-2 cells)] into the cancer patient, $B_i(x_i)$ and $D_i(x_i)$, $i = 1, 2$ are respectively the birth and death rates of x_i, $q_i(x_1, x_2)$ are the specific natural competition functions between cancer and normal cells, $f(w, z)$ denotes the rate of lymphocyte (*LAK*) proliferation due to the induction by lymphokine (*IL*-2), $h(x_2, w)$ the rate of cancer cell destruction by lymphocytes, $e_1(w)$ and $e_2(z)$ are the rates of degradation or elimination of lymphocytes (*LAK*) or lymphokines (*IL*-2) respectively, η and β are constants depicting binding stoichiometry and α_i are

elimination coefficients, the model equations take the form:

$$\begin{cases} \dfrac{dx_1}{dt} = B_1(x_1) - D_1(x_1) - x_1 x_2 q_1(x_1, x_2) \ , \\ \dfrac{dx_2}{dt} = B_2(x_2) - D_2(x_2) - x_1 x_2 q_1(x_1, x_2) - h(x_2, w) \ , \\ \dfrac{dw}{dt} = Q_1 - \alpha_1 e_1(w) + f(w, z) - \beta h(x_2, w) \ , \\ \dfrac{dz}{dt} = Q_2 - \alpha_2 e_2(z) - \eta f(w, z) \ . \end{cases}$$

After postulating suitable regularity and technical growth conditions on the functions involved in the model, the authors prove a series of theorems providing conditions (on the mentioned functions) which guarantee the existence, the local stability, and the possible global asymptotic stability of certain equilibria. Moreover, the above cited paper contains also an analysis of the boundedness of the solutions of the differential equations, as well as the study of the dissipativity of the equations, of their positive-invariance, and even of the persistence character of the system.

Of course, the greatest interest lies in the individuation of a globally asymptotically stable noncancer equilibrium. Between several other results, criteria for such a case are established.

The mathematical tools employed by the authors include linearised stability analysis, the Lyapunov direct method, persistence theory, and Hopf-Andronov-Poincaré bifurcation.

Indeed, bifurcation too is investigated in a section, in which the proliferation function f is assumed to depend also on a parameter μ: $f = f(w, z; \mu)$. Within this context, a Hopf bifurcation is established under certain conditions. Namely, a value of the parameter μ is identified, passing through which a periodic solution is found to bifurcate from a noncancer equilibrium.

Another section of the paper is devoted to studying the case of periodic adoptive transfusions of *LAK* and *IL*-2. Accordingly, Q_1 and Q_2 are assumed to be periodic functions and the Floquet multipliers theory is invoked to establish stability criteria.

Once again, the overall analysis is quite suggestive: different conditions are singled out, under which therapeutic success or therapeutic failure of the anti-cancer immunotherapy are predicted.

The two papers [44] and [45] are quite different for several aspects (the number of differential equations in the models is different; the r.h.s. in the differential equations are exactly specified in first paper and not in [45], where only suitable technical and growth conditions are postulated for them; the results, and this is a major difference, follow in [44] from computational methods, while those in [45] rely on rigorous analytical proofs). In spite of all this, it seems that a fundamental link between these two papers is represented by the typology of results and conclusions which they contain. Which is the essential reason why we selected them as prototypes for finite models.

11.5.3 Other References

Finally, other aspects in the big cancer universe lead to finite models. For example, a class of models described by a system of ordinary differential equations is developed in the chapter by Michelson and Leith in the book [12]. The aim there is to figure out how do tumours grow, how do they react to their adverse environment, how do they control their own growth and manipulate environments to their own advantage. Accordingly, the equations appearing in these models describe the interactive nature of tumour subpopulations (different kinds of cells).

A good introduction to modelling tumour growth and immune response, which brings the reader from the philosophy and methodology of mathematical modelling, through a discussion of several examples and basic models may be found again in the above cited book, in the chapter by Adam.

The development of a mathematical control theory can be recovered in the paper by Swan [50], which is related to finite models of the type we have seen in this section.

11.6 Critical Analysis and Perspectives

This chapter has given a survey of some mathematical models designed to describe the interactions between the immune system and cancer cells. Three classes of models have been described and critically analysed. The first one related to the interactions developed at the cellular level; the second one referred to the kinetic description of large systems of several interacting populations of cells with internal biological structure; the third one referring to the traditional population dynamics framework for cell populations each characterised by a well defined biological activity.

The common guiding line in the analysis of the above models has been that interactions (microscopic dynamics) modify the evolution of the system which end up with a certain asymptotic behaviour. The analysis has been focused on the bifurcation problems related to the two biologically opposite behaviours:

- The effective action of the immune system against cancer cells which ends up with the destruction of the aggressive host
- The progressive inhibition of the immune system due to cancer cells which ends up with the uncontrolled growth of the aggressive host

A critical analysis of the contents of the above sections can be useful to outline some research perspectives which will be brought to the attention of applied mathematicians as challenging, however, difficult targets of mathematical immunology viewed as a new frontier of applied mathematics.

A first criticism refers to the fact that the various models known in the literature refer to different phenomena and representation scales. On the other hand we

have seen that all phenomena are characterised by features at all conceivable scales. Therefore developing a multiscale approach appears to be a relevant research perspective. Indeed, although modelling condensed matter is not dealt with in this chapter, still it is worth recalling that the macroscopic scale refers to phenomena which can be described by models developed in the framework of continuum phenomenological theories, e.g., those of continuum mechanics. These models are generally stated in terms of partial differential equations. A mathematical model which takes into account the above features was proposed by De Angelis and Preziosi [51]. It is plain that continuum models need microscopic cellular descriptions. This may be specifically related to biological rules, i.e., the information which may be transferred from the microscopic to the multicellular scale or to the macroscopic scale, e.g., the role of macrophages in condensed tumours, see Owen and Sherrat [52], [53].

An additional criticism is that models refer to specific physical situations, a precise reference to a general immune competition mathematical theory being missing. Hence, an interesting and challenging research perspective refers to the construction of a general theory suitable to include a large variety of immune competitions such that specific interactions can be cast into the above general framework. This amounts to developing a class of models suitable to include all particular interactions as special cases of general rules.

Finally, we remark that the interaction between mathematics and the sciences of medicine and immunology can certainly take advantage whenever mathematical models refers specifically to therapeutic actions. For instance the control of angiogenesis [54], vaccines [55], replicant viruses [56], and so on. Within such a framework, models, or hopefully a mathematical theory, developed either at the cellular scale or by means of the kinetic description, may be related to the biological mechanisms which effectively are involved in the complex game we are dealing with.

This essentially means developing a mathematical theory of the immune competition suitable to describe the relevant phenomena at the cellular scale. Maybe an interesting research perspective consists in exploiting cellular models to model microscopic interactions in the kinetic models. Dealing with the above topic by methods of kinetic theory, means developing a statistical mechanics theory for interacting subjects with internal intelligent or at least organised microscopic structure. Various interesting papers motivate research activity exploiting the above class of kinetic type equations. Among others, we mention the paper by Hartwell, Hopfield, Leibner, and Murray [57], scientists operating in the field of molecular and cellular biology, which provides various ideas concerning the modelling of large complex biological systems by methods of applied mathematics and physics. The relevant concept proposed in [57], refers to the fact that biological living systems are characterised by specific internal structures, which operate interacting in accordance with classical laws of physics and chemistry. Two sentences reported from [57] clarify the above concept:

- *Although living systems obey the laws of physics and chemistry, the notion of function or purpose differentiate biology from other natural sciences.*

- *Biological systems are very different from the physical or chemical systems analysed by statistical mechanics or hydrodynamics .... the components of physical systems are often simple entities, whereas in biology each of the components is often a microscopic device in itself, able to transduce energy and work far from equilibrium.*

This chapter is concluded by the above statements which contain in a few words a truly challenging research perspective.

11.7 References

[1] Delves, P.J. and Roitt, Y.M., The immune system, *Advances in Immunology* 343, 37-49, 2000.

[2] Forni, G., Foa, R., Santoni, A., and Frati, L., Eds., *Cytokine Induced Tumor Immunogeneticity*, Academic Press, New York, 1994.

[3] Greller, L., Tobin, F., and Poste, G., Tumor hetereogenity and progression: conceptual foundation for modeling, *Invasion and Metastasis* 16, 177-208, 1996.

[4] Stout, R.D. and Suttles, J., *T-Cell Signaling of Macrophage Activation: Cell Contact-Dependent and Cytokine Signals*, Springer, Heidelberg, 1995.

[5] Perelson, A. and Weisbuch, G., Immunology for physicists, *Rev. Modern Phys.* 69, 1219-1267, 1997.

[6] Nossal, G.J., Life, death, and the immune system, *Scientific American* 269, 53-72, 1993.

[7] Kleinstein, S.H. and Seiden, P.E., Simulating the immune system, *Computers and Simulations* 7-8, 69-76, 2000.

[8] Bellomo, N. and Preziosi, L., *Modelling Mathematical Methods and Scientific Computation*, CRC Press, Boca Raton, FL, 1995.

[9] Cercignani, C., Illner, R., and Pulvirenti, M., *Theory and Application of the Boltzmann Equation*, Springer, Heidelberg, 1993.

[10] Bellomo, N. and Lo Schiavo, M., *Lectures Notes on the Generalized Boltzmann Equation*, World Scientific, London, Singapore, 2000.

[11] Bellomo, N. and Pulvirenti, M., Eds., *Modeling in Applied Sciences: A Kinetic Theory Approach*, Birkhäuser, Boston, 2000.

[12] Adam, J. and Bellomo, N., Eds., *A Survey of Models on Tumor Immune Systems Dynamics*, Birkhäuser, Boston, 1996.

[13] Van der Burg, S.H., Offringa, R., and Melief, C.J.M., Viral antigens, in *Principle and Practise of Biological Therapy of Cancer*, 3rd Ed., S.A. Rosenberg, Ed., Lippincot Williams and Wilkins, New York, 2000.

[14] Anichini, A. and Mortarini, R., Il controllo della crescita neoplastica: ruoli dell'immunitá specifica nella risposta alle metastasi, in *Invasione e Metastasi*, G.Bevilacqua, R.Gavazzi, and P.L. Lollini, Eds., 1999.

[15] Burnet, F., *The Clonal Selection Theory of Acquired Immunity*, Vanderbilt University, Nashville, TN, 1959.

[16] Jerne, N.K., The immune system, *Scientific American* 229, 52-60, 1973.

[17] Zorzenon Dos Santos, R.M., Immune responses: getting close to experimental results with cellular automata models, *Annual Review of Computational Physics VI*, D. Stauffer, Ed., 159-202, 1999.

[18] Lollini, P.L., private communication, 2002.

[19] Celada, F. and Seiden, P., A computer model of cellular interactions in the immune system, *Immunology Today* 13, 56-62, 1992.

[20] Forrest, S. and Hofmeyr, S.A., Immunology as information processing, in *Design Principles for the Immune System and Other Distributed Autonomous Systems*, L.A. Segel and I. Cohen., Eds., Santa Fe Institute Studies in the Sciences of Complexity, Oxford University Press, Oxford, 2001.

[21] Perelson, A.S., Ed., *Theoretical Immunology, Part One & Two, SFI Studies in the Sciences of Complexity*, Addison Wesley, Reading, MA, 1988.

[22] Farmer, J.D., Packard, N., and Perelson, A.S., The immune system, adaptation and machine learning, *Physica D* 22, 187-204, 1986.

[23] Dasgupta, D., Ed., *Artificial Immune Systems and Their Applications*, Springer, Heidelberg, 1999.

[24] Kaufman, M., Urbain, J., and Thomas, R., Towards a logical analysis of the immune response. *J. Theor. Biol.* 114, 527-561, 1985.

[25] Weisbuch, G. and Atlan, H., Control of the immune response, *J. Phys. A* 21, 189-192, 1988.

[26] Agur, Z., Fixed points of majority rule cellular automata with application to plasticity and precision of the immune system, *Complex Systems* 5, 351-356, 1991.

[27] Atlan, H. and Cohen, I.R., Eds., *Theories of Immune Networks*, Springer-Verlag, Heidelberg, 1989.

[28] Stewart, J. and Varela, F.J., Morphogenesis in shape-space. Elementary metadynamics in a model of the immune network, *J. Theor. Biol.* 153, 477-498, 1991.

[29] de Boer, R.J., van der Laan, J.D., and Hogeweg, P., Randomness and pattern scale in the immune network: a cellular automata approach, in *Thinking about Biology*, SFI Lectures in Complex Systems, F. Varela and W.D. Stein, Eds., Addison-Wesley, Reading, MA, 1992.

[30] Segel, L.A. and Perelson, A.S., Some reflections on memory in shape space, in *Theories of Immune Networks*, H. Atlan and I.R. Cohen, Eds., Springer, Heidelberg, 63-70, 1989.

[31] Seiden, P.E. and Celada, F., A model simulating cognate recognition and response in the immune system, *J. Theor. Biol.* 158, 329-357, 1992.

[32] Castiglione, F., Mannella, G., Motta S., and Nicosia, G., A network of cellular automata for the simulation of the immune system, *Int. J. of Mod. Phys. C* 10, 677-686, 1999.

[33] Benjamini, E., Coico, R., and Sunshine, G., *Immunology: A Short Course*, Wiley-Liss, New York, 2000.

[34] Castiglione, F., Motta, S., Nicosia G., and Zammataro, L., The effects of an apoptosis mechanism on the immune response, in *Eurosim Conference 2001, Simulation Practice and Theory*, 2003.

[35] Jamin, C., Le Corre, R., Lydyard, P.M., and Youinou, P., Anti-CD5 extends the proliferative response of humane CD5+ B cells activated with anti-IgM and interleukine-2, *Eur. J. Immunology* 26, 57-62, 1996.

[36] Bellomo, N. and Forni, G., Dynamics of tumor interaction with the host immune system, *Math. Comp. Modelling* 20, 107-122, 1994.

[37] Bellomo, N. and De Angelis, E., Strategies of applied mathematics towards an immuno mathematical theory on tumors and immune system interactions, *Math. Models Meth. Appl. Sci.* 8, 1403-1429, 1998.

[38] Arlotti, L., Bellomo, N., and De Angelis, E., Generalized kinetic Boltzmann models: mathematical structures and applications, *Math. Models Meth. Appl. Sci.* 12, 567-596, 2002.

[39] De Angelis, E. and Mesin, L., Mathematical frameworks and applications on tumors and immune system interactions, *Math. Models Meth. Appl. Sci.* 11, 1609-1630, 2001.

[40] Arlotti, L., Gamba, A., and Lachowicz, M., A kinetic model of tumor/immune system cellular interections, *J. Theor. Medicine* 4, 39-50, 2002.

[41] De Angelis, E. and Jabin, P.E., Qualitative analysis of a mean field model of tumor-immune system competition, *Math. Models Meth. Appl. Sci.* 13, 197-220, 2003.

[42] De Angelis, E., Delitala, M., Marasco, A., and Romano A., *Mathl. Comp. Modeling*, 2003.

[43] Kirschner, D. and Panetta, J.C., Modeling immunotherapy of the tumor-immune interaction, *J. Math. Biol.* 37, 235-252, 1998.

[44] Nani, F. and Freedman, H.I., A mathematical model of cancer treatment by immunotherapy, *Math. Biosci.* 163, 159-199, 2000.

[45] Stevenson, H.C., *Adoptive Cellular Immunotherapy of Cancer*, Marcel Dekker, New York, 1998.

[46] Rosenberg, S.A., et al., Observations on the systemic administration of autologous lymphokine activated killer cells (LAK) and recombinant interleukin-2 (rIL-2) to patients with metastatic cancer, *N. Engl. J. Med.* 313, 1485-1495, 1985.

[47] Rosenberg, S.A., Adoptive immunotherapy for cancer, *Scientific American* 62, 1990.

[48] Rosenberg, S.A., Lymphokine activated killer (LAK) cells: a new approach to immunotherapy of cancer, *J. Nat. Cancer Inst.* 75, 595-602, 1995.

[49] Swan, G.W., Role of optimal control theory in cancer chemotherapy, *Math. Biosci.* 101, 237-284, 1990.

[50] De Angelis, E. and Preziosi, L., Advection-diffusion models for solid tumors *in vivo* and related free-boundary problems, *Math. Models Methods Appl. Sci.* 10, 379-408, 2000.

[51] Owen, M. and Sherrat, J., Modelling the macrophage invasion of tumours: effects on growth and composition, *IMA J. Math. Appl. Med. Biol.* 15, 165-185, 1998.

[52] Owen, M. and Sherrat, J., Mathematical modelling of macrophages dynamics in tumours, *Math. Models Meth. Appl. Sci.* 9, 513-540, 1999.

[53] Kerbel, R. and Folkman, J., Clinical translation on angiogenesis inhibitors, *Nature Reviews* 2, 727, 2002.

[54] Nanni, P., Nicoletti, G., De Giovanni, C., Landuzzi, L., Di Carlo, E., Cavallo, F., Pupa, S., Rossi, I., Colombo, M., Ricci, C., Astolfi, A., Musiani, P., Forni, G., and Lollini, P., Combined allogenic tumor cell vaccination and systemic interleukin12 prevents mammary carcinogenesis in HER-2/neu transgenic mice, *J. Exp. Medicine* 194, 1195-1206, 2001.

[55] Jain, R.K., Barriers to drug delivery in solid tumors, *Scientific American* 271, 58-65, 1994.

[56] Hartwell, H.L., Hopfield, J.J., Leibner, S., and Murray, A.W., From molecular to modular cell biology, *Nature* 402, c47-c52, 1999.

Chapter 12

Analysing Hypersensitivity to Chemotherapy in a Cellular Automata Model of the Immune System

Filippo Castiglione, Vera Sleitser, and Zvia Agur
Institute for Medical Biomathematics (IMBM), Bene Ataroth (Israel)

12.1 Overview

Most chemotherapeutic agents have proven to induce hypersensitivity. All four types of allergic reactions have been reported in literature, but type I, or IgE-mediated (see below) is the most common one [1]. In the clinical practice these complications are usually overcome by means of either suitable premedication with antiallergic agents, or by postponing drug administration. Nevertheless, the risk of a severe anaphylactic reaction is a major concern, severity strongly depending on the drug dose and the dosing interval between successive injections [2].

Toxic side-effects of chemotherapeutic drugs have been shown to crucially depend on the dosing interval. Moreover, using mathematical modelling it has been conjectured that intermittent delivery of cytotoxic cell-cycle phase-specific drugs, at intervals equivalent to the mean cell-cycle time of the susceptible host cell population (denoted *Z-Method*), may minimise harmful toxicity without compromising therapeutic effects on target cells [3]. These conjectures have been proven analytically [4,5], and generalised for a large class of chemotherapy functions ([6,7]; see also [8]). The predictions of the *Z-method* have been verified in experiments in lymphoma bearing mice, treated by repeated pulse delivery of the anti-cancer drug 1-β-D-arabinofuranosyl cytosine (ara-C). In these experiments it has been shown that when the dosing intervals of drug delivery roughly coincide with the characteristic marrow cell-cycle time, animals survive and myelotoxicity is significantly reduced. The optimal spacing of repeated treatments was determined by measurements of the kinetics of cell movement through different cell-cycle phases [9–12].

The above experiments showed that it is feasible to control host toxicity by rational drug scheduling. With this general concept in mind, we are set to explore methods for reducing a patient's hypersensitivity to a drug, by considering variations in the drug schedule. As in the above-mentioned works, here too we make use of the power and efficiency of the mathematical modelling research tool.

There are many reasons why modelling allergies is an intricate task. The first and most important of these is that allergic diseases, whose origins have yet to be fully uncovered [13], arise because of a malfunctioning of the immune system, which is known to be among the most complicated natural systems. Moreover, modelling allergies has to embrace different levels of biological organisation, going from the gene level (allergies are likely to have genetic origins), to the cell level, through the complicated machinery of cell signalling. A comprehensive mathematical description of this complexity at one time is quite a challenging task. Nevertheless, models which do not take into account the gene-level but focus on the dynamics of population of cells and molecules of the immune system, have already been able to pinpoint very interesting features.

The model we employ is a generalisation of the stochastic cellular automata (CA) concept [14], in that the entities and the rules are not too simplified or stylised. Indeed a great level of description is implemented. This model has been developed on the tracks of a well known CA model of the immune system [15] which describes

the *humoral* immune response to antigens in the host organism (a downloadable C-language version of the original model which includes also the *cytotoxic* response is available [16]).

This chapter begins with a brief background on the topic of allergies and, in particular, on type I or *IgE-mediated* hypersensitivity reactions. Section 12.2 recalls some basic facts and terms related to allergies and to mathematical models of the immune system. Section 12.3 describes the CA model employed, and the necessary approximations made. The results of the simulations are presented in section 12.4. Finally, in section 12.5 we discuss some implications of our results for the design of chemotherapy administration strategies, which may minimise hypersensitivity to the drug.

12.2 Background

The term *atopic* refers to people suffering certain form of allergy. For reasons that are not yet understood, these people have a predisposition to respond to some environmental antigens (e.g., pollen, mold spores) by producing antibodies of the IgE class (immunoglobulin of class E). Since this trait tends to run in families, it probably has a genetic component. It is estimated that over 30% of the world population is atopic. Moreover, the number of people suffering from atopic diseases is increasing in the industrialised countries, revealing a link between modern life and atopy [2].

In the case of allergy induced during the administration of anti-cancer drugs, the patient develops the same type of hypersensitivity to one or more components of the anti-cancer agents, usually during the first or the second cycle of chemotherapy. Among the known cytotoxic anti-cancer drugs inducing an IgE-mediated reactions we recall *cyclophosphamide* [17], *peplomycin* [18], *hyaluronidase* [19], and *paclitaxel* [20].
Although the literature about such cases of hypersensitivity is quite extensive, few articles discuss the possible causes for this immune reaction. Instead, literature usually focuses on elaborating methods for overcoming the problem by means of temporary treatment interruption, administration of antiallergic substances before and during the therapy, or on the use of desensitisation protocols to attenuate the response and increase the probability of tolerating the drug (see reference [21] and cited).

In recent decades, scientists, clinicians, and epidemiologists have elucidated the intracellular and the cellular mechanisms involved in allergic reactions, including the roles of T helper subsets and interleukins [24]. However, our understanding is still lacking as to the full sequence of events involved in disease development, and to the key factors determining the differences between a person who is allergic to, say, grass pollen and one who is allergic to bee venom. The only agreement seems to be that allergenicity is a consequence of a complex series of interactions involving not only the allergen, but also the dose, the sensitising route, sometimes an adjuvant, and

most importantly, the genetic constitution of the recipient [2,13,22].

Many pathologies have been identified as belonging to the class of allergic reactions. In order to further classify them, Peter Gell and Richard Coombs [23] proposed a classification method which is based on the effector molecules and cells involved in the allergic response [24]. The method distinguishes four classes of allergic disorders:

- Type I, *immediate type* or *IgE-mediated*
- Type II, *antibody mediated*
- Type III, *immune complex mediated*
- Type IV, *delayed type* or *T-helper cell-mediated*

Acute or immediate type I hypersensitivity reaction is a consequence of mediators (histamine, leukotrienes, prostaglandin, etc.) released by mast cells (MC) or basophils triggered via the allergen-mediated cross-linking of cell surface bond immunoglobulin-E (IgE). Convincing evidence has accumulated, suggesting that the immune response to allergens in atopics is biased towards the T helper type 2 (Th2) phenotype, characterised by the production of the interleukin-4 (IL-4) and interleukin-5 (IL-5). These are key cytokines in class switching to IgE (replacing IgG) in B cells and in the accumulation and activation of eosinophils respectively [24]. Allergic IgE responses occur mainly on mucous membrane surfaces in response to *allergens* (i.e., common environmental antigen), which enter the body either by inhalation or ingestion. Typically, such responses manifest themselves in localized symptoms, as hives, eczema, hay fever, food allergies, asthma, and systemic anaphylaxis. Most allergens are small proteins, or protein-bound substances, having a low molecular weight. Common antigens, associated with type I hypersensitive reactions are proteins, such as foreign sera or vaccines, drugs, such as penicillin or sulphonamides, local anaesthetics (most drugs are low molecular weight compounds that are incapable of inducing immune responses, unless conjugated with a larger molecule; these small molecules first react with proteins which work as hapten-carriers to form drug-proteins derivatives) etc., (see [24]).

12.2.1 Immunoglobulins and the Isotype Switch

During the primary response of a normal individual, B cells produce antibodies of the IgM type. Several hours after the onset of IgM production, stimulated by the presence of interferon-γ (IFN-γ), IgG-producing B cells swing into action. Eventually, blood serum concentration of IgG antibodies increases above that of IgM, but as long as the antigen is present in the body, both IgM and IgG antibodies continue to be produced. Upon complete antigen removal, B cell stimulation is shut off and the remaining antibodies are catabolised and broken down. Should the same pathogen with the same antigens attempt to reinvade the body, it will stimulate a faster and

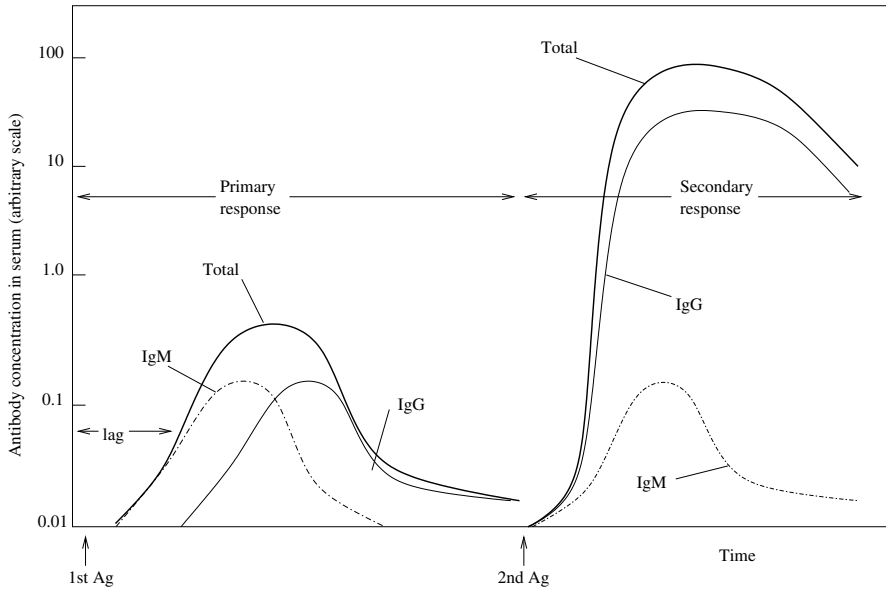

Figure 12.1

Isotype switch during primary and secondary immune response. The concentrations are plotted on a logarithmic scale. The time units are not specified because the kinetics differ somewhat with type of antigen, administration route, species, or strain of animal (adapted from [24]).

stronger antibody production (secondary response in Figure 12.1). This time the IgG antibody producing cells proliferate and release IgG just as quickly as the IgM producing cells. The above pattern of the immune reaction in a normal individual is altered in hypersensitive subjects, mainly by IgE antibodies being produced instead of IgG antibodies. This *isotype switch* takes place in stimulated B cells in the presence of certain cytokines produced by T helper cells [24]. A "normal" isotype switch to IgG occurs if the concentration of interleukin-12 (IL-12) is relatively high, whereas a switch to IgE is dependent on the concentration of IL-4. The problem in having high levels of IgE serum is that they bind to mast cells and basophils through the Fc receptor on the cell membrane, thus *sensitising* these cells. A subsequent exposure to the same allergen induces cross-linking of IgE-bound molecules on sensitised cells. Cross-linking is a term indicating a complex series of events which signal a cell to *degranulate* and release active mediators, such as histamine, serotonin, proteases, eosinophil chemotactic factor (ECF-A), neutrophil chemotactic factor (NCF-A), platelet-activating factor, leukotrienes, prostaglandinis, etc. Finally, the presence of these active molecules provoke a sequence of events, culminating in the symptoms of hypersensitivity. For example, the leukotrienes mediate broncho-constriction, increased vascular permeability, and mucus production (as seen in asthmatics) [24,25].

12.2.2 Cytokines Production and the Role of Th1/Th2 Shift

T helper lymphocytes are mainly classified according to the types of cytokines they secrete [26]. Two distinct kinds of T helper lymphocytes can be distinguished, namely Th1 and Th2 lymphocytes. Th1 lymphocytes participate in cell-mediated immunity. They secrete interleukin-2 (IL-2), IFN-γ, and TNF to enhance inflammation and antiviral responses, and are essential for controlling such intracellular pathogens as *listeria* and *mycobacterium tuberculosis* (the bacillus that causes tuberculosis). In contrast, Th2 lymphocytes provide help to B cells and, in so doing, are essential for antibody-mediated immunity, controlling extracellular pathogens in blood and other body fluids.

Normal immune response requires a balanced activation of Th1 and Th2 lymphocytes. Indeed, many pathologies are related to, or arise from, an imbalance in the activation of these two lymphocyte populations. It has been suggested that the activity of the immune system *in utero*, primed by common environmental allergens crossing the placenta, is very important in determining the individual Th1/Th2 balance and the predisposition to hypersensitivity. This theory states that the immune response of virtually all newborn infants is dominated by type 2 T helper cells and that during subsequent development, the normal infant's immune system shifts in favour of a type 1 T helper cell-mediated response to inhaled allergens. In contrast, in the potentially allergic infant there is a further increase in type 2 T helper cells, which were primed *in utero*. Microbes are probably the chief stimuli of protective type 1 T helper cell immunity [2,22].

A mathematical model of Th1/Th2 balance during adult immune responses has been developed to understand the "decision" of the immune system to trigger a Th1 or Th2 immune response, and how it influences the disease outcome [27]. The model proposes the innate immune recognition as the mechanism for the "decision-making" process. Given this assumption, this model indicates that:

- the default response to pathogens is primarily a Th1 response, followed by a Th1$\rightarrow$Th2 switch, in case of a failure of the Th1 response; and
- antigen dose-dependence of the T helper ratio (high antigen levels promote a Th1$\rightarrow$Th2 switch) and an initial Th1 bias are crucial for the function of selection process.

More simply, in our model, we identify, as a working assumption, the Th2 phenotype as being responsible for hypersensitivity (see paragraph 12.3.1).

Together with Th lymphocytes, the macrophages (MA) are the main source of the different interleukins. Among others, they secrete IL-12 which induces Th differentiation into the Th1 subset. Macrophages are not the only source of IL-12, as any antigen presenting cell (e.g., B cell) is able to secrete IL-12 [24]. The interleukin, IL-12, promotes Th lymphocyte's enhanced secretion of IFN-γ. Conversely,

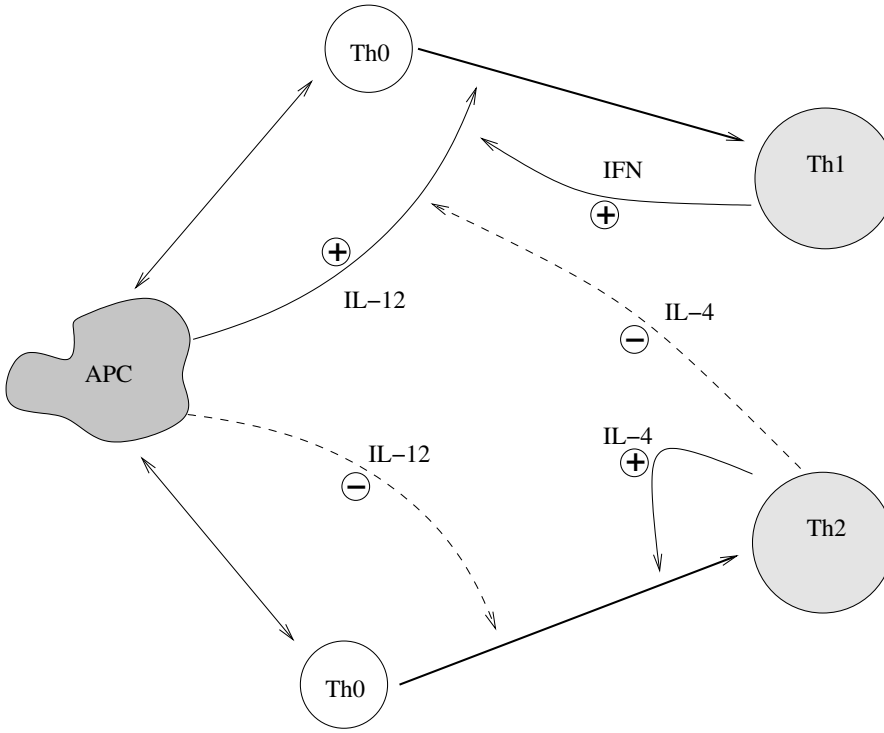

Figure 12.2

Schematic representation of the effects of the cytokines IL-4, IL-12, and IFN-γ and the commitment of Th1 and Th2 cells from the common precursor Th0 in the present model. Dashed lines indicate inhibition, whereas solid lines indicate stimulatory effects.

IFN-γ promotes IL-12 secretion so that there is a positive feedback between these two cytokines (see Figure 12.2). In contrast, by driving the Th response to the Th1 phenotype, IL-12 acts as a suppressive agent of the allergic immune response [28] (observation cited in [29]).

12.2.3 Mathematical Models of the Immune System

The immune system has some unique features, which render it appealing for mathematical modelling:

- It is a highly distributed system, which carries out a complex recognition and classification task

- It evolves and matures using combinatorial, evolutionary and adaptation mechanisms
- It is able to "remember"

Immune system models can generally be classified into continuous models, describing the immune process by sets of differential equations, and discrete models, describing the immune process as a series of interactions in discrete time steps, or utilising combinatorial methods to predict immune properties.

Traditionally, the approach to modelling the immune system involved ODE (ordinary differential equations) or PDE (partial differential equation) [30]. However, in the last two decades discrete mathematical models, and most notably, the CA approach, have become increasingly popular in the theoretical immunology community. These new trends were largely due to the wide-range use of CA in modelling complex phenomena in physics, biology, finance, and, more recently, sociology [31]. Below we briefly overview models belonging to each modelling group. A more detailed review can be found in [30].

12.2.3.1 Continuous Models

Most mathematical models in immunology employ systems of differential equations to describe the dynamic interactions of immune cells and pathogens. The system's description may include equations and parameters for proliferation and death rates of pathogens and lymphocytes, for the transitions between resting and activated states of immune cells, or between naive and memory phenotypes, transitions of the response between humoral and cellular activity, etc. Among the issues addressed using this approach are the maturation of the humoral immune response, exhibited by B cell proliferation and differentiation using clonal selection and somatic hypermutations [32,33], the effect of feedback in monitoring, balancing, and improving the immune response [34], the role of cross-reactive stimulation in maintaining immune memory [35], the threshold ratio between Th memory cells and antigen dose needed to establish T cell memory [36], antiviral immune response in infections, such as hepatitis B, influenza [37,38], HIV [39–42], etc.

12.2.3.2 Discrete Models

One subclass of immune system models uses methods of discrete mathematics to evaluate characteristics of the immune system and to predict its behaviour. Perelson et al. [43] have employed a "shape space" model to study aspects of the immune repertoire: how large should this repertoire be in order to be complete, and what is the probability of recognising foreign vs. self antigens. The shape space model geometrically describes the immunological receptors as points in a multi-dimensional space, each dimension representing a binding parameter such as length, width, charge, etc., and each receptor can bind epitopes within a small "recognition ball" surrounding its complement in the shape space.

A different approach was introduced by Agur et al. [44,45], who analysed the strategy of the humoral immune response as an optimisation problem. Agur et al.

employed dynamic programming methods for investigating the optimal mutation rate function in B cells, which maximises the probability that the required structure of the antigen-binding antibody will be efficiently generated during any immune response. Analytical results have pinpointed a step-function mutation rate as the globally optimal strategy, transition from minimum mutation rate to the maximum biologically possible mutation rate occurring when the size of the best performing B cell clone exceeds a well-defined threshold.

A second subclass of discrete models is that of CA. Discrete in both space and time, these models describe the immune system dynamics by deterministic rules of cells, molecules and their local interactions. In [46] the concept of "evolutionary" experiments *in-machina* (i.e., within computer) was introduced. Thus, computer simulation experiments were performed, where each B cell was represented by a two dimensional cellular automata with variable processing rules. Results of this work suggest that efficient immune response to antigenically homogenous pathogen favours strong contraction in phase space in antibody generation (*one B-cell clone – one antibody*), whereas efficient response to antigenically varying pathogen should favour weak contraction in phase-space in antibody generation (*one B-cell clone – many antibodies*).

These type of experiments can be used prior to any *in vitro* or *in vivo* experiments for qualitatively examining problems in immunology by fast, reproducible, and cheap means. Indeed, Celada and Seiden put forward such a CA simulation model, which attempts to capture "all" the different constituents of the immune system in one comprehensive framework (to be denoted *CS-model*, [15,47,48]). This model has been used to study various phenomena, including the optimal number of human leukocyte antigens (HLA) [48], the autoimmunity and T lymphocytes selection in the thymus [49], antibody selection and hyper-mutation [47], and the dynamics of various lymphocyte populations in the presence of viruses, which are characterised by infectivity, reproduction efficiency, etc., [50]. Formally, the CS-model belongs to a subclass called "stochastic CA."

12.2.3.3 Stochastic Cellular Automata

Most simulators of the immune response are deterministic, assuming that a given set of initial conditions leads to only one end-state. Typically, deterministic models, constituted by a set of differential equations which represent the interactions among immune cells and molecules, are solved iteratively by numerical integration. However, the assumptions underlying the deterministic modelling method cannot represent many intra- and inter-cellular processes, which, typically, are sensitive to the behaviour of a relatively small number of cells and molecules. Under such circumstances any given set of initial conditions can lead to a plurality of end-states. Stochastic CA are models designed to represent the latter systems. In these models the caveats of the deterministic approach are avoided, since they allow for randomness in the activity of the system's operators.

12.3 A Cellular Automata Model of Hypersensitivity

The model to be employed here for studying the role of drug schedules in the eruption of hypersensitivity, is based on the *clonal selection theory* of the Nobel Price laureate F.M. Burnet (1959) developed on the tracks first highlighted by P. Ehrlich at the beginning of the twentieth century.

In our model, a cubic millimetre of blood serum of a vertebrate is mapped onto a two-dimensional $L \times L$ hexagonal lattice (six neighbours), with periodic boundary conditions. Physical proximity is modelled through the concept of lattice-site. All interactions among cells and molecules take place within a lattice-site in a single time step, so that there is no correlation between entities residing at different sites at a fixed time. The diffusion of entities at the end of each time step introduces correlations and is meant to model physical spread of cells and molecules.

Cells are added through an external compartment, which simulate the bone marrow and the thymus. The thymus is implicitly modelled through positive and negative selection of immature thymocytes before they get into the lymphatic system [49]. Major classes of cells of the lymphoid lineage (lymphocytes T helper and cytotoxic, lymphocytes B and deriving antibody-producing plasma cells) and some of the myeloid lineage (macrophages and mast cells) are represented.

The interactions among cells and molecules determine their functional behaviour. They may be *a-specific* (e.g., antigen phagocytosis by monocytes or macrophages, binding by mast cells, etc.) or *specific* according to their affinity or degree of chemical binding strength (e.g., Th interacting with B cells for antigen recognition, etc.). The complete list of interactions is reported in Table 12.1.

In principle, this stochastic CA model allows all cells to interact among themselves. However, in practice, the interactions follow a "greedy" paradigm. That is to say that once two cells successfully interact with each other, they are taken out of the pool of interacting entities for that time step.

Our model is more complex than the majority of the immunological models, as it considers an additional level of description, namely the intracellular processes of antigen digestion and presentation. This *endocytic* pathway is implemented by assuming that the exogenous antigen is digested and attached to the molecules of class II MHC for presentation to the Th's receptors (further details can be found in previous publications about the original CS-model [15] and its modifications [51]).

At each time step of the simulation of our model all cells and molecules can interact locally (i.e., on each lattice site) according to their internal state, represented by suitable internal variables. An interaction between two cells is considered successful if a change in their internal state has occurred.

The present model differs from the original CS-model, mainly in explicitly representing the cytokines. Among the multitude of cytokines involved in an immune response only a subset will be taken into account in the present model (see Figure 12.2).

Table 12.1 Interactions among cells, or cells and molecules; antigen digestion and presentation on class II MHC by APCs. Other modules of the model. (IC = immunocomplex)

Interactions	Entities involved	MHC class involved
B phagocytosis of antigen	B, Ag	
MA phagocytosis of antigen	MA, Ag	
MA phagocytosis of IC	MA, IC	
APC's presentation to Th	MA, B, Th	class II
Immunoglobulins - Ag interaction	IgE, IgG, IgM, Ag	
Sensitisation of MC	MC, IgE	
Degranulation of MC	MC, Ag	
Digestion and presentation	**Entities involved**	**MHC class involved**
B digestion	B	class II
MA digestion	MA	class II
Other procedures	**Entities involved**	
Desensitise MC	MC	
B's isotype switch	B	
Th's class switch	Th	
Clone division	B,Th	
Haematopoiesis	B,Th,MC,MA	
Plasma secretion of immunoglobulins	PLB	
Diffusion	cells and immunoglobulins	

These are the ones which are directly involved in the allergic reactions [52,53] as follows:

- Interleukin-2 (IL-2), which is secreted by stimulated T helper cells. IL-2 is also known as T-cell growth factor (we will be using the acronym T-GF herein, which is not to be confused with the tumour growth factor). It promotes clonal expansion and differentiation of additional T helper and B cells.
- Interleukin-4 (IL-4), which stimulates antibody-producing B-cells to produce IgE instead of IgG. IL-4 inhibits IL-12 released by macrophages and Th1 proliferation. It promotes Th2 clone expansion instead.
- Interleukin-12 (IL-12), which acts in a contrasting manner to IL-4. It promotes Th1 type response and strongly stimulates T cells to synthesise IFN-γ ([54], observation cited in [29]).
- Interferon-γ (IFN-γ), which is secreted by Th1 cells and induces antibody switch to IgG. It also stimulates IL-12 production ([55], observation cited

in [29]) so that there is a positive feedback between IFN-γ and IL-12 (see Figure 12.2).

It is worth noting that two other cytokines which are often mentioned in the literature to be involved in allergic type I reactions, namely IL-13 and IL-5, are not implemented in the present model, for the following reasons:

- IL-13, which is a IL-4 homologue, is only moderately involved in isotype switch and is not involved in Th2 polarization, although it is significant in other proallergic functions.
- IL-5 is ignored for simplicity, since it is involved in the recruitment and development of eosinophils, which are believed to play a central role during the late-phase allergic reaction [56] but which are not taken into account yet. Indeed, in a further work we will investigate the influence of IL-5 and eosinophils on the problem under study.

Homeostasis is explicitly modelled by a mean-reverting process around the initial population of cells (but see [57] for a simple discrete model of blood cells development, where homeostasis is maintained by simple negative feedback on the phase-transition of each proliferating cell):

$$\Delta X_i(t) = \frac{ln2}{\tau_i}(X_i(0) - X_i(t)) \tag{12.1}$$

where $X_i(t)$ is the number of cells or molecules of class i at time t. Equation (12.1) guarantees that, if no antigen is injected into the system, no interactions take place and the system fluctuates around its initial state. The parameter τ_i indicates the half-life of entity i. Most of these values, reported in Table 12.2, are known from the literature [24]. Exceptions are the half-life of memory cells and plasma cells. It is known that some memory cells live for years or even decades, but it is very difficult to actually estimate their half-life [58]. Plasma cells are believed to live for a few days only, but see [58] for a different estimation. We arbitrarily choose to set the half-life of memory cells to six months and those of plasma cells to three days.

The *paracrine* and *autocrine* nature of the action of cytokines is provided by the fact that cytokines release from cells is *local* and *instantaneous*. That is to say that in our model the cytokines are released at the time a cell receives the required signal (mainly during a receptor-binding with another cell), and they are released locally, on the lattice-site where the interaction takes place.
Here we need to make some working assumptions:

- All cells release either the same *basic* amount (indicated by ω) of cytokines or they secrete an *enhanced* number ($\rho \cdot \omega$) of cytokines (see Table 12.3).
- The enhancement corresponds to doubling the rate of secretion (i.e., $\rho = 2$).
- The basic amount ω is equal for all cytokines. This implies that all cytokines have the same ability of exercising their action.

Table 12.2 Half-life of cells and molecules (τ is expressed in days) [24]. Half-life of memory cells is set to six months although it is believed that the immune memory can last for several years. Half-life of the antigen is arbitrarily set to about a year but, in practice, this value does not play a role in our simulations, where antigen is phagocytised by antigen-processing cells in a much shorter period of time. Histamine lasts for less than a minute but, technically, its half-life is constrained by the time resolution adopted, which is eight hours.

Cell	τ	Molecule	τ	Molecule	τ	Molecule	τ
B	3.3	Ag	365	IgM	5	IFN-γ	0.3
Th	3.3	IC	30	IgE	2.5	IL-4	0.3
MA	3.3			IgG	23	T-GF	0.3
MC	3.3					IL-12	0.3
PLB	3.3					HIS	0.3
B memory	180						
Th memory	180						

The antigen injected into the system breaks the equilibrium, bringing the collective dynamics to a metastable state of infection. In other words, once we inject the antigen, some cells move from the inactive state to the active one, through the interaction with other cells or molecules. A cascade of events follows, leading to the clonal expansion of lymphocytes. For example, during the antigen-recognition process, the lymphocytes T helper interact with the antigen presenting cells and eventually enter the mitotic cycle.
The probability for a stimulated B cell to divide at each time step for a maximum of n steps is given by

$$\Pr[\mathrm{B\,divides}] = F_1\left(T_x(t)\right) \cdot F_2\left(T - GF(t)\right), \tag{12.2}$$

where $T_x(t)$ is the total number of cells

$$T_x(t) = B_x(t) + Th_x(t) + MA_x(t) + PLB_x(t) + MC_x(t)$$

in site x at time t,

$$F_1(T_x(t)) = \exp\left(-\frac{T_x^2(t)}{\gamma^2\left(\sum_x T_x(0)\right)^2}\right). \tag{12.3}$$

γ is a constant which determines a size-effect constraint on the clonal expansion,

$$F_2(T - GF(t)) = 1 - \exp\left(-\frac{T - GF_x^2(t)}{\eta^2}\right) \tag{12.4}$$

is the stimulation given by the local amount of cytokines T-GF, and the parameter η represents its efficiency.

Clone division of cells is governed by several parameters. One of these is the number of duplication steps n (i.e., the number of times a cell creates a copy of itself). This parameters is set to $n = 5$. Hence, under suitable conditions (presence of growth factor or absence of inhibitor cytokines), 2^5 cells are created out of the first progenitor activated cell. The parameter γ in Equation (12.3) is chosen to allow a 4- to 15-fold increase of lymphocyte counts during acute infections [24].

After division a B cell matures into either a memory cell or an antibody-producing plasma cell, with probability 1/2.

The probability for a Th cell that has already entered the mitotic cycle to divide is computed taking into account also cytokines' inhibition.

$$\Pr[\text{Th divides}] = F_1(T_x(t)) \cdot F_2(T - GF(t)) \cdot F_3(c), \tag{12.5}$$

where F_1 and F_2 are as in Equations (12.3) and (12.4) respectively, and

$$F_3(c) = \begin{cases} 1 & \text{if } c = 0; \\ \exp(-IL4_x^2(t)/\kappa^2) & \text{if } c = 1; \\ \exp(-IFN_x^2(t)/\kappa^2) & \text{if } c = 2. \end{cases} \tag{12.6}$$

The factor $F_3(c)$ stands for the inhibition of the cytokines IL-4 and IFN-γ, and is dependent on the class $c = 0, 1$, and 2 of the Th cell: If the duplicating Th cell is of class 1 then it is inhibited by IL-4; on the other hand, if it is a Th2 cell then it is inhibited by IFN-γ. If the cell is Th0 then $F_3 = 1$ and there is no inhibition. The parameter κ represents the cytokines inhibition efficiency (note that, for simplicity, κ has been taken equal for both IL-4 and IFN-γ).

The switch between Th's classes depends on the local concentration of cytokines. The probability p of a Th0 cell to become a Th1 or Th2 is given by the relative local amount of IL-4 and IFN-γ

$$p = \left(1 + \frac{IFN_x(t)}{IL4_x(t)}\right)^{-1}. \tag{12.7}$$

This means that Th0→Th2 with probability p whereas Th0→Th1 with probability $1 - p$. If neither IL-4 nor IFN-γ is present in site x, then no switch takes place. Note that in so doing, we are actually embracing the hypothesis that it is not possible for Th1 or Th2 committed cells to switch back to the other class. Hence Th1/Th2 are taken as committed cells.

The isotype switch occurring to B cells is modelled through a sigmoid-Hill function with coefficient m and C,

$$p = \frac{x^m}{C^m + x^m}, \qquad C = \omega,\ m = 2. \tag{12.8}$$

The parameter C has been set to ω, which, in turn, determines the cytokines' secretion rate of cells. The value of parameter m has been arbitrarily chosen equal to two.

The bound between IgE and the Fc receptor on mast cells is stable for a number of weeks [24]. Hence we use a negative-binomial distribution for this event, and

we "desensitise" a mast cell with probability p (meaning that the mast cell loses its IgE bound to Fc receptors). Because the expected value of the negative binomial distribution is $1/p$, we set $1/p = 3$ months, that is $p = 0.0037$, given that a time step is 8 hours, as we will see in the following paragraph.

At the end of each time step, cells and immunoglobulins (but not cytokines which purposely are not assumed to diffuse – in order to match the *autocrine* or *paracrine* nature of cytokines signalling [24]) diffuse from one lattice site to a randomly chosen neighbouring site. Each entity moves independently, the whole process resembling a Brownian motion of particles. It should be mentioned that we are taking equal diffusion coefficients for all modelled entities. Clearly this is only a rough approximation. However, this does not really influence the results, since our model assumes a uniform concentration of cells and molecules.

12.3.1 Choosing Parameters

All the model parameter values are given in Table 12.3. This parameter set is considered here the *standard set of parameters*. In other words, parameter values in Table 12.3 are those used in all simulations, unless specified otherwise. Most of the values have been taken from standard immunology literature. The parameters have been grouped as those whose value was taken from known literature, those which are considered arbitrary and those which determine the initial conditions of the simulation. The values of the half-life, τ, are given in Table 12.2.

Antibody molecules as well as cytokines are handled in "quanta" of concentration, that is, there is a minimum amount of molecules which is taken in bulk within the interaction procedures. These quanta are one milligram per millilitre ($mg/m\mathrm{L}$) for antibodies, one femptogram per millilitre ($fg/m\mathrm{L}$) for cytokines and one nanogram per millilitre ($ng/m\mathrm{L}$) for histamine.
Secretion of monoclonal antibodies by hybridomas, in terms of concentration in plasma, is at about 1-20 $mg/m\mathrm{L}$ during its lifetime [24]. Therefore we set the antibodies secretion rate in plasma to $b = 10\ \mu g/m\mathrm{L}$ per time step, which is, 8 hours.

How to set the initial proportion of Th cells in the class 1 or 2 is a major concern. As a matter of fact this proportion is taken as the criterion for distinguishing hypersensitive people from nonhypersensitive ones. In our model, hypersensitive individuals are characterised by having a larger number of initial Th2 cells. We use two parameters for this purpose: α and β. Thus,

$$
\begin{aligned}
Th0(0) &= \alpha Th(0), \\
Th1(0) &= (1-\alpha)\beta Th(0), \\
Th2(0) &= (1-\alpha)(1-\beta) Th(0),
\end{aligned}
$$

where $Th(0)$ is the total number of helper cells (cfr. Table 12.3). The values of α and β, taken arbitrarily here, are given as initial condition and determine the initial level of susceptibility to the allergen.

Table 12.3 Standard parameter set. The initial amount of cytokines (IL-4, IFN-γ, IL-12, T-GF) is set to zero to indicate normal conditions. ($\mathbb{N}$ and $\mathbb{R}$ indicate integers and real numbers respectively.)

Parameter	Meaning	Range	Value
Known values			
b	Ab secretion rate	$\mathbb{N}$	10 (μg/mL/8h)
n	lymphocytes duplication steps	$\mathbb{N}$	5
ρ	cytokines amplif. factor	$\mathbb{N}$	2
Arbitrary parameters			
η	T-GF efficiency	$\mathbb{R}$	50
κ	cytokines inhib. efficiency	$\mathbb{R}$	10
h	histamine secretion rate	$\mathbb{N}$	1 (pg/mL/8h)
Initial conditions			
L	lattice dimension	$\mathbb{N}$	20
$B(0)$	B's init. population	$\mathbb{N}$	260 (cells/$m\mathrm{m}^3$)
$Th(0)$	Th's init. population	$\mathbb{N}$	875 (cells/$m\mathrm{m}^3$)
$MA(0)$	MA's init. population	$\mathbb{N}$	350 (cells/$m\mathrm{m}^3$)
$MC(0)$	MC's initials	$\mathbb{N}$	300 (cells/$m\mathrm{m}^3$)
γ	size constraint	$\mathbb{R}$	10
$1-\alpha$	fraction of Th0	$[0,1)$	0.9
β	fraction of Th1/Th2	$[0,1)$	0.2
ω	cytokines secretion rate	$\mathbb{N}$	100 (0.1pg/mL)

12.3.1.1 Setting the Scale of Time and Space

The time scale of the model is determined by our assumption that a lymphocyte completes one mitosis cycle in one time step. Since, once stimulated, a lymphocyte divides for about three times a day, our time step corresponds to about 8 hours.

Space is not so simple to define in our model. It is the normal adult blood-cell counts which gives us the reference value. In fact, fixing to about 10^3 the initial lymphocytes' counts our simulation space is taken to be about one $m\mathrm{m}^3$ of blood serum. The only arbitrary value is the initial number of mast cells, which is very low in blood, but high in tissues.

Note that when the initial population of cells is fixed, the lattice dimension L determines the concentration, hence the affinity to the antigen and, in general, the interaction probability.

12.4 Model Validation and Simulation Results

In the first set of simulations we are mainly interested in validating the model suitability for retrieving real-life hypersensitivity. To do so, we first check whether the model can reproduce an immune response, while fulfilling the hallmarks of an IgE-mediated hypersensitive reaction in susceptible individuals. Subsequently, a set of simulations (paragraph 12.4.3) are performed to asses the dependence of the IgE level on both the level of IL-4 and that of IFN-γ [59].
The second set of simulations represents the core of our work. Here we investigate the effect of the allergenic drug dosage and administration schedule on the amount of histamine released by mast cells. Finally, in section 12.5, we briefly discuss the main results and suggest some implications for future drug therapy.

It is worth at this point, to spend few words about the way we use the terms "dose" and "concentration" hereafter. When we say "drug concentration" of, e.g., 2000 $ng/m\mathrm{L}$, we actually mean "the dose whose resulting concentration is 2000 ng in a millilitre of blood after a suitable delay of time," since our simulation space is always a millilitre of blood.

12.4.1 Healthy Subjects: Primary and Secondary Immune Response to a Generic Antigen

There are several ways in which *normal* immune response to a generic antigen can be simulated using our model. For instance one can inhibit the production of IL-4 in the model, thus "knocking-out" IL-4 activity [60]. Another possibility is to force Th cells to be of class 1 only (i.e., $\beta = 1$). Here we mimic a healthy subject by using the first method, that is, we set things so that no IL-4 can be released by Th2 cells. The consequence is a bias towards the Th1 response, i.e., a normal immune response.

The drug administration protocol consists of a first injection at initiation (time zero) and a burst injection at day 40. The drug dose for both injections is calculated so that in one $m\mathrm{m}^3$ the concentration is 2000 $ng/m\mathrm{L}$ (recall paragraph 12.4). Results suggest that the model system reproduces a classical primary and secondary Th1-type, response (Figure 12.3, panels a, b, and c). In panel (a) we see simulation of the blood levels profiles of the interleukins IFN-γ, IL-4, and IL-12. Note that the first increase in all three interleukins is only marginal, occurring 14 days following the first drug challenge. In contrast, the second drug challenge generates a much more significant response in all the simulated interleukins. The level of T-GF is also different during the first and the second response, but the difference from the hypersensitive case (next paragraph) emerges only at the second injection. Panel (b) shows the level of immunoglobulins produced by plasma cells where the IgM type are eventually overtaken by IgG during the second response. Finally, the system

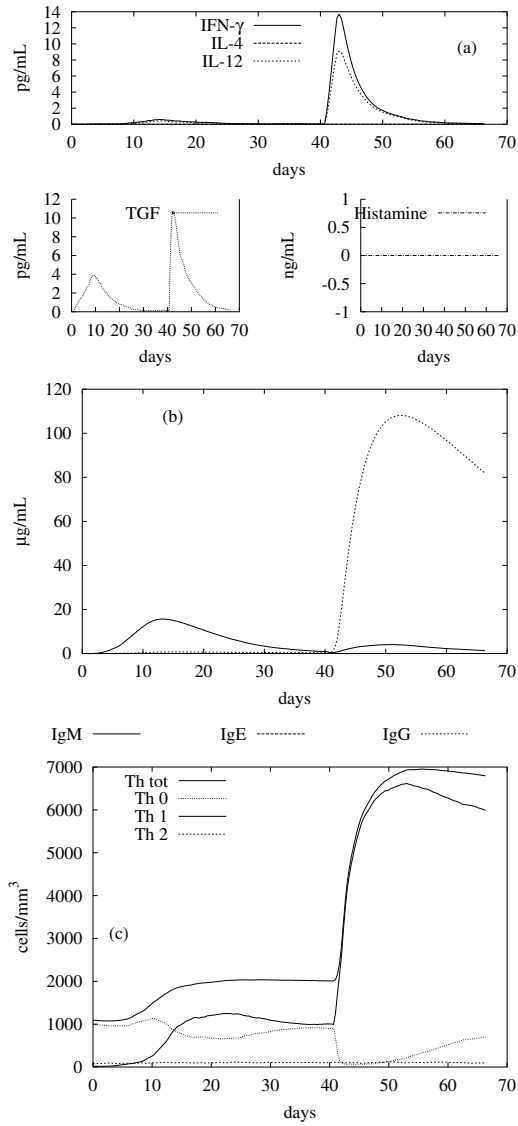

Figure 12.3

Immune response in healthy subjects (or IL-4 knockout mice [60]). Allergenic drug injections are scheduled to be at initiation and in day 40. No histamine is released, because mast cells are not sensitised (not shown) given that no IgEs are secreted (panel (b)). The immune response is of the Th1-type (panel (c)) since IL-4 is absent (panel (a)).

develops immune memory of the Th1-type for the specific antigen (panel (c)). In summary, using our CA tool we retrieve

- the production of antigen-specific IgG antibody (Figure 12.3, panel (b));
- the production of IFN-γ by type 1 Th cells (Figure 12.3, panel (a)); and
- a moderate degree of proliferation of helper cells (Figure 12.3, panel (c)).

Note that in our "healthy subject" model no IgEs are produced (panel (b)) and therefore mast cells do not get sensitised (panel (a)) and no histamine is released (for simplicity we assumed that the basic level of histamine secretion is null).

12.4.2 Allergic Subjects: Sensitisation and Hypersensitivity to a Generic Allergenic Drug

To simulate hypersensitive subjects, who develop a large amount of immunoglobulins of the IgE isotype, we assume an initial Th1/Th2 ratio (i.e., $\beta = 0.2$). Having made this assumption we expect the course of immune response in the hypersensitive individual to be quite different from that of the normal individual. Letting the simulated drug protocol be the same as in the previous experiment, we obtain results as summarised in Figures 12.4 and 12.5. Figure 12.5b shows the population size of Th1-Th2 cells. Comparing results to those displayed in panel (c) of Figure 12.3 one can immediately notice that the initial bias towards higher proportions of Th2 to Th1 suffices for a Th2-type, or allergic response. This result can be interpreted as follows: the first contact with the allergenic drug triggers Th2 cells to release IL-4 (Figure 12.4a). Consequently, increased production of Th2 cells occurs, resulting from the amplified IL-4 production and the inhibited IL-12 and IFN-γ release (Figure 12.4a). In fact, the inhibition of IL-12 prevents the Th0$\rightarrow$Th1 transition so that the Th0$\rightarrow$Th2 transition is now favoured. Increased proportion of Th2 cells, eventually results in the IgG to IgE isotype switch (Figure 12.4b), and IgEs bound to the Fc receptor on mast cell's membrane are crossed-linked by new allergenic drug molecules to degranulate these cells and release histamine (Figure 12.4a bottom right).

In our model at least *two* bounded IgE molecules are required for a mast cell to become sensitised. Figure 12.5a shows the changes, over time, in the proportion of sensitised mast cells. Note, in this figure, that the counts of sensitised mast cells are lower during the first contact with the allergenic drug. This is because IgM are more numerous at the onset. The second injection dosing of allergenic drug finds the system in the Th2-dominant-state so that a larger production of IL-4 induces a large IgE isotype switch of B lymphocytes (Figure 12.4b) with consequent cross-linking and degranulation of already sensitised mast cells. In summary, note that the first response here is mainly IgM, while the second response is dominated by IgE immunoglobulins. Moreover IgGs are virtually absent during the second response,

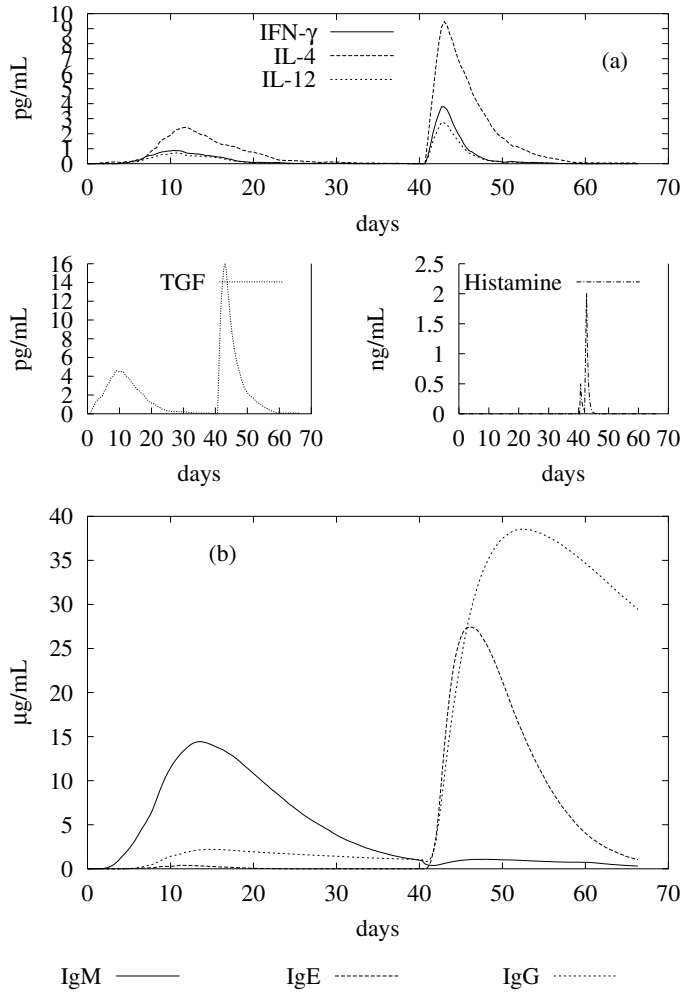

Figure 12.4

Response in hypersensitive subjects. Allergic subjects have a different immune reaction to the allergen compared to healthy (cfr. Figure 12.3). In particular large production of IL-4 which amplify Th0 to Th2 switch (see Figure 12.5) and isotype switch to IgE (panel (b)) with consequent cross-linking (i.e., sensitisation, Figure 12.5) and degranulation with release of histamine (panel (a) bottom right). The parameter $\beta = 0.2$, the injection of allergen is as for Figure 12.3.

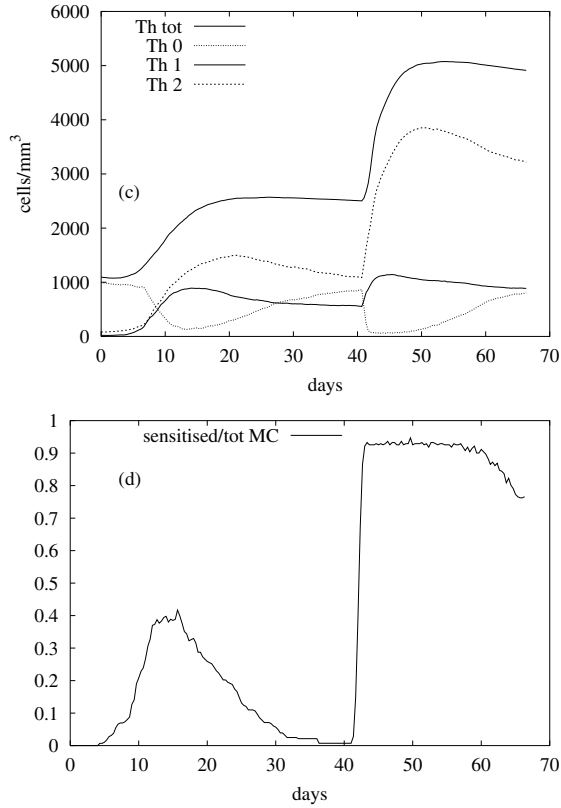

Figure 12.5

Response in hypersensitive subjects. Referring to Figure 12.4, the top panel shows the amplified Th0 to Th2 switch and the bottom panel the sensitisation.

and Th proliferation (Figure 12.5a) is much larger, as compared to that of healthy subjects.

The above simulations validate our model's versatility in reproducing the differences between normal and hypersensitive response.

12.4.3 Effects of IFN-γ and IL-4

To further validate our model we study the effect of IFN-γ and IL-4 on the development of IgE or IgG antibodies (cfr. Figure 12.6). To this end we initiate treatment by injecting a variable amount of IL-4, or a variable amount of IFN-γ. Two weeks later we measure the amount of IgE and IgG produced. Results are shown in Figures 12.6a and 12.6b respectively, where each point is computed averaging the outcome of hundred independent runs.

As expected, the results in Figure 12.6 show that the level of produced IgE is positively correlated with IL-4 dose, since IL-4 not only favours isotype switch to IgE, but also sustains the switch of Th0 to Th2 cells, further producing IL-4 in a positive feedback. In contrast, the level of IgE is negatively correlated with the injected IFN-γ dose, since IFN-γ amplifies the effects of IL-12 released by antigen processing cells, and induces Th0 to undergo a class switch to Th1. In addition, IFN-γ supports isotype switch of B cells to IgG. The inverse results are obtained for the effect of IL-4 and IFN-γ on IgG production. As can be seen in Figure 12.6, our simulation results are in good agreement with real-life observations ([24], observation cited in [59]).

12.4.4 Hypersensitivity Dependence on Drug Dose

In this section we investigate the relationship between the allergenic drug dose and the amount of histamine released. The parameter setting is the same as in the previous experiments, the only difference being the concentration of allergenic drug in blood and the administration schedule.

In these simulations we make use of the knowledge of the "critical histamine level," that is, the amount of secreted histamine above which allergic symptoms appear, whose average value can be defined to be 1 $ng/m\mathrm{L}$ [61]. Nevertheless, it should be mentioned here that in clinical practice the distinction between "normal" and "pathologic" is not so sharp, the threshold of hypersensitivity possibly lying anywhere in the interval 1-10 $ng/m\mathrm{L}$.

In the first simulation experiment we check the effects of the dose of the allergenic drug administered at initiation (denoted *sensitisation*). We do so by varying the sensitisation dose and by measuring the peak value of histamine a few days of simulated time following sensitisation. In Figure 12.7a we plot the average peak of histamine measured within few days after the dosing, as computed over a hundred independent simulations. Results show that the level of histamine release increases proportionally to the sensitising allergen dose. Moreover, a sharp increase above the critical allergic threshold of 1 $ng/m\mathrm{L}$ histamine concentration is found for drug dosing corresponding to about $10^3 ng/m\mathrm{L}$ (cfr. Figure 12.7a) .

Hence a *large dose* of drug, administered in a single shot, is not advisable. Therefore a different method of administration should be considered. This can be,

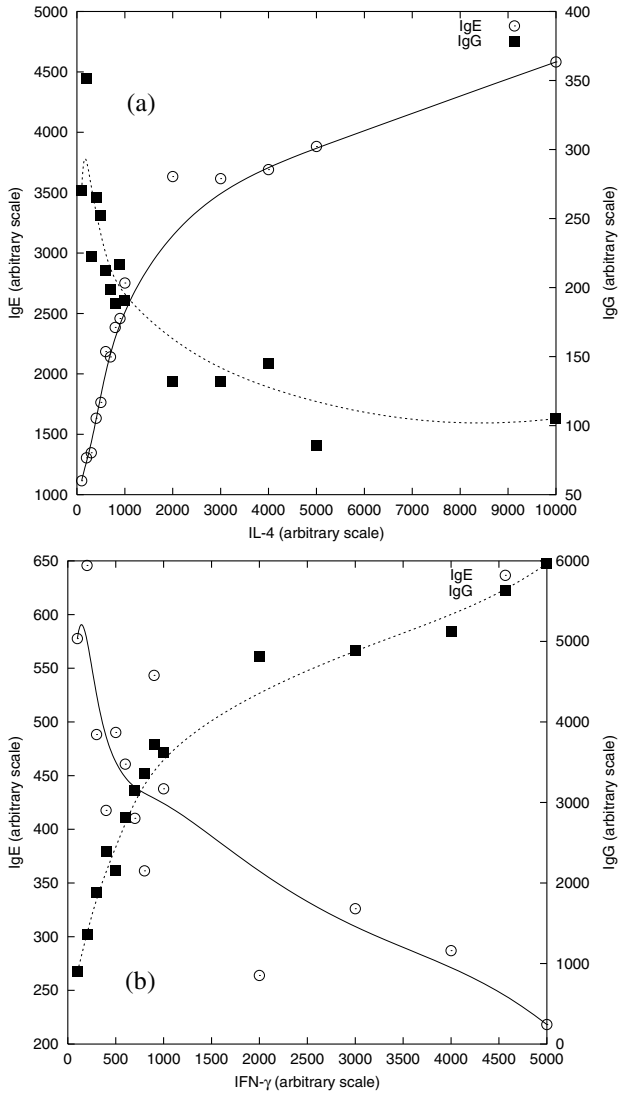

Figure 12.6

IgE and IgG production as a function of the injected IL-4 and IFN-γ doses. IgE production is positively correlated with the injected IL-4 dose and negatively correlated with the dose of IFN-γ. The opposite holds for IgG production. Comparison with *in-vitro* observations is shown (from [24], observation cited in [59]). Concentrations on both axes are given in arbitrary units.

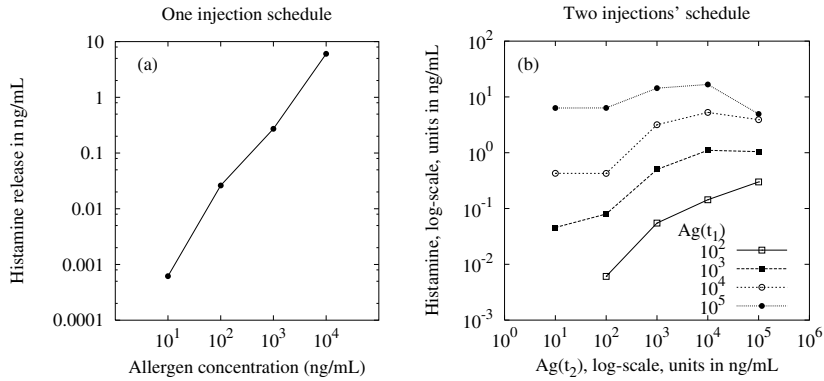

Figure 12.7

Panel (a): Histamine release as a function of the sensitising allergenic drug dose for a single administration. Different doses of allergen are administered at time zero. The corresponding histamine release level increases above the allergic threshold of 1 $ng/m\mathrm{L}$ [61] for an allergenic drug dosing corresponding to the critical concentration of $10^3 ng/m\mathrm{L}$. One hundred independent simulations are averaged; standard deviation is shown as error bars. Panel (b): Histamine release following two allergenic drug dosings of different doses. The plot shows the histamine concentration during the secondary immune response as a function of drug dose in the second dosing $Ag(t_2)$.

for example, administration in divided doses. In order to use our model for studying the effect of such multi-dosing protocols we make another set of experiments.

These simulations are performed according to the following settings: at time 0 we inject the allergenic drug, dose being $Ag(t_1) = 10^2, 10^3, 10^4$, and 10^5 $ng/m\mathrm{L}$. About two weeks later we administer the same variable amount $Ag(t_2)$ (what is called the *challenge*). Thus, in two administrations we check sixteen different dose-schedules $(Ag(t_1), Ag(t_2))$. One hundred independent simulations are performed for each schedule, and the amount of histamine at the peak level *after the second dosing* is measured. Averages are then computed and plotted in Figure 12.7b.

Results in Figure 12.7b suggest a correlation between the first administration dose $Ag(t_1)$ and the amount of histamine released by mast cells. Thus, a sensitisation dose of $Ag(t_1) = 10^4$ $ng/m\mathrm{L}$ risks to stimulate an above-threshold release of histamine, if followed, two weeks later, by a successive dosing above 10^3 $ng/m\mathrm{L}$. It is also interesting to note that a strong sensitisation dosing $(Ag(t_1))$ sets the system to release high levels of histamine, for any positive challenge dose $A(t_2)$ (the points for $Ag(t_1) = 10^5$ remain the same on the log-scale x-axis). This suggests that a larger second dosing is not advisable unless the sensitisation is made with low dosage. In fact, only $Ag(t_1) = 10^2$ and 10^3 $ng/m\mathrm{L}$ remain below the critical level

Table 12.4 Parameters estimated from simulated data shown in Figure 12.8 for Equation (12.9).

Allergen concentration (ng/mL)	a	b	c	d
1000	0.899	3.754	2.662	0.215
2000	2.778	3.422	2.676	0.377
5000	7.330	2.701	2.718	0.715

of 1 ng/mL of histamine after the challenge for the doses tried in this experiment. This result is in line with experimental practice during immunotherapies [2,62].

12.4.5 Dependence of Hypersensitivity on Dosing Interval

In the above experiments we used schedules of two allergenic drug cycles, where the second drug administration was constantly delayed by two weeks. In this section we investigate how the histamine level may change under different intervals between the two cycles $\Delta = t_2 - t_1$. The total drug concentration in a $m\text{m}^3$ in both the sensitisation and the challenge dosing ($Ag(t_1)$ and $Ag(t_2)$, respectively) is set to 1000, 2000, or 5000 ng/mL. We first inject the allergenic drug at time zero and for the second time following a variable delay ranging from 3 days to 100 days. As usual, 100 independent simulations are performed for each setting and the amount of histamine at peak level is measured. Averages are then computed and plotted in Figure 12.8.

Histamine secretion as a function of the dosing interval $H(\Delta)$ is well described by the exponential function

$$H(\Delta) = a \exp\left[-b(\ln(\Delta) - c)^2\right] + d, \tag{12.9}$$

with parameters given as in Table 12.4.

Some of the parameters can be assigned a biological meaning: a depends on the secretion rate of histamine from mast cells (it is expressed in ng/mL/days; cfr. parameter h in Table 12.3), b is a free parameter, whereas d (expressed in ng/mL) determines the asymptotic level of histamine and may be an important estimation of the level of tolerance. Note that the asymptotic value d strongly depends on the half-life of the immune memory. In fact, if memory fades away before the second dosing, a similar response to the first dosing is to be expected.

A most interesting result is obtained when one attempts to estimate the parameter c (expressed in days). This parameter determines the interval, corresponding to the maximum of the function in Equation (12.9), which is attained at $\Delta = e^c$. In all cases simulated here this value corresponds to about two weeks, regardless of the allergenic drug dose. Therefore our model predicts two weeks as the delay one should avoid when setting protocols for chemotherapy, regardless of the drug dosage; how far one should deviate from the two-week delay is a function of the dose (see below).

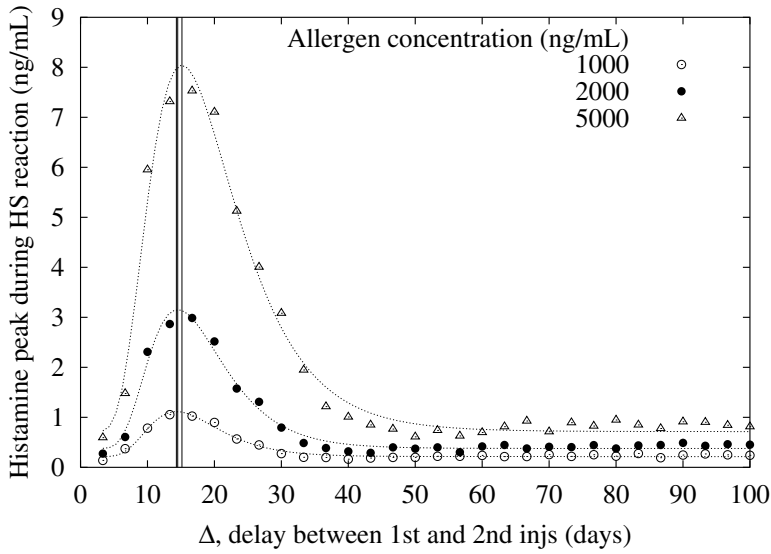

Figure 12.8

Histamine concentration versus $\Delta = t_2 - t_1$. Three regimes are visible: 1) the immune response is still active and wipes out the allergen; 2) large response; and 3) low response because of the decreased number of sensitised mast cells. This stems from the fact that IgE-Fc bound to mast cells can last for e.g., 12 weeks. The 1000 $ng/m\mathrm{L}$ drug-dosage is safe for this two dosings schedule. In contrast, for the 2000 and 5000 $ng/m\mathrm{L}$ drug-dosages there exists a window of durations of the dosing interval, $\Delta_1 - \Delta_2$ (see below), between the two administrations, which increases histamine release above the critical level of 1 $ng/m\mathrm{L}$.

From the simulations in section 12.4.4 we already learned that a safe value for the drug dose would be of 10^3 $ng/m\mathrm{L}$, while 10^4 $ng/m\mathrm{L}$ risks to cause an allergic reaction. Moreover, we already know that for intermediate drug doses there exists a window, for the delay Δ, for which histamine reaches levels above the critical value of 1 $ng/m\mathrm{L}$ which we call now $\tilde{h}$. Performing some simple algebra, using Equation (12.9), we may compute the width of the window as $\Delta_2 - \Delta_1$, where

$$\Delta_1 = \exp\left(c - \sqrt{\frac{1}{b}\ln\frac{a}{\tilde{h}-d}}\right),$$

and

$$\Delta_2 = \exp\left(c + \sqrt{\frac{1}{b}\ln\frac{a}{\tilde{h}-d}}\right),$$

for $a > \tilde{h} - d$ and $d \neq \tilde{h}$. Hence, for example, after estimating the coefficient of the function in Equation (12.9), we can predict whether or not a certain time-schedule

protocol is advisable. For example, for the case of 5000 $ng/m\mathrm{L}$ drug administration, we obtain $\Delta_1 = 5$ .06 days and $\Delta_2 = 45.33$ days.

12.4.6 Fractionating the Drug Dose into Multiple Dosings

We now consider the question whether hypersensitivity reaction can be avoided by further fractionating each drug dosing within a therapy-cycle in a manner equivalent to "applying slow drug administration." In order to address such an issue we perform a set of experiments in which two therapy-cycles are composed of a period of administration of one, two, or three time steps each. Recall that a time step is 8 hours, so that one dosing is equivalent to an 8-hour period of infusion, two dosings are equivalent to a 16-hour period of infusion, and so on. As usual, 100 runs for each scenario are performed, peaks of histamine are measured and averages are shown in Figure 12.9. Plot (a) refers to the total administration of 1000 $ng/m\mathrm{L}$, plot (b) to 3×10^3, and (c) refers to 10^4. As shown, for the case (a) and (b), there is no much difference in the hypersensitivity reaction which results from single or multiple drug dosing of the same total dose. A more significant difference is seen in plot (c), but this is probably due to statistical fluctuations of the results. At this time, given the gross time-resolution adopted in the model (8 hours per time step) we are unable to say if such a result is due to some systematic phenomenon.

12.5 Discussion

Many antitumour drugs have been shown to induce hypersensitive responses. One of the extensively studied examples is the widely used cytotoxic drug, paclitaxel, which is administered in a variety of solid tumour diseases [21,63]. As hypersensitivity to the drug can hamper further therapy, it may be interesting to investigate the effects of the allergenic drug schedule, dose fractionation, dosing interval, and rate of administration, on the resulting symptoms of hypersensitivity. To study these questions we simulated various drug treatment scenarios, employing a CA model of the immune system. Our results are interpreted below hoping to arrive at some practical conclusions for future therapies.

We started by studying the dose effect of a single allergenic drug administration. Figure 12.7a shows that there exists a critical value for the amount of allergenic drug dose for which the allergic threshold of 1 $ng/m\mathrm{L}$ of histamine released is exceeded. This critical concentration is found to lie between 10^3 and 10^4 $ng/m\mathrm{L}$.

We then considered the fractionation of a single dosing into two administration cycles consisting of a single dosing each, and separated by a considerable fixed interval (two weeks). For investigating the effect of the dosage in a schedule of two successive cycles, different schedules are chosen for the simulations reported in Fig-

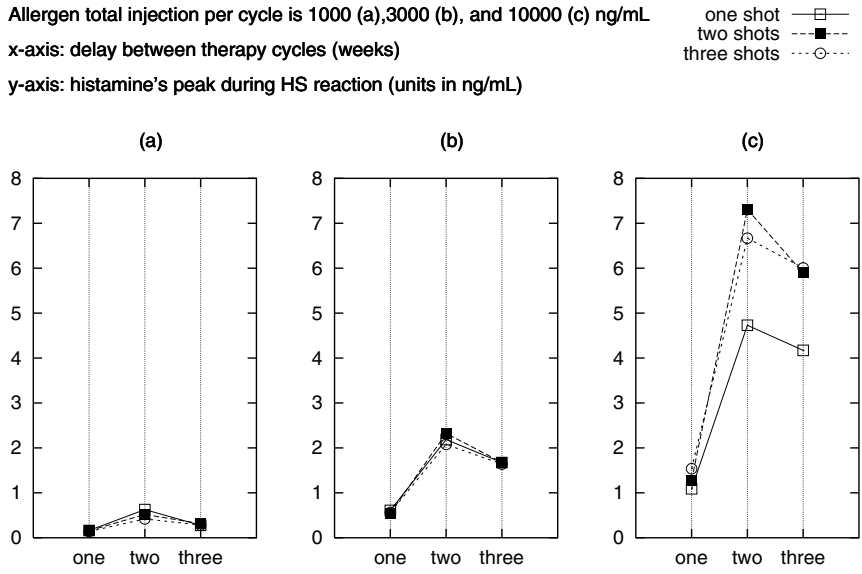

Figure 12.9

Histamine release corresponding to different slow drug administration protocols: two dosing cycles performed at day zero and after one, two, or three weeks. At each cycle, the dosing is performed over a period of 8, 16, or 24 hours. The total amount of allergenic drug is 10^3 $ng/m\mathrm{L}$ in plot (a), 3×10^3 in plot (b), and 10^4 in plot (c). The amount of allergenic drug is equally divided for the period of drug administration, so that, for example, the 16 hour administration in case (a), corresponds to two consecutive dosings (after 8 hours) of 0.5×10^3 $ng/m\mathrm{L}$.

ure 12.7b. Interestingly, we found that the drug dose during the second cycle does not significantly influence the histamine level released by mast cells, if the sensitisation dosing, that is the dosing of the first cycle, is high. The most straightforward explanation for this result is that, due to strong sensitisation, a large number of antibodies are formed, which actually compete for the allergen during the challenge with the sensitised IgE-bound mast cells. Critical concentration of histamine is reached for high drug dosage (even for 10^4 $ng/m\mathrm{L}$), if the challenge is a large dose (for example above 10^3 $ng/m\mathrm{L}$). Note that this is in agreement with the clinical experience in immunotherapeutic protocols: one starts with a small amount of allergen and gradually increases the amount to reach a certain maximum [2]. Indeed, in Figure 12.7b one can easily see that, for equal total drug dose (first dosing + second dosing), the histamine released during the challenge is higher when the first dosing is larger and, vice versa, it is lower for lower first dosing.

The second issue to be discussed is the effect of the allergenic drug dosing interval on hypersensitivity. Replacing the fixed dosing interval of two weeks, we

simulated cycles of therapy with delays of variable number of days between them. The results, summarised in Figure 12.7b, single-out a dosing interval of two weeks as the centre of the peak in histamine release, regardless of the dose of drug injected. The histamine increases above the critical pathological level only if the two cycles are critically distanced, but not if they are very shortly distanced. However, when using a larger amount of drug, both the boundaries of the critical window expand, leftward and rightward reducing the chances for an optimal delay between cycles.

A final question arises when considering prolongation of the drug administration period within a single cycle (i.e., one or more shots). In order to address such an issue we performed a set of experiments in which a therapy-cycle is composed either by a single, two, or three shots. Results are those shown in Figure 12.9. As suggested by this figure, the rate of drug administration of the same total dose has no or little effect on hypersensitivity, if the administered dose is one or three μg/mL. For higher dosage (panel (c)) some effect arises but given the large time scale adopted in our model (8 hours/time step) we are unable to tell more about it.

In summary, our results suggest that in order to avoid allergic reactions to drugs during therapeutic anti-cancer treatments, one should administer a growing dosage of drugs in the same way allergen is administered to the patient during immunotherapies. The interval between successive cycles should be either very short (if the drug dose is low) or very long (if the drug dosage is high) while the question if prolonged period of infusion reduces the risk of allergic reaction remains unanswered.

12.6 Conclusions

Simulations validate the ability of the model to capture the basics of immune phenomena in both normal and drug-hypersensitive individuals. By means of extensive numerical simulations we observe a strong correlation between histamine release and both allergenic drug dosage and the interval between successive dosings.

Varying the interval between successive drug dosings we find that histamine release after the burst dosing has a peak around e^c = two weeks, where c is a constant which seems independent of the allergenic drug dose. This result suggests the existence of an optimal value to be used during anti-cancer therapies.

Our results, however, may be improved in two different directions.

1. At present, we considered only mast cells to be responsible for the allergic reaction. However, it is believed that eosinophils provide further stimulation to the mast cells, inducing degranulation during the late-phase response, which occurs some minutes after the early phase [56]. Therefore, a possible improvement of the model would be to take them into account in order to draw more accurate conclusions.

2. In addition, a finer-grain in the definition of the time-resolution may aid in verifying whether increasing the period of drug administration, within each single

therapeutic cycle may reduce, or, rather, increase the magnitude of hypersensitive reaction.

Acknowledgments

Useful discussion with Prof. Josef Mekori and Prof. Francesca Levy-Schaffer is acknowledged. This work was supported by the European Union Commission through the Human Potential Programme, Contract No HPRN-CT-2000-00105.

12.7 References

[1] Weiss, R.B., Hypersensitivity reactions, *Semin. Oncol.* 19, 458-477, 1992.

[2] Kay, A.B., Allergy and allergic diseases. First Part, *N. Engl. J. Med.* 344, 30-37, 2001.

[3] Agur, Z., Arnon, R., and Schechter, B., Reduction of cytotoxicity to normal tissues by new regimes of phase-specific drugs, *Math. Biosci.* 92, 1-15, 1988.

[4] Cojocaru, L. and Agur, Z., Theoretical analysis of interval drug dosing for cell-cycle-phase-specific drugs, *Math. Biosci.* 109, 85-97, 1992.

[5] Agur, Z. and Dvir, Y., Use of knowledge on $\{\phi_n\}$ series for predicting optimal chemotherapy treatment, *Random & Comp. Dyn.* 2, 279-286, 1994.

[6] Webb, G.F., Resonance phenomena in cell population chemotherapy models, *Rocky Mountain J. Math.* 20, 1195-1216, 1990.

[7] Johnson, M. and Webb, G.F., Resonances in age structured cell population models of periodic chemotherapy, *Int. J. Appl. Sci. Comp.* 3, 57-67, 1996.

[8] Dibrov, B. et al., Mathematical model of cancer chemotherapy. Periodic schedules of phase-specific cytotoxic-agent administration increasing to selectivity of therapy, *Math. Biosci.* 73, 1-31, 1985.

[9] Agur, Z. et al., Zidovudine toxicity to murine bone marrow may be affected by the exact frequency of drug administration, *Exp. Hematol.* 19, 364-368, 1991.

[10] Agur, Z., Arnon, R., and Schechter, B., Effect of the dosing interval on survival and myelotoxicity in mice treated by cytosine arabinoside, *Eur. J. Cancer* 28A, 1085-1090, 1992.

[11] Agur, Z. et al., AZT effect on the bone marrow - a new perspective on the Concorde trials, *J. Biol. Sys.* 3, 241-251, 1995.

[12] Ubezio, P. et al., Increasing 1-b-D-arabinofuranosylcytosine efficacy by scheduled dosing intervals based on direct measurement of bone marrow cell kinetics, *Cancer Res.* 54, 6446-6451, 1994.

[13] Holgate, S.T., Allergic disorders, *British Med. J.* 320, 231-234, 2000.

[14] Ilachinski, A., *Cellular Automata: A Discrete Universe*, World Scientific Publishing Company, London, Singapore, 2001.

[15] Celada, F. and Seiden, P.E., A computer model of cellular interaction in the immune system, *Immun. Today* 13, 56-62, 1992.

[16] http://www.iac.rm.cnr.it/~filippo/cimmsim.html

[17] Aulbert, E. and Schmidt, C.G., Anaphylactic reaction in cyclophosphamide infusion, *Onkologie* 6, 82-83, 1983.

[18] Sakura, H. et al., Occurrence of an anti-peplomycin IgE antibody cross-reacting with bleomycin in a patient with cervical uterine cancer, *Cancer Chemother. Pharmacol.* 23, 333-336, 1989.

[19] Szepfalusi, Z. et al., IgE-mediated allergic reaction to hyaluronidase in paediatric oncological patients, *Eur. J. Pediatr.* 156, 199-203, 1997.

[20] BC Cancer Agency drug database. http://www.bccancer.bc.ca/HPI/DrugDatabase/DrugIndexALPro/Paclitaxel.htm

[21] Essayan, D.M. et al., Successful parental desensitization to paclitaxel, *J. All. Clin. Immun.* 97, 42-46, 1996.

[22] Kay, A.B., Allergy and allergic diseases. Second Part, *N. Engl. J. Med.* 344, 109-113, 2001.

[23] Gell, P.G.H. and Coombs, R.R.A., *Clinical Aspects of Immunology*, 1st Edition, Blackwell Scientific Publications, Oxford, 1963.

[24] Goldsby, R.A., Kindt, T.J., and Osborne, B.A., *Kuby Immunology*, 4th Edition, W.H. Freeman and Company, San Francisco, 2000.

[25] Barnes, K.C. and Marsch, D.G., The genetics and complexity of allergy and asthma, *Immunol. Today* 19, 325-332, 1998.

[26] Mossman, T.R. and Coffman, R.L., Th1 and Th2 cells: different patterns of lymphokine secretion lead to different functional properties, *Annu. Rev. Immunol.* 7, 145-173, 1989.

[27] Bergman, C., van Hemmen, L.J., and Segel, A.L., Th1 or Th2: how an appropriate T helper response can be made, *Bull. Math. Biol.* 63, 405-430, 2000.

[28] Kips, J.C. et al., Interleukin-12 inhibits antigen-induced airway hyperresponsiveness in mice, *Am. J. Respir. Crit. Care Med.* 153, 535-539, 1996.

[29] Magnan, A. et al., Venom immunotherapy induces monocyte activation, *Clin. Exp. Allergy* 31, 1303-1339, 2001.

[30] Perelson, A. and Weisbuch, G., Immunology for physicists, *Rev. Mod. Phys.* 69, 1219-1267, 1997.

[31] de Oliveira, S., de Oliveira, P., and Stauffer, D., *Evolution, Money, War, and Computers - Non-Traditional Applications of Computational Statistical Physics*, Teubner, Stuttgart, 1999.

[32] Bell, G.I., Mathematical model of clonal selection and antibody production, *J. Theor. Biol.* 29, 191-232, 1970.

[33] Bell, G.I., Mathematical model of clonal selection and antibody production II, *J. Theor. Biol.* 33, 339-378, 1971.

[34] Segel, L.A. and Bar-Or, R.L., On the role of feedback in promoting conflicting goals of the adaptive immune system, *J. Immunol.* 163, 1342-1349, 1999.

[35] Antia, R., Pilyugin, S.S., and Ahmed, R., Models of immune memory: on the role of cross-reactive stimulation, competition, and homeostasis in maintaining immune memory, *Proc. Natl. Acad. Sci. USA* 95, 14926-14931, 1998.

[36] McLean, A.R., Modelling T cell memory, *J. Theor. Biol.* 170, 63-74, 1994.

[37] Marchuk, G.I., Romanyukha, A.A., and Bocharov, G.A., Mathematical model of antiviral immune response. II. parameters identification for acute viral hepatitis B, *J. Theor. Biol.* 151, 41-69, 1991.

[38] Marchuk, G.I. et al., Mathematical model of antiviral immune response. I. data analysis, generalized picture construction and parameters evaluation for hepatitis B, *J. Theor. Biol.* 151, 1-40, 1991.

[39] Nowak, M.A. and May, R.M., Mathematical biology of HIV infections: antigenic variation and diversity threshold, *Math. Biosci.* 106, 1-21, 1991.

[40] Perelson, A.S. and Nelson, P.W., Mathematical analysis of HIV-1 dynamics *in vivo*, *SIAM Review* 41, 3-44, 1999.

[41] Kirschner, D.E., Using mathematics to understand HIV immune dynamics, *Notices Amer. Math. Soc.* 43, 191-202, 1996.

[42] Kirschner, D.E. and Webb, G.F., A model for treatment strategy in the chemotherapy of AIDS, *Bull. Math. Biol.* 58, 367-391, 1996.

[43] Perelson, A.S. and Oster, G.F., Theoretical studies of clonal selection: minimal antibody repertoire size and reliability of self-non-self discrimination, *J. Theor. Biol.* 81, 645-670, 1979.

[44] Agur, Z., Mazor, G., and Meilijson, I., Maturation of the humoral immune response as an optimization problem, *Proc. R. Soc. Lond. B Biol. Sci.* 245, 147-150, 1991.

[45] Agur, Z., Mazor, G., and Meilijson, I., *Mimicking the strategy of the immune system: insight gained from mathematics. Theoretical and Experimental Insights into Immunology*, A.S. Perelson and G. Weisbuch, Eds., Springer-Verlag, Heidelberg, 1992.

[46] Agur, Z., Resilience and variability in pathogens and hosts, *IMA J. Math. Appl. Med. Biol.* 4, 295-307, 1987.

[47] Celada, F. and Seiden, P.E., Affinity maturation and hypermutation in a simulation of the humoral immune response, *Eur. J. Immunol.* 26, 1350-1358, 1996.

[48] Seiden, P. and Celada, F., A model for simulating cognate recognition and response in the immune system, *J. Theor. Biol.* 158, 329-357, 1992.

[49] Morpurgo, D. et al., Modelling thymic functions in a cellular automaton, *Int. Immunol.* 7, 505-516, 1995.

[50] Kohler, B. et al., A systematic approach to vaccine complexity using an automaton model of the cellular and humoral immune system, *Vaccine* 19, 862-876, 1999.

[51] Bernaschi, M. and Castiglione, F., Evolution of an immune system simulator, *Comp. Biol. Med.* 31, 303-331, 2001.

[52] Jenmalm, M.C. et al., Allergen-induced Th1 and Th2 cytokine secretion in relation to specific allergen sensitization and atopic symptoms in children, *Clin. Exp. Allergy* 31, 1528-1535, 2001.

[53] Arshad, S.H. and Holgate, S., The role of IgE in allergen-induced inflammation and the potential for intervention with humanized monoclonal anti-IgE antibody, *Clin. Exp. Allergy* 31, 1344-1351, 2001.

[54] Wills-Karp, M., Interleukin-12 as a target for modulation of the inflammatory response in asthma, *Allergy* 55, 113-119, 1998.

[55] Hayes, M.P., Wang, J., and Norcross, M.A., Regulation of interleukin-12 expression in human monocytes: selective priming by interferon-γ of lipopolysaccharide-inducible p35 and p40 genes, *Blood* 86, 646-650, 1995.

[56] Piliponsky, A.M. et al., Human eosinophils induce histamine release from antigen-activated rat peritoneal mast cells: a possible role for mast cells in late-phase allergic reactions, *J. Allergy Clin. Immunol.* 107, 993-1000, 2001.

[57] Agur, Z., Daniel, Y., and Ginosar, Y., The universal properties of stem cells as pinpointed by a simple discrete model, *J. Math. Biol.* 44, 79-86, 2002.

[58] Slifka, M.K. et al., Humoral immunity due to long-lived plasma cells, *Immunity* 8, 363-372, 1998.

[59] Del Prete, G. et al., IL-4 is an essential factor for the IgE synthesis induced *in vitro* by human T cell clones and their supernatants, *J. Immunol.* 140, 4193-4198, 1988.

[60] Kuhn, R., Rajewsky, K., and Muller, W., Generation and analysis of interleukin-4 deficient mice, *Science* 254, 707-710, 1991.

[61] Renz, C.L. et al., Tryptase levels are not increased during vancomycin-induced anaphylactoid reactions, *Anesthesiology* 89, 620-625, 1998.

[62] Secrist, H., DeKruyff, R.H., and Umetsu, D.T., Interleukin 4 production by CD4+ T cells from allergic individuals is modulated by antigen concentration and antigen-presenting cell type, *J. Exp. Med.* 181, 1081-1089, 1995.

[63] Dorr, R.T., *The Annals of Pharmacotherapy*, Harvey Whitney Books Company, Cincinnati, OH, 1994.

Chapter 13

Reaction-Diffusion Systems: A Mathematical Biology Approach

Miguel A. Herrero

Departamento de Matemática Aplicada, Facultad de Matemáticas, Universidad Complutense de Madrid (Spain)

13.1 Introduction

Reaction-diffusion (RD) systems are mathematical models which provide macroscopic descriptions for the dynamics of media in which random motion and chemical reactions are the major players to be kept track of. In a typical situation, an RD system consists of several coupled differential equations, part of which at least involve space and time dependent variables, and are therefore of the type known as partial differential equations. A particularly simple but important case is provided by single scalar equations, of which the linear diffusion equation is arguably the most relevant example.

Reaction-diffusion systems have been extensively studied during the 20^{th} century. While the mathematical analysis of general, nonlinear RD systems is rather involved, in a number of cases of interest in applications RD equations have been shown to possess a wealth of interesting (and often intriguing) behaviours. These correspond to classes of particular solutions, the study of which often goes under the term of pattern formation theory. These notes are intended to provide an introduction to that subject, which plays an important role in many problems in the natural sciences. However, as it will become apparent from the list of contents, our choice is strongly biased in several aspects. First, the selection of topics made pays particular attention to models in biology and medicine. On the other hand, at the methodological level we have focused on the use of asymptotic methods, which are particularly efficient when the underlying dynamics involves different time and space scales. There is no question about other possible approaches having merits of their own. It seems, however, that the material being reported upon in the sequel is of primary interest for any researcher approaching the field of mathematical biology.

The plan of this chapter is as follows. To start, section 13.2 deals with a general overview of RD systems, followed by a short review of results concerning the linear diffusion equation and its relation to random walks. Then, after quickly remarking on asymptotic states for linear and nonlinear systems, we comment on Turing's classical work on diffusion-driven instability generation in linear systems. After that, the section concludes with a description of a simple (but relevant) model of nonlinear pattern formation, the so-called activator-inhibitor system proposed by Gierer and Meinhardt in 1972.

Section 13.3 deals with particular solutions of RD systems of wave type. As a starting point, we review some classical work on scalar, semi-linear diffusion equations, including the groundbreaking 1937 paper by Kolmogorov, Petrovsky, and Piskunov on the existence of travelling waves for a model arising in biology. We then turn our attention to excitable systems which are of particular interest in life sciences, and recall some relevant cases of wave propagation, including pulses, targets, and spiral waves.

Finally, in section 13.4 we present some selected topics on the mathematical analysis of chemotaxis, that is, on motion of micro-organisms driven by the gradient of an attractant (or repellent) chemical signal. After shortly reviewing the problem

of axon growth and neural navigation, we focus on the study of the aggregation properties of a much-studied model, namely the amoeba *Dictyostelium discoideum* (Dd). Phenomena such as chemotactic collapse and stream and spiral motions are considered, always with the help of the asymptotic techniques already introduced in section 13.3.

The material that follows is intended to be suitable for any advanced undergraduate or junior graduate student with some background in differential equations. To keep the flow of the main arguments in the text, lengthy calculations have been omitted, and arguments have been in general condensed. Whenever that occurs, reference is made to those articles or books where additional details can be found.

Last, but not least, I wish to express my sincere thanks to the coordinator of the European Project HPRN-CT-2000-00105, Professor Nicola Bellomo, and to the Director of the Propriano 2001 Summer School on "Using Mathematical Models and Computer Simulation to Improve Cancer Therapy," Professor Luigi Preziosi, for their continuous interest and helpful assistance in all aspects related to the preparation of this work. I am also particularly thankful to Professors Paul Fife and Juan Velázquez for a number of interesting remarks on topics considered in these notes.

13.2 Reaction-Diffusion Systems: Basic Results

In this section we shall recall some relevant facts concerning linear and nonlinear RD systems.

13.2.1 Modelling Assumptions

A reaction-diffusion system of equations is a mathematical formulation of a balance principle. More precisely, let us denote by $u_1, \ldots, u_m$ some quantities depending on space (represented by a vector $\mathbf{x} = (x_1, \ldots, x_n),\ n \geq 1$) and time (denoted by t). A possible rule for the evolution of the $u_i's$ is provided by

$$\frac{\partial u_i}{\partial t} + \nabla \cdot \mathbf{J}_i = f_i(u_1, \ldots, u_m, \mathbf{x}, t)\ , \qquad 1 \leq i \leq m\ . \tag{13.1}$$

The first term on the left of (13.1) corresponds to local variation of the variable u_i, whereas the second term there accounts for transport of u_i within the surrounding medium. In mathematical terms, the notation $\nabla \cdot \mathbf{J}_i$ means the divergence of the quantity $\mathbf{J}_i$, which is termed as the local flux. A typical choice for $\mathbf{J}_i$ is

$$\mathbf{J}_i = -\mathbf{D}^{(i)}(\mathbf{u})\nabla u_i + \sum_{k=1}^{m} \mathbf{v}_{ik}(\mathbf{u})u_k\ , \tag{13.2}$$

where $\mathbf{u} = (u_1, \ldots, u_m)$, and $\mathbf{D}^{(i)}$ is the diagonal matrix $\mathrm{Diag}\{D_1^{(i)}, ..., D_n^{(i)}\}$. The first and second terms in the right of (13.2) are usually referred to as the diffusive and convective components of the flux, respectively: $D_k^{(i)}(\mathbf{u})$ (resp. $\mathbf{v}_{ik}(\mathbf{u})$) are known as the diffusion (resp. convection) coefficients. For instance, assume that $n \geq 1$, $m = 1$ and $\mathbf{D}^{(i)}$, $\mathbf{v}_{ik}$ are constants such that $D_k^{(i)} = D_k > 0$, and $\mathbf{v}_{ik} = \mathbf{v}$ when $i = k$, and $\mathbf{v}_{ik} = 0$ otherwise. Then the transport term in (13.1) is given by

$$\nabla \cdot \mathbf{J} = -\sum_{j=1}^{n} D_j \frac{\partial^2 u}{\partial x_j^2} + \sum_{k=1}^{n} v_j \frac{\partial u}{\partial x_j} .$$

As to the forcing function (13.1), it represents a source (or sink) term, arising for instance from chemical reactions when the u_i denote substances susceptible of recombination. Typical choices for f_i are of a power-like or exponential nature. A simple example, corresponding to the case $n = m = 1$, is provided by $f(u, x, t) = au^k - bu^l$, for some real numbers a, b, k, and l.

13.2.2 Linear Diffusion

A particularly important example of RD systems is the linear diffusion equation, which is obtained by setting in (13.1) $m = 1$, $f = 0$, $v_i = 0$, and $D_i \equiv D > 0$ for $1 \leq i \leq n$. We then obtain

$$\frac{\partial u}{\partial t} = D\triangle u \qquad \text{where} \qquad \triangle u = \sum_{i=1}^{n} \frac{\partial^2 u}{\partial x_i^2} . \tag{13.3}$$

In other words, (13.3) is derived under the assumption that there is no convection in the medium, and the local flux satisfies

$$\mathbf{J} = -D\nabla u ,$$

this last statement being often termed as Fourier's or Fick's law. It is well known that, in order to uniquely determine its solutions, (13.3) has to be supplemented with suitable initial and boundary conditions, thus giving raise to a number of well-posed mathematical problems. One of these is the so-called initial value or Cauchy problem, given by

$$\begin{cases} \dfrac{\partial u}{\partial t} = D\triangle u \qquad \text{when } \mathbf{x} \in \mathbb{R}^n \text{ and } t > 0, \\ \\ u(\mathbf{x}, 0) = u_0(\mathbf{x}) \text{ when } \mathbf{x} \in \mathbb{R}^n ,\ t = 0 . \end{cases} \tag{13.4}$$

Here $u_0(x)$ is a given function, on which only mild requirements need to be assumed. One may directly check that a solution of (13.4) is given by

$$u(\mathbf{x}, t) = (4\pi D t)^{-\frac{n}{2}} \int_{\mathbb{R}^n} e^{-\frac{|\mathbf{x}-\mathbf{y}|^2}{4Dt}} u_0(\mathbf{y})\, d\mathbf{y} , \tag{13.5}$$

where as usual

$$|\mathbf{x}-\mathbf{y}|^2 = \sum_{i=1}^{n} (x_i - y_i)^2 \ ,$$

provided that the integral above converges in some time interval $0 < t < T \leq \infty$. When

$$|u_0(\mathbf{x})| \leq C\, e^{M|\mathbf{x}|^2} \ ,$$

for some positive C and M, (13.5) actually yields the only solution to (13.4) (see for instance [30]). A limit case of particular interest appears when $u_0(\mathbf{x})$ reduces to a pointwise discharge of unit intensity (a Dirac delta, or mass, in mathematical terms), $u_0(\mathbf{x}) = \delta(\mathbf{x}-\mathbf{x}_0)$ for some $\mathbf{x}_0 \in \mathbb{R}^n$. This can be considered as an object satisfying $\int_{\mathbb{R}^n} \delta(\mathbf{x}-\mathbf{x}_0)\, d\mathbf{x} = 1$ but such that $\delta(\mathbf{x}-\mathbf{x}_0) = 0$ for any $\mathbf{x} \neq \mathbf{x}_0$. A conceptually more reassuring alternative consists in considering $\delta(\mathbf{x}-\mathbf{x}_0)$ the limit as $j \to \infty$ of a sequence $\{u_{0j}(\mathbf{x})\}$ of smooth and nonnegative functions, each of which vanishes outside the ball $B_j(\mathbf{x}_0) = \{\mathbf{x} : |\mathbf{x}-\mathbf{x}_0| \leq 1/j\}$ and is such that

$$\int_{\mathbb{R}^n} u_{0j}(\mathbf{x})\, d\mathbf{x} = 1 \ .$$

When such an object is taken as initial value at $t = 0$ in (13.4), (13.5) reduces to

$$\bar{u}(\mathbf{x},t) = (4\pi D t)^{-\frac{n}{2}}\, e^{-\frac{|\mathbf{x}-\mathbf{x}_0|^2}{4Dt}} \ . \tag{13.6}$$

We next remark on two key properties of Equation (13.3), namely its linearity and irreversibility. To begin with, if we consider (13.4) as a black box, which provides a response (output) $u(\mathbf{x},t)$ whenever a stimulus (input) $u_0(\mathbf{x})$ is fed in, formula (13.5) establishes that response is always proportional to stimulus (multiplying $u_0(\mathbf{x})$ by a factor λ yields $\lambda u(\mathbf{x},t)$ as a new solution). Furthermore, any finite linear combination of solutions gives again a new solution, and the same happens when infinite such combinations are considered, provided that convergence of the corresponding series can be established. This fact is the basic idea behind Fourier's celebrated separation of variables technique, which is very useful to solve (13.3) in bounded domains with suitable symmetry, and that consists of looking for solutions of the form

$$u(\mathbf{x},t) = \sum_{j=1}^{\infty} a_j(t) X_j(\mathbf{x}) \ , \tag{13.7}$$

where the $\{X_j(\mathbf{x})\}$ are a countable family of solutions of a suitable eigenvalue problem, and the $\{a_j(t)\}$ are the corresponding amplitudes which modulate them. Both $\{a_j(t)\}$ and $\{X_j(\mathbf{x})\}$ are to be determined upon substitution of (13.7) into the corresponding boundary value problem for (13.3); see for instance [89] for details.

A second important property of (13.3) is irreversibility, i.e., the fact that changing t by $(-t)$ does not leave (13.3) invariant. Actually, the transformed equation thus

obtained is highly unstable. To wit, consider for instance the initial value problem

$$\begin{cases} \dfrac{\partial u}{\partial t} = -\dfrac{\partial^2 u}{\partial x^2} \quad \text{when } x \in \mathbb{R},\ t > 0\ , \\ \\ u(x,0) = e^{ikx} \ \text{ for some } k > 0 \text{ at } t = 0\ . \end{cases} \tag{13.8}$$

A quick check reveals that $u(x,t) = e^{ikx+\Omega t}$ is a solution of (13.8) if

$$\Omega = k^2\ . \tag{13.9}$$

Equation (13.9) is a simple example of a dispersion relation (of which more will be heard in the sequel). It describes the way in which different modes evolve in time (in this case, they are amplified in an exponential way).

A related fact is that solutions to (13.4) do not keep track of most features of their initial values $u_0(x)$. Indeed, (13.5) shows that even if $u_0(x)$ is a highly irregular, discontinuous function, for any positive time t, $u(x,t)$ is infinitely differentiable as a function of x and t. Moreover, if

$$||u_0||_1 = \int_{\mathbb{R}^n} u_0(x)\, dx < \infty\ ,$$

it then follows from (13.5) that

$$\max |u(x,t)| \leq C t^{-\frac{n}{2}} ||u_0||_1 \qquad \text{for some } C > 0\ , \tag{13.10}$$

a strong regularising effect. Notice that (13.10) describes both a smoothening and a flattening effect, since the right-hand side of (13.10) decays algebraically to zero as t increases.

13.2.3 Diffusion and Random Walks

The linear diffusion equation (13.3) is a continuum model of a deterministic nature. This means that if we consider, for instance, problem (13.4) and impose some (mild) assumptions on $u_0(x)$, the corresponding solution is uniquely determined for any subsequent times, by means of formula (13.5). Such determinism at a macroscopic scale (i.e., at a continuum level) is however linked to a random character at a microscopic scale (i.e., at a discrete level) which we shortly discuss below.

Consider for simplicity a one-dimensional random walk, i.e., assume that a particle is moving along a line in the form of a series of steps of equal length, each step being taken either in the left or right direction, with equal probability $\frac{1}{2}$. After taking N such steps, the particle could be at any of the points

$$-N, -N+1, \ldots, -1, 0, 1, \ldots, N-1, N\ .$$

The following question naturally arises: what is the probability $W(m,N)$ that the particle arrives at the point m (m being an integer), after suffering N ($N \geq |m|$) displacements?

Suppose for instance that $m > 0$. Then $W(m,N)$ is the probability of taking $(\frac{N+m}{2})$ steps to the right (indeed, $(N+m)$ must be an even number), out of a total of N steps. It then turns out that

$$\begin{aligned} W(m,N) &= (\text{probability corresponding to an arbitrary sequence of paths}) \\ &\quad \times (\text{number of paths leading to place } m) \\ &= \left(\frac{1}{2}\right)^N \binom{N}{\frac{N+m}{2}} = \left(\frac{1}{2}\right)^N \frac{N!}{(\frac{N+m}{2})!(\frac{N-m}{2})!} \,. \end{aligned} \tag{13.11}$$

Formula (13.11) provides an exact answer, but a very cumbersome one (if you doubt this, try counting from one to 9!). However, in some particular (but relevant) cases, one may trade an exact, unwieldy expression by a merely approximate, but convenient, one. This is the rationale behind many so-called asymptotic methods. For instance, assume that

$$N \gg 1 \qquad \text{and} \qquad \frac{m}{N} \ll 1 \,, \tag{13.12}$$

these symbols meaning "N is very large" and "m/N is very small," are admittedly not the most precise of the statements (see [4] for a careful definition). We then may take advantage of Stirling's formula

$$N! \sim \frac{\sqrt{2\pi N} \cdot N^N}{e^N} \qquad \text{as} \qquad N \longrightarrow \infty \,,$$

(cf. [4] and [29], Chapter II, Section 10), or more precisely of its logarithmic form

$$log(N!) = \left(N + \frac{1}{2}\right) \log(N) - N + \frac{1}{2} \log(2\pi) + O\left(\frac{1}{N}\right) \qquad \text{as} \qquad N \longrightarrow \infty \,, \tag{13.13}$$

to deduce from (13.11) that

$$W(m,N) \sim \left(\frac{2}{\pi N}\right)^{\frac{1}{2}} e^{-\frac{m^2}{2N}} \,, \tag{13.14}$$

provided that (13.12) holds. Here and henceforth we shall freely use the customary asymptotic notations $\sim$ and $O(\cdot)$. For instance, Equation (13.14) means that, under our current assumptions, the ratio of the quantities appearing at both sides of (13.14) tends to one as $N - \to \infty$ (although the difference between these two quantities need not become small for large N). On its turn, $O(\frac{1}{N})$ denotes any quantity which in absolute value may be bounded by $\frac{C}{N}$ for some $C > 0$ as $N \longrightarrow \infty$. Here C may be large, but should not depend on N. If we now set

$$x = ml\,, \qquad t = \frac{N}{n}\,,$$

i.e., if we assume that our particle undergoes n displacements by unit time, and introduce a space variable equal to m times the length $l > 0$ of any displacement (no longer assumed to be of unit value), (13.14) yields

$$W(x,t) \sim (4\pi D t)^{-\frac{1}{2}}\, e^{-\frac{x^2}{4Dt}}\,, \tag{13.15}$$

where

$$D = \frac{nl^2}{2}\,, \tag{13.16}$$

which is a particular case of (13.6) in space dimension $n = 1$. Notice that the mean squared displacement,

$$\langle x^2 \rangle = \int_{-\infty}^{\infty} x^2 W(x,t)\, dx$$

is then such that

$$\langle x^2 \rangle \sim 2Dt\,. \tag{13.17}$$

Relations (13.14) to (13.16) strongly suggest that the continuum equation (13.3) in one space dimension can be considered as a limit model for a one-dimensional random walk when the number of flights N goes to infinity. As a matter of fact, this also happens in higher space dimensions (see for instance [11] for a classical presentation). The random walk just recalled is an example of a stochastic process, a subject for which the reader is referred to [40] and [24] for further information.

13.2.4 General RD Systems: Some Relevant Questions

A type of reaction diffusion system which is often found in applications is the following

$$\begin{cases} \dfrac{\partial u_1}{\partial t} = D_1\, \triangle u_1 + f_1(u_1, \ldots, u_m)\,, \\ \dfrac{\partial u_2}{\partial t} = D_2\, \triangle u_2 + f_2(u_1, \ldots, u_m)\,, \\ \qquad\qquad \vdots \qquad\qquad \vdots \\ \dfrac{\partial u_m}{\partial t} = D_m\, \triangle u_m + f_m(u_1, \ldots, u_m)\,, \end{cases} \tag{13.18}$$

where D_1,D_2,. . .,D_m are given positive constants, and $f_1, \ldots, f_m$ are given (generally nonlinear) functions, whereby coupling between variables $u_1, \ldots, u_m$ is established. Equations (13.18) are said to be of semi-linear type. On setting $\mathbf{f} =$

$(f_1, \ldots, f_m)$, $\mathbf{u} = (u_1, \ldots, u_m)$, and denoting by $\mathbf{D}$ the diagonal matrix with nonzero elements $D_1, \ldots, D_m$, (13.18) is conveniently recast in the form

$$\frac{\partial \mathbf{u}}{\partial t} = \mathbf{D}\triangle \mathbf{u} + \mathbf{f}(\mathbf{u}) \, . \tag{13.19}$$

The system obtained by setting $\mathbf{D} = 0$ in (13.19) is usually referred to as the associated kinetic system.

While general enough to account for a wide number of applications, (13.18) is comparatively simple on mathematical terms, since a number of possible features of the process whose modelisation is intended have been ignored. For instance, we have discarded cross-diffusion (which would yield terms such as $\triangle(u_1 + u_2)$ in (13.18)), nonlinear diffusion (corresponding to operators like $\triangle(u_i^r)$ with $r \neq 1$), gradient-dependent forcing terms of the form $f_j(u_1, \frac{\partial u_1}{\partial x_1}, \ldots, \frac{\partial u_1}{\partial x_n}, \ldots, u_m, \ldots)$, and so on. Recalling our discussion in the previous section, we remark that equations of the form (13.18) can be derived as limit dynamics for systems of moderately interacting, randomly moving particles (cf. [69]). The term "moderately" (or short range) refers to suitable assumptions to be made on the way in which the interaction between individual particles is rescaled as the total population increases to infinity. Details can be found in reference [69].

From a mathematical point of view, looking for general solutions of (13.18) is not easy. For one thing, general representation formulae in the spirit of (13.5) are virtually nonexistent (except when the kinetic terms f_i are linear). Moreover, blow-up may occur, i.e., solutions may cease to exist in finite time. This is most simply illustrated by the ordinary differential equation (ODE for short) $u' = u^2$, which has solutions of the form $u_T(t) = (T - t)^{-1}$ for any $T > 0$. A similar phenomenon has been extensively studied in the presence of diffusion, that is, for equations of the type

$$\frac{\partial u}{\partial t} = \triangle u + u^p \qquad \text{with} \qquad p > 1 \, .$$

Actually in this equation the interplay between the diffusion and kinetic mechanisms has been shown to provide a countable set of spatio-temporal structures when the blow-up time T (at which solutions become unbounded) is approached. However, out of all these, only that having the simplest space structure (characterised by possessing a single maximum in suitable rescaled variables) is stable; see [37] for a discussion of the one-dimensional case.

In general, the existence of solutions to (13.18) can only be obtained for sufficiently small times. This may be achieved by means of various techniques: fixed point methods [31,55], semigroup theory [72], a priori estimates [21,52], etc. We should also mention that when a higher level of nonlinearity is allowed (for instance, when nonlinear diffusion terms as $\triangle(u^2)$ are considered), classical solutions, that is, functions having all the space and time derivatives required to satisfy the system under consideration at any point, need not exist globally in space, even for arbitrarily short times. As a matter of fact, in that case interfaces may appear at which solutions or their derivatives may develop jumps (see for instance [3] for a review on

an important example). Also, the presence of nonlinear convective terms may lead to shock-wave solutions, which exhibit jumps along some moving shock curves or surfaces (cf. [90]).

However, even if general solution formulae are not available, in many cases one is able to detect particular solutions that often play a key role in the dynamics (i.e., the evolution in space and time of solutions). This is clearly illustrated by the following simple example. Consider the ODE

$$u' = u(1-u). \tag{13.20}$$

Equation (13.20) can be explicitly integrated. However, out of all its infinitely many particular solutions, one of them stands out, namely $\bar{u} = 1$. This is readily seen from the approximate picture of solutions recalled in Figure 13.1 below, that can be obtained from elementary considerations

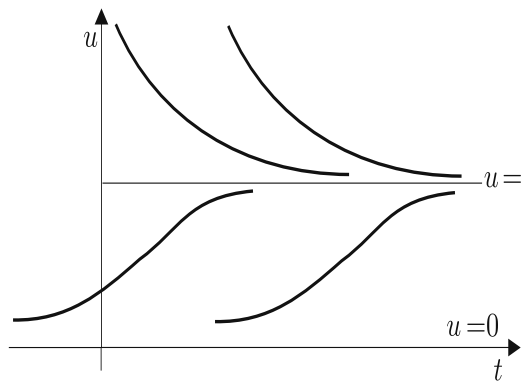

Figure 13.1
The behaviour of solutions of (13.20).

Indeed, $\bar{u} = 1$ is a global attractor for every solution $u \neq 0$ of (13.20). A local (hence weaker) version of this fact, which will be frequently observed in the less trivial examples to follow, is quickly derived by looking for the evolution in time of small perturbations of the explicit solution $\bar{u} = 1$. Namely, let us set

$$u(t) = 1 + z(t) \qquad \text{with} \qquad 0 < |z(0)| \ll 1\,. \tag{13.21}$$

Plugging (13.21) into (13.20), and using the fact that, for small z, $(1+z)^2 \sim 1 + 2z$, we readily see that $z(t)$ satisfies

$$z' = (1+z) - (1+z)^2 \sim 1 + z - 1 - 2z = -z\,.$$

Therefore, at least for small times, $z' \sim -z$, and the subsequent evolution (given approximately by $z(t) = z(0)e^{-t}$) will tend to further damp out the effect of the small perturbation $z(0)$. This is linear stability analysis in a nutshell.

When general systems as (13.18) are considered, a key issue often consists in obtaining relevant particular solutions, that is, solutions displaying asymptotic behaviours that are robust (i.e., do not depend on a particular choice of parameters being made) and at the same time important for the underlying physical or biological problems of which (13.18) is just a model. Consider for instance (13.18) together with initial and boundary conditions for which solutions exist globally in time. In view of our previous remarks, a natural question is the following: what are the possible asymptotics of solutions for large times? Recalling the smoothening feature of linear diffusion illustrated by the regularising effect (13.10), the seemingly obvious answer appears to be that, as time passes, solutions of (13.18) should converge to those of the associated kinetic system, obtained by setting $D_1 = \ldots = D_m = 0$ there.

Indeed, there are many instances in which this is precisely what happens. Consider for instance the case where Ω is a bounded subset of $\mathbb{R}^n\,(n \geq 1)$ with reasonably smooth boundary, and assume that no-flux conditions are imposed on the boundary of Ω, $\partial\Omega$, viz

$$\frac{\partial u_1}{\partial \mathbf{n}} = \ldots = \frac{\partial u_m}{\partial \mathbf{n}} = 0 \qquad \text{at} \qquad \partial\Omega\ ,$$

where $\mathbf{n}$ is the unit normal exterior vector at any point of the boundary $\partial\Omega$. Assume also that our system admits a compact invariant region $\Sigma \subset \mathbb{R}^n$. By this we mean that $0 \in \Sigma$, and if the initial values $\mathbf{u}_0(\mathbf{x}) = (u_{01}(\mathbf{x}), \ldots, u_{0m}(\mathbf{x}))$ lie in the interior of Σ then so does the solution $\mathbf{u} = (u_1, \ldots, u_m)$ for all times $t > 0$. Then it has been shown in [14] that there exits a number $\sigma > 0$, depending on Ω, $\mathbf{f}$, and $D_1, \ldots, D_m$ such that, if

$$\min\{D_1, \ldots, D_m\} > \sigma\ ,$$

then $\mathbf{u}$ converges to $\bar{\mathbf{u}}(t)$ as $t \longrightarrow \infty$, where $\bar{\mathbf{u}}(t)$ satisfies

$$\frac{\mathrm{d}\bar{\mathbf{u}}}{\mathrm{d}t} = \mathbf{f}(\bar{\mathbf{u}}) + \mathbf{g}(t)\ , \qquad \bar{\mathbf{u}}(0) = \frac{1}{|\Omega|}\int_\Omega \mathbf{u}_0(x)\,dx\ , \tag{13.22}$$

$|\Omega|$ denotes the volume of Ω, and $|\mathbf{g}(t)| \leq ce^{-\sigma t}$ for some $c > 0$. Then, for sufficiently large times, (13.18) can be replaced by (13.22) under our current assumptions. As a consequence, asymptotically stable equilibria for

$$\frac{\mathrm{d}\mathbf{u}}{\mathrm{d}t} = \mathbf{f}(\mathbf{u})\ ,$$

conserve that character for the complete RD system (13.19). As it is well known, the former can be characterised as those points $\tilde{\mathbf{u}}$ such that $\mathbf{f}(\tilde{\mathbf{u}}) = 0$, and for which the eigenvalues λ given by

$$|\nabla \mathbf{f}(\tilde{\mathbf{u}}) - \lambda \mathbf{I}| = 0 \,,$$

are such that $\mathrm{Re}\lambda < 0$ (cf. for instance [7] and [12]).

It is now natural to wonder what happens if the assumptions in [14] are not satisfied, something that can be shown to happen if some of the diffusion coefficients in Equation (13.18) are sufficiently small. Then a pattern (that is, an asymptotic state with nontrivial spatial structure) may arise. The simplest candidates for patterns are the stable solutions of the stationary version of (13.18), i.e.,

$$\begin{aligned} D_1 \triangle u_1 + f_1(u_1, \ldots, u_m) &= 0 \,, \\ &\vdots \\ D_m \triangle u_m + f_m(u_1, \ldots, u_m) &= 0 \,. \end{aligned} \tag{13.23}$$

However, in many cases, patterns are hard to come by. Consider for instance the semilinear scalar problem

$$\begin{cases} D \triangle u + f(u) = 0 & \text{in } \Omega \,, \\ \dfrac{\partial u}{\partial \mathbf{n}} = 0 & \text{in } \partial\Omega \,. \end{cases} \tag{13.24}$$

Then it has been shown in [56] that, if Ω is convex in $\mathbb{R}^n$, any nonconstant solution of (13.24) is unstable. A similar result has been shown to hold for the system

$$\begin{cases} d_1 \triangle u + f(u, v) = 0 \,, \\ d_2 \triangle v + g(u, v) = 0 \,, \end{cases} \tag{13.25}$$

(cf. [48]) provided that

$$\frac{\partial f}{\partial v} \leq 0 \,, \qquad \frac{\partial g}{\partial u} \leq 0 \quad \text{in } \Omega \quad \text{and} \quad \frac{\partial u}{\partial \mathbf{n}} = \frac{\partial v}{\partial \mathbf{n}} = 0 \quad \text{in } \partial\Omega \,.$$

However, for any pair $d_1 > 0$, $d_2 > 0$, it is possible to find a domain $\Omega \subset \mathbb{R}^2$ (no longer convex) for which (13.25) possesses a stable, spatially inhomogeneous equilibrium solution [57].

Our previous discussion yields some conditions under which patterns may exist. However, no catalogue of possible patterns has been provided. On the other hand, the question of how a given initial state should evolve into such a pattern has not been addressed. We shall turn our attention to that issue presently.

13.2.5 Linear Theory of Pattern Formation: Turing's Instability

In 1952, A. Turing published a most influential paper [84], in which he argued that reaction-diffusion systems of equations could be actually used as models for

morphogenesis (that is, generation of forms) in living beings. While such approach was not without precedent (see for instance [75]) it certainly gained momentum after Turing's work appeared. The author's vision is concisely described in the abstract of the article:

> "It is suggested that a system of chemical substances, called morphogens, reacting together and diffusing through a tissue, is adequate to account for the main phenomena of morphogenesis. Such a system, although it may originally be quite homogeneous, may later develop a pattern or structure due to an instability of the homogeneous equilibrium, which is triggered off by random disturbances ...",

(cf. [84], p.37). Following [61], we can illustrate this point of view by means of the following simple example. Consider the linear system

$$\begin{cases} \dfrac{\partial u}{\partial t} = \varepsilon \dfrac{\partial^2 u}{\partial x^2} + au - v \ , \\ \\ \dfrac{\partial v}{\partial t} = \sigma \dfrac{\partial^2 v}{\partial x^2} + u - bv \ , \end{cases} \tag{13.26}$$

where a and b are some positive parameters, $\varepsilon \geq 0$, and $\sigma \geq 0$. Consider first the kinetic system obtained by setting $\varepsilon = \sigma = 0$ in (13.26). It certainly has a homogenous equilibrium solution $\bar{u} = \bar{v} = 0$. To study its stability properties, we look for perturbations of the form $u_0 e^{\lambda t}$, $v_0 e^{\lambda t}$ with $0 < |u_0| + |v_0| \ll 1$. Plugging these functions into that kinetic system, we see that the exponent λ is such that

$$\lambda = \frac{1}{2}\{(a-b) \pm ((a+b)^2 - 4)^{\frac{1}{2}}\} \ , \tag{13.27}$$

so that $\bar{u} = \bar{v} = 0$ is asymptotically stable whenever $\mathrm{Re}\lambda < 0$ for both values of λ given in (13.27). It is now easy to draw a stability diagram in terms of the parameters a and b in (13.26) (see Figure 13.2).

Suppose now that we set $\varepsilon = 1$ and $\sigma > 0$, and look for solutions in the form

$$u(x,t) \sim e^{ikx+\lambda t} \ , \qquad v(x,t) \sim e^{ikx+\lambda t} \ , \tag{13.28}$$

for some λ and k. This would correspond to solutions which oscillate in space (with period $\frac{2\pi}{k}$) and decrease (or increase) exponentially in time according to the sign of λ. A quick check reveals that λ satisfies an equation similar to Equation (13.27) when one replaces there a by $a(k) = (a - k^2)$ and b by $b(k) = (b + \sigma k^2)$. Therefore, when k is varied, the point $(a(k), b(k))$ moves over the plane (a, b) describing a straight line consisting of points $(\bar{a}, \bar{b})$ having a slope σ, namely $\bar{b} = b + \sigma(a - \bar{a})$. As σ increases, the motion proceeds toward higher values of $\bar{b}$ and smaller values of $\bar{a}$.

Assume now that we start from a value (a, b) located in the stability domain in Figure 13.2. Then, if $\sigma > 0$ is sufficiently large, we may select values $k > 0$ for which $\mathrm{Re}\lambda(k) > 0$ for one of the eigenvalues λ in Equation (13.28). It then turns out that the oscillatory spatial mode with period $\frac{2\pi}{k}$ will grow, and the stationary

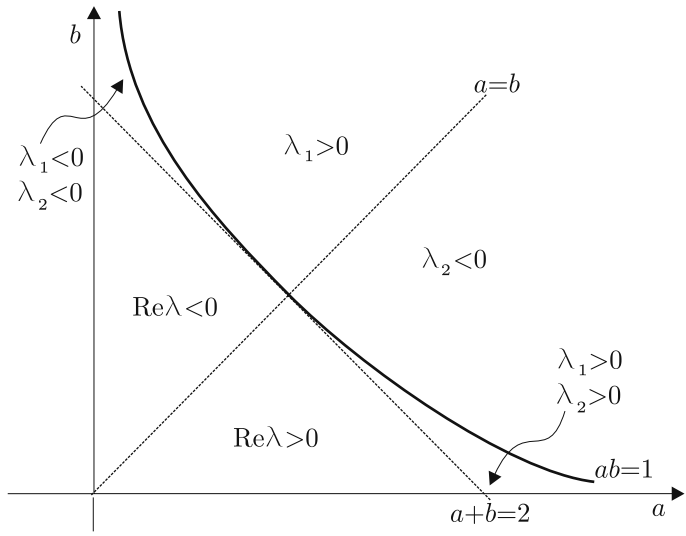

Figure 13.2
The dependence of eigenvalues on coefficients a and b.

state $u = v = 0$ will become unstable with respect to oscillations corresponding to that frequency. Diffusion has therefore destabilised an initially stable homogeneous steady state. This fact is often termed as Turing's instability. The reader is referred to [61], Chapter 5, for a discussion of the various types of instabilities that may arise when systems of type (13.26) are considered in one or two space dimensions.

13.2.6 Nonlinear Pattern Formation: The Activator-Inhibitor Model by Gierer and Meinhardt.

The analysis shortly described in our previous section lies at the heart of the considerable development of the mathematical theory of pattern formation during the last 50 years. Indeed, it is intellectually appealing to think of biological structures (for instance, the limbs of animals) as unfolding out of an almost homogeneous embryo just under the interplay of reaction and diffusion of chemical substances. However, formidable obstacles arise when fitting theory to experiments is attempted (for instance, actual morphogens in animals have proved to be elusive to identification). Even from a merely theoretical point of view, serious difficulties arise at once if linear systems as (13.26) are considered.

Certainly, when it comes to solving equations, linearity is a big bonus. Furthermore, as far as we remain close enough to a given particular solution, any system can be safely approximated by a linear one, namely that obtained by linearising around

such a solution, much as we have done in (13.21). However, such an approximation is no longer valid when perturbations tend to increase, for instance when $\mathrm{Re}\lambda > 0$ in the situation considered in our former section. Once a growing perturbation sets in, there is no way of stopping it in a linear world. To account for actual morphogenesis, one necessarily has to introduce saturation effects, which in mathematical terms amounts to consider nonlinear systems. The price to be paid is that analysis becomes more difficult, a fact that Turing was well aware of. As he explicitly mentions in [84], p. 72, when dealing with nonlinear equations:

> "...The difficulties are, however, such that one cannot hope to have any very embracing theory of such processes, beyond the statement of the equations," although "it may be possible, however, to treat a few particular cases in detail with the aid of a digital computer."

While mathematical analysis and computing have greatly developed since Turing's statement, his remarks continue to provide a sober warning to the limits of quantitative modelling in the life sciences.

However, during the last third of the 20^{th} Century, analysis of nonlinear models in biology has considerably developed. In this trend, a particularly influential model was the activator-inhibitor system proposed in 1972 by Gierer and Meinhardt (cf. [22]) to account for tentacle formation in hydra. This last is a fresh water polyp whose regenerative properties have attracted much attention over the last two centuries (and that incidentally is also mentioned in [84]).

The main idea in [22] consists in considering a type of pattern formation arising from the interplay of two substances. One of them (called activator), $a(x,t)$, is autocatalytic, and at the same time produces an antagonist (inhibitor), $h(x,t)$. This last counteracts the activator a, but diffuses faster than a does into the surrounding medium. The actual interaction between a and h is prescribed so that:

- a local deviation from an average concentration should increase further (otherwise no pattern would be formed), and
- the increase should not go to infinity, but instead the emerging pattern should reach a stable steady state.

To this end, Gierer and Meinhardt proposed the following system

$$\begin{cases} \dfrac{\partial a}{\partial t} = D_a \dfrac{\partial^2 a}{\partial x^2} + \dfrac{ca^2}{h} - \mu a \ , \\ \dfrac{\partial h}{\partial t} = D_h \dfrac{\partial^2 h}{\partial x^2} + ca^2 - \nu h \ , \end{cases} \tag{13.29}$$

(cf. [22,59]), where c, μ, ν, D_a, and D_h are positive constants. Assume for simplicity that $c = \mu = \nu = 1$. Then $a = h = 1$ is an equilibrium solution of Equation (13.29). If the inhibitor concentration is kept constantly equal to one, then $a = 1$ would be an unstable solution of the first kinetic equation in Equation (13.29), that would reduce to

$$a' = a(a-1)\ .$$

However, if we allow h to change, but we assume that it rapidly achieves its equilibrium to a given activator concentration (which amounts to require $D_h \gg D_a$ in Equation (13.29)), then the kinetic equation for a would be instead

$$a' = \frac{a^2}{a^2} - a = 1 - a\ ,$$

for which the corresponding equilibrium $a = 1$ is now a stable one. As stated in [59], "...by a convenient choice of diffusion rates we can achieve local instability with overall stability of the system." It is to be noticed, however, that while numerical simulations in Equation (13.29) are comparatively easy to perform (cf. for instance [59]), the mathematical analysis of (13.29) and related systems (as for instance the model for the unfolding of a planar vascular net proposed in [58]) is yet far from complete in the case of two and three space dimensions; see for instance [78] and [2].

13.3 Wave-Type Solutions

This section is devoted to the study of particular solutions of RD systems. Of these, travelling waves (TW) are specially relevant, since they play a key role in describing propagation phenomena. In a few words, TW are solutions which move at constant velocity without changing shape. We begin by recalling below a classical work which can be rightly considered as the origin of TW theory.

13.3.1 Transition from an Unstable State: The Work by Kolmogorov, Petrovsky, and Piskunov

These authors published their seminal paper [49] in 1937. Motivated by the genetics of natural selection (as described, for instance, in reference [20] quoted therein), they discussed a model to describe the spread of an advantageous gene. In this way they were led to the following problem: to find $v(x,t)$ solution of

$$\frac{\partial v}{\partial t} = k\frac{\partial^2 v}{\partial x^2} + F(v) \qquad \text{when} \quad -\infty < x < \infty\ , \quad t > 0\ , \tag{13.30}$$

$$v(x,0) = H(x)\ , \tag{13.31}$$

where

- F is a continuously differentiable function, such that $F(0) = F(1) = 0$,
- $F(v) > 0$ for $0 < v < 1,\ F'(0) = a > 0,\ F'(v) < a \quad \text{for} \quad 0 < v < 1$,

(13.32)

- $H(x)$ is a discontinuous step function defined as follows :

(13.33)

$H(x) = 0 \quad \text{when} \quad x < 0\,, \qquad H(x) = 1 \quad \text{when} \quad x \geq 0\,.$

The goal of [49] is accurately described by the following excerpts taken from its Introduction:

> "...The domain of densities close to one spreads out, as t increases, from right to left, pushing back the domain of small intensities to the left .... One sees that, as $t \ -\!\!\rightarrow \infty$, the shape of the density curve approaches a limiting shape..." (cf. Figure 13.3 below).

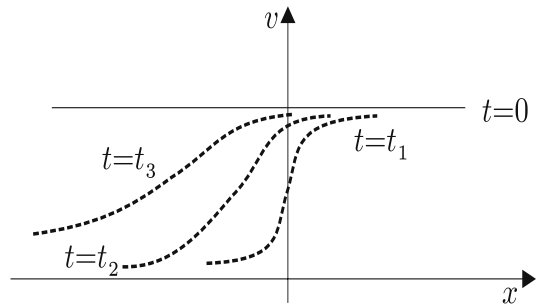

Figure 13.3
The evolution of the density function $v(x,t)$ **at times** $0 = t < t_1 < t_2 < t_3$

> "...The problem is to find this limit shape of the density curve and the limiting rate of its displacement from right to left. One can show that this last is equal to
>
> $$\lambda_0 = 2\sqrt{ka} \qquad \text{with} \qquad a = F'(0).$$"

Note that the kinetic equation associated to (13.30), $v' = F(v)$, has two constant solutions, $v_0 = 0$ and $v_1 = 1$. Of these, the first is unstable, as can be readily

seen from the linearised equation $z' = F'(0)z$. A similar argument shows $v_1 = 1$ to be stable, so that the asymptotics just described above actually correspond to a transition from an unstable state into a stable one.

It is remarkable that the asymptotic speed of propagation of the solution of Equations (13.30) and (13.31) can be computed right away from the knowledge of the diffusion coefficient k and the slope a of function $F(v)$ near $v = 0$. This is rather unusual, as the results in the following sections will show. Incidentally, at this juncture we are taking existence and uniqueness of a solution for granted. This is actually the case, but see the remarks on these issues made at the end of this section.

The approach followed in [49] has become classical, and nowadays is routinely implemented in many problems in applied science. For this reason, some of its main aspects will be briefly sketched here.

To begin with, one looks for solutions of (13.30) of the TW form

$$v(x,t) = v(x + \lambda t) \equiv v(z) \geq 0 \,, \tag{13.34}$$

where λ is unknown, and has to be determined in the course of the analysis. Plugging (13.34) into (13.30), we readily see that $v(z)$ should satisfy

$$\lambda \frac{\mathrm{d}v}{\mathrm{d}z} = k \frac{\mathrm{d}^2 v}{\mathrm{d}z^2} + F(v) \,, \qquad -\infty < z < \infty \,. \tag{13.35}$$

Moreover, since we expect v to behave as indicated in Figure 13.3 above, we should also have that

$$\begin{array}{lll} v(z) - \to 0 & \text{as} & z \longrightarrow -\infty \,, \\ v(z) - \to 1 & \text{as} & z \longrightarrow \infty \,. \end{array} \tag{13.36}$$

Together, (13.35) and (13.36) constitute a nonlinear eigenvalue problem, which has to be simultaneously solved for v and λ. It was shown in [49] that this problem has a solution, unique up to translations, whenever $\lambda \geq \lambda_0 = 2\sqrt{ka}$. This was done by rewriting (13.35) as a system

$$\begin{cases} \dfrac{\mathrm{d}v}{\mathrm{d}z} = p \,, \\ \dfrac{\mathrm{d}p}{\mathrm{d}z} = \dfrac{\lambda p - F(v)}{k} \,. \end{cases} \tag{13.37}$$

Then what is now considered as a standard phase-space analysis was performed. First, one looks for constant solutions of Equation (13.37). These are $(v,p) = (0,0)$ and $(v,p) = (1,0)$. After that, one linearises around them, similarly to what we did for Equation (13.20) in our previous section, to describe the local behaviour of solutions close to these equilibria. When $\lambda \geq 2\sqrt{ka}$, these are as depicted in part $a)$ of Figure 13.4. Having done this, the authors undertook a global analysis, eventually showing that there is a trajectory (v,p) connecting both equilibria, see part $b)$ in Figure 13.4. Such trajectory corresponds to the sought-for travelling wave, when this last is written in terms of the (v,p) coordinates.

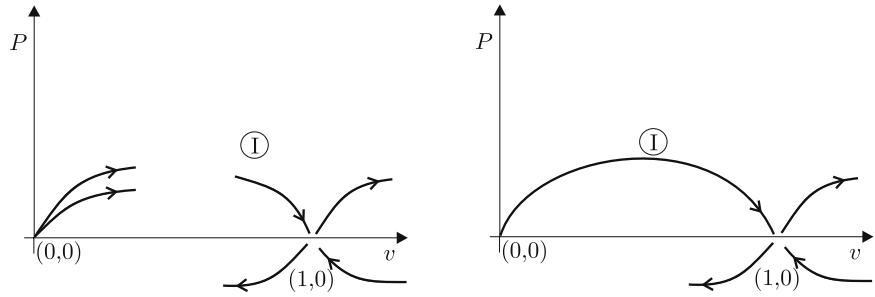

(a) (b)

Figure 13.4

(a) Local portrait of trajectories and equilibria. Point $(0,0)$ is said to be an unstable node, and $(1,0)$ is a saddle point (cf. [7,12] for precise description of these types of equilibria). (b) Global analysis: the trajectory labelled as I corresponds to a TW of (13.30) when $\lambda \geq 2\sqrt{ka}$.

When $\lambda < 2\sqrt{ka}$, trajectories emanating from $(0,0)$ spiral around that point, and cannot therefore provide nonnegative solutions as required in (13.34). The foregoing argument yields the existence of a continuum of TW solutions to (13.30), each of them actually solving the eigenvalue problem (13.35), (13.36) for a value $\lambda \geq \lambda_0$. A key issue in [49] consists of discussing which of these waves is relevant to describe the large-time asymptotics of the problem under consideration. More precisely, the following result is proven in [49] (see also [85]).

There exists a continuously differentiable function $\xi(t)$ such that

$$\xi'(t) - \to \lambda_0 \equiv 2\sqrt{ka} \quad \text{as} \quad t \longrightarrow \infty\,, \quad \text{and} \tag{13.38}$$

$$v(x - \xi(t), t) - \to v_0(x) \quad \text{as} \quad t \longrightarrow \infty\,,$$

where v_0 is the solution of Equations (13.35) and (13.36) corresponding to $\lambda \equiv \lambda_0$. Note however that $\xi(t)$ remains undetermined in (13.38). Actually, this "phase indeterminacy," as is often termed, is a property of the model (13.30), and not merely a technical nuisance. For instance, it is known that

$$v(x - 2t, t) - \to 0 \quad \text{as} \quad t \longrightarrow \infty\,.$$

Furthermore, if $u(x,t)$ is a solution of (13.30) such that $0 < u < 1$ and we assume that $u(x,t)$ converges to some travelling wave as $t \longrightarrow \infty$, and if in addition

$$\lim_{x \to -\infty} e^{\alpha x} u(x,0) = b \neq 0 \quad \text{for some} \quad \alpha \quad \text{with} \quad 0 < \alpha < 1\,,$$

then the velocity of that wave must be $\lambda = (\alpha + \frac{1}{\alpha})\sqrt{ka}$ (cf. [53] for details on these results). Concerning our problem (13.30), (13.31), although it can be said that the x-

profile of $v(x,t)$ approaches that of v_0 (cf. (13.38)), the delicate nature of the results discussed in [53] call attention to possible inaccuracies in any numerical procedure which fail to properly account for the decay of initial values for large $|x|$.

We conclude this section by remarking on the way existence and uniqueness were obtained in [49]. Uniqueness is derived by application of the so-called maximum principle (cf. [21]). Roughly speaking, one assumes the existence of at least two different solutions v_1 and v_2, and considers the equation satisfied by a suitable auxiliary function related to $v_1 - v_2$. Then a contradiction is achieved by examining the sign of the various terms in that equation at the possible local extrema of $v_1 - v_2$.

The existence proof will be briefly sketched below, since it is of a constructive nature, and therefore provides a procedure to approximate the actual solutions. To begin with, let $v_0(x,t)$ be the solution of

$$\begin{cases} \dfrac{\partial v}{\partial t} = k\dfrac{\partial^2 v}{\partial x^2}\,, \qquad -\infty < x < \infty\,, \quad t > 0\,, \\ \\ v(x,0) = H(x)\,. \end{cases} \tag{13.39}$$

Actually, the argument in [49] is carried out for more general initial values than that in Equation (13.39), but consideration of this case is enough for the discussion that follows. A direct check shows that the function

$$\begin{aligned} v_1(x,t) &= v_0(x,t) + \widetilde{v}_1(x,t) \\ &\equiv v_0(x,t) + \frac{1}{2\sqrt{\pi k}} \int_0^t d\eta \int_{-\infty}^{\infty} \frac{e^{-\frac{(x-\xi)^2}{4k(t-\eta)}}}{\sqrt{t-\eta}} F(v_0(\xi,\eta))\, d\xi\,, \end{aligned}$$

is such that $v_1(x,0) = H(x)$ and

$$\frac{\partial v_1}{\partial t} = k\frac{\partial^2 v_1}{\partial x^2} + F(v_0(x,t))\,, \qquad -\infty < x < \infty\,, \quad t > 0\,.$$

A sequence of functions $\{v_i(x,t)\}$ with $i \geq 1$ can be now constructed by means of the rule

$$v_{i+1}(x,t) = v_0(x,t) + \frac{1}{2\sqrt{\pi k}} \int_0^t d\eta \int_{-\infty}^{\infty} \frac{e^{-\frac{(x-\xi)^2}{4k(t-\eta)}}}{\sqrt{t-\eta}} F(v_i(\xi,\eta))\, d\xi\,,$$

and one readily sees that v_{i+1} solves

$$\begin{cases} \dfrac{\partial v_{i+1}}{\partial t} = k\dfrac{\partial^2 v_{i+1}}{\partial x^2} + F(v_i(x,t))\,, \qquad -\infty < x < \infty\,, \quad t > 0\,, \\ \\ v_{i+1}(x,0) = H(x)\,. \end{cases} \tag{13.40}$$

The argument then concludes by showing that $\{v_i(x,t)\}$ converges, as $i \to \infty$, towards a continuous function $v(x,t)$, in such a manner that passing to the limit in Equation (13.40) is allowed, so that $v(x,t)$ turns out to solve (13.30) and (13.31).

13.3.2 Bistable Media

In mathematical terms, bistable media are represented by a scalar, semilinear diffusion equation that has two steady states which are stable under sufficiently small perturbations, and an unstable state between them. An important feature of these media is that a sufficiently strong perturbation may induce a transition between the two stable equilibria. The corresponding solutions are called fronts or trigger waves (cf. for instance [17,61]), and will be shortly discussed below. The simplest reaction-diffusion equation of bistable type can be written as follows

$$\frac{\partial u}{\partial t} = D\frac{\partial^2 u}{\partial x^2} + f(u)\,, \qquad -\infty < x < \infty\,, \quad t > 0\,, \tag{13.41}$$

where $D > 0$, and $f(u)$ is a continuously differentiable function as depicted in Figure 13.5 below. Notice that such function $f(u)$ has two stable equilibria at $u = u_1, u_3$, and an unstable one ($u = u_2$), as can be readily seen from the sign of $f'(u)$ at each of these points. A front (or trigger wave) corresponding to the transition from the state u_1 to the state u_3, and moving with velocity c (say, positive) is a function $u(x,t)$ (if any) of the form $u(x,t) = u(x - ct) \equiv u(\xi)$ which solves (13.41), so that

$$Du'' + cu' + f(u) = 0\,, \qquad -\infty < \xi < \infty\,, \tag{13.42}$$

and

$$u(\xi) - \to u_3 \quad \text{when} \quad \xi \longrightarrow -\infty\,, \qquad u(\xi) - \to u_1 \quad \text{when} \quad \xi \longrightarrow \infty\,. \tag{13.43}$$

A major difference with the case considered in the previous section is that in general there is no more than one wave speed c for which the eigenvalue problem (13.42) and (13.43) can be solved, uniquely up to translations. Such a solution corresponds to a trajectory in the phase space associated to (13.42) joining the two saddle points $(u_1, 0)$ and $(u_3, 0)$. In most cases, the actual value of c can only be computed numerically, again in sharp contrast with the KPP model discussed before. An important exception is provided by the following example

$$\frac{\partial u}{\partial t} = \frac{\partial^2 u}{\partial x^2} + u(1-u)(u-a) \qquad \text{with} \qquad 0 < a < 1\,. \tag{13.44}$$

In this case, the function

$$v(\xi) = \left(1 + e^{\frac{\xi}{\sqrt{2}}}\right)^{-1}\,, \qquad \xi = x - ct\,, \tag{13.45}$$

is a travelling wave with speed

$$c = \sqrt{2}\left(\frac{1}{2} - a\right)\,. \tag{13.46}$$

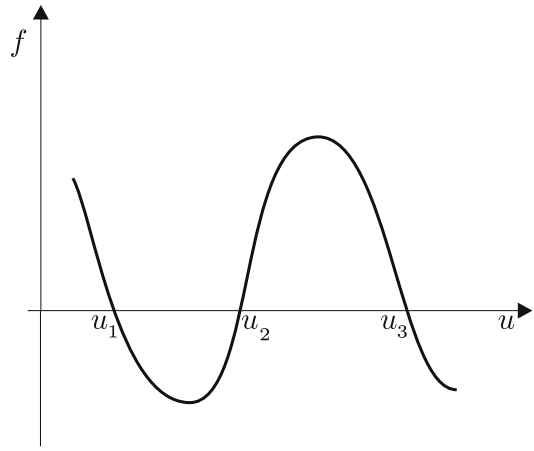

Figure 13.5
A function $f(u)$ characterising a bistable medium.

Notice that the sign of c coincides with that of $(\frac{1}{2} - a)$. Actually, in the general case (13.42) that sign is a feature of the wave motion that can be easily determined from the very beginning. Indeed, on assuming further that $u'(\xi) \; - \!\!\rightarrow 0$ as $\xi \; - \!\!\rightarrow \pm\infty$ (a fact that can be checked a posteriori, and that (13.45) certainly satisfies), we may multiply both sides of (13.42) by $u'(\xi)$ and then integrate from $-\infty$ to ∞ to eventually obtain

$$c = \left(\int_{u_1}^{u_3} f(s) ds \right) \left(\int_{-\infty}^{\infty} (u'(s))^2 \, ds \right)^{-1} , \tag{13.47}$$

so that $\mathrm{sgn}(c) = \mathrm{sgn} \int_{u_1}^{u_3} f(s) \, ds$, and fronts move either way (or remain stationary) according to the actual shape of $f(u)$ in Figure 13.5.

In the general case, besides proving the existence of travelling waves for Equation (13.41), the question naturally arises of ascertaining to what extent such waves, whenever they exist, are relevant for the dynamics of the corresponding equations. More precisely, we may wonder whether fronts are stable, or if they are the only possible propagation patterns in such media, what happens when two such waves collide, and so on. Also, we may be interested in discussing wave propagation for these types of equations in higher space dimensions. This last question will be addressed later on (cf. section 13.3.4). Here we shall briefly consider the question of stability.

Consider again Equation (13.41), and let $\Phi(x - ct) \equiv \Phi(\xi)$ be a travelling wave of that equation, so that $\Phi(\xi)$ solves (13.42). Then, on setting $w = \Phi'(\xi)$, w in turn satisfies

$$A(w) \equiv Dw'' + cw' + f'(\Phi)w = 0 \, . \tag{13.48}$$

Suppose now that we consider solutions initially close to the wave Φ, i.e., such that

$$u(x,t) = \Phi(\xi) + z(\xi,t) \quad \text{with} \quad 0 < |z| \ll \Phi \,,$$

at some initial time. Then, on expanding

$$f(\Phi + z) = f(\Phi) + f'(\Phi)z + \dots \,,$$

we see that to the lowest order, the perturbed function $z(\xi,t)$ should satisfy

$$\frac{\partial z}{\partial t} = A(z) \,,$$

with $A(z)$ as in (13.48). Since this operator has a zero eigenvalue, waves are determined up to translations (as it has already been mentioned), and a natural definition of stability would be this:

$\Phi(\xi)$ is stable if, whenever $z(\xi,t)$ is initially small,

$$(\Phi(\xi) + z(\xi,t)) - \to \Phi(\xi + h) \text{ as } t \longrightarrow \infty, \text{ for some finite constant } h.$$

The stability of fronts solving Equations (13.42) and (13.43) was established by Fife and McLeod in two influential papers (cf. [18,19]). Consider for instance the case when $f(u)$ is as in Figure 13.5 with $u_1 = 0$ and $u_3 = 1$. It is then known that such an equation has a unique (up to translations) monotone travelling front of the form $U(x-ct)$ (see for instance [44]). Suppose now that a continuous function $\varphi(x)$ is given, such that $0 \le \varphi(x) \le 1$, and

$$\lim_{x \longrightarrow \infty} \varphi(x) > u_2 \,, \qquad \lim_{x \longrightarrow -\infty} \varphi(x) < u_2 \,.$$

Then a result in [18] ensures that there exists a finite value x_0 such that the solution of (13.41) over the whole line with initial value $\varphi(x)$ approaches toward $U(x - ct - x_0)$ exponentially in time, and uniformly on x.

There are situations in which the solution of the initial value problem (13.41) will develop into a pair of fronts moving in opposite directions. For instance, let $f(u)$ be as before, and suppose also that $\int_0^1 f(s)\,ds > 0$. Assume now that $\varphi(x)$ is a continuous function such that $0 \le \varphi(x) \le 1$ and

$$\lim_{|x| \longrightarrow \infty} \varphi(x) < u_2 \,, \qquad \phi(x) > u_2 + \eta \quad \text{for} \quad |x| < L \,,$$

where η and L are some positive numbers. Then, as proven in [18], if L is sufficiently large (depending on η and f), there exist constants x_0, x_1, K, and ω (the last two positive) such that the solution $u(x,t)$ of (13.41) with initial value $\varphi(x)$ satisfies

$$\begin{aligned} |u(x,t) - U(x - ct - x_0)| &< Ke^{-\omega t} \qquad \text{when} \quad x < 0 \,, \\ |u(x,t) - U(-x - ct - x_1)| &< Ke^{-\omega t} \qquad \text{when} \quad x > 0 \,, \end{aligned}$$

where $U(x - ct)$ is as in our previous case.

Front waves are known to be the only possible nontrivial patterns of (13.41) (cf. [17,61]). From a biological point of view, bistable media are far from satisfactory for many modelling purposes. In particular, a wave propagating in such medium will leave any point forever excited after reaching it. We shall next see which modifications are to be introduced in this model to dispense with this unwanted feature.

13.3.3 Excitable Systems: Pulses

In rather informal terms, an excitable system can be described by:

- having one stable equilibrium, so that any small enough perturbation around it rapidly decays towards that point, and
- possessing such kinetic terms so as to ensure that any sufficiently large perturbation around the stable equilibrium undergoes a prolonged excursion before eventually returning to it.

In a simple case, an excitable system can be obtained from two coupled equations, corresponding respectively to a bistable medium and a restoring mechanism. As we shall presently see, besides fronts, such systems admit a different type of travelling waves named pulses. These are characterised by the fact that they approach toward the same resting state, both ahead and behind the moving perturbation.

One of the most relevant examples of excitable systems is provided by the FitzHugh-Nagumo (FHN) equations. These were derived as a model simpler than, but qualitatively similar to, the celebrated Hodgkin-Huxley equations for excitation and conduction in nerve (cf. [39] and also [15]). A particular example of the (FHN) equations is the following

$$\frac{\partial v}{\partial t} = \frac{\partial^2 v}{\partial x^2} + z + f(v), \text{ with } f(v) = v(1-v)(v-a) \text{ and } 0 < a < 1 \tag{13.49}$$

$$\frac{\partial z}{\partial t} = \varepsilon v\,, \qquad \text{with} \quad \varepsilon > 0\,. \tag{13.50}$$

In the sequel we shall closely follow the arguments in [10], and look for solutions of Equations (13.49) and (13.50) of the form

$$v(x,t) = v(x+\theta t)\,, \qquad z(x,t) = z(x+\theta t) \qquad \text{for some} \quad \theta > 0\,. \tag{13.51}$$

On setting $\xi = x + \theta t$, we readily see that such solutions should satisfy

$$\frac{\mathrm{d}^2 v}{\mathrm{d}\xi^2} - \theta \frac{\mathrm{d}v}{\mathrm{d}\xi} + f(v) - z = 0\,, \tag{13.52}$$

$$\theta \frac{\mathrm{d}z}{\mathrm{d}\xi} = \varepsilon v\,. \tag{13.53}$$

Equations (13.52) and (13.53) can be transformed into a system of three autonomous, first-order differential equations by writing $\frac{dv}{d\xi} = h$. Hence, the corresponding phase space of variables (v, h, z) is also three-dimensional and its phase portrait (i.e., the plotting of its trajectories) is more involved than the two-dimensional cases considered in our previous sections. However, the analysis of (13.52) and (13.53) greatly simplifies if we assume

$$0 < \varepsilon \ll 1 \, . \tag{13.54}$$

Indeed, introducing a small parameter allows us to make use of singular perturbation techniques, a most powerful tool in analysis (see for instance [4] for a detailed account). From now on, we assume that (13.54) holds, and proceed to describe how a first approximation to a pulse of (13.49), (13.50) can be obtained. What we want is to obtain a solution of the form (13.51), such that the v-component behaves as indicated in the Figure 13.6.

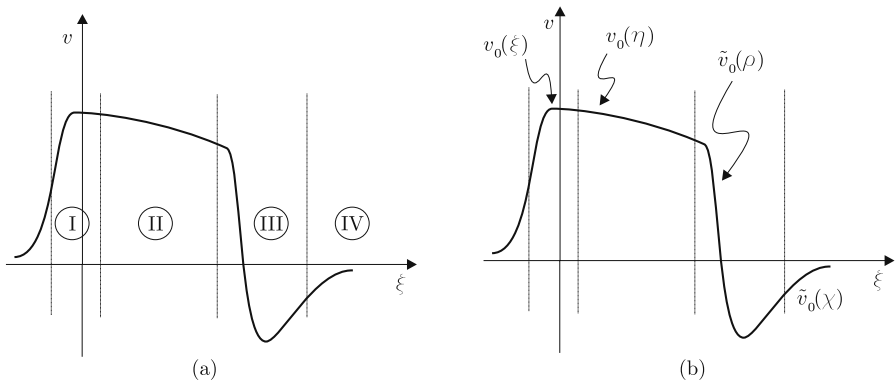

Figure 13.6

(a) The v-component of a pulse solution of (13.49), (13.50). Various relevant regions in the graph of v are denoted as I, II, III, and IV. (b) The detailed structure of the pulse as described in the text.

We now make precise some assumptions on the form of the sought-for pulse. To begin with, we assume $\theta > 0$ to be of order one, and expect $z(\xi)$ to decay to zero as $\xi \longrightarrow -\infty$. Setting $\varepsilon = 0$, we may discard the right-hand side in (13.53) to obtain

$$\frac{\mathrm{d}z}{\mathrm{d}\xi} = 0 \, , \qquad z(\xi) - \to 0 \quad \text{as} \quad \xi \longrightarrow -\infty \, .$$

This gives at once $z(\xi) = 0$, which upon substitution in (13.49) yields

$$\frac{\partial v}{\partial t} = \frac{\partial^2 v}{\partial x^2} + v(1 - v)(v - a) \, .$$

Solving this equation with the condition $v(\xi) - \to 0$ as $\xi \longrightarrow -\infty$, we obtain the analogue of (13.45), viz.

$$v_0 = \left(1 + e^{-\frac{\xi}{\sqrt{2}}}\right)^{-1} , \qquad \theta = \theta_0 = \sqrt{2}\ \left(\frac{1}{2} - a\right) , \tag{13.55}$$

which accounts for the profile of v in Region I in Figure 13.6a. Note that $v_0(\xi) - \to 1$ as $\xi \longrightarrow \infty$, so that $v_0(\xi)$ actually represents a front instead of a pulse. However, $v_0(\xi)$ is easily seen not to provide a uniformly valid approximation for large values of ξ. Indeed, from (13.53) we see that the exact expression for $z(\xi)$ is

$$z(\xi) = \frac{\varepsilon}{\theta} \int_{-\infty}^{\xi} v(r)\, dr \ .$$

Upon replacing $v(r)$ by $v_0(r)$ there, we readily check that z becomes of order one (and therefore cannot be neglected in (13.53)) at distances $\xi = O(\frac{1}{\varepsilon})$. This suggests introducing new variables to analyse Region II in Figure 13.6a as follows

$$\eta = \varepsilon\xi\ ,\ u(\eta,\varepsilon) = v(\xi,\varepsilon)\ ,\ y(\eta,\varepsilon) = z(\xi,\varepsilon)\ . \tag{13.56}$$

Equations (13.52) and (13.53) then transform into

$$\varepsilon^2 \frac{\mathrm{d}^2 u}{\mathrm{d}\eta^2} - \varepsilon\theta \frac{\mathrm{d}u}{\mathrm{d}\eta} + f(u) - y = 0\ , \tag{13.57}$$

$$\theta \frac{\mathrm{d}y}{\mathrm{d}\eta} = u\ . \tag{13.58}$$

On setting above $\theta = \theta_0$ (cf. (13.55)) and $\varepsilon = 0$, we obtain

$$f(u_0) = y_0\ , \tag{13.59}$$

which upon substitution in (13.58) gives $\mathrm{d}\eta = \theta_0 \left[\frac{f'(u_0)}{u_0}\right] \mathrm{d}u_0$, whence

$$\eta = \theta_0 \left[-\frac{3}{2}u_0^2 + 2(1+a)u_0 - a\log|u_0| + C\right] \ , \tag{13.60}$$

besides the trivial solution $u_0 = 0$. Notice that (13.60) defines u_0 as a multivalued function of η. Let us write $u_{\min}$ (resp. $u_{\max}$) to denote the point where $f(u)$ achieves its minimum (resp. its maximum) in $[0,1]$, and let us select $u_0(\eta)$ as the solution of (13.60) in the branch where $u_0 \geq u_{\max}$. This function will describe (to the lowest order) our pulse in terms of v in Region II (cf. Figure 13.6). To allow for matching with Region I, we also require

$$\lim_{\eta - \to 0} u_0(\eta) = v_0(\infty) = 1\ , \qquad y_0(0) = 0\ .$$

From (13.60) we deduce that $u_0(\eta)$ decreases as η increases, but is bounded from below by a positive constant in the branch under consideration. Therefore,

patching together $v_0(\xi)$ and $u_0(\eta)$ still does not provide a uniformly valid representation for the pulse. To this end, we need to introduce a further layer, where a downjump will occur. Suppose that this will happen near a value $\eta = \eta_d$, at which z will achieve a (unknown as yet) value $K_0 > 0$. We then introduce new variables given by

$$\varepsilon\rho = \eta - \eta_d \ , \qquad \widetilde{v}_0(\rho, \varepsilon) = u_0(\eta, \varepsilon) \ .$$

Then, on setting $\frac{d\widetilde{v}_0}{d\rho} = \widetilde{w}_0$, we arrive at

$$\frac{d\widetilde{w}_0}{d\rho} = \theta_0 \widetilde{w}_0 - f(\widetilde{v}_0) + K_0 \ , \tag{13.61}$$

together with boundary conditions

$$\begin{array}{l} \widetilde{v}_0(\rho) - \to \widetilde{\mathrm{U}} \quad \text{as} \quad \rho \longrightarrow -\infty \ , \\ \widetilde{v}_0(\rho) - \to \widetilde{\mathrm{V}} \quad \text{as} \quad \rho \longrightarrow \infty \ , \end{array} \tag{13.62}$$

where $\widetilde{\mathrm{U}} = u_0(\eta_d)$ and $\widetilde{\mathrm{V}}$ are not determined yet. Note that the speed of the downjump has been already fixed, and is equal to θ_0, the corresponding value at the upjump. It is a most remarkable fact that, as shown in [10], this nonlinear eigenvalue problem has a unique solution only for a particular value of K_0. More precisely, in terms of $\widetilde{v}_0$, this solution is

$$\widetilde{v}_0(\rho) = \frac{\widetilde{\mathrm{U}} e^{-h\rho} + \widetilde{\mathrm{V}}}{1 + e^{-h\rho}} \ , \tag{13.63}$$

where

$$\sqrt{2}\, h = \widetilde{\mathrm{U}} - \widetilde{\mathrm{V}} \ , \quad \widetilde{\mathrm{U}} = \tfrac{2+2a}{3} \ , \quad \widetilde{\mathrm{V}} = \tfrac{2a-1}{3} \ , \quad \text{and} \quad K_0 = -2 f_{\mathrm{inf}} \ ,$$

$$\text{with } f_{\mathrm{inf}} \equiv \text{value of } f \text{ at its inflection point, that is} \tag{13.64}$$

$$f_{\mathrm{inf}} = \tfrac{1}{27}(1+a)(2-a)(2a-1) \ .$$

Incidentally, this result is obtained by looking for solutions of Equations (13.61) and (13.62) such that $\widetilde{w}(\widetilde{v})$ is a polynomial: $\widetilde{w}(\widetilde{v}) = \lambda(\widetilde{v} - \mathrm{V})(\mathrm{U} - \widetilde{v})$ for some λ, where V, U are the extreme roots of $f(v) + K = 0$. Since $\theta_0 > 0$, $0 < a < \frac{1}{2}$, and $K_0 > 0$, by (13.64), $\widetilde{\mathrm{V}} < 0$, and to complete the picture a further piece is needed, namely an outer solution which increases from $v = \widetilde{\mathrm{V}}$ at $\eta = \eta_d$ to $v = 0$ as $\eta - \to \infty$. This solution is provided by $\widetilde{u}_0$, where this time the branch where $u < 0$ has to be selected. To deal with the corresponding region, it is also convenient to introduce a new variable by setting $\chi = \varepsilon\rho$. In this way the leading approximation to the v-component of the pulse has been sketched. Higher-order approximations (involving powers of ε in the corrective terms derived) can then be obtained by perturbative analysis, as is done in [10].

Concerning the procedure thus sketched, some remarks are in order. First, Equation (13.57) can be shown to admit also solutions for which

$$\theta = \mathrm{O}(\sqrt{\varepsilon}) \,, \tag{13.65}$$

(see [10], Section 4). Therefore, for given values of a and ε, two pulse solutions are possible: a fast one (with $\theta = \mathrm{O}(1)$) and a slow one (satisfying (13.65)). As the authors of [10] observed, "... it is believed that the larger value of θ corresponds to a stable solution, and the smaller value to an unstable one." As a matter of fact, the stability of fast pulses was later proven in [43]. A second important remark is that pulses are not the only new kind of patterns arising in (13.49), (13.50). For instance, periodic wavetrains can be constructed by methods closely related with those described above. We shall not pursue this matter any further here, and refer instead to [10] and [25] for details.

Let us summarise a bit. We have just recalled how pulses can be constructed for the FHN model (13.49), (13.50) under two key hypotheses: the precise form of $f(u)$ in (13.49) and the small parameter assumption (13.54). This last can be dispensed with (i.e., ε can be taken to be of order one) if, instead of selecting $f(u)$ as in (13.49), we make the explicit choice

$$f(u) = H(u-a) - u \qquad \text{with} \qquad 0 \leq a \leq \frac{1}{2} \,,$$

where $H(s)$ is the step function defined in (13.33). The corresponding study can be found in [76].

To conclude this section, we point out that we have merely scratched at the surface of a large body of results available for pulse propagation in excitable systems. We just refer here to [77] and [45] for further glimpses at the corresponding theory.

13.3.4 Excitable Systems: Targets and Spirals

In our previous sections we have been concerned with waves propagating in one-dimensional media. We shall consider now some particularly relevant structures appearing in higher-dimensional situations. For instance, rotating spirals and concentric circular waves (called targets) are observed in various chemical and biological settings (see for instance [61,63]). We shall define below in a precise manner such types of solutions, describe some reaction-diffusion systems where they appear, and remark on the relevance of these systems from a modelling point of view.

Let us discuss spiral waves first. To this end, consider the following system in two space dimensions

$$\begin{cases} \dfrac{\partial u}{\partial t} = D \triangle u + \lambda(A) u - \omega(A) v \,, \\ \dfrac{\partial v}{\partial t} = D \triangle v + \omega(A) u + \lambda(A) v \,, \end{cases} \tag{13.66}$$

where $D > 0$, and λ, ω are given functions of $A = (u^2 + v^2)^{\frac{1}{2}}$. The system of equation (13.66) is generally referred to as a $\lambda - \omega$ system. A key assumption to be made in (13.66) is the following:

$$\text{for some } a > 0,\ \lambda(A) \text{ is a continuous, decreasing, and positive function in an interval } [0, a), \text{ and } \lambda(a) = 0. \tag{13.67}$$

Condition (13.67) ensures that the kinetic system associated to (13.66) has a stable limit cycle, which corresponds in phase space to a monoparametric family of periodic solutions differing from each other only in a phase shift. Such a limit cycle has amplitude a and frequency $\omega(a)$. It is often convenient to rewrite (13.66) in a more compact manner by setting

$$\mathrm{w} = u + iv\,, \tag{13.68}$$

in which case (13.66) reduces to

$$\frac{\partial \mathrm{w}}{\partial t} = (\lambda + i\omega)\mathrm{w} + D\triangle \mathrm{w}\,. \tag{13.69}$$

It is then natural to look for solutions of the form

$$\mathrm{w} = Ae^{i\phi}\,, \tag{13.70}$$

where A is an amplitude variable, and ϕ is the corresponding phase. Plugging (13.70) into (13.69), one readily sees that A and ϕ should satisfy

$$\begin{cases} \dfrac{\partial A}{\partial t} = A\lambda(A) - DA|\nabla\phi|^2 + D\triangle A\,, \\ \dfrac{\partial \phi}{\partial t} = \omega(A) + \dfrac{2D}{A}(\nabla A \cdot \nabla\phi) + D\triangle\phi\,. \end{cases} \tag{13.71}$$

An m-armed spiral wave of (13.69) is defined as a solution of the form (13.70), where

$$A = A(r)\,, \qquad \phi = \Omega t + m\theta + \psi(r)\,, \tag{13.72}$$

and (r, θ) denote polar coordinates in $\mathbb{R}^2$, $A(r)$, $\psi(r)$ (respectively Ω) are functions (resp. a constant) to be determined, and $m \geq 1$ is a positive integer.

In view of (13.71), the corresponding equations for amplitude and phase read then

$$\begin{cases} D(A'' + \frac{A'}{r}) + A\left(\lambda(A) - D(\psi')^2 - \frac{Dm^2}{r^2}\right) = 0\,, \\ D\left(\psi'' + (\frac{1}{r} + \frac{2A'}{A})\psi'\right) = \Omega - \omega(A)\,. \end{cases} \tag{13.73}$$

System (13.73) has to be supplemented with suitable boundary conditions

$$A(0) = \psi'(0) = 0\,, \qquad A(r) - \to A(\infty) \quad \text{as} \quad r \longrightarrow \infty\,. \tag{13.74}$$

Notice that from this and (13.73) one readily sees that

$$\psi'(\infty) = \left(\frac{\lambda(A_\infty)}{D}\right)^{\frac{1}{2}}\,, \qquad \Omega = \omega(A_\infty)\,, \tag{13.75}$$

which in particular shows that the amplitude at infinity determines the frequency Ω. From now on, we shall set $D = 1$ for simplicity. It has been shown in [13] that, when $m = 1$, there exists a solution of (13.73), (13.74) provided that in addition to (13.67) the following hypothesis is made:

$\omega = \omega(A)$ is continuous in $[0, a]$, and there exist $\varepsilon \geq 0$ and $\mu > 0$ such that

$$|\omega(a) - \omega(A)| \leq \varepsilon(a - A)^{1+\mu} \quad \text{when} \quad 0 \leq A \leq a\,. \tag{13.76}$$

More precisely, the existence proof provided in [13] (which consists in a topological fixed point argument) yields the existence of a logarithmic spiral wave, i.e., a function $w = u + iv$ such that

$$\begin{cases} u \equiv A(\infty)\cos\,\Omega t + \theta + c\log r\,, \\ \\ v \equiv A(\infty)\sin\Omega t + \theta + c\log r\,, \end{cases} \tag{13.77}$$

where

$$c = \frac{1}{a^2}\int_0^\infty sA^2(s)(\omega(A) - \omega(A(s)))\,ds\,.$$

Before a discussion on extensions and improvements of this early result, we remark on the structure requirements made in (13.66) and (13.67). In this respect, it should be noticed that a large class of RD systems can be approximated, in some asymptotic limit, by means of $\lambda - \omega$ equations (cf. for instance [13] and [27]). More precisely, let us follow [27] and consider the system

$$\begin{cases} \dfrac{\partial A_1}{\partial t} = F_1(\mu, A_1, A_2) + \nabla\cdot(D_1(\mu, A_1, A_2)\nabla A_1)\,, \\ \\ \dfrac{\partial A_2}{\partial t} = F_2(\mu, A_1, A_2) + \nabla\cdot(D_2(\mu, A_1, A_2)\nabla A_2)\,, \end{cases} \tag{13.78}$$

where μ represents some nondimensional parameter, and suppose that at some critical value $\mu = \mu_0$ the diffusionless (kinetic) equations, obtained by setting $D_1 = D_2 = 0$ above, are such that a bifurcation from a stable state (A_1^0, A_2^0) to a stable limit cycle occurs (in mathematical terms this is called a Hopf bifurcation). Then, arguing as in [27], Appendix A, we assume $0 < \mu - \mu_0 \ll 1$, and look for solutions of the form

$$A_i \sim A_i^0 + (\mu - \mu_0)^{\frac{1}{2}}A(T, \widetilde{\mathbf{x}})a_i\cos\left(\omega t + \gamma_i + \phi(T, \widetilde{\mathbf{x}})\right)\,, \quad i = 1, 2$$

where $\widetilde{\mathbf{x}} = (\widetilde{x}_1, \widetilde{x}_2) = (\mu - \mu_0)^{\frac{1}{2}}(x_1, x_2)$, a_i and γ_i are suitable constants, and $T = (\mu - \mu_0)t$. Then the overall amplitude and phase $A = (A_1^2 + A_2^2)^{\frac{1}{2}}$ and ϕ are shown to evolve according to the equations

$$\begin{pmatrix} \dfrac{\partial A}{\partial T} \\ \\ A\dfrac{\partial \phi}{\partial T} \end{pmatrix} = \begin{pmatrix} \cos z & -\sin z \\ \\ \sin z & \cos z \end{pmatrix} \begin{pmatrix} \triangle A - A|\nabla\phi|^2 \\ \\ A\triangle\phi + 2\nabla A \cdot \nabla\phi \end{pmatrix} + \begin{pmatrix} A(1-A^2) \\ \\ qA^3 \end{pmatrix} , \tag{13.79}$$

where q and z are certain constants determined from the original system (13.78). In particular, when $D_1 = D_2$, then $z = 0$, and the following $\lambda - \omega$ system is obtained

$$\begin{cases} \dfrac{\partial A}{\partial T} = \triangle A - A|\nabla\phi|^2 + A(1-A^2) , \\ \\ A\dfrac{\partial \phi}{\partial T} = A\triangle\phi + 2\nabla A \cdot \nabla\phi + qA^3 . \end{cases} \tag{13.80}$$

However, since $\omega(A) = qA^2$ in (13.80), condition (13.76) is not fulfilled, and further analysis is required to ensure the existence of spiral waves in this case. In [27], a variety of arguments (analytical and numerical) have been presented to obtain the existence of Archimedean spiral waves of (13.80) (these satisfy $\psi(r) \sim kr$ as $r \longrightarrow \infty$ in (13.72)) for all values of q. More precisely, existence is proven for $q = 0$, which is the startpoint to deal with the case $0 < |q| \ll 1$ via perturbation theory. Spiral waves are also obtained for $|q| \gg 1$, and then a numerical continuation argument is produced to derive the existence of spiral waves for intermediate values of q. The question of the stability of spirals is also addressed, and the author concludes that when $q = 0$, one-armed spirals are stable, while multi-armed ones are not. It is also remarked therein that perturbative arguments strongly suggest that one-armed spirals continue to be stable for small values of $|q|$.

The results just recalled above belong to what could be called early spiral wave theory for excitable systems. This last has greatly developed ever since, and a wealth of analytical and numerical results are now available for a number of model RD systems. We refer to [25,46,61,63,91,92] for further material on that topic.

Before shifting arguments, a further remark is in order. If we change variables in (13.79) by setting $W = Ae^{i\phi}$ (cf. (13.70)), we obtain the so-called Ginzburg-Landau (GL) equation

$$\frac{\partial W}{\partial T} = \alpha W - \beta|W|^2 W + d\triangle W , \tag{13.81}$$

where α, β, and d are some complex coefficients that can be determined from the original system (13.78). This is a particular example of the so-called amplitude equations, that have been extensively used in the physical literature to describe pattern formation resulting from a Hopf's bifurcation in an underlying kinetic system. We

shall not pursue this matter any further here, but refer instead to [51] and [16] for additional information.

We next turn our attention to target patterns. These may be thought of as a travelling wave train of concentric circles propagating from a centre, which is often referred to as a pacemaker. We shall describe below a way of characterising target patterns in RD systems, and from that we will derive some information about media where such a type of wave propagation is sustained.

Specifically, following [26] we consider a system given in vector form by

$$\frac{\partial \mathbf{A}}{\partial t} = \mathbf{F}(\mathbf{A}) + \varepsilon D \triangle \mathbf{A} + \varepsilon \mathbf{g}(\mathbf{x}, \mathbf{A}) \; , \tag{13.82}$$

where $\mathbf{A} = (A_1, A_2)$, $D > 0$, $0 < \varepsilon \ll 1$, and $\mathbf{g}(\mathbf{x}, \mathbf{A})$ is a bounded function of its arguments. On the kinetic term $\mathbf{F}(\mathbf{A})$ we assume conditions so as to ensure that the autonomous system

$$\mathbf{A}' = \mathbf{F}(\mathbf{A}) \; ,$$

has a stable time-periodic solution $\mathbf{B}(t) = \mathbf{B}(t + P)$ for some $P > 0$. Thus (13.82) can be thought of as an example of an RD system where diffusion is small, and small also is the effect of localised impurities, represented by the last term on the right of (13.82). We now introduce a slow-time scale T given by $T = \varepsilon t$, and look for solutions of (13.82) of the form

$$\mathbf{A}(\varepsilon, t, \mathbf{x}) = \mathbf{A}^0(t, T, \mathbf{x}) + \varepsilon \mathbf{A}^1(t, T, \mathbf{x}) + \varepsilon^2 \mathbf{A}^2(t, T, \mathbf{x}) + \dots \; , \tag{13.83}$$

requiring $\mathbf{A}^1, \mathbf{A}^2, \dots$ to be bounded in time. On substituting (13.83) into (13.82) we obtain that $\mathbf{A}^0, \mathbf{A}^1$ should satisfy

$$\frac{\partial \mathbf{A}^0}{\partial t} = \mathbf{F}(\mathbf{A}^0) \; , \tag{13.84}$$

$$\frac{\partial \mathbf{A}^1}{\partial t} - \mathbf{F}_A(\mathbf{A}^0)\mathbf{A}^1 = -\frac{\partial \mathbf{A}^0}{\partial T} + D \triangle \mathbf{A}^0 + \mathbf{g}(\mathbf{x}, \mathbf{A}^0) \; , \tag{13.85}$$

where $\mathbf{F}_A(\mathbf{A}^0)$ denotes the jacobian matrix of $\mathbf{F}(\mathbf{A})$ particularised at $\mathbf{A} = \mathbf{A}^0$. Solving (13.84) gives

$$\mathbf{A}^0 = \mathbf{B}(t + \psi(T, \mathbf{x})) \; , \tag{13.86}$$

where the phase variable $\psi(T, \mathbf{x})$ is to be determined yet. From (13.85) and (13.86) it follows that $\mathbf{A}^1$ has to solve

$$\frac{\partial \mathbf{A}^1}{\partial t} - \mathbf{F}_A(\mathbf{B})\mathbf{A}^1 = -\mathbf{B}' \frac{\partial \psi}{\partial T} + D(\mathbf{B}' \triangle \psi + \mathbf{B}'' |\nabla \psi|^2) + \mathbf{g}(\mathbf{x}, \mathbf{B}) \equiv \mathbf{G}(\psi, \mathbf{x}, t) \; . \tag{13.87}$$

We are interested in bounded solutions of (13.87). To obtain them, a suitable orthogonality condition has to be imposed concerning the right-hand side there. More precisely, by (13.84) and (13.86), we know that the equation

$$\frac{\partial \mathbf{u}}{\partial t} - \mathbf{F}_A(\mathbf{B}(t+\psi))\mathbf{u} = 0 \,, \tag{13.88}$$

has a periodic solution $\mathbf{u} = \mathbf{B}'(t+\psi)$. Since we are requiring (13.86) to be a stable solution of (13.84), we need to impose that all solutions of (13.88) which are linearly independent of $\mathbf{B}'(t+\psi)$ should decay exponentially in time. Under these assumptions, there is a unique row vector $\mathbf{z}^T(t+\psi)$ which is periodic with period P, and is such that, for all t

$$\frac{\partial \mathbf{z}^T}{\partial t} + \mathbf{z}^T \mathbf{F}_A(\mathbf{B}(t+\psi)) = 0 \,, \qquad \mathbf{z}^T(t+\psi)\mathbf{B}'(t+\psi) = 1 \,.$$

Then a solution of (13.87) is bounded in time if and only if

$$\int_0^P \mathbf{z}^T \mathbf{G}(\psi, \mathbf{x}, s)\, ds = 0 \,, \tag{13.89}$$

an orthogonality condition. Incidentally, this is precisely the argument that eventually yields Equations (13.79) or (13.81), except that one has to go up to higher-order terms in the corresponding expansion to be analysed in such case (cf. [27] and [51] for details).

From (13.89), using periodicity we eventually obtain that ψ should satisfy

$$\frac{\partial \psi}{\partial T} = D_1(\triangle\psi + \Gamma|\nabla\psi|^2) + \alpha(\mathbf{x}) \,, \tag{13.90}$$

where

$$\begin{cases} D_1 = \frac{1}{P}\int_0^P \mathbf{z}^T(s) D\mathbf{B}'(s)\, ds \,, \\ \Gamma = \frac{1}{P}\int_0^P \mathbf{z}^T(s) D\mathbf{B}''(s)\, ds \,, \\ \alpha(\mathbf{x}) = \frac{1}{P}\int_0^P \mathbf{z}^T(s)\mathbf{g}(\mathbf{x}, \mathbf{B}(s))\, ds \,. \end{cases} \tag{13.91}$$

Summing all these results up, we have obtained that

$$\mathbf{A}(t, \mathbf{x}) = \mathbf{B}(t + \psi(t, \mathbf{x})) + O(\varepsilon) \,. \tag{13.92}$$

Equations (13.90) to (13.92) can be thought of as providing a description of a distributed medium consisting in a large population of individual oscillators which are weakly coupled by diffusion, the effect of which consists in introducing a phase shift between different points. In particular, Equation (13.90) provides a law for the evolution in time of that shift. The reader is referred to [51,66–68,82] for the derivation of phase equations under different assumptions, as well as for discussing the phenomenon of synchronisation of coupled oscillators.

Having derived (13.90) to (13.92), we are now in a position to discuss the existence of target patterns for (13.82). A first remarkable fact is that for bounded initial conditions, targets can only exist if $\mathbf{g}(\mathbf{x}, \mathbf{A}) \neq 0$. Indeed, assume on the contrary that $\mathbf{g}(\mathbf{x}, \mathbf{A}) = 0$. Then, by (13.91), $\alpha(\mathbf{x}) = 0$. On setting

$$Z = e^{\Gamma\psi} \,, \tag{13.93}$$

(13.91) reduces to

$$\frac{\partial Z}{\partial T} = D_1 \triangle Z \,. \tag{13.94}$$

Therefore the initial value problem for Equation (13.82) can be explicitly solved (cf. formula (13.5)) to give

$$\psi(T, \mathbf{x}) = \frac{1}{\Gamma} \log (4\pi D_1 T)^{-1} \int_{\mathbb{R}^2} \exp \left\{ \frac{\Gamma\psi(0, \mathbf{y}) - |\mathbf{x} - \mathbf{y}|^2}{4D_1 T} \right\} d\mathbf{y} \,.$$

In particular, if $\psi(0, \mathbf{x})$ is bounded, $\psi(T, \mathbf{x})$ converges to a constant as $T - \to \infty$, and asymptotically the medium oscillates with uniform phase shift. When $\psi(0, \mathbf{x})$ is unbounded, however, target patterns can be produced (see for instance (13.34) in [26]).

Consider now the case when impurities are present, i.e., $\mathbf{g}(\mathbf{x}, \mathbf{A}) \neq 0$, when $\alpha \neq 0$ in (13.91). Using (13.93), we obtain this time

$$\frac{\partial Z}{\partial T} = D_1 \triangle Z + \Gamma\alpha(\mathbf{x}) Z \,. \tag{13.95}$$

To solve (13.95), we now separate variables by setting

$$Z(T, \mathbf{x}) = e^{\omega T} \Phi(\mathbf{x}) \,, \tag{13.96}$$

thus obtaining the following eigenvalue problem: to find Φ and ω such that

$$D_1 \triangle \Phi + \Gamma\alpha(\mathbf{x})\Phi = \omega\Phi \,, \qquad \Phi(\mathbf{x}) \text{ bounded in } \mathbb{R}^2 \,. \tag{13.97}$$

To proceed further, we need to introduce additional assumptions on $\alpha(\mathbf{x})$. Basically, we want to solve (13.97) explicitly, and to this end we need $\alpha(\mathbf{x})$ to be a smooth, rapidly decaying function, so that classical spectral theory could be invoked. Assume for instance that $\alpha(\mathbf{x})$ is smooth and compactly supported in a ball $B_R(\mathbf{x}_0) = \{\mathbf{x} : |\mathbf{x} - \mathbf{x}_0| \leq R\}$ for some $\mathbf{x}_0 \in \mathbb{R}^2$ and $R > 0$, and that $\int_{\mathbb{R}^2} \alpha(\mathbf{x})\, d\mathbf{x} > 0$. It is then known (cf. for instance [41,79]) that (13.97) has a finite number $m \geq 1$ of real eigenfunctions $\Phi_1(\mathbf{x}), \cdots, \Phi_m(\mathbf{x})$, which correspond to eigenvalues $\omega_1, \cdots, \omega_m$ such that $\omega_1 > \omega_2 \geq \omega_3 \geq \cdots \geq \omega_m > 0$. Moreover $\Phi_1(\mathbf{x})$ does not change sign. Besides that, there exists a two-dimensional continuum of eigenfunctions $\Phi(\mathbf{k}, \mathbf{x})$. These correspond to eigenvalues $(-D_1|k|^2)$ and are given as the solutions of

$$\Phi(\mathbf{k},\mathbf{x}) = e^{i\mathbf{k}\cdot\mathbf{x}} + \frac{i\Gamma}{4D_1}\int_{\mathbb{R}^2} H_0^{(1)}(|\mathbf{k}|\,|\mathbf{x}-\mathbf{y}|)\alpha(\mathbf{y})\Phi(\mathbf{k},\mathbf{y})\,d\mathbf{y}\ , \tag{13.98}$$

where $H_0^{(1)}$ is the zero-order Hankel function (see [1] for definitions and properties of this special function). Summing up, it follows that the solutions of (13.90) can be represented by means of (13.93), where

$$Z(T,\mathbf{x}) = \beta_1 e^{\omega_1 T}\Phi_1(\mathbf{x}) + \sum_{j=2}^{m}\beta_j e^{\omega j T}\Phi_j(\mathbf{x}) + H(T,\mathbf{x}) - \sum_{j=1}^{m}\gamma_j(T)\Phi_j(\mathbf{x}) + v(T,\mathbf{x})\ , \tag{13.99}$$

and

- $H(T,\mathbf{x})$ is the solution of (13.94), $H(0,\mathbf{x}) = \exp\left(\Gamma\psi(0,\mathbf{x})\right)$,
- $\beta_j = \left(\int_{\mathbb{R}^2}\Phi_j^2(\mathbf{x})\,d\mathbf{x}\right)^{-1}\int_{\mathbb{R}^2}\Phi_j(\mathbf{x})\exp\left(\Gamma\psi(0,\mathbf{x})\right)d\mathbf{x}$,
- $\gamma_j(T) = \left(\int_{\mathbb{R}^2}\Phi_j^2(\mathbf{x})\,d\mathbf{x}\right)^{-1}\int_{\mathbb{R}^2}\Phi_j(\mathbf{x})H(T,\mathbf{x})\,d\mathbf{x}$ when $1 \le j \le m$, and
- $v(T,\mathbf{x})$ is the contribution arising form the continuum spectrum.

(13.100)

Cumbersome as they may appear, these formulae allow for deriving relevant information about the asymptotics of $\Phi(T,\mathbf{x})$. For instance, arguing as in [26] (where suitable estimates on $v(T,\mathbf{x})$ are obtained, and the asymptotic behaviour of eigenfunctions is used), it may be shown that in the region where

$$e^{\omega_1 T - k_1|\mathbf{x}-\mathbf{x}_0|} \ll 1 \quad \text{and} \quad T \gg 1\ , \qquad \text{with} \quad k_1 = \left(\frac{\omega_1}{D_1}\right)^{\frac{1}{2}}\ , \tag{13.101}$$

the function $H(T,\mathbf{x})$ provides the largest contribution in (13.99). One then has that, in such a region

$$\mathbf{A}(T,\mathbf{x}) \sim \mathbf{B}\left(t + \frac{1}{\Gamma}\right)\log H(T,\mathbf{x})\ ,$$

and since $H(T,\mathbf{x})$ converges to a constant for large T, it turns out that whenever (13.101) holds the system eventually approaches toward a spatially constant solution. On the other hand, in the region where

$$e^{\omega_1 T - k_1|\mathbf{x}-\mathbf{x}_0|} \gg 1\ , \qquad T \gg 1\ , \tag{13.102}$$

it is the first term in the right of (13.99) which prevails, and one then has that

$$\mathbf{A}(t,\mathbf{x}) = \mathbf{B}\left((1 + \frac{\varepsilon\omega_1}{\Gamma})t + \frac{1}{\Gamma}\log\Phi_1(\mathbf{x}) + \frac{1}{\Gamma}\log b_1\right) + O(\varepsilon)\ . \tag{13.103}$$

Since

$$\Phi_1(x) \sim C_1(k_1 r)^{-\frac{1}{2}} e^{-k_1 r} \quad \text{for some} \quad C > 1 \,,$$

and $k_1 r \gg 1$ with $r = |x|$, (13.103) yields a target pattern wave (up to corrections of order $O(\varepsilon)$) which is outgoing for $\Gamma > 0$ and ingoing when $\Gamma < 0$. Notice that the initial value $\psi(0, \mathbf{x})$ enters (13.103) only via the phase shift $\frac{1}{\Gamma} \log b_1$.

We conclude by observing that it is possible to perform a similar analysis for impurities $\alpha(\mathbf{x})$ located around two different points $\mathbf{x}_0$ and $\mathbf{x}_1$. Then the precise form of $\alpha(\mathbf{x})$ determines the eigenvalues around $\mathbf{x}_0$ and $\mathbf{x}_1$. In particular, it can be shown that, out of the two emanating targets, it is that having largest first eigenvalues ω_{1i} $(i = 0, 1)$ which eventually takes over. See [26] for details.

13.4 Models of Chemotaxis

In this section we shall deal with some RD systems that have been used to model an important biological activity, namely chemotaxis. By this we refer in general to motion induced by chemical substances, a widely accepted framework to describe the ability of single cells or micro-organisms to sense the direction of external chemical sources, and to migrate towards (or away from) these. Chemotaxis is known to occur in a variety of situations, as for instance during the development of the nervous system, in inflammatory and wound healing responses, and in tumour growth and metastasis, among others. It also plays an important role in the social life of micro-organisms, a subject that will be examined in some detail below. In the following, we shall briefly describe some instances where chemotaxis is a key factor, and will examine some of the mathematical models that have been proposed to provide quantitative and qualitative insight on particular aspects on this phenomenon.

13.4.1 Axon Growth and Neuron Navigation

The nervous system of a person is known to perform a sophisticated set of functions. This requires of a highly complex pattern of wiring among nervous cells (called neurones). The number of these is of the order of 10^{12}, each establishing on average about 10^3 connections (called synaptic contacts) with various targets. Neuronal connections form during embryonic development, when each differentiating neuron sends out an axon, tipped at its leading edge by the growth cone, which migrates through the embryonic environment to meet its target.

Growth cones were first described by Ramón y Cajal in chicken embryos (cf. [73]). These structures are continuously expanding and retracting; this is the way in which growth cones integrate and transduce chemical signals arising from targets and neighbour tissues. In 1893, Ramón y Cajal advanced the so-called chemotactic

hypothesis (cf. [74]), according to which growth cones should be "excitable by substances secreted by some nervous cells," their motion being guided to their eventual targets by "chemical streams." Experimental verification of this conjecture had to wait for a long time; see [83] and [80] for surveys of the aspects involved.

Much is already known about the manner in which neuron navigation occurs. For instance, as explained in [83], axon trajectories appear to be broken into short segments. In this way, reaching a distant target is split into many simpler (and shorter) steps, which all together allow axons to move over comparatively large distances (usually on the order of centimetres, that is, over a thousand times the diameter of each cell body). A second feature stressed in [83] is that the wiring of the nervous system takes place in a stepwise manner. This means that the first axons that develop have to move within an axon-free environment. However, later moving ones have to deal with an expanding media where earlier sailing cells make up a scaffolding network where others should travel along.

Even if large journeys can be broken into shorter legs, the question remains of understanding how each axon navigates any short segment. As described in [83], axons seem to respond to the coordinate action of four types of guidance cues: attractive and repulsive, which can be either short-range or long-range. Long-range attraction and repulsion seem in turn to be produced by diffusible factors, whereas short-range guidance appears to be provided by contact-mediated mechanisms, involving nondiffusible cell surface and extracellular matrix (ECM) molecules. We next proceed to remark on some modelling aspects of long-range, diffusive attraction, or repulsion.

13.4.1.1 Sensitivity, Adaptation, Amplification

A first modelling approach might consist in considering each biological unit (axons in the case recalled above, but possibly lymphocytes or amoebae in the situations to be considered later) as a black box, from which some robust properties are to be expected, irrespective of the precise way in which these are achieved. For instance, for long-range guidance based on the detection of chemotactic gradients to be successful, the organisms involved are expected to fulfill some requirements, namely:

- To be able to respond reliably to small gradients of guidance cues across their surface (sensitivity)

- As migration takes place in a medium where the basal concentration of chemical signals varies by several orders of magnitude, organisms need to constantly re-adjust their sensitivity, a process usually termed as adaptation.

Besides that, in a living environment the detection-orientation system has to allow for high-gain persistent, polarised signalling in response to chemoattractant gradients (amplification).

As a matter of fact, experiments reported in [62] show that under exposure to high levels of netrin-1 of brain-derived neurothropic factor (BDNF), growth cones

of cultured *xenopus* spinal neurones undergo consecutive phases of desensitisation and resensitisation (that is, adaptation) in their ability to detect gradients of netrin-1 of BDNF. Moreover, these cyclic phases of desensitisation and resensitisation are reflected in the zigzag path of alternating attractive and repulsive turning of advancing growth cones towards their source of chemoattractant. However, in the absence of guidance factor, no such type of path is observed, and the growth cone advances in an irregular and unpredictable manner.

A model of amplification in growth cones has been proposed in [60]. It consists in a system of ordinary differential equations involving three variables: a saturating, self-enhancing activator, coupled with two antagonistic equations. Of these, one equilibrates rapidly over the whole cell, causing competition among different surface elements, which is won by those exposed to the highest concentration of external cues. A second antagonistic reaction is assumed to act locally. It has a longer time constant, and produces destabilisation of peaks after they have formed. On the other hand, a model for adaptation different from (but also motivated by) the activator-inhibitor models of [58–60] has recently been proposed in [50,54]. Again, three variables are considered: a response element that can be active (denoted by R^*) or inactive, its total concentration being R_0, and an active excitory (A^*) and inhibitory (I^*) enzymes that catalyse the activation and inactivation of the system. Activation is in turn regulated by receptor occupancy in the cell membrane, which is proportional to the concentration of the local signalling molecule (S). The corresponding set of equations is

$$\begin{cases} \dfrac{\mathrm{d}R^*}{\mathrm{d}t} = -k_1 R^*(t) I^*(t) + k_2 (R_0 - R^*(t)) A^*(t) \ , \\ \dfrac{\mathrm{d}I^*}{\mathrm{d}t} = -k_3 I^*(t) + k_4 (I_0 - I^*(t)) S \ , \\ \dfrac{\mathrm{d}A^*}{\mathrm{d}t} = -k_5 A^*(t) + k_6 (A_0 - A^*(t)) S \ , \end{cases} \tag{13.104}$$

where letter k with different subscripts is used to denote the kinetic constants of the various reactions involved. Assuming the presence in (13.104) of some small parameters, asymptotic limits are identified in [50,54] for which, as $t \longrightarrow \infty$

$$\frac{R^*}{R_0} \ \sim \ C \ \frac{A_0}{I_0} \qquad \text{for some } C > 0 \text{ independent of } S \ ,$$

so that R^* will not depend on the signalling molecule concentration, whence the system will exhibit the adaptation property.

It has been already mentioned that signal processing within the cell is mediated by receptor occupancy at its membrane. In other words, the incoming external cue is captured at some particular places (receptors) scattered over the cell boundary, thus triggering an internal signalling cascade. The physical mechanism by which growth cones sense gradients is a subject deserving considerable attention, and one in which more needs to be known. For instance, in a situation as that of a cell, in which the

energy due to thermal fluctuations is large enough to change the cell motion, the question naturally arises of what are the physical limitations on a cell's ability to sense and respond to changes in its environment. This issue was addressed in the work [5], where a model was produced that provided estimates for the statistical fluctuations in the measuring of concentrations by a small sensing device. From that model, the authors obtained estimates on sensitivity with respect to various factors including a bound on the minimum detectable gradient. This study has been recently taken up in [23], where comparison with experiments and limitations on its predictive value are discussed in detail.

We conclude this section by remarking on a macroscopic, RD-model for axon guidance. Here target cells and growth cones are represented as points in a two- or three-dimensional space, and attention is paid to the change in the concentrations of various chemical signals. More precisely, let us follow [32] and consider the interaction of three types of diffusible substances:

- A chemoattractant u_1 that is released by target cells at a rate σ_1 and has diffusion coefficient D_1
- A chemoattractant u_2 released by the axonal growth cones at a rate σ_2, with diffusion constant D_2
- A chemorepellent u_3 secreted by the axonal growth cones at a rate σ_3 which diffuses with a coefficient D_3

Here we are also denoting by u_1, u_2, and u_3 the concentrations of the signals involved. Assuming that axon growth occurs on a much longer scale than the time needed for diffusive fields to equilibrate (again, a small-parameter hypothesis), the authors of [32] arrive at the following system

$$\begin{cases} \triangle \rho_2 - k_2^2 u_2 = -\dfrac{\sigma_2}{D_2} \displaystyle\sum_\alpha \delta(x - r_\alpha(t)) \, , \\ \\ \triangle \rho_1 - k_1^2 u_1 = -\dfrac{\sigma_1}{D_1} \displaystyle\sum_i \delta(x - x_i) \, , \\ \\ \triangle \rho_3 - k_3^2 u_3 = -\displaystyle\sum_\alpha \sigma_3 \delta(x - r_\alpha(t)) \, , \end{cases} \tag{13.105}$$

where x_i is the fixed position of target cell i, r_α is the location of the α^{th}-growth cone at time t, k_i $(1 \leq i \leq 3)$ is the inverse diffusive length of chemical u_i, and $\delta(x - s)$ denotes Dirac's delta at $x = s$. We refer to [32] for a numerical study of the phenomena of bundling (during navigation) and debundling (on approaching the target). Actually, the analysis made in [32] is concerned with a number of situations, involving not only diffusible signals but also contact interactions, but we shall omit further details here.

13.4.2 Aggregation in Slime Moulds: the Keller-Segel System

The second problem in this section is concerned with morphogenesis, a key feature in the development of multicellular organisms, and already an inspiring motivation behind Turing's seminal work [84]. One of the simplest aspects of morphogenesis is cell aggregation. Indeed, as observed in [65], "... Aggregation phenomena, in which spatially separated cells gather together, form a multicellular group and then proceed to differentiation, are perhaps ideal for studying interactions between cells during morphogenesis. Unfortunately, not many systems are known in which aggregation occurs clearly separated in time from differentiation. Among other reasons, this makes it particularly important to make a detail study of the one *in vivo* system that is well characterised, namely the cellular slime moulds."

The precise biological features of these organisms which are of interest here are succinctly summarised by Bonner ([9], p.62 ; see also [8]) as follows: "... Cellular slime moulds are soil amoebae. They feed as separate individuals on bacteria, and after they have finished the food supply, they stream together to central collection points to form a multicellular individual of thousands of cells. This mass of amoebae moves as a unified "slug" toward light and is also oriented by heat gradients. After this period of migration, the anterior cells turn into stable cells that keep piling onto the tip, while most of the posterior cells turn into spores. The spore mass is slowly lifted into the air as the stalk elongates; the final result is a small fruiting body, in the order of one or two millimetres high, in which a spherical spore mass is supported on a slender stalk made up of large, vacuolate, dead stalk cells ...."

Out of all biological aspects mentioned above, each of which has interest on its own, we shall focus here on aggregation toward "central collection points." More precisely, it is known that when food becomes scarce, some individuals start emitting pulses of a chemical (cAMP $\equiv$ cyclic aminophosphatase in the case of the mould Dictyostellium discoideum, Dd for short). Organisms then proceed to move towards higher concentrations of the substance thus produced, and eventually concentrate into lumps. In the course of motion, experiments reveal a variety of structures: target and spiral waves (of which we have discussed before), but also streaming patterns.

We shall examine now an early continuum model which intends to describe this aggregation stage. It was introduced in 1970 by Keller and Segel (cf. [47]) and, in its simplest version, only two variables are considered. These are the concentration of cells at any point x and time t, to be denoted by $u(x,t)$, and that of the chemical producing aggregation, represented by $v(x,t)$. The conservation equations for $u(x,t)$ and $v(x,t)$ are of the form

$$\begin{aligned} \frac{\partial u}{\partial t} &= -\nabla \cdot \mathbf{J}_u \ , \\ \frac{\partial v}{\partial t} &= -\nabla \cdot \mathbf{J}_v + Au - Bv \ , \qquad A > 0 \ , \ B > 0 \ , \end{aligned} \tag{13.106}$$

where $\mathbf{J}_u$ and $\mathbf{J}_v$ are respectively the fluxes of cell and chemical concentrations,

and terms Au and $(-Bv)$ are particularly simple choices corresponding to chemical production and decay. As to the fluxes, these are assumed to be given by

$$\mathbf{J_v} = -D_v \nabla v \ , \qquad \mathbf{J_u} = -D_u \nabla u + u \nabla \chi(v) \ . \tag{13.107}$$

Here the diffusion coefficients D_u, D_v are positive, and $\chi(v)$ is the so-called chemotactic function, whose gradient attracts cells to gather together. A simple choice is to assume it to be linear, $\chi(v) = \chi v$ for some $\chi > 0$. Putting all pieces together, we eventually arrive at

$$\begin{cases} \dfrac{\partial u}{\partial t} = D_u \triangle u - \chi \nabla \cdot (u \nabla v) \ , \\ \dfrac{\partial v}{\partial t} = D_v \triangle v + Au - Bv \ . \end{cases} \tag{13.108}$$

Equations (13.108) are to be considered in a domain (usually bounded) $\Omega \subset \mathbb{R}^N$. Natural choices for N are $N = 2$ (a reasonable approximation for a Petri dish) and $N = 3$. For the purpose of mathematical analysis, (13.108) has to be supplemented with suitable initial and boundary conditions.

In the case of bounded domains, it is often assumed that there is no flux at the boundary, i.e.,

$$\frac{\partial u}{\partial \mathbf{n}} = \frac{\partial v}{\partial \mathbf{n}} = 0 \qquad \text{for } \mathbf{x} \in \partial\Omega \quad \text{and} \quad t > 0 \ . \tag{13.109}$$

Systems akin to (13.108) can be derived from an interacting stochastic system consisting of many particles, under the assumption that such interaction is of a moderate character when the population size increases to infinity; cf. [81] and also [38,71] for details concerning this derivation.

In the sequel we shall follow [34] to describe some properties of (13.108), a system that despite its simplicity encodes a rich structure. To begin with, one may wonder if the formation of dense cell aggregates (often referred to as chemotactic collapse) is captured at all in the model (13.108). In mathematical terms, this question may be formulated as follows:

Does system (13.108) possess solutions $(u(\mathbf{x}, t), v(\mathbf{x}, t))$ such that $u(\mathbf{x}, t)$ converges to some Dirac mass in finite time, i.e., such that

$$u(\mathbf{x}, t) \ - \!\!\rightarrow M \delta(\mathbf{x} - \mathbf{x}_0) \qquad \text{as} \qquad t \ - \!\!\rightarrow T \ , \tag{13.110}$$

for some $\mathbf{x}_0 \in \Omega$, $T < +\infty$ and $M > 0$?

In this approach, aggregation is represented as a type of blow-up, considered to be the late stage of an instability arising of an initially homogeneous state. As a matter of fact, this early stage can be analysed by means of the techniques recalled in section 13.2.5. To begin with, one has that $u(x, t) = u_0$ and $v(x, t) = v_0$ are constant solutions of (13.108) provided that $Au_0 = Bv_0$. Assume now that $N = 2$ for definiteness, and let us try on (13.108) an expansion of the form

$$u(x,y,t) = u_0 + a\cos(q_1 x + q_2 y)e^{\sigma t} + \cdots ,$$
$$v(x,y,t) = v_0 + b\cos(q_1 x + q_2 y)e^{\sigma t} + \cdots , \qquad (13.111)$$

where the constants a, b, q_1, and q_2 are to be determined. Retaining only linear terms, Equation (13.108) may be replaced in a neighbourhood of (u_0, v_0) by

$$\begin{cases} \dfrac{\partial u}{\partial t} = D_u \triangle u - \chi u_0 \triangle v , \\ \dfrac{\partial v}{\partial t} = D_v \triangle v + Au - Bv . \end{cases} \qquad (13.112)$$

Plugging (13.111) into (13.112) eventually yields

$$\chi u_0 q^2 b - (\sigma + q^2 D_u)a = 0 \quad , \; q^2 = q_1^2 + q_2^2 ,$$
$$-(q^2 D_v + B + \sigma)b + Aa = 0 ,$$

a dispersion relation similar to (but more involved than) (13.9). Since we are interested in nontrivial values of a and b, we need to impose

$$\sigma^2 + \sigma(q^2(D_u + D_v) + B) + q^2(D_u(q^2 D_v + B) - \chi u_0 A) = 0 . \qquad (13.113)$$

It is readily seen that a positive solution of this quadratic equation exists only if

$$0 < q^2 < (\chi u_0 A - BD_u)(D_u D_v)^{-1} ,$$

which in turn requires

$$\frac{\chi A u_0}{BD_u} > 1 . \qquad (13.114)$$

Actually, condition (13.114) implies that homogeneous steady states become (linearly) unstable whenever the initial concentration of cells is large enough.

When (13.113) holds, there exists a continuum of values of q for which (13.114) is satisfied. In particular, there is a value q^* at which the positive root $\sigma = \sigma(q^2)$ of (13.113) achieves a maximum.

Assuming $0 < q^2 \ll 1$, an approximate plot of σ against q^2 can be obtained as shown in Figure 13.7.

The argument just sketched provides a reasonable description of the initial stages of aggregation, that may be considered to be triggered by random perturbations (biological noise) around a given homogeneous state. However, it clearly appears that chemotactic collapse cannot be fully accounted for in such way. Indeed, the validity of this approach is confined to regions where perturbations remain small. As remarked in [65], it cannot be excluded that, after an initial period of

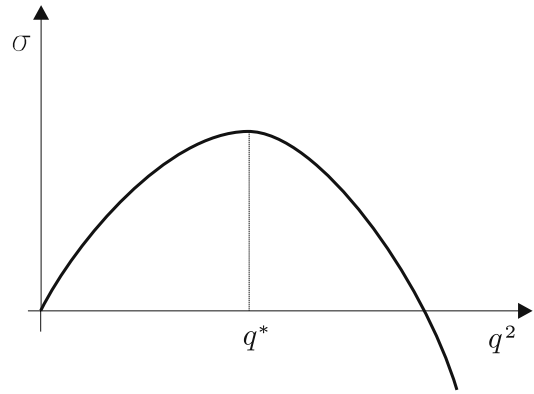

Figure 13.7
The relation between $\sigma(q^2)$ and q^2 for $0 < q^2 \ll 1$.

growth, the system would "settle down to another stationary state, spatially nonuniform, but far from aggregate." After all, this is precisely what was expected from the activator-inhibitor systems mentioned in section 13.2.6. Furthermore, even if some fluctuations would produce solutions that never return to a quiescent state, they could do so in infinite time, or even if blowing up in a finite time, they could do so in a different manner than that prescribed by (13.110).

We now provide a quick overview of known results concerning aggregation properties of system (13.108). As a startpoint, it was shown in [42] that in space dimension $N = 2$, solutions of (13.108), (13.109) exist for all times if the initial density $\bar{u}_0 = |\Omega|^{-1} \int_\Omega u_0(x)\, dx$ is small enough. However, radial solutions corresponding to $\bar{u}_0$ sufficiently large blow up in finite time. The existence of a critical threshold on $\bar{u}_0$ (that can be precisely characterised, see [64]) for blow up to occur is a relevant feature of the two-dimensional case, which is known to be absent when $N = 3$ (see [6] and [33] for results in that direction).

The actual occurrence of chemotactic collapse for radial solutions when $N = 2$ has been shown in [35] (for a simplified version of (13.108) corresponding to the case $0 < D_u \ll D_v$) and in [36,37] (for the general system (13.108) with both diffusion coefficients of order one). The structure of the solution which eventually unfolds into a Dirac's delta is better obtained by asymptotic methods. The basic idea consists in considering separately an inner region, located in a thin layer around the blow-up point (say, x_0), and an external, outer region, where solutions change slowly in time. At the inner region, the solution converges (in rescaled variables) toward a stationary solution of (13.108); the (*a priori* unknown) radius $R(t)$ of this region enters in the form of the scaling required for the stationary solution to eventually form there. At the outer region, our solution can be safely approximated by that of a linearised problem, where all information emanating from the inner region is averaged out in the form of a lumped source term. The radius $R(t)$ is then obtained

by requiring these two approximations (inner and outer) to match at an intermediate region, which overlaps with the inner and outer ones. We refer to [34] for additional details on this strategy, which is fully carried out in references [35–37].

We conclude this section by further remarking on some interesting properties of system (13.108). To begin with, when $N = 3$ a different blow-up mechanism appears. It consists in an imploding, smoothed out shock wave moving towards the blow-up point (cf. [33]). On the other hand, the stability of the chemotactic collapse obtained when $N = 2$ has been extensively discussed in [86], whereas possible regularisations of (13.108) allowing for solutions to be continued beyond blow-up (a natural requirement from a biological point of view) are studied in [87,88]. We also refer to these last two papers for recent mathematical analysis on the Keller-Segel model.

13.4.3 Modelling Some Aspects of Chemotaxis

The previous section was concerned with describing aggregation in slime moulds from a macroscopic point of view. In this way, cells were represented as points, and their individual evolution was reduced to the analysis of their concentration and that of the chemical released during clustering.

While such a crude simplification may be relevant in some contexts, it is far from being realistic in others. In particular, every aspect of the sophisticated processes associated to signal capturing by surface receptors, and its subsequent transduction to trigger a motile response in the cell, were simply ignored. Although these issues are far from being completely elucidated to this day, models have been proposed that partially account for these features. To keep this work within reasonable bounds, only two of them will be briefly described below. In particular, the underlying (and challenging) question of elaborating a comprehensive, multiscale model for Dd will not be addressed here.

The first work to be succinctly commented in the sequel is that by Hagan and Cohen (cf. [28]). Their goal consisted in providing a RD scenario for regulation of cAMP in Dd. They assumed that this can be accounted for in terms of the following variables: the extracellular (resp. intracellular) concentration of cAMP, the intracellular concentration of an inhibitor, and a lumped variable representing concentration of intracellular stored reserves. These are respectively denoted by $\alpha(x,t)$, (resp. $\bar{A}$), C, and S. The interplay of these variables is described in [28] by means of the following system

$$\begin{cases} \dfrac{\partial \alpha}{\partial t} = \bar{q}\bar{l}\bar{A} - p\alpha + D\triangle\alpha \ , \\ \dfrac{\partial \bar{A}}{\partial t} = \bar{f}(\alpha, C) - \bar{l}\bar{A} \ , \\ \dfrac{\partial C}{\partial t} = k(\alpha)S - a(C) - b(C) \ , \\ \dfrac{\partial S}{\partial t} = \dfrac{1}{n}[-k(\alpha)S + a(C)] \ . \end{cases} \tag{13.115}$$

Let us remark briefly on the various terms appearing in (13.115). The first equation therein describes changes in space and time of the concentration of external cAMP. This last increases proportionally (with factor $\bar{q}$) to the rate $\bar{l}\bar{A}$ at which internal cAMP is secreted by the cells. The second and third terms on the right account respectively for degradation and diffusion. The second equation represents synthesis of internal cAMP, and its loss by leaking to the external environment. Activation is due to function $f(\bar{\alpha}, C)$ which is increasing in α, and inhibited by C, so that it eventually saturates in a sigmoid manner (cf. Figure 1 in [28]). The third equation in (13.115) accounts for production of a feedback inhibitor C by catabolism of the stored reserves S (at a α-dependent rate, $k(\alpha)$). C is also recycled (at a rate $a(C)$) to rebuild S, and is lost at a rate $b(C)$. Finally, the last equation describes consumption of the stored reserves S at a rate $(\frac{1}{n})$ times the net production rate of C, and its simultaneous restoring (already discussed).

Of particular importance is the fact that n represents the number of monomers in one polymeric unit of S, so that $n \gg 1$, and we already have a small parameter in (13.115). As pointed out in [28], use of experimental information allows for further separation of scales in the model. For instance, degradation of α is rapid (between $\frac{1}{2}$ and 2 seconds), which suggests setting $p = \frac{1}{\varepsilon}$ with $0 < \varepsilon \ll 1$. Production of intracellular cAMP seems also to be fairly rapid (about 15 seconds). On the other hand, production of inhibitor occurs at a much slower pace (about 100 seconds). Furthermore, since $n \gg 1$, S is depleted only in a very slow scale (of the order of hours). Thus, on setting $ql = \varepsilon\bar{q}\bar{l}$, $\delta\bar{f}(\alpha, C) = f(\alpha, C)$, $l = \delta\bar{l}$ with $0 < \varepsilon \ll \delta \ll 1$, (13.115) can be recast in the form

$$\begin{cases} \dfrac{\partial \alpha}{\partial t} = \dfrac{1}{\varepsilon}(ql\bar{A}\alpha) + D\triangle\alpha \ , \\ \dfrac{\partial \bar{A}}{\partial t} = \dfrac{1}{\delta}(f(\alpha, C) - l\bar{A}) \ , \\ \dfrac{\partial C}{\partial t} = k(\alpha)S - a(C) - b(C) \ , \\ \dfrac{\partial S}{\partial t} = \dfrac{1}{n}[-k(\alpha)S + a(C)] \ . \end{cases} \tag{13.116}$$

One then may argue as follows. Since α evolves in a faster time scale than $\bar{A}$, it is always near equilibrium with $\bar{A}$, so that $\alpha \sim ql\bar{A}$. From the first equation in (13.116) we then obtain that

$$\alpha = ql\bar{A} + \varepsilon\left(D\triangle\alpha - \frac{\partial\alpha}{\partial t}\right) \sim ql\bar{A} + \varepsilon\left(D\triangle(ql\bar{A}) - ql\frac{\partial\bar{A}}{\partial t}\right)$$
$$\sim ql\left(\bar{A} + \varepsilon(D\triangle\bar{A} - \bar{A})\right) . \qquad (13.117)$$

We next consider the second equation in (13.116) and set there

$$A = ql\bar{A} \quad , \quad F(\alpha, C) = qlf(\alpha, C) .$$

Taking advantage of (13.117) and using Taylor's expansion on $F(\alpha, C)$, we obtain

$$\delta\frac{\mathrm{d}A}{\mathrm{d}t} = F(\alpha, C) - lA \qquad (13.118)$$
$$= F(A, C) - lA - \frac{\varepsilon}{\delta}F_A(A, C)\left(F(A, C) - lA\right) + \varepsilon DF_A(A, C)\triangle A + \dots .$$

Arguing in a similar way for the third equation in (13.116), we are able to reduce the original system (13.115) to one consisting of three equations, namely

$$\begin{cases} \delta\dfrac{\partial\bar{A}}{\partial t} = F(A, C) - lA + \varepsilon DF_A(A, C)\triangle A , \\ \dfrac{\partial C}{\partial t} = k(A)S - a(C) - b(C) + \varepsilon DSk'(A)\triangle A , \\ \dfrac{\partial S}{\partial t} = \dfrac{1}{n}[-k(A)S + a(C)] . \end{cases} \qquad (13.119)$$

Moreover, since S changes little in time, we may consider (13.119) as consisting essentially of its first two equations, and having a slowly varying parameter there. The reduced system thus obtained can be analysed in two steps. First, we may drop the (small) diffusivity terms, and then consider the ODE system thereby obtained. Keeping track of the variation of S, it is then possible to classify the corresponding equilibrium states and describe the resulting dynamics in phase space. At a second stage, we introduce back the weak coupling due to diffusion, to characterise the onset of pulse and spiral patterns in the reduced system (13.119) (cf. [28], p. 885-898).

A question also addressed in [28] is the need of a rule connecting external cAMP concentration with cell motion. This is assumed to be that cells move in the direction opposite to cAMP wave propagation. In this way, evidence for the formation of streams can be obtained in the following manner. Suppose that cells are migrating toward a distant aggregation centre located on the x-axis. We can then write A and C in the form

$$\begin{cases} A(t, x) = \widetilde{A}(\omega_0 t + \psi(\tau, x), S_0) + \dots , \quad \tau = \varepsilon t , \\ C(x, t) = \widetilde{C}(\omega_0 t + \psi(\tau, x), S_0) + \dots , \end{cases} \qquad (13.120)$$

(recall Equations (13.82) to (13.90) in the previous section). Here $\psi(\tau, x)$ is the phase shift, that may be assumed to be in the form of a plane wave near the origin: $\psi \sim kx + \gamma\tau$ for some k, γ; w_0 is the average of $\omega(S(x))$, a frequency determined by the local value of $\omega(S(x))$, and S_0 is the average value of $S(x)$. Assuming $\omega(S(x))$ to be almost constant and equal to ω_0 except in a small region: $x^2 + y^2 < r_0^2$, we may write $\psi(\tau, x)$ in the form

$$\psi(\tau, x) = kx + \gamma\tau + P(\tau, x, y) \, , \tag{13.121}$$

where P represents the perturbation caused by the inhomogeneities of $\omega\,(S(x))$ around the origin. From Equations (13.119) to (13.121), it is possible to estimate the term $(\nabla\psi - (k, 0))$ which represents the relative direction field of the cell motion, to eventually produce a streaming pattern as that in Figure 8 in [28].

We conclude this section by succinctly describing a model containing elements already incorporated in [28] together with the explicit consideration of a (possibly large) population of moving organisms, as in the system studied in [32] and recalled in section 13.3.1. More precisely, we follow [70] and consider a family of n organisms, assumed to be approximately circular, moving on a two-dimensional space. The position of any cell is then characterised by the location of its centre, $R_i(t) = (x_i(t), y_i(t)) \equiv r_i(t)$ with $1 \leq i \leq n$. The model in [70] describes Dd cells which can produce cAMP and move towards a cAMP gradient according to the following rules: Dd cells have membrane receptors that can be either active or inactive. In the active state, the receptors can bind external cAMP, thereby stimulating the synthesis of cAMP inside the cell. This intracellular cAMP is then leaked outside the cell, where it stimulates cAMP receptors, thereby closing a feedback loop. On the other hand, receptors become inactive as a result of prolonged exposure to high cAMP concentrations, which allows for refractory periods in the cell. In mathematical terms, we introduce three variables: $\rho(r, t)$ (fraction of cAMP receptors in active state), $\beta(r, t)$ (concentration of intracellular cAMP), and $\gamma(r, t)$ (concentration of extracellular cAMP) and state the following relations among them

$$\begin{cases} \varepsilon_1 \dfrac{\partial \rho}{\partial t} = (-f_1(\gamma)\rho + f_2(\gamma)(1-\rho)) \displaystyle\sum_{i=1}^{n} \delta(r - R_i(t)) \, , \\ \varepsilon_2 \dfrac{\partial \beta}{\partial t} = (s_1 \Phi(\rho, \gamma) - \beta(r, t)) \displaystyle\sum_{i=1}^{n} \delta(r - R_i(t)) \, , \\ \dfrac{\partial \gamma}{\partial t} = D \triangle \gamma + \dfrac{1}{\varepsilon_3}(s_2 \beta - \gamma) \displaystyle\sum_{i=1}^{n} \delta(r - R_i(t)) \, . \end{cases} \tag{13.122}$$

Here functions f_1, f_2, and Φ are given, and a number of parameters appear which allow for separation of scales in suitable asymptotic limits. For instance, arguments are given in [70] to assume that the second equation in (13.122) is in a

quasi-steady state (that is, the internal cAMP dynamics are very fast). Then (13.122) can be reduced to

$$\begin{cases} \varepsilon_1 \dfrac{\partial \rho}{\partial t} = (-f_1(\gamma)\rho + f_2(\gamma)(1-\rho)) \displaystyle\sum_{i=1}^{n} \delta(r - R_i(t)) \ , \\ \dfrac{\partial \gamma}{\partial t} = D \triangle \gamma + \dfrac{1}{\varepsilon_3}(s\Phi - \gamma) \displaystyle\sum_{i=1}^{n} \delta(r - R_i(t)) \ . \end{cases} \tag{13.123}$$

As in the case previously examined (cf. [28]), a locomotion rule needs yet to be added to (13.123) to account for cell motion. Some choices for such rules are discussed in [70], but to give merely a glimpse of the problems therein considered, we just comment on one of these. Let $\mu = \mu(\rho, \gamma)$ be such that $\mu = 0$ if the following conditions are met: either $\rho < \rho_0$ for some critical value ρ_0, or $|\nabla \gamma| < \theta_0$ for some $\theta_0 > 0$; we take $\mu = 1$ otherwise. Then motion of the cells can be described by the equation

$$\frac{\mathrm{d}R_i}{\mathrm{d}t} = \mu \frac{\nabla \gamma}{|\nabla \gamma|} \ , \qquad \text{for } i = 1, \ldots, n \ . \tag{13.124}$$

The mathematical analysis of (13.123), (13.124) with $n \gg 1$ is rather involved. However, numerical simulations seem to be comparatively easier. A number of them were performed in [70], which show occurrence of various types of patterns, including stream formation and spiral motion, in suitable ranges of the parameters appearing in (13.123), (13.124).

13.5 References

[1] Abramowitz, M. and Stegun, I.A., *Handbook of Mathematical Functions*, Dover, New York, 1972.

[2] Andreucci, D., Herrero, M.A., and Velázquez, J.J.L., On the growth of filamentary structures in planar media, Preprint, 2002.

[3] Aronson, D.G., The porous medium equation, in *Nonlinear Diffusion Processes*, A. Fasano and M. Primicerio, Eds., Springer Lecture Notes in Mathematics n$^{\mathrm{o}}$ 1224, 1-46, Heidelberg, 1985.

[4] Bender, C.M. and Orszag, S.A., *Advanced Mathematical Methods for Scientists and Engineers*, Springer Verlag, Heidelberg, 1999.

[5] Berg, H.C. and Purcell, E.M., Physics of chemoreception, *Biophysical J.* 20, 193-219, 1977.

[6] Biler, P., Local and global solvability of some parabolic systems modelling chemotaxis, *Adv. Math. Sci. Appl.* 8, 297-308, 1998.

[7] Birkhoff, G. and Rota, G.C., *Ordinary Differential Equations*, John Wiley & Sons, New York, 1989.

[8] Bonner, J.T., *The Cellular Slime Molds*, Princeton Univ. Press, Princeton, NJ, 1967.

[9] Bonner, J.T., *Sixty Years of Biology*, Princeton Univ. Press, Princeton, NJ, 1996.

[10] Casten, R.G., Cohen, H., and Lagerstrom, P.A., Perturbation analysis of an approximation to the Hodgkin-Huxley theory, *Quart. Appl. Math.* Vol. XXXII, 4, 365-402, 1975.

[11] Chandrasekhar, S., Stochastic problems in physics and astronomy, *Rev. Modern Physics* 15, 1-85, 1943.

[12] Coddington, E.A. and Levinson, N., *Theory of Ordinary Differential Equations*, McGraw-Hill, New York, 1995.

[13] Cohen, D.S., Neu, J.C., and Rosales, R.R., Rotating spiral wave solutions of reaction-diffusion equations, *SIAM J. Appl. Math.* 35, 536-547, 1978.

[14] Conway, E., Hoff, D., and Smoller, J., Large time behaviour of solutions of systems of nonlinear reaction-diffusion equations, *SIAM J. Appl. Math.* 35, 1-16, 1978.

[15] Cronin, J., *Mathematical Aspects of Hodgkin-Huxley Neural Theory*, Cambridge University Press, London, New York, 1987.

[16] Cross, M.C. and Hohenberg, P.C., Pattern formation outside of equilibrium, *Rev. Modern Physics* 65, 854-1090, 1993.

[17] Fife, P.C., *Mathematical Aspects of Reacting and Diffusing Systems*, Springer Lecture Notes in Biomathematics n^o 28, Heidelberg, 1979.

[18] Fife, P.C. and McLeod, J.B., The approach of solutions of nonlinear diffusion equations to travelling front solutions, *Arch. Rat. Mech. Anal.* 65, 335-361, 1977.

[19] Fife, P.D. and McLeod, J.B., A phase plane discussion of convergence to travelling fronts for nonlinear diffusion, *Arch. Rat. Mech. Anal.* 75, 281-314, 1981.

[20] Fisher, R.S., *The Genetical Theory of Natural Selection*, Oxford University Press, Oxford, 1930.

[21] Friedman, A., *Partial Differential Equations of Parabolic Type*, Robert Krieger Co., Malabar, FL, 1983.

[22] Gierer, A. and Meinhardt, H., A theory of biological pattern formation, *Kybernetik* 12, 30-39, 1972.

[23] Goodhill, G.J. and Urbach, J.S., Theoretical analysis of gradient detection by growth cones, *J. Neurobiol.* 41, 230-241, 1999.

[24] Grimmet, G. and Stirzaker, D., *Probability and Random Processes*, Oxford University Press, Oxford, 2001.

[25] Grindrod, P., *Patterns and Waves*, Oxford University Press, Oxford, 1991.

[26] Hagan, P.S., Target patterns in reaction-diffusion systems, *Adv. in Appl. Math.* 2, 400-416, 1981.

[27] Hagan, P.S., Spiral waves in reaction-diffusion equations, *SIAM J. Appl. Math.* 42, 762-786, 1982.

[28] Hagan, P.S. and Cohen, M.S., Diffusion induced morphogenesis in the development of Dictyostellium, *J. Theor. Biol.* 93, 881-908, 1981.

[29] Hairer, E. and Wanner, G., *Analysis by Its History*, Springer, Heidelberg, 1996.

[30] Hellwig, G., *Partial Differential Equations*, Teubner, Stuttgart, 1977.

[31] Henry, D., *Geometric Theory of Semilinear Parabolic Equations*, Springer Lecture Notes in Mathematics 840, Heidelberg, 1981.

[32] Hentschel, H.G.E. and van Ooyen, A., Models of axon guidance and bundling during development, *Proc. R. Soc. London B*, 266, 2231-2238, 1999.

[33] Herrero, M.A., Medina, E., and Velázquez, J.J.L., Finite-time aggregation into a single point in a reaction-diffusion system, *Nonlinearity* 10, 1754-1793, 1997.

[34] Herrero, M.A., Asymptotic properties of reaction-diffusion systems modelling chemotaxis, in *Applied and Industrial Mathematics*, R. Spigler, Ed., Kluwer Acad. Pub., Dortrecht, 89-108, 2000.

[35] Herrero, M.A. and Velázquez, J.J.L., Singularity patterns in a chemotaxis model, *Math. Ann.* 306, 583-623, 1996.

[36] Herrero, M.A. and Velázquez, J.J.L., Chemotactic collapse for the Keller-Segel model, *J. Math. Biol.* 35, 177-196, 1996.

[37] Herrero, M.A. and Velázquez, J.J.L., A blow-up mechanism for a chemotactic model, *Ann. Scuola Norm. Sup. Pisa, Ser. IV*, vol. XXIV, 633-683, 1997.

[38] Hillen, T. and Othmer, H.G., The diffusion limit of transport equations derived from velocity-jump processes, *SIAM J. Appl. Math.* 61, 751-775, 2000.

[39] Hodgkin, A.L. and Huxley, A.F., A quantitative description of membrane current and its application to conduction and excitation in nerve, *J. Physiology (London)* 117, 500-544, 1952.

[40] Hoel, P.G., Port, S.C., and Stone, C.J., *Introduction to Stochastic Processes*, Houghton Mifflin Co., Boston, 1972.

[41] Ikebe, T., Eigenfunction expansions associated with the Schrödinger operators and their applications to scattering theory, *Arch. Rat. Mech. Anal.* 5, 1-34, 1960.

[42] Jäger, W. and Luckhaus, S., On explosions of solutions to a system of partial differential equations modeling chemotaxis, *Trans. Amer. Math. Soc.* 329, 819-824, 1992.

[43] Jones, C.K.R.T., Stability of the travelling wave solution of the FitzHugh-Nagumo system, *Trans. Amer. Math. Soc.* 286, 431-469, 1984.

[44] Kanel, Y.I., On the stabilization of solutions of the Cauchy problem for equations arising in the theory of combustion, *Mat. Sbornik* 59, 245-288, 1962. See also *Sov. Math. Dokl.* 1, 513-516, 1960, and *Sov. Math. Dokl.* 2, 48-51, 1961.

[45] Keener, J.P., Waves in excitable media, *SIAM J. Appl. Math.* 39, 528-548, 1980.

[46] Keener, J.P., A geometrical theory for spiral waves in excitable media, *SIAM J. Appl. Math.* 46, 1039-1056, 1986.

[47] Keller, E.F. and Segel, L.A., Initiation of slime mold aggregation viewed as an instability, *J. Theor. Biol.* 26, 399-415, 1970.

[48] Kishimoto, K. and Weinberger, H.F., The spatial homogeneity of stable equilibria of some reaction-diffusion systems on convex domains, *J. Diff. Equations* 58, 15-21, 1985.

[49] Kolmogorov, A., Petrovsky, I., and Piskunov, N., Study of the diffusion equation with growth of the quantity of matter, and its application to a biology problem. *Bul. Moskovskovo Gos. Univ.* 17, 1-26, 1937, (in Russian). English translation in *The Dynamics of Curved Fronts* P. Pelcé, Ed., Academic Press, New York, 1988.

[50] Krishnan, J., Iglesias, P.A., and Ma, L., Spatial sensing of chemotactic gradients: a reaction-diffusion approach, preprint (2002).

[51] Kuramoto, Y., *Chemical Oscillations, Waves and Turbulence*, Springer Series in Synergetics, Heidelberg, 1984.

[52] Ladyzenskaja, O.A., Solonnikov, V.A., and Uraltseva, N.N., *Linear and Quasilinear Equations of Parabolic Type*, Transl. Math. Monographs. vol. 23, AMS, Providence, RI, 1968.

[53] Larson, D.A., Transient bounds and time-asymptotic behavior of solutions to nonlinear equations of Fisher type, *SIAM J. Appl. Math.* 34, 93-103, 1978.

[54] Levchenko, A. and Iglesias, P. A., Models of eukaryotic gradient sensing: applications to chemotaxis of amoebae and neutrophils, *Biophysical J.* 82, 50-63, 2002.

[55] N. G. Lloyd, *Degree Theory*, Cambridge University Press, London, New York, 1978.

[56] Matano, H., Asymptotic behaviour and stability of solutions of semilinear diffusion equations, *Publ. RIMS, Kyoto Univ.* 15, 401-454, 1979.

[57] Matano, H. and Mimura, M., Pattern formation in competition-diffusion systems in nonconvex domains, *Publ. RIMS, Kyoto Univ.* 19, 1049-1079, 1983.

[58] Meinhardt, H., Morphogenesis of lines and nets, *Differentiation* 6, 117-123, 1976.

[59] Meinhardt, H., *Models of Biological Pattern Formation*, Academic Press, New York, 1982.

[60] Meinhardt, H., Orientation of chemotactic cells and growth cones: models and mechanisms, *J. Cell Science* 112, 2867-2874, 1999.

[61] Mikhailov, A.S., *Foundations of Synergetics I*, Springer Verlag, Heidelberg, 1994.

[62] Ming, G.-L., Wang, S.T., Henley, J., Yuan, X.B., Song, H.J., Spitzer, N.C., and Poo, M.M., Adaptation in the chemotactic guidance of nerve growth cone, *Nature* 417, 411-418, 2002.

[63] Murray, J.D., *Mathematical Biology*, Springer, Heidelberg, 1993.

[64] Nagai, T., Blow-up of radially symmetric solutions to a chemotaxis system, *Adv. Math. Sci. Appl.*, 1-21, 1995.

[65] Nanjundiah, V., Chemotaxis, signal relaying, and aggregation morphology, *J. Theor. Biol.* 42, 63-105, 1973.

[66] Neu, J.C., Chemical waves and the diffusive coupling of limit cycle oscillators, *SIAM J. Appl. Math.* 36, 509-515, 1979.

[67] Neu, J.C., Coupled chemical oscillators, *SIAM J. Appl. Math.* 37, 307-315, 1979.

[68] Neu, J.C., Large populations of coupled chemical oscillators, *SIAM J. Appl. Math.* 38, 305-316, 1980.

[69] Oelschläger, K., On the derivation of reaction-diffusion equations as limit dynamics of systems of moderately interacting stochastic processes, *Prob. Theor. Rel. Fields* 82, 565-581, 1989.

[70] Oss, C.V., Panfilov, A.V., Hogeweg, P., Siegert, F., and Weijer, C.J., Spatial pattern formation during aggregation of the slime mould Dictyostellium discoideum, *J. Theor. Biol.* 181, 203-213, 1996.

[71] Othmer, H.G., and Hillen, T., The diffusion limit of transport equations II: chemotaxis equations, *SIAM J. Appl. Math.* 62, 1222-1250, 2002.

[72] Pazy, A., *Semigroups of Linear Operators and Applications to PDE*, Springer, Heidelberg, 1983.

[73] Ramón y Cajal, S., Sobre la aparición de las expansiones celulares en la médula embrionaria, *Gaceta Sanitaria de Barcelona* 12, 413-419, 1890.

[74] Ramón y Cajal, S., La retine des vertébrés, *La Cellulle* 9, 119-258, 1893.

[75] Rashewsky, N., An approach to the mathematical biophysics of biological self-regulation and cell polarity, *Bull. Math. Biophys.* 2, 15-25, 1940.

[76] Rinzel, J. and Keller, J.B., Travelling wave solutions of a nerve conduction equation, *Biophysical J.* 13, 1313-1337, 1973.

[77] Rinzel, J. and Terman, D., Propagation phenomena in a bistable reaction-diffusion system, *SIAM J. Appl. Math.* 42, 1111-1137, 1980.

[78] Rothe, F., *Global Solutions of Reaction-Diffusion Systems*, Springer Lecture Notes in Mathematics n^o 1072, Heidelberg, 1984.

[79] Schiff, L.I., *Quantum Mechanics*, McGraw-Hill, New York, 1968.

[80] Song, H.-J. and Poo, M.-M., The cell biology of neuronal navigation, *Nature Cell Biol.* 3, E81-E88, 2001.

[81] Stevens, A., The derivation of chemotaxis equations as limit dynamics of moderately interacting stochastic many-particle systems, *SIAM J. Appl. Math.* 61, 183-212, 2000.

[82] Strogatz, S.H., From Kuramoto to Crawford: exploring the onset of synchronization in populations of coupled oscillators, *Physica D* 25, 1-20, 2000.

[83] Tessier-Lavigne, M. and Goodman, C.S., The molecular biology of axon guidance, *Science* 274, 1123-1133, 1996.

[84] Turing, A. M., The chemical basis of morphogenesis, *Phil. Trans. R. Soc. London* 237, 37-72, 1952.

[85] Uchiyama, K., The behaviour of solutions of some nonlinear diffusion equations for large times, *J. Math. Kyoto Univ.* 18, 453-508, 1978.

[86] Velázquez, J.J.L., Stability of some mechanisms of chemotactic aggregation, *SIAM J. Appl. Math.* 62, 1581-1633, 2002.

[87] Velázquez, J.J.L., Point dynamics in a singular limit of the Keller-Segel model. To appear in *SIAM J. Appl. Math.* A preprint can be downloaded at `http://www.mat.ucm.es/deptos/ma`.

[88] Velázquez, J.J.L., Well posedness of a model of point dynamics for a limit of the Keller-Segel system. Submitted for publication 2002. A preprint can be downloaded at `http://www.mat.ucm.es/deptos/ma`.

[89] Weinberger, H.F., *A First Course in Partial Differential Equations*, Dover, New York, 1995.

[90] Whitham, G.B., *Linear and Nonlinear Waves*, Wiley Interscience, New York, 1974.

[91] Winfree, A.T., *The Geometry of Biological Time*, Springer Verlag, Heidelberg, 1980.

[92] Winfree, A.T., *When Time Breaks Down*, Princeton Univ. Press, Princeton, NJ, 1987.